NASA CR 71506

VOYAGER SPACECRAFT SYSTEM

FINAL TECHNICAL REPORT

VOLUME B
ALTERNATE DESIGNS CONSIDERED FOR FLIGHT SPACECRAFT AND HARDWARE SUBSYSTEMS

prepared for

JET PROPULSION LABORATORY
CALIFORNIA INSTITUTE OF TECHNOLOGY
PASADENA, CALIFORNIA

UNDER
CONTRACT NO. 951111
JULY 1965

THE BOEING COMPANY • AERO-SPACE DIVISION • SEATTLE, WASHINGTON

THE BOEING COMPANY

SEATTLE, WASHINGTON 98124

LYSLE A. WOOD
VICE PRESIDENT-GENERAL MANAGER
AERO-SPACE DIVISION

July 29, 1965

Jet Propulsion Laboratory
California Institute of Technology
4800 Oak Grove Drive
Pasadena, California

Gentlemen:

This technical report culminates nearly three years of Mariner/Voyager studies at Boeing. During this time, we have gained an appreciation of the magnitude of the task, and feel confident that the experience, resources and dedication of The Boeing Voyager Team can adequately meet the challenge.

The Voyager management task is accentuated by three prime requirements: An inflexible schedule of launch opportunities; the need for an information-retrieval system capable of reliable high-traffic transmission over interplanetary distances; and a spacecraft design flexible enough to accommodate a number of different mission requirements. We believe the technical approach presented here satisfies these design requirements, and that management techniques developed by Boeing for space programs will assure delivery of operable systems at each critical launch date.

Mr. E. G. Czarnecki has been assigned program management responsibility. His group will be ably assisted by Electro-Optical Systems in the area of spacecraft power, Philco Western Development Laboratories will be responsible for telecommunications, and the Autonetics Division, North American Aviation will provide the auto-pilot and attitude reference system. This team has already demonstrated an excellent working relationship during the execution of the Phase IA contract, and will have my full confidence and support during subsequent phases.

This program will report directly to George H. Stoner, Vice President and Assistant Division Manager for Launch and Space Systems. Mr. Stoner has the authority to assign the resources necessary to meet the objectives as specified by JPL.

The Voyager Spacecraft System represents to us more than a business opportunity or a new product objective. We view it as a chance to extend scientific knowledge of the universe while simultaneously contributing to national prestige and we naturally look forward to the opportunity of sharing in this adventure.

Lysle A. Wood

Lysle A. Wood

INTRODUCTION

CONTENTS

CONTENTS
(Cont.)

INTRODUCTION

In fulfillment of the Jet Propulsion Laboratory (JPL) Contract 951111, the Aero-Space Division of The Boeing Company submits the Voyager Spacecraft Final Technical Report. The complete report, responsive to the documentation requirements specified in the Statement of Work, consists of the five following documents:

VOLUME	TITLE	BOEING DOCUMENT NUMBER
A	Preferred Design Flight Spacecraft and Hardware Subsystems	D2-82709-1
	Part I	
	Section 1.0 Voyager 1971 Mission Objectives and Design Criteria	
	Section 2.0 Design Characteristics and Restraints	
	Section 3.0 System Level Functional Descriptions of Flight Spacecraft	
	Part II	
	Section 4.0 Functional Description for Spacecraft Hardware Subsystems	
	Part III	
	Section 5.0 Schedule and Implementation Plan Section 6.0 System Reliability Summary Section 7.0 Integrated Test Plan Development	
B	Alternate Designs Considered--Flight Spacecraft and Hardware Subsystems	D2-82709-2
C	Design for Operational Support Equipment	D2-82709-3
D	Design for 1969 Test Spacecraft	D2-82709-4
E	Design for Operational Support Equipment for 1969 Test Flight Spacecraft	D2-82709-5

For convenience the highlights of the above documentation have been summarized to give an overview of the scope and depth of the technical effort and management implementation plans produced during Phase IA. This summary is contained in Volume 0, Program Highlights and Management Philosophy, D2-82709-0. A number of supporting documents are provided to furnish detailed information developed through the course of the contract and to provide substantiating reference material which would not otherwise be readily available to JPL personnel. Additionally, a full scale mock-up of the preferred design spacecraft has been assembled. This mock-up, shown in Figure 1, has been delivered to JPL. The mock-up has been provided with the view that it would be of value to JPL in subsequent Voyager Spacecraft System planning. Mr. William M. Allen, President of The Boeing Company, Mr. Lysle A. Wood, Vice-President and Aero-Space Division General Manager, Mr. George H. Stoner, Vice-President and Assistant Division Manager responsible for Launch and Space Systems activities, and Mr. Edwin G. Czarnecki, Voyager Program Manager, are shown with the mock-up.

During the three-month period covered by Contract 951111, Boeing has:

1) Performed system analysis and trade studies necessary to achieve an optimum or preferred design of the Flight Spacecraft.
2) Determined the requirements and constraints which are imposed upon the Flight Spacecraft by the 1971 mission and by the other systems and elements of the project, including the science payload.
3) Developed functional descriptions for the Flight Spacecraft and for each of its hardware subsystems, excluding the science payload.

Figure 1: Preferred Design Mockup

Left to Right:

William M. Allen
Edwin G. Czarnecki
Lysle A. Wood
George H. Stoner

4) Determined the requirements for the Flight Spacecraft associated Operational Support Equipment (OSE) necessary to accomplish the Voyager 1971 mission.

5) Developed a preliminary design of the OSE.

6) Developed functional descriptions for the OSE.

7) Determined the objectives of a 1969 test flight and the design of the 1969 Test Flight Spacecraft using the Atlas/Centaur Launch Vehicle. An alternate test flight program is presented which utilizes the Saturn IB/Centaur Launch Vehicle.

8) Developed functional descriptions for the Flight Spacecraft Bus, and its hardware subsystems, and OSE for the 1969 test spacecraft.

9) Updated and supplemented the Voyager Implementation Plan originally contained in the response to JPL Request for Proposal 3601.

The Voyager Program Management Team, shown in Figure 2, is under the direction of Mr. Edwin G. Czarnecki. Mr. Czarnecki is the single executive responsible to JPL and Boeing management for the acoomplishment of the Voyager Spacecraft Phase IA, and will direct subsequent phases of the program. He reports directly to Mr. George H. Stoner who has the authority to commit those corporate resources necessary to fulfill JPL's Voyager Spacecraft System objectives.

Although Boeing has a technical management capability in all aspects of the Voyager program, it is planned to extend this capability in depth through association with companies recognized as specialists in certain fields. Use of team members to strengthen Boeing's capability was considered early during preproposal activities. The basic concept was to

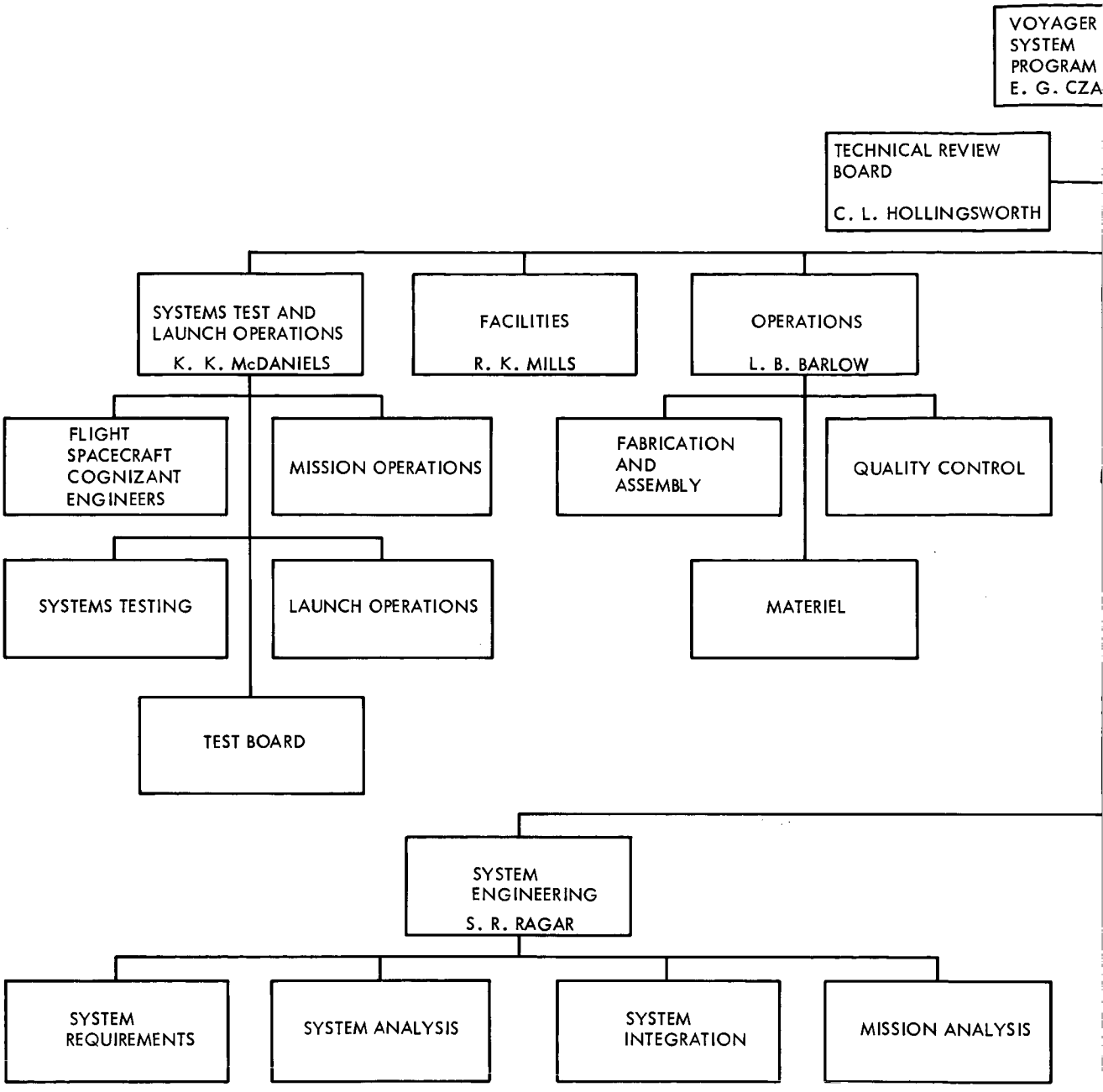
VOYAGER
SYSTEM
PROGRAM
E. G. CZA
TECHNICAL REVIEW
BOARD
C. L. HOLLINGSWORTH
SYSTEMS TEST AND
LAUNCH OPERATIONS
K. K. McDANIELS
FACILITIES
R. K. MILLS
OPERATIONS
L. B. BARLOW
FLIGHT
SPACECRAFT
COGNIZANT
ENGINEERS
MISSION OPERATIONS
FABRICATION
AND
ASSEMBLY
QUALITY CONTROL
SYSTEMS TESTING
LAUNCH OPERATIONS
MATERIEL
TEST BOARD
SYSTEM
ENGINEERING
S. R. RAGAR
SYSTEM
REQUIREMENTS
SYSTEM ANALYSIS
SYSTEM
INTEGRATION
MISSION ANALYSIS

10

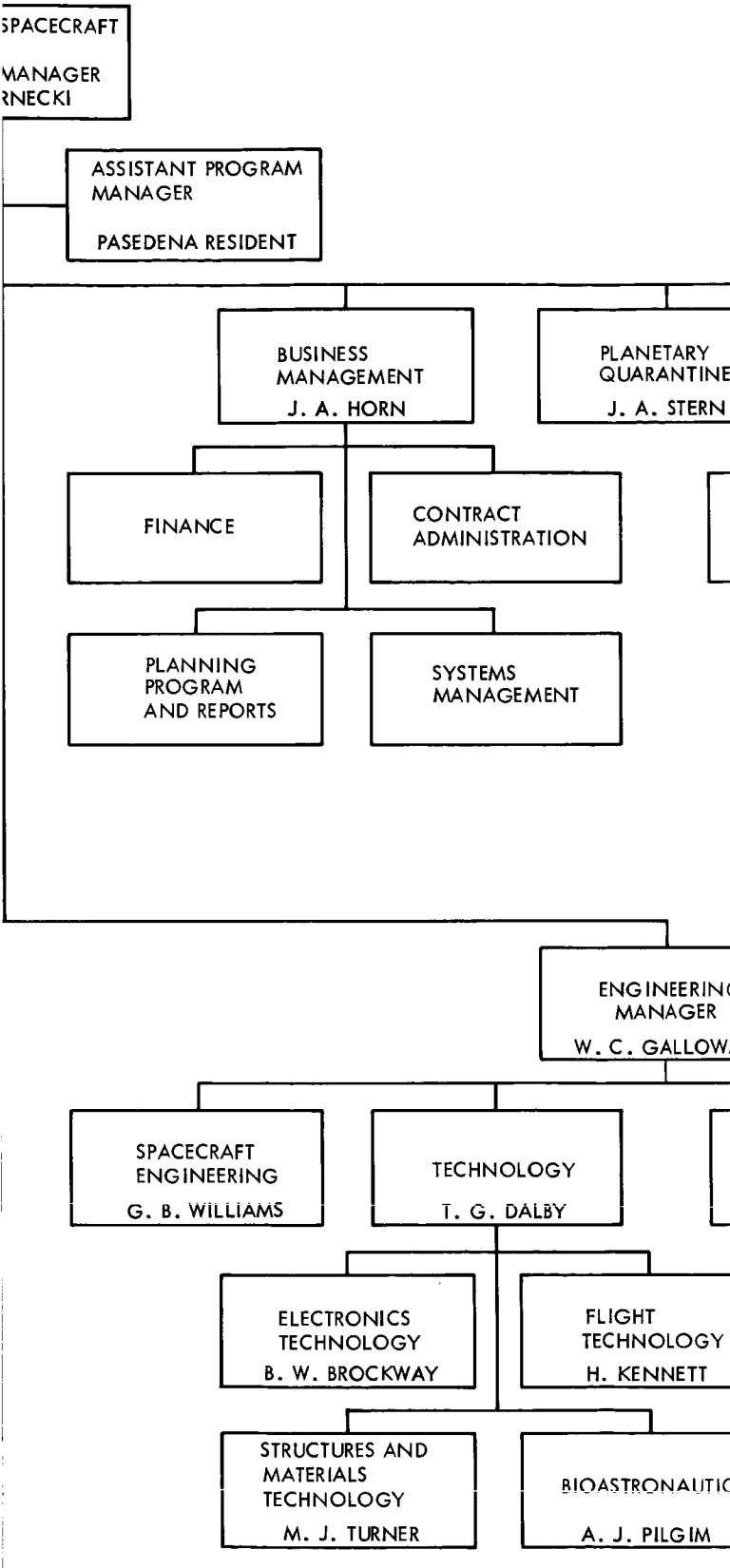
SPACECRAFT
MANAGER
RNECKI
ASSISTANT PROGRAM MANAGER
PASEDENA RESIDENT
BUSINESS MANAGEMENT
J. A. HORN
PLANETARY QUARANTINE
J. A. STERN
FINANCE
CONTRACT ADMINISTRATION
PLANNING PROGRAM AND REPORTS
SYSTEMS MANAGEMENT
ENGINEERING MANAGER
W. C. GALLOW
SPACECRAFT ENGINEERING
G. B. WILLIAMS
TECHNOLOGY
T. G. DALBY
ELECTRONICS TECHNOLOGY
B. W. BROCKWAY
FLIGHT TECHNOLOGY
H. KENNETT
STRUCTURES AND MATERIALS TECHNOLOGY
M. J. TURNER
BIOASTRONAUTIC
A. J. PILGIM

Spacecra

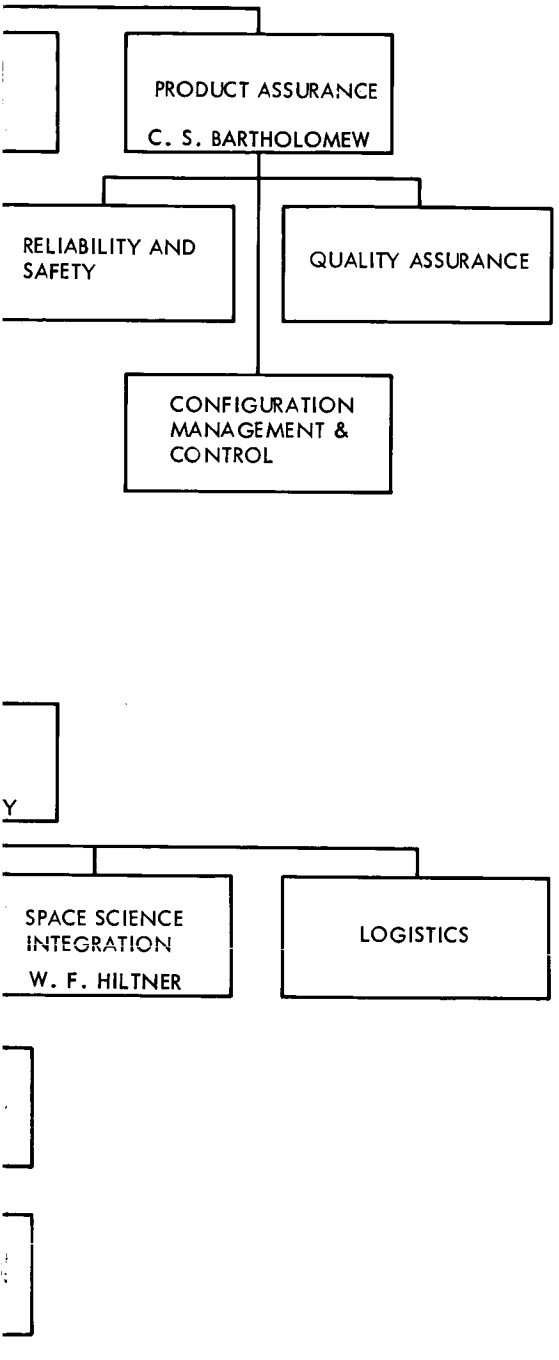

Figure 2 Boeing Voyager
ft Systems Management Structure

add team members who would complement Boeing experience and capability, and significantly improve the amount of quality of technical and management activities. Based upon competitive considerations including experience and past performance and giving strongest emphasis to technical qualifications and management willingness to support the Voyager effort, Autonetics, Philco Western Development Laboratories, and Electro-Optics Systems were chosen as team members. This team arrangement, subject to JPL approval, is shown in Figure 3. The Flight Spacecraft design and integration task to be accomplished by this team is illustrated in Figure 4. Discussions leading to the formation of this team were initiated late in 1964, formal work statement agreements have been arrived at, and there has been a continuous and complete free exchange of information and documentation permitting the Boeing team to satisfy JPL's requirements in depth and with confidence.

<table>
<tr><td colspan="3">BOEING VOYAGER TEAM

VOYAGER SPACECRAFT AND SPACE SCIENCES PAYLOAD INTEGRATION CONTRACTOR

The Boeing Company
Seattle, Washington

Mr. E. G. Czarnecki - Program Manager</td></tr>
<tr><td>SUBCONTRACTOR

Autonetics, North American Aviation
Anaheim, California

Autopilot and Attitude Reference Subsystem

Mr. R. R. Mueller
Program Manager</td><td>SUBCONTRACTOR

Philco, Western Development Lab.
Palo Alto, California

Telecommunication Subsystem

Mr. G. C. Moore
Program Manager</td><td>SUBCONTRACTOR

Electro-Optical Systems, Inc.
Pasadena, California

Electrical Power Subsystem

Mr. C. I. Cummings
Program Manager</td></tr>
</table>

Figure 3

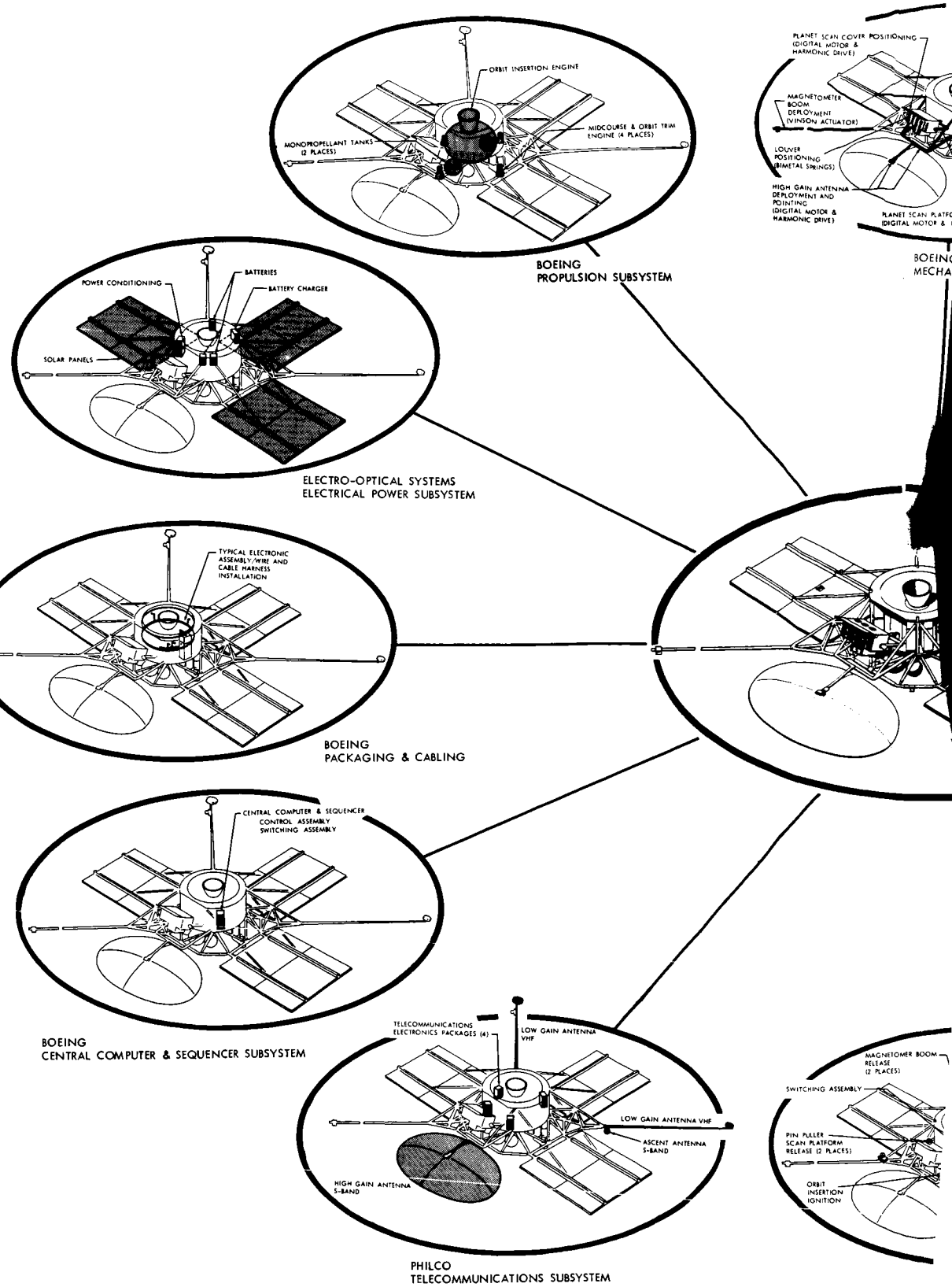
ORBIT INSERTION ENGINE
MIDCOURSE & ORBIT TRIM ENGINE (4 PLACES)
MONOPROPELLANT TANKS (2 PLACES)
BOEING
PROPULSION SUBSYSTEM
PLANET SCAN COVER POSITIONING (DIGITAL MOTOR & HARMONIC DRIVE)
MAGNETOMETER BOOM DEPLOYMENT (VINSON ACTUATOR)
LOUVER POSITIONING (BIMETAL SPRINGS)
HIGH GAIN ANTENNA DEPLOYMENT AND POINTING (DIGITAL MOTOR & HARMONIC DRIVE)
BOEING
MECHA
BATTERIES
POWER CONDITIONING
BATTERY CHARGER
SOLAR PANELS
ELECTRO-OPTICAL SYSTEMS
ELECTRICAL POWER SUBSYSTEM
TYPICAL ELECTRONIC ASSEMBLY/WIRE AND CABLE HARNESS INSTALLATION
BOEING
PACKAGING & CABLING
CENTRAL COMPUTER & SEQUENCER CONTROL ASSEMBLY SWITCHING ASSEMBLY
BOEING
CENTRAL COMPUTER & SEQUENCER SUBSYSTEM
TELECOMMUNICATIONS ELECTRONICS PACKAGES (4)
LOW GAIN ANTENNA VHF
LOW GAIN ANTENNA VHF
ASCENT ANTENNA S-BAND
HIGH GAIN ANTENNA S-BAND
PHILCO
TELECOMMUNICATIONS SUBSYSTEM
MAGNETOMER BOOM RELEASE (2 PLACES)
SWITCHING ASSEMBLY
PIN PULLER SCAN PLATFORM RELEASE (2 PLACES)
ORBIT INSERTION IGNITION

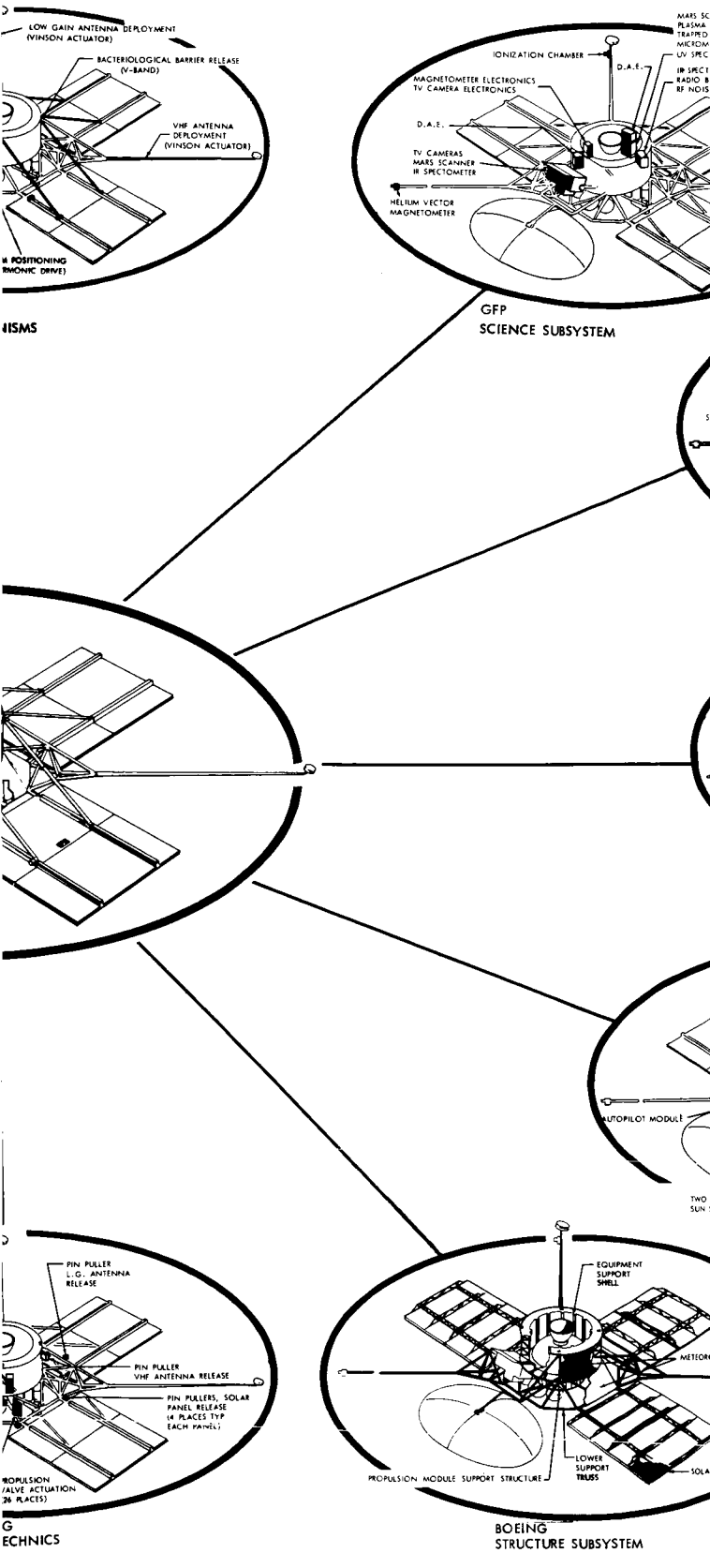

Figure 4: Voyager Flight Spa

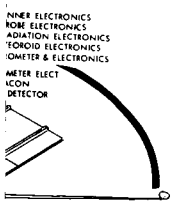

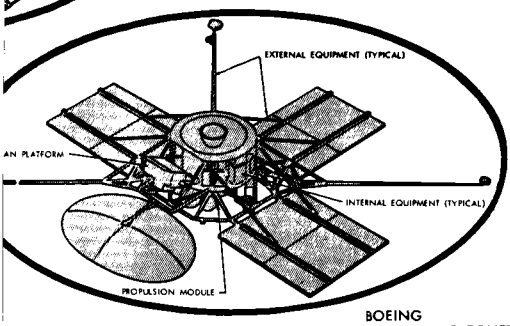

BOEING
TEMPERATURE CONTROL
SUBSYSTEM

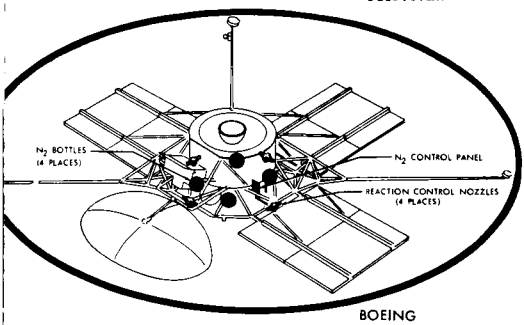

BOEING
REACTION CONTROL
SUBSYSTEM

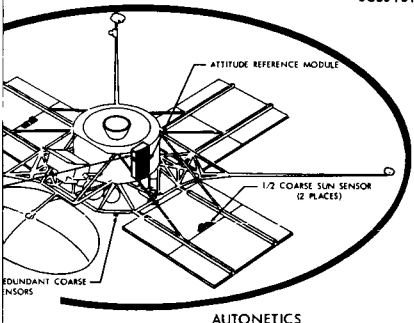

AUTONETICS
AUTOPILOT AND ATTITUDE REFERENCE

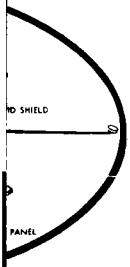

cecraft Subsystem Integration

Alternate mission objectives, design characteristics, and system and subsystem designs for the Voyager Spacecraft System are presented in this volume. In addition, the bases on which a preferred system was selected are discussed. The choice of a preferred method or technique from among the various alternates was based heavily on considerations of mission success (reliability), state-of-development of equipment, weight, safety, and versatility (applicability to various missions). The effects of these considerations may be summed in the statement that the intent of the Voyager development was to apply conservative engineering practice to the use and careful extension of present-day knowledge, techniques, and equipment to provide a spacecraft and system with the greatest possible capabilities.

In this study of alternate systems and subsystems and in the selection of the preferred designs, the JPL documents 45 and 46 (Mission Specification and Mission Guidelines) and EPD's (particularly 250, 277, and 139) were used so extensively and so universally that if they were to be listed as applicable documentation, it would be necessary to call them out in each and every section. It was believed to be unnecessary to do this; however, they are to be considered part of every section.

Alternate missions for the Voyager Spacecraft were considered in terms of reduced objectives which might be attained despite occurrence of certain critical, but not totally disabling, malfunctions of the spacecraft. These considerations indicate that substantial value could be derived from a mission despite such malfunctions.

Variations in overall system design were treated in terms of (1) the effects on spacecraft configuration, particularly in terms of inclusion of a planet sensor, derived from navigation and guidance error analyses; (2) alternate spacecraft configurations, particularly as they affect weight, reliability, equipment accessibility, and system versatility; and (3) effects on design of a spacecraft due to a possible requirement for sterilization (or other special treatment) of all or part of the spacecraft in order to meet with satisfactory confidence the requirement on Mars contamination. Results of the sterilization study indicate a possibility of substantial change in spacecraft equipment depending on the outcome of further refinements in the analyses of contamination events and probability of occurrence of such events.

Development of preferred designs for the various subsystems required consideration of a number of alternatives. Some of the most significant aspects of these studies are discussed in the following paragraphs.

Before proceeding with optimization of a radio communications subsystem, a brief study was made of the potential of laser communications through 1971. The result indicated that, as implied by JPL, laser communications could not reasonably be considered during this period. Optimization of an S-band radio communications system was concerned primarily with incorporation of the largest antenna that was feasible, with selection of a final power amplifier, and with the best use of selective redundancy. The selection of a power amplifier placed particular emphasis on power level and type of device. (A 50 watt traveling wave tube was selected on the basis of development status; however, if the state-of-development of

solid state power sources were further advanced, they would have been very attractive by virtue of their potential high reliability.) Studies of system reliability considered use of redundant critical components and fail-safe switching as well as careful selection of components. Studies were also made of modulation and coding techniques in order to develop a method which would minimize formatting and coding/decoding problems yet provide a significant improvement in transmission capability.

Electrical power generation by nuclear and radioisotope converters was considered briefly in order to evaluate the state of such developments in comparison with that of solar photovoltaic systems. It was determined that no reasonable alternate to the photovoltaic power source is presently available. Optimization of the solar photovoltaic system included consideration of alternate panel designs, of various types of power conditioning equipment, and of batteries. Nickel cadmium batteries were disqualified from consideration because of their weight and the large magnetic dipole moment they could produce.

Studies of propulsion for midcourse correction, orbit insertion (including thrust vector control) and for orbit trim considered liquid fuel engines of both the mono- and bipropellant types and solid fuel motors of several shapes and propellant types. The studies emphasized reliability and development status of the various items of hardware. Results indicated that the monopropellant system would be a desirable choice for midcourse correction and orbit trim maneuvers and that the orbit insertion requirements for tne period 1969 through 1973 could only be satisfied within the specified weight limitation of 3500 pounds by a solid fueled motor.

Thrust vector control techniques for such a motor were investigated extensively; and it was decided to recommend secondary fluid injection.

Engineering mechanics includes thermal control, packaging and cabling, structure, mechanisms, and pyrotechnics. Studies in these fields led to selection of a method of thermal control using conventional space-facing louvers that provide a high degree of thermal independence between individual packages, making it possible to modify the equipment load on the spacecraft with minimum redesign. The packaging and cabling concept, together with the structure design, provides excellent accessibility to spacecraft equipment and mechanisms consistent with the desire to keep total weight at or near a minimum value. Mechanisms were selected primarily on the basis of reliability and development status. A considerable study was made of methods for firing pyrotechnic devices because of the relatively large number of such devices required for the Voyager spacecraft and the requirement for extremely reliable operation. The study indicated that a method using silicon transistor switching which was developed for the NASA-Langley Lunar Orbiter provided the highest reliability as well as the lowest weight.

Consideration of the attitude control subsystem, consisting of sensors, autopilot, and reaction control devices indicated that redundant sensors having different failure modes could be used for most functions. Choice of autopilot and reaction control equipment emphasized the use of reliable, proven techniques and equipment.

Study of the central computer and sequencer indicated that this device could have a major effect on the versatility of the spacecraft, i.e., the ease with which the spacecraft could be adapted to various missions. Consideration of various means of implementing the central computer and sequencer indicated that a special-purpose memory-oriented computer offered many advantages and that such a device was developed for and would be space-proven by virtue of its use on the NASA-Langley Lunar Orbiter. Further study showed that the Lunar Orbiter central computer and sequencer could be adapted to the Voyager requirements with relatively small modifications and that this approach appeared to offer the best means of satisfying system requirements.

In conclusion, major alternatives were evaluated for all spacecraft subsystems and a preferred design selected in each case. In total, no state-of-the-art extensions are needed for the preferred configuration and the selections are conservative and generally available and proven hardware.

CONTENTS

1.0 MISSION OBJECTIVES AND DESIGN CRITERIA

No exceptions were taken to the mission objectives presented in the JPL Voyager specification, therefore, only alternate mission objectives resulting from planetary vehicle malfunctions were considered. Of the many conceivable malfunctions, the consequences of three (failure to separate the Flight Capsule, failure of one or two of the three solar panels to deploy, and failure of the high-gain antenna to deploy or to point) are particularly pertinent to development of alternate mission objectives. This is because they are critical, single-thread operations. These malfunctions would preclude attainment of all mission objectives, but some of these objectives might be attained if alternate design criteria were used.

1.1 CAPSULE SEPARATION FAILURE

In the event of Flight Capsule separation failure, three potential alternative missions that will salvage scientific or engineering data from the flight are:

1) Flyby along the design approach trajectory;
2) Flyby using a closer aim point than the design trajectory;
3) Insertion of the capsule and spacecraft into a highly elliptic orbit.

Planning of alternates to cover such an eventuality requires examination of:

1) Scientific values of the various alternates;
2) Extent of modifications -- in terms of effect on weight and performance -- to the basic Flight Spacecraft design.

Results of the evaluation indicate that limited benefit may be obtained from the flyby modes. The mode involved in the insertion into a highly elliptical orbit has a major disadvantage because the Planetary Vehicle would be required to have a ΔV capability substantially greater than that provided by the nominal design.

An assumed scientific instrumentation package per Section 4.5, Volume A, was used for evaluation. A qualitative analysis was made to determine the effects of each alternate mission on the information acquired from this hypothetical science payload. Table 1-1 contains the results of this analysis and lists the two parameters used to assess each alternate mission:

1) Coverage -- The degree to which the area of interest is covered. This factor reflects the ability to make meaningful interpretation of the data obtained;
2) Quality of data -- The quality of data obtained with respect to that obtainable in the course of a normal successful mission.

For purposes of this comparative analysis, all instruments are assumed to have an adequate view of the planet at all times. Limitations are discussed in detail below.

Flyby Powered Mode--In general, considerations of thermal heating on the spacecraft coupled with guidance positioning uncertainties (± 500 kilometers) limit the minimum approach altitude to 1000 kilometers. A low-altitude passage could result in the requirement for camera image motion compensation. Analysis of what this means in terms of potential design

Table 1-1: SCIENTIFIC VALUE OF ALTERNATE MISSIONS

MISSION	HIGH ELLIPTIC ORBIT		FLYBY--NONPOWERED		FLYBY--POWERED	
INSTRUMENT	COVERAGE	DATA QUALITY	COVERAGE	DATA QUALITY	COVERAGE	DATA QUALITY
TV Cameras	A	M	I	M	I	M
Mars Scanner	A	M	I	I	I	I
IR Spectrometer	A	A	M	M	M	M
Dual-Frequency Radio Beacon	A	A	A	A	A	A
UV Spectrometer	A	A	M	M	M	M
Mars RF Noise Detector	A	A	I	A	I	A
Magnetometer	A	A	M	A	M	A
Plasma Instrument	A	A	M	A	M	A
Trapped Radiation Detector	A	A	M	A	M	A
Micrometeorite Detector	A	A	M	A	M	A
Ionization Chamber	A	A	M	A	M	A

COVERAGE
- I - Inadequate
- M - Marginal
- A - Adequate

DATA QUALITY
- I - Inadequate
- M - Moderate Degradation
- A - Adequate

modifications must await final definition of the science payload package.

Placement of the spacecraft on a close-approach flyby can be accomplished in two ways:

1) A deflection maneuver wherein the aim point, $|\bar{B}|$, is altered. The ΔV requirement for such a maneuver is on the order of 10 meters per second or less assuming that separation is desired 5 days prior to encounter. This velocity requirement is well within the capability of the proposed midcourse and orbit propulsion system.
2) A retromaneuver wherein the approach velocity, VHP, is reduced maintaining the basic trajectory aim point. Retrovelocity requirements range from 750 to 1000 meters per second for the 1971 mission, which requires utilization of the orbit insertion propulsion motor.

For the proposed spacecraft design, the solid motor is aligned with the nozzle pointing directly at the flight capsule, precluding the accomplishment of this maneuver. Location of the motor in this position was due to conservative design considerations of the heat radiated to the solar panels during orbit insertion firing (See Section 4.4.1). If the heat load can be reduced through design modifications and/or applying a special coating reflective to the exhaust wavelengths without solar panel performance degradation, the motor may be pointed away from the capsule, allowing it to be fired with the capsule attached.

Examination of a shadow graph (Figure 1-1) for the proposed spacecraft design shows that the view of planet-oriented sensors is completely blocked

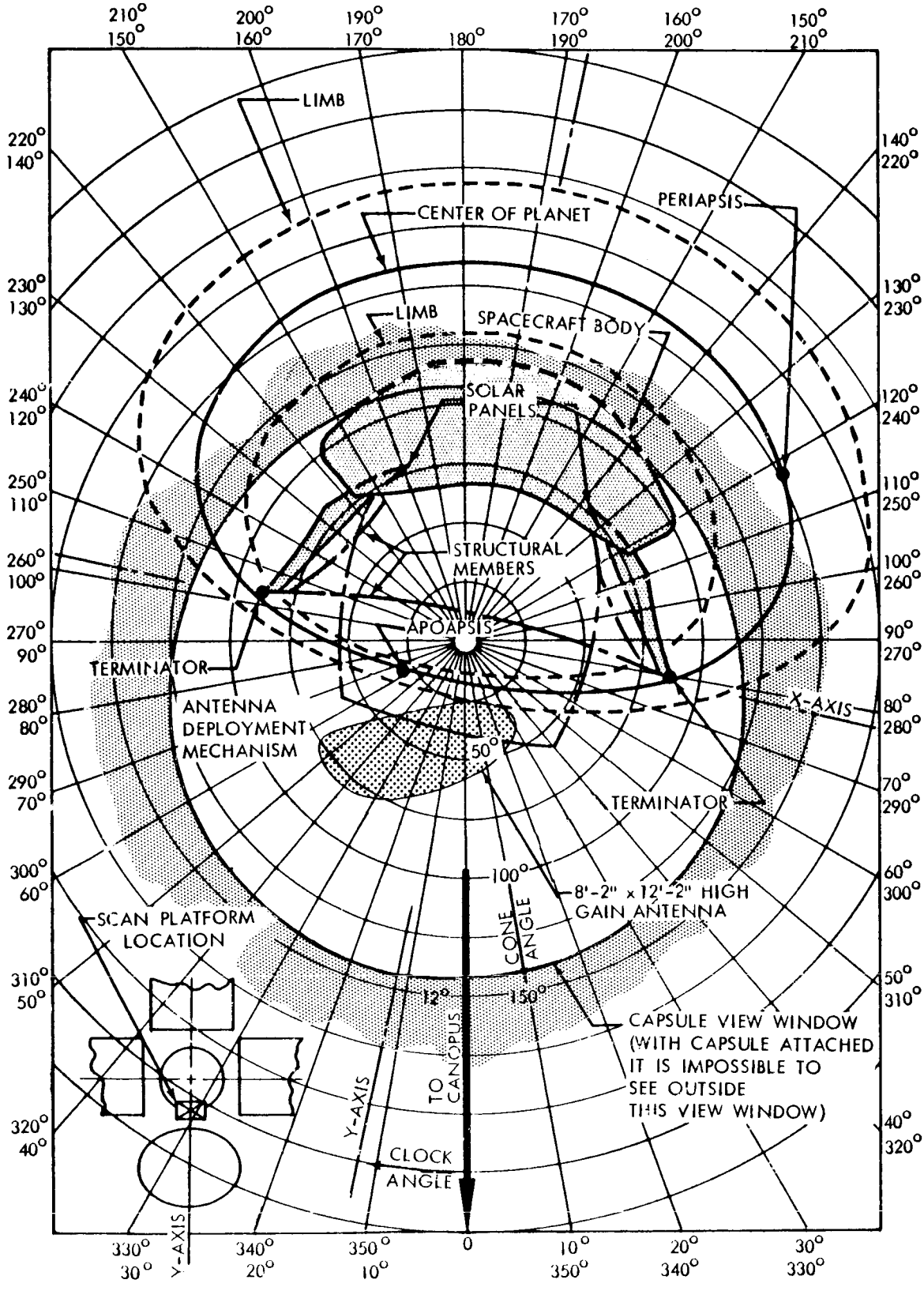

Figure 1-1: TYPICAL SCAN PLATFORM VIEW CAPABILITY

at periapsis vicinity with the flight capsule attached and the vehicle Sun-oriented. However, pictures may be taken by breaking the Sun reference lock and stabilizing the spacecraft on the IRU. With regard to nonscanning sensors, the presence of the capsule will generally either perturb the absolute scale value or reduce the instrument field of view. Analysis of these effects must await final science payload definition.

Flyby Unpowered Mode--For this mode, the spacecraft continues on the approach trajectory without alteration. The value of picture data would be reduced from that associated with the powered flyby mode.

Orbital Mode--Constraints imposed on a Mars orbit insertion maneuver are:

1) The orbit must have a 50-year minimum lifetime consistent with the Mars contamination criteria;
2) The orbit must be stable from the standpoint of astronomical perturbations. A maximum orbit period of 100 hours was assumed to satisfy this constraint.

The ability to insert both the capsule and spacecraft into a Mars orbit depends primarily upon the capability of the spacecraft orbit-insertion propulsion system because of the greater mass involved. Figure 1-2 illustrates orbit insertion ΔV requirements as a function of arrival VHP for various elliptical orbits. The orbits are described in terms of orbital period and are based on minimum periapsis altitudes consistent with the contamination constraint.

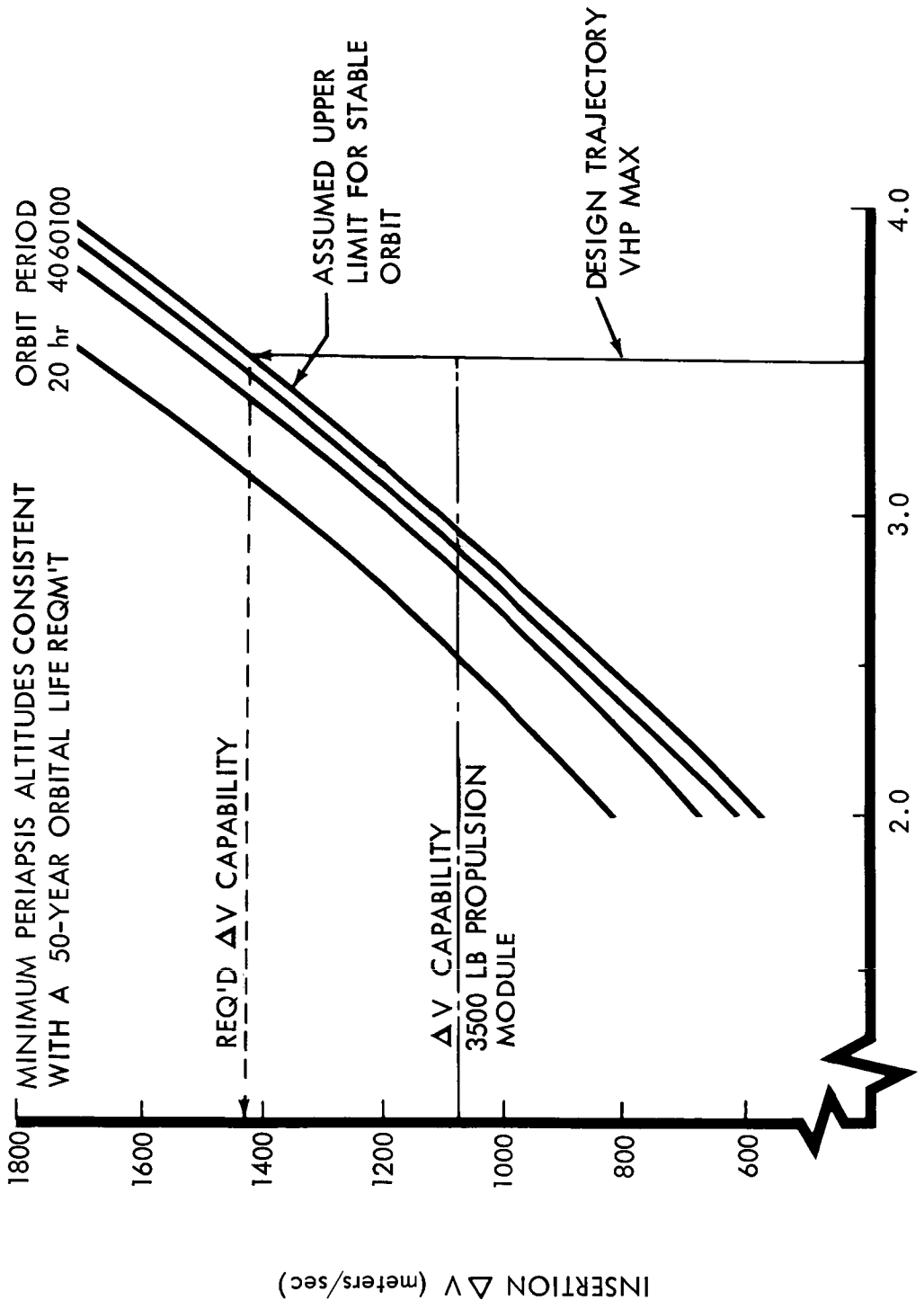

Figure 1-2: Orbital Capability — Capsule + Spacecraft

As shown, the 3500-pound propulsion system design makes it impossible to achieve orbital insertion of the spacecraft and capsule under any but the most favorable approach conditions (VHP $\leq$ 2.95 kilometers per second). To achieve minimum orbital conditions at the design trajectory velocity (VHP = 3.5 kilometers per second, maximum) requires an additional 350 meters per second ΔV capability. Thus, to facilitate this alternate mission mode, not only must the insertion engine be reoriented, as indicated above for the flyby retro mode, but also the propulsion system must be resized with an attendant increase in total vehicle weight of approximately 1200 pounds.

1.2 PARTIAL DEPLOYMENT OF SOLAR PANELS

The purpose of this analysis is to determine the extent to which mission objectives may be attained in the event that the solar panels do not all properly deploy. Conceivable failures could result in power generation capabilities ranging from 0 to nearly 100 percent of nominal power. For this study, two levels of failures were analyzed, which resulted in two power-level points. These were where two of the six panels (Configuration 945-6026 described in Volume A) are out of commission and where four of the panels are inoperative. If more than four panels were inoperative, there would not be enough power available for the basic planetary spacecraft housekeeping needs, and the mission objectives could not be met. If less than two panels were out of commission, the mission objectives as presented in the specifications could be met.

The capability of accomplishing partial or all mission objectives at reduced power levels is discussed below.

Case 1 (Two Panels Inoperative)--For this example, the four remaining solar panels would be capable of generating approximately 430 watts

of power at Mars distance. Considering no solar cell degradation, this amount of power is sufficient to:

1) Provide power for planetary spacecraft housekeeping requirements;

2) Transmit all engineering and science data during the cruise phase;

3) Recharge the batteries after midcourse maneuvers;

4) Provide required power for capsule separation, insertion of spacecraft into Mars orbit, and operation of all scientific instruments in orbit;

5) Transmit engineering and science data in Mars orbit. It is probable that some alteration of the data transmission schedule would be required since battery power as well as solar panel power would probably be required to handle the high data transmission modes.

Case 2 (Four Panels Inoperative)--Two operating panels would be capable of generating approximately 215 watts of power at Mars distance, again considering no solar cell degradation. This power generating capability is sufficient to:

1) Provide all planetary spacecraft housekeeping power requirements.

2) Provide limited communications during the cruise phase. Batteries would be required to furnish part of the power during data transmission. As a result, data transmission would have to be intermittent to permit battery recharge.

3) Provide midcourse maneuvers, flight capsule separation, and flight spacecraft injection into Mars orbit.

4) Operate scientific subsystems in Mars orbit.

5) Provide intermittent transmission of data to Earth during orbiting phase. The quantity of data would be severely limited since the

communications subsystem would have to be periodically shut off to recharge the batteries.

No spacecraft design modifications are required to handle this malfunction condition. Reprogramming of the DAS and CC&S would probably be required to incorporate a different data readout format and power cyclic operation; this capability presently exists within the CC&S. Battery reliability will be degraded in this mode of operation because of the large number of charge-discharge cycles required.

1.3 HIGH-GAIN ANTENNA FAILURE

This analysis considers the condition wherein the high-gain antenna fails to deploy or suffers a subsequent malfunction. The analysis examines the accomplishment of various mission objectives in light of this failure.

Conditions imposed on the study are: (1) the low-gain antenna is fully functional, (2) the DSIF 210-foot antenna is available, and (3) the telemetry data modes, as presented in Section 4.1, Volume A, can be used. These modes applicable to the low-gain antenna are summarized in Table 1-2.

If the high-gain antenna fails before encounter, alternate telemetry data modes would have as their primary objective the transmission of data to enhance Flight Capsule deployment. Therefore, engineering data from the Flight Spacecraft and capsule are of primary concern. The cruise science data are of secondary importance at this point in the mission and would be sacrificed if necessary to achieve capsule insertion. Data Mode 1 would provide the Flight Spacecraft and capsule engineering data telemetry

Table 1-2: LOW-GAIN ANTENNA TELEMETRY DATA MODES

Data Mode	Data Rate (bps)	Data Transmitted	Range at Grey-Out (km)	Range at Blackout (km)
1	22-2/9	Flt S/C Engrg Data (11-1/9) Flt Capsule Engrg Data (11-1/9)	100×10^6 **	54×10^6 * 180×10^6 **
2	133-1/3	Flt S/C Engrg Data (11-1/9) Flt Capsule Engrg Data (11-1/9) Cruise Science Data (111-1/9)	-	32×10^6 * 100×10^6 **
3	133-1/3	Flt S/C Engrg Data (11-1/9) Flt Capsule Engrg Data (11-1/9) Stored Flt Capsule Engrg Data (111-1/9)	-	32×10^6 ** 100×10^6 *
4	5-5/9	Flt S/C Engrg Data (5-5/9)	195×10^6 **	295×10^6 **

* 85-foot DSIF Antenna

** 210-foot DSIF Antenna

through Mars encounter; consequently, no new alternate data mode would be required for this function. Mode 2, which provides cruise science data at the rate of 111-1/9 bits per second, cannot be used at the encounter range. Alternate data modes with science data rates less than 111-1/9 bits per second could be employed to extend science coverage beyond the 100-million-kilometer range.

After capsule separation, emphasis shifts to the orbital phase of the mission. Throughout this phase, spacecraft engineering, science, and capsule relay data are normally transmitted. As indicated above, Mode 1 provides adequate communications into the orbital phase of the mission. At this point, the relative emphasis would normally shift from the engineering to the science data, necessitating higher transmission rates. Table 1-2 shows the range capability of the low-gain antenna for several data bit rates. At the 22-2/9-bps rate, blackout occurs approximately 3 weeks after encounter. The short orbital-phase operates in the grey-out region.

With the lower rate of 5-5/9 bps, 1 month is available from encounter to grey-out and an additional 2.5 months until blackout. This limited capability at encounter will necessitate careful consideration of alternate data modes. The low data rates available exclude the acquisition of any large amount of data from the television or Mars scanner science instrumentation. Selective sampling of the other various science instruments could be employed depending on the relative priority of each investigation. The actual amount of data retrieved and the capsule data relay function

would ultimately depend on the trade between data rate and time available from encounter to blackout.

Detailed analysis of alternate telemetry data modes and the system modifications associated with each must await final science payload definition. It is apparent, however, that the low-gain antenna would afford a limited opportunity to acquire science data in orbit if the high-gain antenna fails.

CONTENTS

2.0 DESIGN CHARACTERISTICS AND RESTRAINTS

This section presents discussions and analysis of three alternate design and functional requirements considered in the course of establishing ground rules. In all instances, the requirements of the Mission Specifications were adhered to. However, analyses were conducted to determine if, by altering these requirements, improvements in performance, cost, or schedule could be realized.

The following subjects were analyzed and are reported herein.

1) Extension of the launch azimuth;

2) Design loads for spacecraft structure;

3) Materials and hazard factors for pressure vessels.

2.1 LAUNCH AZIMUTH EXTENSION

An analysis was conducted for the purpose of examining launch azimuths in excess of 71 degrees east of north. In particular, the work was directed to evaluating the performance gain resulting from extension of launch azimuth to 45 degrees east of north while maintaining a maximum C_3 of 18 km^2/sec^2. For Voyager missions later than 1971, the launch period is limited by the C_3 of 18 km^2/sec^2 boundary rather than by the 33-degree |DLA| boundary.

Figure 2-1 is a plot of Saturn IB/Centaur payload performance as a function of launch azimuth. Launch azimuth can be extended to 45 degrees at the expense of reducing the weight margin by a factor of approximately 2.5. A decrease in allowable weight margin of this magnitude must be traded against the potential benefit obtained by: (1) the increased

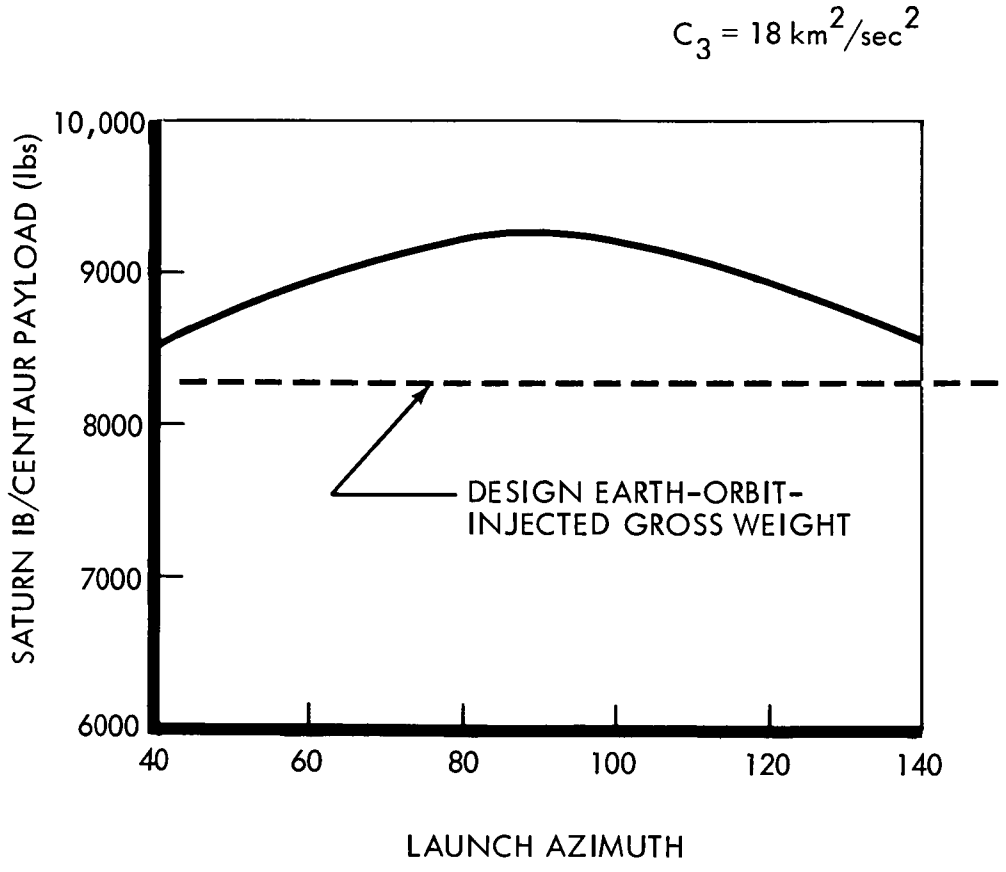

Figure 2.1: Saturn IB/Centaur Performance

daily launch window afforded; (2) the increased launch period available; and (3) a reduction of the excess hyperbolic velocity (VHP) at Mars encounter. Items (2) and (3) require further analysis since the launch window afforded by a 71-degree launch azimuth restraint is more than adequate to meet the 1-hour window constraint given in the Mission Specification (refer to Section 3.1 of Volume A).

Figure 2-2 presents curves of VHP plotted as a function of arrival date at Mars and launch date. Superimposed on the curves are boundary conditions of the booster performance (C_3 = 18 km^2/sec^2) and two launch azimuth limits. The |DLA| (declination of launch asymptote) values of 33 and 50 degrees correspond to launch azimuths of 71 and 45 degrees, respectively. A further boundary is shown on the plot, namely, the minimum DLA shall be no less than 5 degrees (for tracking purposes). Extensions in available launch periods are afforded by utilizing a DLA limit of 50 degrees.

The final factor analyzed was the extent to which the VHP at Mars could be reduced by considering |DLA| values of up to 50 degrees. Referring to Figure 2-2, it can be seen that by moving the launch date to the left, a reduction in VHP is possible for a fixed launch period and a constant arrival date. Figure 2-3 illustrates the advantages gained in terms of the design velocity increment required to insert into Mars orbit. The example chosen was for a fixed-arrival-date trajectory (November 1, 1971) with a 50-day launch period, a Mars insertion-periapsis-altitude of 2700 kilometer, and an orbital period of 18 hours. As seen in the figure, the design-orbit insertion-propellant loading can be reduced by

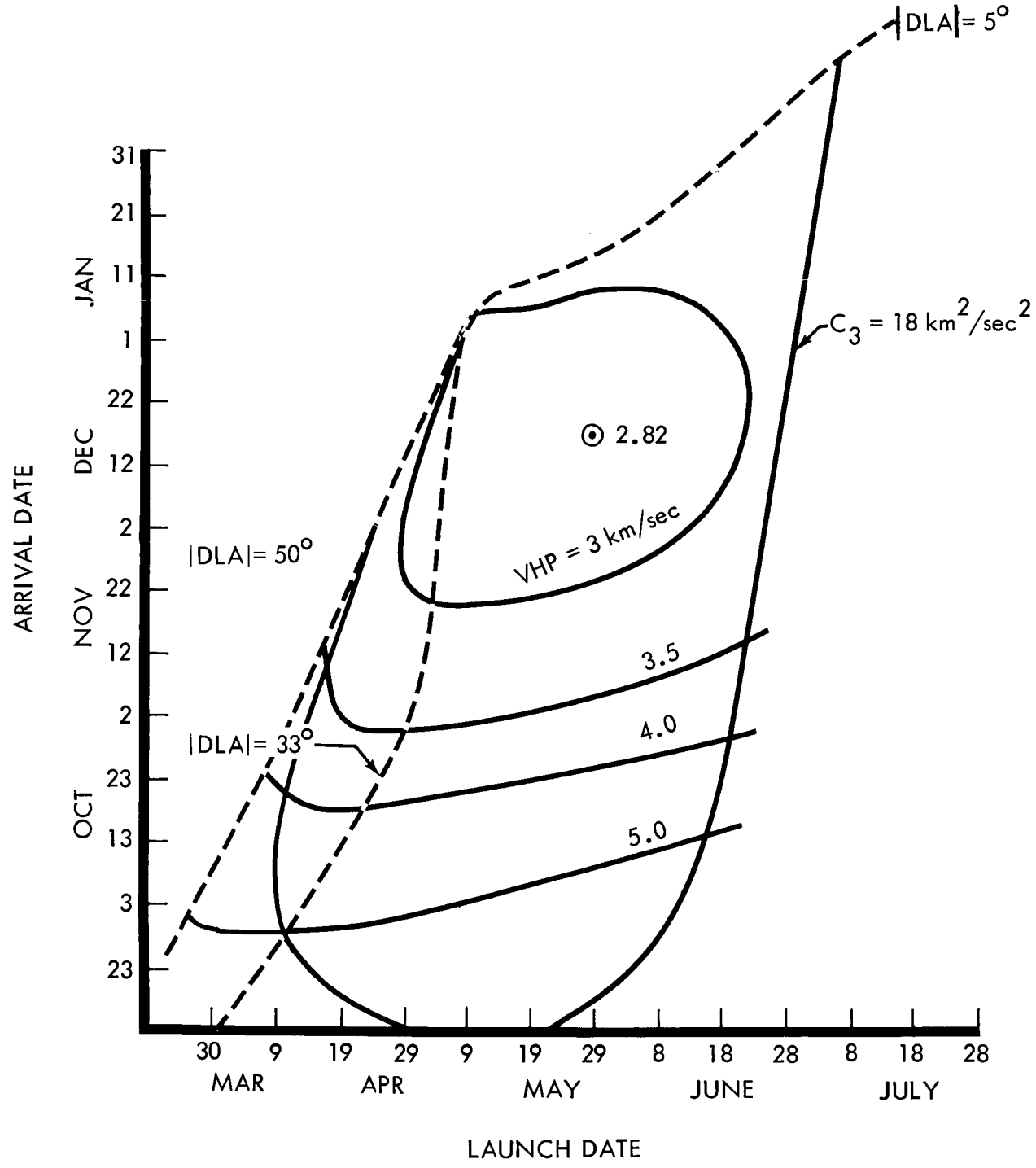

Figure 2.2: Basic Trajectory Chart

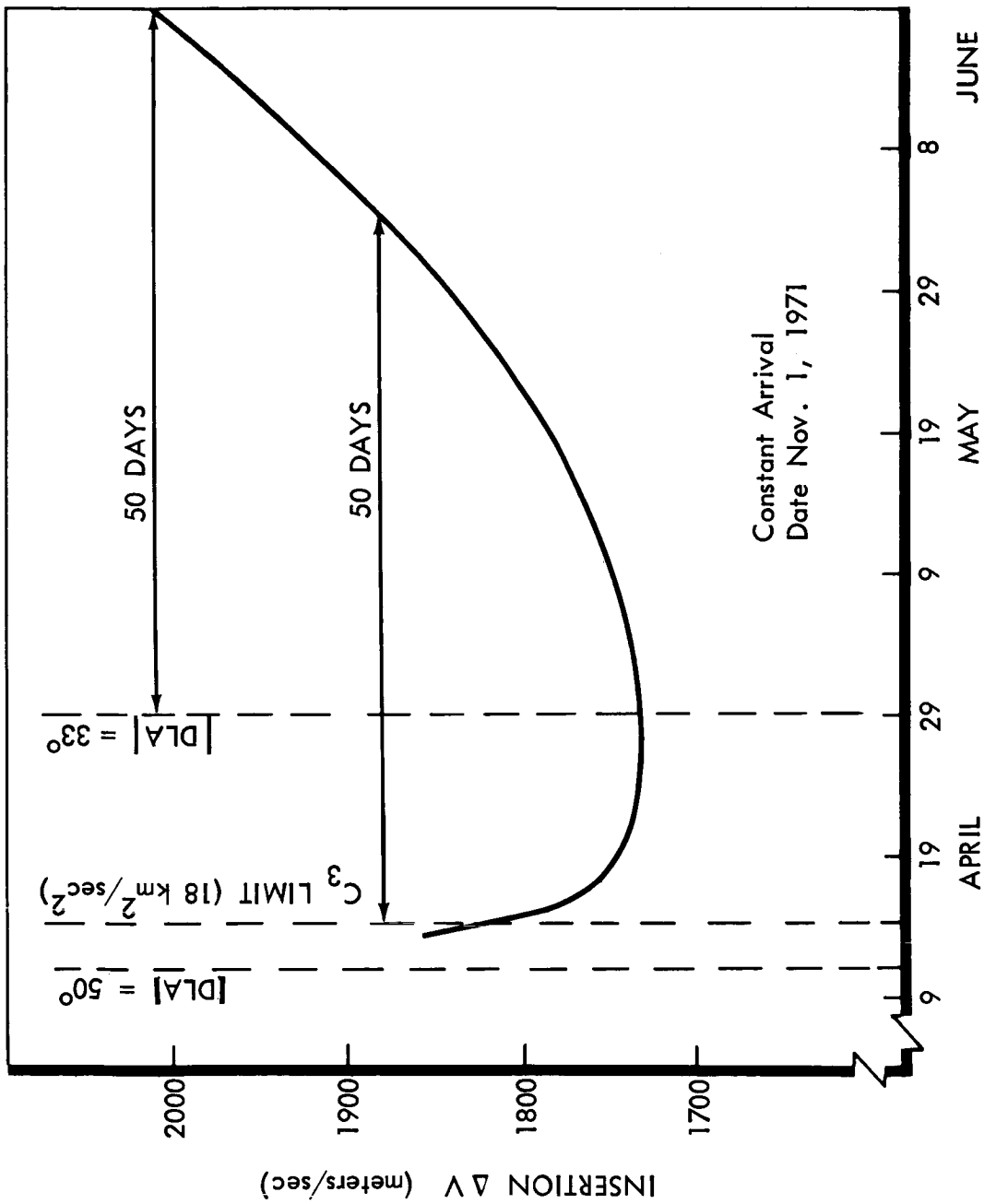

Figure 2.3: Effects of DLA on Design ΔV Requirements

130 meters per second by extending the DLA range. This provides a 5-percent increase in available weight in Mars orbit. For a nominal in-orbit burn-out weight this is about 150 pounds.

2.2 DESIGN LOADS FOR SPACECRAFT STRUCTURE

Re-evaluation of the dynamic loading environment indicated that a structural weight reduction (relative to that based on the specification design load) could be justified by detailed analysis. The specified vibration inputs are of such a nature that excitation of the cantilever resonances will occur. This condition arises when the exciting frequency coincides with one of the fixed-base natural frequencies of the Planetary Vehicle. The response modes may be either lateral-bending or axial modes. Under these conditions the Planetary Vehicle presents a very high impedance to the vibration exciter; therefore, the spacecraft structural loads are very large and are highly dependent on structural damping. However, the actual loading conditions imposed by the launch vehicle are not strongly dependent on structural damping since the loads result from transient events or sustained acceleration rather than steady sinusoidal excitation.

Analyses of the dynamic response (based on considerations of significant events from launch to Mars orbit insertion) revealed that critical loading conditions exist during the launch phase. Existing data on engine transients, launch vehicle response, flight test experience, and launch vehicle structural capability were used. Conservative factors as high as 5 were introduced where data or analysis were considered insufficient. The use of these data and criteria are believed sufficient to ensure

that the structural capability of the Planetary Vehicle will be compatible with that of the launch vehicle.

On the basis of the study of dynamic response conditions outlined above, the following alternate loading conditions (expressed as limit load factors) result:

CONDITION	LIMIT LOAD FACTORS	
	Axial	Lateral
Launch Release	+1.2 g	±2 g
S-IB Cut-off	+4.3 g	±1 g
	-2.2 g	±1 g

Consideration of these load factors in the preliminary structural design of Spacecraft Model 945-6026 resulted in a weight reduction of 150 pounds relative to the design incorporating the specification loads.

2.3 REQUIREMENTS FOR PRESSURIZED VESSELS

The Voyager Mission Specification requires the use of Ti-6Al-4V titanium alloy in the annealed condition, and a hazard factor of 1.76 for vessels to be pressurized in the vicinity of personnel. The weight of nitrogen tankage based on these requirements is 128 pounds total.

The alternate requirements listed below were considered with respect to possible weight reductions and their influence on structural reliability. The results show that the use of Ti-6Al-4V either in the heat-treated

condition or with alternate hazard factors can provide substantial weight reductions.

Alternate Requirement	Hazard Factor	Material Condition	Weight per tank (lbs)
1*	1.76	Annealed	32.0
2	1.76	Heat Treated	27.4
3	1.60	Heat Treated	25.3
4	1.40	Annealed	25.8

*Specification Requirement

Requirement No. 2 allows a nitrogen tank weight reduction of 18.4 pounds total by the substitution of heat treatment for annealing. Neither the base metal nor weld is critical for explosive failure but the greater toughness of the annealed material is sacrificed. Requirement No. 3 (design criteria for the Lunar Orbiter and Dyna-Soar programs) results in a weight reduction of 26.8 pounds total. Neither the base metal nor the weld is critical for explosive failure. Requirement No. 4, which produces approximately the same weight reduction as No. 2, appears to be most promising of the alternates considered. Although the hazard factor has been reduced to 1.40, the toughness of the annealed condition has been retained and the design weld, rather than the base metal, is critical, this is consistent with the JPL requirement. Requirement No. 4 provides a weight reduction for the nitrogen tanks of about 25 pounds.

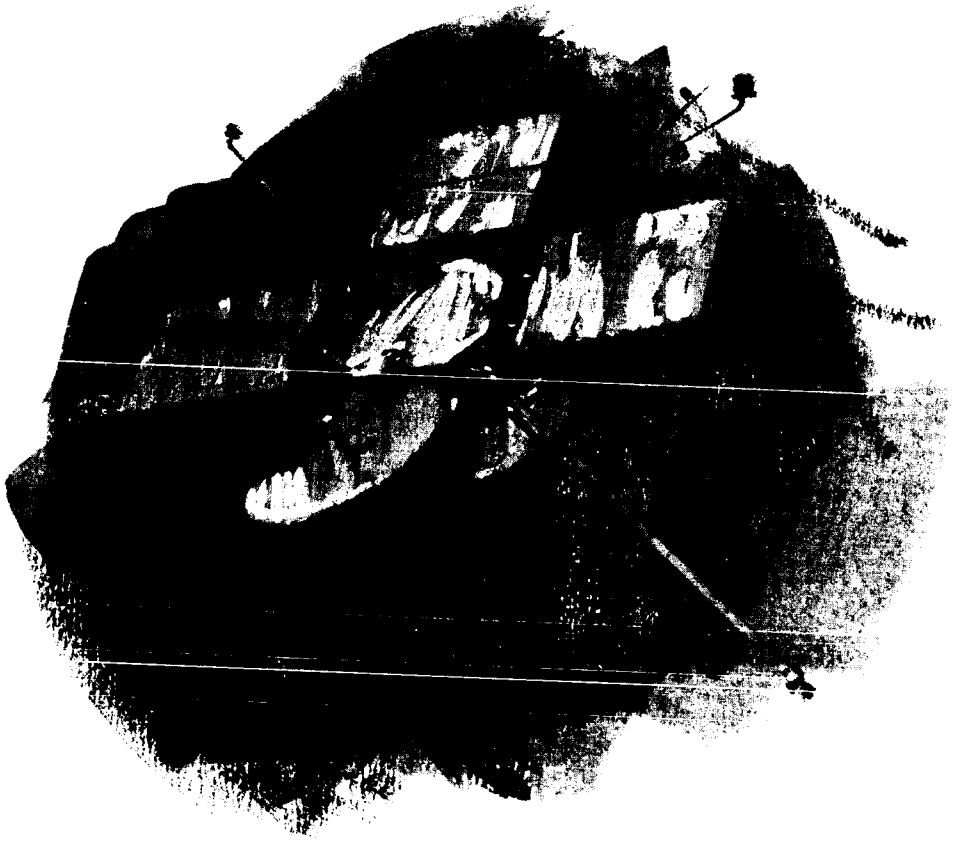

CONTENTS

3.0 ALTERNATE SYSTEM PHILOSOPHIES AND MECHANIZATIONS INCLUDING TRADEOFFS

Consideration of alternate Voyager systems involved the following three major elements:

1) Navigation and guidance analysis to determine maneuver strategy and onboard sensor requirements.
2) Alternate spacecraft configurations with attendant variations in performance of subsystems.
3) Planetary quarantine studies as they reflect on the need to accommodate sterilization or other special treatment of all or part of the spacecraft.

The navigation and guidance analyses have led to the conclusion that the accuracy of DSIF doppler data is sufficient to satisfy navigation and guidance requirements and that little advantage, for 1971 or for later missions, would accrue from adding a planet sensor to the spacecraft.

A number of spacecraft configurations and layouts were studied; of these all but three were discarded rather quickly as being inconsistent with the engineering conservatism required for the program. Of the three configurations studied in detail, the chosen one places the Flight Capsule ahead of the spacecraft in order to minimize structural weight (and in compliance with JPL specifications); provides the largest antenna of the three configurations; and has the most favorable equipment mounting provisions.

The planetary quarantine studies were directed toward evaluating the need for alternate sterilizable spacecraft designs. More data are needed before a firm conclusion can be drawn from these studies, but it appears that (1) the spacecraft propulsion subsystem should be sterilized (because of planetary contamination by ejecta) and that (2) some treatment of the spacecraft should be carried out to reduce its total microbial load at takeoff. These measures would be necessary in order to provide reasonable confidence of meeting the requirement on probability of Mars contamination.

3.1 GUIDANCE AND NAVIGATION PERFORMANCE TRADES

Summary--A navigation and guidance subsystem does not exist as such, but rather the navigation and guidance functions are satisfied through command of several subsystems, both on the ground and on the spacecraft. The functions required are the estimation of the past, present, and future state of the spacecraft; comparison of this state with the desired state; and computation of required velocity changes and associated timing (within spacecraft performance and mission constraints). The particular means of fulfilling the navigation and guidance functions impose various requirements on the mission operation and on the design of certain subsystems.

To establish these requirements and to establish the navigation and guidance capability for each mission phase, the following trades and analyses were performed:

1) Injection accuracy and ΔV for first midcourse correction versus parking orbit geocentric angle.
2) Midcourse orbit determination capability, attainable guidance accuracy, and ΔV requirements versus maneuver sequence and maneuver control accuracy.
3) Orbit determination capability during approach to Mars using DSN and using DSN augmented with planet tracker data.
4) Accuracy of orbit insertion versus control accuracy.
5) Orbit determination capability in the Mars orbiting phase for DSN only and DSN augmented by horizon scanner data.
6) Investigation of the problems associated with early convergence in the solution for the orientation of the orbit about the line of

sight, using DSN doppler data only.

7) Analysis of ΔV requirement and attainable orbit parameter accuracy for orbit trim.

Based upon these analyses and trades, the following conclusions have been reached:

1) Short parking orbits ($<$20 minutes) are desirable to keep midcourse ΔV requirement down.

2) Nominal midcourse correction times of 5, 25, and 175 days from launch should be selected to provide near optimal midcourse orbit determination capability. Encounter accuracies and ΔV requirements are relatively insensitive to variations in the nominal maneuver sequence.

3) The addition of planet tracker data does not greatly improve the orbit determination capability during the approach to Mars for the 1971 mission. With the improved definition of the Mars gravitational constant and ephemeris that will be achieved from the 1971 mission, the contribution of onboard-sensed data will be even less for subsequent missions.

4) The desired guidance accuracies can be met with the following control accuracy:

   1 σ pointing : 0.6 degree

   1 σ ΔV proportional: 1%

   1 σ ΔV resolution: midcourse and orbital trim: 0.01 meter per second
   orbit insertion: 4.5 meters per second.

5) The ΔV requirements are 75 meters per second for midcourse and 100 meters per second for orbit trim.

6) The dominant error in the initial determination of the orbit about Mars is in the position of the node in the plane normal to the Earth-Mars line, using either DSN only or DSN augmented with observations by a horizon scanner. The position of the node is determined to within a 1-σ error of 0.15 degree in 2 days and 0.03 degree in 3 days, using DSN only. The error is reduced to 0.02 degree in one orbital period when the DSN is augmented by the angle measurements. After 3 to 4 days of tracking, the contribution of the angle measurements becomes insignificant.

7) The solution for position of the node, using DSN only, converges steadily after 1 day of tracking, if the solution for all parameters is unbiased by the estimation procedure. Further development in estimation procedures is required to fully exploit the precision of the doppler data.

8) Initial uncertainties in the major physical constants do not significantly affect the orbit determination capability.

3.1.1 Analysis Assumptions and Techniques

During an actual mission, maneuver parameters are essentially free variables selected to satisfy mission requirements, and the navigation and guidance process is, therefore, adaptive to the specific mission. However, some premission analysis is required to obtain information on the following:

1) Orbit determination capability during the several mission phases;

2) Desired nominal maneuver strategies including;

   a) The number and timing of midcourse velocity corrections,

b) Aim point biasing requirements to satisfy the contamination constraint,

c) Expected number and timing of orbit trim maneuvers;

3) Resultant state accuracies;

4) Maneuver ΔV requirements;

5) Constraints on maneuver execution control accuracy.

An encounter accuracy of $\pm$ 500 kilometers or less in the $\underline{B}\cdot\underline{T}$ - $\underline{B}\cdot\underline{R}$ plane is desired, based on three midcourse corrections (nominally). It is further desired that the maneuvers be performed to a 1-percent accuracy for medium to large maneuvers and to an accuracy of 0.01 meter per second for maneuvers in the neighborhood of 0.1 meter per second. The 1-percent desired accuracy leads to pointing and ΔV - proportional errors of 0.010 radian and 1 percent, respectively.

The mission is broken into five phases: boost and injection, midcourse, approach to Mars, Mars orbit insertion, and Mars orbit. The results of analyses of each of these phases are presented in the following sections.

3.1.2 Boost and Injection

The analysis of midcourse navigation and guidance starts with trans-Mars trajectory injection errors. These errors are most critical in the areas of midcourse ΔV requirements and initial aim-point selection. The purpose of this analysis is to provide estimates of the injection errors expected from the Centaur vehicle. Since the Centaur has autonomous guidance with no updates from the Saturn vehicle or the ground, the random

errors at injection into the trans-Mars orbit are functions of the Centaur guidance system components only. The injection errors were estimated from a postulated set of component errors, using the Boeing Inertial Guidance Error Analysis program. The 1-sigma component errors assumed and the position and velocity errors at injection versus geocentric parking angle are shown in Figure 3-1. The injection errors projected to 5 days after injection are shown in Figure 3-2. The corresponding midcourse ΔV requirement at 5 days to correct for the random injection errors is also shown in Figure 3-2. The correction is slightly higher than the velocity deviation and increases directly with parking orbit duration.

The results represent expected Centaur capability. However, they should be viewed as being optimistic for two reasons. First, the nominal Centaur accuracy has not been proven, and, second, there is always a possibility of a nonabortive off-nominal injection.

Some data are available on the Agena in this area, but no such data are presently available for the Centaur. As faults that cause off-nominal operation are found, they are usually corrected, thereby reducing the probability of future off-nominal injections. However, some consideration must be given to bad but nonabortive injections in fixing the limit on parking angle and in the estimation of the actual midcourse ΔV requirements.

ASSUMED COMPONENT ERRORS

- ACCELEROMETER:
  - BIAS $5(10^{-5})g$
  - SCALE FACTOR $7(10^{-5})g/g$
  - MISALIGNMENT
    - IN PLANE 6 sec
    - NORMAL 8 sec
- GYRO DRIFTS:
  - CONSTANT .04°/hr
  - SPIN UNBALANCE .2°/hr/g
  - INPUT UNBALANCE .1°/hr/g
- INITIAL PLATFORM ALIGNMENT:
  - LEVEL 10 sec
  - AZIMUTH 10 sec

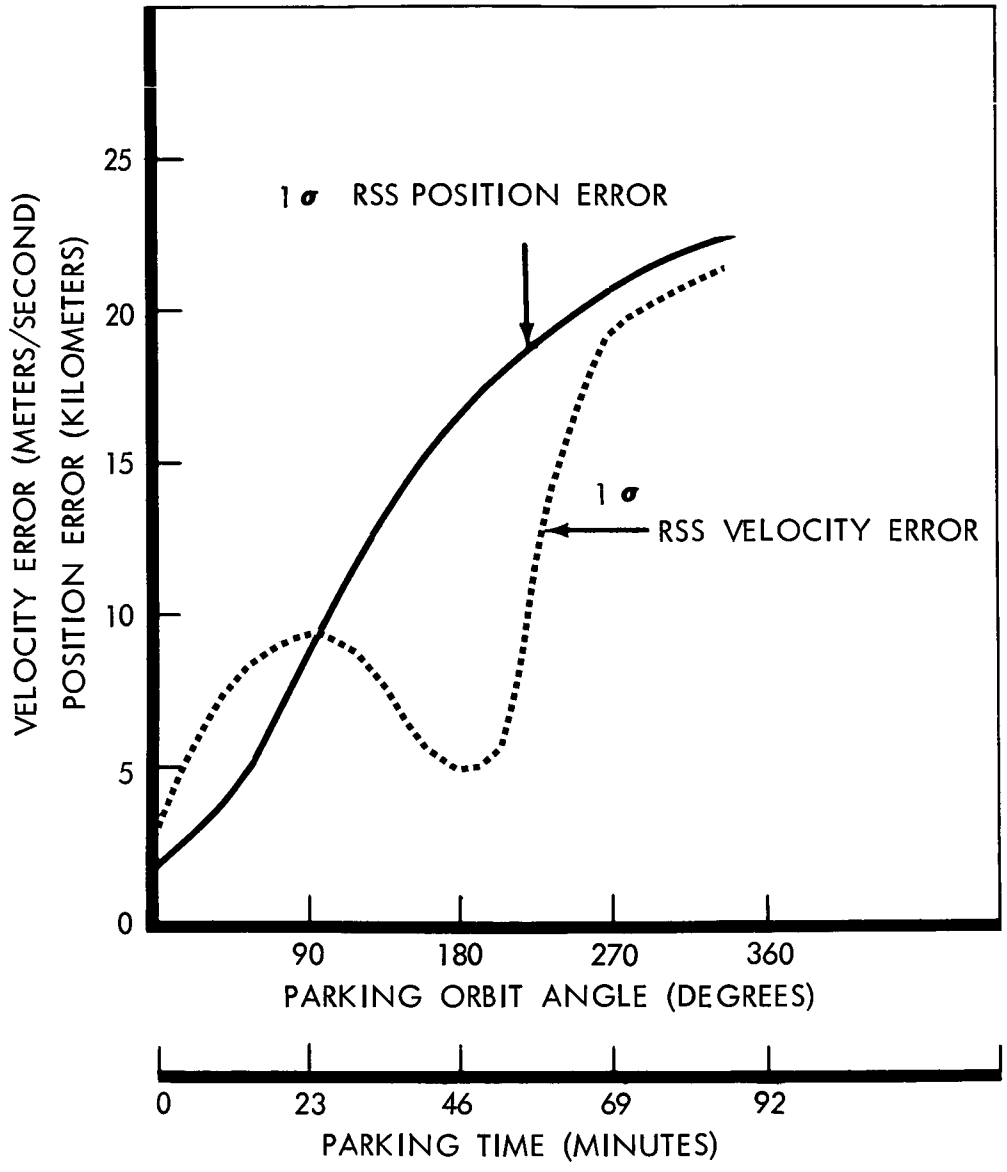

Figure 3-1: Trans-Mars Orbit Injection Errors Versus Parking Angle in Earth Orbit

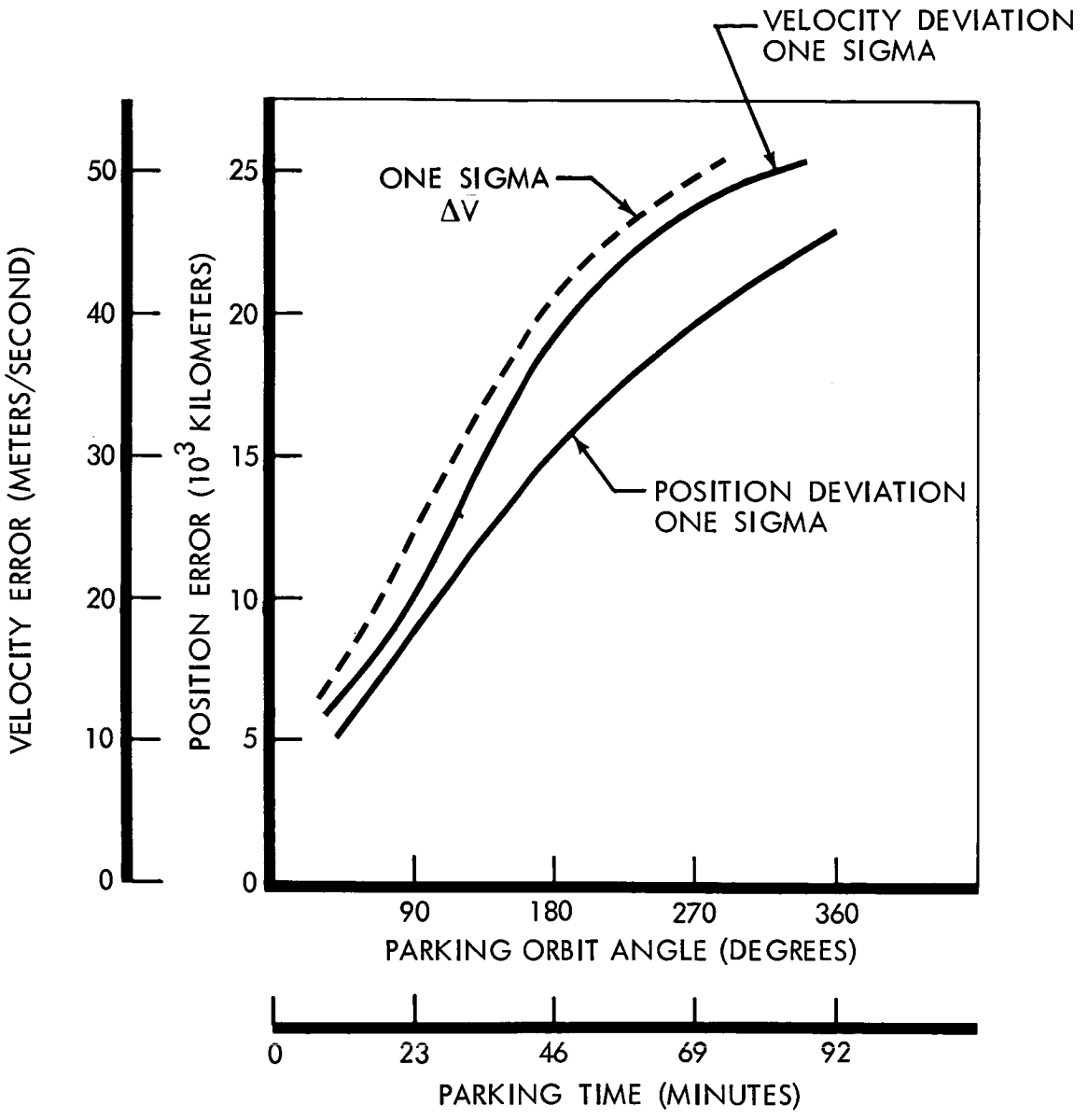

Figure 3-2: Trans-Mars Orbit Injection Errors Projected to 5 Days in Midcourse

3.1.3 Midcourse Navigation and Guidance

The prime objectives of premission midcourse navigation and guidance analyses are to provide data from which to determine the following:

1) Accuracy of knowledge of the spacecraft state at past, present, and future times;
2) Accuracy to which the spacecraft trajectory can be controlled;
3) Maneuver strategies, based upon Items 1) and 2) and contamination constraint, that provide desired encounter accuracies and satisfy contamination constraint at all times;
4) The ΔV requirements;
5) The velocity-correction execution-control accuracy requirements;
6) The sensitivity of results to accuracy of a prior knowledge of the values of model parameters.

The general restraints and assumptions governing the analysis are:

1) The DSN will be utilized for orbit determination and guidance-command generations;
2) The nominal midcourse correction sequence will include three corrections with one early (2 to 10 days after injection) to correct for Centaur injection inaccuracies, and one fairly late to achieve the desired encounter accuracy;
3) No constraint exists on the orientation of the spacecraft for a velocity correction;
4) The 1 in 10,000 Mars contamination probability constraint must not be violated.

3.1.3.1 Orbit Determination Uncertainties

The assumptions regarding the accuracy and use of DSN and the a priori information used for the midcourse orbit determination analysis are given in Table 3-1. The analysis was performed using the weighted-least-squares technique for solving for the six components of vehicle position and velocity, the gravitational-constant-mass product of Earth, the astronomical unit and the gravitational-constant-mass product of Mars.

The a priori state vector covariance matrix was the matrix obtained in the analysis of Section 3.1.2 for a parking orbit angle of 65 degrees or a time in orbit of 17 minutes. This corresponds to about a 90 degree geocentric angle from Earth launch point or a time from launch of about 27 minutes.

To account for disturbance in knowledge of state due to imperfect control at midcourse maneuvers, the velocity errors were increased by a factor of 10^2 (velocity covariance multiplied by 10^4 and position-velocity covariance by 10^2) to obtain the a priori state covariance for navigation after each midcourse correction.

The estimated position and velocity uncertainties relative to Earth during the first 5 days after launch are shown in Figure 3-3. These results show that, after about 2 days of tracking after launch, the orbit determination (OD) errors have essentially leveled out. The first midcourse correction can, therefore, be planned at some point after 2 days. For the remainder of the analysis, a first correction at 5 days is assumed.

Table 3-1: NAVIGATION ANALYSIS ASSUMPTIONS

Trajectory

215-day Type I trajectory (May 14, 1971, to December 15, 1971)

Tracking Times

Mission Time (Days)	Stations	Sample Interval (Minutes)
0 - 2	Goldstone	1
	Woomera	1
	Johannesburg	1
2 - 5	Goldstone	3
	Woomera	3
	Johannesburg	3
5 - 210	Goldstone	5
210 - 214	Goldstone	3
	Woomera	3
214 - 215	Goldstone	1

Tracking Accuracy

$1\sigma_{\dot{r}}$ = 0.001 meter/second

A Priori Physical Constant Uncertainties (Nominal)

$1\sigma_{GME}$ = 2 km^3/sec^2

$1\sigma_{GMM}$ = 1000 km^3/sec^2

$1\sigma_{AU}$ = 300 km

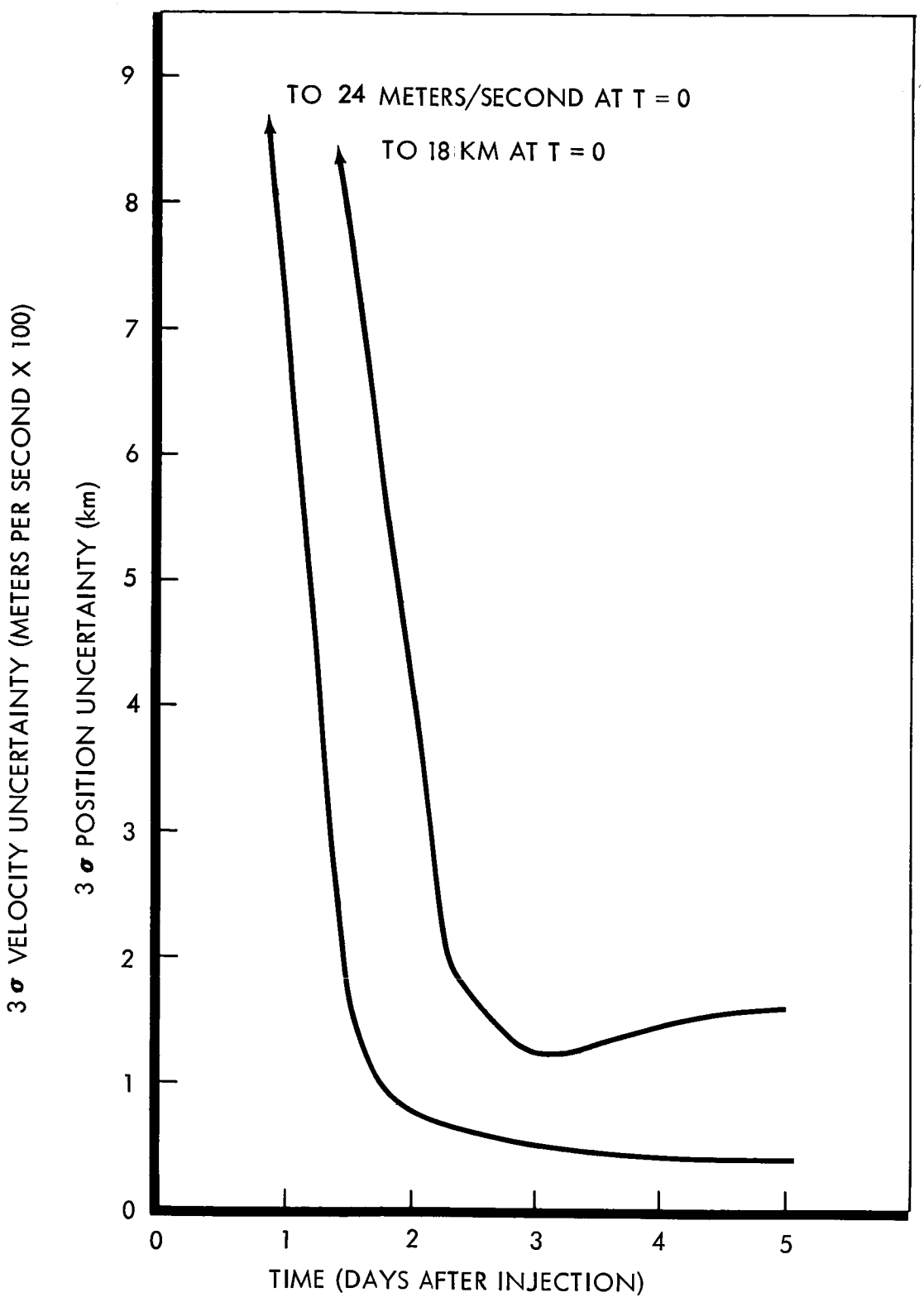

Figure 3-3: DSIF OD Uncertainty During First Five Days

The estimated uncertainties after a first correction at 5 days and after second corrections at various times are shown in Figure 3-4. In all cases examined, the velocity was accurately determined within 25 days after the correction. The level of error, however, increases slightly as the second correction is made later and later. The capability to redetermine position shows a marked sensitivity to the second correction time. In practically all cases, however, the position uncertainty is near minimum at about 175 days.

The estimated OD uncertainties after a third midcourse correction are depicted in Figure 3-5 through 3-7 for various second-correction and third-correction times. As the third correction is made later in the mission, the redetermination of the orbit becomes progressively more difficult. Redetermination after the third correction is also quite sensitive to the second midcourse correction time. From this standpoint, an early second midcourse correction is desirable.

The trends in improvement of physical constants are shown in Figures 3-8 and 3-9. The cases plotted are for midcourse corrections at 5, 25, and 175 days. The nominal a priori estimates for error in the constants are given in Table 3-1. In the analysis, these a priori values were varied within the following limits:

σ_{GME} 0.5 to 2.0 km^3/sec^2

σ_{GMM} 1.0 to 1000 km^3/sec^2

σ_{AU} 100 to 300 km

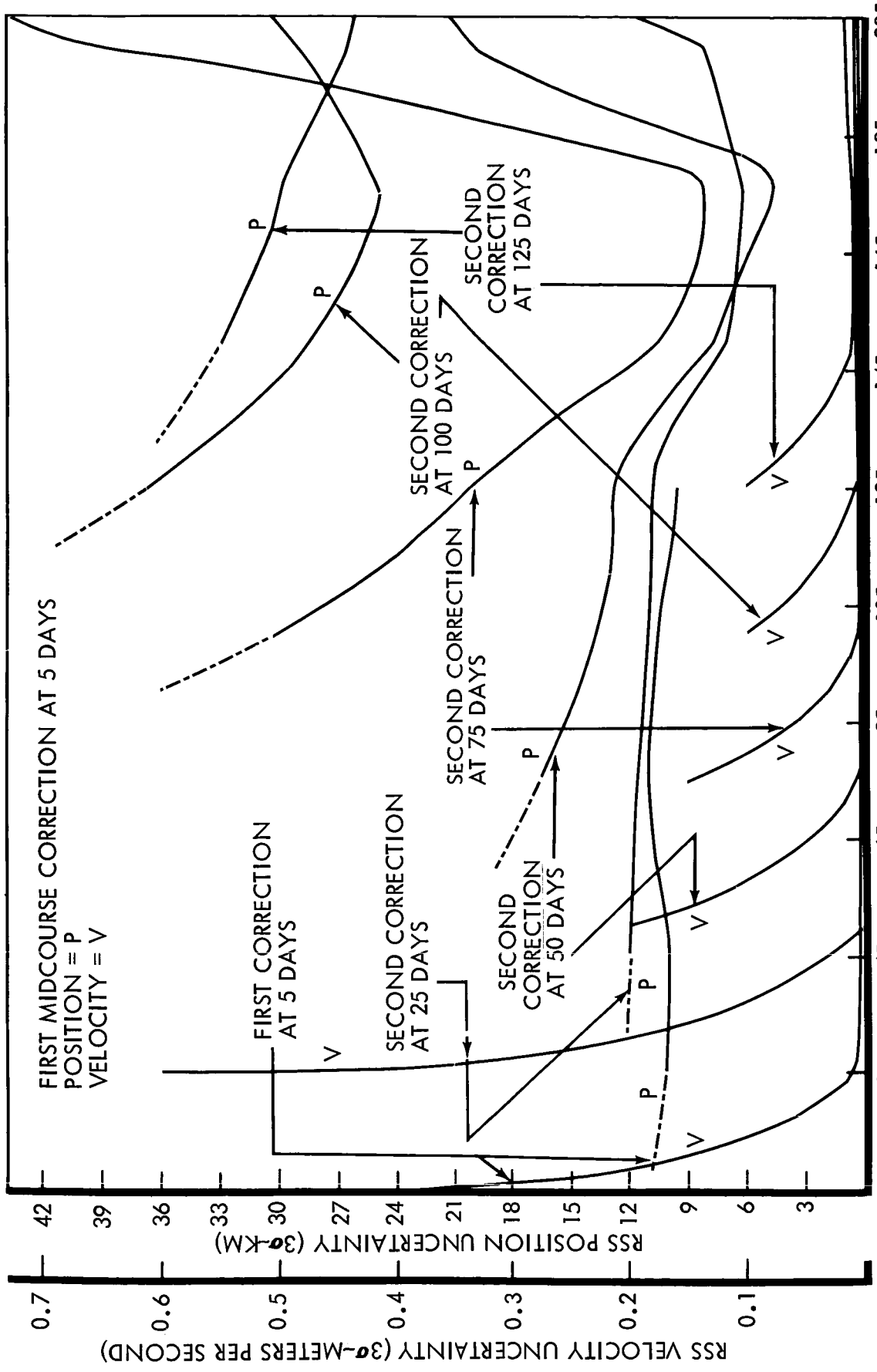

Figure 3-4: DSIF Orbit Determination Accuracy — Midcourse

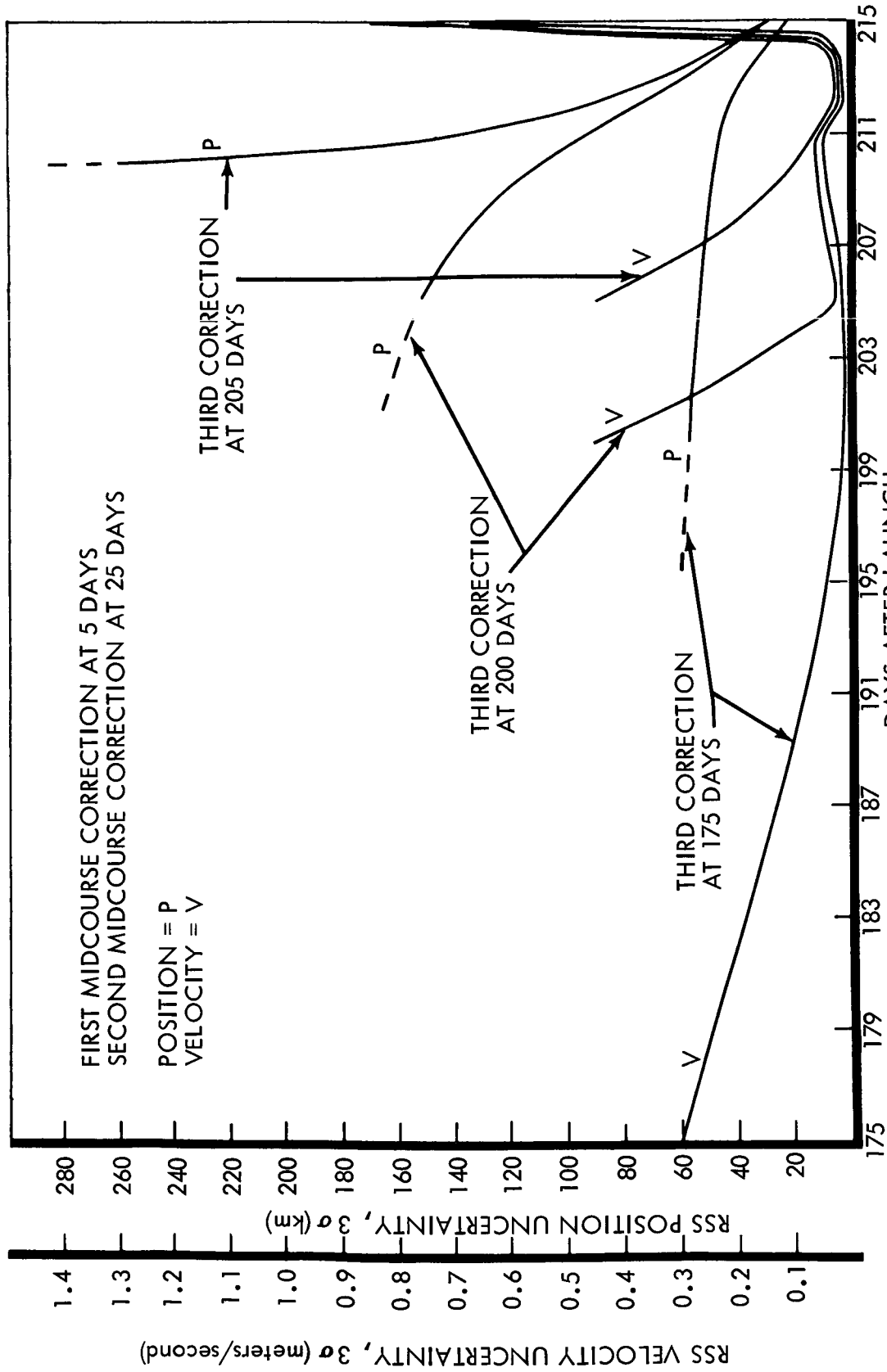

Figure 3-5: DSIF Orbit Determination Accuracy — Midcourse

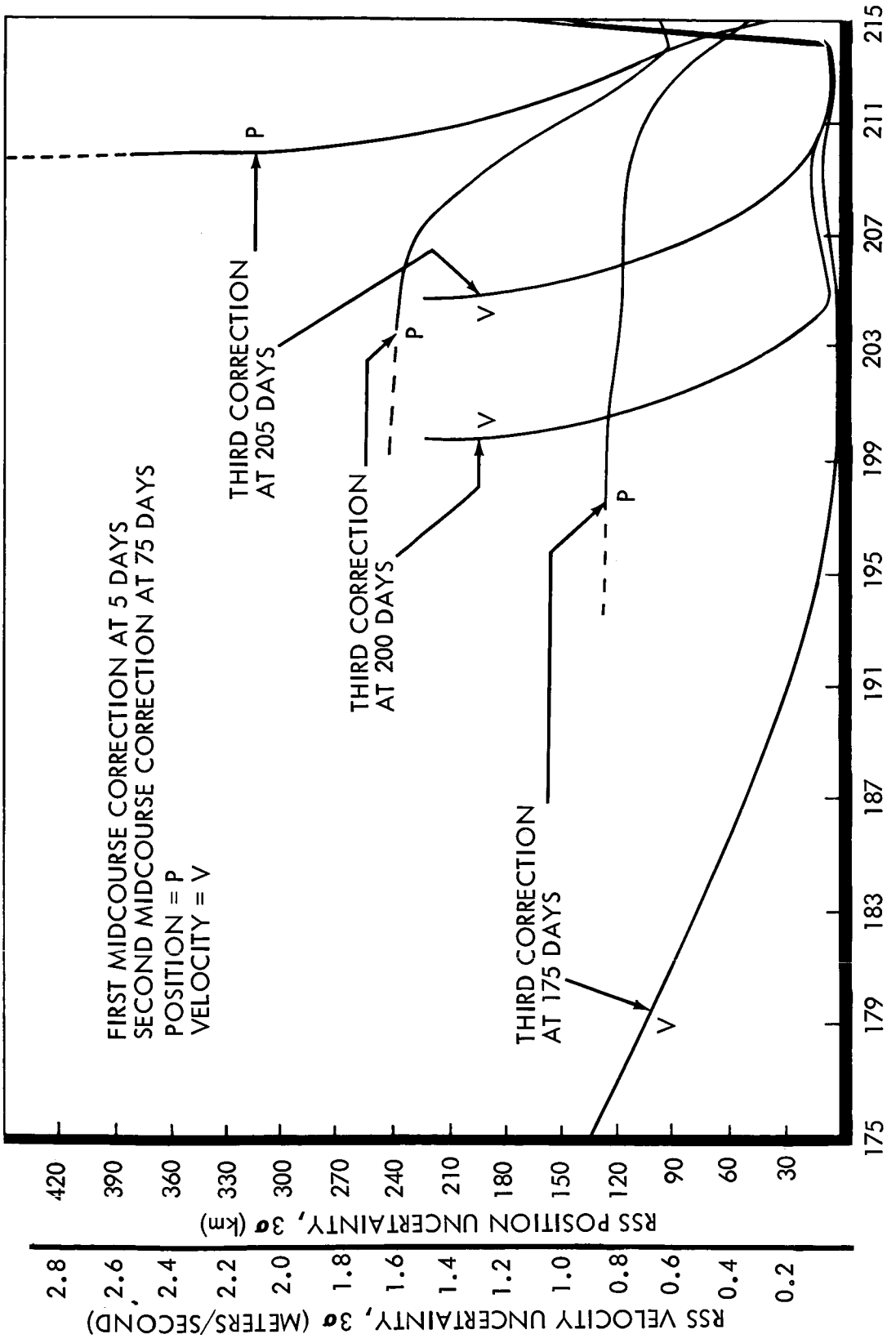

Figure 3-6: DSIF Orbit Determination Accuracy — Midcourse

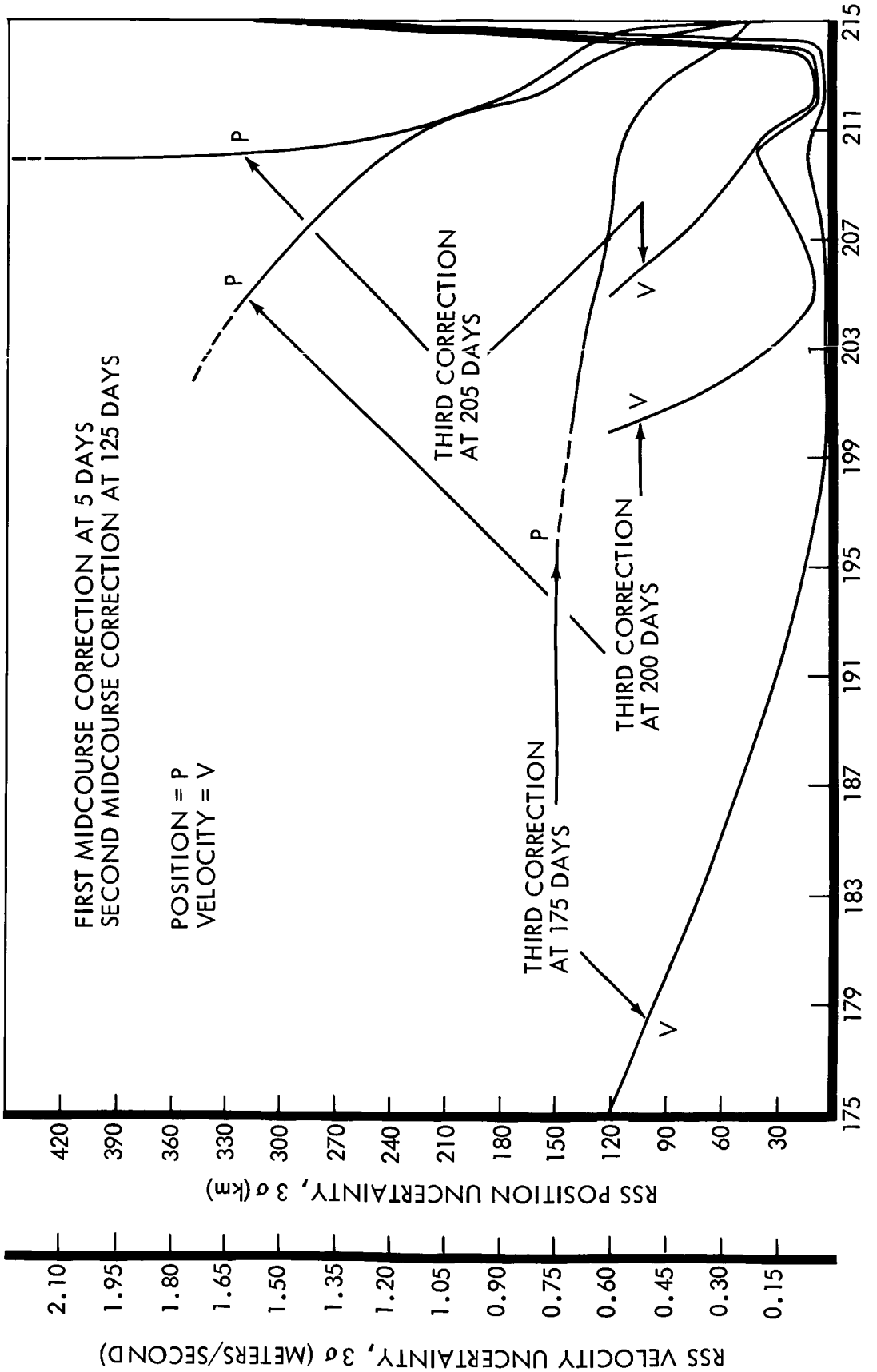

Figure 3-7: DSIF Orbit Determination Accuracy — Midcourse

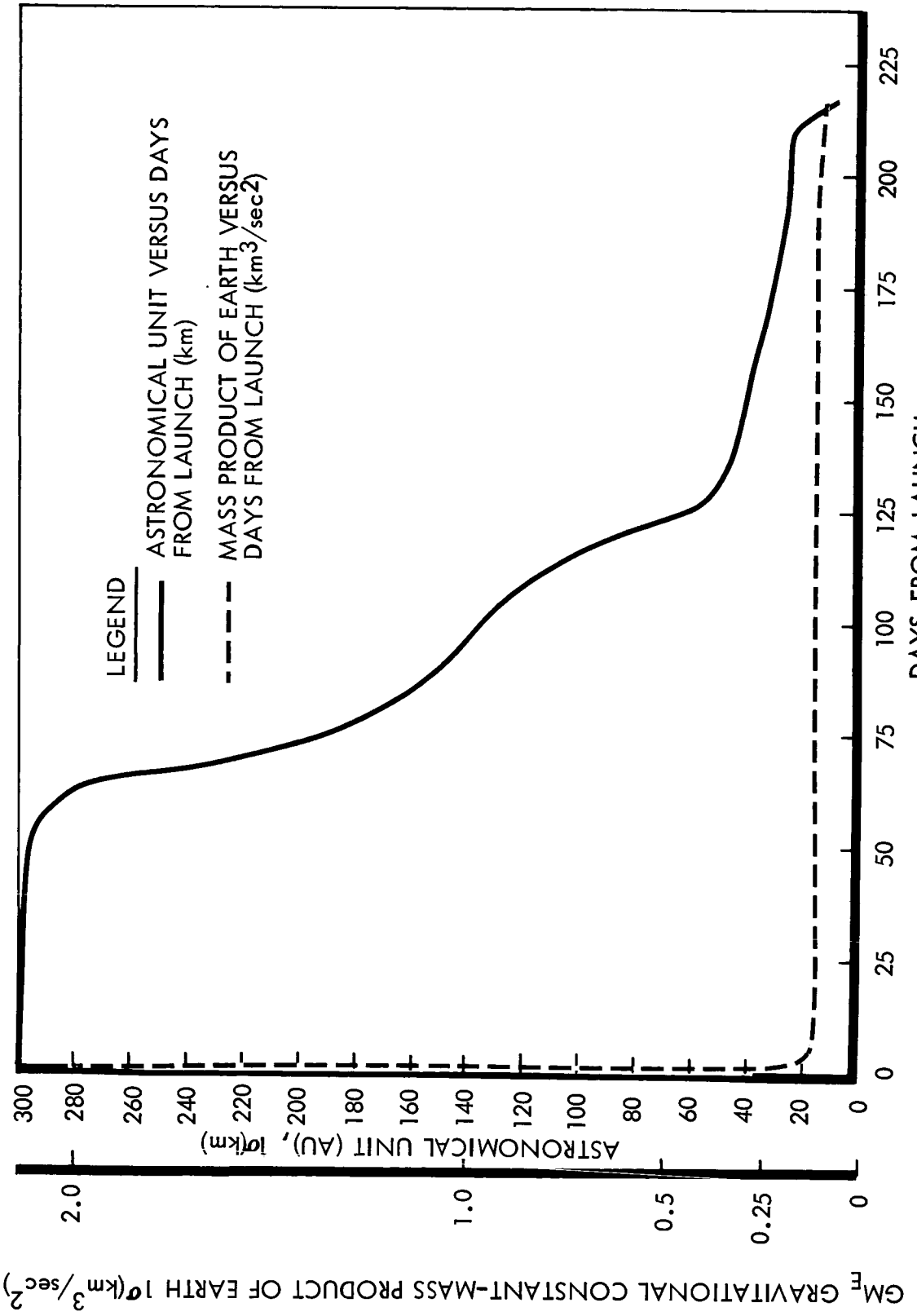

Figure 3-8: Physical Constant Uncertainties

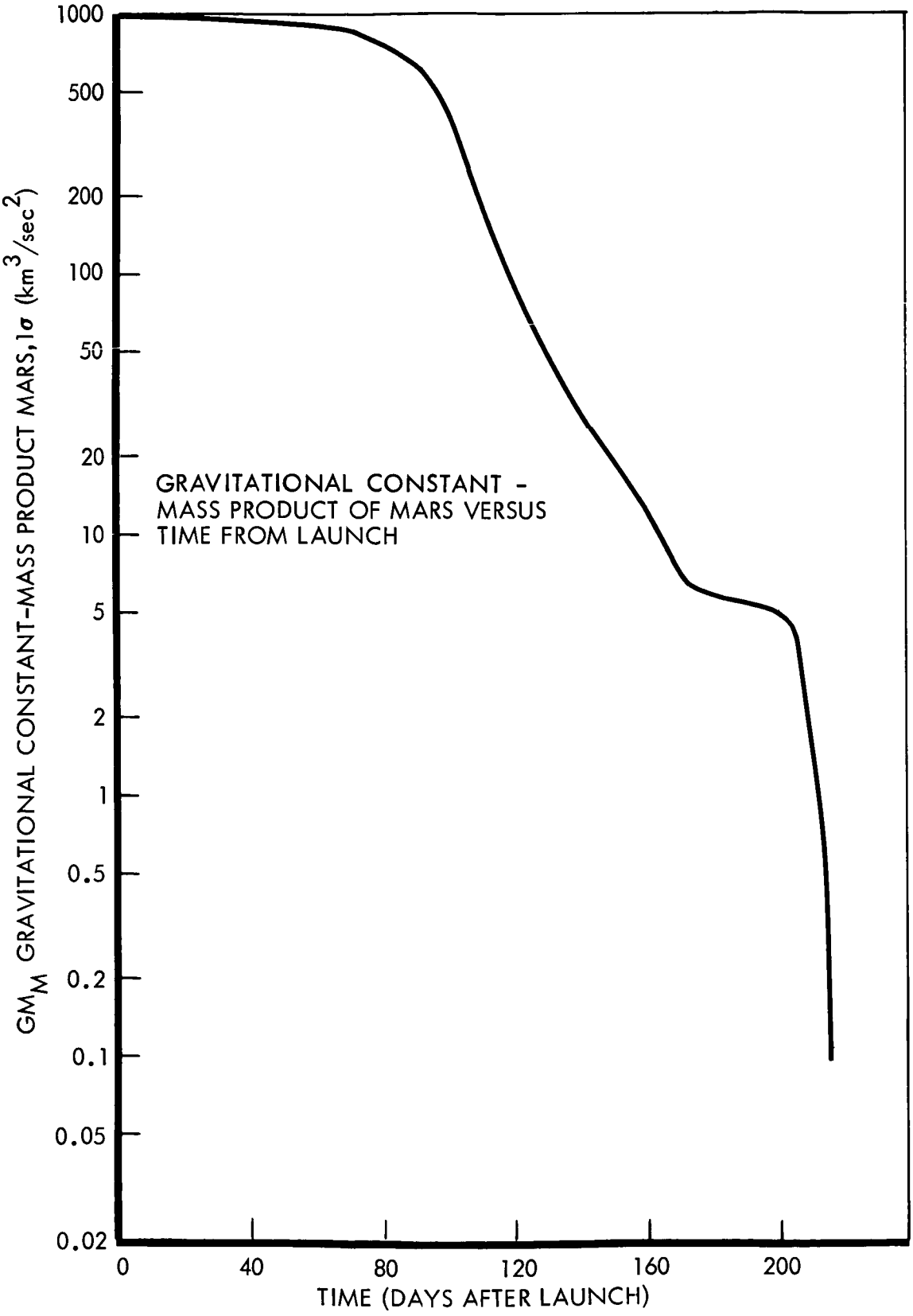

Figure 3-9: Physical Constant Uncertainties

The resulting errors in the constants after completion of tracking were within the following ranges:

$$0.05 \lesssim \sigma_{GME} \lesssim 0.12 \ km^3/sec^2$$

$$0.1 \lesssim \sigma_{GMM} \lesssim 1.0 \ km^3/sec^2$$

$$10 \lesssim \sigma_{AU} \lesssim 40 \ km$$

Although the model was incomplete (that is, a number of error sources were not considered), it may be concluded that the constants can probably be determined to the following accuracies:

$$\sigma_{GME} < 0.15 \ km^3/sec^2$$

$$\sigma_{GMM} < 1.0 \ km^3/sec^2$$

$$\sigma_{AU} < 50 \ km$$

The gross effect of different a priori estimates on the total orbit determination (OD) uncertainties was not striking. As soon as a constant began to disturb the trajectory, the high precision of the doppler measurements allowed significant updating of the parameter value, thus keeping its effect on navigation uncertainty low.

The results presented in this section have not included effects due to Mars ephemeris uncertainties, which are expected to be on the order of 50 to 100 kilometers in position. The Mars ephemeris can (and will) be included in the parameters to be determined and, in light of the sensitivity of the measurement to GMM, the measurements should be quite sensitive to Mars ephemeris and, therefore, allow significant improvement. Reprocessing of the Mariner '64 tracking data with the ephemeris

as parameters should allow significant improvement, also. However, as a conservative estimate of the navigation accuracy relative to Mars during midcourse, the expected ephemeris error can be root-sum-squared with the errors relative to Earth.

3.1.3.2 Midcourse Guidance Accuracy Analysis

The midcourse guidance analysis technique can be described generally as follows. The injection errors are mapped to the first midcourse correction time as an estimate of the expected deviations from the nominal trajectory at that time. These errors and the guidance law provide the information for estimation of the ΔV required to correct the trajectory such that the desired terminal conditions are satisfied.

Tracking data is assumed to have been accumulated after injection such that the navigation errors at the correction time are considerably smaller than the mapped injection errors. However, some error still exists in the knowledge of vehicle position and velocity. In addition, the maneuver itself cannot be executed perfectly and therefore, the knowledge of vehicle state is further corrupted by the execution errors. The combined navigation and control errors are mapped to the second correction time and are used in the same manner that the injection errors were used at the first correction time. The process is then repeated at the second correction time. After each correction, the errors are mapped to the terminal parameter space. Subsequent corrections are handled in the same manner.

The guidance law used gives the velocity to be gained as:

$$\underline{V}_g = G \, \Delta \underline{p} - \Delta \underline{V}$$

where:

$\underline{V}_g$	=	velocity to be gained vector (column)
G	=	3 x 3 matrix of guidance coefficients
$\Delta \underline{p}$, $\Delta \underline{V}$	=	deviation of position and velocity from nominal at the correction time.

The guidance coefficient matrix, G, depends on the type of control and the terminal parameters to be controlled. For this analysis, the $\underline{B}$ plane parameters, $\underline{B} \cdot \underline{T}$ and $\underline{B} \cdot \underline{R}$ and the flight time, T_f, were selected as terminal parameters to be controlled. The ΔV estimate for a given correction is made by computing

$$1\sigma \ \Delta V = \left[\text{Trace (Expected value of } \left\{\underline{V}_g \ \underline{V}_g{}^T\right\})\right]^{1/2}$$

The measure of required ΔV for the correction is found as:

$$\Delta V = 3 \ (1\sigma \ \Delta V)$$

The magnitude of the execution control source errors were taken nominally to be:

1σ	pointing error	=	10 milliradians
1σ	proportional velocity error	=	1 percent
1σ	nonproportional velocity error	=	0.01 meter per second

The results of the analysis are shown in Table 3-2.

Table 3-2: Nominal Midcourse Analysis Results

CORRECTION 1ST	2ND	3RD	1σ T_F	1σ B_{MAX}	1σ B_{MIN}	θ MAX	1σ ΔV
INJECTION							
5			0.917	4933.54	403.024	26.907	15.64
5	25		0.035	194.007	19.746	26.902	0.278
5	25	175	0.003	19.854	3.987	26.512	0.101
5	25	200	0.001	8.389	3.671	25.382	0.272
5	25	205	0.001	6.457	3.655	23.980	0.409
5	50		0.027	157.360	26.905	26.663	0.376
5	50	175	0.003	20.900	4.378	25.944	0.079
5	50	200	0.001	9.314	3.494	24.679	0.212
5	50	205	0.001	7.396	3.044	23.720	0.318
5	75		0.020	133.554	40.611	26.313	0.535
5	75	175	0.003	23.456	7.781	28.551	0.062
5	75	200	0.001	12.819	3.401	34.854	0.168
5	75	205	0. 001	10.951	2.684	37.538	0.253
5	100		0.016	119.694	56.289	26.140	0.756
5	100	175	0.003	23.311	11.481	28.911	0.054
5	100	200	0.001	10.374	5.711	39.830	0.144
5	100	205	0.001	8.297	4.429	49.624	0.216
5	125		0.01	108.919	20.439	26.533	0.107
5	125	175	0.00	23.036	15.264	29.660	0.049
5	125	200	0.001	9.507	7.073	45.302	0.132
5	125	205	0.001	7.433	5.488	60.644	0.198

1σ B_{MAX} = Semimajor axis of dispersion ellipse in miss plane, km

1σ B_{MIN} = Semiminor axis of dispersion ellipse in miss plane, km

θ_{MAX} = Angle between semimajor axis of ellipse and the T axis, degrees

1σ T_f = Standard deviation of flight time in hours

1σ ΔV = ΔV to correct 1σ dispersions for the last correction listed

The second correction time was varied from 25 to 125 days after launch and the third correction from 175 to 205 days after launch.

As the time of the second or third midcourse correction increases, the expected encounter errors go down and the ΔV requirements go up.

The Mars ephemeris error has not been considered in this analysis. Its effect can be approximated by root-sum-squaring the ephemeris error with the encounter error. When this is done, the encounter errors are dominated by this error source for all three-midcourse-correction sequences, but the control uncertainties dominate for the first two corrections. It can also be concluded that any plausible sequence of three corrections satisfies the 500 kilometer, 3σ, encounter-accuracy requirement and, in fact, provides nominal encounter accuracies only slightly over 300 kilometers, 3σ, if the Mars ephemeris error is assumed to be a pessimistic 100 kilometers, 1σ.

The actual selection of the nominal maneuver sequence proceeds as follows. It is desirable to make the first correction as early as possible for two prime reasons. First, it is desirable to provide reasonable encounter dispersions early in the mission. Second, the earlier the first correction the less the ΔV required. This is especially important for poor injections. The OD analysis results show the OD uncertainties leveling off at about 2 days. Therefore, the first correction would probably be executed not long after that. It is somewhat arbitrary in the nominal case because the ΔV requirement

is not very sensitive to changes of a day or two in the first correction time. For this example, 5 days is selected as the nominal first correction time. The second correction should be made as early as possible after the first to keep the ΔV requirement down and to improve the orbit redetermination for the remainder of the mission. An early second correction also acts as a backup for a possible poor first correction. The analysis results indicate that a second correction at 25 days satisfies these desires.

The third correction normally would be as late as possible to improve encounter accuracy. However, the analysis shows encounter accuracy to be relatively insensitive to the time of the third correction. More important, it is desirable to have the third correction early to improve the orbit-redetermination capability before capsule deflection and encounter. The OD uncertainties reach a minimum in the neighborhood of 175 days and the OD capability after 175 days is considerably more acceptable than for later third corrections. Also, setting the third correction before 175 days could require the execution of a ΔV impulse less than 0.1 meter per second, thereby establishing a difficult control problem. The third correction should, therefore, be set nominally at 175 days.

The sensitivity of the guidance accuracy to control errors was investigated for the nominal maneuver sequence selected above. The effects are quoted for an assumed 100 kilometers, 1σ, Mars ephemeris error.

Tightening the pointing-accuracy requirement to 0.005 radian or relaxing it to 0.015 radian affected the encounter accuracy after the first correction only. A 10-percent reduction and increase, respectively, was obtained in the semimajor axis of the encounter ellipse and a 40 percent variation in the semiminor axis. The second and third correction accuracies were essentially uneffected because of the small ΔV magnitudes involved. It may be concluded, therefore, that there is no good reason to tighten the pointing accuracy requirement and, in fact, it might be relaxed to about 1 degree without significant degradation of the mission.

Tightening the ΔV-proportional error requirement to 0.5 percent again affected mainly the accuracy resulting from the first correction, yielding about a 40 percent improvement in the semimajor axis and none in the semiminor axis. Relaxing the requirement to 2 percent caused 100 and 30 percent increase in the semimajor axis of the encounter dispersion for the first and second corrections respectively. It can, therefore, be concluded that no strong case can be made for increasing the ΔV-proportional accuracy requirement, but that a relaxation could produce a significant adverse effect on the encounter accuracy after the first and second correction.

Reducing the ΔV resolution error by a factor of three affected only the second-correction resultant accuracies. About 30-percent improvement in the semimajor axis was obtained. Relaxing this error is not practical because of the small ΔV magnitude involved in the last two corrections.

It may be concluded that the control accuracy requirements of 0.010 radian, 1σ, in pointing; 1.0 percent, 1σ, in V-proportional errors; and 0.01 meter per second, 1σ, in resolution; provide good control, but that the pointing accuracy requirement could be relaxed to about 1 degree. Tightening, if possible, of the resolution accuracy would be good for the last two corrections because of the small ΔV magnitudes and would provide for the distinct possibility of meeting the desired encounter accuracies with only two corrections at 5 and 25 days. This would also improve the OD capability significantly. The exectuion of the nominal three-correction case will require 48 meters per second ΔV for random error correction. In keeping with past experience concerning nonabortive failures, raising the requirement to 75 meters per second is plausible.

The above discussion is based on the use of an axial accelerometer for velocity metering. The possibility of using timed burns should also be considered. Use of timed burns would essentially increase the ΔV-proportional errors to a few percent, but would reduce the resolution error since a significant contributor is the accelerometer integrator resolution. The two error changes act in opposition. Larger encounter errors would be expected after the first correction, but little degradation would be noticed for the nominal three-correction case.

3.1.3.3 Aim-Point Selection

The present constraint on probability of impact of the spacecraft at encounter is 1×10^{-5}. Because the 3σ error dispersions of the 25- and 175-day trajectory corrections are small compared with the required

insertion altitude for a 50-year lifetime orbit, these maneuvers do not contribute (apart from malfunctions) to the probability of impact at encounter. Postponing the malfunction considerations, it remains that, if the heliocentric injection or the 5-day trajectory correction aim points are at the nominal 175-day aim point, the probability of impact at encounter is greater than 1×10^{-5}. The problem is to select these two aim points so as to meet the constraint and also minimize the probability of needing the additional corrections at 25 and 175 days.

Nominal error dispersions for the heliocentric injection maneuver and the 5-day correction are projected to the Mars R-T plane where they are described by means of constant probability density contours (ellipses) of the density function for intersection of the approach asymptote with the plane. Varying the aim points primarily moves the density function over the R-T plane without changing its size or angular orientation significantly. The Mars capture zone and preferred orbit insertion area (target area), projected into the R-T plane, were drawn to the same scale as the ellipses. Transparent overlays of the injection and 5-day trajectory correction error dispersion ellipses were used along with tables of the bivariate normal distribution function to compute the probability of impact at encounter, and probability of encounter in the target area, as a function of aim-point location.

Since the ratio of the major to minor axes of the injection dispersion is about 100:1, (435,000 to 5010 kilometers), it is reasonable to pass the minor axis of the injection dispersion ellipses through the nominal

aim point, then bias the major axis on the target-area side of Mars. For the 5-day correction dispersion, it appeared most desirable to pass the major axis of the dispersion ellipses through the nominal aimpoint, and bias the minor axis away from Mars.

The next step in the solution was to write an equation, using nominal reliability values for the corrections, which properly related the impact probabilities to one another and to the correction reliabilities. This was done by using a Markov tree diagram of the maneuver outcomes.

By choosing the maximum probability of impact at encounter, first for the injection and then for the 5-day correction, the closest possible aimpoints for each was found. It then was apparent that more probability of target encounter was to be gained per increase in impact probability by aiming the 5-day correction as close as possible, and moving the injection aim point away as far as necessary.

Figure 3-10 shows the location of the two aim points selected, along with their respective 3σ ellipses. The $\bar{R}$ and $\bar{T}$ components of the aimpoints are -13,500 kilometers and +17,500 kilometers, respectively, at injection; and +9000 and +22,200 kilometers at 5 days.

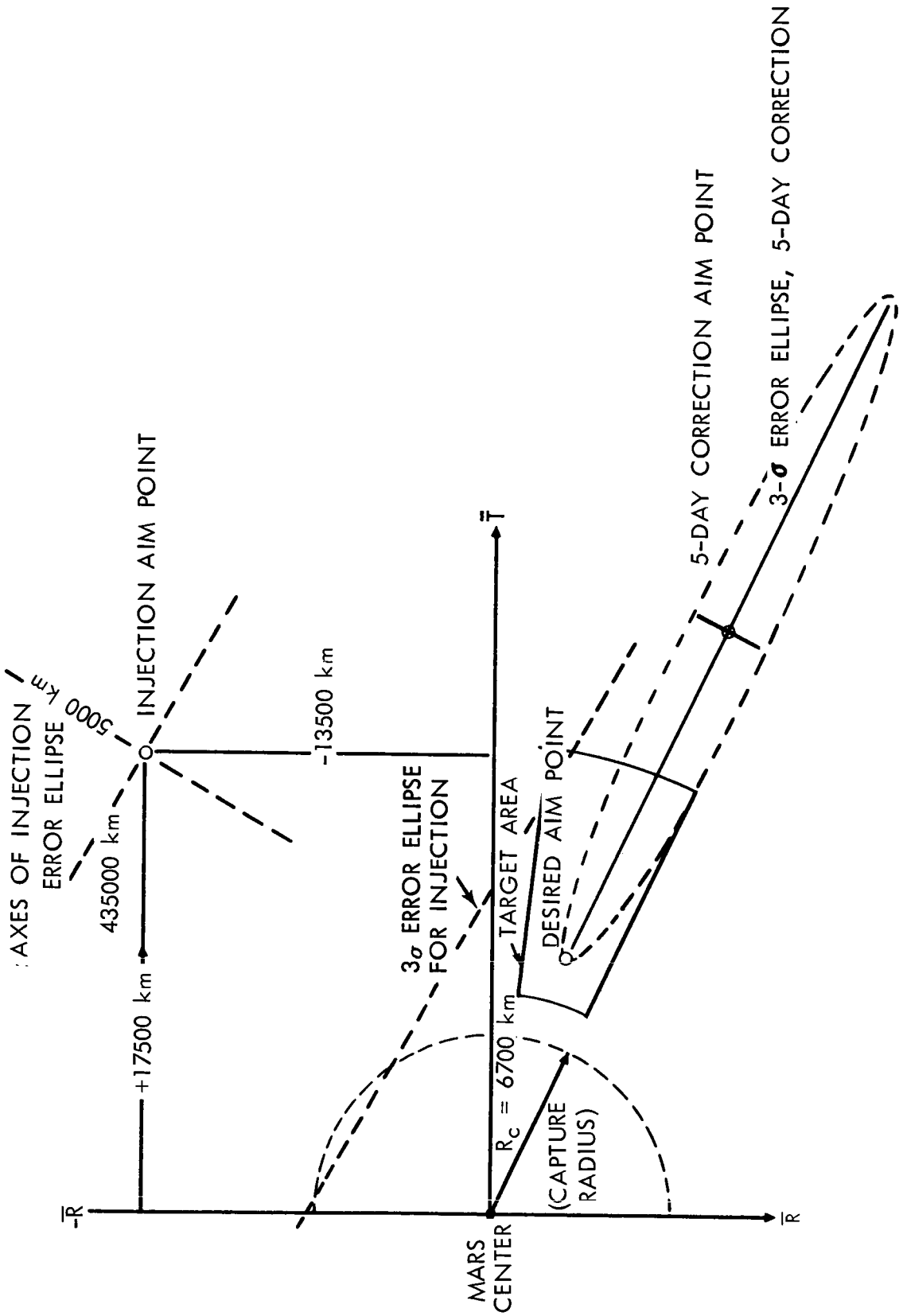

Figure 3-10: Optimum Aim Points At Injection And At 5 Days

3.1.4 Mars-Approach Orbit Determination Uncertainties

The basic question to be resolved in connection with the Mars-approach-phase navigation is whether or not an onboard sensor should be included to augment ground-based tracking.

To answer this question, an effort has been made to look beyond the 1971 mission to the later missions when conditions have changed. To this end, the analysis of navigation accuracies has been performed parametrically so that results may be extrapolated to the later launch opportunities. Quantities treated parametrically are the error sources that contribute to navigation errors, namely, random measurement errors, measurement biases, physical constant uncertainties, and Mars ephemeris errors. The results of the analysis indicate that an onboard sensor does not offer a sufficient advantage over ground-based tracking to justify the added complexity.

The only type of onboard sensor considered is one that measures local vertical to Mars relative to inertial space. This might be accomplished with TV as described in G.E. final report to JPL on Voyager (Document 645D933). Alternatively, a simpler but less accurate system such as a planet tracker might be used.

The error-analysis program used utilizes an estimation procedure due to Kalman. In addition to the position and velocity errors, the errors in determining a maximum of five biases are obtained. Also, near Mars, errors in determining the ephemeris of Mars are obtained. The resultant number of state variables is 17.

To investigate the desirability of including a local vertical sensor to augment DSIF, six configurations were examined. These six configurations include various doppler and angular measurement accuracies as given in Table 3-3. The accuracy given for angular sensor D corresponds to accuracies quoted in Document 645D933 by G.E. for a TV system. The other angular sensor corresponds to some hypothetical planet tracker, which is presumably less complex than the TV system. A bias error in locating the center of Mars of 100 kilometer per axis has been assumed for both C and D. The 0.01 meter per second doppler accuracy indicated corresponds to the present performance of the DSN. The projected accuracy for the doppler measurement in 1971 is 0.001 meter per second sampled once per minute. The 0.0025 meter per second accuracy quoted in the table makes a conservative allowance for this expected improvement. The data rate assumed is one observation per hour.

The physical constants considered in the solution are Earth gravitational constant, solar radiation pressure, Mars gravitational constant, and doppler scale factor. The doppler scale factor uncertainty is due to both the uncertainty in the astronomical unit and in the speed of light. Values of these uncertainties used in the analysis are given in Table 3-3.

A successful orbiter mission in 1971 is likely to reduce the ephemeris error of Mars and the physical constant uncertainties. For this reason, all six sensor configurations were examined with an order-of-magnitude reduction in the ephemeris error and physical constant uncertainties. The exception to this is uncertainty in the effects of solar radiation pressure, since the effective spacecraft area uncertainty is not likely to decrease as a result of previous missions.

Table 3-3: Approach Phase Error Analysis Data

RANDOM MEASUREMENT ERRORS					
Sensor	rms Error Sources	Time Between Measurements			
DSIF — doppler	A. 0.01 m/sec	Near Planet	1 min	Interplanetary	1 hr
	B. 0.0025 m/sec		1 min		1 hr
Local Vertical	C. 0.3 degree		1 hr		1 hr
	D. 0.02 degree		8 hr		8 hr

LOCAL VERTICAL MEASUREMENT BIAS
Uncertainty in location of center of Mars: 100 km* per axis

SENSOR CONFIGURATIONS ANALYZED		
1. A	3. A plus D	5. B plus C
2. A plus C	4. B	6. B plus D

INITIAL PHYSICAL CONSTANT UNCERTAINTIES (PARTS PER MILLION)			
Constant	Uncertainty	Constant	Uncertainty
1. Earth gravitational constant	2.5	3. Mars gravitational constant	1000
2. Sun gravitational constant	1	4. Doppler scale factor (A.U.)	1

MARS EPHEMERIS ERROR — 100 km IN EACH COORDINATE			
Trajectory Data			
Launch Date:	May 13, 1971	Mars orbital inclination	40 degrees
Arrival Date:	December 14, 1971	Mars periapsis altitude	2640 km

* This is the accuracy used by C. R. Gates and H. J. Gordon of J.P.L. in "Planetary Approach Guidance," a paper in Journal of Spacecraft and Rockets, 1965.

Figure 3-11 and 3-12 give the navigation accuracy that may be expected from the six sensor configurations considered. The projected periapsis altitude error has been taken as the most meaningful measure of performance. In each case, angular measurements were started 10 days from periapsis passage, and the doppler sampling period was decreased from 1 hour to 1 minute at the sphere of influence of Mars (1.5 days to periapsis passage). The curves of Figure 3-11 represent navigation accuracies using current doppler accuracies. Figure 3-12 gives navigation accuracies for sensor configurations utilizing an improved doppler measurement accuracy. In the Voyager application, only the region prior to 5 hours to encounter is applicable because injection maneuver computations cannot be initiated at a much later time. An improvement in doppler accuracy (Sensor Configuration 4) gives a negligible improvement over current doppler accuracies (Sensor Configuration 1).

The upper curves in the two figures represent the accuracies with the ephemeris error and physical constant uncertainties given in Table 3-3. The lower curves represent the accuracies with the ephemeris error and Mars physical constant uncertainties reduced by an order of magnitude. When the ephemeris error is 100 kilometers, an improvement in navigation accuracy of approximately 30 percent is realized by augmenting the doppler measurement. However, when the ephemeris error is reduced, the local vertical measurement gives a negligible improvement.

The relative insensitivity of periapsis altitude error to improved measurement accuracies is due to the effects of Mars ephemeris errors. The 100-kilometer ephemeris error corresponds to an angular uncertainty of

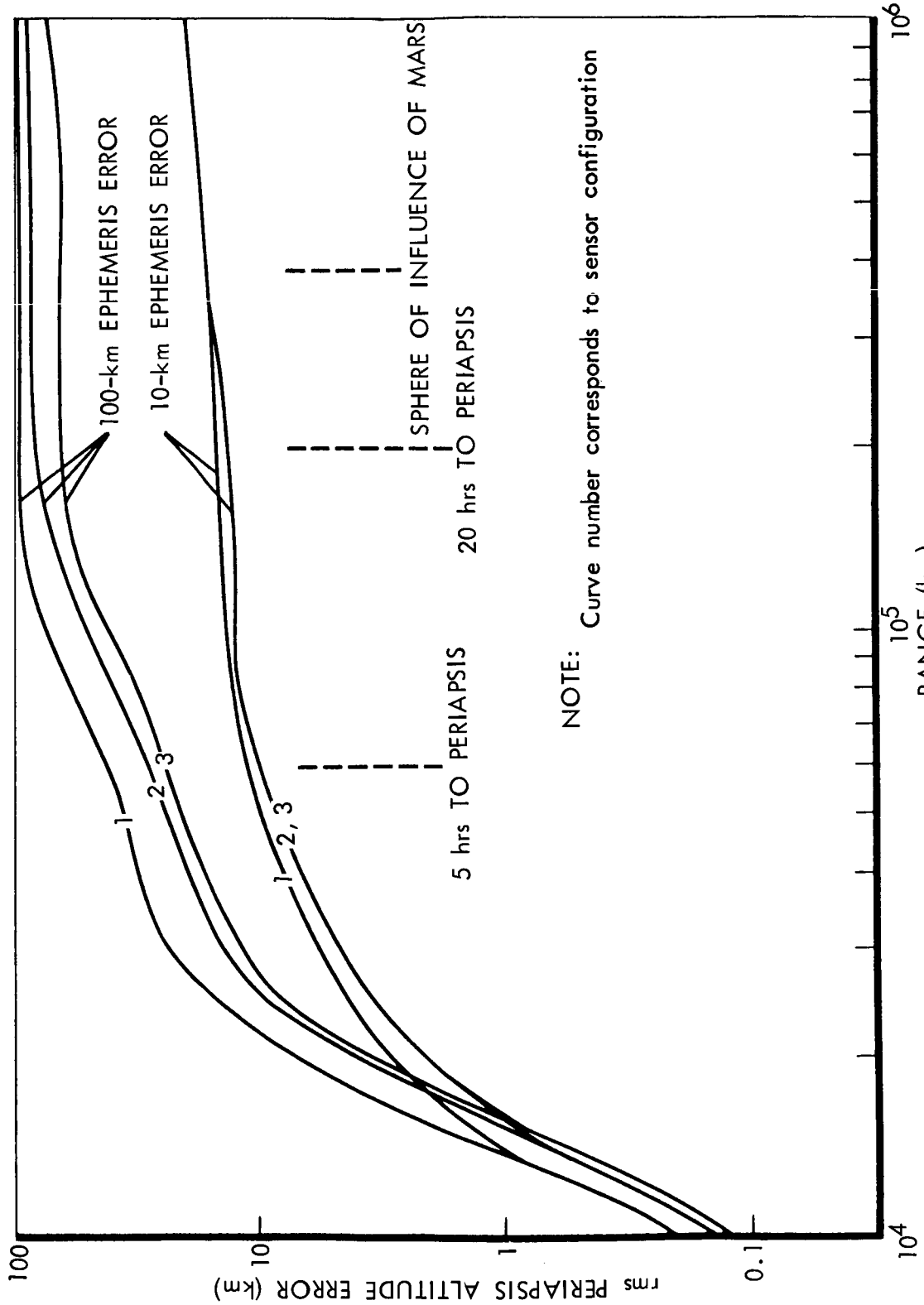

Figure 3-11: Approach-Phase Navigation Accuracies

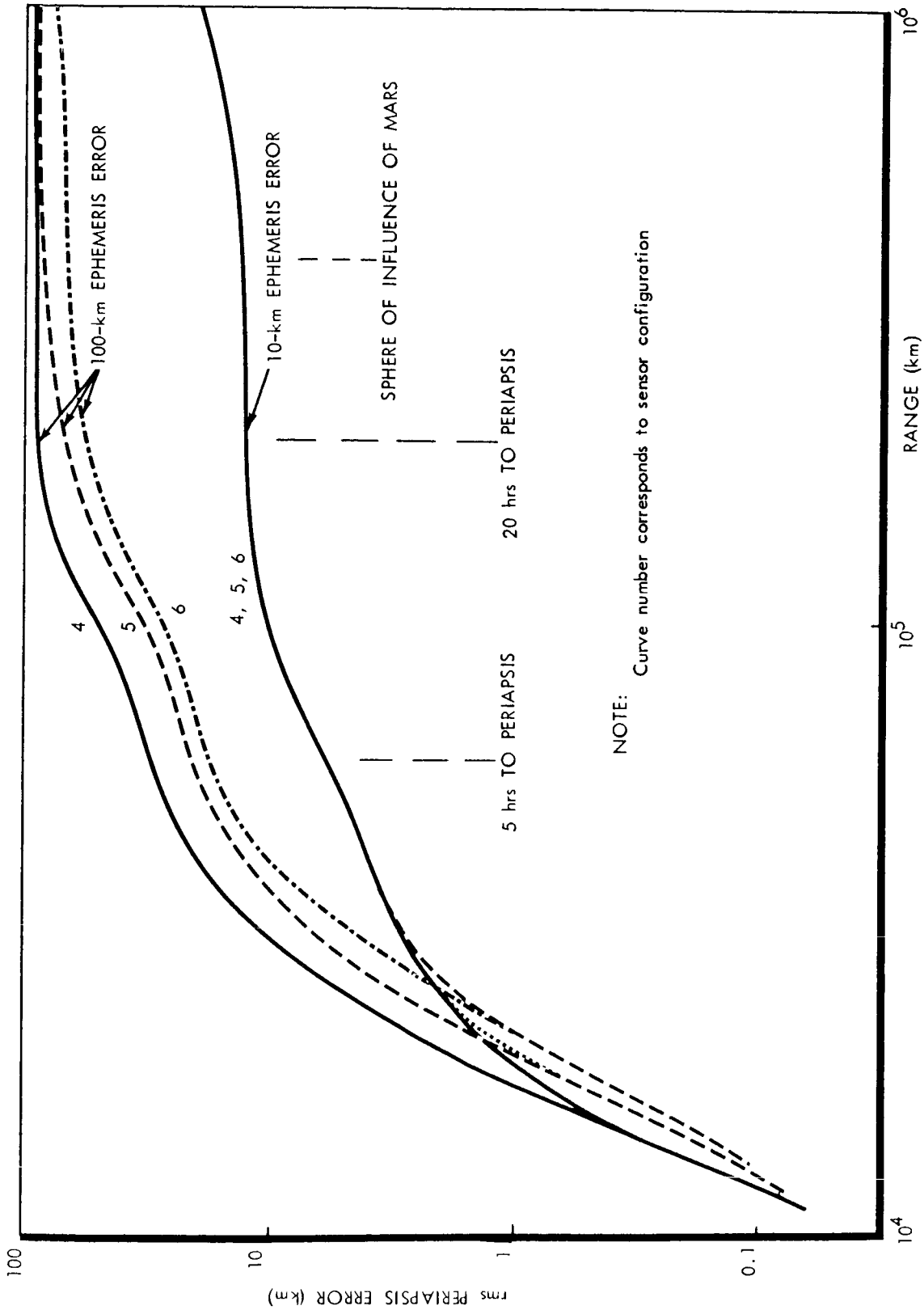

Figure 3-12: Approach-Phase Navigation Accuracies

Mars position of 0.1 of a second of arc. The doppler measurement is unable to resolve the ephemeris error until the gravitational effect of Mars on the spacecraft is appreciable. The local vertical measurement is of limited use in determining the ephemeris error because of the assumed 100 kilometer bias error in locating the center of the planet.

Because it is likely that the physical constant uncertainties and measurement bias errors will change during the Voyager program, it is desirable to know the effect of changes of these physical constants on the performance of the navigation system. By utilizing the information contained in the error-covariance matrix of the system-state vector, it was possible to obtain parametric data on the variation of accuracy with physical constant uncertainties and measurement bias errors. Figures 3-13 to 3-15 show the effect of altering the standard deviation of each source error. The lack of sensitivity of altitude error to physical constant uncertainties again points out the dominance of the Mars ephemeris error. Sensor configurations that employ a local vertical measurement are also sensitive to an uncertainty of the location of the center of Mars. From Figure 3-14, if this uncertainty could be decreased from 100 to 10 kilometers, a 50 percent reduction in periapsis altitude error would result. However, for the 10-kilometer ephemeris-error case (Figure 3-15), such a high sensitivity does not exist because the planet center uncertainty has the same effect on a local vertical measurement as does the ephemeris error.

Graphs such as Figure 3-13 give the parametric effect of the uncertainties in physical constants at a point during the approach phase. Figure

3-16 gives the sensitivity of the projected periapsis altitude error as a continuous function of range from periapsis. This graph corresponds to the slope of Figure 3-13 at the (1.0, 1.0) point. The graph shows that the insensitivity of periapsis altitude error to physical constant uncertainties is maintained throughout the approach phase.

Aside from navigation accuracies, the accuracy of the determination of physical constants is also of interest. Table 3-4 gives the final determination accuracies of the physical constants at 2 hours from periapsis passage. The only significant advantage of the local vertical measurement is better determination of Mars gravitational constant for the least accurate doppler. For the more accurate doppler, the advantage is not as great. An improvement in the determination of the doppler scale factor (AU and speed-of-light uncertainties) is also possible with the inclusion of the local vertical measurement. However, better accuracy of the doppler scale factor for later missions is not needed to improve navigation accuracy in the critical region prior to 5 hours from periapsis passage.

To verify the results of the statistical analysis, Monte Carlo simulation of the approach-phase navigation was performed. The covariance matrix was initialized with diagonal elements consistent with the statistical analysis of the approach phase. The trajectory was started at the sphere of influence of Mars. The program used does not solve for Mars ephemeris errors. However, this should not effect the basic question of convergence of estimated position to the nominal. Figure 3-17 gives the results of simulations for Sensor Configuration 1. The Monte Carlo and statistical errors agree quite well.

In conclusion, the two reasons why an onboard sensor might be of value to the Voyager Mission are to corroborate DSN results and to improve approach orbit determination capability.

Studies, including a study by Gates and Gordon[1], have shown that onboard data can, in fact, corroborate the DSN results under nominal conditions. However, if the data from the two are in strong disagreement, then greater reliance must be placed upon the DSN data because it is a proven system, thus detracting from the value of onboard data for corroboration purposes.

It is also found that Mars-approach orbit determination capability is improved for the 1971 mission by using onboard sensed data. However, the expected navigation accuracies using the DSN only are sufficient for the 1971 mission. Furthermore, assuming a successful mission, the model improvement attainable from DSN data during the 1971 mission would render onboard data of negligible value for subsequent missions.

---

[1] Gates, C. R., and H. J. Gordon, Planetary Approach Guidance, Technical Report No. 32-631, Jet Propulsion Laboratory, California, Institute of Technology, Pasadena, California, June 30, 1964.

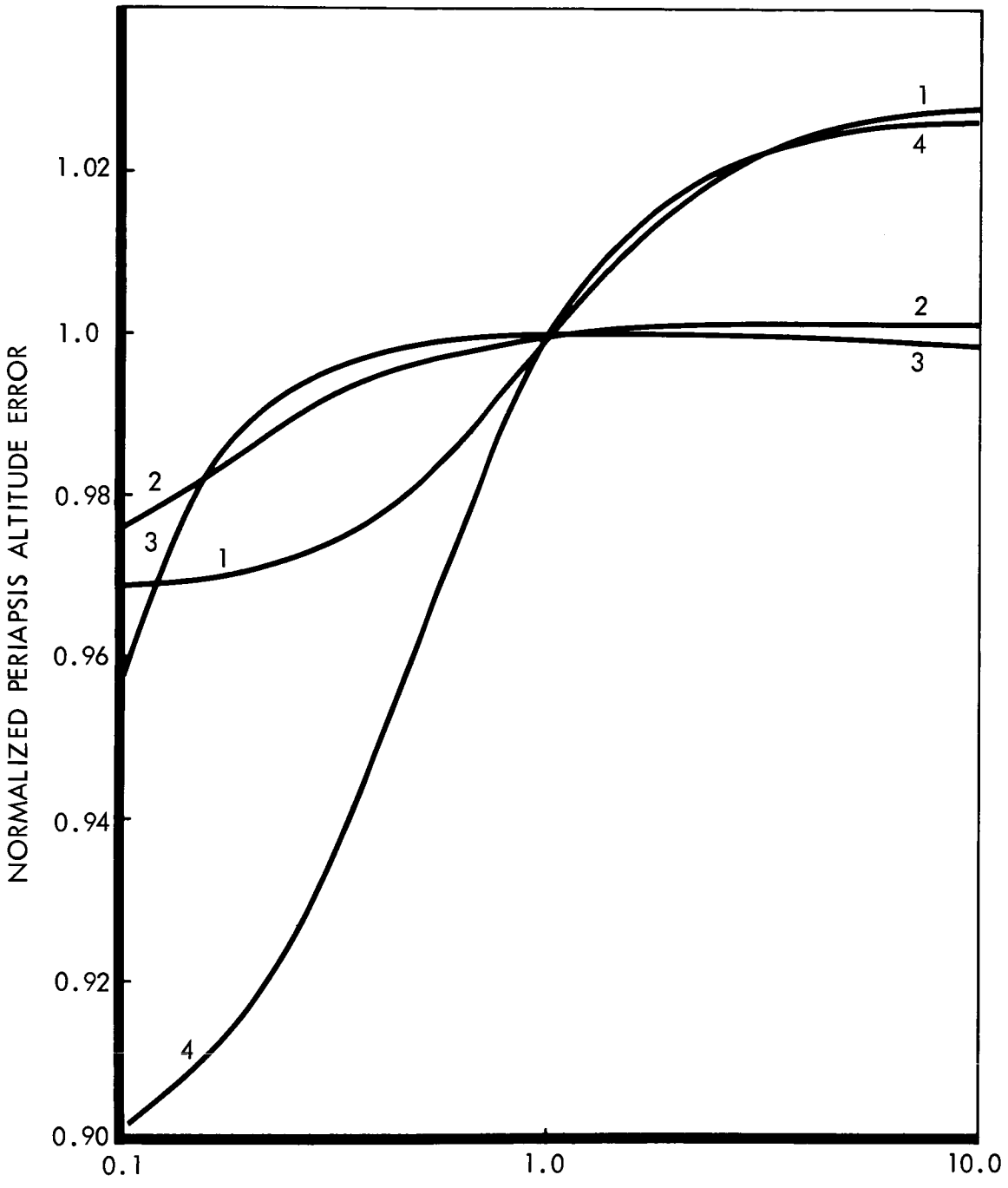

CURVE:

1 — EARTH'S GRAVITATIONAL CONSTANT
2 — SUN'S GRAVITATIONAL CONSTANT
3 — MARS' GRAVITATIONAL CONSTANT
4 — DOPPLER SCALE FACTOR (A.U.)

ALTITUDE ERROR NORMALIZATION FACTOR = 42.3 km
STOP DATA 5 hrs FROM PERIAPSIS PASSAGE

Figure 3-13: Performance Sensitivity — Sensor Configuration 1

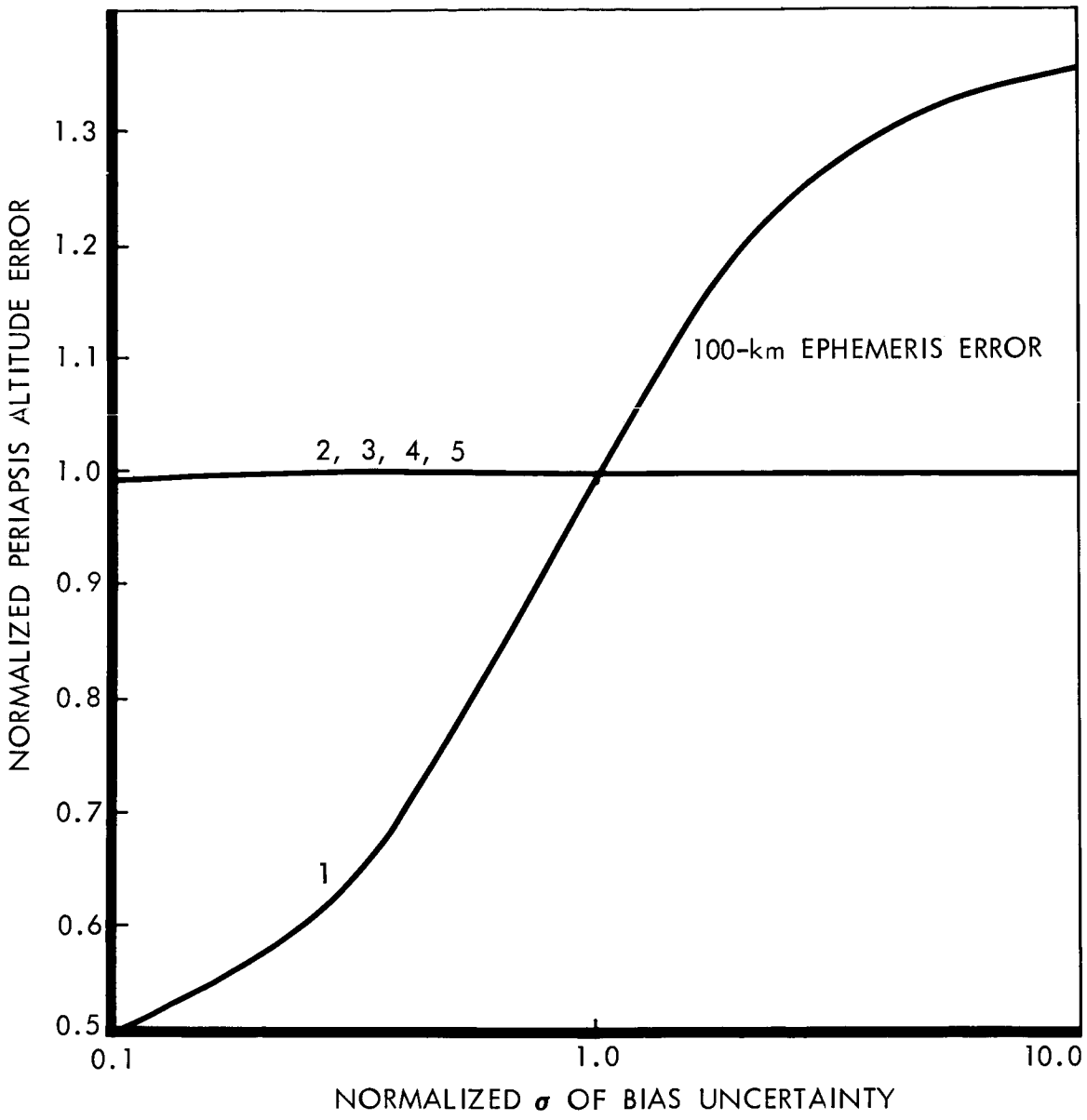

CURVE:

1 — BIAS ON ANGULAR MEASUREMENT IN ORBIT PLANE
2 — SUN'S GRAVITATIONAL CONSTANT
3 — MARS' GRAVITATIONAL CONSTANT
4 — DOPPLER SCALE FACTOR (A.U.)
5 — BIAS ON ANGULAR MEASUREMENT OUT OF ORBIT PLANE

ALTITUDE ERROR NORMALIZATION FACTOR = 65 km
STOP DATA 20 hrs FROM PERIAPSIS PASSAGE

Figure 3-14: Performance Sensitivity — Sensor Configuration 3

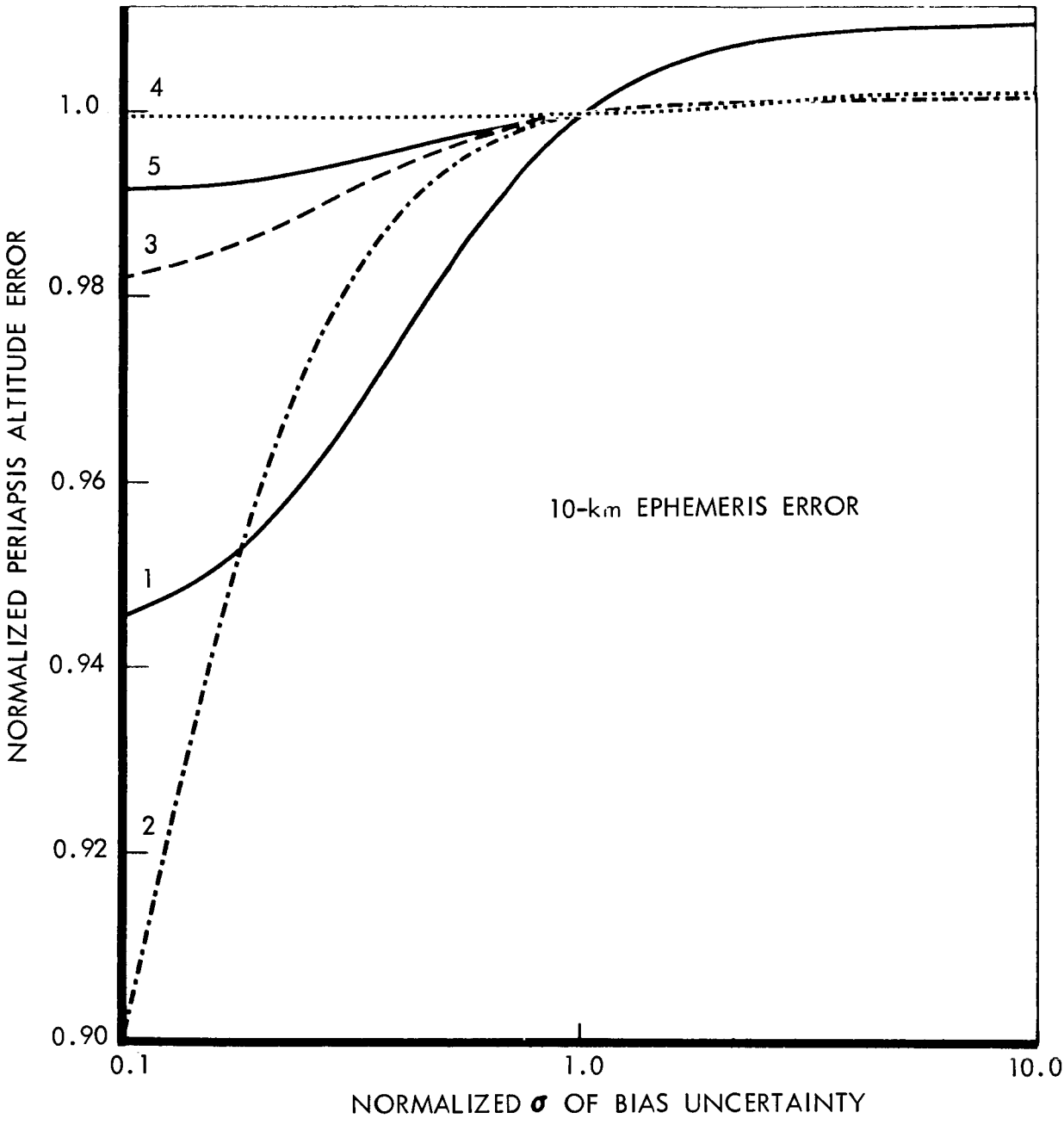

CURVE:

1 — BIAS ON ANGULAR MEASUREMENT IN ORBIT PLANE
2 — SUN'S GRAVITATIONAL CONSTANT
3 — MARS' GRAVITATIONAL CONSTANT
4 — DOPPLER SCALE FACTOR (A.U.)
5 — BIAS ON ANGULAR MEASUREMENT OUT OF ORBIT PLANE

ALTITUDE ERROR NORMALIZATION FACTOR = 13 km
STOP DATA 20 hrs FROM PERIAPSIS PASSAGE

Figure 3-15: Performance Sensitivity — Sensor Configuration 3

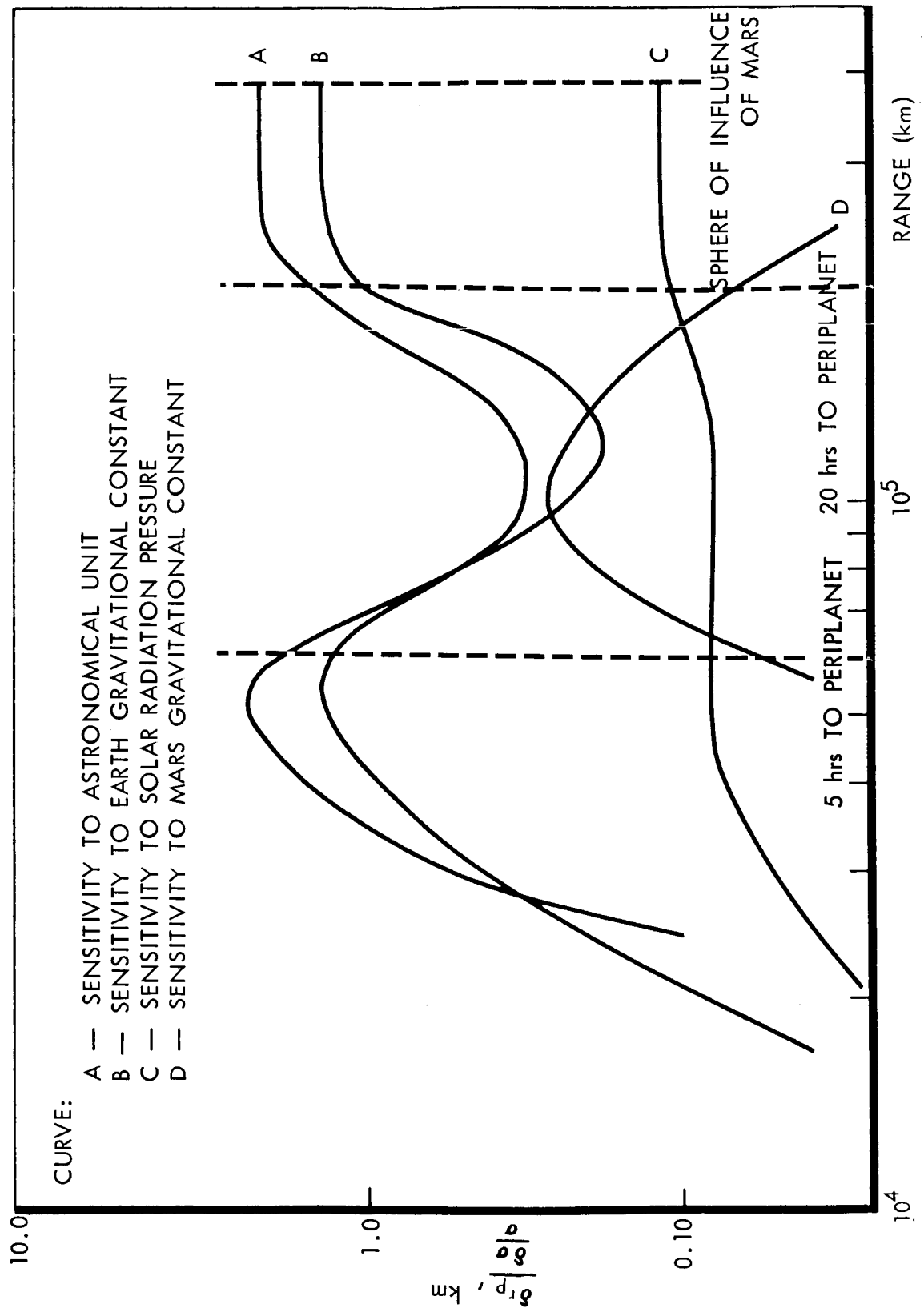

Figure 3-16: Approach-Phase Sensitivity Of rms Periplanet Altitude Error To Normalized Bias Variances

Table 3.4: Final Determination Of Physical Constant Uncertainties — Approach Phase
(2 Hours From Periapsis Passage)

SENSOR CONFIGURATION	PHYSICAL CONSTANT: SUN'S GRAVITATIONAL CONSTANT (PARTS PER MILLION)	PHYSICAL CONSTANT: MARS' GRAVITATIONAL CONSTANT (PARTS PER MILLION)	PHYSICAL CONSTANT: DOPPLER SCALE FACTOR (AU) (PARTS PER MILLION)	R.S.S. MARS EPHEMERIS ERROR - km
Initial Value	1.0	1000	1.0	173
1	0.21	28.8	0.43	96
2	0.21	14.7	0.27	77.5
3	0.21	14.4	0.27	74.5
4	0.2	10.9	0.19	56.5
5	0.19	7.1	0.08	44.3
6	0.19	7.1	0.08	44

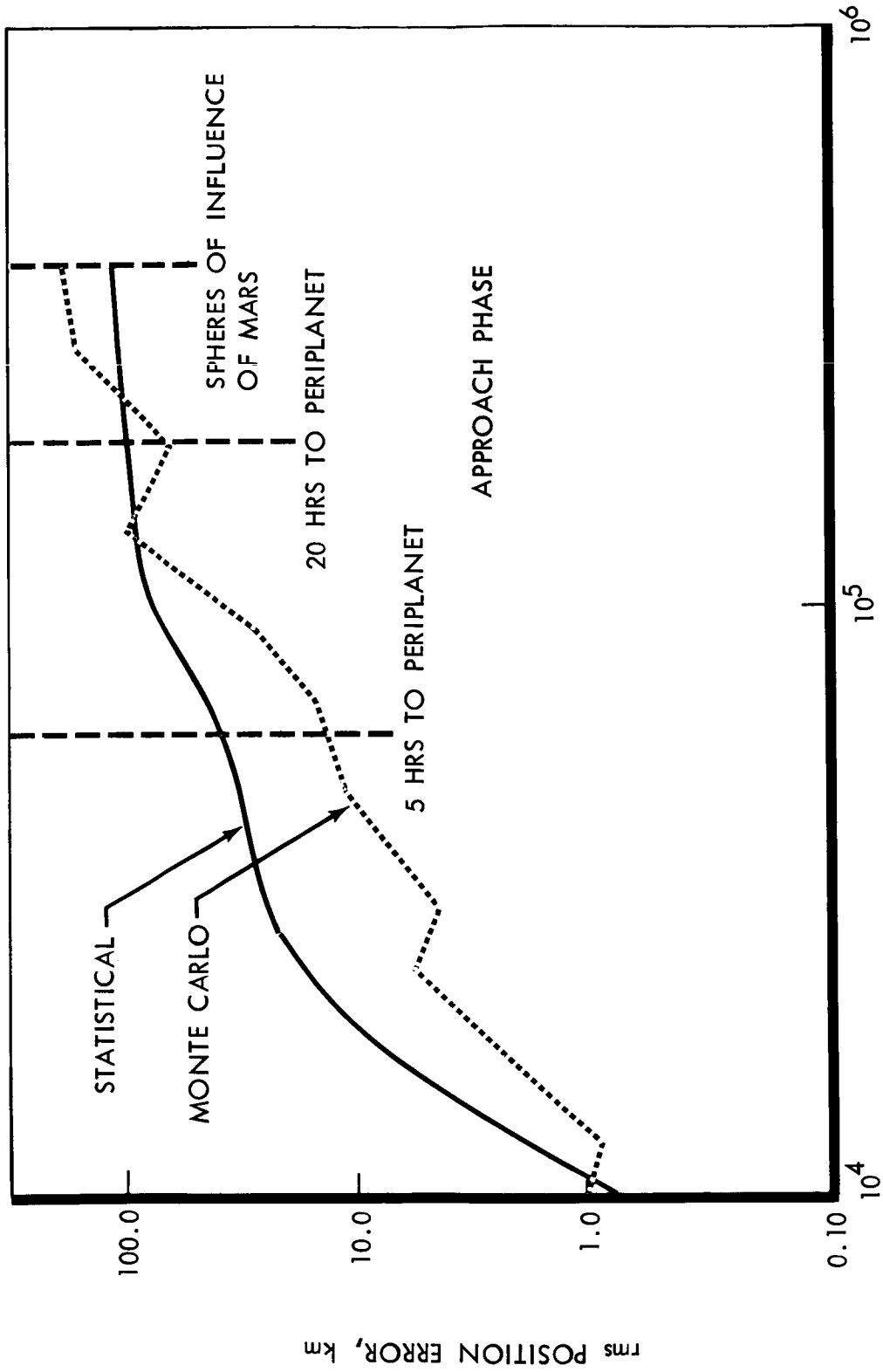

Figure 3-17: rms Radial Component of Position Error vs Range-Sensor Configuration 1

3.1.5 Orbit Insertion

Analyses, such as are presented in JPL EPD 250, have shown that little is gained by using an optimum thrust profile for orbit insertion, and that, in fact, the simple fixed-direction-in-space thrust is essentially as "optimum" as any method. The results presented in Table 3-5 are based on this method of orbit insertion.

The object of the analysis was to determine the relative significance of the navigation uncertainties at insertion and the uncertainties in state due to execution of the insertion maneuver. The sensitivity of the total uncertainty after insertion to control accuracy allows a judgment to be made regarding the allowable control errors.

The orbit determination uncertainties just prior to insertion are assumed to be 50 kilometers and 2.5 meters per second in each of the three axes. This is consistent with the results of the approach navigation analysis. The control accuracies were initially taken as the nominal accuracies discussed for the midcourse maneuvers but with a resolution error of 4 meters per second. The resultant errors in orbit parameters for a typical orbit are shown in Table 3.5.

Table 3-5: ORBIT INSERTION ERRORS--18-HOUR ORBIT

PARAMETER	a*	e	I*	W_p	Ωn
1 σ Due to Navigation	922	0.016	0.015	0.011	0.003
1 σ Due to Control	179	0.004	0.005	0.001	0.002
Total 1σ	939	0.017	0.016	0.011	0.004

*a in kilometer, angles in radians

Examination of the sensitivity of the errors to component error sources reveals high sensitivity to increases in gyro drift and torquing errors (pointing error). A drift rate of 0.5 degree per hour produces almost 10 times the error due to control in Table 3-5, based on a 4-hour maneuver sequence prior to burn. Drift rates on the order of 0.1 degree per hour or less are compatible with the nominal pointing tolerance.

From this analysis, there appears to be no reason to place more severe requirements on the maneuver control for insertion than the accuracies selected for midcourse maneuvers.

The possibility of using accelerometers for cross-axis control was investigated. No significant advantage accrues for the 1971 mission. Some advantage may appear for later missions when physical constant and Mars ephemeris uncertainties have been significantly reduced and the control uncertainties become more important relative to the navigation uncertainties.

3.1.6 Orbit-Phase Orbit Determination and Guidance

3.1.6.1 Orbit Determination

Previous studies indicated that the DSN, utilizing doppler data only, is adequate for determining the parameters of the Voyager orbit about Mars, if a solution delay time of up to 1 week can be tolerated. The principal objective of the study reported in this section was to determine the delay time by establishing the rate of convergence in the solution of the initially indeterminate parameter, the longitude of the node in the plane normal

to the line of sight. The study results show that the solution for longitude of the node on an 18-hour orbit converges steadily after 1 day of tracking. The estimate of the 1-σ error is 0.15 degrees after 2 days in orbit and 0.03 degree after 3 days in orbit, given range-rate errors of 0.01 meter per second, 1 σ. When range rate is augmented by onboard measurements of local vertical to Mars, (accurate to 0.1 degree, 1σ), the 1-σ error in the node is reduced to 0.02 degree in one orbital period. After 4 days in orbit, the contribution of the onboard measurements to solution accuracy becomes insignificant.

Both differential correction and deterministic methods of solution were applied in the analysis. While a sophisticated differential correction process is required to fully extract the information contained in a redundant set of data, the deterministic methods are valuable for producing initial parameter estimates.

3.1.6.2 Differential Correction, DSN Only

The several orbit-determination programs applied in the analysis of the midcourse and approach phases of mission are written in single precision and solve for vehicle state variables in cartesian coordinates. Two kinds of problems were encountered in the attempt to use these programs for analysis in the orbital phase. In the Monte Carlo mode, initial convergence generally could not be achieved. In the analysis mode, which assumes convergence, the error covariance matrices become ill-conditioned. It was thought that the precision of computations and the choice of coordinate system were the causes of the problems. Therefore, a double-precision simulation of Kalman differential correction of the Keplerian orbital

elements was developed as a tool for analysis. An advanced version of the program, which includes the physical constants and Mars-Earth relative velocity in the parameter set, is still under development.

3.1.6.3 Initial Solution, DSN Only--The results presented in this section are for the nominal orbit shown in Figure 3-18. The orbit has an eccentricity of 0.635 and is inclined at 78 degrees to the plane normal to the Mars equatorial plane. Figure 3-19 shows the curve of velocity normal to the plane of the sky. No significant variation in orbit-determination capability was noted for plane orientation variations of $\pm$ 20 degrees about the nominal and for period variations from 13 to 20 hours.

The double-precision program was applied in the following sequences of iterations:

1. A series of iterations at low data rate (one observation per hour or a fewer number of observations in selected regions of the orbit), solving for five orbital elements only.
2) A series of iterations at higher data rates, solving for the five orbital elements in a rotating coordinate system that keeps the reference plane coincident with the plane of the sky. In the advanced version of the program, the physical constants and the Mars-Earth relative velocity will be included in the solution on these iterations. The rotating coordinate system minimizes the effect of the ambiguity in the longitude of the node.
3) An iteration at low data rate solving for all parameters but confining the data points to regions in which the contribution of

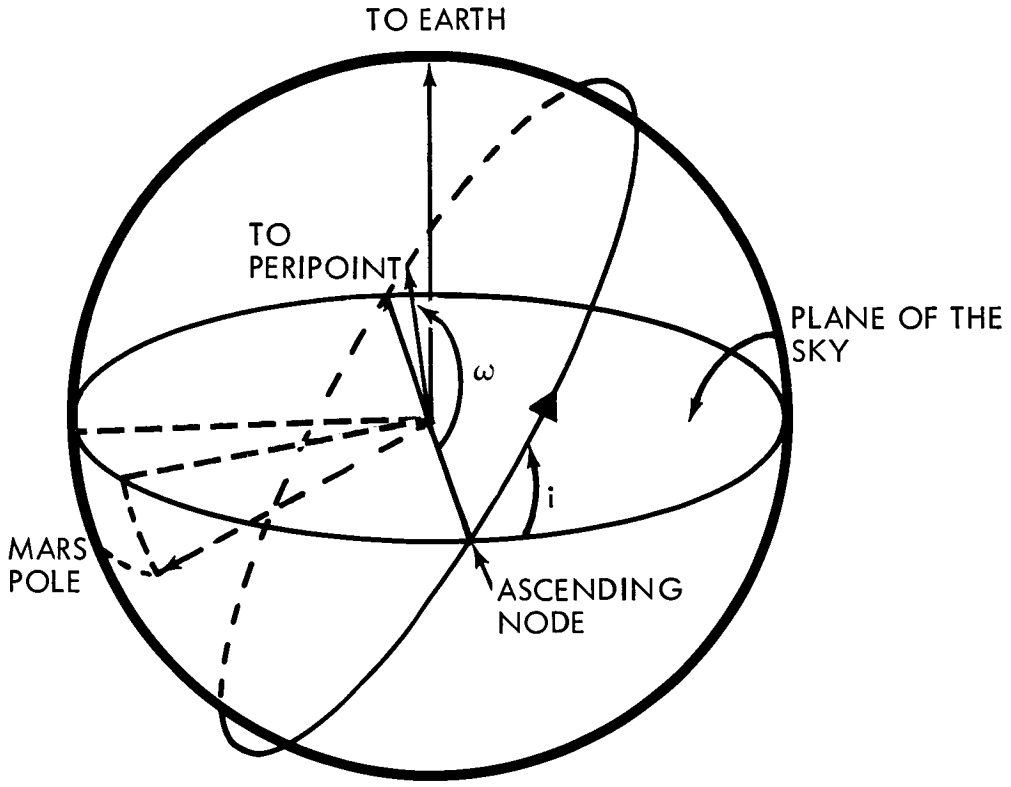

PARAMETER	MARS EQUATORIAL	PLANE OF THE SKY
INCLINATION, i	39.98°	77.74°
ASCENDING NODE, Ω	17.24°	164.6°
ARGUMENT OF PERIPOINT, ω	313.5°	155.5°
SEMIMAJOR AXIS (a)	16596.3 km	
ECCENTRICITY (e)	0.6349	
PERIOD	18.02 hours	

Figure 3-18: Nominal Orbit

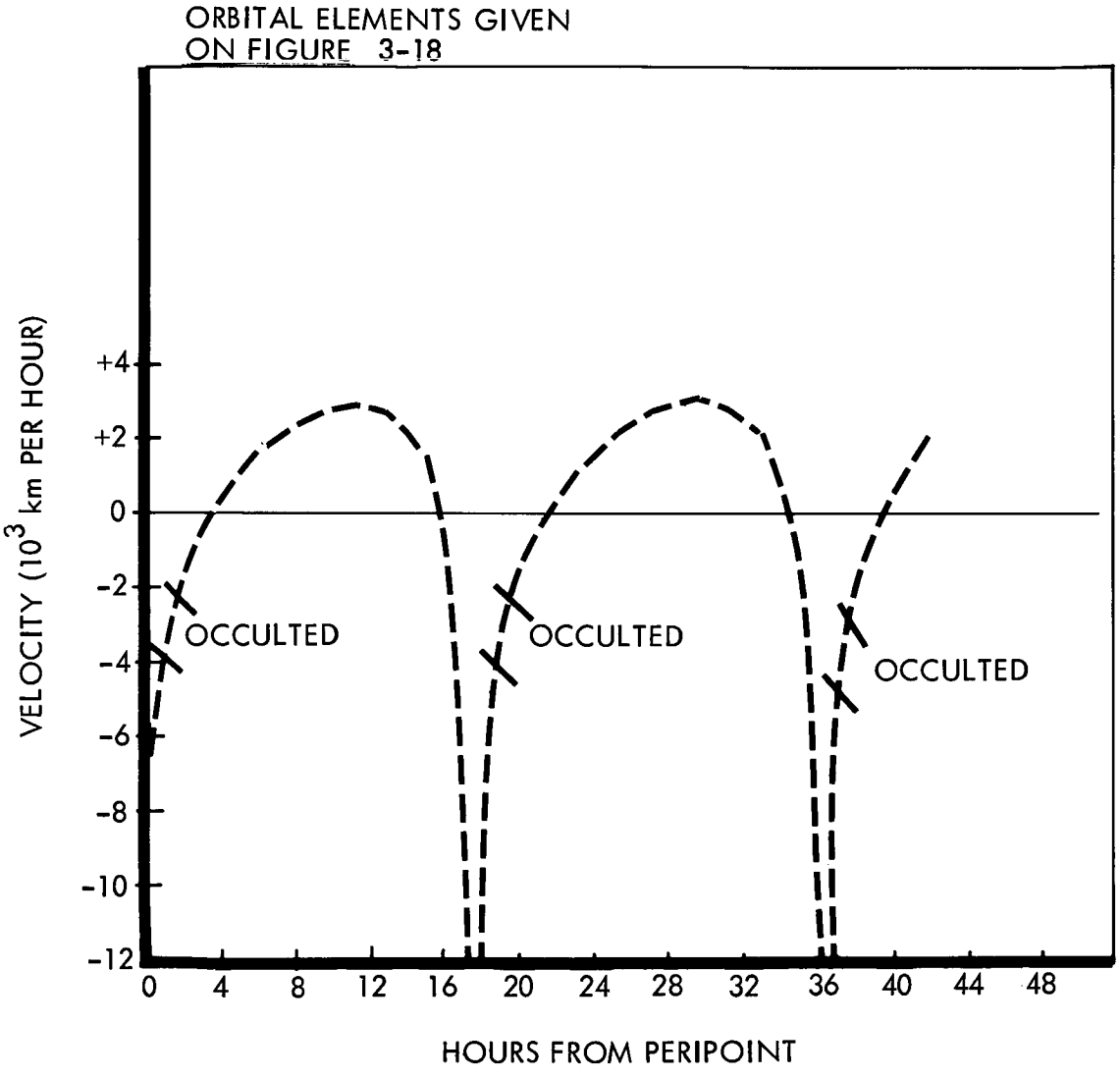

Figure 3-19: Orbital Velocity Normal to the Plane of the Sky ($\dot{z}$)

longitude of node error to the range-rate residuals is high relative to the residuals due to the uncertainty in the other parameters.

The most important conclusion drawn from the application of the above procedure was that the principal problem remaining is development of a method that fully exploits the inherent precision of the doppler data. Reasonably good solutions were obtained, but there is evidence that better results can be achieved. On the initial iterations, it was necessary to estimate the covariance matrix of parameter errors after each iteration by testing the residuals over the first orbital period in a trial and error process. This, or something equivalent to it, is necessary because the covariance matrix as well as the solution generated by the Kalman filter is biased by the nonlinearities of the problem. This is most in evidence initially when the error in the parameter estimate is greater. A better procedure for starting and maintaining convergence to an unbiased estimate is under investigation. It consists essentially of the following steps:

1) Generation of the first estimate for five orbital elements by application of the classical method of determining orbits of binary stars (discussed in Section 3.1.6.8).
2) Generation of an initial error covariance matrix in the five elements by applying the classical least-squares method on reduced parameter sets, using data at selected regions of the orbit, and starting with the estimate generated in the first step.
3) Iteration with the Kalman estimation procedure, solving for physical constants and five orbital elements, possibly with introduction of second-order terms in the region near periapsis where the sensitivity

of range rate to error in the parameters is many times greater than at other points on the orbit. The sensitivities of range rate to deviations in semimajor axis and in inclination are shown in Figures 3-20 and 3-21. The extreme nonlinearity near periapsis occurs in the sensitivity of range rate to each of the orbital elements. Data in this region could be more effectively utilized if second-order effects are considered.

3.1.6.4 Solution for Five Orbital Elements

Table 3-6 shows the solution obtained on a sample run and is typical of the results on other runs. The first iteration shown was obtained after adjustment by trial and error in the initial parameter error covariance matrix. Note that a reduction of range-rate error from 0.01 to 0.001 meter per second had a negligible effect on the solution errors of the first iteration. Likewise, no effect at either error level was produced by using different error samples on this iteration. This shows conclusively that the process was controlled by the filter coefficients rather than by the range-rate error. The second iteration shown was obtained after again adjusting the covariance matrix by trial and error, choosing the one of several which produced the smallest rms residual over one orbital period. The solution error on this iteration is about five times lower for range-rate error of 0.001 than for 0.01 meter per second. Variations in the range-rate error sequences did not significantly affect the solution error levels. The error estimates are conservative in that the data rate used was only four observations per hour, whereas 60 per hour are available. It is concluded that in a perfect model the 1-σ errors after two

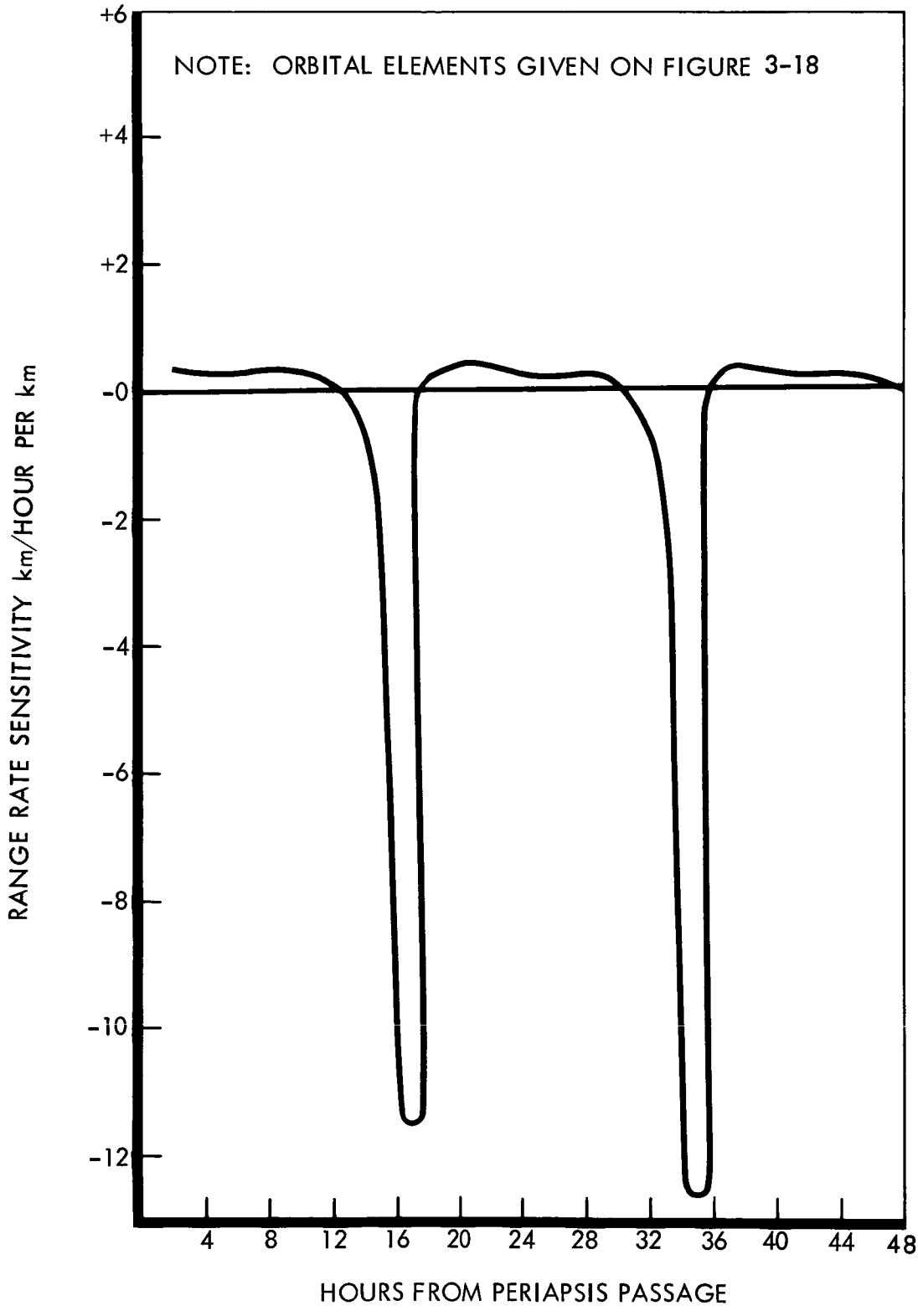

Figure 3-20: Sensitivity of Range Rate to Semimajor Axis (a)

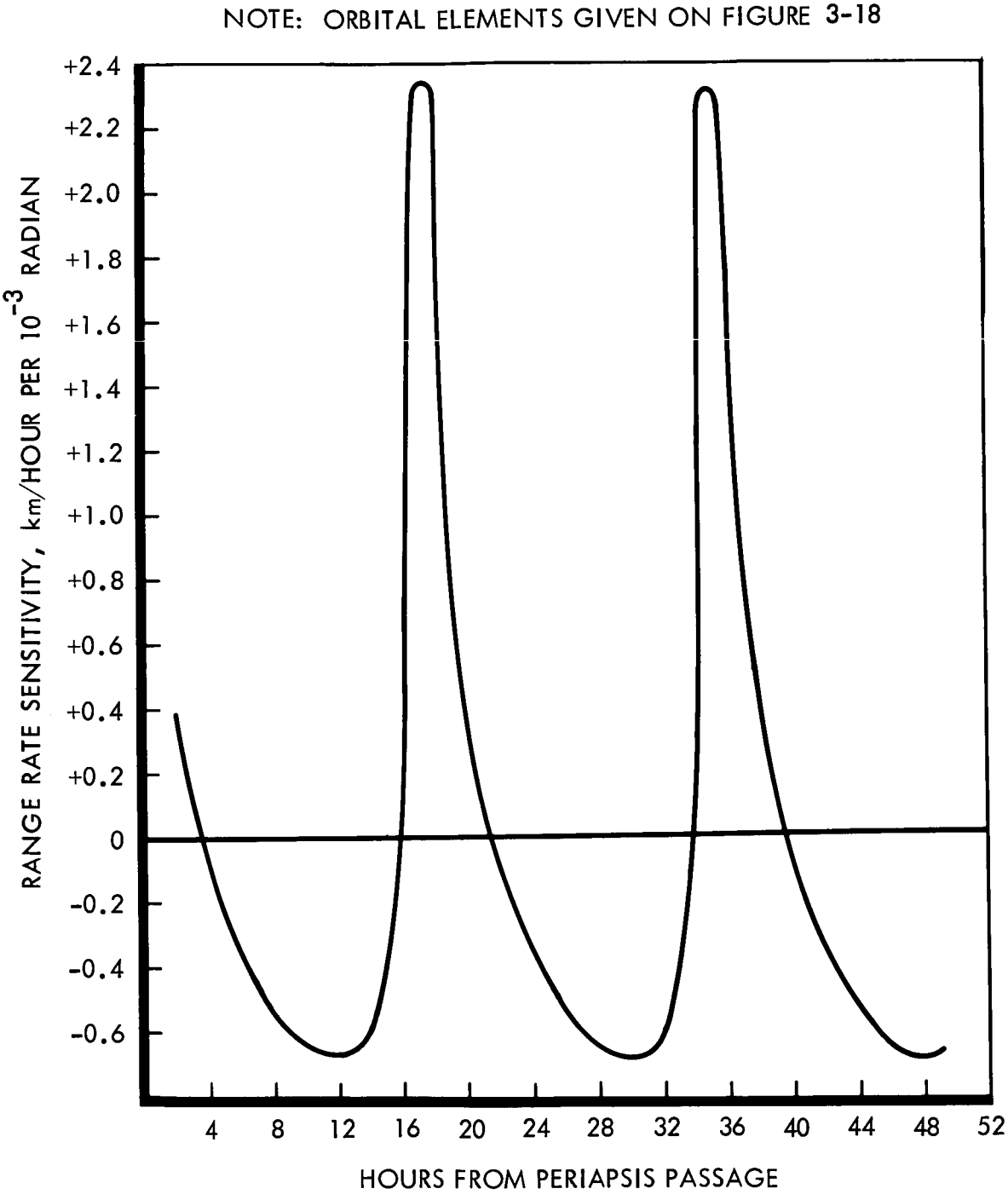

Figure 3-21: Sensitivity of Range Rate to Inclination to the Plane of the Sky (i)

Table 3-6: A Sample Solution Using DSN Doppler Data in a Modified Kalman Filter

		TIME (hrs)	Δa (KM)	Δe	Δt_p (hrs)	$\Delta \omega$ (RADIANS)	Δi (RADIANS)	COMMENTS
$\delta R^{\bullet} = 0.01$ METER/SECOND	ITERATION 1	0	205	-.015	-.005	-.02	-.02	• REF PLANE FIXED AND $\Delta\Omega$ FIXED AT 0.035 RADIAN. • DATA RATE: 1 OBS/ HOUR
		4	27	-.003	.0043	.004	-.024	
		8	-56	.001	-.0014	-.002	-.0136	
		12	-0.8	$.2 \cdot 10^{-3}$	-.0015	$.2.10^{-3}$	.0013	
		18	-0.33	$-.2 \cdot 10^{-4}$	$.2 \cdot 10^{-4}$	$-.1.10^{-3}$	-.0005	
		30	-0.33	$-.1 \cdot 10^{-5}$	$.2 \cdot 10^{-4}$	$.6 \cdot 10^{-4}$	-.0003	
	ITERATION 2	0	-0.33	$-.1 \cdot 10^{-5}$	$.2 \cdot 10^{-4}$	$.6.10^{-4}$	$-.0003_4$	• ROTATING REFERENCE SYSTEM TO MINIMIZE EFFECT OF $\Delta\Omega$ • DATA RATE: 4 OBS/ HOUR
		4	-0.01	$-.1 \cdot 10^{-4}$	$.8 \cdot 10^{-5}$	$-.8.10^{-5}$	$.7.10^{-4}$	
		8	0.02	$-.1 \cdot 10^{-4}$	$.9 \cdot 10^{-5}$	$.3.10^{-4}$	$.9.10^{-4}$	
		12	-0.06	$.7 \cdot 10^{-6}$	$.1 \cdot 10^{-4}$	$-.7.10^{-5}$	$-.2.10^{-4}$	
		18	0.003	$.2 \cdot 10^{-6}$	$.4 \cdot 10^{-4}$	$-.2.10^{-5}$	$.1.10^{-4}$	
		30	$-0.8 \cdot 10^{-3}$	$-.2 \cdot 10^{-6}$	$.2 \cdot 10^{-5}$	-10^{-6}	$-.6.10^{-5}$	
$\delta R^{\bullet} = 0.001$ METER/SECOND	ITERATION 1	0	205	-.015	-.005	-.02	-.02	• REF PLANE FIXED AND $\Delta\Omega$ FIXED AT 0.035 RADIAN • DATA RATE: 1 OBS/ HOUR
		4	22	-.003	.0043	.0036	-.024	
		8	-50	$.8 \cdot 10^{-3}$	-.0014	-.002	-.0134	
		12	-0.8	$.1 \cdot 10^{-3}$	-.0013	$.2.10^{-3}$	.0009	
		18	-0.3	$-.2 \cdot 10^{-4}$	$.2 \cdot 10^{-4}$	$-.1.10^{-3}$	-.0005	
		30	-0.3	$-.3 \cdot 10^{-5}$	$.2 \cdot 10^{-4}$	$.6.10^{-4}$	-.0003	
	ITERATION 2	0	-0.3	$-.3 \cdot 10^{-5}$	$.2 \cdot 10^{-4}$	$.6.10^{-4}$	$-.0003_4$	• ROTATING REFERENCE SYSTEM TO MINIMIZE EFFECT OF $\Delta\Omega$ • DATA RATE: 4 OBS/ HOUR
		4	-0.05	$-.1 \cdot 10^{-4}$	$.2 \cdot 10^{-4}$	$.2.10^{-5}$	$-.8.10^{-4}$	
		8	+0.05	$-.6 \cdot 10^{-5}$	$.2 \cdot 10^{-4}$	$.3.10^{-5}$	$.4.10^{-4}$	
		12	0.06	$.9 \cdot 10^{-6}$	$.1 \cdot 10^{-4}$	$.2.10^{-6}$	$.3.10^{-4}$	
		18	$-0.1 \cdot 10^{-3}$	$.7 \cdot 10^{-7}$	$-.8 \cdot 10^{-6}$	$.2.10^{-6}$	$-.1.10^{-5}$	
		30	$-0.2 \cdot 10^{-3}$	$.13 \cdot 10^{-7}$		$.2.10^{-6}$	$-.7.10^{-6}$	

orbits of tracking are of the following order: 1) Semimajor axis $\pm 10^{-3}$ km; 2) Eccentricity $\pm 10^{-6}$; 3) Time at Periapsis $\pm 10^{-5}$ hour; 4) Argument of Periapsis $\pm 10^{-6}$ radian; and 5) Inclination $\pm 10^{-6}$ radian.

3.1.6.5 The Solution for Physical Constants and Mars-Earth Relative Velocity Solution for model parameters in the double-precision program has not been satisfactorily tested. The problem was analyzed with a single-precision program using a Kalman estimation formulation that solves for six vehicle state variables and four physical constants. The physical constants are the gravitational constant of Mars, doppler scale factor (AU), bias in the doppler measurement caused by Mars ephemeris uncertainties, and the primary oblateness term of the gravitational potential. The program did not operate satisfactorily on range-rate data only, so the analysis results are based on runs using both range rate and measurements of local vertical. Because of the precision of the range-rate measurement, it is probable that the measurements of local vertical contribute insignificantly to the accuracy of the determination of all of the physical constants except perhaps the oblateness term. Range rate is sensitive to the oblateness term through the rotation of the line of apsides and through the variation of the orbit inclination to the plane of the sky. For the nominal orbit, the advance of the line of apsides is 0.5 degree per day, while the regression of the line of nodes in the Mars equator is estimated at 0.37 degree per day. The component of the nodal regression that appears in the inclination to the plane of the sky is about 0.2 degree per day. The doppler measurement, therefore, is sensitive to 80 percent of the effect of oblateness. The estimated errors in position at periapsis and in the physical constants after one orbit of tracking

are summarized in Table 3-7. A substantial improvement was realized in each of the physical constants except the primary Mars gravitational constant. Note that the improvement in doppler scale factor and bias was the same for the 10-to-1 range of range-rate error from 0.001 to 0.01 meter per second. This indicates that the results were limited by the method of analysis rather than the range-rate measurement precision, supporting the earlier conclusion that further development in the method of analysis is required.

3.1.6.6 Solution for Longitude of the Node

The point at which solution for longitude of the node is introduced depends on the magnitude of the range-rate residuals produced by the errors in all of the other parameters versus that produced by the error in longitude of the node. The sensitivity of range rate to deviations in longitude of the node for the nominal orbit is plotted in Figure 3-22. Figure 3-23 shows that range rate is sufficiently sensitive to an error in longitude of the node of 0.1 degree to produce a residual in certain regions of the orbit that is well above that of the RSS of the residuals in all other parameters, given the order of error achieved in the runs shown in Table 3-6. It was found that solution for longitude of the node converged with initial errors in the other parameters an order of magnitude greater than this. Estimated errors versus time in orbit are plotted in Figure 3-24. The uncertainty is reduced to within 0.15 degree in 2 days and 0.03 degree in 3 days. This represents a conservative estimate of performance in that it is believed to be feasible to develop a method of analysis which will produce better initial conditions in the other parameters. On the other hand, the analysis neglects the error in

Table 3-7: POSITION AND MODEL UNCERTAINTIES AFTER ONE ORBIT OF TRACKING

Range Rate and Local Vertical Measurements Processed in Kalman Filter

CONFIGURATION $\sigma_{\dot{R}}$ M/SEC	CONFIGURATION σ_{θ} DEGREES	1 σ POSITION ERRORS AT PERIAPSIS IN LOS*	RADIAL	NORMAL	MARS GRAVITATIONAL CONSTANT	DOPPLER SCALE FACTOR	DOPPLER BIAS	MARS OBLATENESS
0.01	0.3	0.08	0.2	3.0	99.6	0.6	8	1958
0.01	0.03	0.04	0.2	0.5	95	0.6	8	471
0.0025	0.03	0.01	0.2	0.5	92	0.6	8	477
Assumed Initial Model Uncertainties in Parts Per Million					100	1.0	100.0	2000

*LOS = Line of Sight

NOTE: ORBITAL ELEMENTS GIVEN ON FIGURE 3-18

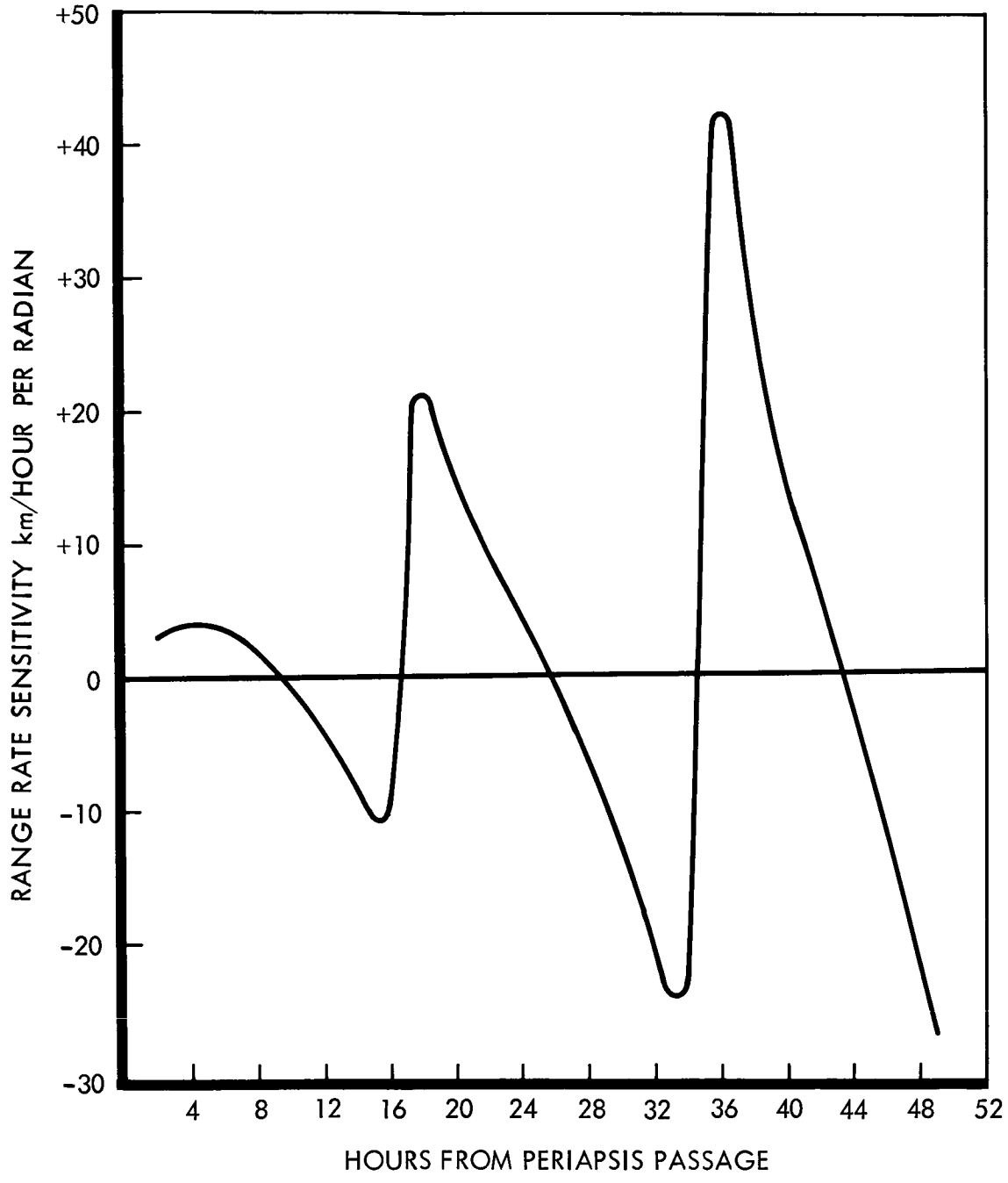

Figure 3-22: Sensitivity of Range Rate to Longitude of Nodes in the Plane of the Sky

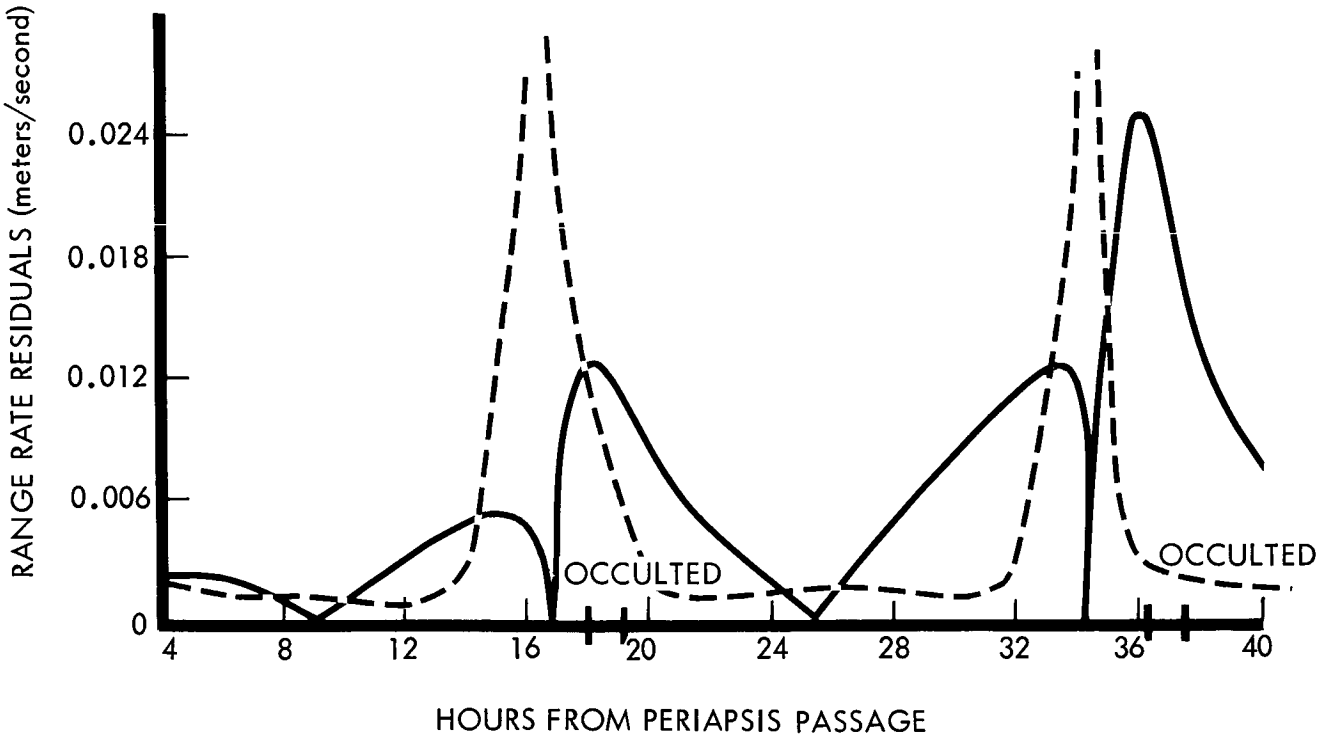

— — RSS RESIDUAL FOR: SEMIMAJOR AXIS ERROR = 0.01 km
ECCENTRICITY ERROR = 10^{-6}
ARGUMENT OF PERIAPSIS ERROR = 10^{-6} rad
INCLINATION ERROR = 10^{-6} rad
TIME ERROR = 10^{-6} hours

——RESIDUAL FOR LONGITUDE OF NODES DEGREE ERROR OF 0.1°

Figure 3-23: Range Rate Residuals Versus Time and Parameter-Error Levels

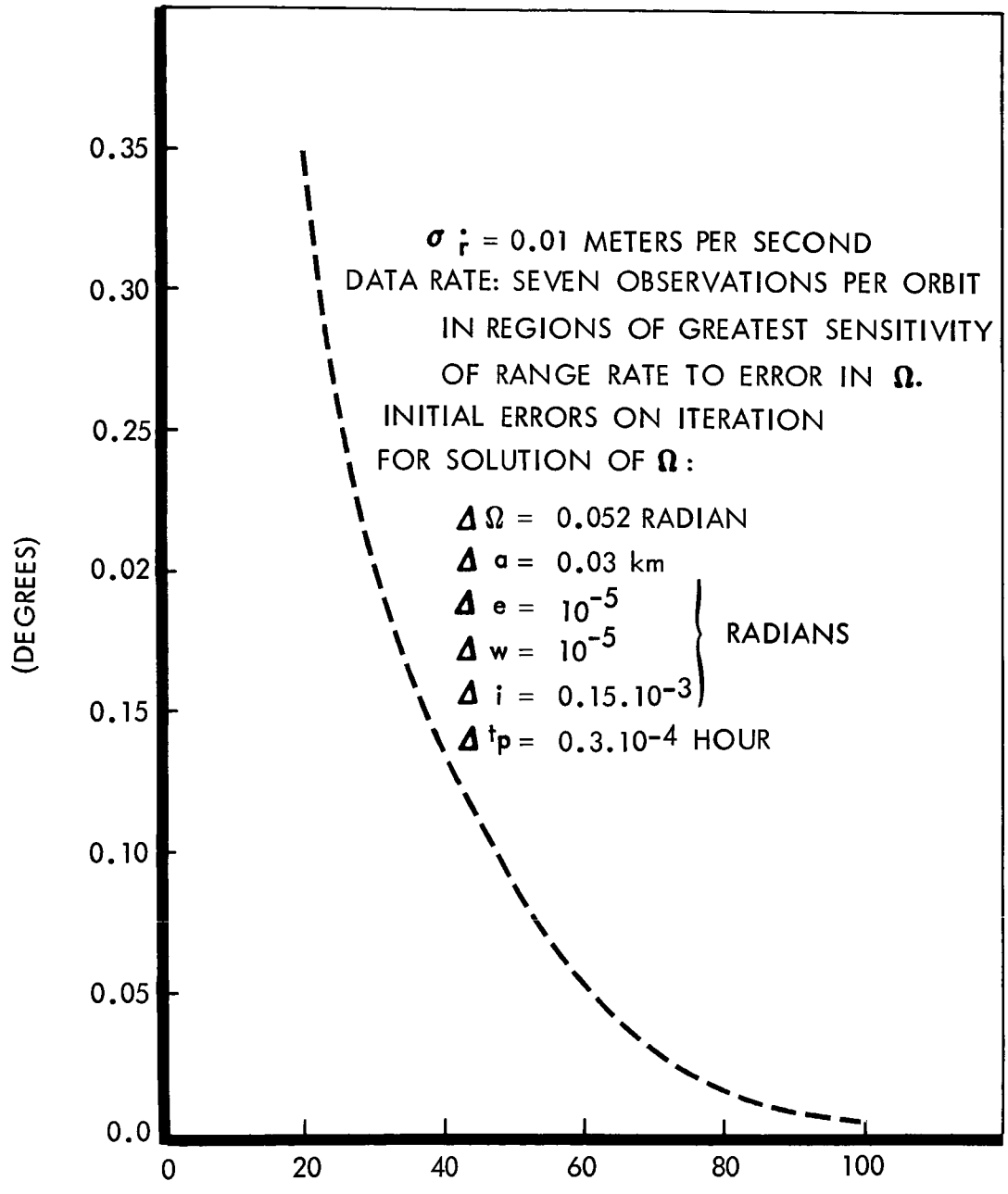

Figure 3-24: Error in Longitude of Nodes in the Plane of the Sky Ω Using DSN Doppler Data Only

Mars velocity relative to Earth, which must be solved for simultaneously with longitude of the node, and may result in some degradation in accuracy. Another factor that makes the estimate of performance conservative is that the analysis was for a spherical Mars. For the nominal orbit geometry, the effective rate of rotation of the Mars-Earth line relative to the node is increased by about 80 percent by the regression of the node due to Mars oblateness. The node is regressing at least 0.37 degree per day relative to the Mars equator, while the Mars-Earth line is progressing at the rate of 0.45 degree per day, so the relative rate of rotation is 0.82 degree per day. This increases the sensitivity of range rate to errors in the node substantially over that assumed in the analysis.

3.1.6.7 DSN Augmented by Onboard Data

The initial solution for the inplane parameters and inclination to the plane of the sky is not improved when the DSN range-rate data is augmented by measurements of the direction of local vertical with a 1- σ error of 0.1 degree. A solution for longitude of the node good to 0.02 degree is obtained in one orbit. After 4 days of tracking further improvement in the DSN solution by the local vertical data is negligible.

3.1.6.8 Deterministic Orbit Determination

As indicated in the previous section, the differential correction method of orbit determination is simplified if a good initial estimate is available. The principal technique studied for this consists of determination of five of the six orbital elements from one orbit of doppler data by application of the classical method of determining orbits of binary stars.

The sixth element, the longitude of the ascending node relative to the plane of the sky, is determined from two or more orbits of data separated in time. As the line of sight rotates, the inclination and longitude of the node vary in the rotating cartesian system of which the line of sight is an axis. These quantities are utilized as measurements in an estimation procedure to determine the initial node angle and the angles of rotation. Table 3-8 lists the 1σ parameter errors found with 0.001 meter per second 1σ error in range rate with a perfect model and with an uncertainty in the Mars primary gravitational constant and with a doppler bias.

Table 3-8: ORBIT DETERMINATION ERRORS
(CLASSICAL BINARY STAR METHOD)

Mars Gravitational Constant Bias	Doppler Bias	Orbital Element 1σ Errors				
		a, km	e	w	i	t_p
0	0	0.001	$1.5.10^{-5}$	0.005^o	0.001^o	0.013 min
20 Parts Per Million	3 m/sec	0.1	0.002	0.1^o	0.1^o	0.3 min

The results obtained show that this method is very useful for providing initial estimates and for monitoring the process by providing mean values of the orbital elements. These solution errors are well below the uncertainties in the estimate of orbit parameters based on midcourse and injection-phase statistics. The longitude of the node was estimated with a 1σ error of 0.3 degree in two orbits and 0.1 degree in four orbits. This also will provide a useful check on the differential correction process.

3.1.6.9 Summary of Conclusions

The principal conclusions of the orbit determination study are:

1) The dominant error in orbit determination is in the position of the node in the plane normal to the Earth-Mars line. Using doppler data only, the node is determined with a 1σ error of 0.15 degree in 2 days and 0.03 degree in 3 days. The error is reduced to 0.02 degree in 1 orbit when the doppler data is augmented by onboard measurements of local vertical good to 0.1 degree, 1σ. After 4 days of tracking, the contribution of onboard measurements becomes insignificant. On the nominal orbit, the position error due to 0.03 degree error in the node is 3 kilometers near periapsis and 15 near apoapsis.

2) Further development is required to devise an orbit-determination method that fully exploits the inherent precision of the doppler measurement.

3) Next to uncertainty in position of the node, the dominant error in initial determination of the orbit is the cumulative effect of parameters not included in the initial model. These will be of two classes: those not anticipated and those with individual effects below the detection level of the system within a few days of observation.

3.1.7 Orbit Trim

Because of uncertainties in Mars encounter conditions and orbit insertion control, the orbit attained will most probably not satisfy the mission requirements and constraints. In fact, the orbit insertion analysis indicates that errors in the semimajor axis of the orbit can be as large

as 1000 kilometers, 1 - σ, under nominal conditions. It is necessary, therefore, to provide capability to perform orbit trim maneuvers.

The most likely sequence of maneuvers will include two velocity corrections, one to correct periapsis altitude and one to correct the semimajor axis.

The ΔV requirement for orbit trim and the accuracy to which the trim can be accomplished were estimated based on the nominal results of the insertion and orbit determination analyses, and the nominal 1 percent accuracy for each maneuver. The semimajor axis adjustment required 75 meters per second (3σ) ΔV and the periapsis adjustment (performed at apoapsis) requires 15 meters per second (3Δ) ΔV. Upon completion of both maneuvers, the periapsis radius was within 5 kilometers, 3σ, of the desired radius, and the semimajor axis was within 30 kilometers, 3σ, of the desired value.

Control of other parameters is not warranted with the possible exception of the inclination. However, it is not anticipated that the 2 degree, 1σ, inclination error that is obtained will be significant.

3.2 Voyager Flight Spacecraft Layouts and Configurations

Summary--Numerous Flight Spacecraft configurations were investigated to perform the 1971 through 1977 missions. Three of these configurations are discussed in this section. They are identified by Boeing model numbers as follows:

1) Model 945-6026--Preferred configuration;
2) Model 945-6016--Similar to preferred configuration except for package mounting and antenna size;
3) Model 945-6015--Spacecraft forward of capsule.

Configuration Model 945-6026 was selected as the preferred design because it was found to excel in the features discussed below. This configuration consists of three basic elements: 1) a cylindrical structure, around which the electronic equipment is mounted; 2) truss module which attaches to the launch vehicle; 3) a central module within the cylindrical support and truss, consisting of all propulsion and reaction control subsystem components. This arrangement provides excellent access to the electronic assemblies and propulsion subsystem. This results in ease of installation, maintenance, and testing, and improves the reliability of the spacecraft. This model incorporates a large (8' 2" x 12' 2") paraboloidal antenna that provides for data rates consistent with real-time transmission. Modular construction of subsystems allows for complete checkout prior to installation in the spacecraft. For example, the propulsion and reaction control subsystems are assembled in

a single subassembly, which can be fabricated, tested for type approval and flight acceptance, and installed as an entity. The configuration can accommodate various electronic assembly sizes, allowing versatility in their arrangement to permit optimum grouping of electronic functions for simple interfaces, and for testing and installation. Further, it allows for thermal control and center-of-gravity control. The orientation of the orbit-insertion engine minimizes potential temperature and contamination effects on the solar panels and other spacecraft elements. The configuration allows clear views for scientific data gathering, including near-complete coverage of the planet during orbit while remaining on celestial reference. The versatility of the configuration will accommodate mission changes or changes to the subsystems, such as increased solar-panel area. It is also easily adaptable to the 1969 test program for Atlas-Centaur. The configuration provides the versatility to accommodate the equipment anticipated to meet the 1971 through 1977 mission requirements while complying with the mission specification.

Two other configurations studied include Model 945-6016 and Model 945-6015. Model 945-6016 is similar to the Mariner IV spacecraft in construction and electronic assembly mounting. Model 945-6015 is the result of precontract studies and does not meet the mission-specification spacecraft envelope, but does meet the specified nose fairing envelope. This configuration offers some advantages in capsule size and solar-panel and boom stowage but was not selected as the preferred design due to excessive adapter weight and noncompliance with the specification spacecraft envelope.

3.2.1 Model 945-6026

This configuration is shown in Figure 3-25. Three basic modules make up the spacecraft: equipment-support module, the propulsion/reaction control module, and the lower support truss module.

The equipment-support module is a cylindrical stiffened shell located directly below the capsule and attached to the lower support truss structure. This shell is approximately 5 feet in diameter and has the equipment packages mounted on its exterior surface. Each package is handled as an entity at a deliverable subsystem level and can be located around the periphery as required by thermal balance and center-of-gravity requirements. Thermal-control louvers are installed outside of the exterior surface of each package as required. An insulating blanket supported by an aluminum retainer provides thermal insulation as well as meteoroid protection. This arrangement provides for maximum accessibility for installation, maintenance, repair, inspection, and testing. The cylindrical surface provides 42 square feet of area for mounting equipment packages, with approximately 20 percent reserve to accommodate alternate scientific payloads or changes to the mechanization of subsystems. The outer surface (57 square feet) provides a radiator area nearly twice that required to maintain a proper thermal balance.

Four longerons are provided within the equipment support module to provide a four-point support system for the capsule loads.

A propulsion/reaction control module is located in the center of the equipment-support module and lower support truss structure. This module

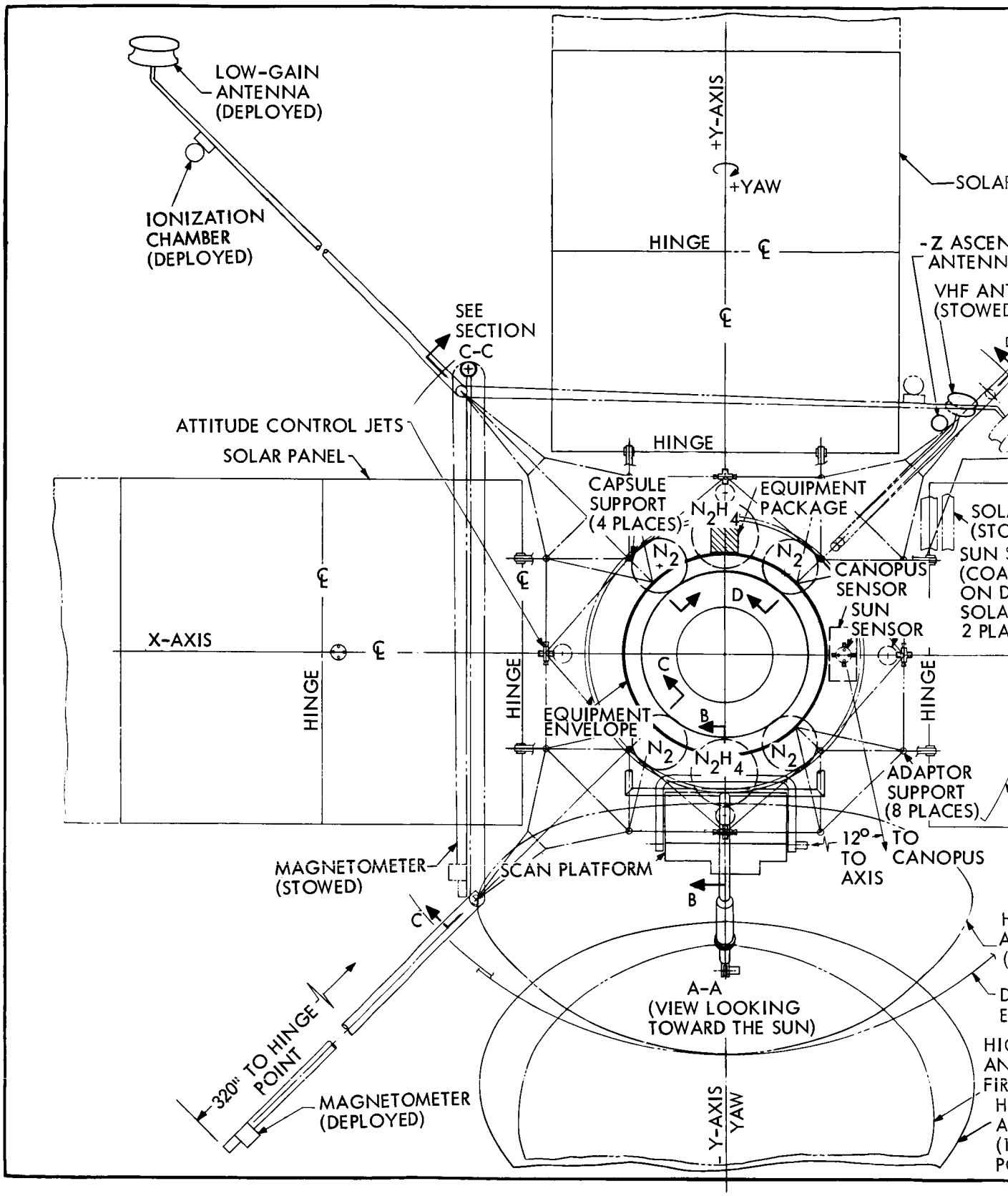
LOW-GAIN ANTENNA (DEPLOYED)
IONIZATION CHAMBER (DEPLOYED)
SEE SECTION C-C
ATTITUDE CONTROL JETS
SOLAR PANEL
+Y-AXIS
+YAW
HINGE
-Z ASCEN ANTENN
VHF AN (STOWED
HINGE
CAPSULE SUPPORT (4 PLACES)
N_2H_4
EQUIPMENT PACKAGE
N_2
N_2
CANOPUS SENSOR
SUN SENSOR
SOL (STO
SUN (COA ON D SOLA 2 PLA
X-AXIS
HINGE
HINGE
HINGE
D
C
B
EQUIPMENT ENVELOPE
N_2
N_2H_4
N_2
ADAPTOR SUPPORT (8 PLACES)
12° TO AXIS
TO CANOPUS
MAGNETOMETER (STOWED)
SCAN PLATFORM
B
C
A-A
(VIEW LOOKING TOWARD THE SUN)
320" TO HINGE POINT
MAGNETOMETER (DEPLOYED)
Y-AXIS YAW

710

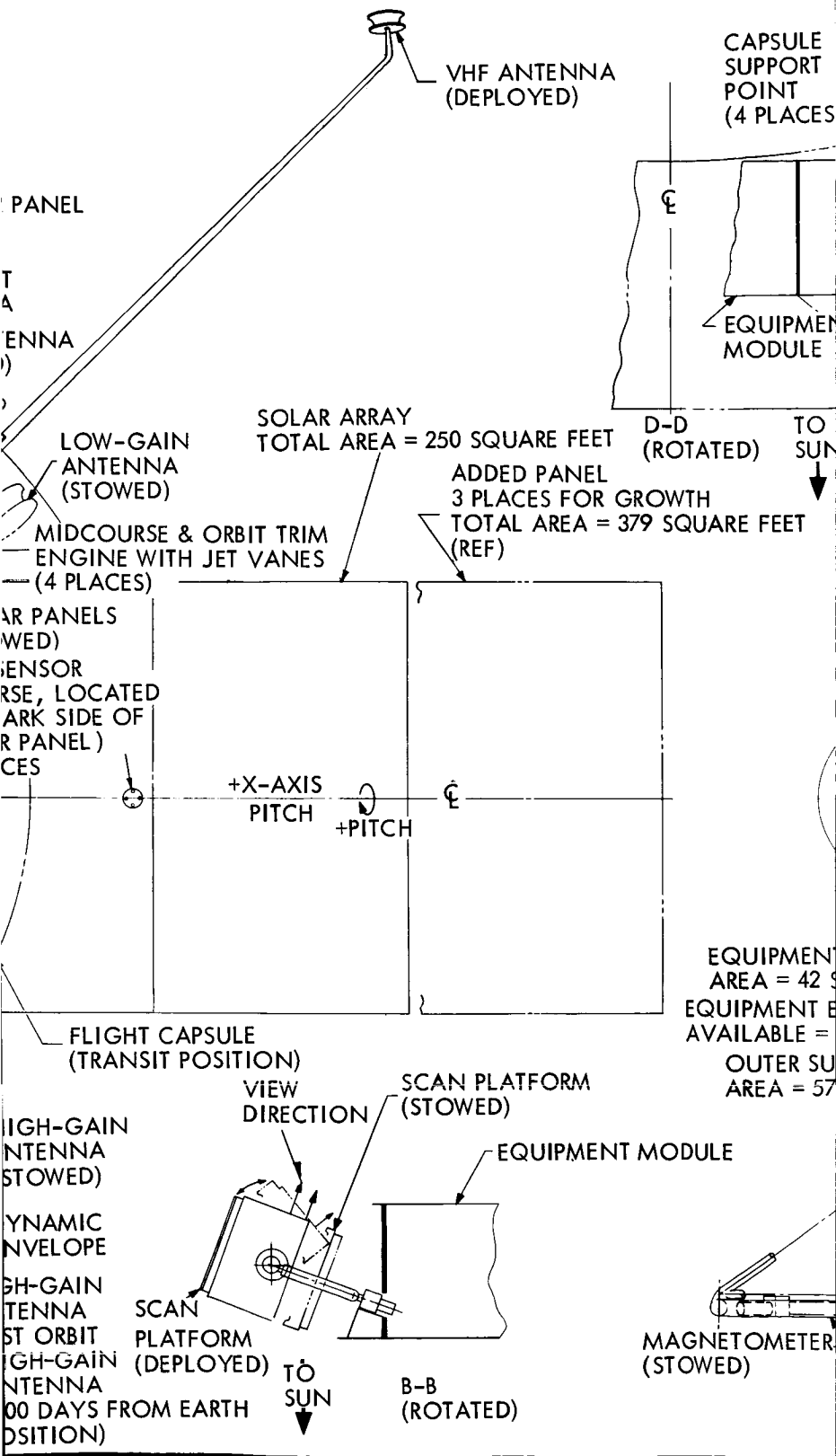
VHF ANTENNA
(DEPLOYED)
CAPSULE
SUPPORT
POINT
(4 PLACES
PANEL
ENNA
)
EQUIPMEN
MODULE
D-D
(ROTATED)
TO
SUN
LOW-GAIN
ANTENNA
(STOWED)
SOLAR ARRAY
TOTAL AREA = 250 SQUARE FEET
ADDED PANEL
3 PLACES FOR GROWTH
TOTAL AREA = 379 SQUARE FEET
(REF)
MIDCOURSE & ORBIT TRIM
ENGINE WITH JET VANES
(4 PLACES)
AR PANELS
WED)
ENSOR
RSE, LOCATED
ARK SIDE OF
R PANEL)
CES
+X-AXIS
PITCH
+PITCH
EQUIPMEN
AREA = 42
EQUIPMENT E
AVAILABLE =
OUTER SU
AREA = 57
FLIGHT CAPSULE
(TRANSIT POSITION)
VIEW
DIRECTION
SCAN PLATFORM
(STOWED)
IGH-GAIN
NTENNA
STOWED)
EQUIPMENT MODULE
YNAMIC
NVELOPE
GH-GAIN
TENNA
ST ORBIT
GH-GAIN
NTENNA
00 DAYS FROM EARTH
DSITION)
SCAN
PLATFORM
(DEPLOYED)
TO
SUN
B-B
(ROTATED)
MAGNETOMETER
(STOWED)

71 (2)

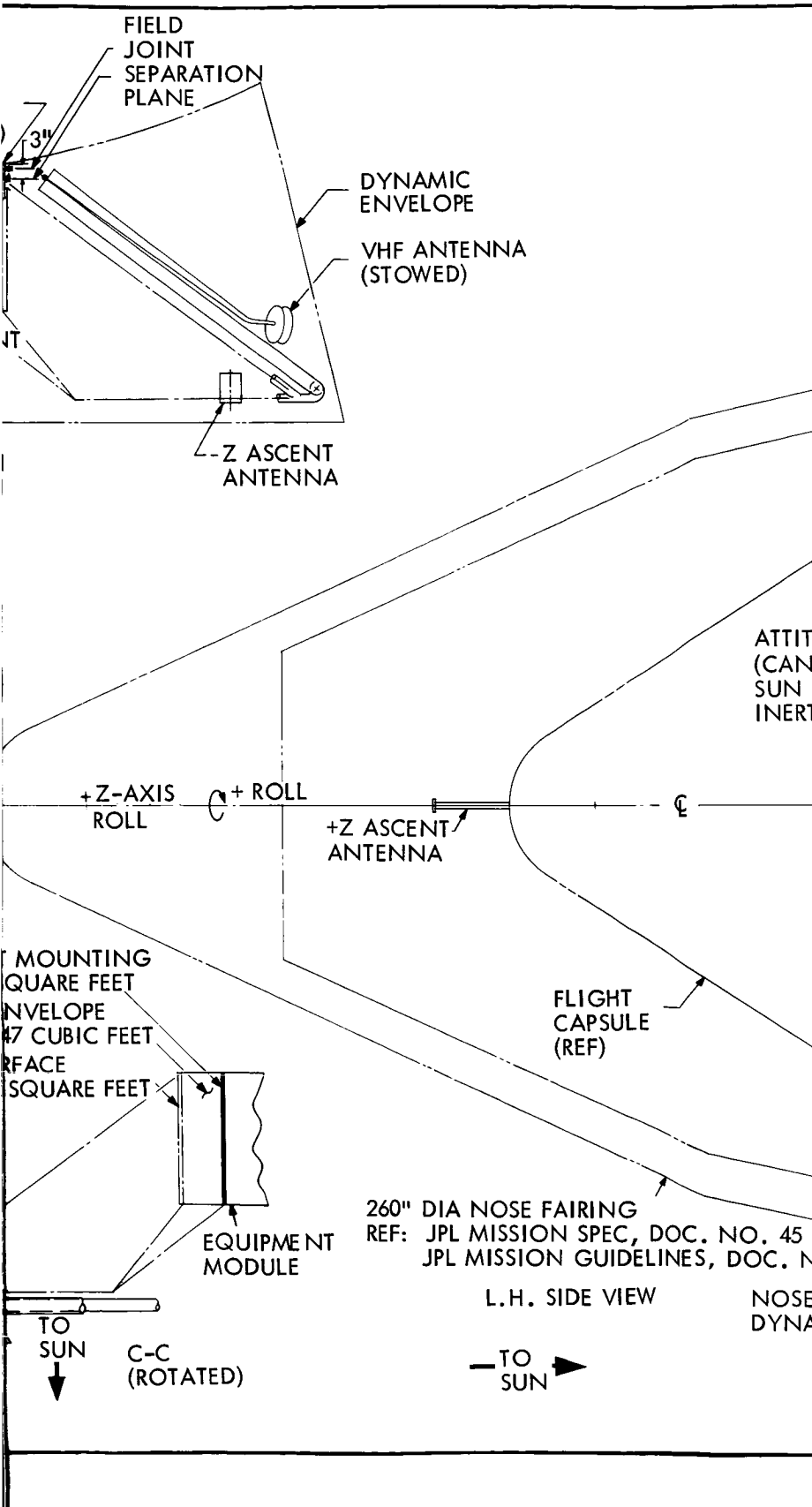
FIELD
JOINT
SEPARATION
PLANE
3"
DYNAMIC
ENVELOPE
VHF ANTENNA
(STOWED)
-Z ASCENT
ANTENNA
+Z-AXIS
ROLL
+ ROLL
+Z ASCENT
ANTENNA
FLIGHT
CAPSULE
(REF)
260" DIA NOSE FAIRING
REF: JPL MISSION SPEC, DOC. NO. 45
JPL MISSION GUIDELINES, DOC. N
L.H. SIDE VIEW
EQUIPMENT
MODULE
TO
SUN
C-C
(ROTATED)
TO
SUN

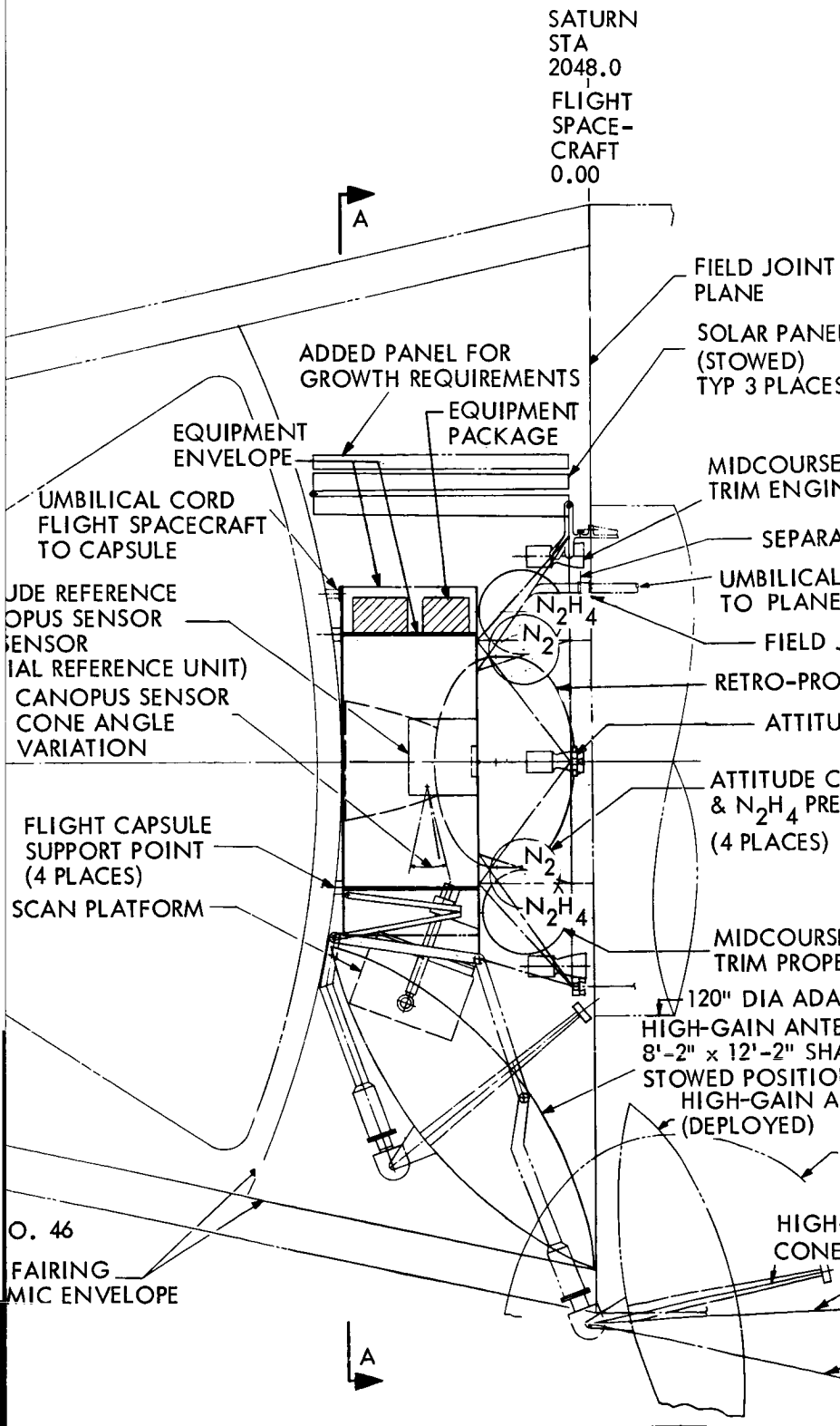

Figure 3-25

71 (4)

& ORBIT
IE, WITH JET VANES (4 PLACES)

TION PLANE

CORD – LAUNCH VEHICLE
TARY VEHICLE

OINT

PULSION ENGINE (SOLID)

DE CONTROL JETS (4 PLACES)

ONTROL GAS
SSURANT

& ORBIT
LLANT

TER
NNA
PED PARABOLIC
N
NTENNA

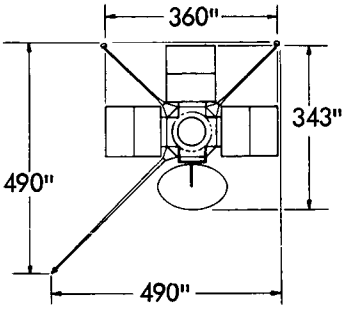

SPACECRAFT DEPLOYED
(VIEW LOOKING TOWARD SUN)

HIGH-GAIN ANTENNA
FIRST ORBIT POSITION

GAIN ANTENNA 100-DAY ACQUISITION
= 14°, CLOCK = 210°
HIGH-GAIN ANTENNA
240TH ORBIT
CONE = 18°, CLOCK = 265°
HIGH-GAIN ANTENNA
FIRST ORBIT
CONE = 43°, CLOCK = 283°

Voyager Flight Spacecraft

consists of a solid-propellant orbit-insertion engine with fluid injection for thrust-vector control, four 50-pound thrust monopropellant engines to perform midcourse and orbit trim maneuvers, and a cold-gas (N_2) reaction control system with a single level of thrust providing attitude control. Two monopropellant tanks and four cold-gas (N_2) tanks are located symmetrically about the X and Y axes to maintain center-of-gravity control. The monopropellant tank pressurant is stored in the same tank that provides the cold-gas (N_2) supply for the reaction control subsystem. The orbit-insertion engine is oriented with the nozzle in the direction of the +Z axis to ensure minimum thermal and contamination effects during engine operation. The midcourse engine and reaction control jets are oriented with their exhaust directed in a -Z direction and away from the spacecraft. This module can be completely assembled, bench-checked, leak-tested, or test fired as a complete unit prior to installation in the spacecraft.

The truss module supports the equipment-support module, propulsion module, solar panels, and low-gain antenna, VHF antenna, and magnetometer booms. This module provides the load-carrying capability between the planetary vehicle and the 120 inch diameter Centaur adapter. The truss-type structure provides maximum access for installation, maintenance, repair, inspection, and testing of the propulsion module.

Solar panels that provide 258 square feet of gross panel area (236 square feet net area) are mounted and stowed vertically on three sides of the spacecraft. Each panel consists of two segments (86 square feet)

and an actuator for deployment following Centaur separation. The solar panels are attached at the base of the lower support truss structure, allowing sufficient clearance between the panels and capsule to permit backface radiation of excess panel heat. With the addition of one segment to each panel, an increase of 129 square feet of area can be added with sufficient clearance of the dynamic envelope.

A single 8'2" by 12'2" paraboloidal high-gain antenna is installed along the Y axis. This antenna is provided with two-axis orientation capability and has a clear field of view of Earth during all portions of the mission for which it is intended to be used. The solar pressure effects of this antenna are balanced by the solar panel on the opposite side of the spacecraft. The dynamic clearance of this antenna with the nose-fairing envelope is a minimum.

The low-gain and VHF antennas are supported from a truss network off the base of the lower support truss structure. The VHF antenna is folded, stowed, and secured diagonally alongside one of the support truss members. The low-gain antenna is stowed in a horizontal position along side of and at the base of the solar panels. This antenna and boom are secured by the VHF-antenna support truss during the boost phase. When deployed, these antennas will be positioned between the solar panels. Two ascent antennas are provided for launch and early phases of the mission. One is located on the VHF basic truss support structure and the second antenna is mounted on the nose of the capsule.

The magnetometer is mounted on a 27-foot-long boom and is supported in a manner similar to the low-gain and VHF antennas. However, it is stowed in a horizontal position alongside of and at the base of the solar panels. This boom is secured by the low-gain antenna support truss during the boost phase.

The scan platform is located on the Y axis. It has a two-axis gimbal drive that, when deployed, has the capability to view the entire planet from practically any point in the orbit. A shadow graph of the scan platform's field of view is shown in Figure 3-26. Shaded areas indicate occulation by spacecraft elements.

The Canopus sensor is located on the +X axis. Its sighting direction is in a plane rotated 12 degrees counter clockwise from the -Y axis. This location for the Canopus sensor is chosen to provide the scan platform with the maximum possible views of the planet while the spacecraft remains locked on its celestial references. The resulting spacecraft orientation provides the antennas with proper views.

Redundant fine Sun sensors are located at the base of the equipment-support module and adjacent to the Canopus sensor and inertial-reference unit in the attitude-reference subsystem assembly. Grouping of these units allows them to be mounted on a single chassis thereby reducing alignment tolerances to a minimum. The coarse Sun sensor is mounted on the base of the spacecraft. A second set of coarse Sun sensors is mounted on the dark side of the solar panels on the X axis. These sensors are used during initial acquisition of the Sun.

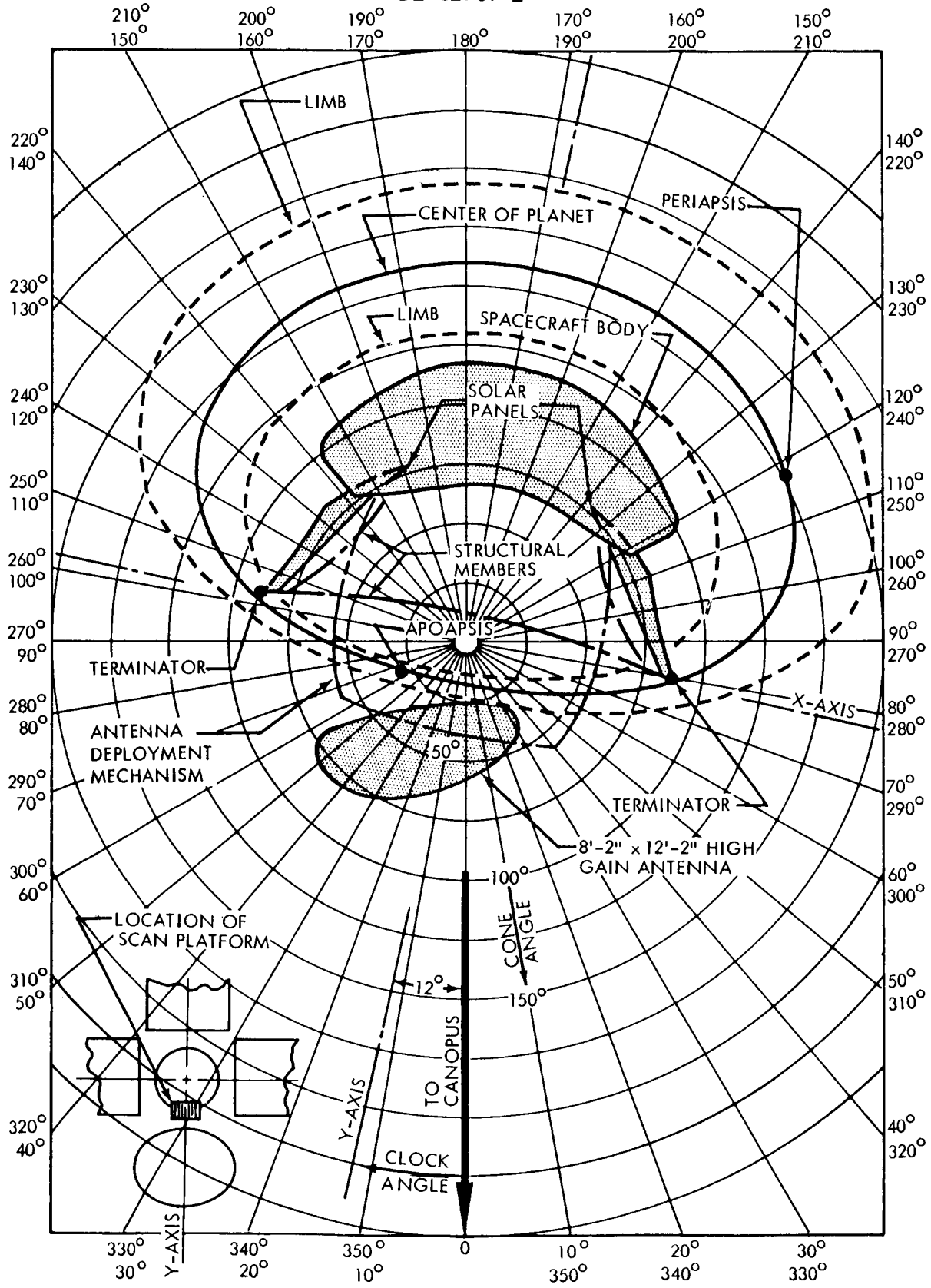

Figure 3-26: 945-6026 First Day of the 18-Hour Orbit Period (Toward Sun)

3.2.2 Model 945-6016

This configuration is shown in Figure 3-27. An octagonal equipment module is attached through exterior fittings to the launch-vehicle adapter. This module, with approximately 80 cubic feet of potentially usable volume, is constructed of eight vertical truss beams, a circumferential ring at the base and top, and shear panels on each of the eight flat faces. These shear panels are used as radiators (65-square-foot area) for the rejection of excess heat to space and for meteoroid protection of the interior subsystems. Electronic subassemblies are attached directly to the radiating surface. Louvers are installed on the exterior side of the radiators for temperature control. The combination of shear, equipment mounting, and radiator panel all into one panel will result in limited access for maintenance, repair, and testing.

The equipment-module volume is 80 cubic feet, but thermal control requirements for heat radiation to space may prevent the use of this entire volume. The large volume provides the ability to relocate assemblies for mass balancing to control the center-of-gravity location, and permits growth to accept design adaptations to suit later missions.

A propulsion module is located directly ahead of the equipment module. It consists of a bipropellant system that has a high-thrust engine located on the center line for orbit insertion, and four low-thrust engines located on the X and Y axes for midcourse maneuvers and thrust vector control of the orbit-insertion engine. The propellant tank arrangement provides for a controlled center of gravity. This module also contains the reaction control subsystem tanks and high-pressure

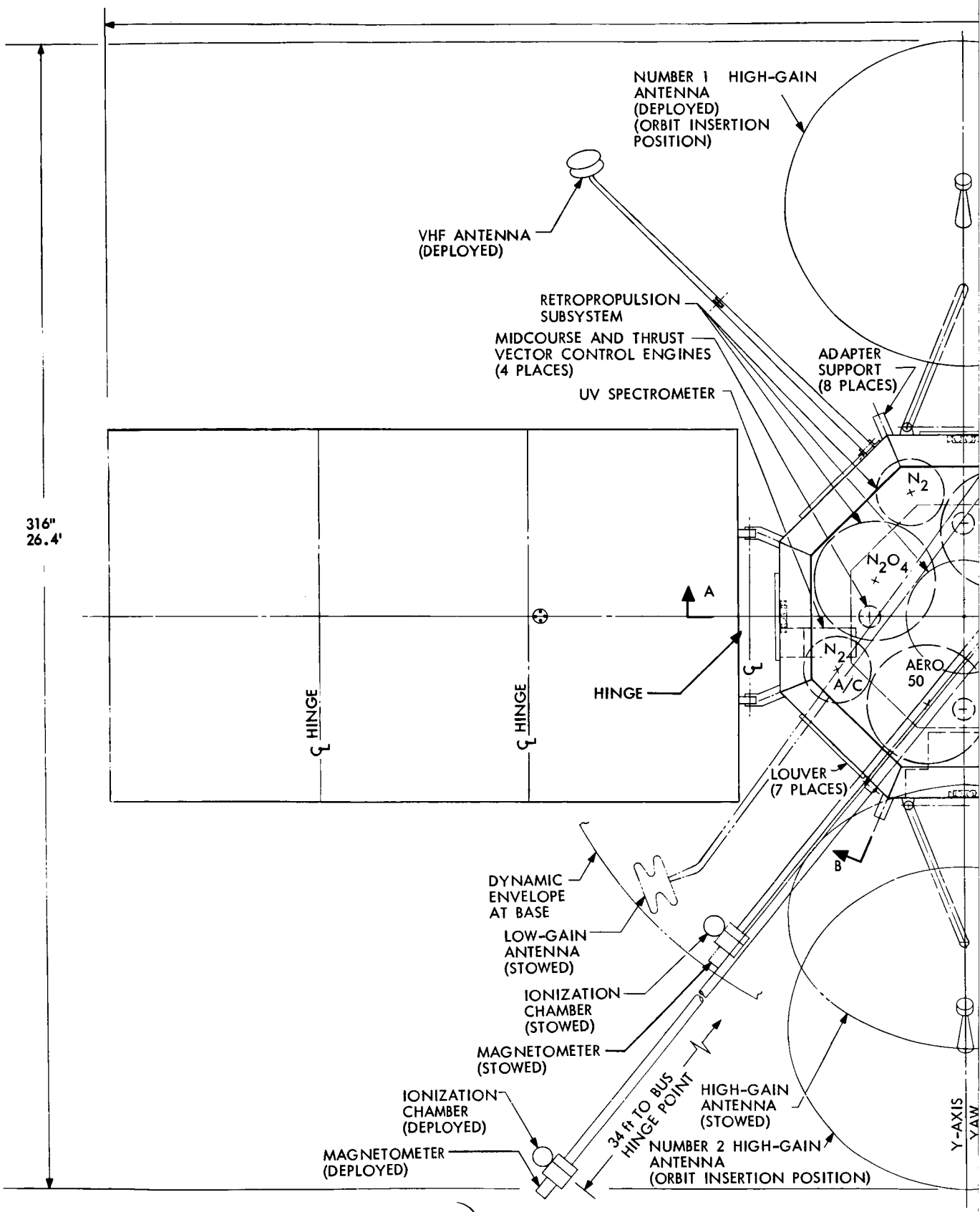
NUMBER 1 HIGH-GAIN ANTENNA (DEPLOYED) (ORBIT INSERTION POSITION)
VHF ANTENNA (DEPLOYED)
RETROPROPULSION SUBSYSTEM
MIDCOURSE AND THRUST VECTOR CONTROL ENGINES (4 PLACES)
UV SPECTROMETER
ADAPTER SUPPORT (8 PLACES)
316" 26.4'
HINGE
HINGE
HINGE
A
B
N_2
N_2O_4
N_2
A/C
AERO 50
LOUVER (7 PLACES)
DYNAMIC ENVELOPE AT BASE
LOW-GAIN ANTENNA (STOWED)
IONIZATION CHAMBER (STOWED)
MAGNETOMETER (STOWED)
IONIZATION CHAMBER (DEPLOYED)
MAGNETOMETER (DEPLOYED)
34 ft TO BUS HINGE POINT
HIGH-GAIN ANTENNA (STOWED)
NUMBER 2 HIGH-GAIN ANTENNA (ORBIT INSERTION POSITION)
Y-AXIS YAW

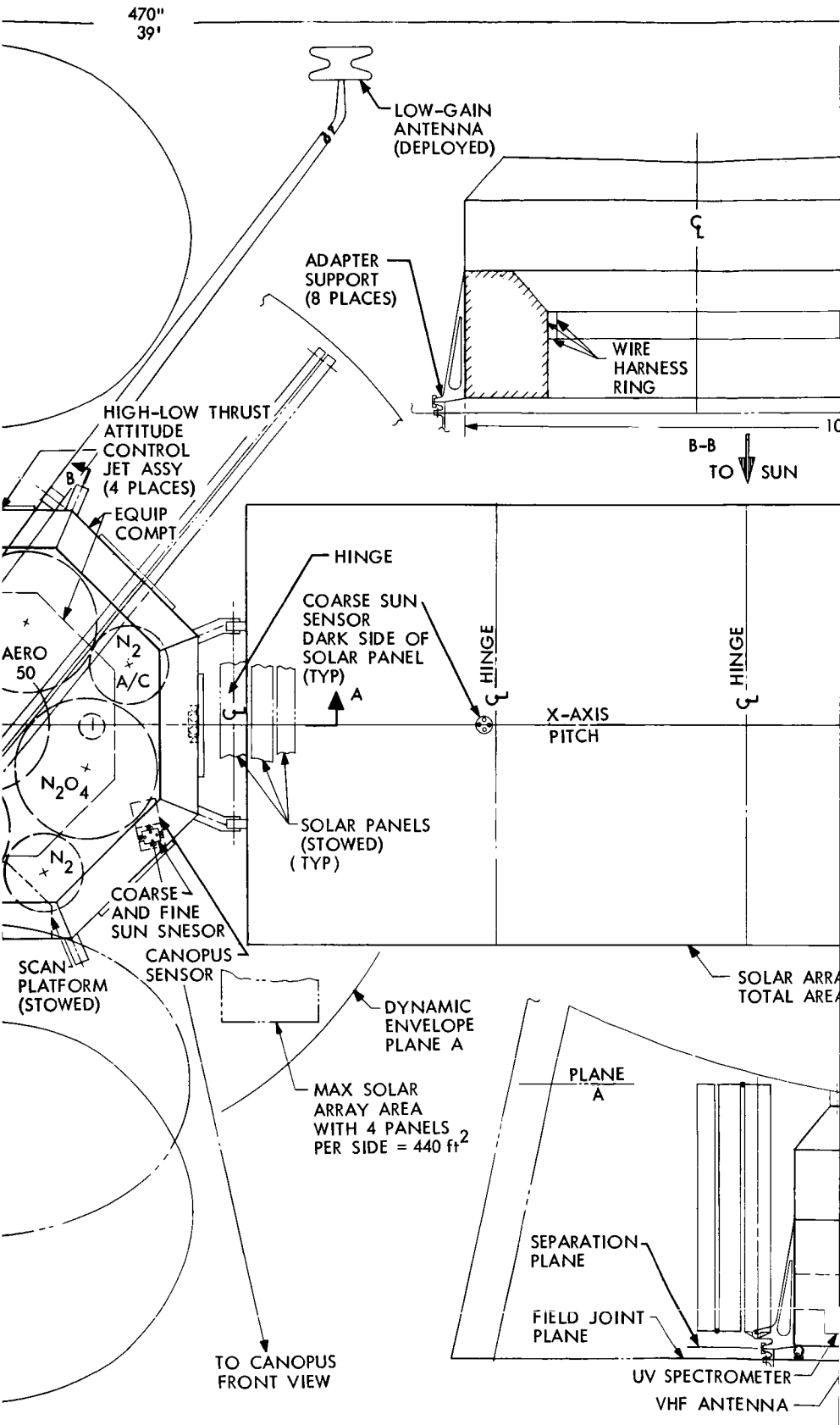
470"
39'
LOW-GAIN ANTENNA (DEPLOYED)
ADAPTER SUPPORT (8 PLACES)
WIRE HARNESS RING
B-B
TO SUN
HIGH-LOW THRUST ATTITUDE CONTROL JET ASSY (4 PLACES)
EQUIP COMPT
HINGE
COARSE SUN SENSOR DARK SIDE OF SOLAR PANEL (TYP)
A
HINGE
HINGE
AERO 50
N_2
A/C
X-AXIS
PITCH
N_2O_4
SOLAR PANELS (STOWED) (TYP)
N_2
COARSE AND FINE SUN SNESOR
CANOPUS SENSOR
SCAN PLATFORM (STOWED)
SOLAR ARRA
TOTAL AREA
DYNAMIC ENVELOPE PLANE A
MAX SOLAR ARRAY AREA WITH 4 PANELS PER SIDE = 440 ft^2
PLANE A
SEPARATION PLANE
FIELD JOINT PLANE
UV SPECTROMETER
VHF ANTENNA
TO CANOPUS FRONT VIEW

7 9 (2)

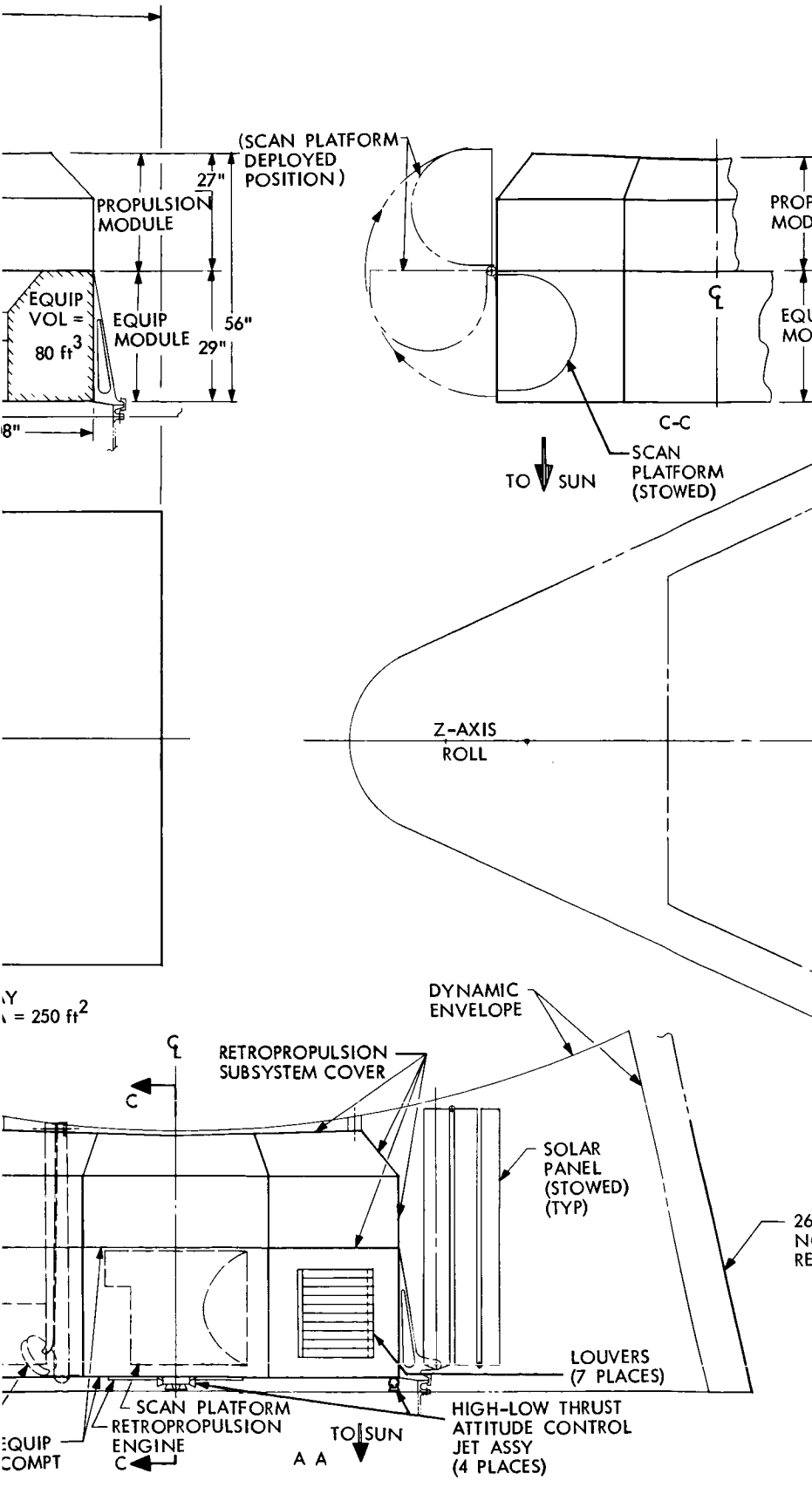
(SCAN PLATFORM DEPLOYED POSITION)
27"
PROPULSION MODULE
EQUIP VOL = 80 ft3
EQUIP MODULE
56"
29"
8"
C-C
TO SUN
SCAN PLATFORM (STOWED)
Z-AXIS ROLL

= 250 ft2
DYNAMIC ENVELOPE
RETROPROPULSION SUBSYSTEM COVER
SOLAR PANEL (STOWED) (TYP)
LOUVERS (7 PLACES)
SCAN PLATFORM
RETROPROPULSION ENGINE
EQUIP COMPT
TO SUN
HIGH-LOW THRUST ATTITUDE CONTROL JET ASSY (4 PLACES)

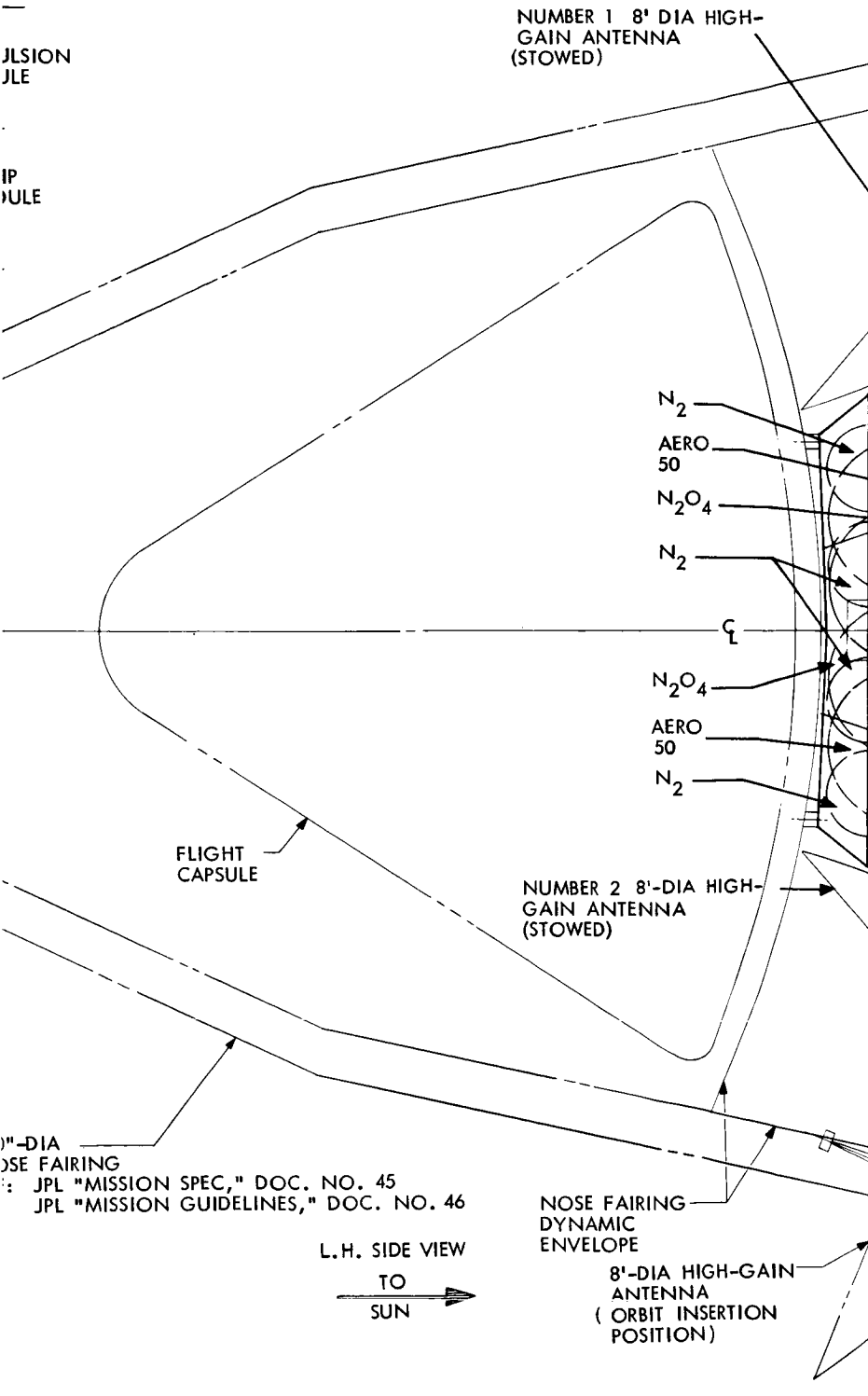
NUMBER 1 8' DIA HIGH-GAIN ANTENNA (STOWED)
N_2
AERO 50
N_2O_4
N_2
$\mathcal{C}_L$
N_2O_4
AERO 50
N_2
FLIGHT CAPSULE
NUMBER 2 8'-DIA HIGH-GAIN ANTENNA (STOWED)
NOSE FAIRING DYNAMIC ENVELOPE
8'-DIA HIGH-GAIN ANTENNA (ORBIT INSERTION POSITION)
L.H. SIDE VIEW
TO SUN

Figure 3-27:

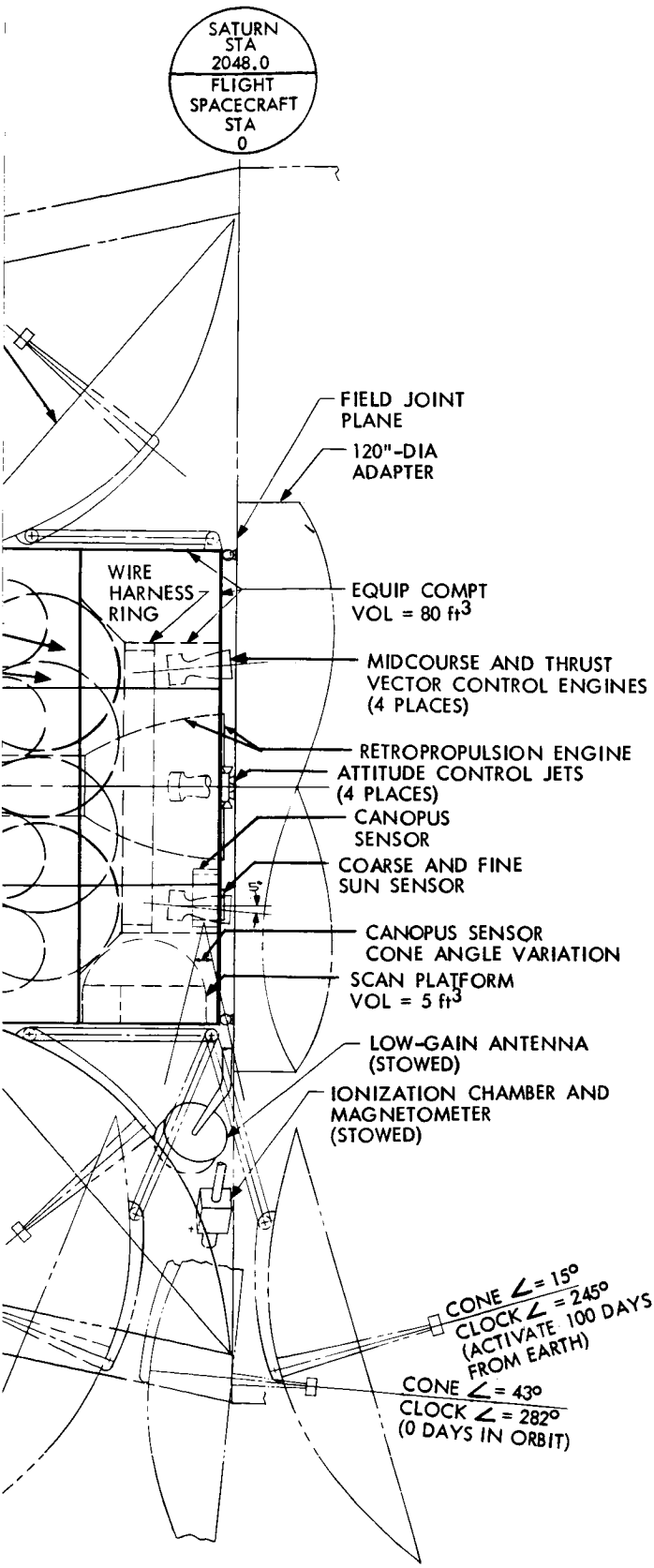

Model 945-6016 Voyager Flight Spacecraft

components. The propulsion module is supported on the equipment module by a set of crossbeams that, in turn, support the tankage, orbit insertion engine, and support structure for the low-thrust engines. This module can be installed as a complete unit.

The reaction control subsystem uses cold-gas (N_2) and has a high-low-thrust jet assembly mounted on the equipment module base on each of the control axes.

A truss structural system surrounds the propulsion module to provide an eight-point support for the capsule. This truss has an upper frame 80 inches in diameter at the capsule interface. The capsule support structure must be removed prior to removal of the propulsion module.

Solar panels that provide 258 square feet of gross area are mounted and stowed vertically on two sides of the spacecraft. Each panel consists of three segments (129 square feet) and single-action actuators provide for deployment. The solar panels are attached in a manner similar to Model 945-6026. However, with the orbit-insertion engine plume directed in the -Z direction, an exhaust plume impingement problem will exist. Addition of one solar panel segment per side provides an additional 86 square feet of area, if future mission requirements so dictate.

Two eight-foot-diameter paraboloidal high-gain antennas are installed on the Y axis. These antennas are provided with two-axis-orientation capability resulting in a clear field of view of Earth for all portions of the mission including maneuvers when proper roll of the spacecraft

is programmed. The second high-gain antenna was installed for redundancy and for solar pressure balancing purposes. The low-gain antenna and magnetometer booms are stowed under the spacecraft and are deployed away from the spacecraft between the high-gain antenna and solar panel. The VHF antenna is stowed in a vertical position alongside the spacecraft and deployed between the high-gain antenna and solar panel.

A scan platform is stowed internally on the Y axis. When deployed, this platform has two-axis-orientation capability resulting in the ability to view the planet from practically all points in the orbit as can be seen from the shadowgraph in Figure 3-28.

The Canopus sensor is located between the X and Y axes with its line of sight directed 12 degrees counterclockwise from the -Y axis. This position of the Canopus sensor is chosen for the same reasons stated for Model 945-6026.

The fine Sun sensor and coarse Sun sensor are located at the base of the equipment module and adjacent to the Canopus sensor and inertial reference unit in a manner similar to Model 945-6026. A second set of coarse Sun sensors is mounted on the dark side of the solar panels for initial Sun acquisition.

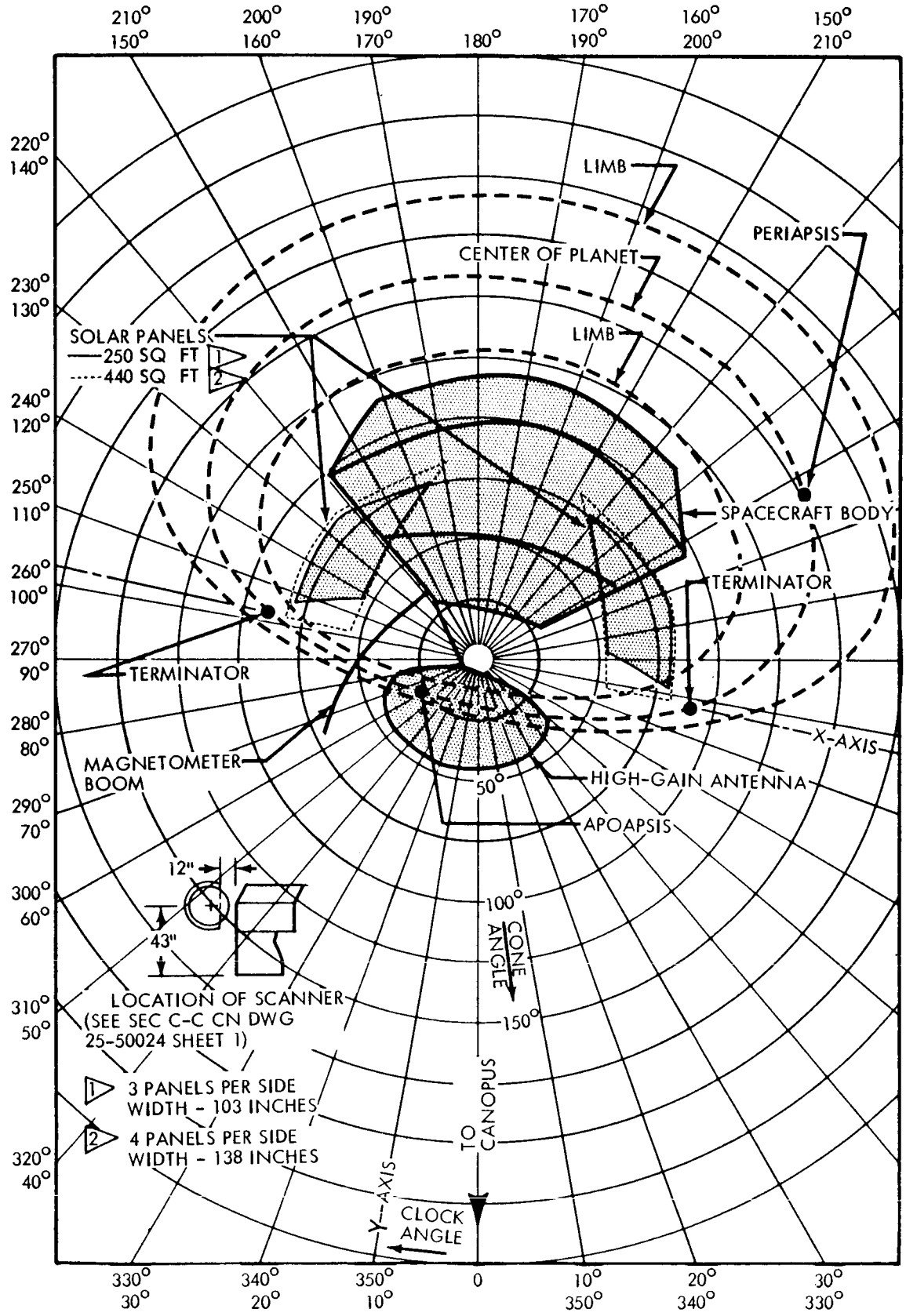

Figure 3-28: 945-6016 18-Hour Orbit Period 0-Days (Toward Sun)

3.2.3 Model 945-6015

This configuration is a result of precontract studies and does not meet the mission-specification spacecraft envelope, although it does fit within the specified nose-fairing envelope. Its features are included here for comparison with the specification compliant configurations since several features of this arrangement are superior to the capsule-ahead-of-spacecraft arrangement. However, the large weight penalty associated with the adapter, and noncompliance with the specification precludes its selection as the preferred design.

The configuration is shown in Figure 3-29. The spacecraft is located ahead of the capsule and supported by an adapter that also houses and supports the capsule. The adapter is mounted directly to the launch vehicle. This arrangement provides for spacecraft loads to be independent of capsule weight and for maximum capsule diameter. The adapter also provides meteoroid protection for the capsule. Solar panels are folded down along the side of the adapter providing for four panels of 250 square feet total area. Each panel has a single deployment hinge line. Antennas and science booms are easily stowed along the adapter with single action deployment. The equipment module is directly ahead of the adapter and will accommodate either internally or externally mounted equipment. This module can fit in the Surveyor nose fairing for 1969 testing.

The propulsion module is located directly ahead of the equipment module and is constructed as an independent module that will include the reaction control subsystem high-pressure components.

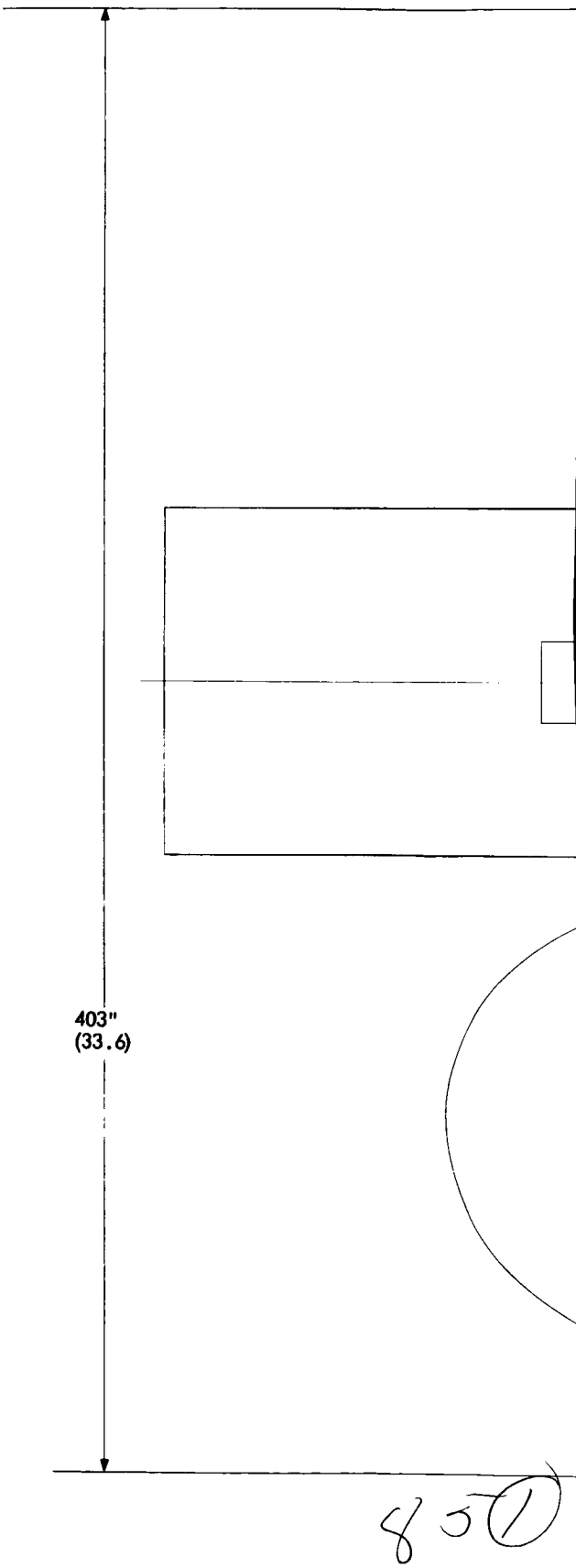

851

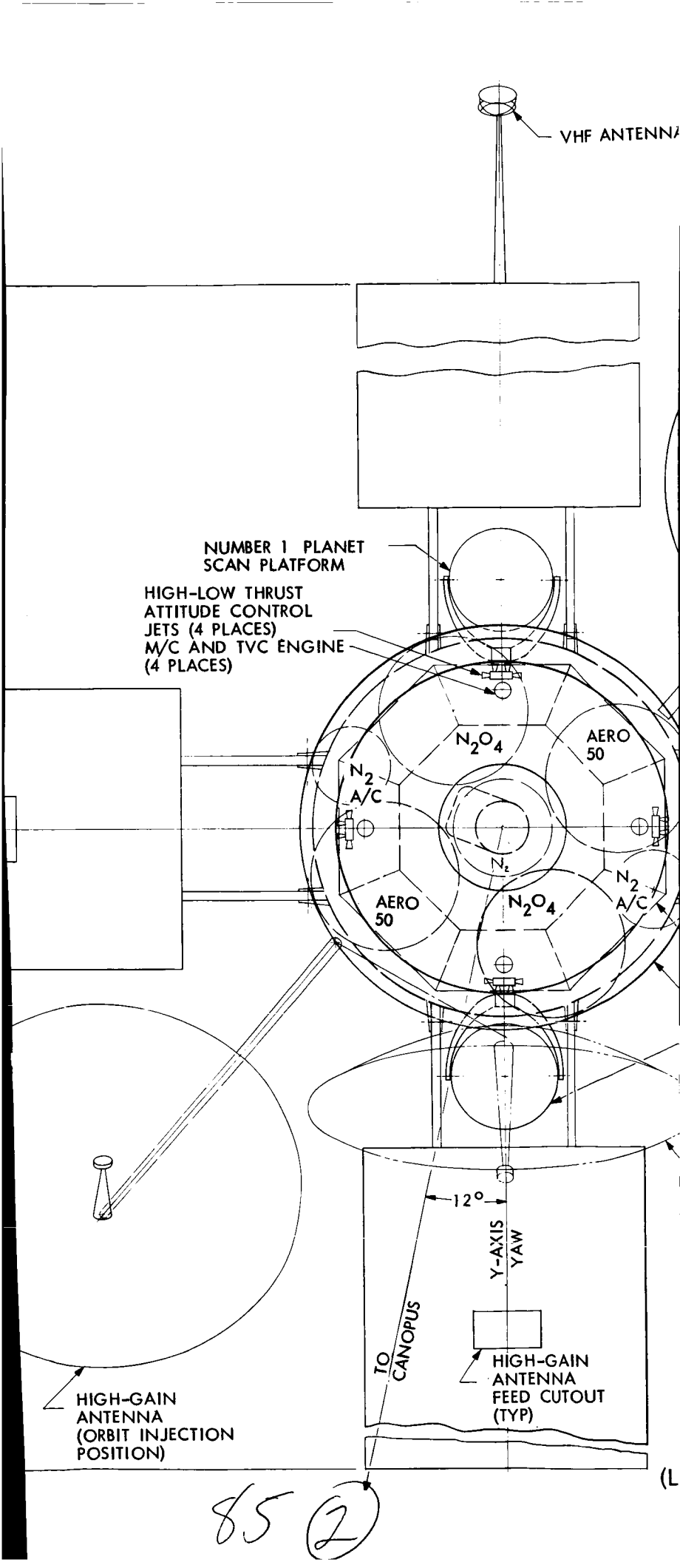
VHF ANTENNA
NUMBER 1 PLANET SCAN PLATFORM
HIGH-LOW THRUST ATTITUDE CONTROL JETS (4 PLACES)
M/C AND TVC ENGINE (4 PLACES)
N_2O_4
AERO 50
N_2 A/C
N_2
AERO 50
N_2O_4
N_2 A/C
12°
Y-AXIS YAW
TO CANOPUS
HIGH-GAIN ANTENNA FEED CUTOUT (TYP)
HIGH-GAIN ANTENNA (ORBIT INJECTION POSITION)
85 (2)

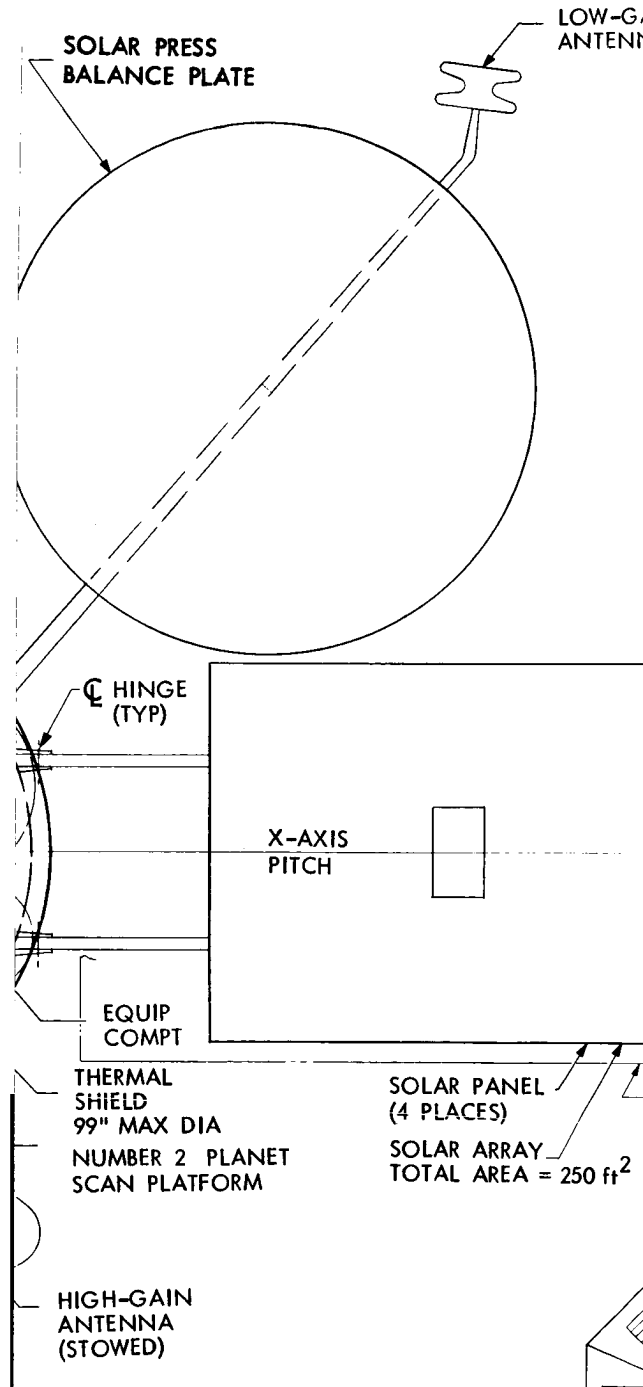

FRONT VIEW
OOKING AWAY FROM SUN)

85 (3)

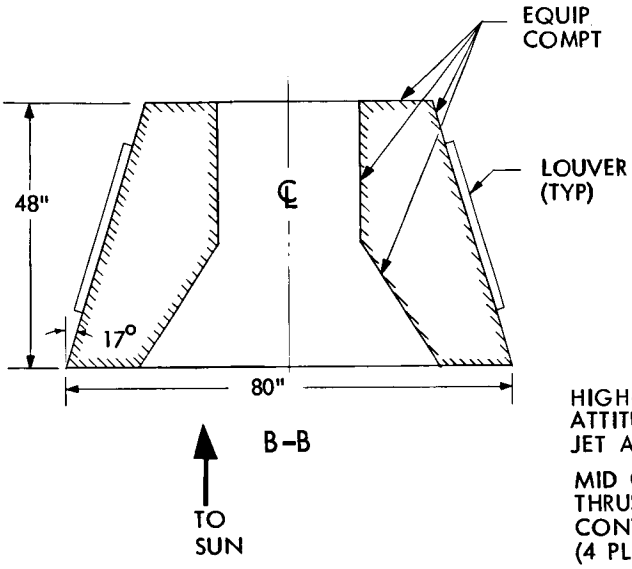

HIGH-LOW THRUST ATTITUDE CONTROL JET ASSY - 4 PLACES

MID COURSE AND THRUST VECTOR CONTROL ENGINE (4 PLACES)

RETROPROPULSION SUBSYSTEM

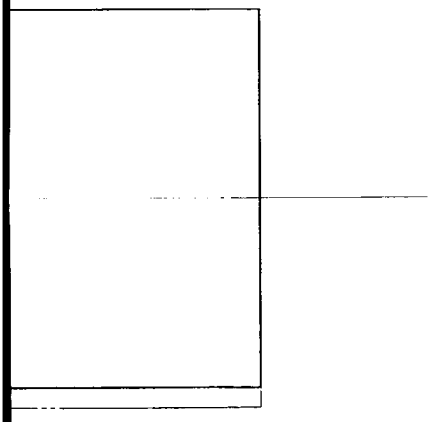

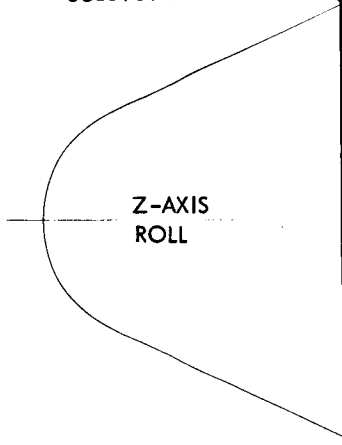

MAX SOLAR PANEL ENVELOPE (TOTAL AREA = 300 ft^2)

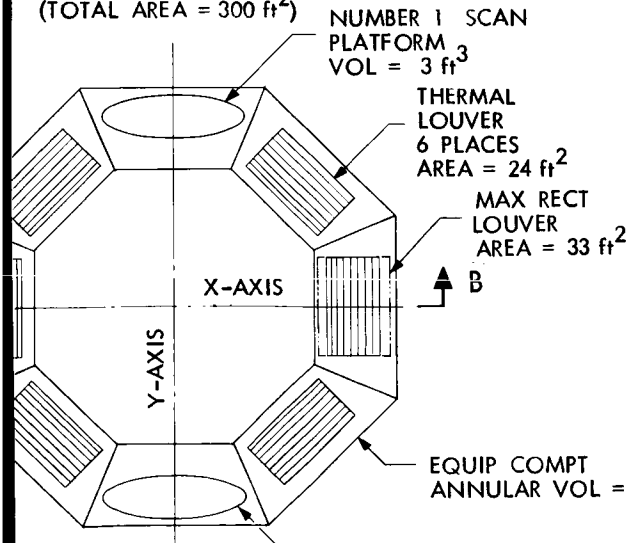

A-A

CONE ∠ = 15
CLOCK ∠ = 24
(ACTIVATE AT
DAYS FROM E

CONE ∠ = A
CLOCK ∠ =
(0 DAYS IN

T
SU

85 4

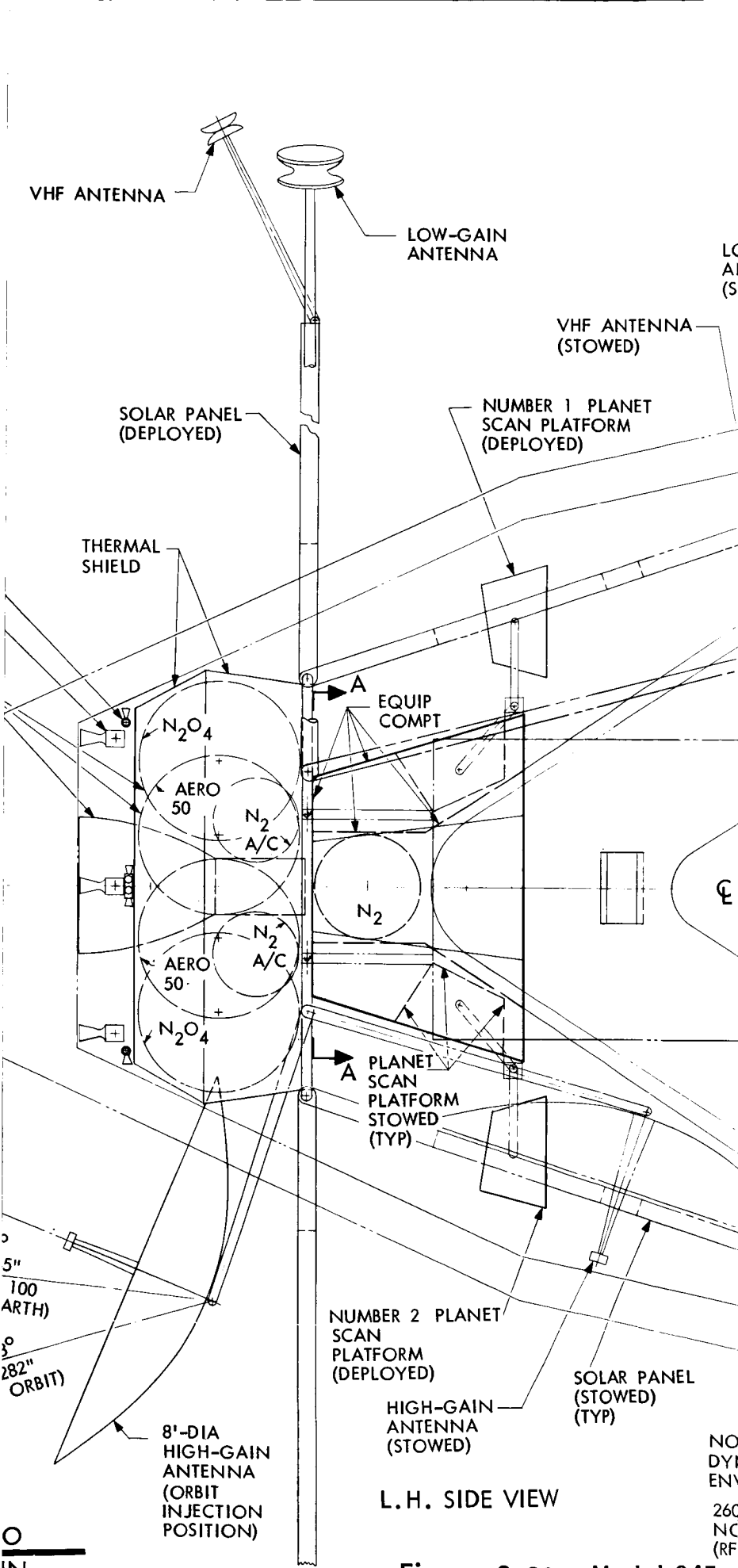

Figure 3-29: Model 945-(

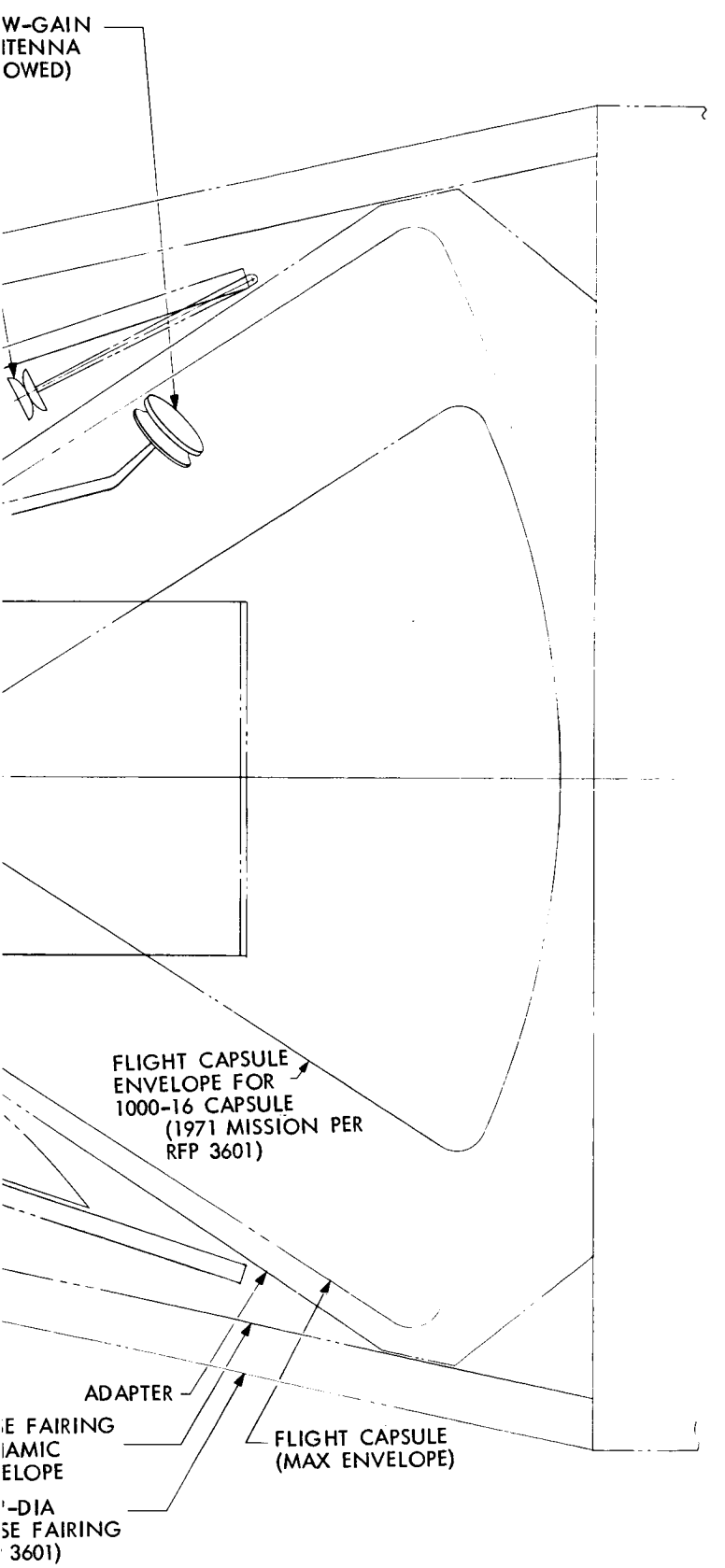

015 Mars Exploration Flight Spacecraft

The major advantages have been stated above. The disadvantages of this configuration are:

1) Large adapter weight--approximately 1400 pounds;

2) Dynamic loads on spacecraft are higher due to distance above launch-vehicle interface;

3) Large Planetary-Vehicle inertia;

4) Large inertia and center-of-gravity change after capsule separation.

3.2.4 Justification for Selection of Preferred Design

This section compares each of the alternate configurations on the basis of meeting overall program objectives. The design that best meets these objectives is the preferred design. To compare the configurations, four "measures of effectiveness" were used: probability of mission success, technical risk, spacecraft weight, and configuration design. In addition, the cost of each alternate configuration was estimated.

3.2.4.1 Measures of Effectiveness

Probability of mission success measures the ability of the system to reach and maintain an orbit around Mars for 6 months, and to return data to Earth. It is assumed that a success will be registered if these events are accomplished, and the quantity and quality of data are within acceptable limits. The ability of the system to acquire and return data within these limits is, therefore, measured separately.

Technical risk measures the probability that the spacecraft and its

components will be completely operational and meet their performance, reliability, and cost requirements by the launch date. Technical risk can be minimized by the use of an approved parts list that contains only proven highly reliable state-of-the-art parts. Such a list has been developed and is being used. Parts not on the list can be added if required, subject to successful demonstration during exhaustive tests under specified conditions of operation and environment.

Spacecraft weight has been used as a measure of configuration efficiency. In this comparison, all allocated spacecraft weight has been used. Where the nominal configuration weight fell below the allocation, redundant parts were added to improve the probability of mission success. This addition was accomplished as described in Section 3.10 of D2-82709-1.

Configuration design has been used to measure the degree to which each configuration satisfies the following major competing design variables and features:

1) Reliability;
2) Mass Properties;
3) Views;
4) Versatility.

Reliability--The spacecraft configuration has an important influence on the reliability level that can actually be achieved. This influence manifests itself in four ways:

1) The provisions for adequate redundancy;
2) The provision for adequate access;

3) The provision for modular construction of subsystem assemblies;

4) Simplicity of construction, operation, and interfaces.

Mass Properties--The mass properties of the spacecraft are affected by an efficient configuration arrangement. The arrangement has a direct effect on the following:

1) Center-of-gravity control;

2) Spacecraft inertia;

3) Spacecraft weight.

Views--Proper views must be provided for scientific instruments, electrical power, attitude references, antennas, and thermal-control radiators.

Versatility--A versatile spacecraft will accommodate revised missions, alternate launch vehicles, alternate scientific payloads, or changes to the mechanization of subsystems. This versatility directly influences the exterior shape and volume allocations that will accommodate equipment changes.

3.2.4.2 Configuration Comparison

Figure 3-30 compares the assessments of the three configurations against three of the five measures of effectiveness (probability of success, spacecraft weight, and configuration design) and against the remaining measures of effectiveness (data acquisition and recovery, and technical risk). No appreciable difference in the assessments existed. In addition,

CRITERIA	SPECIFICATION	CONFIGURATION		
		945-6015	945-6016	945-6026
PROBABILITY OF SUCCESS				
Total Mission	None	0.02	0.14	0.25
Through 30 days in orbit	0.45	0.17	0.47	0.62
Through Injection	0.65	0.24	0.73	
Through Capsule Separation	0.80	0.37	0.71	0.83
DATA ACQUISITION AND RECOVERY				
Orbital Periapsis (km)	None	2700		
Orbit Period (hour)	None	18 hours		
Coverage	Contiguous & repeat in 30 - 90 days	Contiguous and repeat in 30 days		
Occultation				
Sun (Days to Occultation)	30	55		
Canopus	1-2 hrs/orbit	Meets spec. for minimum of 180 days		
Earth	No data transmission degradation	No data transmission degradation		
Data Rate (bits/sec)		48000		
TECHNICAL RISK	Minimize Risk	All parts from preferred list		
SPACECRAFT WEIGHT (lbs)	5500	6660	5550	5500
COST		About Same		
CONFIGURATION DESIGN		79	97	111

Figure 3-30: Evaluation Summary

the cost of each configuration was very nearly the same. The configuration choice was, therefore, made on the basis of the three measures of effectiveness shown in Figure 3-30.

Probability of success is tabulated in Figure 3-30 and is plotted in Figure 3-31. It can be seen that configurations 945-6026 and 945-6016 meet the probability-of-success specification in all respects. The values of probability of success were obtained using a severe definition of success that considered a mission to be successful only while all possible data was being received (i.e., during orbit around Mars, all instruments were required to be in operation). For comparison, a second curve for these configurations is plotted in Figure 3-30 which considers the mission successful while all major spacecraft systems and any scientific instruments are functioning.

The spacecraft weight for Model 945-6015 exceeds the allocation by over 1000 pounds. The effect of this overweight condition is reflected in a probability of success of 0.02 for the 180-day mission. This low probability occurred because no weight was available for improvement of mission success. Conversely, the probability of success was high for 945-6016 and 945-6026 because these configurations have nominal weights that are less than the allocation, and all weight between this nominal and the allocation was used to maximize mission success. On the basis of probability of success and spacecraft weight, the configuration choice was narrowed to Models 945-6016 and 945-6026.

Configuration design ratings are tabulated in Figure 3-32. The rating

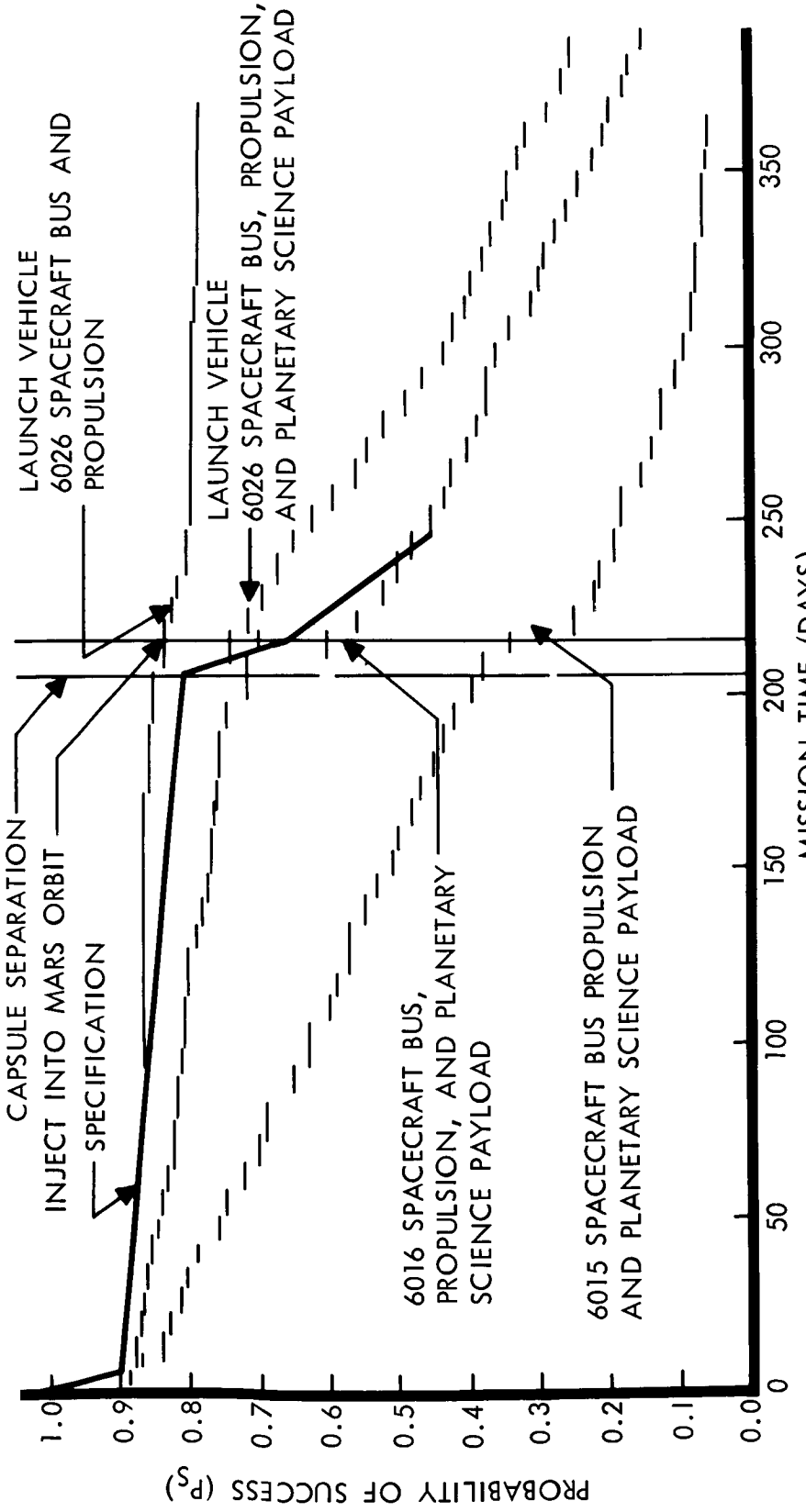

Figure 3-31: Probability Of Mission Success Comparison

	ENVELOPE	RELIABILITY				MASS PROPERTIES			VIEWS	VERSATILITY			TOTAL
		REDUNDANCY	ACCESS	MODULAR CONSTRUCTION	SIMPLICITY	CG	INERTIA	WEIGHT		EQPMT VOL	EXT. SHAPE	EQPMT CHANGES	
945-6026	10	9	10	10	9	9	9	10	9	9	9	8	111
945-6016	10	8	7	7	8	8	8	9	7	8	8	9	97
945-6015	0	0	7	10	7	8	7	7	6	9	9	9	79

Figure 3-32: Configuration Design

is based on a scale of one to ten with ten being the most desirable. A summary of the ratings is shown in Figure 3-30. It can be seen that Model 945-6026 has the most desirable rating.

From the above overall ratings, Model 945-6026 has been chosen as the preferred configuration.

3.3 PLANETARY QUARANTINE ANALYSIS

Summary--Evaluations and analyses were conducted of events on the Voyager program that could result in contamination of Mars. Probability apportionments to each event were made within the overall planetary quarantine constraint that the probability of contamination for a 50-year period be less than 1 in 10,000 for any single launch. The probability allocations for accidental impact of the Centaur booster case, capsule canister, and of the Flight Spacecraft at encounter are met by biasing the aiming points. The selected range of orbits for the Flight Spacecraft is such that the probability of impact from orbit decay in less than 50 years is less than the allocated probability.

As a result of a series of analyses on the remaining events, it appears that the planetary quarantine constraint can only be met through treatment of the Flight Spacecraft to reduce microbial load. Analysis of Mars contamination by means of emissions from the orbit-insertion and orbit-trim propulsion systems indicates that the Planetary Quarantine constraint will be violated if these systems are not treated to reduce microbial load. Analyses relative to the probability of Mars contamination by means of meteoroid ejecta also indicate a need for treatment of the exposed surface areas of the spacecraft to reduce microbial load in order to meet the planetary quarantine constraint.

Complete sterilization of the spacecraft has definite advantages from the high-resolution data-gathering standpoint, and from the value to

subsequent missions. However, state-of-the-art problems exist for certain electronic components and subsystems and with certain materials as to their compatibilities with the heat-sterilization (135°C for 24 hours) and ethylene-oxide decontamination treatments. Additional problems associated with maintenance of sterility during subsequent handling, checkout, and launch operations are also recognized.

Sterilization of only those portions of the spacecraft that appear to be offenders, as far as Mars contamination is concerned, may be a tenable answer to meeting the planetary quarantine constraint. However, this approach gives rise to unique problems. These include recontamination at shroud separation and outgassing of nonsterile components. In addition, this approach also has the same problems of handling after treatment as those mentioned for the complete sterilization approach.

On the basis of the results of the analyses and consideration of the sterilization treatment techniques, it is considered prudent at this time to plan for sterilization of all the propulsion and attitude-control systems as the preferred concept. In addition, intensified study efforts to refine the analyses of Mars-contamination probabilities and to assess the ramifications of sterilization of the total Flight Spacecraft are needed. Expansion of the current JPL programs of investigating temperature tolerance of electronic parts and components, as well as specific study efforts relative to sterilization in the forthcoming Voyager Project, Phase IB, appear appropriate.

3.3.1 Applicable Documents

Jet Propulsion Laboratory Specifications--

XSO-30275-TST-A	Environmental Test Specification Compatibility Test for Planetary Dry Heat Sterilization Requirements
GMO-50198-ETS-A	Environmental Test Specification Compatibility Tests for Ethylene Oxide Decontamination Requirements
ZPP-2010-SPL-A	Electronic Part Sterilization Candidates for Spacecraft Application

Other--

GE 635D801, Vol. V	Sterilization, Voyager Design Study, Missile & Space Division of GE, 1963
NASA CR-191	Studies for Sterilization of Space Probe Components, Wilmot Castle Company, 3/65
NASA Management Manual Instruction 4-4-1	NASA Unmanned Spacecraft Decontamination Policy, September 1963
Space Science Board, Nat. Acad. Sci.	Draft Minutes, Conference on Hazard of Planetary Contamination, 28 July 1964
Aerojet General Corp. SNP 65564-2	Voyager Retropropulsion Technical Report, June 1965
Godding, R.M. & Lynch, V.H.	Viability of Bacillus Subtilus Spores in Rocket Propellants, App. Micro., 13 January 1965
NASA Report CR 54201	Meteoroid Protection for Spacecraft Structures, 1965
NASA TND2828	Determination of Design Meteoroid Mass For a Sporadic and Stream Meteoroid Environment, May 1965
Autonetics, T5-1161.1/ 3061 A, B & C	Voyager Attitude Reference and Autopilot Subsystems Investigation, 1965
Philco, WDL-TR-2531	Mars Mission Communication Analysis, 1965
U.S. Federal Standard No. 209	Federal Specification "Clean Room and Work Station Requirements, Controlled Environment", 16 December 1963

Dynamic Science Corp. SN-37	Sterilization Handbook, Final Report, NASw-777, August 1964
G.E. 645D4362	Design Criteria for Planetary Spacecraft to be Sterilized by Heating, First Quarterly Progress Report, NAS8-11372, September 1964
Bell Aircraft Corp. AFFTC-TR-60-5	Research and Development on the Basic Design of Storable High Energy Propellant Systems and Components, Declassified, 16 June 1960
Nowitzky, A.N. Johnson Publishing Co.	Spacecraft Sterilization Techniques and Equipment, 1965

Boeing--

D2-82724-1	Voyager Reliability, 1965
D2-82733-1	Planetary Quarantine Studies, July 1965
D2-82734-1	Materials & Processes for Voyager Phase IA, 1965

3.3.2 Planetary Quarantine Considerations

The JPL specification states, "The probability that Mars is contaminated prior to the calendar year 2021 as a result of any single launch shall not be greater than 1 in 10,000. Consideration shall be given to the implication of this requirement on the Centaur stage, the spacecraft, the capsule, and all emissions, ejecta, etc.".

The complex task of achieving a probability of Mars contamination of less than 1 in 10,000 for any single launch requires consideration of all of the events which can contribute to planetary contamination. These events, which have been evaluated and analyzed, include: accidental Centaur impact, accidental capsule canister impact, violation of the biological barrier and contamination of the capsule, accidental impact by the flight spacecraft, either at encounter or as a result of

orbit decay within the specified 50-year period, contamination of the planet from emissions of the orbit-insertion or orbit-trim propulsion systems or from the attitude control system, and contamination by ejecta resulting from meteoroid impact of the spacecraft.

The principal organisms of concern in this study have been bacterial and fungal spores. Viruses do not appear to be a primary problem for consideration since they are reported to have a relatively low resistance to the various sterilization techniques contemplated for use. This resistance is comparable to that of vegetative bacterial cells. For this reason viruses have not been considered explicitly in the Planetary Quarantine Analysis.

3.3.3 Distribution of The Constraint Probability

If the probability that each contributing subevent contaminates Mars were 10^{-4}, the probability of Mars contamination as a result of a single launch would be greater than 10^{-4}. Therefore, contributing probabilities were defined by a probability analysis of the possible contaminating events, and then the total constraint probability was distributed among the probabilities so defined. This analysis is presented in D2-82733-1, Planetary Quarantine Studies.

Initial distribution of the 10^{-4} constraint probability among the contributing probabilities is made on the basis of engineering judgment. This discussion indicates the considerations bearing on this initial choice of subconstraint values and presents the subconstraints in relation to the total constraint.

3.3.3.1 The Mars Contamination Constraint Probability

Because the constraint probability is a small number (0.0001) a large percentage change in this probability is also a small number. Thus, although the COSPAR (Draft Minutes, Space & Science Board, NAS, July 28, 1965) preferred values (less than 10^{-4} for the probability of a viable organism on board a spacecraft intended for landing and no greater than 3×10^{-5} for the probability of accidental impact of an unsterilized spacecraft) seem little different from the JPL (NASA) requirement (10^{-4} for the mission from launch) there could actually be a large percentage difference in the two constraints. The COSPAR constraint, however, is not so inclusive as the JPL (NASA) constraint, and therefore would leave room for uncertainty as to the requirements for the Centaur, the canister, and the spacecraft non-impact contamination considerations.

3.3.3.2 Optimal Selection of Subconstraint Probabilities

If a sterilized Flight Capsule is assumed, then Flight Spacecraft impact and non-impact contamination probabilities are the most difficult to reduce adequately to meet the planetary quarantine constraint.

Difficulty in reducing the spacecraft impact probability is primarily due to the fact that reduction of the probability of impact from orbit also reduces the probability of obtaining satisfactory orbiter data. A secondary consideration is that a large reduction of the probability of impact at encounter greatly increases the required biasing of the injection and first trajectory correction aim points, and thereby increases fuel requirements, later trajectory dispersions, and final aim point biasing, which also decreases orbiter data expectations.

Spacecraft nonimpact contamination (by propulsion exhaust products, and meteoritic spalling) can apparently be avoided only by heat treatment and/or sterilization of various parts of the Spacecraft. The contributing factors are interrelated and, as in the case of aim point biasing, a multivariate extremization analysis is required to optimize the system constraints with respect to mission success, cost, and value to subsequent missions.

Optimal distribution of the total constraint probability to the probabilities dependent on the involved factors discussed above is obviously not possible without extensive analysis of a quite well defined system. Thus an iterative technique is inevitable.

The approach adopted at this point is to allow spacecraft considerations the major portion of the total constraint probability.

3.3.3.3 Initial Allocation of Subconstraint Probabilities

In line with the above reasoning, the probability of Mars contamination by an unsterilized Flight Spacecraft was limited to no more than 6×10^{-5}. Because Centaur booster and sterilization canister impact did not appear difficult to avoid, probability of contamination from these sources was limited to 1×10^{-5}, allowing 3×10^{-5} as the ultimate contribution by the Flight Capsule lander.

It has been difficult to determine whether spacecraft impact or nonimpact considerations deserve the largest portion of the 6×10^{-5} subconstraint for the spacecraft. Therefore, the allocation of 3×10^{-5}

to each of the Spacecraft contributions was made. This places the probability of accidental impact of the unsterilized Spacecraft at the same figure as that preferred by COSPAR, 3×10^{-5}.

Further probability analyses have been made of the events already mentioned. These analyses are included in D2-82733-1. The resulting initial allocations, estimated values, and derived probability relationships are shown on the chart in Figure 3-33.

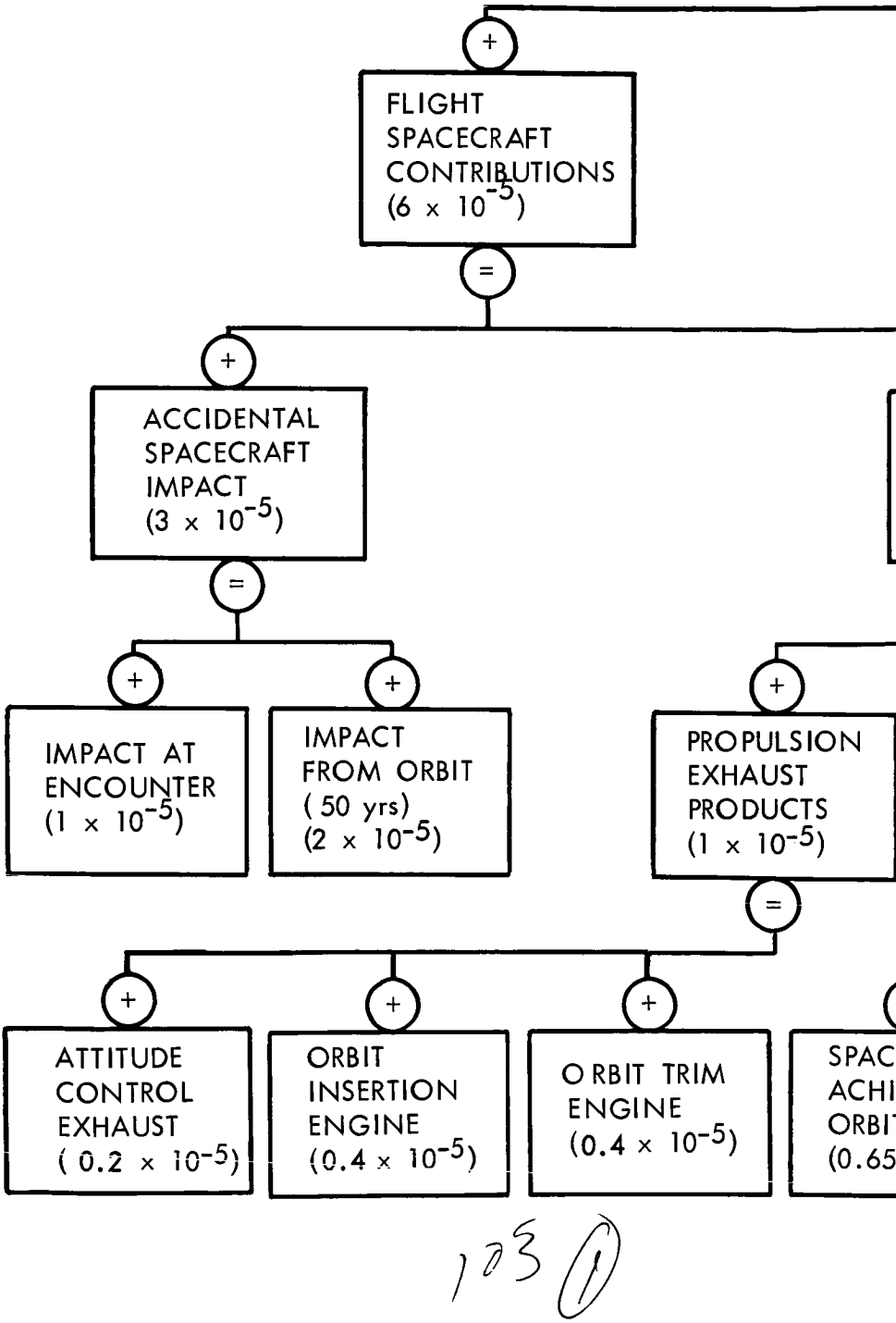
+
FLIGHT SPACECRAFT CONTRIBUTIONS (6×10^{-5})
=
+
ACCIDENTAL SPACECRAFT IMPACT (3×10^{-5})
=
+
IMPACT AT ENCOUNTER (1×10^{-5})
+
IMPACT FROM ORBIT (50 yrs) (2×10^{-5})
+
PROPULSION EXHAUST PRODUCTS (1×10^{-5})
=
+
ATTITUDE CONTROL EXHAUST (0.2×10^{-5})
+
ORBIT INSERTION ENGINE (0.4×10^{-5})
+
ORBIT TRIM ENGINE (0.4×10^{-5})

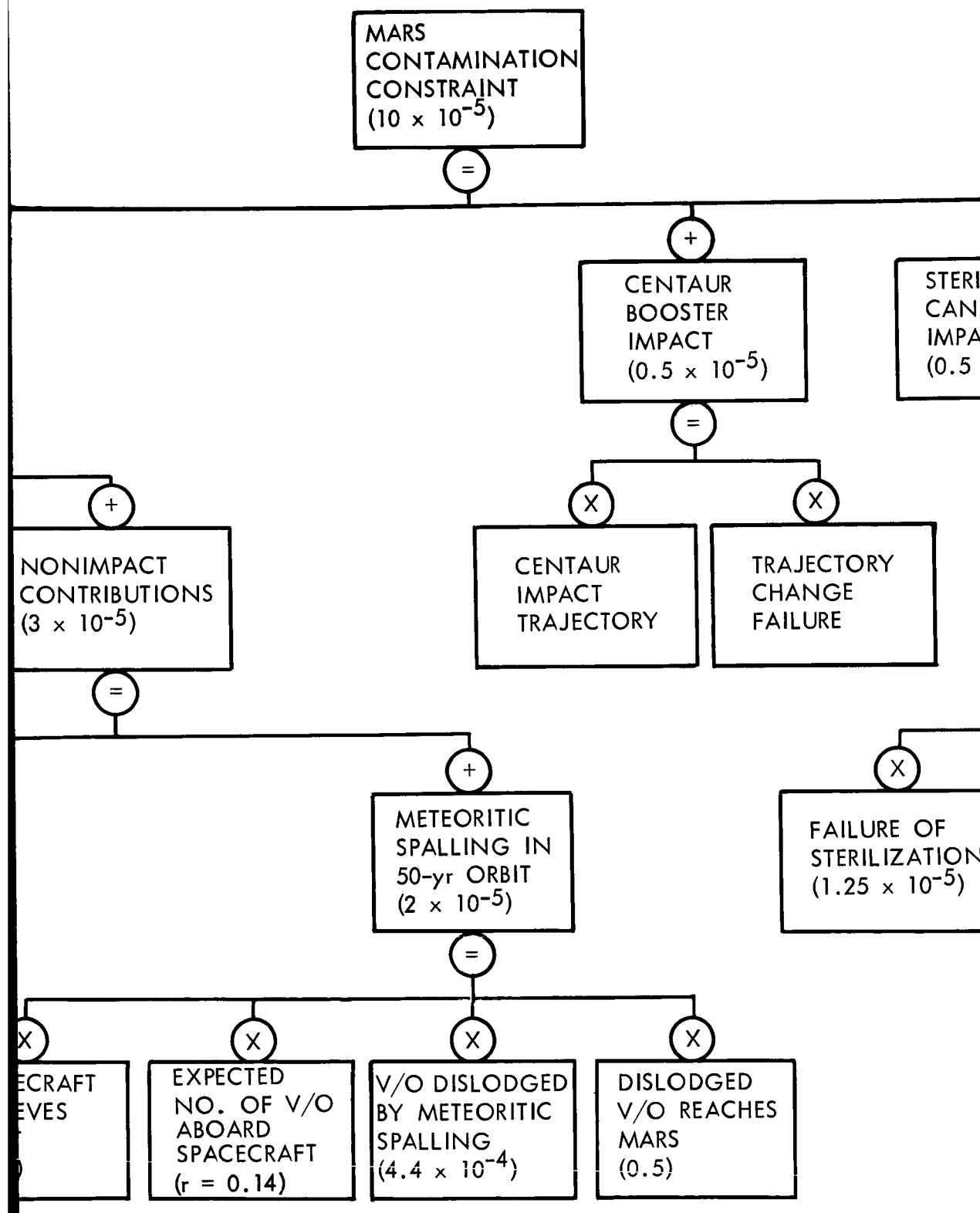
MARS CONTAMINATION CONSTRAINT (10×10^{-5})
=
+
CENTAUR BOOSTER IMPACT (0.5×10^{-5})
=
X
CENTAUR IMPACT TRAJECTORY
X
TRAJECTORY CHANGE FAILURE
+
NONIMPACT CONTRIBUTIONS (3×10^{-5})
=
+
METEORITIC SPALLING IN 50-yr ORBIT (2×10^{-5})
=
X
EXPECTED NO. OF V/O ABOARD SPACECRAFT ($r = 0.14$)
X
V/O DISLODGED BY METEORITIC SPALLING (4.4×10^{-4})
X
DISLODGED V/O REACHES MARS (0.5)
X
FAILURE OF STERILIZATION (1.25×10^{-5})

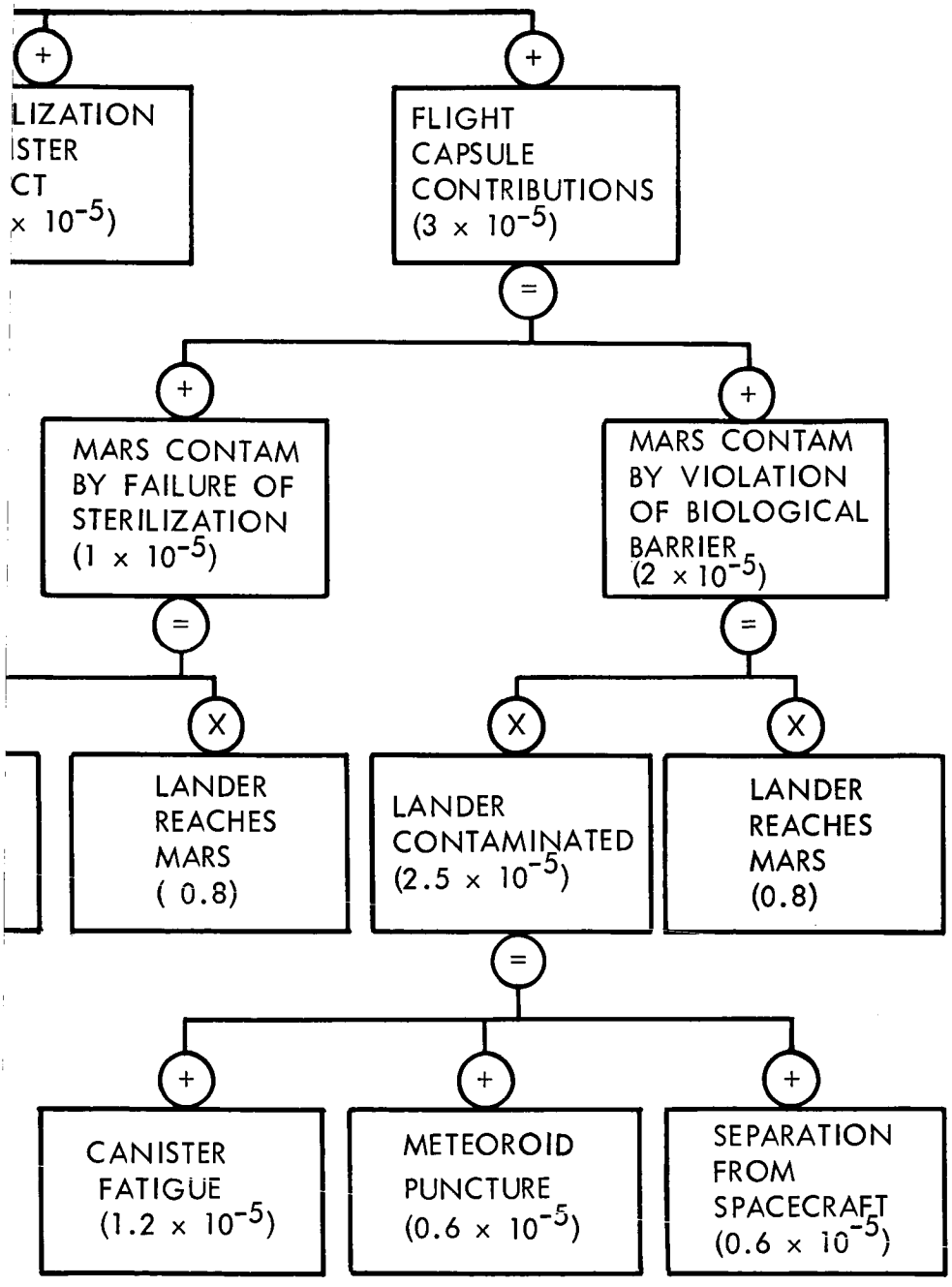

Figure 3-33: Initial Distribution of Constraint Probability to Contributing Event Probabilities

3.3.4 Possible Contaminating Events

Each of the events, presented in Section 3.3.3 which could result in contamination of the planet Mars are discussed below.

3.3.4.1 Accidental Impact of Centaur Booster, Capsule Sterilization Canister, and Flight Spacecraft at Encounter

To meet the planetary quarantine requirement, consideration has been given to accidental impact of the Centaur booster case, the Capsule sterilization canister, and the Flight Spacecraft at encounter. To reduce the probability of these occurrences, the aim points for the Planetary Vehicle trajectory have been biased so as to provide a high probability of a nonimpact trajectory.

The Centaur booster is separated shortly after leaving Earth orbit. In addition to being on a biased trajectory, the Centaur retro capability, discussed in Volume A, Section 3.5, will be activated after separation to ensure the probability of impact with Mars of 0.5×10^{-5} or less.

The Flight Capsule and Sterilization Canister separation occurs approximately 10 days before encounter. The forward section of the canister is separated prior to release of the Flight Capsule. Separation of the capsule requires reorientation of the Planetary Vehicle to eject the capsule on a Mars impact trajectory. After this the vehicle attitude is returned to its normal cruise orientation and the aft section of the canister is separated. With the Planetary Vehicle on a nonimpact trajectory at time the canister sections are separated, the probability of their impacting Mars at encounter is 0.5×10^{-5} or less.

By properly biasing the aim points of the Planetary Vehicle, the probability of accidental impact of the spacecraft at encounter is 1×10^{-5} or less.

3.3.4.2 Accidental Impact of the Spacecraft From Orbit

Insertion of the spacecraft into Mars orbit is not to be commanded unless the lifetime of the resulting orbit extends for at least 50 years, with a probability satisfying the subconstraint of less than 2×10^{-5} for impact of the spacecraft from orbit.

The final aim point is selected, as discussed in Section 2.4, Volume A, so that there will be a high probability of being able to command orbit insertion.

3.3.4.3 Violation of Barrier and Contamination of Flight Capsule

Mars contamination resulting from the Flight Capsule can be attributed to failure of capsule sterilization or contamination of the capsule due to violation of the biological barrier. This might happen because of canister fatigue or meteoroid penetration or at time of capsule separation. The separation of the sterilization canister and maintenance of the contamination requirements are responsibilities of the Flight Spacecraft contractor. The probability of contamination during separation is allocated as 0.6×10^{-5}. This low probability is realized by means of a highly reliable separation mechanism (0.999999+ as presented in Volume A, Section 6).

3.3.4.4 Contamination Due to Propulsion Exhaust Products

The probability of contamination due to the propulsion systems for orbit insertion, orbit trim, and attitude control must not exceed 1×10^{-5} (as established in Section 3.3.3). An assessment of contamination probabilities for each of the three systems is made under the assumption that probability of contamination is equal to the product of probability of spore ejection (either alone or with other material) and probability of capture by the Martian atmosphere.

Orbit Insertion Propulsion System--The proposed orbit insertion propulsion system is a solid propellant motor which is designed to operate at an average chamber pressure of 500 psia for 90 seconds. The motor design incorporates a buried nozzle and a freon injection thrust vector control system. The possible sources of spores or material containing spores includes the liquid freon, igniter assembly, igniter pellets, solid propellant, nozzle seal, throat insert, insulation, and nozzle materials.

During Voyager orbit insertion the following materials are ejected:

1) Freon leakage after TVC system activation (approximately 2 seconds before ignition);
2) Nozzle seal, igniter assembly and possible unburned igniter pellets;
3) Unburned propellant during ignition and tail-off (notably aluminum) because of low combustion efficiency at low pressure;

4) Throat insert material by erosion;

5) Rubber insulation from the motor chamber; and

6) Silica phenolic from the nozzle and nozzle extension.

During normal operation gas temperatures vary from over 3000°C in the chamber to about 1000°C at the nozzle exit. The spores will take approximately 1 millisecond to pass through the nozzle, and will typically be at a higher temperature than the surrounding gas. It is expected that this extreme thermal environment will result in a total kill, although no adequate basis exists for determining kill probability for such short time durations. Spores passing through the thin boundary layer near the relatively cool wall will probably have no better chance for survival than in the core. The boundary layer temperature is greater than the core temperature except for a small part of the laminar sublayer. The velocities are small in the sublayer and, hence, the time required to pass through the nozzle is increased.

In addition to ejection during normal ignition, steady operation, and tail-off, ejection of the above materials can occur in the event of motor malfunction. The failure rate of motor components are listed in Table 3-9.

The most probable malfunction which could result in the ejection of viable spores during the orbit insertion maneuver is the loss of the throat insert. The estimated failure rate is reported by Aerojet to be 3 in 10,000 (component reliability of 0.99969). Single component

Table 3-9: MOTOR COMPONENT RELIABILITY

Reference: Proposal SNP 65564-2, June 1965, Aerojet General Corporation

Component	Failure Rate			Probability of Occurrance on Voyager
	Tests 1-10	Tests 11-20	Tests 20-	
1. Case	0.06122	0.03703	0.01149	0
2. Insulation	0.03415	0.00990	0.00245	0
3. Propellant	00	0	0	
4. Igniter	00	0	0.00411	0.5
5. TVC	0.2600	0.03266	0	
6. Nozzle Approach	0.10126	0	0	
7. Nozzle Throat	0.23626	0.12281	0.00255	0.5
8. Nozzle Exit	0.09396	0.04545	0	
9. Nozzle Extension	0.00000	0	0	

Predicted Failure Rate for Each Voyager Component = 0.000310

Motor Failure Rate = 0.0028 (9 Components)

Note: Potential Hazards Not Accounted for Include the Effects of Radiation and Hard Vacuum for 6-9 Months.

reliability is selected as representative of probability for ejection of material which contains spores. This occurrence could result in the ejection of the throat, nozzle, unburned propellant fragments varying in size from microns to inches, and free spores.

Of the spores ejected alive during orbit insertion, the fraction which arrives at the planet alive depends first, on the probability of capture by the Martian atmosphere, and secondly, on the severity of the thermal environment during entry. In addition to free spores, many of the spores imbedded in small particles can be expected to survive because of their small ballistic coefficients (M/C_DA). Several typical conditions encountered by spores and fragments during Mars entry are shown in Table 3-10. From the data presented in this table and spore thermal death time relationships (Figure 3-39) it becomes evident that the conditions of entry are not sufficiently severe to cause death of all entering spores. It is therefore concluded that the loss of the throat insert would almost certainly result in contamination. The probability of this occurrence alone exceeds the allowable contamination probability allocated to propulsion systems. Therefore, the reduction of microbial load of all orbit insertion system components and propellants is necessary to meet the allocated probability and, at this point in time, sterilization appears to be the most prudent course.

Orbit Trim Propulsion System--Possible sources of contamination from the liquid monopropellant engine include the fuel (hydrazine), catalyst bed, internal hardware, and nozzles. The temperature of the propellant when passing over the catalyst ranges from 1380°C to 880°C, and

Table 3-10: Entry Parameters

$\frac{M}{C_D A}$ (SL/FT^2)	SPORE DIAMETER (FEET)	BUS FRAGMENT DIAS. (FEET)
0.01	—	10^{-3}
10^{-4}	$3.28\ (10)^{-7}$	$3.28\ (10)^{-5}$
10^{-8}	$1.31\ (10)^{-4}$	—

	$\frac{M}{C_D A}$ (SL/FT^2)	V e (FT/SEC)	γ_e°		TIME (SECONDS)	TEMP (°R)	
	0.01	12000	-90	FRAGMENTATION	28.6	2050	KILL
	0.01	12000	-5		318	1300	
	0.01	6000	-90		57	1120	
	0.01	6000	-5		632	610	SURVIVE
SPORES	10^{-4}	12000	-90		28.6	820	
	10^{-4}	12000	-5		318	460	
	10^{-4}	6000	-90		57	410	
	10^{-4}	6000	-5		636	230	
	10^{-8}	12000	-90		10^4	300	
	10^{-8}	12000	-5		10^4	300	
	10^{-8}	6000	-90		$2(10)^4$	300	
	10^{-8}	6000	-5		$2(10)^4$	300	

then decreases to -20°C at the nozzle exit. Spores contained in the propellant would take about 4 milliseconds in passing over the catalyst bed before entering the nozzle. Although this thermal environment appears severe, total microbial kill is improbable. No accurate estimate of kill probability for such short time durations is known.

A second possible source of contamination from the hydrazine occurs from leakage. It is estimated that the mass loss from leakage which will reach Mars is about 0.01 percent of the total propellant mass. Nearly all spores emitted with this leakage are expected to be captured alive.

Other sources of contamination from this system are the internal hardware, catalyst pellets, and the nozzles. The probability that viable spores ejected during orbit trim maneuvers will contaminate is estimated to be approximately 80 percent. An analysis of the probability that live spores will be ejected (which is a function of the microbiological burden of the system and the probability of spore survival during the expulsion process) is not available at this time. Considering the high probability of spore survival at entry conditions and the apparent improbability of total kill during expulsion, sterilization of this entire propulsion system is recommended at this time.

Attitude Control System--Unlike the orbit insertion and orbit trim systems, the attitude control system is a cold thrust device; hence, no spores will be thermally annihilated in either the chamber or nozzle.

Initial estimates indicate approximately 2 percent of the nitrogen will be expended during that part of the trans-Mars trajectory for which spore capture is possible and 19 percent will be used during orbit. (One-half of the 19 percent is conservatively assumed to be captured.) A further 25 percent will leak out within the 50 years of orbit lifetime (based on 10^{-3} lbm/day). Approximately 36 percent of the spores initially in the nitrogen are estimated to reach Mars alive. Thus, sterilization of the nitrogen, internal hardware, and nozzles are required to meet the established quarantine requirements.

3.3.4.5 Analysis of Meteoroid Hits and Fragmentation

Meteoroid impact on any portion of the spacecraft will result in the ejection of material from the spacecraft. Under conditions of hypervelocity impact, the material can be dislodged in several ways. The pressures and temperatures generated in the immediate vicinity of the impact are sufficiently high to cause the material to behave like a fluid. Fragments of both the projectile and the target material are ejected radially outwards and backwards from the point of impact. High-speed photographs of hypervelocity perforation of thin sheets show this phenomenon quite clearly. Even after penetration is complete material continues to be ejected from the surface due to momentum trapped by the passage of reflected high-intensity stress waves. If the target sheet is thick enough to prevent complete penetration compression waves that emanate from the bottom of the crater are reflected as tension waves from the free surface at the back of the sheet. The stresses generated are frequently high enough to cause tension failures of the material

resulting in spall fragments tearing loose from the sheet. Particularly in the case of brittle materials, several spalls may be formed if the stresses are sufficiently high. The velocity of spall fragments is limited by the velocity of stress wave propagation. An upper limit is one-half the shear wave velocity, which in the case of aluminum is approximately 5000 fps.

If the target is a laminated structure composed of several elements bonded together, each boundary provides a surface from which reflections can take place. The relative strengths of the reflected and transmitted stress waves as well as the material properties of the adjoining media determine the size and velocity of the spall fragments. Solar cell cover glass will shatter and release fragments that may be as large as several square millimeters.

The solar panels are representative of a layered medium, and consequently are subject to spallation when struck by a high velocity particle. Figure 3-34 shows the result of impact by a 2×10^{-4} gram particle at 4 km/sec. The area immediately adjacent to the point of impact has been crushed, whereas, the surface farther away shows both radial and circumferential cracks as well as the spalled area. The fragment size varies from approximately 10^{-6} grams to 10^{-3} grams and the ejecta velocity ranges between 0.5 and 10 km/sec.

When a meteoroid strikes a thin sheet the particle is fractured and a spray cone of high velocity debris emerges from the back of the sheet.

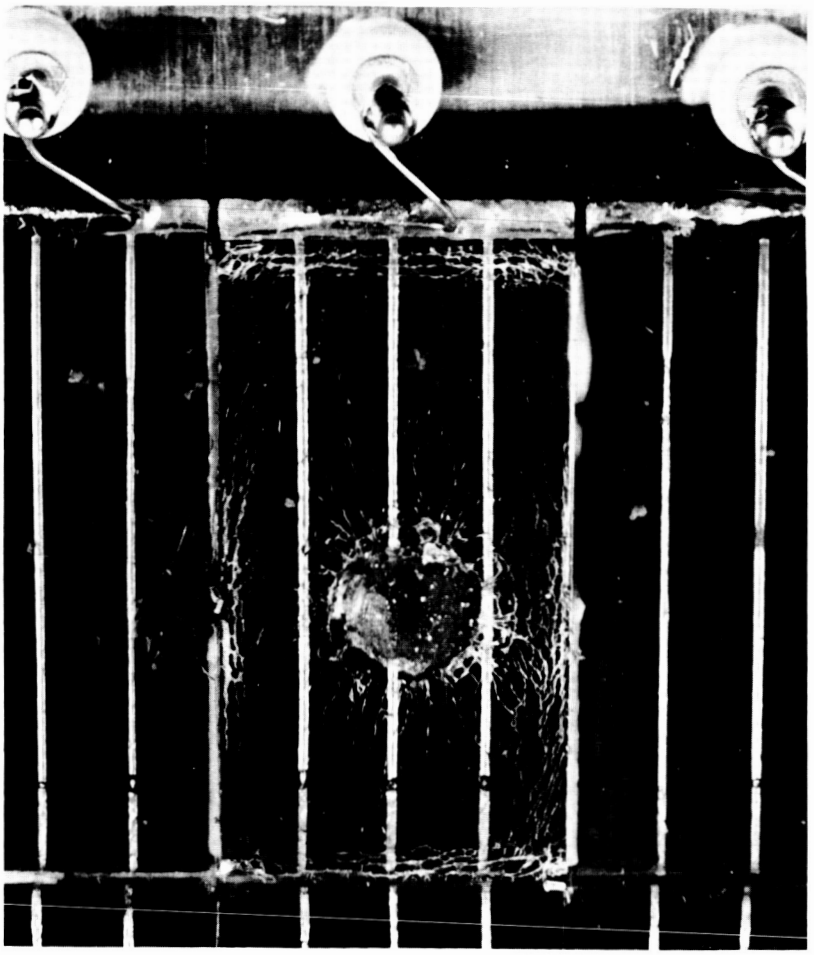

PROJECTILE: 2×10^{-4} gram GLASS SPHERE, DENSITY = 2.2 g/cc

VELOCITY: 4 km/sec

Figure 3-34: Simulated Meteoroid Impact Test
Solar-Panel Face Impact

If these fragments impinge on a second sheet, the resulting damage is a large ragged hole produced by overlapping perforation.

Ejecta from the high gain antenna are produced by the phenomenon of multisheet perforation (NASA Report CR.54201, 1965). Fragmentation of rock-like projectiles will occur only for velocities in excess of 4 km/sec. Data from this report indicates that only particles larger than 10^{-4} grams will penetrate both surfaces of the antenna.

The significance of the problem can be put into perspective by considering a specific case. For the purpose of this study the spacecraft has been divided into several areas that are determined by the type of ejecta produced upon impact. The most critical areas are the solar panels and the high-gain antenna. The estimates of the ejected material and ejecta velocity are shown in Table 3-11.

The lower portion of Figure 3-35 shows the probability of at least one impact for various meteoroid masses as a function of time. The upper portion gives the average number of impacts on the same area. The area considered is 250 square feet, which is approximately equal to the area of the solar panels. The meteoroid flux is taken from the near-Mars environment and is given by $\log N_A = -1.0 \log m_A - 11.70$ (Volume A, Section 2.2.4.8, Meteoroid Environment). The chart shows that nearly 10 impacts by a mass of 10^{-4} grams (or greater) can be expected during a 6-month period. The probability of at least one such impact is virtually 100 percent. Under these conditions, many hundreds of

Table 3-11

Meteoroid Mass	Ae, Area of Ejected Material	
	Solar Panels	High-Gain Antenna
grams	cm^2	cm^2
1.0 and larger	---	---
10^{-1} " "	20	1
10^{-2} " "	210	12
10^{-3} " "	680	122
10^{-4} " "	1170	1422
10^{-5} " "	1780	1422
10^{-6} " "	2990	1422
V_e = ejecta velocity	V_e = 0.5 km/sec for $m \leq 10^{-4}$ V_e = 10 km/sec for $m > 10^{-4}$	V_e = 10 km/sec for $m \geq 10^{-4}$

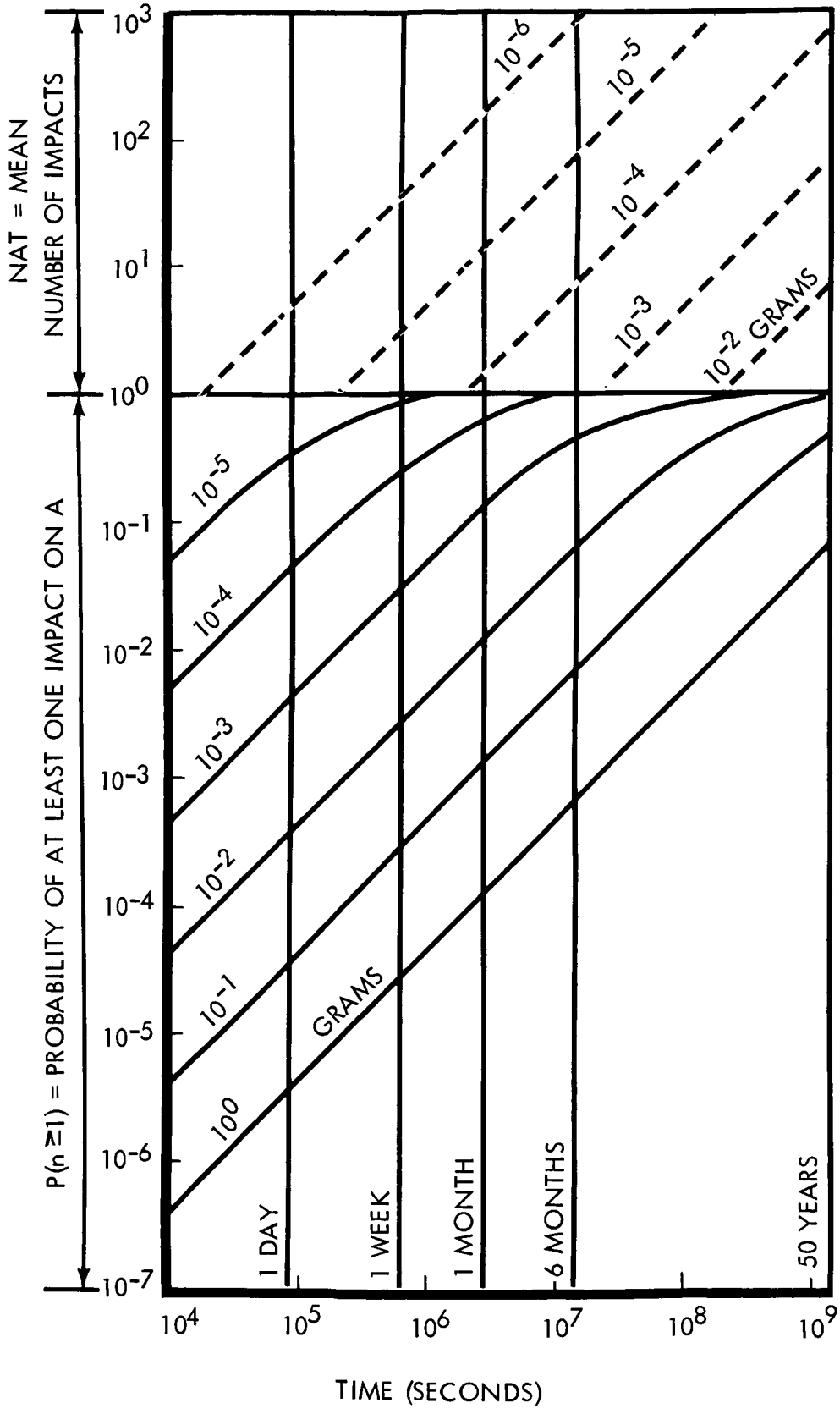

Figure 3-35: Meteoroid Impacts on Solar Panels

small particles will be ejected from the exposed surfaces during 50 years in orbit. Each of these fragments provides a potential vehicle for transporting a viable organism to the Martian surface.

Contamination implies that a viable organism survives entry into the Martian atmosphere. Survival probabilities are established by comparing the time-temperature history of the entering particle with time-temperature-kill data (Figure 3-39). The time-temperature history is a function of the particle mass, shape and geometry as well as entry angle and velocity. Table 3-10 shows that at least under one condition ejecta fragments will survive entry into the Martian atmosphere. The table also shows that particles approximately of spore size will also survive entry.

Impact of the exterior surface of the Spacecraft Bus can be neglected for purposes of this study. These surfaces will be either bare metal or metal covered by high emissivity paint for thermal control purposes. Hypervelocity cratering of metallic targets is accompanied by pressures in the megabar range and temperatures in excess of 1000^{o}K. The ejecta produced are all in the molten state and are believed to contain no viable organisms. A certain amount of the thermal control coating will be dislodged by spalling upon impact, however, the quantity of this material is negligible when compared to the ejecta from the solar panels and the antenna.

Microbiological Burden--The following analysis has been used to determine the requirement for spacecraft decontamination so that the planetary quarantine is not violated due to ejecta generated by meteoroid impact. Spacecraft contamination is specified by the expected number of viable organisms (v/o) surviving heat (or other appropriate) treatment, under the assumption that organism-survival probability is described adequately by the Poisson distribution. The allowable density of micro-organisms on the spacecraft is obtained by use of a derived expression for P_1, the probability of Mars contamination by meteoritic ejecta of the orbiting spacecraft.

The derived expression for P_1 is

$$P_1 = P_o \left[1 - \exp(-r P_2 P_3)\right]$$

where;

P_o = the probability that the spacecraft achieves a 50-year (lifetime) orbit.

$P_2 = \frac{A_e}{A_T}$, the ratio of area affected by meteoritic spalling to total spacecraft area, under the assumption that a viable organism has equal probability of being on any part of the total area for a period of 50 years.

P_3 = the probability that a dislodged v/o reaches Mars.

r = the number of microorganisms per spacecraft.

The initial allocation of the total allowable probability of Mars contamination (10^{-4}) sets P_1 at 2×10^{-5}. P_o must be greater than 0.65, by JPL specifications.

Thus, $P_1/P_o = 1 - \exp(-r P_2 P_3)$ is very small and the approximation $P_1/P_o = r P_2 P_3$ holds with negligible error.

The allowable number of microorganisms is now specified by:

$$r = \frac{P_1}{P_o P_2 P_3}$$

The total area of surfaces of the spacecraft is very nearly 10^7 cm^2. Using the estimates for A_e from Table 3-11

$$P_2 = \frac{(2.99 + 1.42) \times 10^3}{10^7} = 4.41 \times 10^{-4}$$

The probability of particle capture is a function of the ejecta velocity vector. Considering that all directions are equally likely and the range of ejecta velocity, P_3 is taken as 0.5. Therefore;

$$r = \frac{2 \times 10^{-5}}{(0.65)(4.41 \times 10^{-4})(0.5)} = 1.40 \times 10^{-1}$$

The above result is of course a function of the near Mars meteoroid environment. It is important to recognize that this environment is subject to some uncertainty. If the conservative environment used should prove to be too severe by a factor of 10, P_2 becomes 4.56×10^{-5} and the equation for r becomes

$$r = \frac{2 \times 10^{-5}}{(0.65)(4.56 \times 10^{-5})(0.5)} = 1.35$$

It can be seen (Figure 3-36) that the calculation is relatively insensitive to estimates of the environment. Even if the ratio of ejected (contaminated) area to the total spacecraft area were to decrease by a factor of 100 ($P_2 = 4.4 \times 10^{-6}$) the allowed number of v/o per spacecraft would

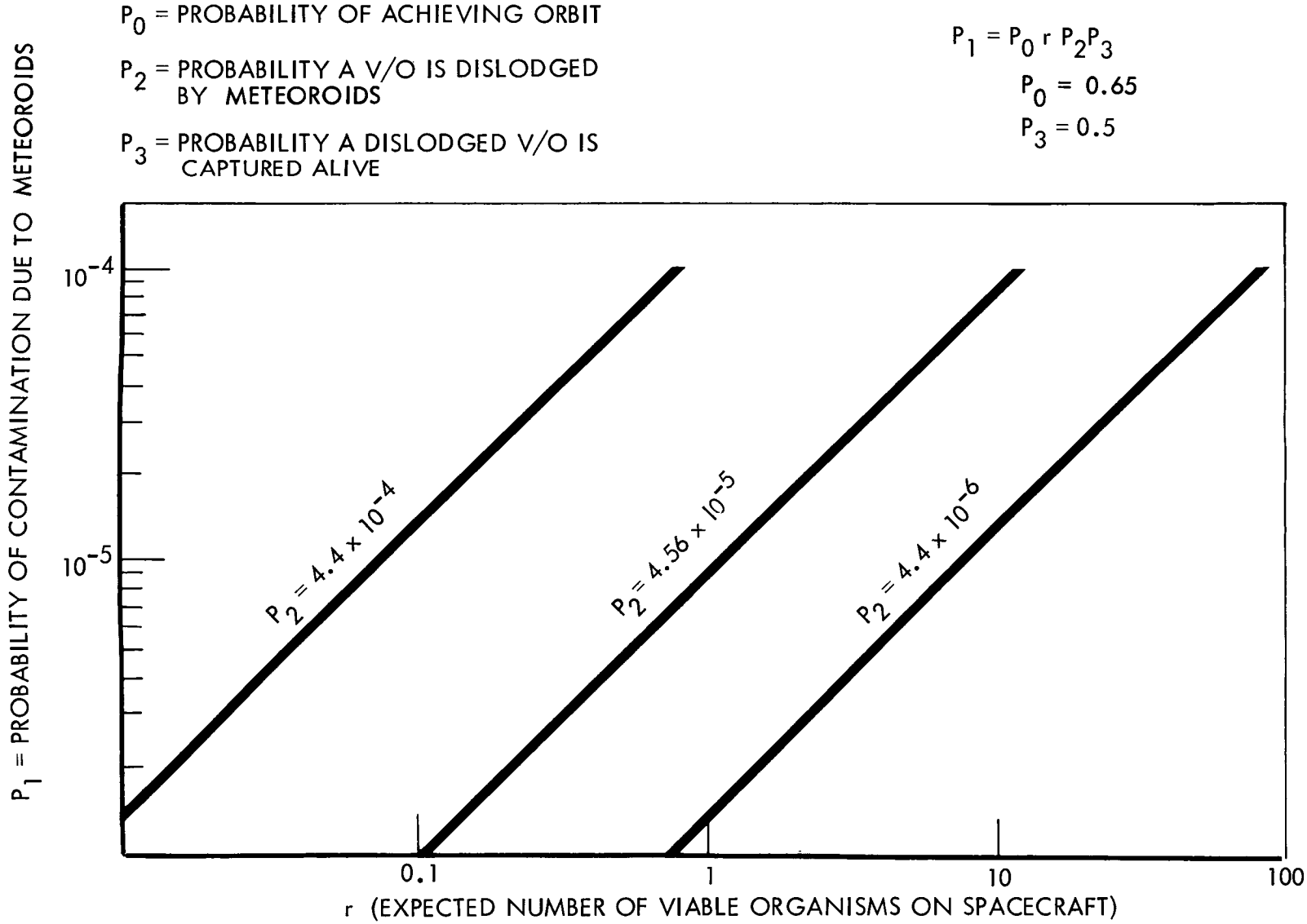

Figure 3-36: Mars Contamination Due to Meteoroids vs Spacecraft Contamination

be approximately 14. It can therefore be concluded that the number of v/o per spacecraft must be reduced to a very small number ($r \simeq 1$) although sterilization is not required.

The Effect of Short Period Changes in the Environment--The critical meteoroid environment is due to the asteroidal contribution. It has been shown in Volume A, Section 2.2.4.8, that the asteroidal component exceeds the cometary component by a factor of 30 in the range of interest. The cometary flux is representative of the mean sporadic meteor flux seen at Earth. It is well known that there are periods of intense meteor activity associated with passage through one of the meteor streams. Although the showers raise the yearly average by less than a factor of 2, the possibility of unknown streams at Mars cannot be discounted. Enhancement factors for the major known meteor streams have been tabulated by Kessler and Patterson (NASA TND2828, 1965). These data show that magnification factors of 6 to 8 are possible for short periods in the mass range above 10^{-2} gram.

Extrapolation of these values to Mars is difficult. Figure 3-37 shows five of the known showers whose orbit probably crosses the orbit of Mars.

The meteor stream orbits shown were chosen from the tabulation of major meteor showers, using the criterion that their inclinations to the ecliptic are small (specifically, $\leq 6.8^{\circ}$); and, since the inclination of Mars orbit is less than 2 degrees, these streams, assuming some

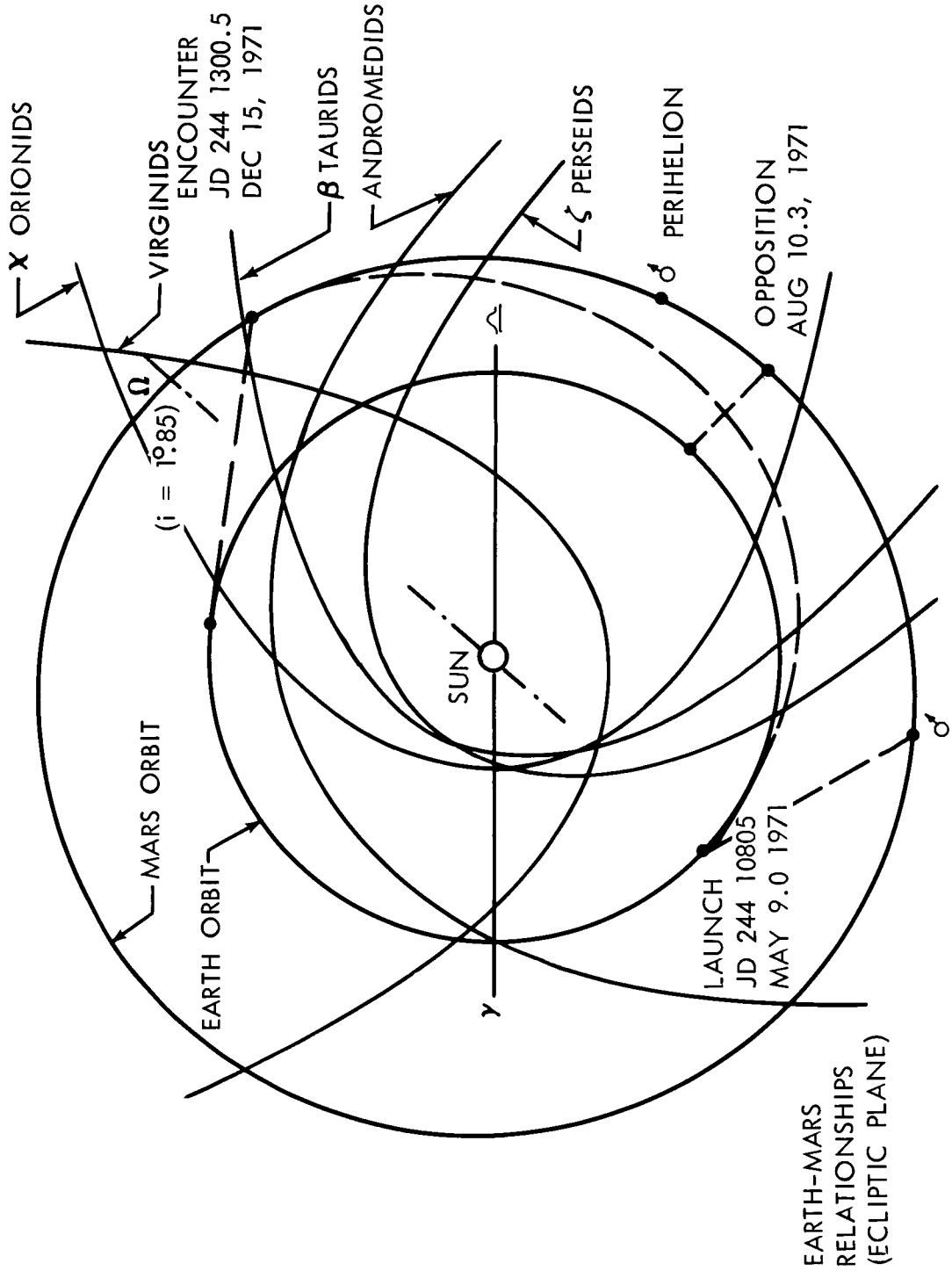

Figure 3-37: Meteoroid Streams

dispersion, have the highest probability of encountering Mars orbit. That this may happen in the case of the Taurids was predicted by Whipple in 1940.

The meteor orbits shown were calculated from the orbital elements and plotted in the plane of the ecliptic as if their inclinations were zero. With the low inclinations used, little error results. Orbits of other prominent streams with higher inclinations were not plotted because of the low probability of intersecting Mars orbit and to avoid congesting the plot.

Of the nine streams considered with inclinations ≤ 6.8 degrees (the several Taurid branches were assumed to be adequately represented by the β Taurids), five are shown as indicated below:

Streams	Inclination (degrees)	Longitude of Perihelion (degrees)
Andromedids	6.8	113
ξ Perseids	0	137
β Taurids	6	162
χ Orionids	0.9	185
Virginids	5	280

The other four (α Capricornids, N. ι Aquarids and two branches of the S. ι Aquarids) are not shown because their longitudes of perihelion are such (45 to 99 degrees) that there is less probability of their being encountered by Voyager in transit or at Mars, compared with those shown.

The design environment refers to asteroidal debris. Meteoroid showers are composed exclusively of cometary particles. If the shower component at Mars were double that observed at Earth, the effect would be to increase the average sporadic background by a factor of three. However, the estimated asteroidal component exceeds the average cometary contribution by more than a factor of 10. Even if the most intense streams known on Earth were present at Mars, the maximum increment would be a factor of 20 to 30 for a period of a few hours in the mass range above 10^{-2} gram. Therefore, unless the present estimate of the asteroidal contribution proves to be high by more than one order of magnitude, it is safe to neglect the effect of meteor showers.

3.3.5 Microbiological Considerations

In Section 3.3.3, above, analyses of the contaminating events lead to requirements for meeting the associated subconstraints. The necessary action for meeting the subconstraints regarding impact of unsterilized vehicles and vehicle sections has been indicated. Also, the method of satisfying the subconstraint on contamination of the Flight Capsule at separation has been referenced. However, only the requirements have been specified so far as the subconstraints relating to thrust exhaust products and meteoritic spalling are concerned.

These requirements cannot be met by trajectory alteration, since an orbit that adequately precludes contamination from these sources must remain so far from Mars as to be relatively useless for data purposes. Mechanical methods also fail, as containment of exhaust products is impractical and meteorites are unavoidable.

Thus, no alternative to sterilization of the thrusting systems is apparent; furthermore, at least a significant reduction of the expected number of viable organisms on certain spacecraft surfaces exposed to meteoritic spalling must be achieved. Conceptually, the surest way to realize an adequate solution to these problems is to sterilize the entire Flight Spacecraft. However, serious practical problems arise when this is contemplated. Nevertheless, some solution must be found. The most promising candidates are therefore examined and evaluated.

3.3.5.1 Specified Heat Sterilization

Complete spacecraft sterilization requires a terminal dry heat soak of 135°C for 24 hours, as specified in the JPL Specification XSO-30275-TST-A. This specification further requires that all spacecraft parts to be sterilized pass a qualification test of three cycles of dry heat soak at 145°C for 36 hours. The application of these procedures to the spacecraft imposes limitations on the selection of materials and parts for design.

The severity of these limitations is not apparent solely from the specifications, as qualification tests and terminal sterilization may require exterior temperatures considerably higher than 145°C, and exposure times far in excess of 36 hours in order to reach thermal isolation points. These higher outside temperatures increase the probability of heat damage. Therefore, parts and materials should be selected so that the required temperature is achieved throughout as rapidly as possible and with a minimum of thermal gradients.

Materials--Thermal treatments affect the mechanical properties of metals and thus put some restrictions on their allowable heat treatment. Nonmetals and electrical connectors are degraded, electrical solders may become soft and reactive, and electrical and optical properties of solar panel sections may be affected. Additional discussion is presented in Boeing Document D2-82734-1, Section 5.0.

Orbit Insertion Propulsion System--Materials can be selected for the case, liner, nozzle and thrust vector control that are compatible with the required heat treatment cycle. The principal concern is with the propellant, igniter, and the chemical and mechanical interaction of the reactive and inert portions of the engine. Limited data indicates that propellants and pyrotechnic devices can be made available which by themselves can withstand thermal sterilization. A detailed analysis and test program will be required to establish that the assembled system can withstand the thermal cycle. Foremost will be consideration of detonation during heat treatment from auto-ignition or catalytic reaction. Changes in the propellant due to shrinkage, mechanical flow due to softening and polymerization or depolymerization will have to be investigated. Separation of the propellant liner case from mechanical forces resulting from either chemical reaction or thermal expansion also require investigation. It will be required to trade long heat-up times, desired to minimize thermal stresses and to get the heat into the propellant, with shorter total time at elevated temperatures desired to minimize chemical reactions and interactions. There will also be a design trade between the use of high-efficiency thermal insulations around the case and engine to prevent overheating of the structure during firing and a requirement for good thermal paths during sterilization. Because of the possibility of explosive detonation, the sterilization heat treatment will have to be conducted in a remote area. Additional discussion of sterilization of solid propellants is presented in Section 4.3.5 of this document.

Orbit Trim Propulsion System--It is possible to construct the system from materials that are compatible with thermal sterilization. It will be necessary to develop and qualify squibs to meet the multiple cycle component qualification tests. Hydrazine can withstand thermal sterilization as shown in Figure 3-38. Tanks must be kept extremely clean to prevent catalytic decomposition. The entire system will have to be evaluated by analysis and tested to ensure that there are no deleterious chemical or mechanical interactions. Trades will be required between sterilization of the entire unit with the propellant in the tanks (desired for minimizing the probability of recontamination) and separate sterilization of subcomponents and propellant (desired for minimizing thermal and chemical reactions and interaction).

Experimental results reported by Godding and Lynch (Applied Microbiology, Volume 13, July 1964) indicate that Bacillus subtilis cannot live in either monomethyl or dimethyl hydrazine for extended periods. Considering these results, possible sporicidal properties of hydrazine should be investigated further.

Attitude Control System--The system can be designed with materials which are compatible with thermal sterilization. The comments made for orbit trim propulsion system with respect to analysis, test, qualification, and trades also apply to the attitude control system. Trades between system sterilization versus component sterilization involve considerations of the heavy tanks and valves required for the complete system sterilization and the possibility for contamination during component assembly.

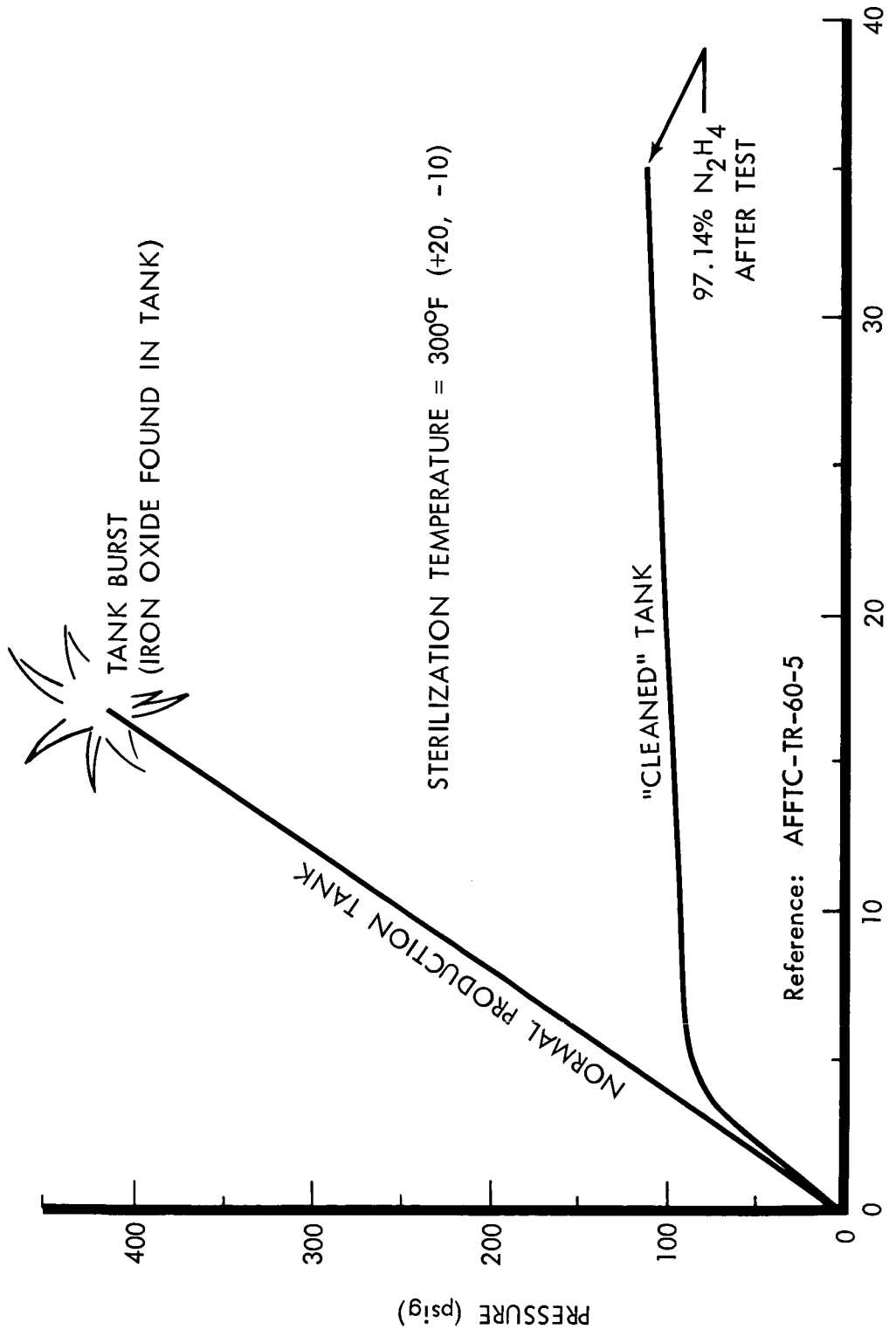

Figure 3-38: Effect Of Sterilization On Hydrazine (N_2H_4)

Electronic Parts and Components--Most problems anticipated with electronic components resulting from sterilization heat treatments appear to be resolvable. The capability of electronic parts to withstand heat sterilization without degradation is currently being investigated. JPL is leading this investigation with industry participation (JPL Specification ZPP-2010-SPL-A). Boeing and Philco Western Division Laboratories are currently testing electronic parts for JPL. The test programs consist of life tests (10,000 hours) after exposure to the sterilization heat cycle (maximum 145°C temperature, six cycles). Detailed discussions concerning electronic component sterilization are presented in Autonetics Document, T5-1161.1/3061 A, B, and C; and Philco Document WDL-2531.

Voyager typical parts and potential materials were reviewed considering the thermal sterilization compatibility test requirements. The following comments are made on parts considered to be problems.

1) Transponder

   a) Resistors--Carbon resistors have a storage temperature of 150°C.

   b) Capacitors--Tantalum foil capacitors have a storage temperature of 125°C. Temperatures in excess of 125°C would decrease the life and reliability of the capacitors. Ceramic feed-through and standoff capacitors have epoxy and seals and are rated at 125°C. Temperatures of 145 $\pm$ 2°C would affect the seals. Mica feed-through and standoff capacitors which are hermetically sealed will withstand 145°C. Ceramic capacitors which have epoxy-or wax-impregnated phenolic resin coatings are rated at 125°C. When exposed to 145 $\pm$ 2°C, the coating will tend to

degenerate. Porcelain or glass capacitors can be used and will withstand 145°C.

c) Chokes and Coils--The chokes are rated at a maximum of 125°C. The insulation on the wire and the molding material will not withstand a temperature of 145 ±2°C. It is possible to obtain chokes and coils with an insulation that will withstand higher temperatures.

d) Connectors--Connectors having insert insulation of glass-filled dially phthallate, silicon rubber, teflon, or glass will withstand 145 ±2°C.

2) Recorder

a) Resistors and Capacitors--See transponder.

b) Tape--Critical above 125°C.

c) Transformers--Transformers can be obtained with Type H insulation which would allow the temperature range to 180°C.

d) Motor--The motor should be designed with Class H insulation.

3) Telemetry Processor

a) Capacitors--See transponder--ceramic capacitor.

b) Crystal--The specification for the crystal would have to specify a storage temperature in excess of 145 ±2°C, although stability of the crystal characteristics after 145°C storage is not well established.

4) Tunnel Diode Preamplifier

a) Ferrites--The specification should specify the storage temperature in excess of 145°C. The curie temperature of ferrites varies between 100°C and 500°C.

Preliminary investigation of the telecommunications components, parts, and materials revealed the following critical areas in order of criticality: (1) magnetic tapes; (2) magnetics, i.e., transformers, inductors, and coils; (3) encapsulauts, i.e., organic plastics; and (4) capacitors.

For the electromechanical and electrooptical components, heat soak will cause failure of the cadmium sulphide cell used in the Canopus trackers and the Sun sensors, will cause failure of the indium solder used in the Autonetics electromagnetic accelerometer, and will cause reliability degradation of the permanent magnet in the electromagnetic accelerometer. These sensitive components (which are all in the attitude reference module) must be removed from the spacecraft during heat sterilization and must either be manufactured in a sterile fashion or sterilized by other means.

Silver Cadmium Batteries--Thermal heat treatment and qualification of the silver cadmium batteries require further study. The plastic cell case is incapable of sustaining the sterilization temperature. If a metal can is used, welding of the lids creates magnetic characteristics. Currently, the separator within the cell is a cellulose material that prevents silver migration. This material is severely attacked by the electrolyte at elevated temperatures. To obtain sterilizable batteries, new materials must be developed and tested. Additional sterilization in selecting the spacecraft battery are discussed in Section 4.2 of this document.

3.3.5.2 Alternate Sterilization Considerations

Spacecraft sterilization as discussed above imposes severe design and material constraints on the Flight Spacecraft. A large lead time is necessary to develop adequate materials and methods so as to meet these constraints. This suggests that serious consideration be given to establishing alternate sterilization requirements that will reduce the severity of the constraints.

Time-Temperature Trade Technique--A reduction in the temperature required for the heat cycles will increase the variety of materials and parts that can be considered for use in the design of the spacecraft without reducing reliability. Assuming a spacecraft microbial load of 10^9 microorganisms and a "D" value (see Figure 3-39) of approximately 290 minutes at 125°C, an exposure time of 63 hours meets the same 10^{-4} probability constraint as does the 135°C/24 hours cycle. Similarly, with "D" values for 120°C, an exposure time of 108 hours meets the 10^{-4} probability constraint.

The longer time periods required for heat soaks at lower temperatures can be compensated for if the come-up heating and cooling periods are shortened. Heating and cooling time may be reduced by designing thermal pathways into the vehicle; however, these will alter the thermal balance and the environmental control of the spacecraft and could prove disadvantageous.

These considerations do not alleviate the problem and require time for additional analysis and examination.

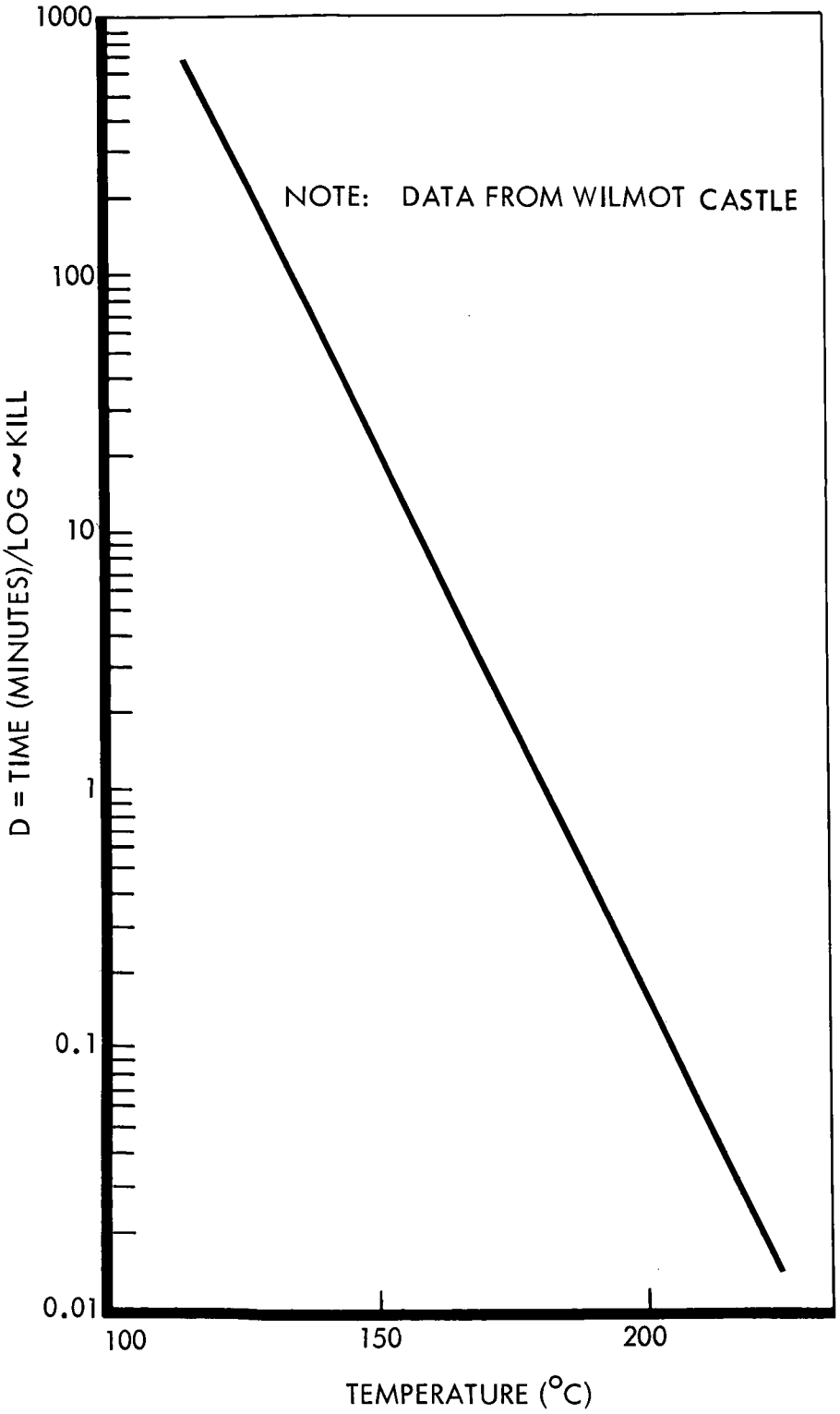

Figure 3-39: Dry Heat Soil Sterilization (120→160°C)

Parts Sterilization and Sterile Assembly Techniques--The sterilization of parts and the use of aseptic assembly techniques can be considered. Although this technique has been useful in some commercial enterprises and academic environments, the lack of sufficient data from aerospace manufacturing operations precludes a recommendation at this time. Therefore this technique will require additional study.

3.3.5.3 Spacecraft Decontamination

Several methods are available to decontaminate spacecraft, thereby reducing microbial loading. These methods include ethylene-oxide treatments for surface decontamination, radiation exposures, lower temperature heat treatment and the use of clean rooms to maintain low contamination levels during manufacture.

Ethylene Oxide Treatment (ETO)--The specified ETO treatment (JPL spec. GMO-50198-ETS) is exposure to a gaseous mixture of 12-percent ETO and 88-percent Freon 12 (or Genetron 12) at 35% relative humidity. Parts and materials are to be qualified to one of three levels, capable of withstanding 48 hours exposure (24 hours at 24°C and 24 hours at 40°C), capable of withstanding 24 hours at 24°C, and capable of withstanding 24 hours at 40°C.

Material and handling problems are associated with the use of ethylene oxide. Special facilities and safety regulations must be instituted to protect the personnel that are associated with the gas, since it is both toxic and flammable. Its use requires closed containers and complete purging of air before and after exposure.

ETO reacts to some extent with most materials. The reaction is not well defined, especially for sensitive elements where trace contamination can cause long-range difficult to detect effects. ETO is polymerized by oxides and some metallic and organic surfaces to form a film or residue. This residue can degrade components (especially optical and thermal control surfaces) directly or by subsequent reaction during exposure to the operating environment. ETO must be excluded from all propulsion and gas systems since it is not only reactive, but any polymerized material would foul valves and lines. Reaction products, though not destructive to prime components, can migrate to sensitive elements such as electronics where they may react or cause deposits with late reactions. Trapped ETO or polymerized products would promote incompatible material reactions.

In general, use of ETO would require an extensive program to evaluate material and component reactions. The probability that unpredicted reactions might occur is high. It is recommended, therefore, that ETO be used as a surface decontaminant only when absolutely necessary.

Radiation--Ionizing radiation has been considered for decontaminating the spacecraft. Radiation kill of microorganisms may be described by an exponential curve similar to that describing thermal kill; however, the doses required to ensure death are so high that damage would likely occur to the spacecraft components. This method of decontamination does not, therefore, appear to be desirable at the present time.

Heat Treatment--The application of heat soak techniques to achieve decontamination can be readily applied during manufacturing operations by

using a chart such as that in Figure 3-39. The orders-of-magnitude reduction desired can be multiplied by the "D" value in exposure time, thus, reaching the desired level of contamination.

Any desired level of decontamination and probability can be achieved by selecting applicable temperatures and exposure times.

Clean Room Manufacture--A major factor that dictates the time required to sterilize or decontaminate a space vehicle is the total microbial loading that is present on that vehicle. Figure 3-40 illustrates the concept that death of a microbial population can be plotted as a logarithmic function. This type of curve is observed when death is caused by either heat or radiation. It can be seen that the lower the microbial loading, the shorter is the time required to sterilize or decontaminate.

The use of clean rooms may be one way of decreasing the microbial loads on spacecraft during manufacturing. Laboratory investigations have been conducted in Boeing clean rooms to determine the number of microorganisms present on surfaces and in the air. The results of these studies demonstrated a significant decrease in the number of organisms in the clean room areas over that normally found in manufacturing areas.

3.3.5.4 Maintenance of Decontaminated or Sterilized Condition

Maintenance of the reduced bacterial load of the spacecraft through assembly and launch will require continuing study. Definition and delineation of operational techniques and required equipment must include consideration of all possible sources of recontamination.

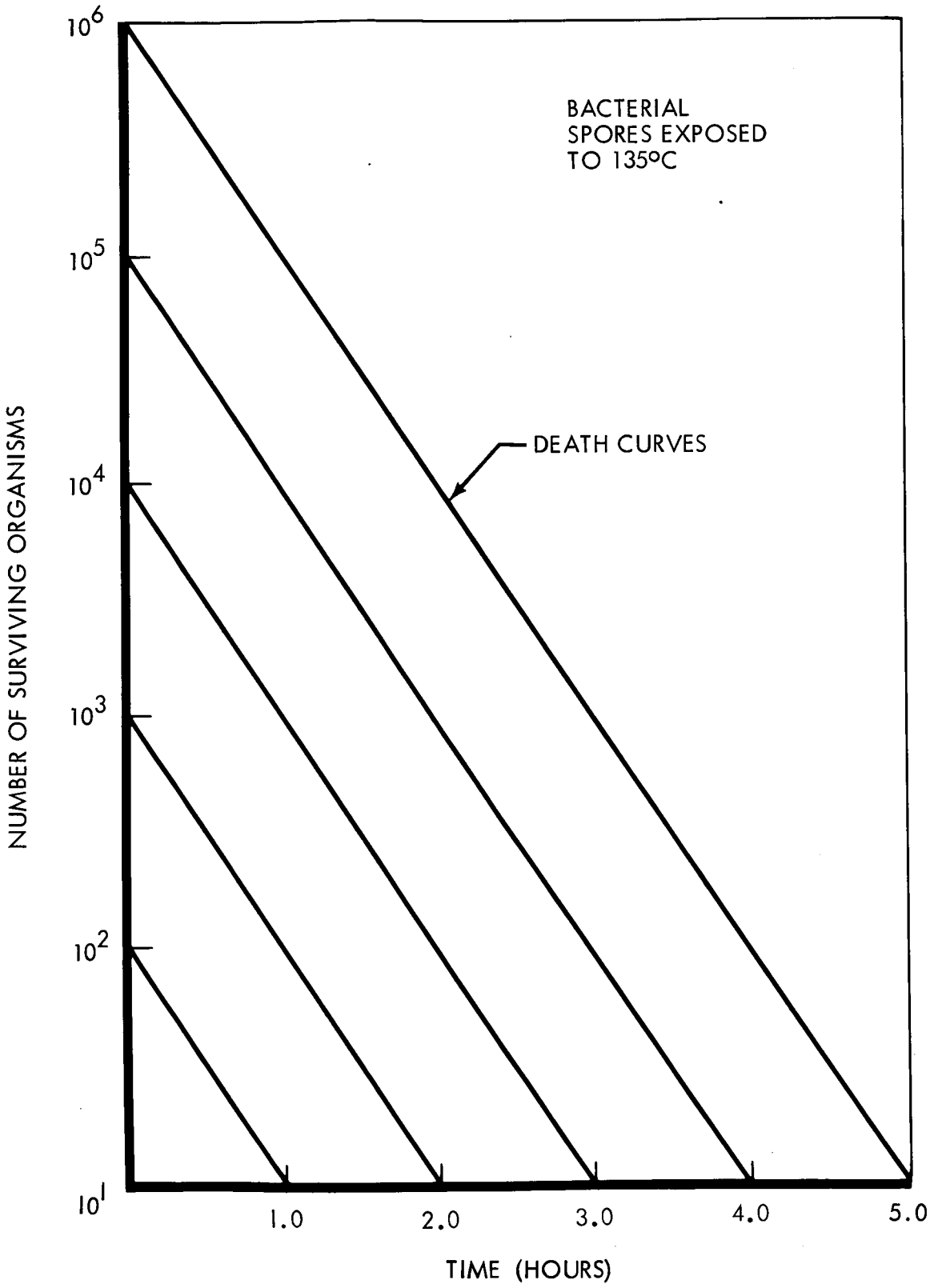

Figure 3-40: Typical Microbial Thermal Death Curve

Throughout manufacturing, storage, handling, and transportation, a level of cleanliness consistent with the decontamination requirements selected will be necessary to keep the recontamination potential to a minimum. If a selected parts sterilization approach is used, special handling and assembly techniques will have to be developed to retain sterility. If a terminal heat treatment of the spacecraft is used, the problems associated with transportation to the pad, assembly on the pad, and maintenance of the decontaminated condition on the pad will have to be defined and resolved. As an alternate consideration, it may prove advantageous not to decontaminate the spacecraft until assembled on the pad.

Considerations for decontamination of the shroud inner surface indicates the necessity of a closure barrier during transportation to the pad and installation over the spacecraft, in addition to the requirement for a barrier between spacecraft and Centaur. The provision of sterile conditioned air around the entire spacecraft and within the shroud after installation on the Centaur is another requirement to be further evaluated.

Sealing the shroud after installation has been considered, but it is recognized that this approach would create a pressure condition after launch. Other problems related to maintenance of the decontaminated condition of the spacecraft include contamination from the shroud exterior surface during launch, shroud separation after launch, booster exhaust products, and outgasing of the various subsystem electronic packages. Particularly during boost, the outflow of gas from the internal components may carry biological contamination to the decontaminated surfaces. Thermal

insulations and partially sealed electronic packages will continue to out-gas for several minutes after boost termination. The amount of contamination can be reduced by controlled venting of these gases.

The operational problems associated with maintaining the decontaminated condition require additional study and evaluation before they can be fully incorporated into the probability analysis of the mission.

3.3.6 Conclusions

The analyses presented in this section have indicated that reduction in the microbial load of the Flight Spacecraft appears necessary to comply with the planetary quarantine constraint. This conclusion has been confirmed by the "fault-tree" failure-mode analysis presented in Boeing Document D2-82724-1, Section 3.7.

Complete sterilization of the spacecraft has definite advantages from the high resolution data gathering standpoint and from the value to subsequent missions. However, state-of-the-art problems exist for certain electronic components and subsystems and with certain materials as to their compatibility with the heat sterilization (135°C for 24 hours) and ethylene oxide decontamination treatments. Additional problems associated with maintenance of sterility during subsequent handling checkout and launch operations are also recognized.

Selected part sterilization of only those portions of the spacecraft, which appear to be the offenders as far as Mars contamination is concerned,

may be a tenable answer to meeting the planetary quarantine constraint. However, this approach gives rise to unique problems. These include recontamination at shroud separation and outgassing of nonsterile components. In addition, this approach also has the same problems of handling after treatment as those mentioned for the complete sterilization approach.

Further study is needed to refine the analyses relative to Mars contamination probabilities from propulsion and attitude control systems emission and from ejecta from meteoroid impace. In addition, analytical and laboratory studies of system sensitivity to probability allocations, meteoroid impace occurrence and spalling effects, initial microbial loading on spacecraft, clean room applications to reduce the initial microbial load and microbial planetary entry dynamics are needed. Also, further investigation and understanding of operational problems and equipment handling techniques associated with recontamination are required before accurate microbial loading limits can be established. Only then can correct heat treatments be specified that will reduce the microbial load on the spacecraft to a level that will satisfy the appropriate probability allocation.

As a result the preferred spacecraft concept for compliance with the planetary quarantine constraint allocation at this time includes only heat sterilization of all flight spacecraft propulsion devices. Refinement of the analyses and further consideration of the operational problems are necessary before specific constraints should be imposed on spacecraft surfaces and protruberances subject to meteoroid impact.

CONTENTS

4.0 ALTERNATE DESIGNS CONSIDERED- FLIGHT SPACECRAFT AND HARDWARE SUBSYSTEMS

Alternate designs considered for each subsystem and the reasons for selection of each of the preferred designs are given in this section. The preferred subsystems are described in Volume A. The primary considerations in the choice of a preferred subsystem were reliability, safety, performance, weight, state-of-development, power requirements, and versatility in application to various missions.

The communications studies include (1) a brief consideration of optical communications using lasers and (2) consideration of radio communications in terms of effective radiated power, modulation techniques, and state-of-development of various items of equipment. Study of electrical power sources included an investigation of the status of radioisotope power converters and detailed work on solar panel design, batteries, and electrical power conditioning and distribution systems for solar photovoltaic systems.

Propulsion subsystems condisered included both mono- and bipropellant engines for midcourse correction, for thrust vector control during orbit insertion, and for orbit trim. Studies of propulsion for orbit insertion considered liquid mono- and bipropellant and solid propellant engines of various configurations. Engineering mechanics involved consideration of various means of thermal control associated with different spacecraft configurations; the choice of a structural concept consistent with the desire to minimize weight and yet provide good equipment assessibility and thermal control; the study of mechanisms from the standpoint of reliability, weight, and state-of-development; and the investigation of methods for maximizing the reliability and safety features of pyrotechnic equipment.

Review of sensors for the Voyager Spacecraft included consideration of a number of types of instruments in order to provide a redundant system with elements having different failure modes. Consideration of the uto-pilot and reaction control equipment was based heavily on reliability and space-proven development status.

The design of a central computer and sequencer was evaluated in terms of the following three concepts: (1) a fixed-wired timer-oriented unit; (2) a special purpose memory-oriented computer; and (3) a general purpose memory-oriented computer. These were evaluated in terms of reliability, development status, and versatility, and particular attention was given to equipment of the type based on the JPL Mariner designed and tested for the NASA-Langley Lunar Orbiter.

4.1 TELECOMMUNICATIONS

Summary--The communication system selected for Voyager is a fully redundant conventional S-band system using coded data modulation, a 50-watt traveling-wave tube (TWT), and a 8' x 12' paraboloidal high-gain antenna. This coupled with the DSIF 210-foot ground antenna, provides a capability for real-time transmission of high-rate scientific data (48,000 bits per second) for approximately 3 months after encounter in the nominal case.

Two tape recorders allow storage of a total of 2×10^8 bits for those periods when Earth transmission is prevented by occultation, or when link margins will not support high-rate transmission.

Exceptional system versatility is supplied by the wide variety of operational modes available. A low-noise tunnel diode preamplifier in the radio subsystem allows reception of ground commands through the omnidirectional low-gain antenna for the entire mission if the 100 KW DSIF transmitter is used, thus allowing for corrective action when the link through the high-gain antenna is not operational for any reason.

The possible alternatives for a deep-space communications link in the 1969-71 period are optical systems and conventional microwave systems. An examination of the state of the art for both approaches results in the following conclusions:

1) a) A reliable optical communications system for this time period can provide only a 50 kilobits per second data rate at interplanetary ranges because of limitations in laser power output. Higher power outputs are available only at considerable sacrifice in reliability.

   b) A microwave system can provide approximately this same data using available technology.

2) The optical system will weigh from 700 to 1000 pounds as compared to less than 300 pounds for the microwave system.

3) The optical system will require development of a completely new global network of ground stations. In addition, an extensive development and test program will be required on all elements of the space vehicle system.

An S-band microwave system is recommended for the initial Voyager flights with further study of an optical system for 1975 or later.

The nominal output data rate from the science data automation system is 50,000 bits per second from the planetary scan instruments. It is desirable to match the transmission rate of the telecommunications system to the data-output rate of the science system to provide real time data return to earth.

To accomplish this requires maximum use of the microwave technology that will be available in 1966.

There are essentially four ways to increase the data-transmission rate of a microwave data link:

1) Use more efficient modulation techniques;

2) Increase transmitted power;

3) Increase the combined transmitting and receiving antenna gain;

4) Decrease the receiver noise temperature.

By effective use of all four approaches, a data rate of approximately 50,000 bits per second can be achieved for at least the early portion of the Voyager '71 mission.

A study of possible modulation techniques reveals that a gain of approximately 2 db over the current Mariner system can be achieved by the use of a (16,5), bi-orthogonal code for the data on a PSK/PM coherent link. Consideration was given to more expanded codes. However, the use of a (32,6) or higher order code provides an additional gain of not more than 1 db at a cost of, (1) greatly increased complexity, particularly in ground equipment; and (2) a transmission bandwidth increase of two or more.

The power output from space vehicle transmitters has been limited to about 10 watts by available power tubes on past and current probes. A technology survey indicates that 50 to 100-watt tubes can be developed to the prototype stage in 1966. This is true of both TWT's and electrostatically focused klystrons. Other devices (triodes, amplitrons, solid-state amplifiers) appear to have limitations in power output, reliability, or efficiency in this time period. A 50-watt TWT was

selected as the preferred design for the following reasons:

1) It represents the greatest extrapolation to a new design from existing tubes that is consistent with the policy of engineering conservatism adopted for the Voyager program.

2) Increasing the transmitter power level from 50 to 100 watts would result in a Spacecraft weight penalty of approximately 200 lbs. For the additional electrical power and thermal control.

The limitations in payload weight have effectively limited space vehicle and antenna size on current space probes. The use of the Saturn 1B/Centaur booster for Voyager permits an increase in antenna size up to the 8- to 12-foot region. Although this requires tighter vehicle attitude control and precise antenna pointing, these do not appear to be limiting conditions. It is believed that a gain of approximately 34 db can be realized by an 8- by 12-foot paraboloid. This is the largest rigid, nonsegmented,nonfolding antenna that can be accommodated with the Boeing-designed Voyager Spacecraft inside the launching shroud. Larger unfurlable antennas were considered but were rejected primarily on the basis of the complexity and potential unreliability of the unfurling or erecting mechanisms. Also, larger diameter antennas create significant reaction-control-system penalties because of the tighter limit cycle required to maintain total pointing tolerances.

Current DSIF improvement programs will take care of the remaining items. The planned 210-foot antennas will provide an additional 8 db of gain. An additional 2 to 3 db in system sensitivity is provided by the lower noise temperature of these antennas.

Other system configuration problems examined in detail include receiver configuration and data-storage techniques. Inclusion of a low-noise preamplifier in the receiver provides a command reception capability on the low-gain antenna at encounter ranges in conjunction with 10-kilowatt ground transmitter and to end-of-mission with a 100-kilowatt transmitter thus increasing reliability of command reception and mission success probability. Parametric, tunnel diode, transistor and TWT preamplifiers were examined. The tunnel diode was selected primarily on the basis of highest predicted reliability. It also ranked favorably in terms of weight and cost.

Although tape recorders present a reliability problem, they still provide the best choice for large-capacity data storage. Achievement of a real-time capability for at least part of the mission after encounter decreases absolute dependence on recorder operation. They will still be used for backup in this mode and as a prime element in lower rate modes.

The logical procedure followed to develop the preferred configuration is illustrated in Figure 4.1-1.

To summarize, a spacecraft communication system using a 50-watt power amplifier, an antenna approximately 8 feet by 12 feet and coded data modulation, operating with the 210-foot antennas at the Deep Space Stations, can provide a 48,000-bit per second data rate for a period from 10 days to 3 months after Mars encounter, depending on whether system tolerances are at worst case or nominal conditions.

4.1.0 Applicable Documents

1. "The Deep Space Network," JPL, EPD 283, July 1965

2. NASA/Langley Letter, Ref. B/L-97, from T. N. Barton to The Boeing Company, dated October 22, 1964, ATTN: R. J. Helberg, Subject: "NASA Contract NAS1-3800-Lunar Orbiter Project Communications Subsystem, DSIF 10-Mc IF Characteristics"

3. Martin, B. D., "The Mariner Planetary Communication System," Jet Propulsion Laboratory, Report No. 32-85, May 15, 1961

4. Springett, J. C., "Telemetry and Command Techniques for Planetary Spacecraft," Technical Report No. 32-495, January 15, 1965

5. Viterbi, A. J., "On Coded Phase-Coherent Communications," IRE Transactions, Vol. SET-7, pp. 3, March 1961

6. Nutall, A. H., "Error Probabilities in Equi-correlated M-ary Signals under Phase-Coherent and Phase-Incoherent Reception," IRE Transaction Vol. IT-8, pp. 305, July 1962

7. "Mars Mission Communication Analysis," WDL-TR-2531, Philco Western Development Laboratories, Palo Alto, California, July 1965

8. "Mars Mission Communication Analysis," WDL-TR-2531, Philco Western Development Laboratories, Palo Alto, California, July 1965

9. Peterson, W. W., "Error-Correcting Codes," MIT-WILEY, 1961

10. Mitchell, M. E., "Simple Decoders and Correlators for Cyclic Error-Correcting Codes," IRE Transactions, Vol. CS-10, pp. 284, September 1962

11. "Voyager Design Study," GE Document 63 SD801, Part 1, Volume III, pp. 1-162, General Electric Co., October 15, 1963

12. Wozencraft, J. M. and G. Reiffen, Sequential Decoding, Technology Press and John Wiley, N.Y., 1961

13. Stiffler, J. J., "Space Programs Summary," No. 37-26, Vol. IV, Jet Propulsion Laboratory, April 30, 1964, p. 243

14. Davenport, W. B., and W. L. Root, Random Signals and Noise, McGraw-Hill, pp. 266, 1958

15. Springett, J. C., "Telemetry and Command Techniques for Planetary Spacecraft," Technical Report No. 32-495, Jet Propulsion Laboratory

16. Stiffler, J. J., "Synchronization Methods for Block Codes," IRE Transactions, Vol. II-8, pp. 525, September 1962

17. Jaffe, R. M., "Digilock Telemetry System for the Air Force Special Weapons Center's Blue Scout Jr.," IRE Transactions, Vol. Set-8, pp. 44, March 1962

18. EPD 283, "The Deep Space Network," Jet Propulsion Laboratory, July 1965

19. GMS-50109-DSN-A, "Design Specification, Telecommunications Development, GSDS Command System, Ground Subsystem (Command Verification Equipment)," JPL, October 1964

20. Preliminary Voyager '71 Mission Specification, JPL Project Document No. 45, JPL, May 1965

21. Davenport, W. B., Jr., "Signal to Noise Ratios in Band Pass Limiters," Journal of Applied Physics, Vol. 24, No. 6, June 1953

22. Springett, J. C., "Telemetry and Command Techniques for Planetary Spacecraft," JPL-T.R. No. 32-49J, January 15, 1965

23. Viterbi, A. J., "Phase-locked Loop Dynamics in the Presence of Noise by Fokker-Planck Techniques," Proc. IRE, December 1963, pp. 1737

24. Gilchrist, C. E., SPS 37-16, Vol. IV, August 1962, pp. 87

25. (tunnel diode amplifier) Micro-State Electronics Corp., "Proposal on Low Noise Preamplifier," P1-85-A

26. (tunnel diode amplifier) International Microwave Corp., "Proposal on Tunnel Diode Amplifiers," 70311

27. (TWTA - File No. Watkins-Johnson 65-P-3106), Technical Discussion to Modify the WJ-269 or WJ-295

28. (Endless Loop Transports), Various Telephone Conversations

29. Reel-to-Reel Transports Kinelogic Corp., "High Capacity Space Borne Tape Transport"

30. Raymond Industries, "Proposal for High Capacity Magnetic Tape Recorder"

31. Traveling-Wave Tube Amplifier - RCA Microwave & PWR Tube Div., "The Design and Development of 100 Watt TWT," IP 345 - Also Hughes Microwave Tube Division, "Proposal for Philco Corp.," R-5341

32. Bodner, M. G., et al., "The Satellite TWT," BSTJ, July 1963, pp. 17030-17048

33. (Electrostatically Focused Klystron Amplifier), Eitel-McCullough Inc., "Technical Proposal for a 50 Watt Power Amplifier" ESFK

34. The Amplitron Raytheon Company, "Development of a 70 Watt S-Band Amplitron," PT 567 & PRP 1873

35. Triod Amplifier

36. Boeing Report D5-13122, "Study to Determine Feasibility of Designing a 20 Watt UHF Solid State Transmitter"

37. Boeing Report D2-90775-1, "Analysis of an Optical Communication System for Mars Exploration"

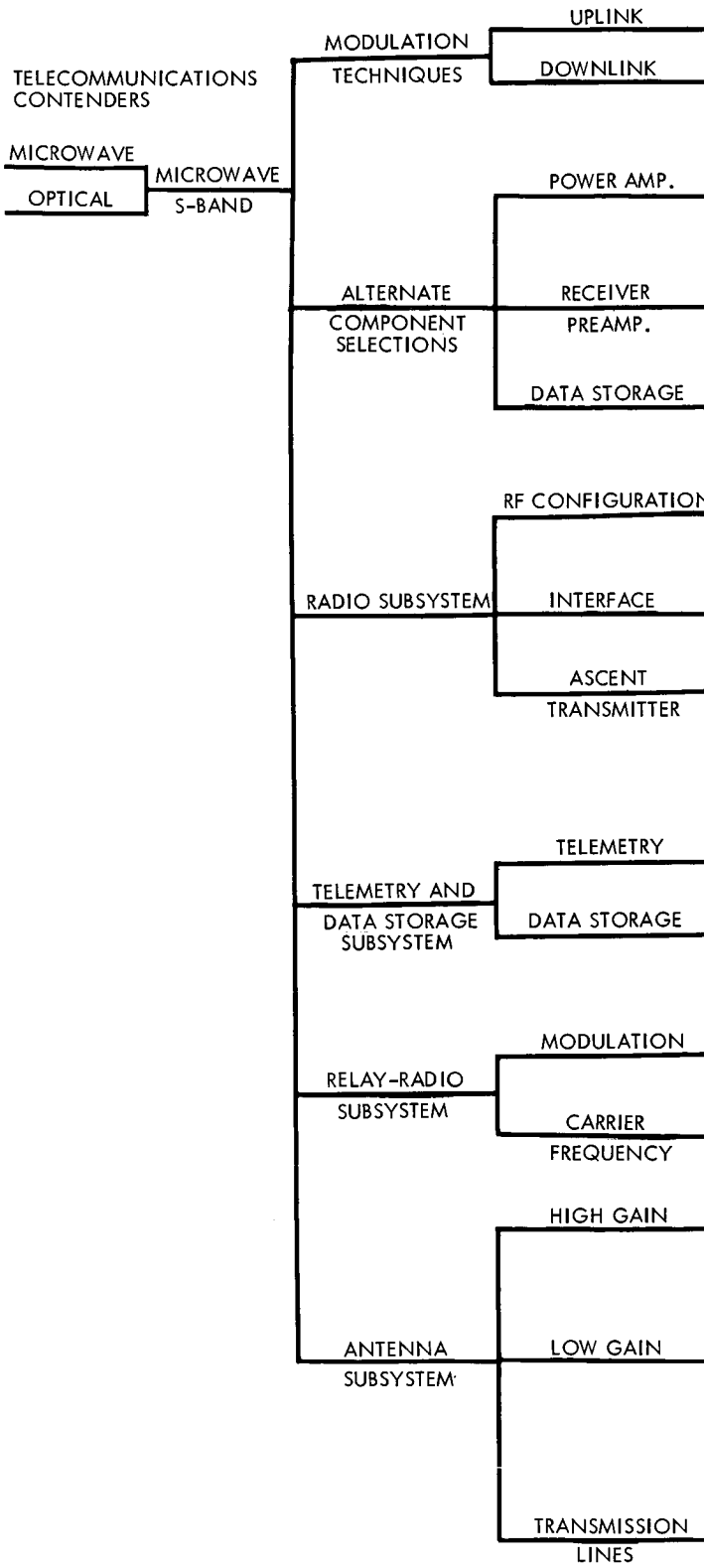
TELECOMMUNICATIONS CONTENDERS
MICROWAVE
OPTICAL
MICROWAVE
S-BAND
MODULATION TECHNIQUES
UPLINK
DOWNLINK
ALTERNATE COMPONENT SELECTIONS
POWER AMP.
RECEIVER PREAMP.
DATA STORAGE
RADIO SUBSYSTEM
RF CONFIGURATION
INTERFACE
ASCENT TRANSMITTER
TELEMETRY AND DATA STORAGE SUBSYSTEM
TELEMETRY
DATA STORAGE
RELAY-RADIO SUBSYSTEM
MODULATION
CARRIER FREQUENCY
ANTENNA SUBSYSTEM
HIGH GAIN
LOW GAIN
TRANSMISSION LINES

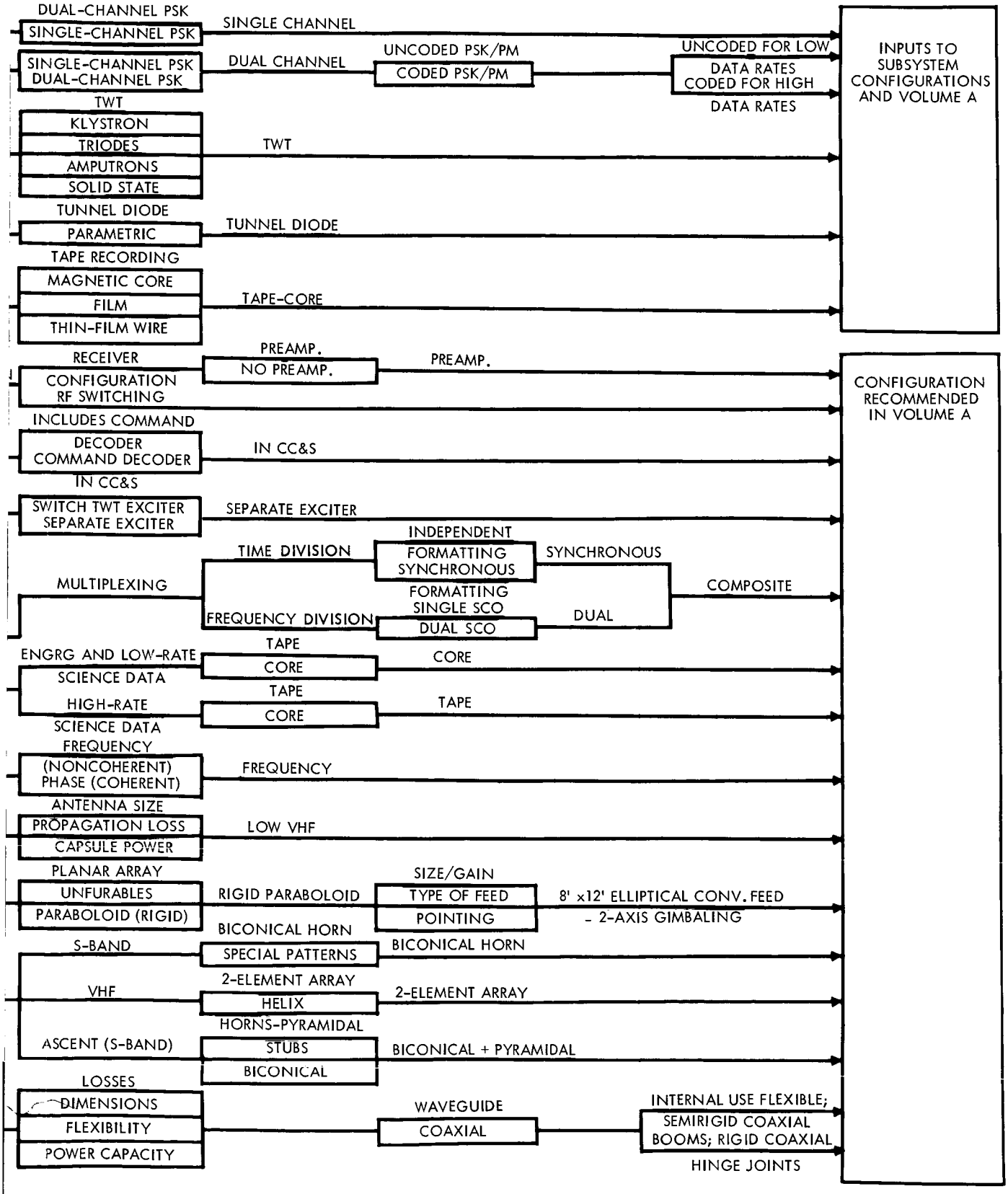

Figure 4.1-1: Telecommunications Logic Diagram

4.1.1 Alternate Telecommunications Subsystems Considered

4.1.1.1 Descriptions

Optical Telecommunications Subsystem--At the present time optical communications represents the only feasible alternative to a microwave link for deep-space exploration. The optical technologies involved have now developed to the point that implementation of a deep-space optical link within the next 10 years appears feasible. Therefore, it is necessary to examine the potential advantages, if any, of such a system as compared to a conventional microwave link and to weigh these advantages against the technological development problems associated with optical communications.

The elements of a two-way deep-space optical communications system are as follows. The spaceborne unit consists of a large Cassegrainian optical system, sensors for receiving Earth-to-vehicle communications and tracking signals, a gas-phase laser transmitter and electro-optical modulator, and a laser-beam deflector. The ground station consists of a large segmented mirror coupled to a tracking receiver. An array of electronically coupled small mirrors also has some promise. A CW laser beacon is slaved to the tracking receiver and pointed in the direction of the space vehicle.

Microwave Telecommunications Subsystem--Microwave links are the accepted standard for current and planned deep-space probe communications. The

required hardware has reached a well-advanced stage of development and production. In particular, a very elaborate ground-station complex has been developed on a global basis and is fully operational. The general characteristics and configuration of a microwave link are well known. The most significant difference from an optical system is the substitution of a microwave power amplifier and receiver for the laser transmitter and optical detector.

4.1.1.2 Competing Characteristics'

Reliability--The reliability of an optical system is determined by the laser transmitter at present. For a system based on 1966 state-of-the art freeze, gas-phase lasers (He-Ne) exist that are highly stable with operational lifetimes currently in excess of 1 year. However, their power output is low (0.01 to 0.1 watt), effectively limiting the bandwidth of the system to, at most, 50 kilobits.

In comparison to the optical system, the microwave power amplifier is the critical reliability element. Traveling-wave tubes have demonstrated lifetimes in excess of 30,000 hours and have estimated MTBF's up to 150,000 hours. Data-handling portions of the two systems will be comparable in complexity and reliability.

Data Rate--An optical communication system can offer a data rate of 50 kilobits per second at distances covering the whole 1971 mission profile with mid-1966 state-of-the-art components. As noted in the previous section, this limitation is primarily a function of the laser transmitter.

The data rate of a microwave system is limited primarily by the transmitted power, combined transmitting and receiving antenna gain, and by the effective receiving-noise temperature. The receiving station capabilities are reaching practical limits with low-noise preamplifiers and the development of 210-foot-diameter receiving antennas. Development of higher power TWT's and other power tubes suitable for spaceborne use, together with larger vehicle antennas made possible by increased total payload weight, promise much higher data than achieved on current probes. For a 1971 mission using 1966 technology, data rates approaching 50 kilobits per second can be achieved. In this time period, the optical system does not appear to provide a significant data-rate advantantage.

Weight--The total weight of the spaceborne optical subsystem is high, principally because of the structure required to support the optical system and because of the weight of the Sun shield. It is difficult to establish an exact weight, but a reasonable estimate based on previous Orbiting Astronomical Observatory studies and on the Optical Technology Study places the total weight of the spaceborne subsystem (excluding data storage and encoding equipment) at 700 to 1000 pounds.

Microwave system weight varies significantly as a function of the amount of redundancy incorporated to increase realiability. A fully redundant system operating in the 20- to 50-watt power output range can be mechanized for a 1969-1971 period for a weight of less than 300 pounds including all antennas and data-storage equipment. This is a three to one advantage over the optical system in this time period.

Development Status--The hardware components necessary for implementation of an optical system with a 50-kilobit per second data rate should be available by mid-1966 from current R & D programs. However, plans for development and test of a spaceborne system cover a much longer time scale, which is not compatible with the schedule for Voyager system development.

An optical system will also require development of a number (probably 8 to 10) ground-based receiving stations to provide approximate all-weather capability. The most significant factor here with respect to a 1971 mission is that the system is not compatible with the DSIF.

A global network of S-band ground stations for deep-space communication (the DSIF) is well developed and in full operation. Additional stations and improvements to existing stations are already under development. Thus, no major new development is required to support Voyager missions.

Complete microwave telecommunications systems have been space-proven on numerous space programs, including the current Mariner IV flight. Areas requiring further development are as follows:

1) Power amplifiers -- devices to operate reliability at power outputs of 20 to 50 watts are required:
2) Data recorders improved both in reliability and total storage capacity are required:
3) Larger high-gain, steerable antennas must be developed to maximize data rates.

A technology survey reveals that the above problems will be solved in the immediate future by existing or planned programs.

4.1.1.3 Logic of Selection

The use of a microwave system for the 1971 Voyager mission is dictated by the following considerations:

1) An optical system requires the development of a complete new ground station network.

2) A reliable optical system using 1966 technology imposes a weight penalty of several hundred pounds but does not offer a signficant improvement in data rate over a microwave system. An extensive development and test program would be required on all elements of the system.

3) A minimum of new development is required for a high-data-rate microwave system. The technology for this development is much more advanced than it is for the optical system.

It is recommended that further studies be carried out on the development of a deep-space optical communication system for Voyager missions in the post-1975 time period.

For additional data on optical system characteristics, performance and development status, see Boeing Document D2-90775-1 "Analysis of An Optical Communications System for Mars Exploration."

4.1.2 Data-Link Modulation, Coding and Synchronization Techniques

This section discusses the various modulation, synchronization and coding techniques investigated for application to the Voyager 1971

spacecraft-to-Earth telemetry data link. Of primary interest has been the selection of carrier modulation parameters, subcarrier frequencies, subcarrier modulation parameters, data bit rates, coding parameters, and the evaluation of performance measures for the various alternate approaches considered. The primary goal in selection of specific parameters has been to maximize the quantity of data that can be successfully acquired by the Deep Space Network (DSN) during the nominal 6 month planetary encounter.

4.1.2.1 Telemetry System Requirements

Functional Requirements and Objectives--These include:

- Accept and store engineering and scinetific data from the Flight Capsule and Flight Spacecraft.
- Multiplex, encode, and transmit engineering and cruise science data at bit rates from 400 to 20 bits per second consistent with available link performance.
- During Mars Orbit, record video data during periapsis pass and readout during remaining orbit period at rates up to 8000 bits per second, consistent with available link performance.
- During early Mars orbit, transmit real-time video data at a 48,000 bits per second (optional).
- During cruise and encounter, provide an emergency low-rate data mode to extend the communication range of the system.

Design Constraints--Spacecraft-radiated signals must be compatible with the DSN equipments and techniques as specified in EPD-283 as follows:

1) Four switch-selectable bandwidths are provided in the receiver telemetry channel. Filters providing these bandwidths have a center frequency of 10 Mc with amplitude characteristics as follows:

BANDWIDTH	
1 db	3 db
3.3 Mc	6.0 Mc [1]
420 kc	600 kc
20 kc	30 kc
4.5 kc	7 kc

2) An IF output at 50 Mc with a 10-Mc bandwidth can be furnished if needed.

3) Three carrier tracking loop effective noise bandwidths are available:

Threshold $2B_{LO}$	Strong Signal
12 cps	120 cps
48 cps	255 cps
152 cps	500 cps

Performance Measures --These are:

1) Available data rates at maximum range;

2) Total acquirable data during 6 month Mars orbit phase;

3) Number of discrete data rates used.

4) The telemetry-data signal-to-noise-ratio in a 1-cps noise bandwidth required for the specified bit error rates of $P_b^e = 5 \times 10^{-3}$.

[1] See Exhibit A. (pages 4.1-197 and 198)

5) The telemetry-sync signal-to-noise ratio in a sync-loop threshold noise bandwidth.

6) Carrier and telemetry acquisition times at threshold.

4.1.2.2 Alternate Carrier Modulation Techniques

The choice of carrier modulation for the down link is constrained by the basic requirement for DSN compatibility which dictates the use of a coherent phase-modulated RF carrier. Three basic carrier-modulation techniques have been considered:

1) A single coherent carrier modulated by a single PSK subcarrier;

2) A single coherent carrier modulated by two PSK subcarriers;

3) Two carriers, a coherent one modulated by a single PSK subcarrier for low-rate data, and a non-coherent carrier biphase modulated by the high-rate video data.

Figure 4.1-2 illustrates the power spectra associated with these three approaches.

Single Carrier, Single Data Subcarrier Approach, Alternate A--This approach considers a system in which data from all sources are time multiplexed into a single PCM bit stream which biphase modulates a subcarrier. At least six different bit rates between 20 and 48,000 bits per second are desired to accommodate the various mission phases and data sources. Subcarrier frequencies are chosen to be powers-of-two multiples of the selected bit rates to simplify the subcarrier modulator configuration. The primary advantages of this approach are the need for a single subcarrier modulator in the spacecraft, a single subcarrier

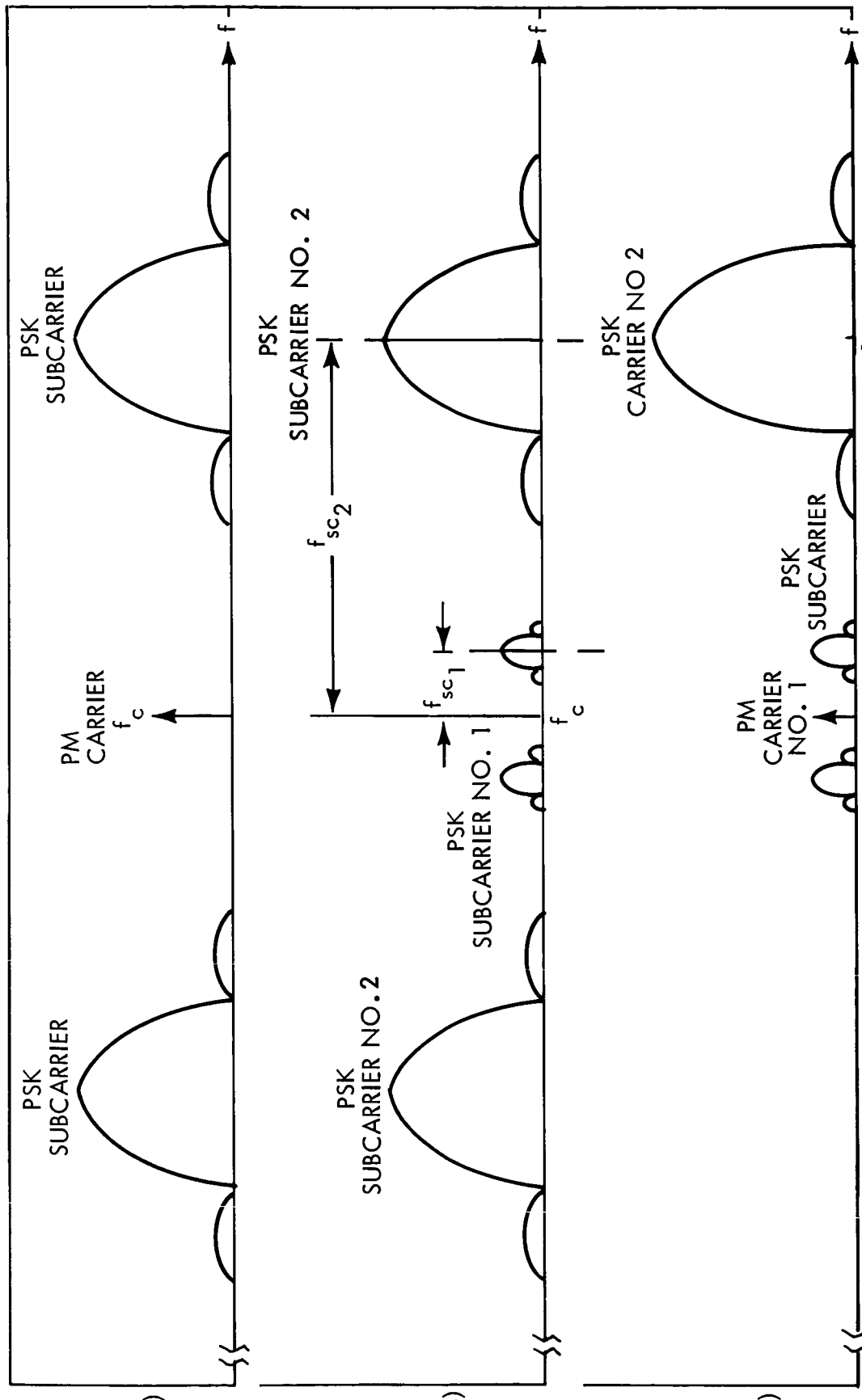

Figure 4.1-2: Alternate-Carrier-Modulation RF Spectra

demodulator in the spacecraft, a single subcarrier demodulator on the ground, minimum interference with range signals, and efficient usage of available side band power. A major disadvantage is the complexity required in the data system to multiplex asynchronous data from several sources into a single bit stream. A complete discussion of the various data multiplexing and formating techniques considered may be found in Section 4.1.6.

Single Carrier, Two Data Subcarrier Approach, Alternate B--To simplify the data multiplexer, this approach considers the use of two data subcarriers to permit frequency multiplexing of asynchronous data sources. Engineering and cruise science data are transmitted throughout the mission at bit rates between 20 and 400 bits per second on a lower subcarrier while planetary science data are transmitted on a second subcarrier. This approach permits, in addition to a simplified multiplexer, more flexibility in the encoding and synchronization of the critical planetary science data. The use of more than two subcarriers was rejected because of the resulting degradation in the data channels for only a small additional degree of flexibility in the multiplexer. The major disadvantages of the two subcarrier approach are a nominal 0.6 db increase in the total power required at the data channel threshold and the need for an additional subcarrier modulator in the vehicle.

Two Carrier, Single Data Subcarrier Approach, Alternate C--To overcome the relative inefficiency of the frequency division multiplexed (FDM) data system, the use of a second carrier offset by a constant frequency from the coherent carrier has been considered. This approach combines

the advantages of simplified multiplexing and efficient power utilization. Its prime disadvantages is the need for an additional exciter in the spacecraft and an additional RF demodulator on the ground.

Recommended Approach--The performance of the three approaches in terms of total RF power threshold requirements is indicated in Table 4.1-1 for Modes 5a and 6. These numbers were generated by optimizing the modulation parameters for each alternate and noting the resulting total power required at the design threshold. Table 4.1-2 summarizes the important parameters associated with each approach and indicates that the single carrier/two subcarrier approach is the preferred technique. Alternate A (single carrier, single subcarrier) was eliminated because of the resulting complexity of the multiplexing system, while Alternate C was excluded because of possible conflict with the DSN. However, Alternate C is attractive and deserves more detailed treatment since it affords a possible improvement in performance over the referenced configuration of 1.9 db.

4.1.2.3 Alternate Subcarrier Modulation and Coding Techniques

The choice of a near-optimum subcarrier modulation technique for each data rate is essential if the design goal of maximum information transfer is to be realized.

Phase-shift-keying (PSK) or biphase subcarrier modulation is proposed for all telemetry modes. This selection is based on the superiority of PSK to all other binary signaling techniques, on the simplicity of the

Table 4.1-1: Comparison of Carrier Modulation Techniques for Modes 5a, 6

MODE 5c CODED	A		B			C		
	CARRIER	SUBCARRIER	CARRIER	SUBCARRIER #1	SUBCARRIER #2	CARRIER #1	SUBCARRIER #1	CARRIER #2
1. REQUIRED ST/N/B, $(S/N)_{2B_{Lo}}$, db	15.0	+ 5.0	15.0	7.2	5.0	15.0	+ 7.2	5.0
2. BIT RATE, B = 1/T, $2B_{Lo}$	10.8	+39.2	10.8	26.0	39.0	10.8	+26.0	39.0
3. REQUIRED S/NO PER CHANNEL, db	25.8	+44.2	25.8	+33.2	44.0	25.8	+33.2	44.0
4. MODULATION INDEX, RAD	--	1.5	--	0.56	1.44	--	1.5	1.57
5. MODULATION LOSSES, db	5.8	2.0	6.0	13.7	2.9	5.8	2.0	--
6. P_{c_1}/P_t, P_{c_2}/P_t, db	--	--	--	--	--	9.3	9.3	0.5
7. INTERMODULATION LOSSES IN TWT, db	--	--	--	--	--	0.5	0.5	0.5
8. TOTAL S/NO REQUIRED, db	+31.6	+46.2	+31.8	+46.9	+46.9	+41.4	+45.0	+45.0

MODE 6 CODED	A		B			C		
1. REQUIRED ST/N/B, $(S/N)_{2B_{Lo}}$, db	+15.0	+ 5.0	+15.0	+ 7.2	+ 5.0	+15.0	+ 7.2	+ 5.0
2. BIT RATE, B = 1/T, $2B_{Lo}$, db $2B_{Lo}$	+10.8	+46.8	+10.8	26.0	46.8	+10.8	26.0	46.8
3. REQUIRED S/NO PER CHANNEL db	+25.8	+51.8	+25.8	+33.2	+51.8	+25.8	+33.2	+51.8
4. MODULATION INDEX, RADIANS	--	1.5	--	0.5	1.5	--	--	--
5. MODULATION LOSSES, db	5.8	2.0	+ 6.4	+15.1	+ 2.5	5.8	2.0	--
6. P_{c_1}, P_t, P_{c_2}/P_t, db	--	--	--	--	--	16.7	16.7	0.1
7. INTERMODULATION LOSSES IN TWT, db	--	--	--	--	--	0.5	0.5	0.5
8. TOTAL S/NO REQUIRED, db	+31.3	+53.8	+32.2	+48.3	+54.3	+48.8	+52.4	+52.4

ITEMS:

6 = RATIO OF POWER IN UNMODULATED RF CARRIER TO TOTAL POWER AT THE OUTPUT OF THE TWT

8 = TOTAL POWER-TO-NOISE DENSITY AT RECEIVER INPUT TO MEET INDIVIDUAL CHANNEL THRESHOLDS, FOR THE MODULATION PARAMETERS SHOWN = ITEMS 1,+2,+5,-6,+7

Table 4.1-2 ALTERNATE CARRIER MODULATION TECHNIQUES -- COMPETING CHARACTERISTICS

Considerations Alternates	Channel	RF Power Threshold S/N_O, db Mode 5a	Mode 6	Range at Greyout 2) 10^6 nm	Spacecraft Equipment	Ground Equipment	Choice	Effective Threshold Improvement, db Mode 5a	Mode 6
A	Carrier	+31.6	+31.3	470	Requires complex data[4] multiplexer, and format generator, single subcarrier and carrier modulators.	Requires single turnable subcarrier demodulator and PCM system.	Unacceptable	+ 0.0	+ 0.0
	Data	+46.2	+53.8						
B	Carrier	+31.8	+32.2	465	Simplifies multiplexing, storage and formating problems, requires second subcarrier biphase modulators	Requires dual tunable subcarrier demodulators, dual PCM systems	Preferred Approach	- 0.7	- 0.5
	Data #1	+46.9	+48.3						
	Data #2	+46.9	+54.3						
C	Carrier #1	+41.4	+48.8		Simplifies multiplexing, storage and formating problems, requires additional RF exciter and hybrid combiner at input to TWT.	Requires auxiliary carrier Biphase demodulator operating from 1st or 2nd IF of DSN Receiver.	Alternate Approach	+ 1.2	+ 1.4
	Data	+45.0	+52.4	600					
	Carrier #2	+45.0	+52.4						

NOTES:
1) Thresholds based on system noise temperature of 35°K.
2) Based on Mode 5a.
3) Alternate C thresholds include 0.5 db loss due to TWT Intermodulation Products.
4) See Section 4.1.7, Volume B for discussion of alternate multiplexer.

modulation process, and on the successful application of this technique to many recent telemetry systems including Pioneer, Mariner R, and Mariner C. Several variations of the basic PSK techniques described below have been considered with respect to each bit rate required by Voyager.

Figure 4.1-3 presents the theoretical bit-error-rate performance versus the signal energy to noise density ratio ST/N/B at the input to the subcarrier demodulator required for the following modulation techniques.

Uncoded Coherent PSK--Uncoded coherent PSK is a technique in which a subcarrier is a biphase modulated $\pm\pi/2$ radians by NRZ data whose bit rate is a coherent sub-multiple of the subcarrier. The theoretical bit error rate for coherent PSK is shown as Curve No. 2 in Figure 4.1-3 and is based on the use of coherent subcarrier demodulation, matched filter bit detection, and zero error in the subcarrier and bit rate reference signals. Practical biphase demodulator-detectors that perform to within 1 db of the theoretical curve are available from several sources for a wide range of bit rates and subcarrier-to-bit-rate ratios. Performance of these units deteriorates at very low bit rates (below 10 bits per second) because of the difficulty of implementing the matched filter and bit sync circuits, and because of the resulting large subcarrier-to-bit-rate ratios.

An inherent disadvantage of coherent PSK is that conventional subcarrier demodulators, including both the square-law and the Costas or I-Q type demodulators, generate a subcarrier reference frequency that may be

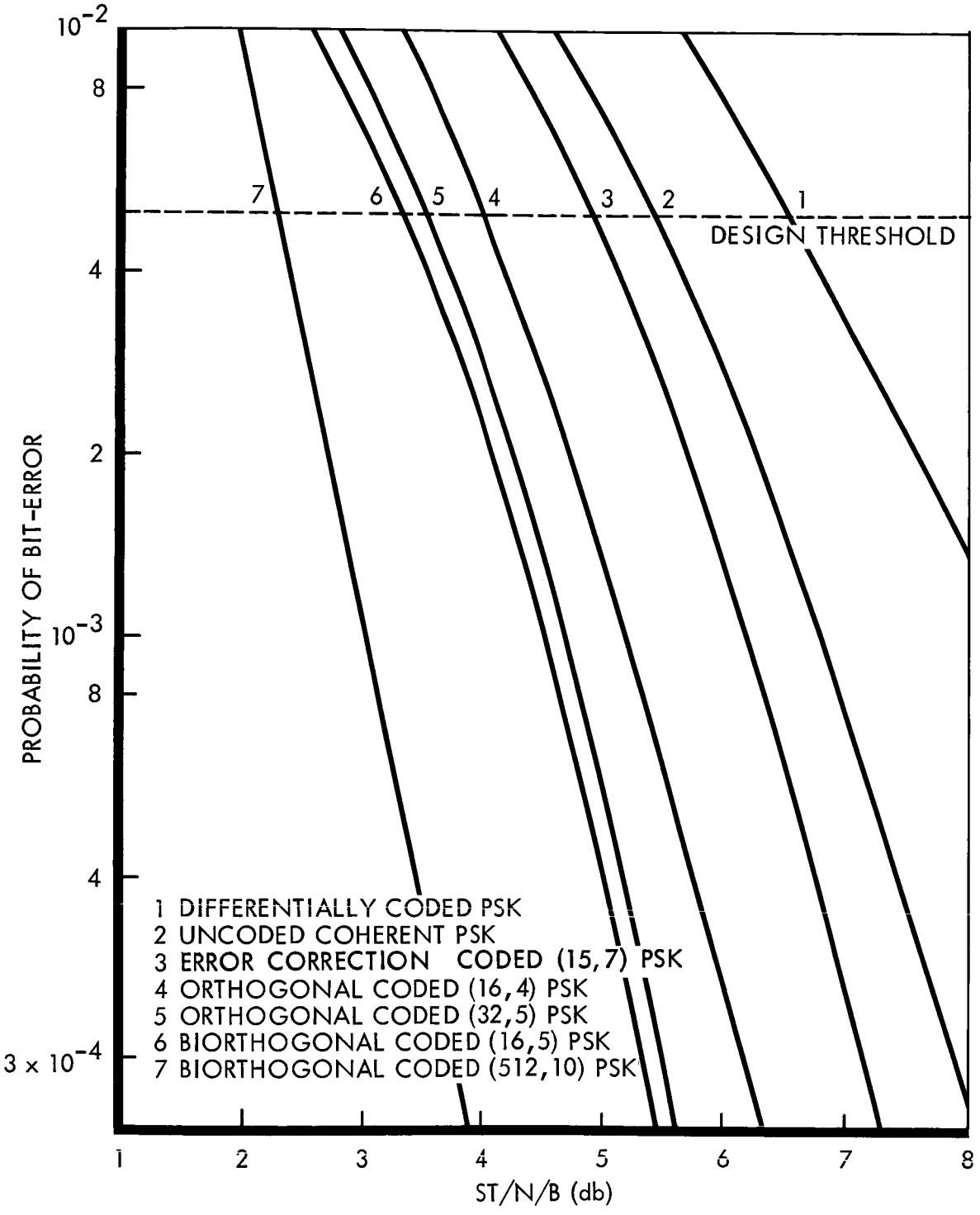

Figure 4.1-3: Bit Error Rates vs ST/N/B

either in phase or 180 degrees out of phase with the received signal. The effect of this ambiguity is to invert the output data when the reference is out of phase.

Techniques used in the past to resolve this demodulator ambiguity include the use of NRZ-M coding, the addition of pseudo-noise sequences to the data, and the use of frame sync words that may be detected with high confidence in either polarity. These techniques are described below.

Differentially Coded PSK--One method for eliminating the subcarrier reference ambiguity mentioned above is to use differentially coded (NRZ-M) data (i.e., to transmit a transition for a "1" and no transition for a "0"). This technique requires at most, several extra flip-flops in the vehicle encoder. On the ground the received PSK is demodulated and converted to NRZ by sensing the received data transitions as "1's."

Since the location of a transition in the data is independent of the phase ambiguity in the demodulator, the NRZ-M to NRZ code converter can regenerate the original data for either 0 or 180 degree subcarrier reference phase. However, the use of NRZ-M coding has the effect of degrading the bit error rate for a given ST/N/B since one error in the channel causes two errors in the output. Similarly, a slipped cycle in the reference loop will cause two errors in the output data. The resulting bit error rate curve for NRZ-M data is plotted as Curve No. 1 in Figure 4.1-3 and indicates a degradation of ST/N/B at $P_b{}^e = 5 \times 10^{-3}$

of 1.2 db over coherent PSK. Most current PSK systems make use of NRZ-M to eliminate the additional complexity and operational disadvantages of an NRZ system. For power-limited systems such as Voyager, 1.2 db is significant, and one must look at alternate techniques for resolving subcarrier-phase ambiguities.

Pseudo-Noise Coded PSK--One such technique, developed by JPL[3] and used on Mariner II and other minimum-power deep-space probes, adds a pseudo-noise (PN) sequence to the data either on a separate subcarrier (two channel) or by modulo-two addition with the data (single channel). In either case, the state of the PN sequence is detected and used to establish the proper subcarrier, bit, and (in some cases) word synchronization. Springett[4] has described the single- and the double-channel systems and justifies the additional complexity of these systems over conventional PSK on the basis of near-optimum performance at very low bit rates.

The two-channel PN system is particularly attractive for application to the Voyager low-data-rate telemetry Modes 1 and 4 because of the absence of data ambiguities for real-time decommutation of engineering data, because of a nominal 1.2 db advantage over NRZ-M coding, and because of the proven performance of this type of system on Mariner C at comparable low bit rates.

NRZ PSK with Ambiguity Resolution--The additional complexity in the spacecraft of the PN/PSK system can be avoided for all but the very-low-data-rate channels by programming the frame sync word detector in the

PCM ground equipment to detect the sync word in either polarity and to select the proper data polarity at the output of the PCM bit detector. Since most general-purpose PCM equipment can be supplied with this capability, the major disadvantage of this technique is the loss of all remaining data in a frame whenever the subcarrier loop locks in the incorrect phase. The amount of data lost due to improper subcarrier lock can be estimated from the expected time between false locks and the number of bits per telemetry frame. For the Voyager telemetry formats, a false lock every 200th frame would result in a loss of data equivalent to the loss of data if NRZ-M were used.

Coherent PSK with Biorthogonal Block Coding--If the PCM data is divided into k-bit words, and each of the resulting $M = 2^k$ binary words is transmitted as a coded n-symbol word and detected on the ground in an optimum M'ary detector, a significant improvement in a bit-error-rate performance can be realized. Viterbi[5] and Nuttall[6] have derived the theoretical performance of such systems in terms of signal error probability, the signal-energy-to-noise-density ratio, the number of possible words, and the cross-correlation coefficients of the selected code words. Viterbi[7] has calculated the theoretical performance of such systems and summarizes the theory, performance, and implementation problems associated with binary-coded biorthogonal, orthogonal, and transorthogonal systems applicable to Voyager. The bit-error-rate performance of representative block-coded systems has been shown in Figure 4.1-3 for the following codes:

1) Orthogonal, n = 16, k = 4, M = 16;

2) Orthogonal, n = 32, k = 5, M = 32;

3) Biorthogonal, n = 16, k = 5, M = 32;

4) Biorthogonal, n = 512, k = 10, M = 1024.

Note that, to make the comparison with binary systems valid, both ordinate and abcissa have been normalized by the data bit rate $1/T_b$.

A coded biorthogonal(16,5) system was selected as the most appropriate coding technique to evaluate for Voyager. The performance and implementation of such a system has been described in supporting documents by Viterbi. The theoretical ST/N/B improvement of this system over uncoded coherent PSK for a $P_e^b = 5 \times 10^{-3}$ is +2.1 db as shown in Figure 4.1-3. The realizable improvement for the proposed Voyager bit rates and formats varies from 1.6 to 2.2 db. This improvement is equivalent to an increase in available bit rate at maximum range by a factor approximately 1.5 or to an increase in range at the nominal design bit rate by approximately 50×10^6 kilometers. Since Mars is receding at an approximate rate of 10^6 kilometers per day, a coded system will permit transmission at a given bit rate for an additional 50 days.

Coherent PSK with Error-Correction Coding--An alternate form of block coding is one in which each k-bit data word is coded into an n-bit transmitted word such that resulting $M = 2^k$ code book is a cyclic group with distance properties[9] that may be used on the ground to detect and correct errors. On the ground, the PSK subcarrier is demodulated and the received data is detected on a bit-by-bit basis. The reconstructed redundant PCM stream is fed to an error-correcting device that corrects certain patterns of random errors and decodes the n-bit transmitted words into appropriate k-bit words. Several methods have been used to

MODE	TELEMETRY CHANNEL DATA TYPE & RATES	CHANNEL	SUBCARRIER FREQUENCY	PHAS PEAK MIN
1	SPACECRAFT ENGINEERING @11-1/9 bps CAPSULE ENGINEERING @11-1/9 bps	CARRIER SYNC DATA	 200 cps 400 cps	 0.32 1.15
2 OR 3	SPACECRAFT ENGINEERING @ 11-1/9 bps CAPSULE ENGINEERING @ 11-1/9 bps CRUISE SCIENCE @ 111-1/9 bps OR STORED SPACECRAFT ENGINEERING	CARRIER DATA	 533-1/3 cps	 1.26
4	SPACECRAFT ENGINEERING @ 5-5/9 bps	CARRIER SYNC DATA	 50 cps 100 cps	 0.63 1.17
5A	SPACECRAFT ENGINEERING @ 66-2/3 bps CRUISE SCIENCE @166-2/3bps CAPSULE ENGINEERING AND SCIENCE @166-2/3 bps	CARRIER LOWER UPPER	 1.6 kc 102.4 kc	 0.50 1.30
5B	SAME AS 5A	CARRIER LOWER UPPER	 1.6 kc 102.4 kc	 0.66 1.26
5C	SAME AS 5A	CARRIER LOWER UPPER	 1.6 kc 102.4 kc	 0.77 1.15
6	SAME AS 5A	CARRIER LOWER UPPER	 9.6 kc 614.4 kc	 0.45 1.35
COMMAND	SINGLE CHANNEL SYSTEM	CARRIER SYNC DATA	 (NOTE 1)	 0.80

NOTE 1 : CHARACTERISTICS ASSUMED FOR SINGLE-CHANNEL COMMAND SUPPLIED TO JPL UNDER CONTRACT NO 950416 (PHLICO)
NOTE 2 : GOVERNS LINK THRESHOLD

Table 4.1-5: Te

E DEVIATION, RADIANS		CARRIER MOD LOSS P_c/P_t, db	SYNC OR SUBCARRIER MOD LOSS P_{sc1}/P_t, db	UPPER SUBCARRIER MOD LOSS P_{sc2}/P_t, db	MISSION PHASE	
NOM	MAX					
0.35 1.27	0.38 1.41	$-4.7^{+1.0}_{-1.1}$	$-13.6^{+1.7}_{-1.6}$	$-3.3^{+0.5}_{-0.6}$	LAUNCH ACQUISITION MANEUVERS	152 12
1.40	1.54	$-4.9^{+1.0}_{-1.3}$	$-2.4^{+0.4}_{-0.4}$		CRUISE & POST-MANEUVER OPTION	12
0.70 1.30	0.77 1.43	$-6.5^{+1.4}_{-1.5}$	$-8.0^{+1.6}_{-1.8}$	$-5.0^{+0.9}_{-1.0}$	EMERGENCY, CRUISE OR ENCOUNTER	5 0
0.56 1.44	0.62 1.58	$-6.0^{+1.2}_{-1.5}$	$-13.7^{+1.9}_{-2.3}$	$-2.9^{+0.5}_{-0.6}$	PRIMARY ENCOUNTER AND ORBITAL	12 48
0.73 1.40	0.80 1.54	$-6.2^{+1.3}_{-1.5}$	$-11.3^{+1.8}_{-1.9}$	$-3.6^{+0.6}_{-0.7}$	OPTIONAL LATE ORBITAL	1
0.85 1.28	0.93 1.41	$-5.8^{+1.2}_{-1.2}$	$-9.3^{+1.6}_{-1.6}$	$-4.4^{+0.7}_{-0.8}$	OPTIONAL LATE ORBITAL	12
0.50 1.50	0.55 1.65	$-6.4^{+1.4}_{-1.9}$	$-15.2^{+2.1}_{-2.6}$	$-2.7^{+0.5}_{-0.6}$	OPTIONAL ENCOUNTER AND ORBITAL	1
0.89	0.98	$-1.8^{+0.3}_{-0.5}$	$-4.8^{+0.6}_{-0.8}$		ALL PHASES	2

DETECTOR AS

31

lemetry and Command Modulation Mode Parameters

$2B_{Lo}$ cps	$(\frac{S}{N})2B_{Lo}$, db	INFO BIT RATE, BPS	TRANS-MITTED BIT RATE, BPS	EFFECTIVE $\frac{ST}{N/B}$, db	P_e^b, EFFECTIVE BIT ERROR RATE
, 48.0, .0).5	9.0 14.0 ± 0.5	22-2/9	22-2/9	7.6 ± 0.5	5×10^{-3}
.0	15.0	133-1/3	133-1/3	7.2 ± 0.5	5×10^{-3}
.0 .5	6.0 14.0 ± 0.5	5-5/9	5-5/9	7.7 ± 0.5	1×10^{-2}
.0 .0	15.0	400 8000	400 25,600	7.2 ± 0.5 5.0 ± 0.5	5×10^{-3} 5×10^{-3}
.0	15.0	400 4000	400 12,800	7.2 ± 0.5 5.0 ± 0.5	5×10^{-3} 5×10^{-3}
.0	15.0	400 2000	400 6,400	7.2 ± 0.5 5.0 ± 0.5	5×10^{-3} 5×10^{-3}
.0	15.0	400 48,000	400 153,600	7.2 ± 0.5 5.0 ± 0.5	5×10^{-3} 5×10^{-3}
).0 .0	9.0 db 15.0 db (NOTE 2)	1	1	$10.5\ ^{+0.5}_{-0.0}$	1×10^{-5}

implement the error-correcting devices[10] which are digital, all solid-state, and relatively compact compared to the multiple matched filter correlation detectors required to detect a biorthogonal coded system.

The principal disadvantage of error-correction coding for Voyager is that long block lengths and, therefore, a less reliable spacecraft encoder must be used to achieve an error-rate improvement comparable with that available from biorthogonal coding. General Electric II has proposed a (73,45) (n,k) Bose-Chaudhuri code and has indicated an ST/N/B improvement of approximately +1.2 db for $P_e^b = 5 \times 10^{-3}$ and an encoder with approximately five times as many components as required by the biorthogonal encoder. The use of a (15,7) error-correcting code would require an encoder roughly equivalent to the biorthogonal encoder and would yield an ST/N/B improvement of only 0.5 db as compared to 2.1 for the biorthogonal system. The performance curve for a (15,7) error-correcting coded system has been plotted as curve No. 3 in Figure 4.1-3 for comparison with other proposed techniques.

Convolution Coding--Convolution coding and sequential decoding are techniques originally described by Wozencraft and Reiffen[12]. Viterbi has described convolutional coding and compares its performance to that of orthogonal coding. This technique is not recommended for Voyager because of the excessive code lengths and resulting encoder complexity necessary to achieve reliable decoding, and because the theoretical performance of such systems has not yet been verified in practical hardware design.

Recommended Coding Technique--The recommended modulation and coding techniques for the various Voyager telemetry are summarized in Table 4.1-3.

The relative improvement in the telemetry channel thresholds due to the use of biorthogonal coding for Modes 5 and 6 is shown in Table 4.1-4. Note that the threshold ST/N/B ratios shown include degradations due to the use of the lower subcarrier for coded word synchronization. These degradations have been calculated and tabulated in Volume A., Section 4.1.4.

4.1.2.4 Synchronization Techniques

To achieve near-optimum performance with the modulation and coding techniques described above, several types of timing or synchronization signals are needed at the receiver. These include:

1) A locally generated subcarrier frequency that is coherent in phase with each received subcarrier;
2) A locally generated bit sync signal that is coherent in phase with the data-bit transitions;
3) A locally generated word sync signal that identifies the first bit in each word in the bit stream;
4) Locally generated frame sync signal that identifies the first word in each frame of telemetry data.

Subcarrier Synchronization--A locally generated subcarrier reference for subcarrier demodulation may be generated by operating on the data subcarrier or by transmitting a second subcarrier that is coherently

Table 4.1-3: TELEMETRY MODE MODULATION AND CODING TECHNIQUES

Mode	Channel	Bit Rate, bps	Subcarrier, cps	Technique
1	Low Rate Data	22-2/9	200/400	PN Coded PSK-Two Channel
2	Cruise Data	133-1/3	533-1/3	Coherent PSK
3	Cruise Data	133-1/3	533-1/3	Coherent PSK
4	Emergency Low Rate	5-5/9	50/100	PN Coded PSK-Two Channel
5	Cruise and Capsule Data	400	1.6K	Coherent PSK
	Planetary Science	8/4/2K	102,400	Bi-Orthogonal (16,5) Coded Coherent PSK
6	Cruise and Capsule Data	400	9.6K	Coherent PSK
	Planetary Science	48K	614,400	Bi-Orthogonal (16,5) Coded Coherent PSK

Table 4.1-4 DATA LINK IMPROVEMENT DUE TO CODING

	ALTERNATES	CODED			UNCODED		
	CHANNEL	CARRIER	DATA #1	DATA #2	CARRIER	DATA #1	DATA #2
MODE 5a	Required ST/N/B, $(S/N)_{2B_{Lo}}$, db	+15.0	+ 7.2	+ 5.0	+15.0	+ 7.2	+ 7.2
	Bit Rate, B = 1/T, $2B_{Lo}$, cps	+10.8	+26.0	+39.0	+10.8	+26.0	+39.0
	Required S/No per Channel, db	+25.8	+33.2	+44.0	+25.8	+33.2	+46.2
	Modulation Index, rad	--	00.56	1.44	--	0.54	1.60
	Modulation Losses, db	6.0	13.7	2.9	6.6	15.3	2.3
	Total S/No Required, db	+31.8	+46.9	+46.9	+32.4	+48.5	+48.5
	IMPROVEMENT	+ 0.6	+ 1.6	+ 1.6	--	--	--
MODE 6	Required ST/N/B, $(S/N)_{2B_{Lo}}$, db	+15.0	+ 7.2	+ 5.0	+15.0	+ 7.2	+ 7.2
	Bit Rate, B = 1/T, $2B_{Lo}$, cps	+10.8	+26.0	+46.8	+10.8	+26.0	+46.8
	Required S/No Per Channel, db	+25.8	+33.2	+51.8	+25.8	+33.2	+54.0
	Modulation Index, rad.	--	0.5	1.5	--	0.5	1.5
	Modulation Losses, db	6.4	15.1	2.5	6.4	15.1	2.5
	Total S/No Required, db	+32.2	+48.3	+54.3	+32.2	+48.3	+56.5
	IMPROVEMENT	--	--	+ 2.2	--	--	--

related to the data subcarrier. Stiffler[13] has compared the two techniques for the case of a double-frequency subcarrier tracking loop and concludes that it is preferable to use the squaring loop rather than to divide power between data channel and a separate sync channel. Squaring loops have, in fact, been used in bit synchronizers and biphase demodulators for a number of years for the demodulation and detection of biphase signals. A disadvantage of the squaring loop is that the square-law device at the input exhibits the familiar small-signal suppression effect derived by Davenport[14]. If the SNR loss through the square-law device is to be kept small, then the SNR at the input to the device must be kept about +0 db, and the predetection bandpass filter must be sufficiently narrow to realize the desired input SNR at the data-channel threshold. For uncoded PSK, this constraint does not present a practical problem. For the PSK channels described here, the data-channel threshold is +7.2 db in a bandwidth equal to the bit rate so that a predetection filter bandwidth of four times the bit rate would yield a predetection SNR of +1.2 decibels. The relationship between the input and output SNR's for the square-law device is

$$\frac{S}{N}_o = \frac{(S/N)_i^2}{2\left[1+2(S/N)_i\right]}$$

where:

$\frac{S}{N}_o$ = Output signal-to-noise ratio

$\frac{S}{N}_i$ = Input signal-to-noise ratio

from which the $(S/N)_o$ into the double-frequency loop will be -6.5 db in a bandwidth of four times the bit rate, which is adequate for the

double-frequency loop if the ratio of data bit rate, $1/T_b$, to loop bandwidth, B_L, is large.

However, for the coded PSK technique proposed here, the data-channel threshold is defined as +5 db in $1/T_b$ cps. Since the coded bit rate, $1/T_c$, is actually 16/5 times $1/T_b$, the signal-to-noise ratio in a predetected filter bandwidth equal to $4/T_c$ will be -6 db and the $(S/N)_o$ in the double subcarrier tracking loop referred to $4/T_c$ will be -16.8 db. Thus, to limit the phase jitter on the subcarrier reference to $\sigma_n = 0.2$ radian, and, therefore, to maintain the loop SNR in $2B_{L_o}$ above +9 db, the required ratio of the coded bit rate to loop bandwidth is:

$$Q = \frac{1}{T_c B_l} = +9 + 3 + 10.8 = +22.8 \text{ db} = 111.$$

For the lowest coded data rate, proposed for Voyager $1/T_c = 6400$ bps so that $B_L < 53.5$ cps. Since the proposed subcarrier frequency is 102,400 cps, the loop will operate at 204,800 cps. These numbers are comparable to the parameters for the JPL range-clock tracking loop and do not appear to be a serious design problem. However, the narrowness of the loop may require manual or automatic sweep acquisition at the DSIF since the initial frequency uncertainty of the subcarrier and loop VCO's may exceed $2B_L$.

As an alternate approach to the mechanization of the subcarrier demodulator, one should consider the use of a Costas demodulator. The Costas demodulator is more complex than the square loop, but it has a distinct advantage over the square loop in that there is no predetection threshold effect.

In conclusion, either the Costas or the square-loop subcarrier demodulator can be used for demodulating both the coded and the uncoded PSK suabcarriers.

Bit Synchronization Techniques--Bit synchronization is required for uncoded PSK signals to establish the time at which each bit decision is to be made. The last few years have seen considerable improvements in hardware designed to recover bit sync directly from the data and to reconstruct the data stream in a matched filter detector. Several suppliers will guarantee the signal-to-noise performance of their equipment to within 1 db of the theoretical bit error rate versus bit-energy-to-noise-density curve for bit rates from 10 bps to 10^6 bps. Several suppliers have delivered detectors that combine the functions of subcarrier demodulation and bit reconstruction.

The JPL-developed pseudonoise[15] PSK systems successfully combine subcarriers and bit synchronization into a composite signal. The detectors for these systems, in effect, use the correlation properties of the PN sequence to resolve the multiple ambiguities between the data subcarrier and the coherent bit stream. Springett has justified the development of the PN sync system in terms of its superior performance to conventional PSK at very low bit rates.

For the lowest bit rates presently considered for Voyager ($5\text{-}^5/_9$, and $22\text{-}^2/_9$ bps) the exact margin of superiority is difficult to determine from the data that JPL has published on the Mariner and Pioneer

telemetry systems. The primary justification, therefore, for recommending the use of the two-channel PN system for Voyager's low-bit-rate data is the flight-proven status of this system.

Word Synchronization--The proposed bi-orthogonal coding technique depends for its improvements on word-by-word detection. The word detection depends in turn on the existence of a stable local word clock that identifies the beginning of each word. Several techniques for regenerating the word clock on the ground have been considered. These include:

1) The use of a comma-free code book and the computational techniques required to detect a periodic component at the word rate in the voltage produced by cross-correlating the received data in all possible overlaps with a reference sync word.
2) The addition of a PN sequence to the data in such a way that on the ground, the sequence can be acquired, tracked, and detected to establish the word clock.
3) The addition of a frequency multiplexed signal to the transmitted baseband that is periodic with the word rate or with a simple multiple of the word rate.

The first technique, which has been suggested by Stiffler[16], is based on a probabilistic argument that is difficult to verify. Digilock[17], a similar technique implemented several years ago, was successful in acquiring data, but required considerably more computation to establish synchronization that had been originally anticipated.

The second technique could be implemented in a manner similar to the single-channel PN system described previously. The major disadvantage of this approach is the excessive bandwidths that would be required to obtain an adequate PN-bit-to-transmitted-bit-rate ratio, and the additional complexity of the spacecraft hardware.

The third technique, the use of a transmitted reference, has the advantage of simplifying the additional encoding and decoding equipment required. This technique usually requires a division of power to realize the separate sync channel. For application to Voyager, however, this technique is particularly attractive since a lower subcarrier is required for the low bit rates, and its frequency has been chosen to be a coherent multiple of the word rate. In addition, the bit rate of the lower data channel is a coherent submultiple of the coded word rate and may be used to resolve ambiguities that will occur in the lower subcarrier in Modes 5b and 5c. Because the lower data channel is not coded, the ST/N/B in the lower channel subcarrier demodulator will be normally +7 db higher than that in the coded channel subcarrier demodulator.

This technique has been selected for the preferred design and is reflected in the threshold analysis in section 4.1.4, Volume A, where a 0.6 db loss is allocated to the coded subcarrier demodulator, and 0.3 db to the word detector.

Frame Synchronization--For both the coded and uncoded data channels, conventional PCM frame sync techniques will be used with bipolar detection to resolve the subcarrier phase ambiguities as described previously. A discussion of the equipment required to implement the telemetry ground system is contained in Volume C.

4.1.2.5 Selection of Operating Modes

The major performance parameters of the recommended telemetry system have been summarized in Table 4.1-5. This section discusses the selection of these parameters and describes the resulting telemetry system performance.

Mode 1--Low Bit Rate--Mode 1 parameters have been chosen to realize a minimum bit rate capability of at least 20 bps through the end of encounter. The actual bit rate proposed, 22-2/9 bps, results from the choice of coherent PSK subcarrier modulation with double-channel PN sync on 400-cps and 200-cps subcarriers, respectively. A 63-bit PN sequence per data word is used with 9 PN bits per data bit and 7 data bits per word. This technique was selected to achieve near-optimum performance at low bit rates and low signal-to-noise ratios, to provide unambiguous detection at both bit and word formats in real time, and to take advantage of flight-proven hardware developed for Mariner C. The bit rates and subcarriers indicated above fall within the range of parameters specified for Mariner C.

A sinusoidal subcarrier is recommended for the data channel since only one bit rate is involved and the equipment simplifications in going to a squarewave subcarrier are insignificant. The selection of subcarrier deviations, ST/N/B's, SNR's, and threshold bandwidths are described in Volume A.

Modes 2 and 3--Engineering and Cruise Science--The parameters for Modes 2 and 3 have been chosen to realize a minimum bit rate requirement of 120 bps. The actual bit rate proposed, 133-1/3 bps, has been chosen as a convenient submultiple of the basic CC&S clock frequency. Unambiguous real-time decommutation is not as desirable in these modes as in Mode 1 so that the PN sync channel is omitted and coherent PSK modulation is used on a 533-1/3 cps subcarrier to yield a 4:1 subcarrier-frequency-to-bit-rate ratio. NRZ bit coding is used with a bipolar sync word detector that selects the correct data polarity at the output of the bit detector.

Mode 4--Emergency Low Data Rate--Mode 4 parameters have been chosen to meet minimum telemetry margins throughout the cruise phase in case of a failure in the High-gain-antenna system. A 5-5/9-bps data rate, together with 50-cps and 100-cps sync and data subcarriers, results in a system identical to that for Mode 1 except for a 4:1 scaling of all coherent clocks and timer references.

Mode 5--Planetary Science--More than 95 percent of the data acquired by the Voyager will be transmitted to the Earth in Modes 5 and 6. Therefore, particular attention has been given to the selection of the

parameters for those modes that maximize the amount of data that can be successfully acquired by the DSN. Because of the difficulty of multiplexing spacecraft and capsule engineering data, with planetary science data, two separate subcarriers are used, a lower one at 1600 bps, biphase modulated by 400 bps engineering data, and an upper one at 102,400 kilocycles biphase modulated by 2000, 4000, or 8000-bps coded planetary science data. The recommended coding technique employs a (16,5) bi-orthogonal coded alphabet that can be generated in a simple and reliable spacecraft encoder and requires a detector on the ground comparable in complexity to existing equivalent stored-program PCM ground equipment. Note that the word synchronization signal for the proposed near-optimum M'ary detector is generated from the lower subcarrier demodulator to simplify the ground equipment implementation. The principal reason for the selection of this technique is a significant increase in the amount of data that can be acquired during encounter for a nominal increase in system complexity.

Mode 6-Planetary Cruise Real-Time Data--Mode 6 parameters have been chosen to achieve real-time relay of planetary science data from Mars to the DSN. An information bit rate of 48 kbps is proposed for the planetary data, equivalent to a transmitted bit rate of 153.6 kbs and a subcarrier of 614.4 kbs. The subcarrier was chosen to yield a binary-subcarrier-to-bit-rate ratio of 4:1. The resulting RF bandwidth is 1.5 megacycles, including the first sidebands, and 3.8 megacycles including the third-order sidebands. Because of the 3.3 megacycle bandwidth restriction on the DSIF, a lower subcarrier was considered to reduce the required RF bandwidth. The possible phase distortion due to frequency

foldover effects and interference with the lower subcarrier at 9.6 kilocycles led to the selection of the high subcarrier frequency.

4.1.3 Command Link Modulation Analysis

This section will summarize the performance analysis of the single-channel and two-channel command detector and recommend a preferred design. Supporting analysis can be found in the Philco WDL Analysis Document WDL-TR-2531, "Mars Mission Communication Analysis."

4.1.3.1 Requirements and Constraints

The spacecraft command equipment must be compatible with the DSN equipment and techniques 18, 19, 20 so that the following constraints apply:

1) Modulation format is PCM/PSK/PM.
2) Carrier component may not be totally suppressed.
3) A coherent PN sequence is used for bit sync information.
4) Data rate is 1 bit per second.

On the basis of these constraints, the detailed analyses may be confined to the JPL-developed two-channel and single-channel system.

4.1.3.2 Modulation Spectrum

Two-Channel System--The two-channel system transmits the data on a sinusoidal subcarrier at 2fs and the PN sequence on a square-wave subcarrier also at 2fs. The transmitted signal can be represented as:

$$f_c(t) = \sin \left[\omega_c t + x_d\, a_d(t) \sin 2\pi\, 2f_s t + y_s\, a_s(t)\, s(2f_s t) \right]$$

where

ω_c = RF carrier frequency

x_d, y_s = deviation ratio of data and sync signals, respectively

$a_d(t)$, $a_s(t)$ = data and PN sync binary sequences, respectively

$s(2f_s t)$ = square wave at frequency $2f_s$

After carrier demodulation, the relative amounts of power for each signal are as follows:

P_c = carrier power = $J_o^2(x_d) \cos^2(y_s) P_t$

P_d = data power = $2J_1^2(x_d) \cos^2(y_s) P_t$

P_s = sync power = $J_o^2(x_d) \sin^2(y_s) P_t$

There are many more spectrum components. These, however, are either excluded by the receiver bandwidth or appear together with the data signals as noise of very low amplitude.

Single Channel System--The single-channel system transmits both the data and the PN sequence mod-2 combined on a single sinusoidal subcarrier at a frequency $2f_s$. The transmitted spectrum for a square wave subcarrier is:

$$f_c(t) = \sin\left[\omega_c t + \phi\,(D \oplus PN \oplus 2f_s)\right]$$

or for a sinusoidal subcarrier.

$$f_c(t) = \sin\left[\omega_c t + \phi\,(D \oplus PN^* \cos(2\pi f_s t)\right]$$

where

$D \oplus PN^*$ = the composite sync and data binary stream of amplitude $\pm$ 1.0

ϕ = carrier modulation index.

At the carrier demodulation output, the recovered power for the signals of interest is:

P_c = carrier power = $J_o^2(\phi) P_t$

P_{cs} = composite data signal = $2J_1^2(\phi)\ P_t$

P_t = total power

All higher-order components occur as harmonics of the fundamental subcarrier frequency. Since these components are, in general, of low magnitude (-17 db or lower), no attempt is made to recover them. Filters in the receiver demodulator are then just wide enough to pass the desired terms.

4.1.3.3 Hardware Degradation Characteristics

Bandlimiting and Limiter Suppression--Under conditions of low SNR, a limiter will produce signal suppression. To keep limiter suppression[21] at a minimum, bandpass filters are inserted at points 1 and 2 in Figure 4.1-4 and points 3 and 4 in Figure 4.1-5. These filters are made as narrow as possible to maximize the SNR into the limiters following the filters. As a minimum, the filters would be designed to pass only the fundamental component of the data signal, in which case they also exclude 0.91 db of the total received data power when the subcarrier is a square wave.

Noisy Signal Crossmultiplication--As shown in Figure 4.1-5, upon entering the detector, the single-channel signal is operated on by PN and $PNOf_s$ to produce $\pm f_s \angle 90^\circ$ and $\pm 2 f_s$. Both these signals are noisy and are crossmultiplied to produce f_s. This crossmultiplication of noisy signal produces an SNR degradation that has been calculated by Springett

the SNR of the signal to the crossmultiplier.

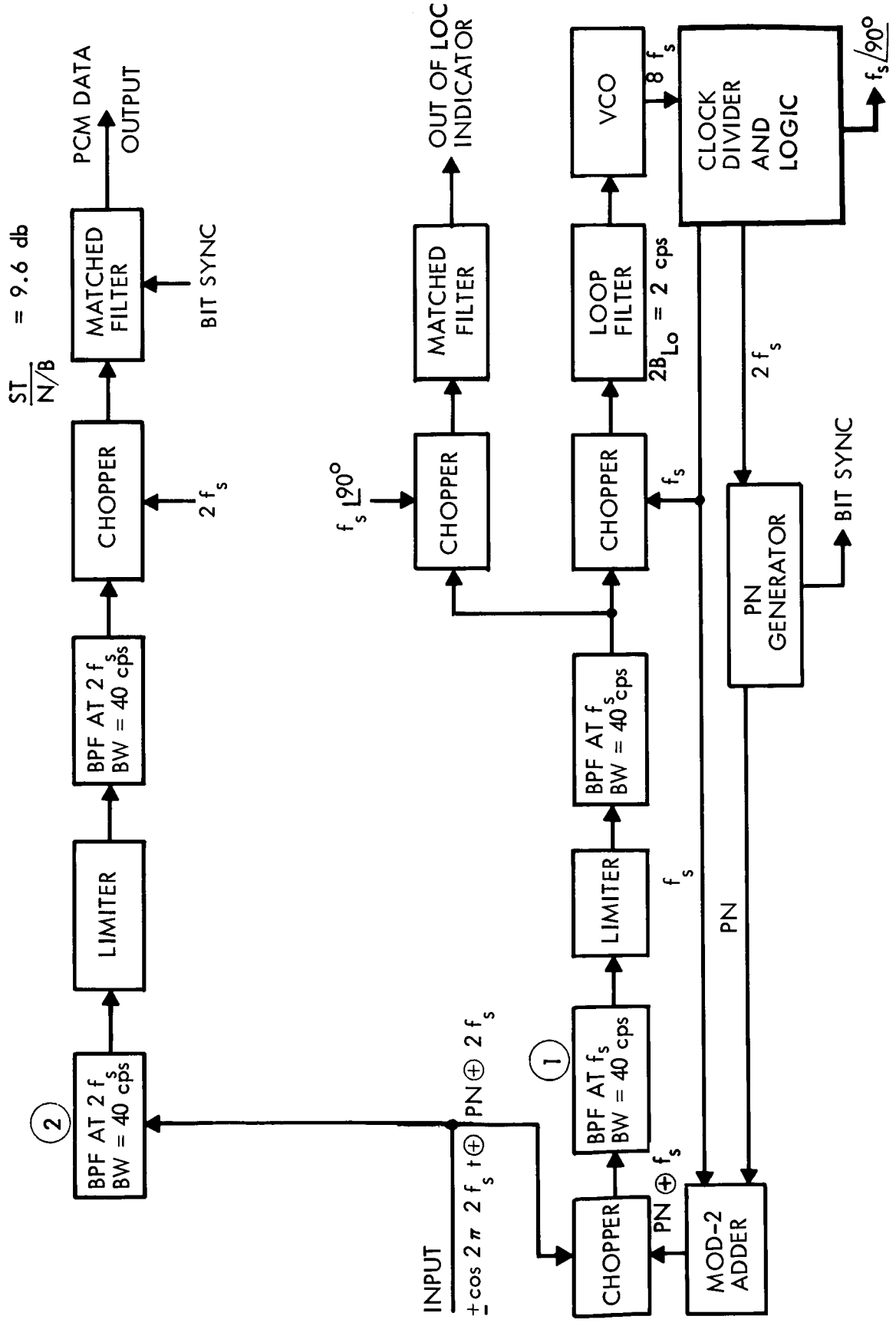

Figure 4.1-4: Two-Channel Command Detector — Simplified Block Diagram

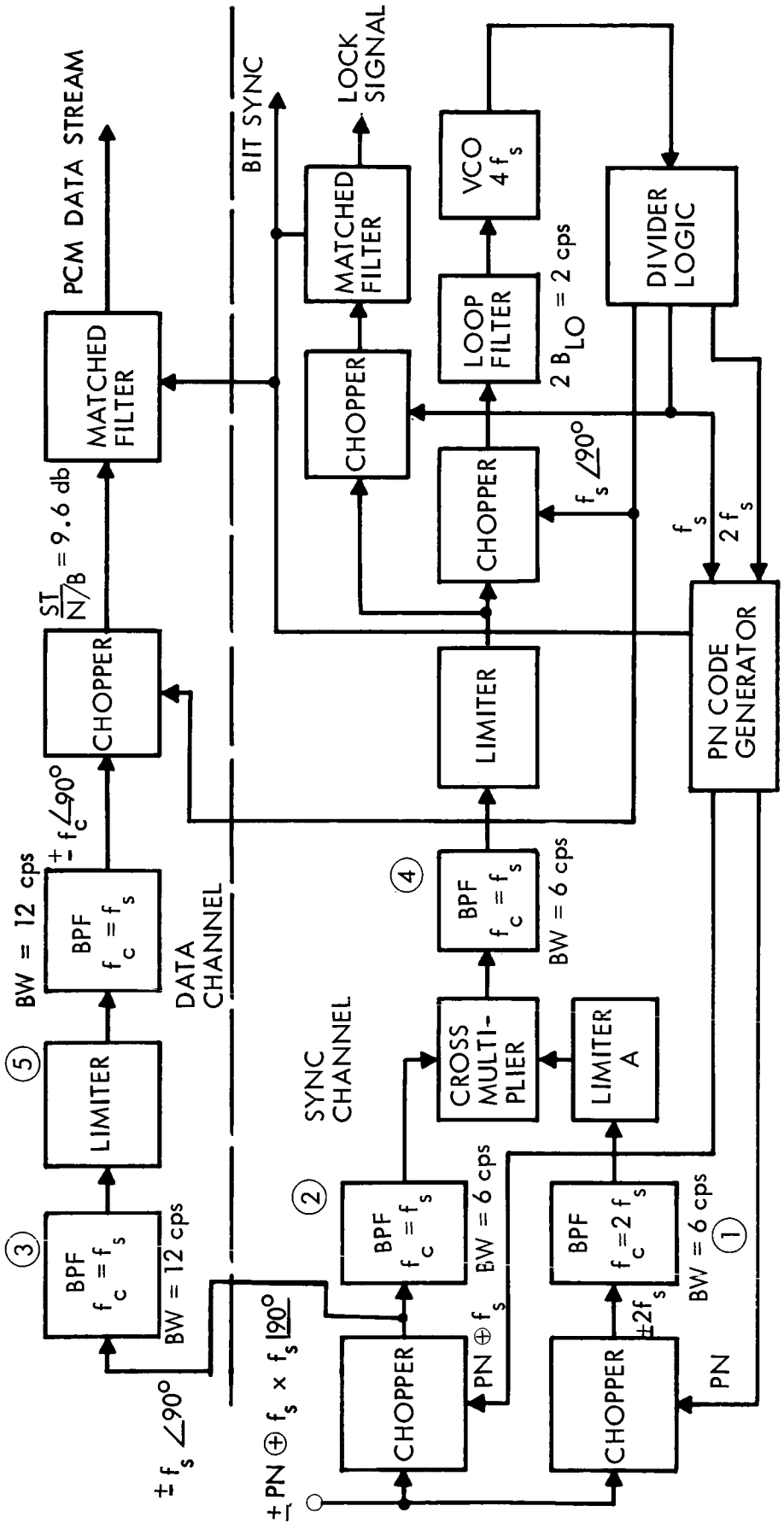

Figure 4.1-5: Single-Channel System Detector — Simplified Block Diagram

Carrier Phase Jitter--Carrier loop phase error will be produced by noise in the loop, doppler offset, doppler rate, and oscillator instaaility. Degradations due to jitter on the carrier have been analyzed by Viterbi[23] and Gilchriest[24]. Section 4.1.4.3, Volume A, shows that a value of 9db in 2 B_{LO} has been used. This value results in a carrier phase jitter of 0.37 rad rms with an attendant subcarrier degradation of 0.64 db. Doppler offset can be reduced by proper choice of transmitting frequency. Doppler rate during command periods will be so low that it will have negligible effect. Therefore, these two factors will not be treated here.

Subcarrier Phase Jitter--The data channel of the single-channel system, as built by Philco for JPL under Contract 950416, utilizes a data sampling technique that reduces the degradation effects of subcarrier phase error in the subcarrier demodulation operation, as shown by Gilchriest. This technique not only reduces the jitter degradation, but also degrades the operation of the matched filter as derived below.

The probability of error out of a matched filter detector is based on the $\frac{ST}{N_o}$ at its input. For the unsampled signal case, with T = bit period, and N_o = the noise density, S is a function of $\frac{A^2}{2}$, where A is defined as the peak amplitude of the sinusoidal subcarrier. For the case of the 50 percent sampled signal (K = 0.5), the effective integration period is T/2 and S becomes a function of the rms value of the sine wave between + 45° and + 135°. That is,

$$S = \frac{2A^2}{T}\int_{\pi/4}^{\frac{3\pi}{4}} \left(\cos \frac{2\pi t}{T}\right)^2 dt = 0.409A^2,$$

so that the sampling degradation is

$$\frac{\frac{ST}{N_o}\text{ nonsampled}}{\frac{ST}{N_o}\text{ sampled}} = \frac{A^2 T}{2 N_o} \times \frac{N_o}{0.409\, A^2 T} = 0.86 \text{ db}$$

Consider now the effect of subcarrier phase jitter. Gilchriest's results (K = 1) show that for any jitter larger than 0.2 rad rms, it pays to use this sampling technique. For instance, if the phase jitter in the sync loop is 0.5 rad rms, the total improvement is: nonsampled jitter loss minus sampled jitter loss minus sampling loss, or:

Improvement = 2.6 - 0.3 - 0.86 = 1.44 db

Bit Sync Jitter--In the case of both the two-channel system and the single-channel system, the subcarrier frequency is much higher than the bit rate. Since the sync jitter is equal to the subcarrier phase jitter multiplied by the ratio of sync to subcarrier frequency, its value will be so low that it may be ignored.

4.1.3.4 System Power Requirement

Based on the preceding discussion, a detailed analysis of both the single-channel and two-channel system can be made. The analysis is based on the implementations of the detectors as shown in Figures 4.1-4 and 4.1-5. The results are shown in Table 4.1-6 and 4.1-7. The input signal-to-noise ratios agree well with measured result. The major analysis error probably occurs in the calculation of the various jitters in the phase-locked loops where a sinusoidal error function has been assumed. It is known that the error function of the single channel is complex and depends on the system implementation.

Because in the single-channel system both sync and data are derived from the same signal, the supplied SNR is the same for both channels

Table 4.1-6: SIGNAL-TO-NOISE RATIO REQUIREMENTS FOR SYNCHRONIZATION

	SINGLE CHANNEL	TWO CHANNEL
$2B_{LO}$, cps	2.0	2.0
SNR in $2B_{LO}$, db	14.0	14.0
$2B_L$, cps	3.39	5.5
Jitter in Loop, rms rad	0.187	0.236
B_{if}, Bandpass Filter Bandwidth	6	40
Limiter Output SNR in B_{if}, db	+9.22	+ 1.0
Limiter Degradation, db	-2.22	- .78
Crossmultiplier Degradation, db	+ 3.1	-
Limiter A Degradation	-2.46	-
Sync Jitter Loss	+ 0.8	+ 1.1
Band Limiting Loss	-	+ 0.91
Carrier Jitter Loss	+ 0.64	+ 0.6
Input SNR in B_{if} Required	+ 9.08	+ 2.87
Required Input SNR in $2B_{LO}$, db	+ 13.86	+15.87
Required Input SNR in 1 cps, db	+16.86	+18.87

Table 4.1-7: SIGNAL-TO-NOISE RATIO REQUIREMENTS FOR DATA DEMODULATION

	SINGLE CHANNEL	TWO CHANNEL
Matched Filter Input SNR in 1 cps, db	9.6	9.6
Subcarrier Jitter, rms rad	0.187	0.236
Jitter Loss for Sampling at k = 0.5, db	0.00	0.2
Sampling Loss, db	0.86	0.86
B_{if}, Bandpass Filter Bandwidth, cps	12	40
Output SNR in B_{if} of Limiter db	-0.33	-5.34
Limiter Suppression, db	-0.59	+0.29
Input Chopper Jitter Loss, db	0.8	-
Carrier Jitter Loss, db	0.64	0.64
Required Input SNR in 1 cps, db	11.31	11.59

at the input to the detector. Based on the SNR requirements for the two channels, as indicated in Tables 4.1-6 and 4.1-7, the data channel is being supplied approximately 6 db better SNR than required assuming a perfect sync reference. This is necessary to reduce sync loop jitter and provide a bit error rate of 1×10^{-5}, or, stated differently, to ensure detector operation above sync loop threshold (WDL-TR-2531, "Mars Mission Communication Analysis").

4.1.3.5 Modulation Efficiency Comparison, Single-Channel Versus Two-Channel System

To determine the relative efficiency of the two systems, we determine the ratio P_{T1}/P_{T2}, the total power required for the single channel to the power required for the two-channel system. Operating under the constraint that the single-channel carrier power P_{c1} equal the two-channel carrier power P_{c2}, we write

$$P_{c2} = J_o^2(\theta_d)\cos^2(\theta_s)P_{T2} = J_o^2(\phi)P_{T1} = P_{c1}$$

where θ_d and θ_s are the modulation indices of the sine wave data subcarrier and the square-wave sync subcarrier, respectively and ϕ is the modulation index of the single channel sine wave subcarrier.

From Section 4.1.3.4, we see that the required data input signal powers, P_{sc1} and P_d, for the single- and two-channel systems are within a few tenth db so that

$$P_d = 2J_1^2(\theta_d)\cos^2(\theta_s)P_{T2} = 2J_1^2(\phi)P_{T1} = P_{sc1}.$$

Combining these two equations results in $\theta_d = \phi$.

Similarly, we find from the same section that the required sync input power ratio

$$\frac{P_{s2}}{P_{s1}} = 2db = \frac{J_o^2(\theta_c)\ \sin^2(\theta_s)}{2J_1^2\ (\phi)} = \frac{P_{T2}}{P_{T1}} = 1.6$$

Combining this with the carrier power constraint equation we find that

$$\frac{3.2J_1^2(\phi)}{J_o^2(\phi)} = \tan^2\ \theta_s$$

Using the value $\phi = 0.89$ rad as derived in Section 4.1.4.3, Volume A, we find that

$$\theta_s = 0.7 \text{ rad} \quad \text{and} \quad \theta_c = 0.89 \text{ rad}$$

so that from above

$$\frac{P_{T1}}{P_{T2}} = \frac{J_o^2\ (0.89)\ \sin^2\ (0.7)}{3.2\ J_1^2\ (89)} = -1.89 \text{ db}$$

which shows that the single-channel system performs better by a factor of 1.89 db.

4.1.3.6 Sine Wave/Square Wave Subcarrier Modulation Trade

The question of whether to use square wave or sine wave subcarrier must also be resolved. In the command link one need not consider the additional implementations required for obtaining phase-coherent sine waves from a digital source, since all generation equipment is on the ground and only one data rate is required. The choice, therefore, can be made upon modulation efficiency only.

The relative power remaining in the subcarrier $\frac{P_{s/c}}{(P_T)}$ and in the carrier $\frac{P_c}{P_T}$ after the carrier-modulation/demodulation process is given by

$$\frac{P_{s/c}}{P_T} = \frac{8}{\pi^2} \sin^2(\theta), \text{ and } \frac{P_c}{P_T} = \cos^2(\theta)$$

for the square wave subcarrier case and

$$\frac{P_{s/c}}{P_T} = 2J_1^2(\phi) \quad \text{and} \quad \frac{P_c}{P_T} = J_o^2(\phi)$$

where θ and ϕ are the peak carrier deviation for the square and sine wave subcarriers, respectively.

The $\frac{8}{\pi^2}$ factor in the square wave subcarrier term is due to the band limiting effect of the bandpass filters in the data and sync legs of the demodulator (Figure 4.1-5).

Under the constraint that the power in the carrier channel be the same for both cases, we plot (Figure 4.1-6) ϕ versus θ, and the relative power in the square wave subcarrier versus θ, as well as the power of the sine wave subcarrier versus θ. In the area of interest $0.3 < \theta < 1.0$ radians or $0.4 < \phi < 1.5$ radians, it is seen that the sinewave subcarrier offers better performance. At low values of index, the improvement is up to 0.9 db.

4.1.3.7 Conclusions and Recommendations

The analysis shows that the single channel detector outperforms the two channel system by a margin of up to 1.9 db. Implementation complexity, reliability, weight, and power requirements do not differ

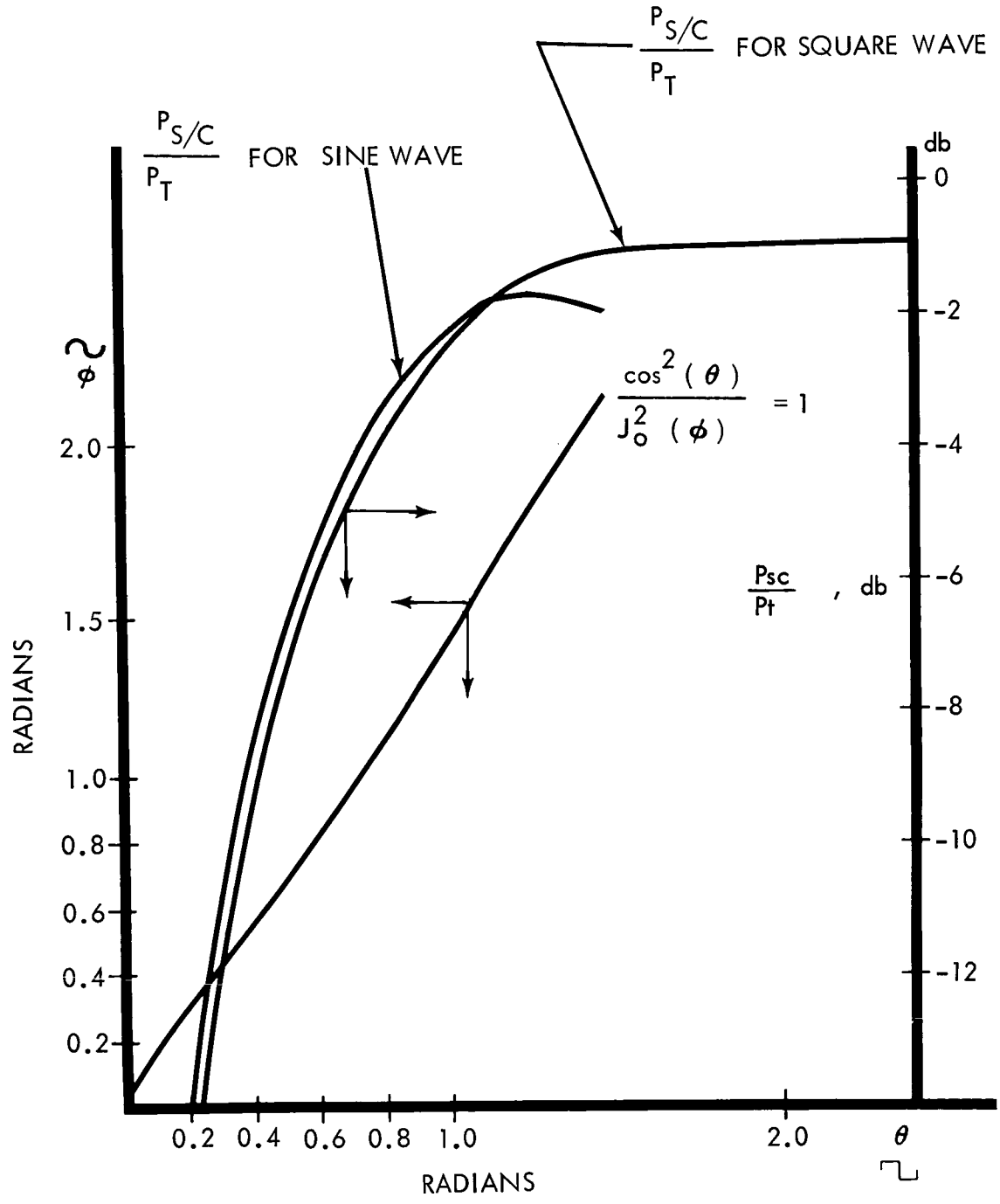

Figure 4.1-6: Single Channel System — Power for Sine and Square Wave Subcarriers with Equal-Carrier-Power Constraint

for the two detectors. Both single- and two-channel detectors have been built in a flight hardware configuration.

On the basis of the above analysis and discussions, the single-channel command detector is recommended as the preferred design for the Voyager mission.

4.1.4 Alternate Component Mechanization Considered

Because the configuration of the Telecommunications System is established by the Voyager characteristics and restraints, the most significant trades are involved in the selection of techniques and components for use in mechanization of the selected design. This section describes the alternate mechanizations of the pre-amplifier, data storage, power amplifier, and switching device.

The selection of the preferred design is based on the following criteria listed in approximate order of importance:

1) Confidence in reliability based on status of development
2) Inherent reliability based on use of proven technology and material
3) Suitability for use in deep space applications based on simplicity, efficiency, electrical performance, external magnetic fields, and survivability of environmental conditions
4) Other factors unique to specific components

The information contained in this section is based on a comprehensive survey of those companies whose past performance and continuing developmental work might qualify them for participation in the Voyager Program. Although the list is not complete, sufficient information has been obtained to provide objective confirmation of the evaluation.

Power amplifiers and data storage devices have been recognized as problem areas requiring long lead time development by both the

Department of Defense and the National Aeronautics and Space Administration. Design and development contracts have been awarded to some of the contractors who have been consulted. It was attempted to be as objective as possible on conducting the supplier survey, however; the existence of development contracts for certain devices must be considered in the weighting factor assigned to the criteria for selection. Although performance and test data are quoted from selected suppliers, this does not imply that any selection of source has been made at this time.

4.1.4.1 S-Band Receiver Preamplifier Trade Study

Summary--The purpose of this section is to define and compare the various devices capable of performing a low-noise S-band preamplifier function for the Voyager mission. Four devices were surveyed; the tunnel diode amplifier, the transistor amplifier, the parametric amplifier, and the low-noise traveling wave tube. Of these, the tunnel diode amplifier was selected.

Required Amplifier Characteristics and Tentative Specifications--

1) The required characteristics will be as follows:
   a) Center frequency; 2113 ± 5Mc
   b) Magnetic and reliability requirements as listed in Section 2.2, Vol. A for equipment aboard the Voyager vehicle
2) The tentative specifications will be:
   a) Gain; 15 ± 1db over all operating conditions
   b) Bandwidth; 10 Mc minimum at 3 db points

c) Noise Figure; 2-5 db over all operating conditions

d) Impedance; 50 ohms, VSWR maximum 1.2:1 for input and output

e) Dynamic Range; Threshold to --50 dbm

f) Phase Instability (nominal); Less than 2 degrees peak in $2B_{LO}$=cps

g) Phase Instability versus Vibration (above nominal); Less than 0.5 degree peak/g in $2B_{LO}$=100 cps

h) Phase Shift versus Temperature (above nominal); ± 10 degrees maximum

Alternative Device Discussion--All four of the devices considered are capable of providing the required 15 db of gain with a maximum noise figure of 5 db or less. The significant device parameters differ, however, as detailed in the following paragraphs. Table 4.1-8 is a listing of the pertinent parameters of each of these devices.

1) The Tunnel Diode Amplifier (TDA)

A TDA can be supplied by either Micro State Electronics Corporation[25] or International Microwave Corporation[26], which will meet or exceed the required specifications. The TDA is illustrated in Figure 4.1-7 operating with a 4-port circulator. The important active element is the negative conductance -G, presented by the tunnel diode when properly biased in an appropriate microwave circuit. The reflection coefficient from the negative conductance has an absolute value greater than one, indicating gain. The circulator separates the incoming signal from the amplified outgoing signal. The second circulator section shown on the right in Figure 1--4.1.7 ensures that the amplifier will be stable regardless of the input or output terminations.

DEVICE TYPE:	MAXIMUM NOISE FIGURE INCLUDING 10 db 2nd STAGE	GAIN / 3 db BAND WIDTH	DYNAMIC RANGE (OUTPUT LEVEL) FOR 1 db COMP	ESTIMATED SIZE AND WEIGHT (WITH MAGNETIC SHIELDING)	POWER REQUIRED (EXCLUDING ANY TEMPERA-TURE CONTROL)	M PR
GERMANIUM TUNNEL DIODE AMPLIFIER (TDA)	4.9 db MAXIMUM INCLUDING 4-PORT CIRCULATOR	15 db / 120 mc	-21 dbm	6 x 6 x 5 IN. 4 lbs	180 mw 15 ma at 12v d.c.	~ A SH (M SH
TRANSISTOR AMPLIFIER (ANTICIPATED CHARACTER-ISTICS)	5 db	18 db / 50 mc	0 dbm	1 x 1 x 4 in. <1 lb NO SHIELD-ING REQUIRED	80 mw 12 ma at 6 v d.c.	N FO FI
PARAMETRIC AMPLIFIER (PAR AMP)	2.0 db INCLUDING 4-PORT CIRCULATOR	15 db / 50 Mc	-5 dbm	6 x 6 x 6 in. 6 lb INCLUDING S/S PUMP	S/S - 10w KLYSTRON 17-27w	~ AT SH (M SH
LOW-NOISE TRAVELING WAVE TUBE AMP (TWTA)	4.7 db	19 db / 2 Gc	-5 dbm	13 x 6 x6 in. 20-25 lb	1 w	~ 20 SH (M SH

AGNETIC OPERTIES	VIBRATION, SHOCK, AND ACCELERATION DATA	TEMPERATURE RANGE OPERATING STORAGE	SAFE INPUT POWER LEVEL	PHASE STABILITY
500 GAMMA 9 in. W/O IELDING UST BE IELDED)	TEST DATA: 60 g, 7 ms 250 g, 1 ms } SHOCK 20-2000 cps at 3 oct/min 20-g VIBRATION 60 g, 2 min ACCELERATION	W/O COMPENSATION -25 to + 75°C -40 to +80°C	50 mw cw	TEST DATA: $\Delta\phi = 4.6^\circ$ T = 20° C $\Delta\phi = 0.8^\circ$ at 1 db GAIN COMPRESSION
ONE EXCEPT OR CURRENT ELDS	NO DATA, BUT ANTICIPATE NO FUNDAMENTAL PROBLEM MEETING SPECIFICATIONS	-25 to +75°C -60 to +80°C W/O COMPENSATION	NO DATA	NO DATA
500 GAMMA 9 in. W/O ELDING UST BE ELDED)	NO DATA, BUT ANTICIPATE NO FUNDAMENTAL PROBLEM MEETING SPECIFICATIONS WITH SOLID-STATE PUMP, THE PROBLEM IS SIMILAR TO THE TDA	-25 to +75°C W/COMPENSATION OR ANY 30° INTERVAL W/O COMPENSATION -40 to +80°C	1w cw	$\pm$ 0.5° OBTAINED WITH UNLEVELED AND UNLOCKED PUMP. TEMP CONTROL MAY BE REQUIRED
2 GAUSS AT in. W/O ELDING UST BE ELDED)	SINUSOIDAL VIBRATION TESTED TO: 0.10 in. D.A. 5-45 cps 10g 45-2000 cps SHOCK: 30 g, 11 ms (FURTHER TEST AND REDESIGN MAY BE REQUIRED)	-54° to +85°C -54° to +85°C	0.5w cw	INPUT VOLTAGE CHANGE OF 10% YIELDS $\Delta\phi = 60^\circ$

Table 4.1-8: Preamplifier Performance Characteristic Chart

CONDUCTION COOLING	OPERATING VSWR INPUT / OUTPUT	GAIN STABILITY	COSTS * (THOUSANDS OF DOLLARS)
YES	2:1 / 1.2:1	$\Delta G = \pm 1$ db -10° to +55°C G = + 2 db -25° to + 75°C W/O COMPENSATION	$2-3
YES	NO DATA	NO DATA	$2-4
YES	2:1 / 1.2:1	TEMPERATURE, PUMP POWER, AND FREQUENCY SHOULD BE COMPENSATED	$12-15 INCLUDING KLYSTRON P/S AIRCRAFT TYPE UNIT
YES	2:1 / 1.5:1	GAIN STABILITY REQUIRES P/S REGULATION	2 at $65

*LESS ENVIRONMENTAL TESTING COSTS

The gain of the germanium TDA is a function of the temperature and may vary as much as $\pm$ 2 db through the interval of -25°C to + 75°C. A gain variation of $\pm$ 1 db occurs through the interval of -10°C to +55°C. These gain fluctuations may be reduced and the temperature extremes expanded through the use of temperature compensation and heaters. The entire circulator as well as the tunnel diode module will require temperature control and will consume approximately 10 watts.

A phenomenon that may make temperature control desirable, depending on the final environmental specifications, occurs with the circulator. One vendor reports that circulators used with TDA's will change characteristics at temperatures below -40°C. These permanent changes are slight, but do adversely affect the amplifier's performance through a change in the VSWR presented at the tunnel diode port.

A gallium-antimonide tunnel diode can be substituted for the germanium tunnel diode. This will reduce the maximum noise figure from 4.9 db to 4.3 db (including a 10 db second stage). The noise figure and gain of the gallium-antimonide unit are very temperature-sensitive and require temperature control. In addition, the reliability of the gallium-antimonide TDA is not as well documented as that of the germanium TDA.

Additional isolation in front of the TDA to ensure stability over all environmental conditions is desirable in the absence of temperature control. This will involve an additional third circulator section in front of the amplifier (5-port circulator). This added section will increase the noise figure by virtue of the added insertion loss, to 5.1 db and decrease the amplifier input VSWR from 2:1 to 1.25:1.

The TDA's circulator produces a magnetic field of approximately 500 gamma at 9 inches. For the Voyager mission a standard TDA will require magnetic shielding or compensation. It is estimated that an adequate shield will add 2 pounds to the TDA for a total weight of four pounds.

With regard to shock, vibration and acceleration, the TDA has been tested for other programs to levels that approach the Voyager tentative specifications. TDA's have been space qualified for such programs as ITT's ComSat and JPL's Mariner "C". Additional environmental testing, will be required.

The TDA has a very low parts count as indicated in Figure 4.1-7, with the tunnel diode being the least reliable of the circuit elements. The normal failure involves an open- or short-circuited tunnel diode. In a failed mode, the amplifier will have an insertion loss of from 1 to 6 db. The TDA is a very reliable device, with an estimated MTBF (based on life tests) of 25,000 hours and is often warranted for 18 months or 13,000 hours.

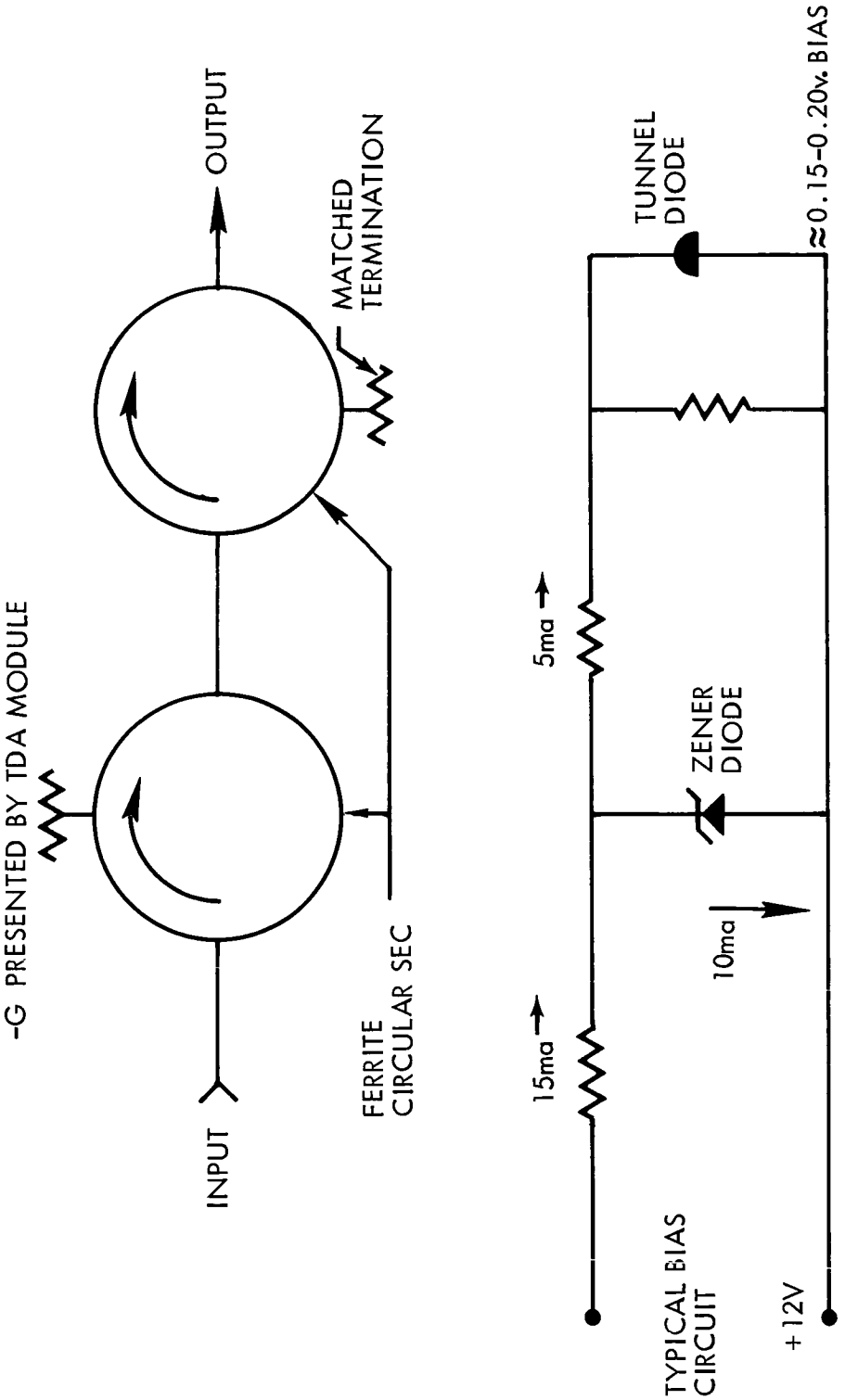

Figure 4.1-7: Tunnel Diode Amplifier

The TDA is well developed and is finding wide application in space. Typical cost is $2000, neglecting magnetic shielding costs and other additional measures taken to boost reliability.

2) The Transistor Amplifier

Recent work being performed at the General Electric Company and at Motorola indicates that low noise S-band transistor amplifiers will be fully developed within 1 year. The anticipated noise figure is 4 db. Such an amplifier would be very small, lightweight, with no magnetic shielding problems, and a small power requirement.

3) The Parametric Amplifier (Par Amp)

The Par Amp is a negative conductance device similiar to the TDA except that a higher frequency pump source is required. The negative conductance is derived from a varactor modulated by a pump source and coupled to a signal circuit and an idler circuit. A four-port circulator is used to separate the incoming and amplified signals.

The parts count is much higher than for a TDA. If either a klystron or a solid-state pump source is provided, the amplifier is quite reliable. It is estimated that a well-designed parametric amplifier can easily achieve an MTBF of 12,000 hours.

The primary failure mode is a loss of pump power. The second most important failure mode is an open-circuited varactor. In

both of these cases, the amplifier presents an insertion loss of about 3 db.

The Par Amp is generally more gain-sensitive to temperature changes than the TDA and would require temperature control. It is anticipated that a total primary power requirement of 20 watts will be needed to operate a temperature controlled Par Amp.

The Par Amp uses a circulator and hence will have the previously mentioned TDA circulator problems. Specifically, there are permanent characteristic changes that have been noted with circulators below -40°C. In addition, the circulator will have to be magnetically shielded.

If the Par Amp is temperature controlled, a five-port circulator will not be necessary to insure stability over the environmental extremes. The extra circulator section is necessary, however, just as with the TDA, if the input VSWR is to be brought below 2:1.

The greatest asset the Par Amp could contribute to the Voyager mission is in the area of performance with its lower noise figure. A standard Par Amp would have a noise figure of 2 db and cost about $12,000 to $15,000.

The Par Amp has not yet reached full design maturity in the area of environmental tests and thus does not enjoy as much confidence for space applications as the TDA.

4) Low Noise Traveling Wave Tube Amplifier (TWTA)

The Watkins-Johnson - 269 TWTA [27] can be adapted to meet the required amplifier characteristics and specifications with the exception that it may not meet the shock and vibration levels.

This tube is similar to power TWT's that have been space-qualified for other missions. Some vibration, shock, and acceleration tests have been made, but tube redesign and more tests will be required.

The tube will require considerable magnetic shielding (presently produces 2 gauss at 20 inches) and to meet the VSWR requirement it must be preceded by an isolator requiring further magnetic shielding. The fully shielded weight is anticipated to be 20 to 25 pounds.

The TWT power supply requires careful regulation to hold the phase and gain changes within the specified tolerances.

The primary failure mode for the TWTA is power supply failure with its relatively high parts count. This is followed by filament problems in the tube itself. Tube or power supply failure will cause 60 to 80 db attenuation of the received signal.

The tube is designed for a 35,000 hour life and costs approximately $32,500.

Selection Logic--The TDA was selected over the other 3 devices primarily on the basis of reliability and development status. Secondary supporting considerations are weight and cost.

The remaining three devices under consideration all lack the evidence of flight-proven performance and extensive testing. The reliability of the TDA is highest because of its simplicity.

The weight and cost of the TDA is second only to the transistor amplifier, which should not be considered at this time due to its uncertain availability.

4.1.4.2 Data Storage Component Trades

The purpose of this trade study is to examine the various data storage devices and techniques applicable to the Voyager mission. The storage devices investigated were magnetic tape recorders, core memories, plated wire memories; and thermoplastic, photoplastic, aluminized plastic, and phototape recorders. Redundant magnetic tape recorders were selected for planetary science data and magnetic core storage buffers for spacecraft engineering, cruise science, and capsule data.

Mission Data Storage Requirements and Constraints--The baseline telemetry and data storage subsystem, which uses two data subcarriers

and synchronous formating, requires large bulk storage of planetary science data and buffer storage of spacecraft engineering, and capsule data. If only one data subcarrier with serial multiplexing of all types of data were used, then additional buffer storage elements would be required.

The planetary science storage requirements are:

1) Maximum practical storage capacity
2) High reliability
3) A large record/playback rate ratio
4) Playback synchronized with a clock reference.

The first requirement is necessary because acquisition of planetary science data at each periapsis can easily exceed 10^8 bits. Reliable operation of this storage component is essential to preserve planetary science data for delayed transmission and as a precautionary backup in the real time mode. The input rate is relatively fixed and is much higher than can be transmitted in all delayed transmission modes. The input rate is 50 kbps and the lowest output rate is 2 kbps. On playback the data is subjected to block encoding which requires synchronization to a fixed clock reference.

The capsule and spacecraft engineering storage components have similiar requirements. For the synchronous formating of the telemetry and data storage subsystem, data playback from these devices must be time-multiplexed with other data sources on a fixed-word basis (i.e., 7

bits per word). This implies that these storage devices must output short bursts of data in a sequential manner (under control of a reference clock) without by-passing any stored data (a continuous running tape recorder cannot be utilized). Expected Earth out-of-contact times (due to maneuvers, occulations, etc.) will require a minimum storage of 72 x 10^3 bits for spacecraft engineering data, and capsule data.

All the storage devices are allowed to operate on a sequential access basis. Data that is read in first is read out first. There is no requirement for random-access readout.

In addition to the requirements listed, the following factors must be considered in selecting candidate storage components:

1) Weight, volume, power consumption
2) Availability of space-qualified units for the 1969 and 1971 launch dates
3) Performance parameters
4) Environmental constraints as stated in Section 2.2, Vol. A.

Description of Alternate Devices--In the following paragraphs the advantages and disadvantages of the four storage techniques will be compared.

Magnetic Tape Recorders--The three types of recorders under consideration are a) endless loop transports, b) reel-to-reel transports and c) incremental motion transports.

Endless Loop Transports [28]

1) Storage capacity is limited to less than 10^7 bits, recorded on mylar-backed tape one-half inch wide or less.

2) Adjacent layers of tape rub against one another as tape unwinds from a specially profiled tape spool. Dry lubrication has been found necessary to provide smooth tape flow.

3) With a closed loop configuration, it is possible to record the entire data and then arrive at the starting point for playback.

4) Endless loop recorders require actuation during the launch phase to avoid the possible problem of tape spillage.

5) Loop recorders are inherently unidirectional devices.

6) Loop recorders have been used where volume requirements preclude the use of the reel-to-reel approach.

Reel-to-Reel Transports 29 and 30

1) Data capacity of 10^9 bits for flight hardware has been achieved.

2) A peripheral tape drive or an iso-elastic drive provides a controlled tape tension as tape pack diameters change. Bi-directional operation is inherent with motor reversal. Either Mylar or H Film (Kapton) drive belts may be used.

3) Record-to-playback ratios as high as 1200:1 have been attained in current spacecraft units. Speed ratios over a range of 10:1 or less are obtained by frequency division of the power supplied to a single motor. Larger ratios are more difficult to achieve and require separate record and playback drive motors with associated coupling mechanisms.

4) Transport power consumption is approximately proportional to tape speed. Average input power is of the order of 15 watts at 30 inches per second for operation with synchronous-hysteresis motors.

5) While reproduce speeds as low as .01 inches per second have been used, this is not generally compatible with a large number of record channels. This results in a low output signal of from 50 to 100 microvolts and may impose a severe burden upon the electronic amplifiers.

6) Two methods of recording are notable:

   a) Input data is serial NRZ digital clock encoded and sequentially recorded with head track switching. Track 1 is recorded with tape moving in the forward direction; Track 2 with the tape moving in the reverse direction; Track 3 in the forward direction, etc. This system requires only one record and one playback amplifier, but additional track switching circuitry.

   b) Serial input data is converted to a parallel format, recorded on multiple tracks with a separate track for synchronization, and on readout is converted from the parallel to a serial stream. Currently this method uses a separate record and playback amplifier for each channel in addition to the shift registers for conversion.

7) Random access has not been used in spacecraft recorders. Limited access may be achieved by track selection with serial record.

8) Long-term speed stability is assured by driving the 2-phase motor power from a dc-to-ac inverter synchronized to an internal 400 cps reference frequency. The short-term stability, i.e., wow and

flutter, jitter, etc., depends on the response of a phased locked loop reclocking system. The vendor survey states that a jitter figure of less than 3 percent peak-to-peak is within the current state-of-the-art.

Incremental Motion Transport

1) Incremental tape motion is applicable to either the endless loop or reel-to-reel recorder. Drive is generally with a fast response printed circuit motor. Start is triggered from a suitable sync pulse. Both motor acceleration and deceleration are precisely controlled with essentially constant velocity during readout of the bit or word.
2) With the incrementing technique, playback below 0.1 inches per second can be achieved.

Core Memories--Toroidal ferrite cores strung on wires are presently used as storage elements in very large memories at computation facilities and for relatively small memories in satellites and spacecraft. The following are some noteworthy characteristics:

1) Packing density is presently approximately 500 bits per cubic inch for complete memories with up to 100,000 bits capacity. Density increases to 5000 bits per cubic inch for larger memories, presently limited to less than 10^7 bits.
2) These memories may be organized for random access, or more simply for temporary storage of serially acquired data.
3) Readout is nondestructive.

Plated Wire Memories--New storage techniques are evolving, which exploit magnetic and magneto resistive effects. The plated wire memory stores information bits according to the magnetization of a plated wire. Ones and zeros are stored as clock-wise and counter clock-wise magnetization. The following characteristics have been noted:

1) Packing density is approximately 500 bits per cubic inch for complete memories with up to 100,000 bits capacity. For larger memories, up to at least 10^8 bits, the density increases to 5000 bits per cubic inch.

2) The mechanical construction is simple. The bit line and sense line are combined into a single wire. Large tolerances make for inexpensive construction.

3) Switching energy is about 1/200 of that required for a 50-mil-OD, 30-mil-ID ferrite core. Signal output is nominally $\pm$ 10 mv.

4) Readout is nondestructive.

5) The wire memory tolerates severe environments. Certain sub-assemblies have operated over a temperature range of -20°C to +100°C, withstood impact forces to 140G and vibration from 10 to 60 cps to 40 G peak.

While plated wire memories hold potential for future missions because of their relative high storage capacities, ruggedness and simplicity, they cannot be considered for use on the Voyager because of the status of development and the absence of test data. Current research models with sufficient storage capacity for Voyager would require four times as much power as a magnetic tape recorder of the same capacity.

Thermoplastic, Photoplastic, Aluminized Plastic and Photo Tape Recorders--These are advanced recording techniques that show considerable promise in the future. Both thermoplastic and photoplastic techniques are characterized by extremely high bit packing densities (up to 10^7 bits per square inch has been achieved for thermoplastic recording). However, both techniques use special processing for recording and reading which require large bulky equipment. Both the aluminized plastic and photo tape techniques are characterized by moderate bit packing densities (2500 bits per square inch is feasible for aluminized plastic recordings). The total weight and volume required for recorders utilizing these techniques is somewhat less than required for thermoplastic and photoplastic recorders.

Power requirements for recorders using these techniques are higher, by a factor of at least four, than magnetic tape and core memory devices.

Two characteristics of recorders using these techniques discourage their use for the Voyager requirements. Compared to other candidate storage devices such as magnetic tape recorders, core and plated wire memories, these recorders require a relatively large weight volume and power. The most important disadvantage is that these techniques are relatively new and have not been fully developed. After an extensive review with manufacturers developing these techniques, it has been concluded that usable, reliable spacecraft recorders cannot be developed and qualified in time for the 1969 and 1971 Voyager launch dates.

Logic of Selection--The storage devices for the Voyager mission can be considered in terms of a large storage device (10^8-10^9 bits of planetary science data) and two smaller storage devices (10^5-10^6 bits each for capsule and spacecraft engineering data). The parametric curves of Figure 4.1-8 compare the types of devices examined on the basis of weight, power, volume, and storage capacity. Reliability and availability (state of development) are considered separately.

The selection of the optimum storage device for the particular data storage requirement of the Voyager spacecraft was based on the curves of Figure 4.1-8 and an evaluation of the reliability, availability, operating characteristics and cost of each device. The curves of Figure 4.1-8 show which device will supply the data storage capacity required and then the choice can be made to minimize weight, power, and volume.

Planetary Science Storage Device--The reel-to-reel magnetic tape recorder is chosen because it will handle the 10^8 bits required and has flight experience. The weight, power, and volume parameters also are most reasonable for this technique. Thermoplastic and photoplastic techniques may become applicable for later Voyager missions if they can be space-qualified.

Capsule Data and Spacecraft Engineering Data Storage Devices--The core memory and the plated wire memory have much the same characteristics with respect to weight, volume, and power dissipation. Both memory types are very applicable to the Voyager storage requirements for engineering data. In addition, the performance parameters of interest are almost identical.

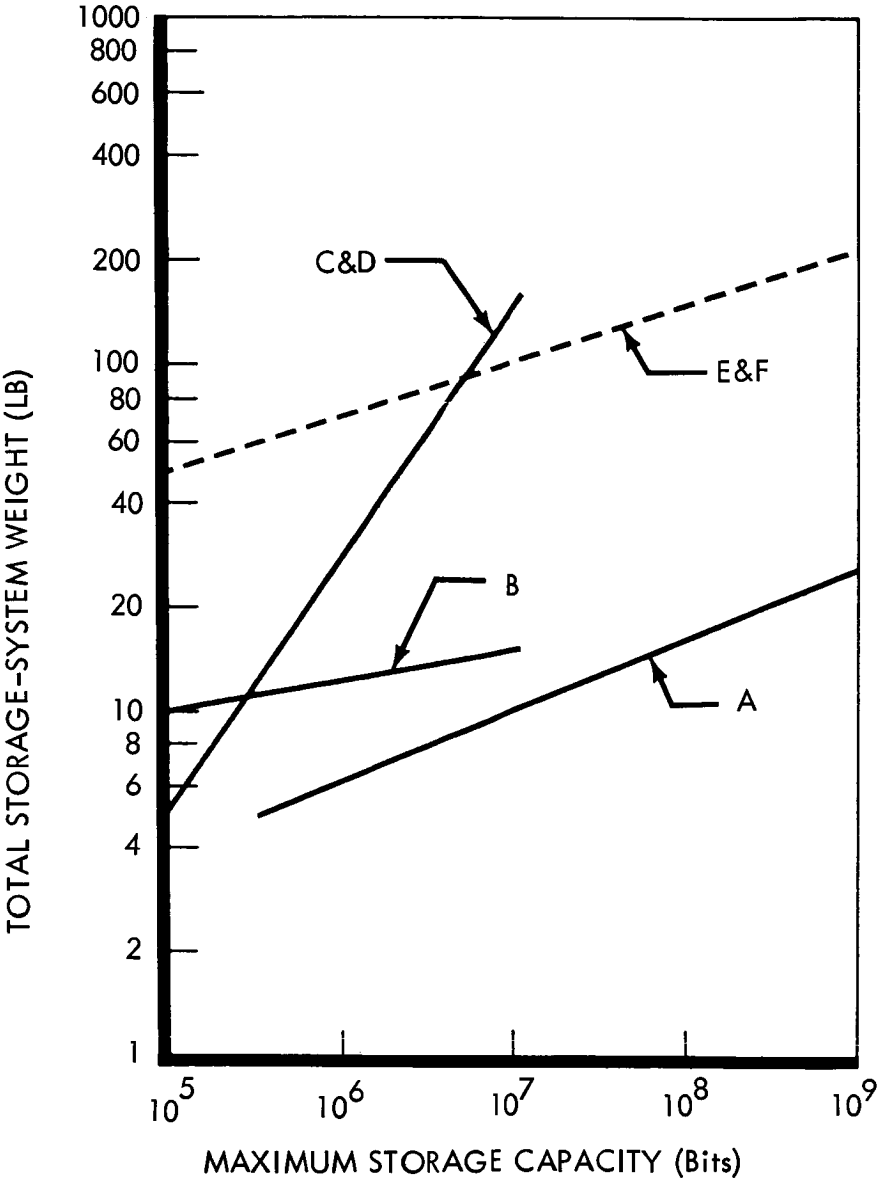

LEGEND:

CURVE A — REEL-TO-REEL RECORDER
CURVE B — ENDLESS LOOP RECORDER
CURVE C — CORE MEMORY
CURVE D — PLATED WIRE MEMORY
CURVE E — THERMO-PLASTIC RECORDER
CURVE F — PHOTO-PLASTIC RECORDER

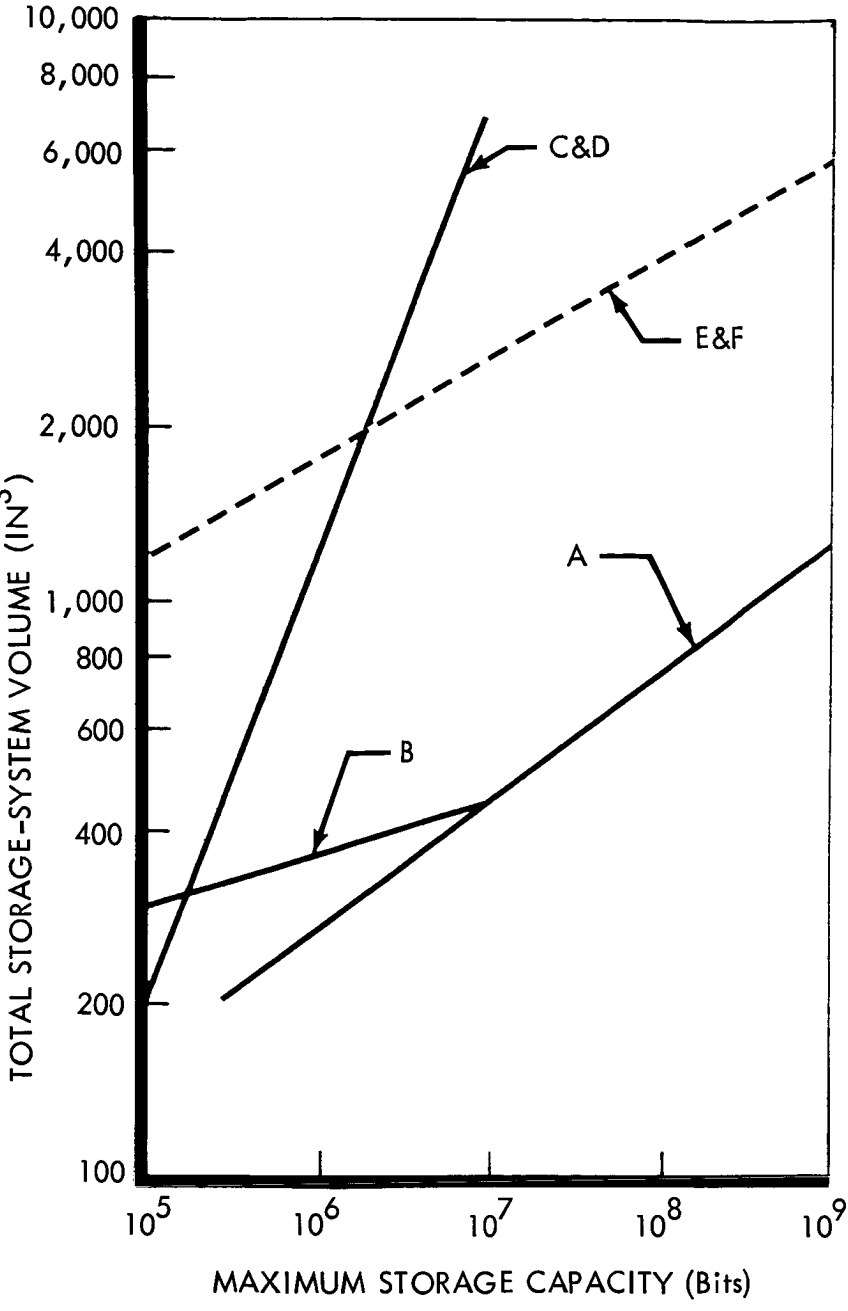
10,000
8,000
6,000
4,000
2,000
1,000
800
600
400
200
100
TOTAL STORAGE-SYSTEM VOLUME (IN^3)
C&D
E&F
A
B
10^5
10^6
10^7
10^8
10^9
MAXIMUM STORAGE CAPACITY (Bits)

Figu

4121

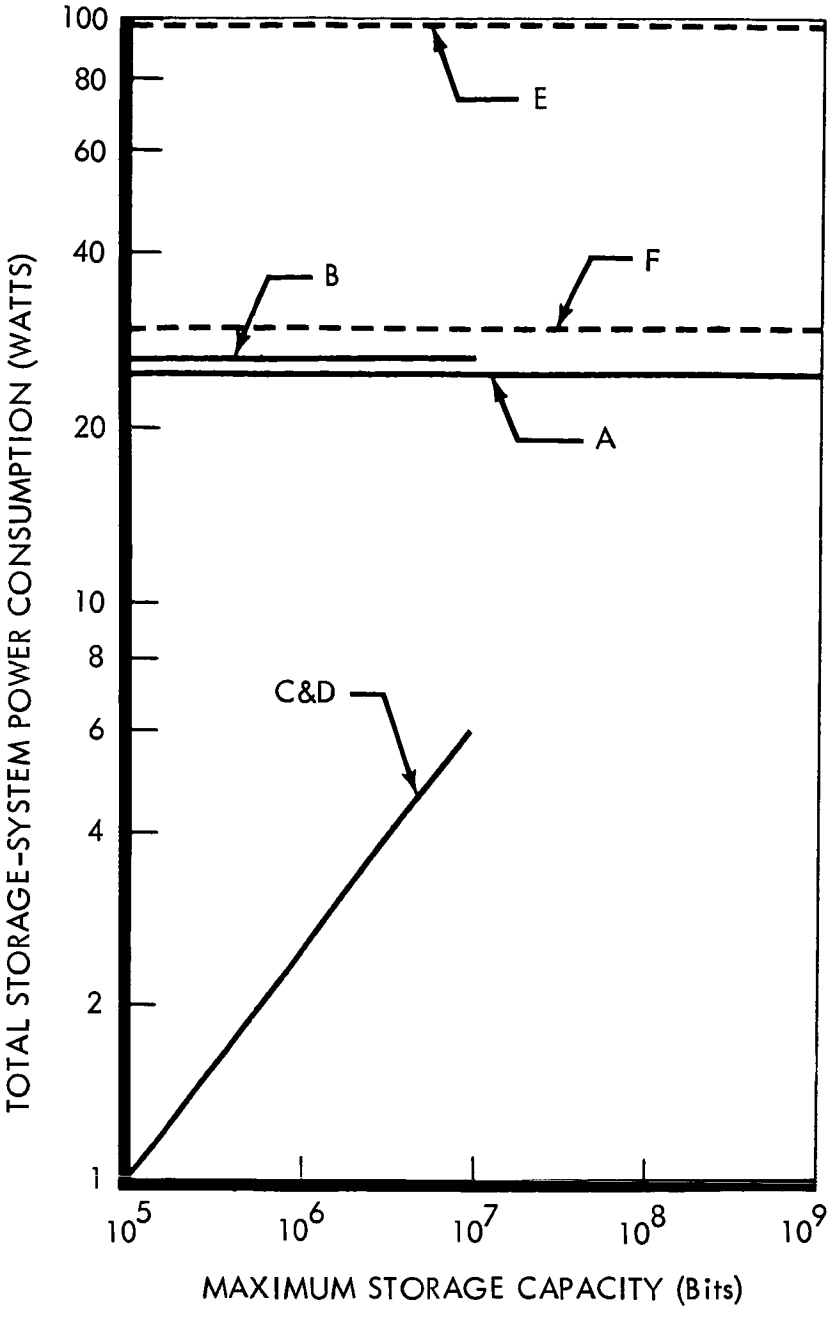

NOTE: TAPE RECORDER POWER CONSUMPTION BASED ON 30-ips RECORD SPEED

re 4.1-8: Comparison of Recorder Characteristics

Because the competing characteristics are so similar, factors such as availability, reliability, and past qualification for spacecraft usage must be considered. Core memories have proven to be reliable and qualified models are available for the 1969 and 1971 Voyager launch dates. Plated wire memories are relatively new and development is incomplete. It is on this basis that the recommendation is made that core memories be utilized for the applicable Voyager storage requirements.

4.1.4.3 Power Amplifier - Component Trade Study

The purpose of this trade study is to select the most appropriate power amplifier device for the Voyager mission. The three output power levels of 20, 50, and 100 watts which are consistent with system constraints were considered. The amplifier devices investigated include the traveling-wave tube (TWT), electrostatically focused Klystron (ESFK), Ion Focused Klystron (IFK), amplitron, cavity triode, and an all-solid state transmitter. The 50 watt TWT has been selected as the preferred design with a 50-watt ESFK as a first alternate.

Required Characteristics--The required characteristics for the power amplifier are listed below:

Power Output and Gain (assuming no more than 500 mw drive power)

Power Output	Gain
20 watts	20 db or more
50 watts	20 db or more
100 watts	20 db or more
Frequency	2295 ±5 mc
Bandwidth	5 mc minimum

Environmental Requirements--As specified in Section 2.2, Vol. A.

Decision Criteria--In deciding upon the best power amplifier for the 20, 50 and 100 watt power level, the following general criteria, listed in order of importance were considered.

1) Reliability

2) Weight

3) Availability (State of Development)

4) Cost

5) Performance

Discussion of Alternative Devices--This section will discuss the advantages and disadvantages of six different approaches to the power amplifier design.

Traveling-Wave Tube Amplifier [31]--The TWTA is the most frequently used amplifying device for today's space projects requiring an RF power output of 2 or more watts. It has been used in Syncom, Surveyor, Apollo, Pioneer, Mariner (Mars), Application Technology Satellite, Early Bird, and Lunar Orbiter. Thus, the tube has accumulated extensive development, space qualification, and life test history, which provides greater reliability assurance for this device than for any of the other competing devices.

Vacuum tubes exhibit two types of failures, sudden or catastrophic and wear-out. Catastrophic failures such as open circuit of the heater or rupture of a vacuum seal are mainly due to manufacturing defects and usually occur within the first few hundred operating hours. Tubes with this sort of weakness may be selected out by

seasoning tests. It is generally accepted that the wearout life of a TWT is largely determined by a loss of emission from the cathode. To achieve long operating life, a cathode must be operated at very low current densities (less than 250 ma/cm^2) [32] and all cathode poisoning agents must be removed. The operating temperature of the cathode (normally between 700 and 725°C) is also very important. Bell Laboratories studies show that increasing the cathode temperature only 25°C above the optimum temperature will reduce tube life by one-half.

Hughes has 5 of its 394H 20 watt tubes on continuing life test. To date, these devices have accumulated over 1500 hours each without failure. The 20-watt tube is closely related to its 10-watt predecessor. Hughes has seven 10-watt tubes with 22,000 hours each on life test. RCA has ten 11-watt tubes with 27,000 hours continuous testing on each. Watkins-Johnson has nine 13-watt tubes with 30,000 hours each on life test. Because there is a close generic relationship between these 10 to 13 watt tubes and a higher power design, the life data provides a high confidence level in the TWTA for the Voyager mission.

The anode and helix voltages of a TWTA must be well regulated (better than 0.5 percent) to provide proper focusing and beam synchronism with the r-f wave on the helix (input signal). Power supply variations will cause defocusing and a corresponding increase in helix interception current. An excessive increase of current will heat the helix and is associated with output power sagging. The TWT will generally work with up to 3:1 output VSWR without damage to the device. The power supply is required to supply 3 or 4 high voltages plus heater power.

The traveling-wave tubes' size and weight range from 10 cubic inches and 1 pound for a 20W device to 15 cubic inches and 2.5 pounds for proposed 50 and 100W devices. The major increase in the size and weight from the 20 watt package (package is defined to include power supply) to the 100 watt package would be the size of the required power supply.

TWTA's can be developed that will meet all the requirements listed except for the stray magnetic field requirements. A typical X-band PPM TWT was measured at Philco WDL and found to have a stray field of 400 to 600 gamma at 12 inches. It was estimated that this tube could be compensated to reduce the field by a factor of 3 (reducing field to approximately 130 to 200 gammas). Reducing the magnetic field to the desired level at all orientations from the tube and at the specified distance would be extremely difficult. However, past experience at Hughes indicates that the total field in any selected direction may be reduced to very low levels by using compensating magnets. In the Pioneer program, the Hughes 349H tube was selectively compensated so that at a distance of six feet in a specific direction, the field was approximately 0.1 gamma. Mounting two TWTA's antiparallel will ease the compensation problem.

Electrostatically Focused Klystron (ESFK or Klystron) Amplifier [33]-- Recent developments have been made by Litton Industries on a (20w) klystron tube, Model No. L-3910, using electrostatic focusing in place of magnetic focusing. This klystron has an electron gun (cathode), a converging element, cavities separated by Einzel lenses and a collector. The beam is propagated from the electron gun through the cavity areas,

focused by the alternate lenses, and received by the collector. Rf power is coupled out through an iris.

The number of cavity resonators is determined by the desired gain and bandwidth. The cavities are copper plated to provide efficient heat transfer. A depressed collector model is being built by Litton and its efficiency should be approximately 40 percent at the 50 watt level. The method of focusing provides ion drainage which assists in eliminating ion back-bombardment of the cathode, thus increasing cathode life.

Since the electron beam is focused by the electrostatic lenses, the magnetic field of this klystron would consist only of the stray field from the materials used in the tube construction and from current loops in the power supply.

The required cavity size for S-band klystrons makes the device rather large (approximately 4.5 diameter by 5 inches length) with a weight of 2.5 to 3 pounds for a 20 watt device. The 50 to 100 watt device would be approximately 4.5 inches in diameter by 5 inches in length with a weight of 3.5 to 5 pounds.

Because the output power is directly proportional to the anode voltage (with no defocusing effect), variation in voltage can be used for multiple power output modes.

This tube has not been space-qualified and, although it appears doubt that the device will exhibit an operating life comparable to the

TWT, this has not yet been demonstrated. The cathode wearout should be no problem as the tube operates at low cathode-loading densities of 72 ma/cm^2 for the 20 w device to 128 ma/cm^2 for the 100 w device.

If it were not for its early stage of development, the ESFK would perhaps be the best choice for Voyager mainly because of its potentially long life and low stray magnetic field. In any case, the ESFK is more appropriate at the 100-watt level or higher. This is mainly due to the fact that beam formation, beam interaction, and beam collection are physically separated and that the rf interaction structure is extremely rugged in a thermal as well as mechanical sense.

The Amplitron [34]--The amplitron is a cross-field backward wave amplifier developed by Raytheon. It has a high-plate efficiency of 55 to 60 percent with a stage gain of 14 to 17 db. To provide over 20 db gain two amplitrons must be cascaded.

Magnets are required for focusing the amplitron and a stray magnetic field of 200 gamma has been measured.

The size of an amplitron assembly is approximately 6 inches by 7 inches. A 20 watt package weighs 5.5 pounds.

The long-term reliability of the amplitron is questionable. The device is sensitive to input drive and output loading.

With the re-entrant electron stream used by the amplitron, the cathode is subject to high ion back-bombardment. The Raytheon calculations

that indicate a long-life cathode for the amplitron do not allow for the back-bombardment and it is doubtful that this device will live up to its predicted life of 33,000 hours. The lack of reliability of this device is sufficient to disqualify it from consideration at this time.

Ion Focused Klystron (IFK)--This tube was developed by the Sperry Rand Corporation many years ago and has been used extensively in microwave repeater systems. Tubes have operated continuously for as long as 78,000 hours without failure. However, life test data in a space environment does not exist.

The tube does not require a focusing magnet and the development of a long-life, 50-watt tube is presently within the state of the art.

This tube must be disqualified at this time because of its low gain (less than 20 db) and because little, if any, development work has been conducted on tubes with power capabilities of 20 watts or greater.

Triode Amplifier -- The ceramic triode, in conjunction with input and output resonant cavities may be used in an amplifier that can provide up to 50 watts power output. However, because of the low gain of these tubes (10 to 13 db per stage) 2 stages are necessary. A 2-stage amplifier is estimated to have a 40 percent efficiency (device and heater power - not including power supply efficiency). A special cathode has been developed by Siemans and Halske AG, a German firm, which is potentially capable of a 50,000 hour life. The tube, however, suffers from Barium deposition on the grid and anode structure which causes detuning of the rf circuits. As a result, net tube life is predicted to be approximately 10,000 hours.

Because of the complexity associated with two amplifier stages and because the expected tube life is too short for this application, the ceramic triode is not considered to be a good candidate for the Voyager telemetry power amplifiers.

Solid State Transmitter[35]--A solid-state transmitter would consist of a VHF crystal oscillator, a VHF power amplifier, and several UHF varactor multiplier stages. Such a system has the potential for very high reliability and would require neither magnetic focusing nor a high voltage converter. A total efficiency of 10 percent is predicted. It is presently within the state of the art to develop such a transmitter with 20 watts output at 2/Gc. However, it will be necessary to operate the power transistors and the varactors near their maximum power ratings, and it is questionable whether the potential reliability could be achieved under those conditions. Long operating life requires the use of transistors and varactors that have been derated below their normal operating levels. If this derating is applied to existing devices, it is not obvious that the required 20-watt output can be obtained. Within 1 year, devices with the required characteristics will very likely be available.

Recommended Power Amplifier--The TWTA, operating at 50 watts output, has been selected as the preferred design. This device is not the most desirable from a magnetics standpoint because it requires magnetic focusing. However, the extensive development, space qualification, and life test history on the TWT places it in a unique category. None of the competing devices with the performance required have been space qualified.

The recommended approaches at each power level considered are:

	20 Watts	50 Watts	100 Watts
First Choice	TWTA	TWTA	ESFK
Second Choice	ESFK	ESFK	TWTA

4.1.4.4 Switching Devices

The purpose of this trade is to select the most appropriate rf switch device for the Voyager mission. Devices under consideration include the ferrite (circulator), diode, and mechanical switches.

Requirements--The prime requirement for rf switches in the rf subsystem is reliability. This factor is amplified by the difficulty in applying redundancy to the switching devices. Other factors of weight, performance, cost and magnetic field will be secondary to reliability and have little weighting.

Description of Alternate Devices--The mechanical switch is constructed as a coaxial line with provision for moving and opening a small section of the conductor. The device is normally operated by a magnetic solenoid to overcome a spring resistence. The unit can be made latching or non-latching. The latching configuration is most desirable for Voyager because power is required only during the switch operation.

A ferrite circulator switch is a three-port device with nonreciprocal transmission properties controlled by an external magnetic field. A signal entering the first port will circulate in a given direction; the process is reversed by reversing the applied magnetic field. An ideal

property of the circulator is that it can perform a diplexer function (transmitter and receiver) for signals traveling in different directions.

An isolator function can be provided by applying a permanent magnetic field (as compared to an applied electromagnetic field) and terminating one port in a load.

A third switch for consideration is the rf diode switch. A change in diode electrical characteritstics provides a transmission line impedance change that passes or reflects the rf energy. Present diode switches are limited in power-handling capacity and cannot be used for the 50-watt antenna line function.

Device Comparison--A comparison of mechanical and circulator switches was made, based upon an SPDT configuration for both devices. Factors evaluated were reliability, weight, availability, cost, performance, and magnetic field. Because the mechanical switch has moving parts, it is much less reliable than its ferrite counterpart. In addition, the switch provides a mechanical separation in the off position and presents an extremely high VSWR. This effect could cause a mismatch to an adjoining unit (diplexer, etc.) still being used. The primary disadvantage of the circulator switch is the low isolation presented to the off path. Thirty decibels is typical, but ferrite material sensitivity to temperature causes a degradation at reduced temperatures

(-10 to -25°C) to 20 decibels. When higher isolation is required, the units must be cascaded.

A circulator switch failure would most likely occur from a loss in magnetic field causing the device to become a power divider with a 3-decibel loss, while the mechanical switch may fail in either closed or open position.

Logic of Selection--Based on the criteria presented, the preferred switch for Voyager application is the ferrite circulator device. The choice is based primarily on the increased reliability of the circulator due to the absence of moving parts. The amount of isolation required will depend on the specific application. Cascading of circulators for isolation presents increasing forward-insertion loss (0.2 decibel per section). This could be reason to reject the circulator if the full 80-decibel mechanical switch isolation is required.

4.1.5 Radio Subsystem

Development of a functional radio system capable of satisfying the Voyager requirements necessitates maximum utilization of redundancy and internal switching logic, consistent with size and weight limitations, to meet reliability requirements.

Of prime concern in the design of a radio system as complex and sensitive as the anticipated Voyager system is the assurance that sufficient isolation is included among functional components. Particular attention must be given to such items as:

1) Elimination of spurious emissions, noise, and RFI at the receiver input frequency generated by the exciter and power amplifier.
2) Sufficient isolation to eliminate possible received signal interference from the high-gain antenna when the receiver is operating from the low-gain antenna.
3) Elimination of signal interference caused by undesired high-gain antenna leakage when transmitting on the low-gain antenna.

Elimination of spurious signals at the receiver input can be provided through careful filtering at the exciter and power amplifier outputs. Narrowband filters (20 megacycles typical) between the exciter and power amplifier eliminate harmonic and spurious frequencies (the output spectrum contains signals at 19 megacycles intervals about the carrier due to modulation of the carrier by the VCO or auxiliary oscillator). Isolators should be placed at the exciter and launch transmitter outputs to eliminate instabilities due to load fluctuations. A band-reject filter is necessary at the output of the traveling wave tube amplifier

to reject the contribution of output noise at the receiver frequency. A band-reject rather than a bandpass design is chosen to provide maximum rejection consistent with minimum insertion loss. In addition, the band-reject filter has a low Q at the transmitter frequency and is less susceptible to rf voltage breakdown.

Transmitter and receiver leakage through the high-gain antenna is primarily due to the ferrite circulator switches which allow some leakage through the "off" path (20 db typical loss over the anticipated environmental extremes) and reflected energy circulating back through the device in an undesired direction. Typical would be the case of desired low-gain transmission through CS1 and the diplexer. (Section 4.1.5.3). Referring to Figure 4.1-10, Circulator Switches 1, 2, and 3 provide 60 db minimum isolation to a signal passing directly to the high-gain antenna (approximately 34 db gain and hence 26 db difference between low-gain and high-gain radiated power). However, if CS4 were not included, transmitter energy would be completely reflected by the preselector and the isolation would fall to an unacceptable 40 db. CS4 also provides isolation to the high-gain-antenna-derived signal at the receiver frequency when transmitting on a high-gain antenna and receiving on the low-gain antenna.

Consideration in the design of a final amplifier must be given to such factors as rf power level, outgassing, and transfer of heat dissipated by the power amplifier. The required rf power level will be a function of transmission losses and desired data transmission rates. A 50-watt traveling wave tube amplifier (Section 4.1.4.3) has been selected as the

preferred design for the amplifier. The required power level could be reduced through elimination of transmission switching losses (dual antenna transmission/reception, etc.) but system reliability and versatility would be affected.

4.1.5.1 Exciter Mechanization

Two alternate exciter mechanizations are indicated in Figure 4.1-9. Configuration I includes completely redundant exciters, isolators, and bandpass filters. Activation of either exciter is accomplished through application of d.c. power to the respective power supply. A second alternate (Configuration II) is also indicated. The obvious approach is to switch either exciter to the bandpass filter. The single ferrite circulator switch would also provide the required output isolation function for either applied exciter. Configuration II is simpler and lighter, but less reliable since the switch and filter yield nonredundant series elements. Characteristics of Configuration II relative to I can be summarized as follows:

Reliability	Configuration I is 33 percent more reliable
Weight	Configuration II is 3.0 pounds lighter
Availability	No change
Cost	Configuration II cost is less due to reduction of 2 components
Performance	Little change--Configuration II switch requires 30 milliwatts additional continuous power
Magnetic Field	Configuration II is less due to the replacement of two isolators by one circulator switch

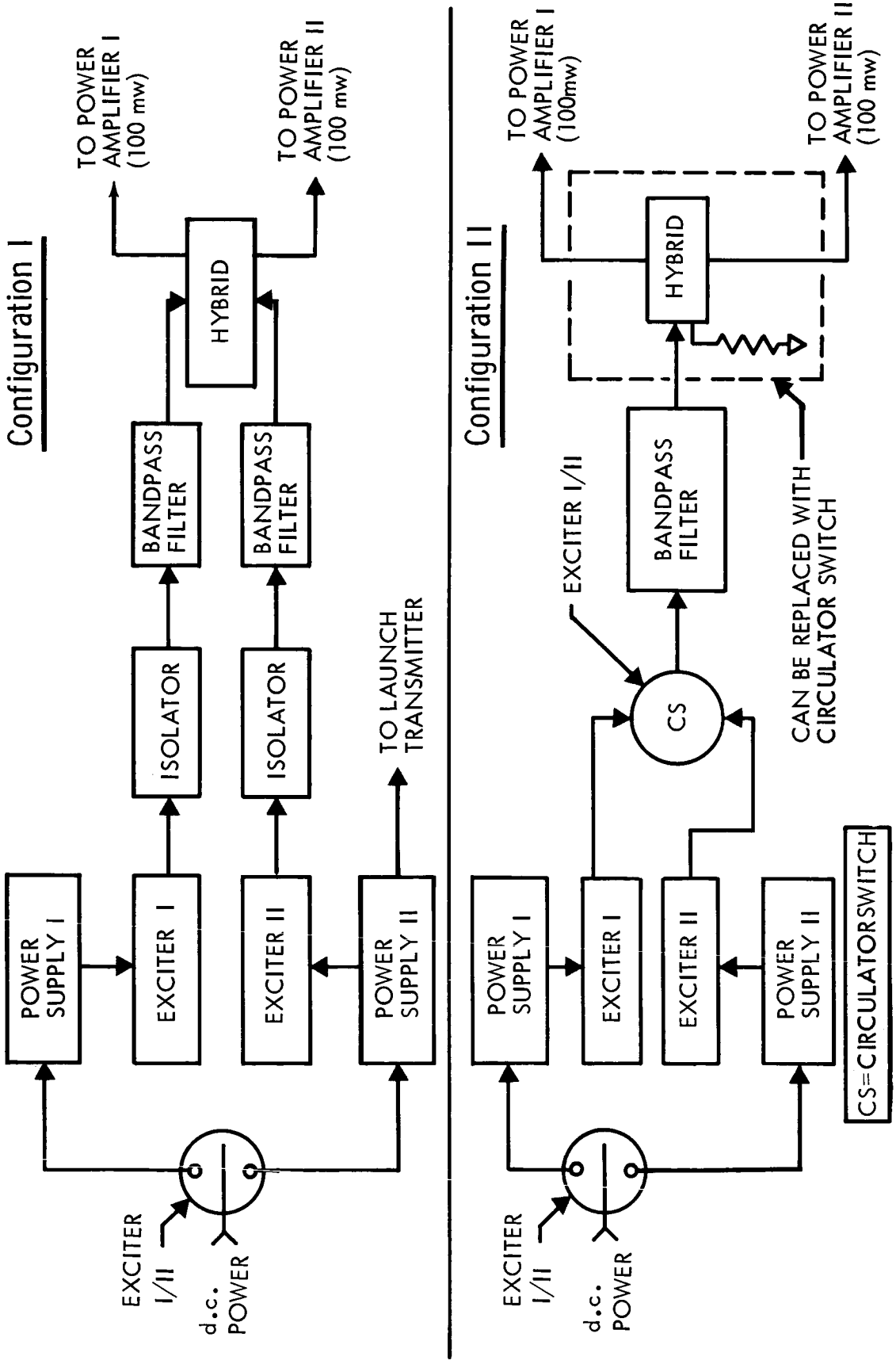

Figure 4.1-9: Exciter Mechanizations

An alternate of Configuration II would replace the 3 db hybrid by a circulator switch. This would reduce the required exciter power by 3 db and provide a d.c. power saving of approximately 1.5 watts. However, reliability would be reduced due to an additional switch function. Configuration I is the preferred design because of the increased reliability for a slight weight penalty.

4.1.5.2 Launch Transmitter Mechanization

Due to the rf power levels and TWT amplifier high voltages, the power amplifier is not utilized during launch and ascent through critical pressure. A separate, low-voltage, solid-state unit (launch transmitter) is utilized during the first 20 to 30 hours of the mission to allow complete outgassing of the spacecraft and power amplifier elements. This approach is necessary since the TWTA (Section 4.1.4.3) cannot operate in a low power mode at extremely reduced voltages. In Configuration I (Figure 4.1-10) this transmitter (less power supply) is completely separated from the normal mission components.

An alternate approach (Configuration II) utilizes a single solid-state unit that can be switched at the output to provide the launch or power amplifier exciter function. Although this configuration has a slight weight improvement, it is less reliable for both the launch and cruise operations. In the launch mode, a switch has been added in place of an isolator. In the cruise mode, both the switch and an attenuator have been added. Since it is not feasible to drop the power in the solid-state exciter, the unit must run at the 1-watt output level when in use, thereby increasing the input power requirements. However, this could be

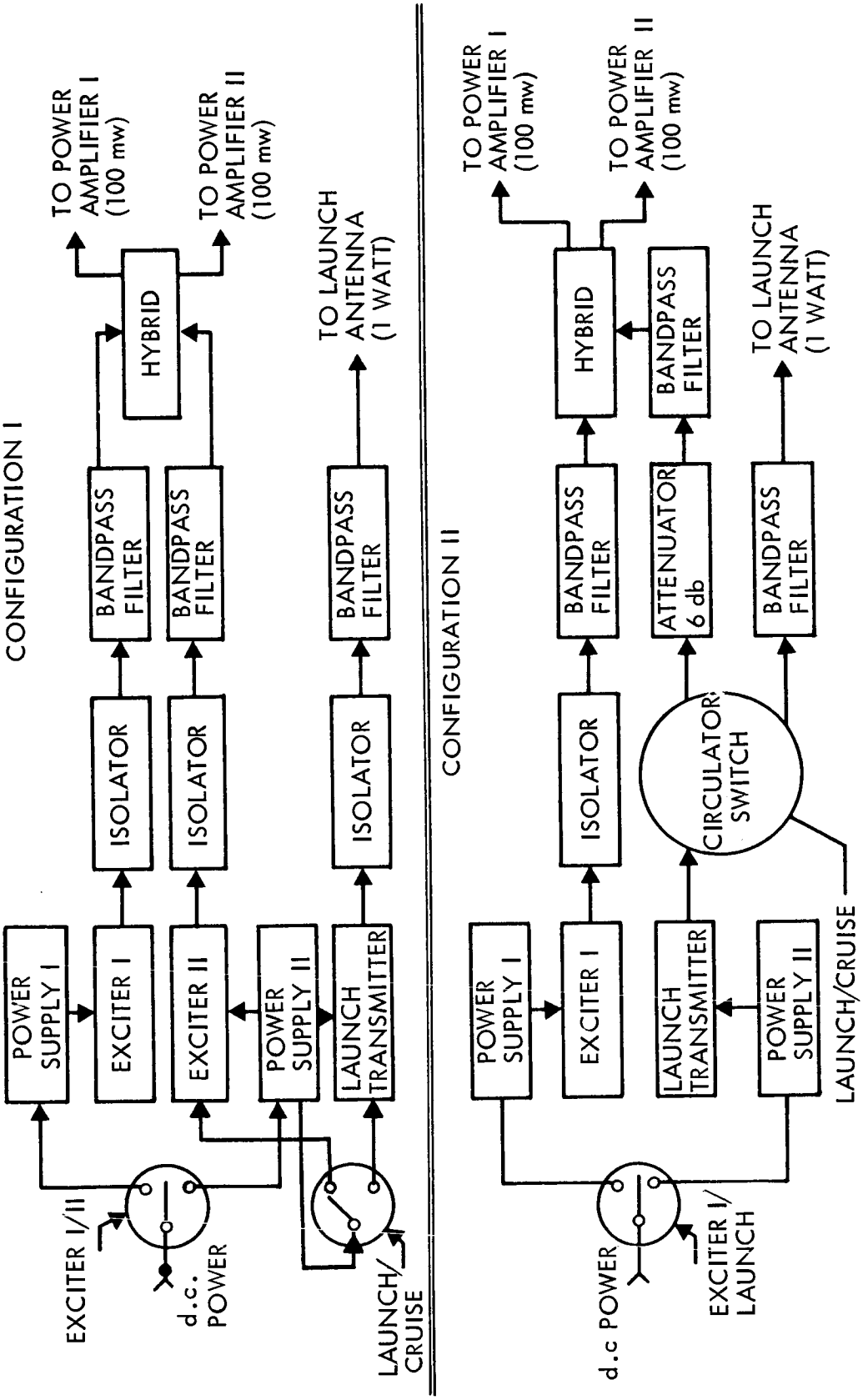

Figure 4.1-10: Launch-Transmitter Mechanizations

a secondary effect if high-power units were used as a backup to the lower power exciter. Comparative characteristics relative to the two configurations can be summarized as follows:

Reliability, Launch	Configuration I is 2 percent more reliable
Reliability, Cruise	Configuration I is 7 percent more reliable
Weight,	Configuration II is 2.5 pounds lighter
Availability	No change
Cost	Configuration II cost is less due to the elimination of an exciter
Performance	Configuration II requires 15 watts additional power if exciter I fails
Magnetic Field	Less in Configuration II due to elimination of one ferrite device
Other Considerations	Increased thermal load for Configuration II if Exciter I fails

Since reliability has the highest weighting, Configuration I is the preferred design even though there is a slight weight disadvantage.

4.1.5.3 Antenna Switching Mechanization

The antenna switching mechanization provides the function of coupling both receiver and transmitter to the desired high-gain or low-gain antenna. The desired operational modes are:

1) Transmit low-gain, receive low-gain;

2) Transmit high-gain, receive low-gain;

3) Transmit high-gain, receive high-gain.

A possible switching mechanization is indicated (Configuration I) in Figure 4.1-11. The design is based on ferrite circulator switch utilization for all S-band switching functions. As discussed in Section 4.1.6.1,

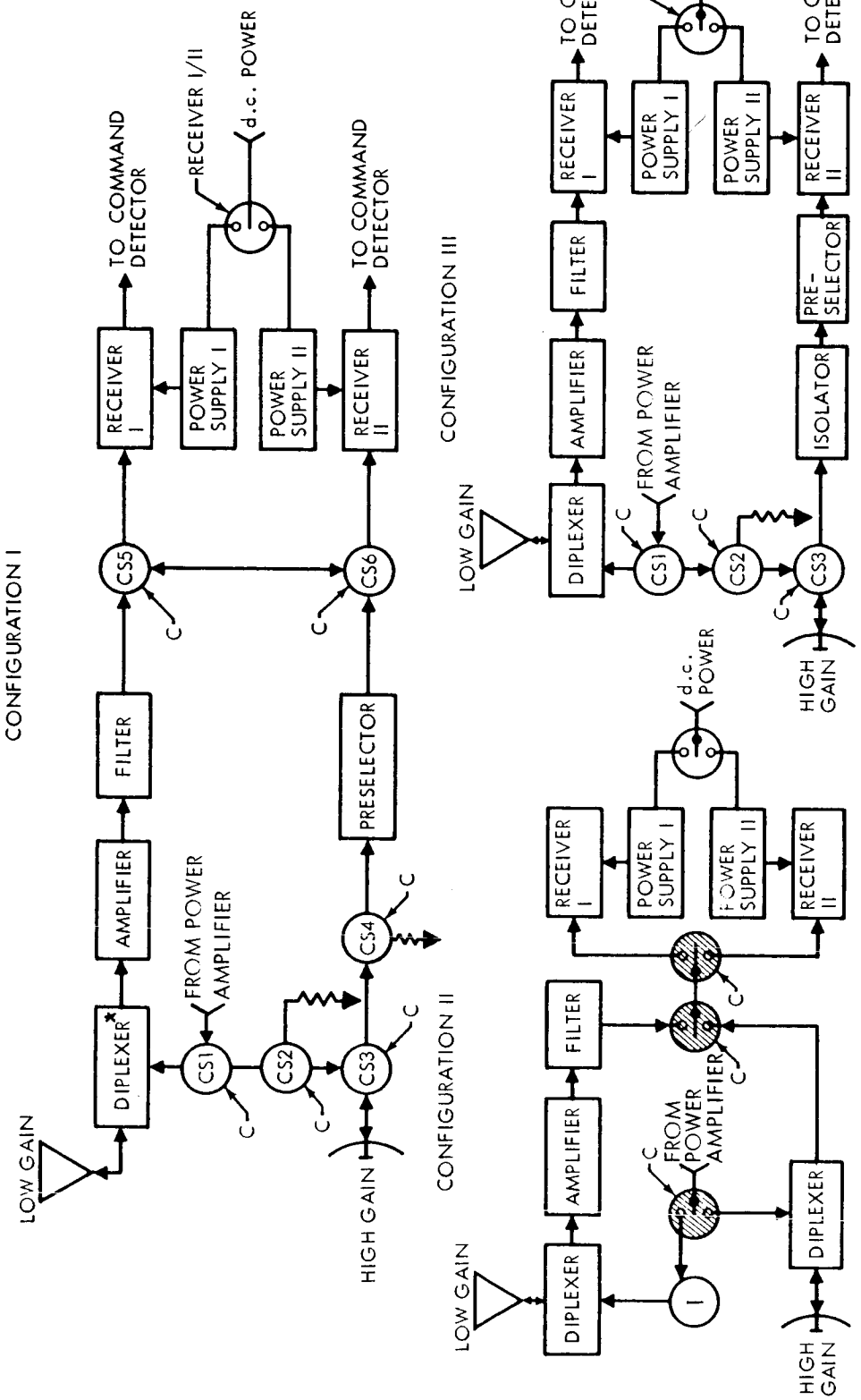

Figure 4.1-11: Antenna Switching Mechanization

two additional units (CS2 and CS4) are provided for required high-gain antenna received and transmitted signal isolation when low-gain antenna utilization is desired. CS1 provides the transmitter switching function between low-gain and high-gain antennas. CS5 and CS6 allow utilization of either receiver on either antenna. CS3 could be a simple circulator rather than a circulator switch if it did not have to provide additional isolation to the high-gain path during low-gain transmission. In practice, CS1/CS2, CS3/CS4, and CS5/CS6 would be configured as three 4-port circulators. This technique allows internal common junction connection improving weight and reliability through the deletion of cabling and connectors.

Configuration II replaces the ferrite circulator switches with mechanical-coaxial units. The isolation of mechanical switch units is considerably higher than their ferrite counterparts (70 to 30 db versus 20 db). The disadvantage of this device (Section 4.1.4.4) is the decreased reliability due to its mechanical moving parts. One coaxial switch is utilized to switch the power amplifiers between antennas. It provides sufficient isolation in the off direction to eliminate high-gain antenna leakage when transmitting in the low-gain mode. An isolator is provided at the transmitter low-gain diplexer input to eliminate diplexer mismatch and characteristic change during the receive low-gain and transmit high-gain mode. Table 4.1-9 indicates the criteria trades between this configuration and Configuration I.

The approach indicated in Configuration III is a simplification of Configuration I through the removal of CS5 and CS6. This technique provides

Table 4.1-9: ANTENNA SWITCHING MECHANIZATION ALTERNATES
CHANGES FROM CONFIGURATION I

CRITERIA	CONFIGURATION II	CONFIGURATION III	CONFIGURATION IV
Reliability	(see Table 4.1-10)		
Weight	5-pound reduction	3.5-pound reduction	1.0-pound increase
Availability	Requires development of Hi-Reliability Coaxial Switches	No change	No change
Cost	Increased development cost	Less due to fewer components	Slightly higher due to additional component
D.C. Power	7 watts during switching versus 30-milliwatts continuous	90-milliwatt reduction	30-milliwatt continuous addition
Insertion Loss	0.3 db higher in transmit low-gain antenna mode	0.2 to 0.4 db improvement in high-gain reception	0.2 db improvement in transmit; 0.2 db degradation in receive low-gain antenna mode
Magnetic Field	Less due to elimination of two ferrite devices	Less due to elimination of two ferrite devices	Higher due to an additional circulator

simplicity and weight reduction at the expense of dual receiver redundancy for each antenna. Since there is no coupling between receivers at the input, and receiver II is not powered during low-gain operation, CS4 can be replaced by an isolator. This device eliminates reflected transmitter power from the preselector being radiated through high-gain antenna during low-gain antenna transmission. A comparison to Configuration I of this mechanization is indicated in Table 4.1-9.

Configuration IV would replace the Configuration I low-gain antenna diplexer with a circulator and preselector. This technique provides slightly improved transmitter insertion loss at the expense of increased receiver loss plus increased complexity and magnetic field. The alternate criteria is summarized in Table 4.1-9.

Configuration I has been selected as the preferred design approach at this development stage. Configuration II requires heavy dependence on coaxial switches, which do not have the flight proven history of their ferrite counterparts. Configuration III yields a sizable reliability reduction for a slight decrease in weight. Configuration IV provides little electrical improvement for the decreased reliability and increased weight.

4.1.5.4 Radio Subsystem Redundancy

The optimum radio system for the Voyager application will yield the most reliable configuration consistent with the required electrical

characteristics and weight available. The design approach is to begin with a single-thread system and provide redundancy to the least reliable components until the desired reliability goal is achieved. Figures 4.1-12 and 4.1-13 represent the approach utilized for the following discussion.

Single Thread--The single thread (nonredundant) failure rate was estimated to be 4588 bits (failures per 10^8 hours). Since the reliability of each individual component is weighted by the effective mission operational time requirement, the product of failure rate (λ) and effective mission time (λt) is used as the figure of merit for reliability improvement criteria. (Where time is the same in comparisons, failure rate (λ) is used as a relative figure of merit for reliability improvement, e.g., subcomponent module failure rate comparisons.)

The components of the single-thread design are ranked as follows in respect to failure rate, λ , and λt products.

Items of major interest that require improvement include the power amplifier, receiver, exciter, command detector, and preamplifier, in that order . It should be noted that due to the short requirement time, the launch transmitter, which is ranked third in failure rate, is ranked 10th in λt and hence not considered as critical.

Subcomponent Redundancy--An investigation was performed to determine which, if any, of the component failure rates could be improved through active or standby subcomponent redundancy (i.e., redundancy on the part, circuit, and module level).

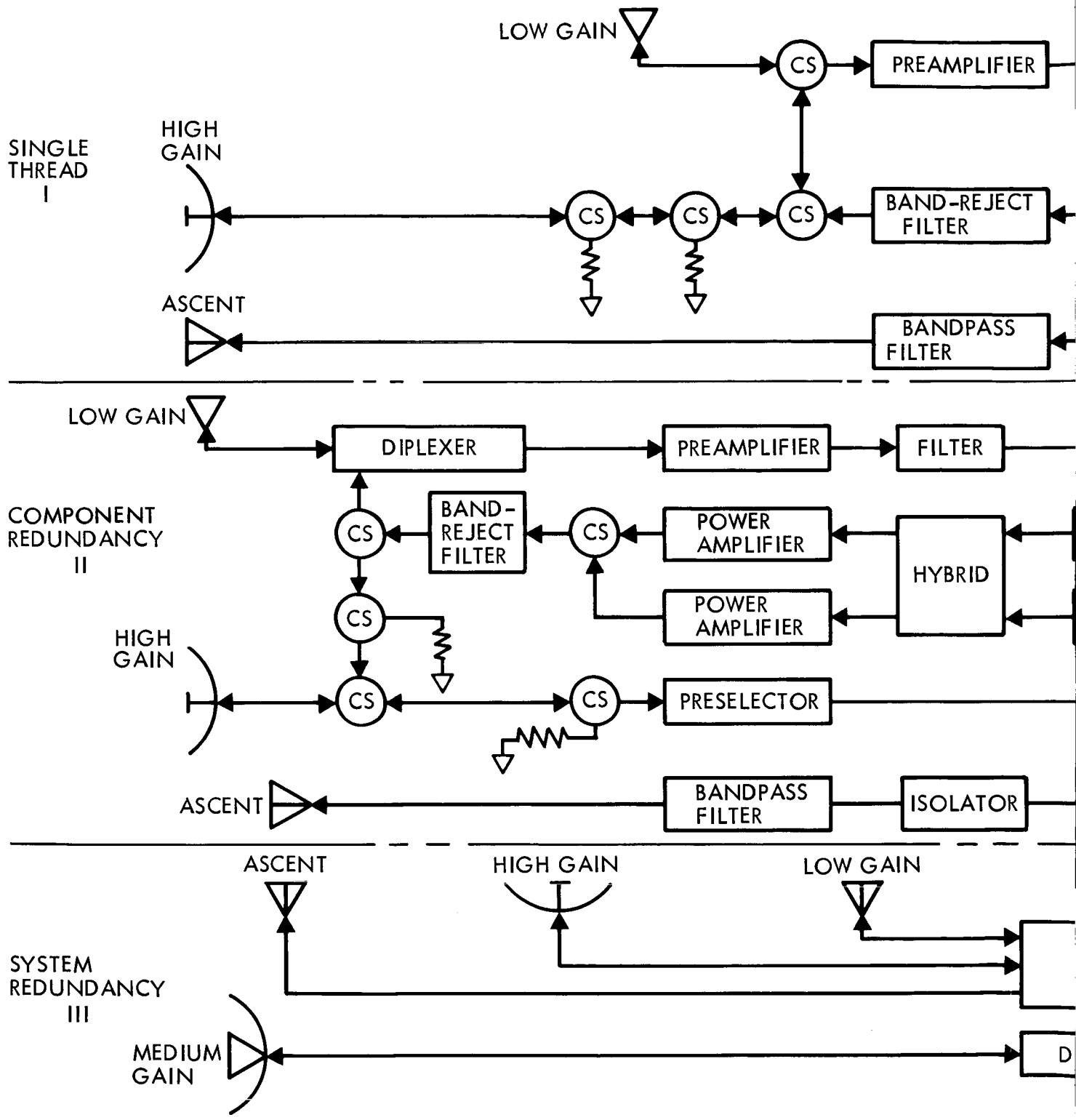

* APPLICABLE TO SUBCOMPONENT REDUNDANCY

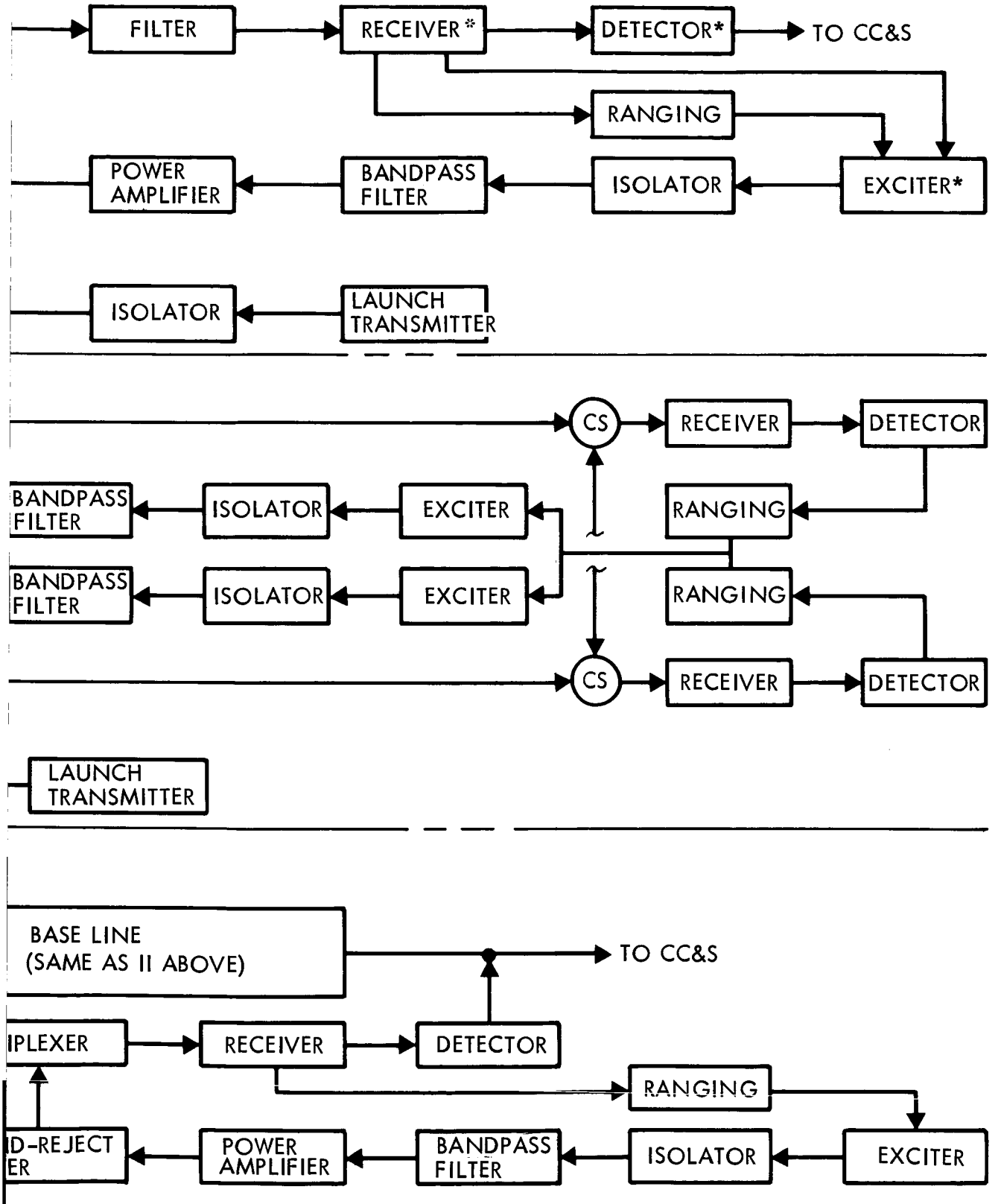

Figure 4.1 - 12: Radio System Redundancy Configurations

I SINGLE THREAD

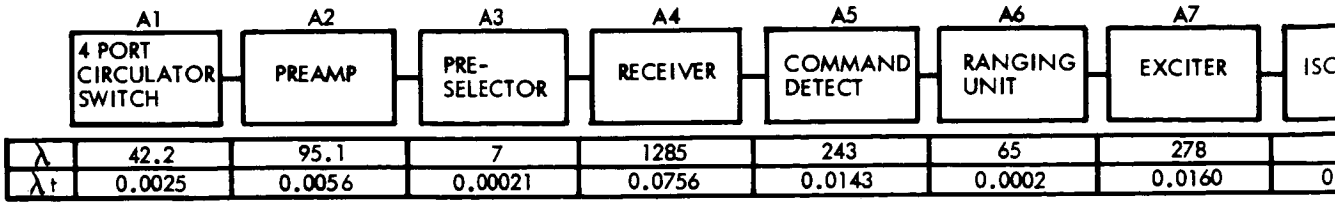

λ	42.2	95.1	7	1285	243	65	278
λt	0.0025	0.0056	0.00021	0.0756	0.0143	0.0002	0.0160

II SUBCOMPONENT REDUNDANCY

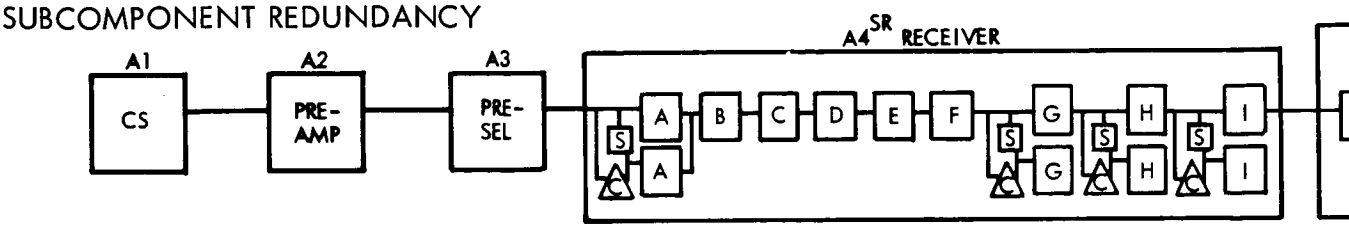

λ	519
λt	0.0304

III COMPONENT REDUNDANCY

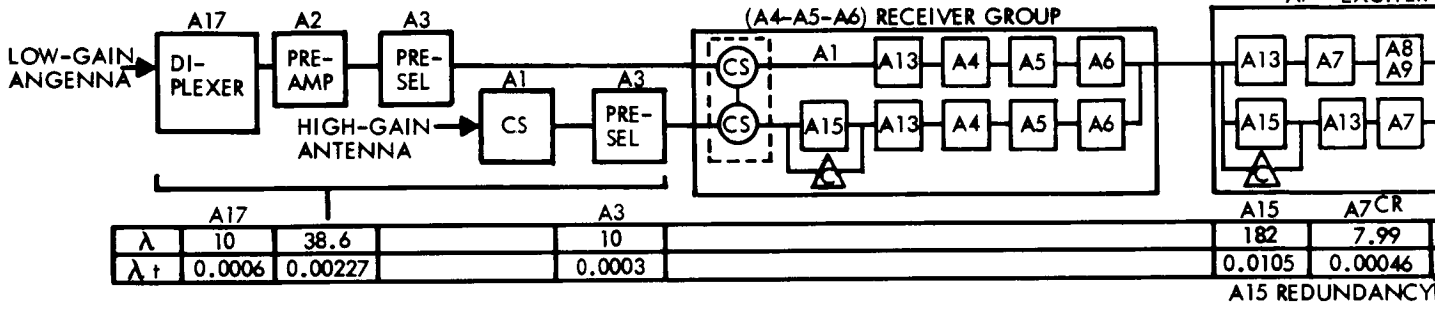

	A17			A3		A15	$A7^{CR}$
λ	10	38.6		10		182	7.99
λt	0.0006	0.00227		0.0003		0.0105	0.00046

A15 REDUNDANCY

IV SUBSYSTEM REDUNDANCY

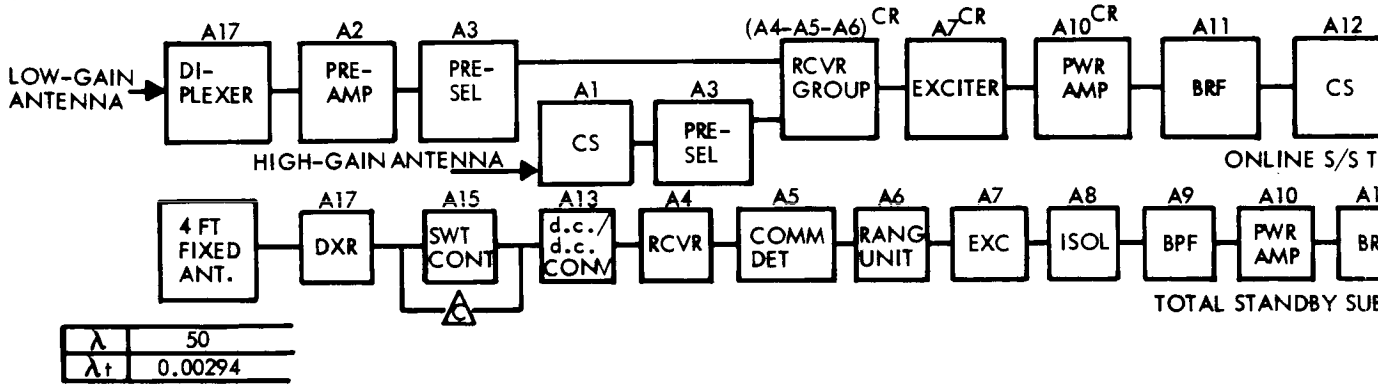

λ	50
λt	0.00294

NOTES:
1. λ = BITS = FAILURES PER 10^8 HOURS
2. SR = SUBCOMPONENT REDUNDANT
3. CR = COMPONENT REDUNDANT
4. CS = CIRCULATOR SWITCH
5. S = SENSE-SWITCHING LOGIC
6. C = BACKUP COMMAND FROM CC&S, $P_S = 0.99$
7. $A4^{SR}$ MODULE IDENTIFICATION
   - A - MIXER PREAMPLIFIER
   - B - 47.8 mc IF
   - C - 9.56 mc XTAL FILTER
   - D - 9.56 mc IF AMP
   - E - PHASE DETECTOR
   - F - AGC DETECTOR
   - G - FREQ DIVIDER
   - H - V.C.O.
   - I - X36 MULTIPLIER
8. $A5^{SR}$ MODULE IDE
   - A - SYNC CIRC
   - B - DATA DET
   - C - INLOCK IN CIRCUITS

1090

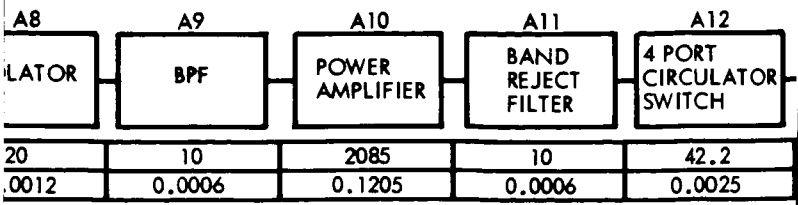

20	10	2085	10	42.2
.0012	0.0006	0.1205	0.0006	0.0025

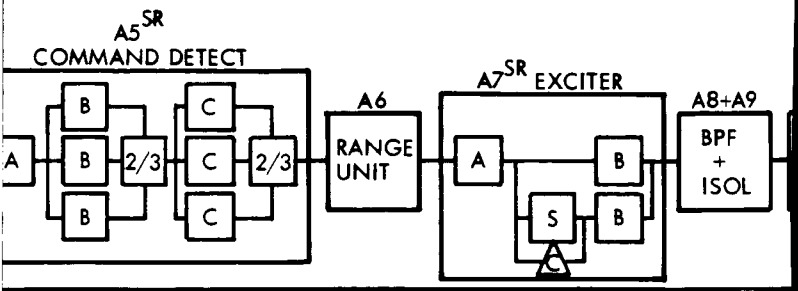

196		123.5	
0.0119		0.00712	

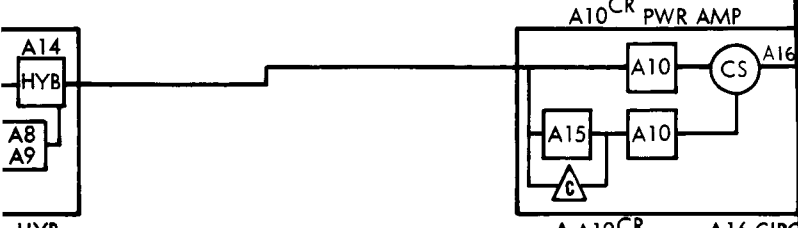

HYB		ΔA10CR	A16 CIRC
20		118.6	21.1
0.0012		0.00683	0.0012

CONTROL WITH d.c./d.c. CONVERTER (PARALLEL REDUNDANT-ACTIVE)

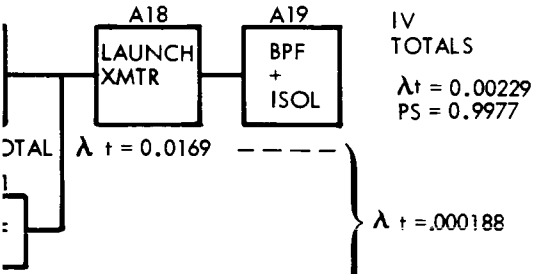

IV
TOTALS

$\lambda t = 0.00229$
PS = 0.9977

CONFIGU
I SINGLE T
II SUBCOMI LEVEL RE
III COMPON REDUNDA
IV SUBSYSTE REDUNDA COMPON REDUNDA
*PLUS 10-2

NTIFICATION
UITS
IRCUITS
IDICATOR

9. A7SR MODULE IDENTIFICATION
   A - AUX OSCILLATOR
   B - X30 MULTIPLIER

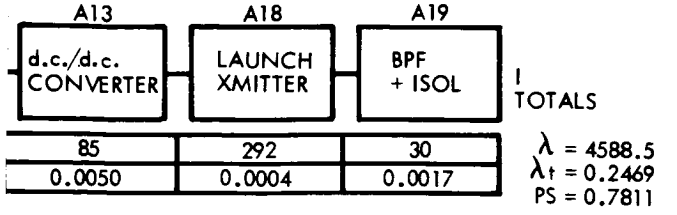

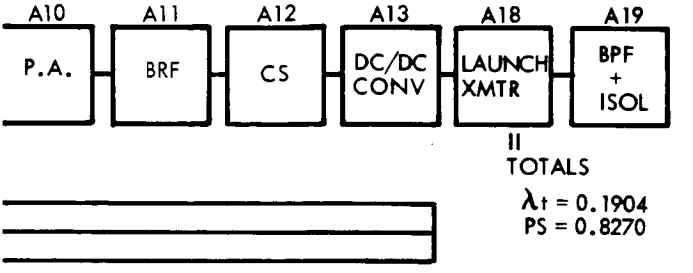

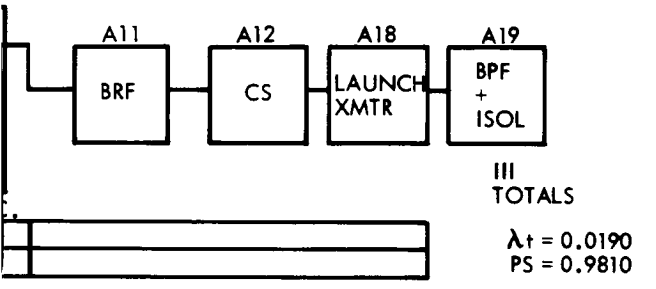

SUMMARY

RATION	$P_S(t)$	λ_t	λ IMPROVEMENT OVER I	WEIGHT (LB)
THREAD	0.7811	0.2469	1.0	46
PONENT DUNDANCY	0.8270	0.1904	1.3	56
IENT LEVEL ANCY (ONLY)	0.9810	0.0190	13	87
M LEVEL ANCY (WITH IENT LEVEL ANCY)	0.9977	0.00229	108	126*
0 POUNDS ADDITIONAL ANTENNA WEIGHT				

Figure 4.1-13: Radio Subsystem Alternate Redundancy Configurations

λ (BITS)	RANK	COMPONENT	λt	λt RANK
42.2	9	Four-Port Circulator Switch	0.0025	7
95.1	6	Preamplifier	0.0056	5
7.0	12	Preselector	0.00021	11
1285	2	Receiver	0.0756	2
243	5	Command Detector	0.0143	4
65	8	Ranging Unit	0.0002	12
278	4	Exciter	0.0160	3
20	10	Isolator	0.0012	8
10	11	Bandpass Filter	0.0006	9
2085	1	Power Amplifier	0.1205	1
10	10	Band-Reject Filter	0.0006	9
42.2	9	Four-Port Circulator Switch	0.0025	7
292	3	Launch Transmitter	0.0004	10
20	10	Isolator	0.000024	13
10	11	Bandpass Filter	0.000012	14
85	7	D.c.-to-d.c. Converter	0.0050	6
4588	Total			

Power Amplifier--The power amplifier ranks number one in λt, but subcomponent redundancy is not a practical approach to reliability improvement. Most of the failure rate (88 percent) is in the tube itself. The d.c.-to-d.c. converter with its high-voltage power switching circuits, is adaptable to subcomponent redundancy techniques.

Receiver--The S-band receiver ranks second in λt. The subcomponent ranking is as follows:

λ(BITS)	RANK	SUBCOMPONENTS
342	1	A - Mixer Preamplifier
86.6	7	B - 47.8 MC IF Amplifier
109.7	5	C - 9.56 MC XTAL Filter
93.9	6	D - 9.56 MC IF Amplifier
55.7	9	E - Phase Detector
72	8	F - AGC Detector
152	3	G - Frequency Divider
146	4	H - Voltage Controlled Oscillator (VCO)
226	2	I - X36 Multiplier
1285 Total		

Standby redundancy in the mixer preamplifier, frequency divider, VCO, and X36 multiplier results in a factor of 2.5 improvement for an equivalent failure rate of 519 bits. However, the practical consideration of submodule failure detection, switching, and interfacing must be considered.

The majority of the mixer preamplifier failure rate is attributed to the mixer diodes. Since it is not practical to provide redundant diodes due to the required mixer balance, the entire mixer preamplifier would have to be made redundant (circulator input switch plus parallel outputs). The X36 multiplier failure rate is similar to the mixer in that a microwave varactor diode is the major failure rate contributor. Again, the entire subcomponent would be made redundant for a single diode backup.

The VCO and frequency divider each have multiple outputs making paralleling or switching extremely impractical.

The conclusion can be drawn that the subcomponent redundancy within the receiver is wasteful in size, weight, and complexity and is not the desired approach.

Exciter--The exciter ranks third in λt. Its high failure rate is primarily derived from the microwave output diode. Subcomponent redundancy would require paralleling the X30 multiplier portion of the exciter and combining the output in a hybrid or circulator switch. This technique would provide an improvement of 2.2 times, reducing the total failure rate to 123 bits. The approach of paralleling an entire multiplier to protect one diode is wasteful and should not be utilized unless absolutely necessary.

Command Detector--The command detector is ranked fourth in λt. The subcomponent rating for the detector is summarized as follows:

BITS	RANK	COMMAND DETECTOR SUBCOMPONENTS
176.4	1	Synchronization Circuitry
37.1	2	Data Detection Circuitry
29.5	3	In-Lock Indicator Circuitry
243 Total		

The synchronization circuitry does not lend itself to redundancy mechanization. Majority voting can be implemented in the data detector and in-lock indicator circuitry, but this results in only a 1.19 improvement in

reliability to 202 bits. This improvement of the command detector by subcomponent-level redundancy was rejected as introducing too much complexity for the improvement realized.

Preamplifier--The preamplifier ranks fifth in λt. It consists of a tunnel diode and ferrite circulators. There is no practical way to lend subcomponent redundancy to this unit.

Summary--If subcomponent redundancy were applied to each applicable item previously discussed, the total single-thread system reliability would be improved by a factor of 1.27 times to a λt of 0.1904 and a probability of success of 0.8270. However, due to the complexity of internal sensing and switching plus the other characteristics described, it is felt that redundancy at the subcomponent level would introduce too much complexity for the improvement realized.

Component Redundancy--Referring to the initial single-thread component ranking table, the components are now addressed on a component redundancy level. Offline, inactive, standby redundancy was used instead of parallel active techniques to provide higher reliability within reasonable limits on weight, power consumption, interference generation, and sensing and control mechanization.

Power Amplifier--The power amplifier ranks first in probability of failure. Standby redundancy with one additional power amplifier (including its high-voltage d.c.-to-d.c. converter) results in an improvement in reliability

of 17.6 times for a λt of 0.00683. This places it below the command detector, which is ranked fifth in λt product.

Receiver--The receiver is addressed next since it is now first in λt ranking. Analysis of the redundancy mechanization of the receiver led to the conclusion that the command detector and ranging unit components, ranked 4 and 12, respectively, should be grouped with the receiver. The rationale was based on maintaining a reliable interface between the receiver and the two units. Another factor is the inability to detect whether the command detector has failed. The lowest risk approach was to group the three components and sense the VCO level in the receiver with automatic switchover backup from the CC&S if phase lock acquisition is not accomplished within a specified period of time, e.g., 29 hours. Standby redundancy of the receiver group, i.e., receiver command detector and ranging unit, resulted in a total λt improvement of 18 times over the single-thread λt for a λt of 0.00524. This places the receiver below the redundant power amplifier.

Exciter--The exciter with standby redundancy including a d.c.-to d.c. converter, signal level failure sensing, and switchover control with command backup was improved by a factor of 40 for a λt product of 0.0004.

Summary--Diminishing returns on improvement of reliability of individual components as a function of weight increase requires consideration of improvement at the subsystem level. The total improvement in the radio subsystem (Configuration III) using component-level redundancy only, was a factor of 13 times, for λt of 0.019 and a probability of success of 0.9810.

Subsystem Level--Further reliability improvement mechanization was addressed using an independent single-thread subsystem in standby to be automatically programmed on by the CC&S if an inhibit command is not received within a specified time. This configuration requires a fixed medium-gain (4-foot-diameter) antenna to realize the maximum functional backup of the radio subsystem. The launch transmitter is not included since its λt product is low due to its short functional time requirement. An improvement of 109 times was realized over the single-thread configuration using the component level. Weight constraints appear to preclude this configuration, however.

Summary--Table 4.1-10 summarizes the reliability improvements of the various configurations. The preferred design is the mechanization utilizing component redundancy (Configuration III) since it provides the most reliability improvement consistent with weight increase.

Further analysis of the mechanization problems will be required to ensure that this is the optimum configuration in the context of overall system requirements.

4.1.6 Alternate Telemetry and Data Storage Subsystems

4.1.6.1 Basic Consideration and Requirements Affecting Alternate Choices

The Voyager telemetry data that is to be transmitted to the DSN stations originates from eight separate sources:

1) Engineering multiplexer and encoder--spacecraft engineering data;

2) DAS (cruise science experiments)--cruise science data;

Table 4.1-10: ANTENNA SWITCHING MECHANIZATION RELIABILITY COMPARISONS*

FUNCTION	CONFIGURATION II	CONFIGURATION III	CONFIGURATION IV	
I. Receive and Transmit Low Gain				
a) Receive Function	+29	+312	+4.5	%
b) Transmit Function	+7	0	+11.6	%
c) Total	+41.5	+299	+4.3	%
II. Receive Low-Gain, Transmit High-Gain				
a) Receive Function	+29	+312	+4.5	%
b) Transmit Function	-12	0	0	%
c) Total	+25	+181	+2.8	%
III. Receive High-Gain, Transmit High-Gain				
a) Receive Function	+10	+274	0	%
b) Transmit Function	+13	0	0	%
c) Total	+21	+251	0	%

* Configuration I is more reliable by percentages indicated.

3) DAS (planetary science experiments via planetary recorder)--planetary science data;

4) Capsule via hardline--capsule engineering data;

5) Capsule via Relay Radio Link--capsule engineering data;

6) Spacecraft engineering storage--stored spacecraft engineering data;

7) Capsule engineering storage--stored capsule engineering data;

8) DAS (planetary science experiments)--real-time planetary science.

Four of the data sources that represent separate and independent data acquisition systems are:

1) Spacecraft multiplexer and encoder;

2) Capsule;

3) DAS cruise science;

4) DAS planetary science.

Each of these data sources is characterized by different types and numbers of channels, bit rates, frame lengths, and synchronization techniques. In addition, the ability to synchronize the generation of capsule data with an on-board reference is lost after capsule separation.

Mission requirements and communication-channel-capacity constraints during the several mission phases establish the need for six basic telemetry modes. Each mode is characterized by the transmission of different combinations of data at different bit rates. This requirement is shown in Table 4.1-11.

In consideration of alternate subsystem configurations, emphasis must be placed on reliability and simplicity. Also to be considered are such

Table 4.1-11: Minimum Telemetry Data Requirements

MODE	MISSION PHASES	DATA TO BE TRANSMITTED	MINIMUM TRANSMISSION RATE
1	LAUNCH, ACQUISITION CRUISE, MANEUVER	SPACECRAFT ENGINEERING DATA	10 (bps)
		CAPSULE ENGINEERING DATA	10 (bps)
2	CRUISE	SPACECRAFT ENGINEERING DATA	10 (bps)
		CAPSULE ENGINEERING DATA	10 (bps)
		CRUISE SCIENCE DATA	100 (bps)
3	POSTMANEUVER OPTION	SPACECRAFT ENGINEERING DATA	10 (bps)
		CAPSULE ENGINEERING DATA	100 (bps)
		STORED SPACECRAFT ENGINEERING DATA	50 (bps)
4	EMERGENCY CRUISE OR ENCOUNTER	SPACECRAFT ENGINEERING DATA	THE MAXIMUM THE CHANNEL WILL ALLOW
5A	PRIMARY ENCOUNTER AND ORBITAL	SPACECRAFT ENGINEERING DATA	10 (bps)
		CAPSULE ENGINEERING DATA	100 (bps)
		STORED CAPSULE ENGINEERING DATA	50 (bps)
		CRUISE SCIENCE DATA	100 (bps)
		PLANETARY SCIENCE	THE MAXIMUM THE CHANNEL WILL ALLOW
5B	OPTIONAL LATE ORBITAL	SAME AS 5A	THE MAXIMUM THE CHANNEL WILL ALLOW
5C	OPTIONAL LATE ORBITAL	SAME AS 5A	THE MAXIMUM THE CHANNEL WILL ALLOW
6	OPTIONAL ENCOUNTER AND ORBITAL	SAME AS VA WITH THE EXCEPTION THAT REAL-TIME PLANETARY SCIENCE IS TRANSMITTED	SAME AS 5A WITH THE EXCEPTION THAT PLANETARY SCIENCE TRANSMISSION IS AT THE REAL-TIME RATE

factors as weight, volume, and power dissipation. In addition, the candidate alternate subsystem configurations should not impose excessive design constraints on the telemetry and data storage interface subsystems.

The preferred design uses two subcarriers to transmit all the data. Planetary science data in block encoded form modulates a high-frequency subcarrier. The cruise science data, spacecraft engineering data, capsule data and recorded engineering and capsule data are synchronously time multiplexed into a specific format. The composite signal modulates a low-frequency subcarrier. Byphase modulation is used for both subcarrier modulations. In Modes 1 and 4 (low bit-rate modes), two-channel PN/PSK-modulation techniques are used to facilitate the recovery of data synchronization signals at the receiving stations.

Redundancy is used on the part level in the engineering multiplexer/encoder. In addition, subsystem component redundancy in the form of two planetary science recorders is used.

4.1.6.2 Subsystem Mechanizations Considered

Data Multiplexing--In considering the basic requirements as documented by Table 4.1-11, the major task involved is the multiplexing of several data sources. Several techniques exist to implement the multiplexing requirements:

1) All data sources are frequency multiplexed;
2) All data sources are time multiplexed and incorporate independent formating.

3) All data sources are time multiplexed and incorporate synchronous formatting;

4) Combination of frequency and time multiplexing-- the time-multiplexed data incorporates synchronous formatting;

5) Combination of frequency and time multiplexing--the time-multiplexed data incorporates independent formatting.

Independent formatting implies that in the time-multiplexing technique, one data source is transmitted while the other data sources are being stored in buffers. Transmission is at a bit rate equal to the sum of the bit rates of the individual data sources. Thus, all data sources are eventually transmitted at an average rate equal to the rate at which they arrive at the telemetry and data-storage subsystem. The duration of transmission of each data source is relatively large (i.e., many frames). Thus, this form of formatting is simply a time-sharing of the channel in a given sequence with no attempt to establish a new encompassing format.

Synchronous formatting is similar to independent formatting with the big exception that only a fixed number of bits from each data source is transmitted before the next data source is selected. The number of bits transmitted at a time from each source is proportional to the incoming data rate of each source. Each complete sequence of transmission is identified by a transmitted synchronizing signal. Thus a new encompassing format is generated.

Frequency multiplexing implies that each data source has a separate subcarrier.

All Data Sources Frequency Multiplexed--Figure 4.1-14 illustrates a telemetry and data-storage subsystem in which all the data sources operate on separate subcarriers. The only subcarrier that is shared, S/C_2, is modulated by either the stored capsule or stored engineering data.

The enginerring data at 10 bps modulates the two-channel PN/PCM/PSK modulator. When the capsule is on the spacecraft, it is assumed that capsule data can be synchronized with engineering data (both referenced to the CC&S clock sources). This being the case, the low bit rate (10 bps) capsule data can be transmitted on a single subcarrier modulation channel because bit synchronized information can be derived from the engineering channel.

Planetary science and cruise science data are always simultaneously transmitted when in orbit. In the block encoded configuration the planetary science data requires transmitted word synchronization for proper data detection. This synchronization can be achieved by choosing the cruise science data subcarrier (S/C_4) as an even multiple of the planetary science word rate.

Switch S_3 is used to establish Mode VI. Switch S_4 is used to eliminate block coding of the planetary science data. Switch S_1 selects the required storage device for transmission of stored data and Switch S_2 selects either the capsule hardline or the telemetered capsule data. The positioning of all these switches as well as the choices of subcarrier frequencies are all configured by commands from the CC&S.

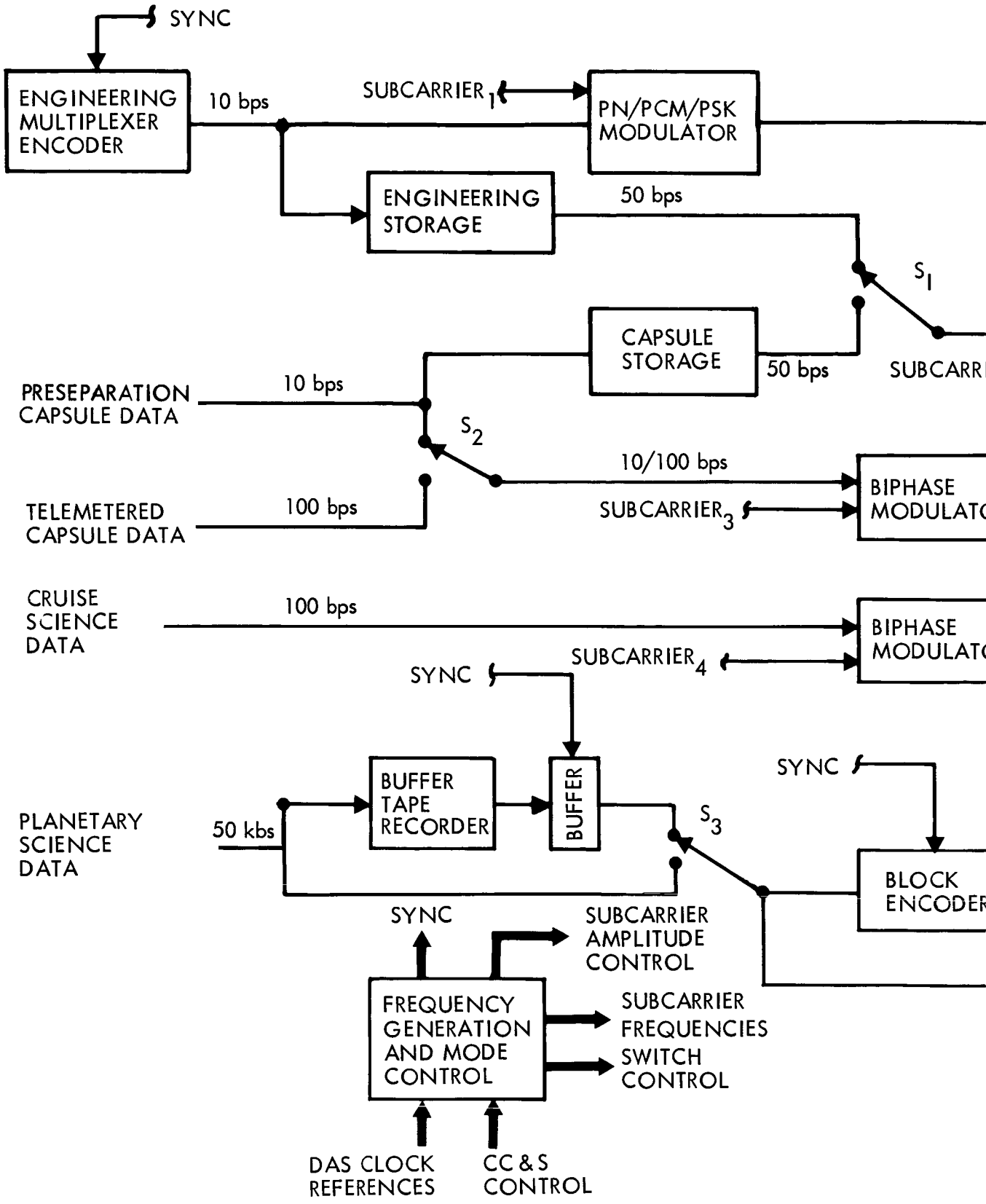
SYNC
ENGINEERING MULTIPLEXER ENCODER
10 bps
SUBCARRIER 1
PN/PCM/PSK MODULATOR
ENGINEERING STORAGE
50 bps
S1
CAPSULE STORAGE
50 bps
SUBCARR
PRESEPARATION CAPSULE DATA
10 bps
S2
10/100 bps
BIPHASE MODULAT
TELEMETERED CAPSULE DATA
100 bps
SUBCARRIER 3
CRUISE SCIENCE DATA
100 bps
BIPHASE MODULAT
SUBCARRIER 4
SYNC
SYNC
BUFFER TAPE RECORDER
BUFFER
S3
PLANETARY SCIENCE DATA
50 kbs
BLOCK ENCODER
SYNC
SUBCARRIER AMPLITUDE CONTROL
FREQUENCY GENERATION AND MODE CONTROL
SUBCARRIER FREQUENCIES
SWITCH CONTROL
DAS CLOCK REFERENCES
CC&S CONTROL

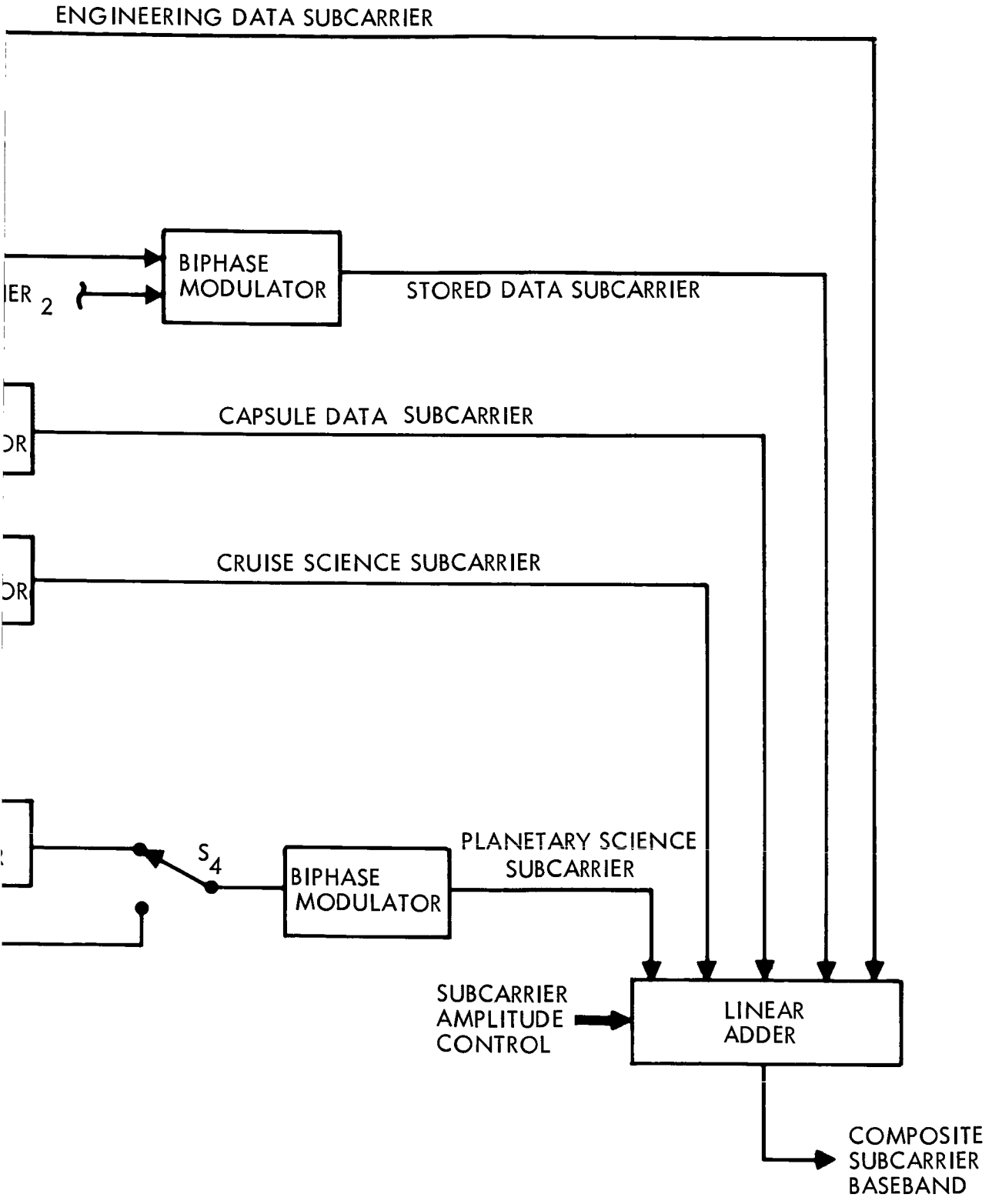

Figure 4.1-14: Subsystem Configuration With Data Sources Frequency Multiplexed

All Data Sources Time Multiplexed with Independent Formatting--Figure 4.1-15 illustrates a telemetry and data storage subsystem in which all the data sources are time multiplexed on to one subcarrier. The subcarrier is bi-phased modulated by the composite data. The data sources to be transmitted during any particular telemetry mode time-share the subcarrier. When one data source is being transmitted, the other data sources (that are to be transmitted during the mode) are being loaded into buffer storages. The read-out rate of each buffer is equal to the sum of the data rates of each source. The duration of readout from each buffer is relatively large and may include many frames of data.

Identification as to which particular buffer is being read out at any particular time can be accomplished in two ways. A long identification code can be transmitted just prior to the start of readout of any particular buffer or the start of any particular buffer readout can by synchronized to the frame synchronization of the individual data sources. The latter approach implies that frame identification circuits must be included in the electronics associated with each buffer.

To implement this multiplexing approach and satisfy the telemetry mode requirements, four additional buffers are required.

Switch S_1 selects either the capsule hardline or telemetered capsule data as the capsule data source. Switch S_2 by-passes the planetary science buffer as required in Mode VI. Switch S_3 by-passes the block encoder when encoding of the planetary science data is not required.

Since only one subcarrier is employed, word synchronization for the block-encoded planetary science data must be derived from the data itself.

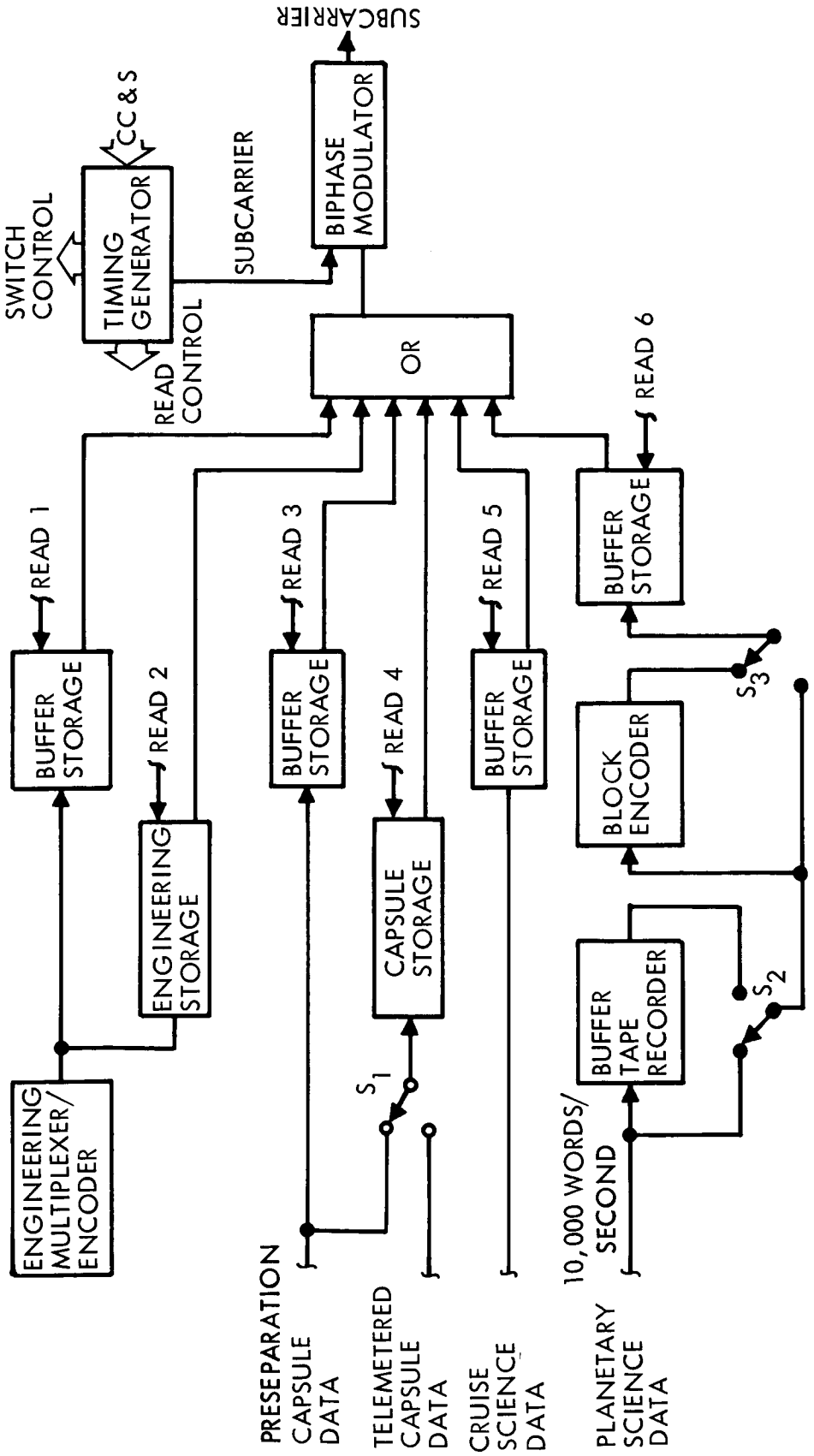

Figure 4.1-15: Configuration With Data Sources Time-Multiplexed & Independent Formatting

All Data Sources Time Multiplexed with Synchronous Formatting--Figure 4.1-16 illustrates a telemetry and data storage subsystem in which all the data sources are synchronously time multiplexed on one subcarrier which is biphase modulated by the composite data. The operation is similar to the operation of the recommended configuration (two subcarriers with synchronous formatting) with the exception that the planetary science data is included in the master time-multiplexing format.

In order to include the planetary science data in the multiplexing plan, the addition of a small buffer is required to accumulate a block of planetary science data while other data sources are being transmitted.

Combination of Frequency and Time Multiplexing with Synchronous Formatting--Figure 4.1-17 illustrates a telemetry and data storage subsystem in which the planetary science data modulates a high-frequency subcarrier and the other data sources (in a synchronously time-multiplexed format) modulate a low-frequency subcarrier. Two different low-frequency subcarrier arrangements exist: that required for Mode 1 and Mode 4 in which the modulation is PN/PCM/PSK, and that required for the remaining modes.

The subsystem illustrated in Figure 4.1-17 represents the recommended subsystem configuration and is described in Volume A, Section 4.1.1.

Evaluation of the Various Multiplexing Techniques--Several major considerations influence the choice of data multiplexing:

1) Simplicity to increase reliability (minimization of parts and subsystem components);

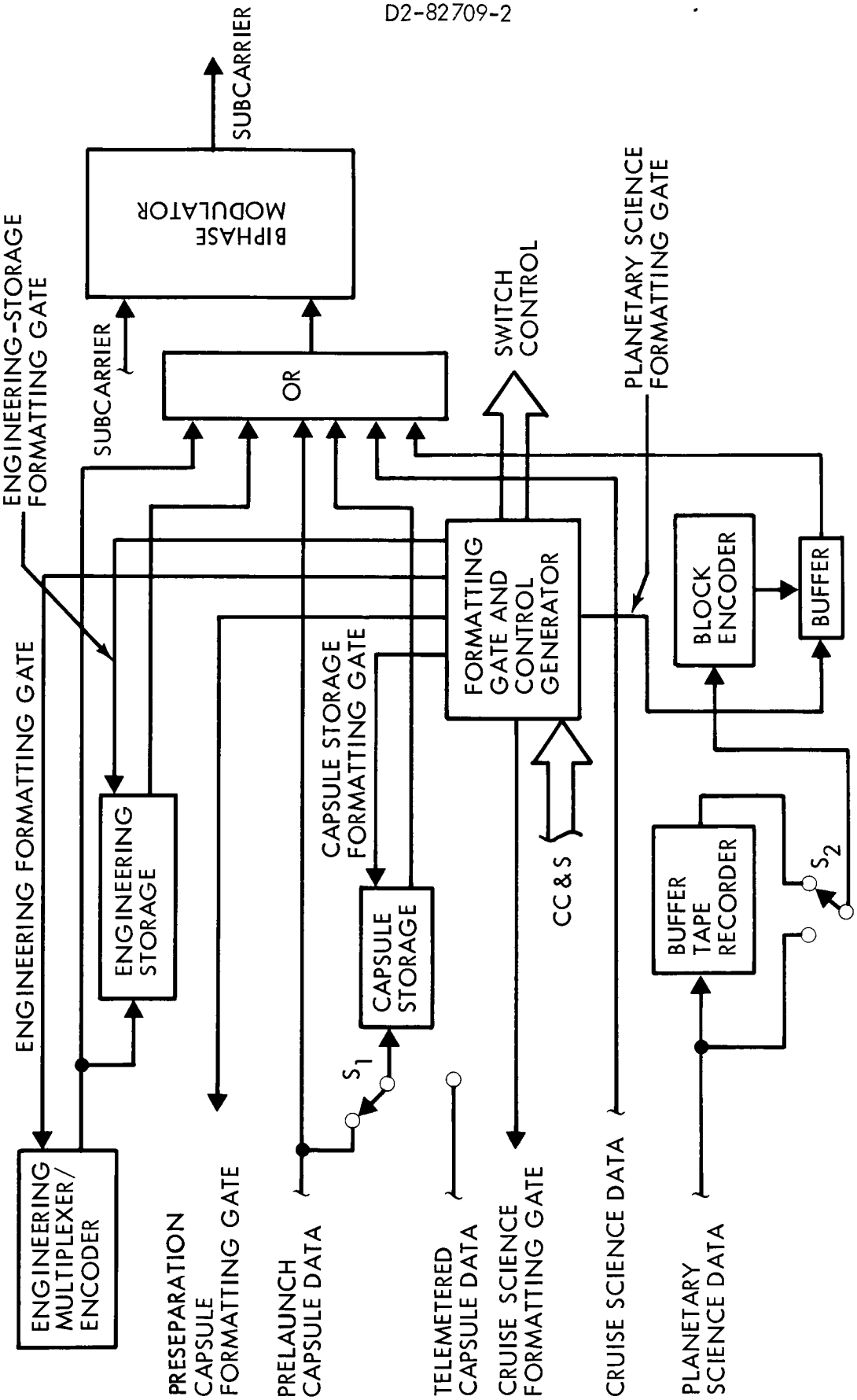

Figure 4.1-16: Configuration With Data Sources Time-Multiplexed & Synchronous Formatting

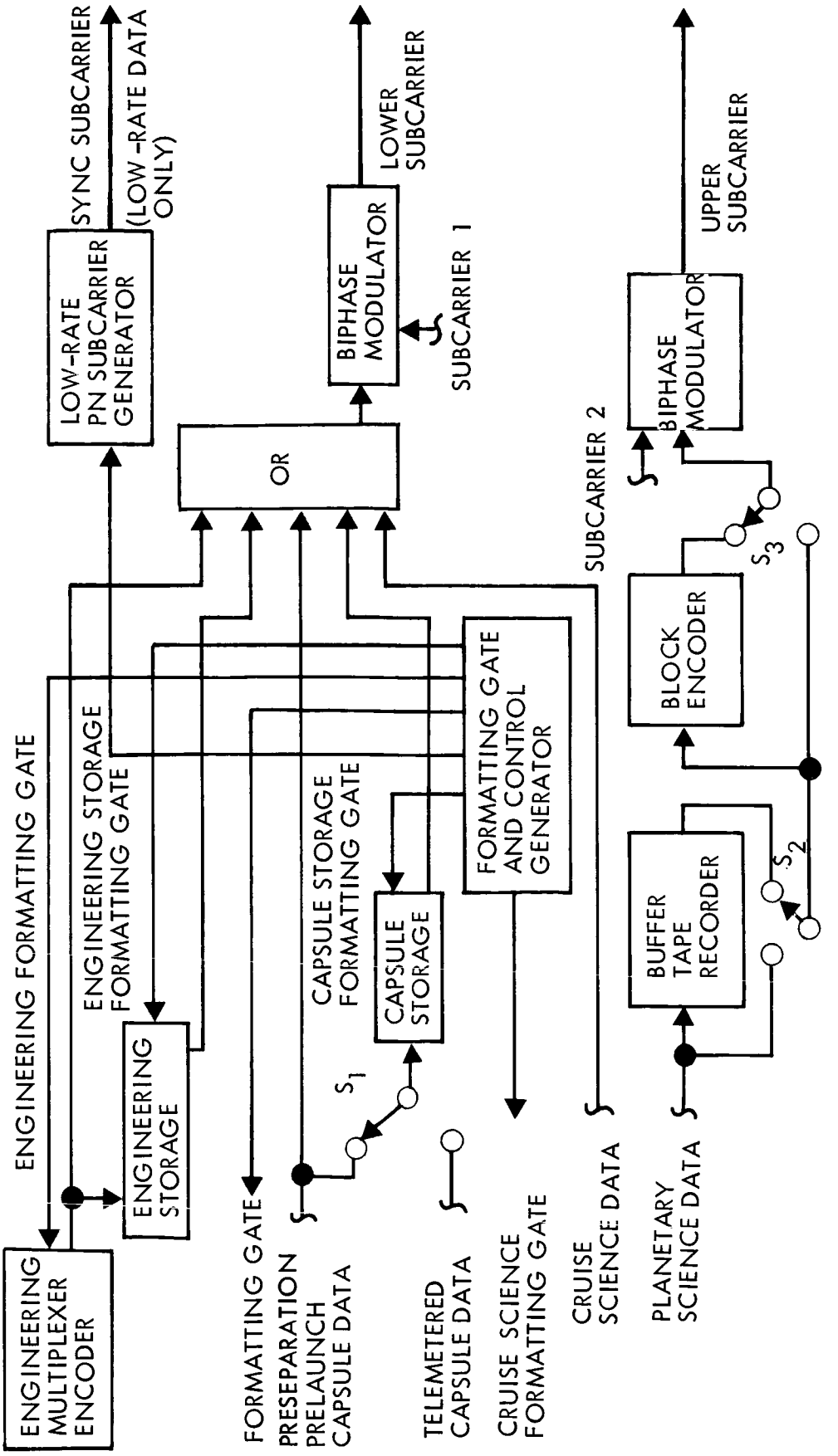

Figure 4.1-17: Synchronous Formatting — Two Subcarrier Configuration

2) Maximizing the amount of data transmitted for a given amount of power;

3) Adaptability thru the use of redundancy;

4) Minimization of weight, volume, and power dissipation;

5) Minimizing the interface control signals with other spacecraft subsystems.

With the exception of 2), the separate subcarriers multiplexing technique is as good or superior to the other candidate multiplexing methods. In respect to item 2), however, this approach is costly in available data bandwidth. Each subcarrier would require extra power to synchronize its ground detector. Hence, to maximize the link bit rate, a maximum reasonable use of time division multiplexing is required.

The first design approach, therefore, was to multiplex all data sources on one subcarrier. While this is possible, the circuit complexity becomes forbidding. This is because the planetary science data can have different formats depending on the experiment and because its data rate is much higher than the other sources. The resulting frame length is much longer. In order to get a sufficient percentage of frame synchronization information, the frame-synchronization pattern must be referred to the data train with the majority of bits. For example, one can insert a low bit-rate multiplexer output during a TV line retrace without reducing the picture quality in the least and still retain good synchronization. However, the reverse would not work. Sufficient number of synchronization bits would not be available at the slower rate. If only a picture line frame were required, the problem of mixing the data would still be difficult because of the above reasons. However, other formats, such as IR, UV, or photospectrometer may be used as

well. Timing and length of these formats are not known (being subject to ground command) and will be of necessity of an intermittent nature.

Mixing of the lower bit rate data in the planetary science subsystem before recording is another approach. This must be discarded because of the 1000-to-1 ratio in the bit rates and the intermittent operation.

Mixing of the low rate data at 10 bps with picture data at 8000 bps would require a line scan or master format of about 2800 bits. By putting the planetary science data on a separate subcarrier, the master format was reduced to 91 bits, including a 7-bit synchronization word with a corresponding significant reduction in logic elements. Thus, a reasonable compromise was found. This was to time-division multiplex all data except planetary science on one subcarrier and put the planetary science data on a separate subcarrier. This system was then detailed and found to be easily implemented.

Time-division multiplexing will be done with data words synchronized as much as possible (frame synchronization requires excessive buffering to accomplish). A short frame of 13 words is sufficient to accomplish the task of multiplexing the data during the six modes of data transmission. One word is for master-frame synchronization and the other 12 words are for data. Subsystem gating functions to channel the bit rate to the various subsystems are easily generated using outputs from a 13-count binary string. These functions are controlled by mixing with the mode control functions in "AND" gates.

The six different required modes are changed by shifting a different control word into the mode command register from the central computer and

sequencer. The different control functions, gating functions, oscillator frequencies, bit rates, and filter selections all depend on the particular pattern of the mode command code. Limiting the format to a fixed length resulted in simplification of the switching since a fixed length counter could be employed, thus improving the reliability.

From the communications link standpoint, the two-subcarrier approach offers some advantages. The major advantage is that a 5 or 6 decibel improvement can be effected in the lower channel by turning the upper frequency planetary science subcarrier off when it is not needed. Also, when both subcarriers are on, the subcarrier from the lower channel will be used to synchronize the word rate of the upper channel. It would be possible to turn the upper channel on only during playback of the planetary science recorder, thus improving lower channel link performance.

Study was also made of independent formatting versus synchronous formatting. Considerable buffer storage is needed to accomplish this. Synchronous formatting is recommended on the Voyager to eliminate bulky storage buffers as well as unnecessary time delays and time coding problems. Synchronous formatting is now being used successfully on the Boeing Lunar Orbiter.

It is therefore concluded that the maximum possible use of synchronous formatting with all data, except planetary science, time division multiplexed on one subcarrier and the planetary science recorded playback on a separate subcarrier will result in the most reliable data handling system. It will also have the mission operational advantage of being easy to control to maximize the amount of received data for the available power and time.

Information is presented in Table 4.1-12 to compare the major problem areas on a qualitative basis.

4.1.6.3 Data Compression

Use of data compression techniques for the Voyager spacecraft engineering and science data and the relayed capsule data can offer the following possible advantages:

1) Increased transmission of information for a given bit rate constraint,
2) Decreased bit rate and, consequently, improved link margin, for a given information transmission requirement.

The disadvantages of data compression are the increased complexity and, hence, a reduction of reliability and an increase of weight, volume, and power.

Several data compression techniques can be used. Considering the weight, volume, and power dissipation constraints; feasible techniques that can be employed are delta modulation, and zero and first order compression (with prediction or interpolation) with a fixed or variable aperture.

The spacecraft engineering data, capsule data, cruise science data, and planetary science data all represent measurement of different phenomena. For this reason, these data sources would be subjected to different degrees and possible different forms of data compression. In the preferred design, the spacecraft engineering data, capsule data, and cruise

Table 4.1-12: COMPETING CHARACTERISTICS

	rf Link Efficiency	Buffer Storage Required	Master Frame Format Generator	Mission Operations Flexibility	Single Thread Reliability
1. All Data Sources Frequency Multiplexed	Poor	None	None	More than Required	0.855
2. All Data Sources Time Multiplexed with Independent Formatting	Best	10^5 Bits	Buffer Dump Timing Interlock System	Difficult to Implement	0.734
3. All Data Sources Time Multiplexed with Synchronous Formatting	Best	50 Bits	3000 Bits Long	Difficult to Implement	0.811
4. Combination of Frequency and Time Multiplexing with Synchronous Formatting	Good	50 Bits	91 Bits Long	Meets Requirements	0.815*

* Reliability is 0.896 for the Volume A configuration.

science data are all time multiplexed. The complexity of a data compressor operating on the time multiplexed signal with different compression requirements for each of the data types would be extremely high. It is therefore concluded that if any or all of the data sources are to be subjected to data compression, the compression should be done on an individual basis.

There are certain advantages in performing the data compression at the data sources where the data points are sampled and encoded. The principal advantage is that the different control signals that sample the data points can also serve as the access signals to storage devices where the past history of data is stored. This leads to the conclusion that if independent data compressors are used for the planetary science and capsule data, they should be physically located in the DAS subsystem and in the capsule respectively.

Since it has been concluded that the telemetry and data storage subsystem should not have any data compression responsibility for planetary science, cruise science, or capsule data, data compression for the spacecraft engineering data is now addressed.

For the preferred design, engineering data is transmitted at the average rate of 11 1/9 bps for Modes 1, 2, and 3, 66 2/3 bps for Modes 5 and 6, and 5 5/9 bps for Mode 4. In Modes 2 and 3, and in Modes 5 and 6, the total transmission rates are 133 1/3, and 400 bps respectively, thus it is seen that the engineering data is a small fraction of the total data transmitted during these modes. Mode

4 is an emergency mode with a low probability of usage. With the exception of Mode 1, it is therefore concluded that use of compression to reduce the transmitted bit rate cannot be effectively traded off for the weight, volume, and power required and the increased complexity.

The logic thus far has concluded that if data compression is employed in the telemetry and data storage subsystem, then it must be for the purpose of increasing the number of sampled spacecraft engineering data points without increasing the transmitted bit rate.

An extensive engineering telemetry list has been compiled that defines the required sampling points, their sampling rate, and the precision of sampling required. This requirement was reduced to an engineering bit rate that was compatible to the channel capacity for all the telemetry modes. Since there is a capability to transmit all the required data, no requirement for data compression exists because of limited transmission channel capacity.

Because of all the above reasons discussed, the final conclusion is that data compression is not recommended in the telemetry and data storage subsystem.

4.1.6.4 Redundancy

Redundancy Considerations and Alternatives for the Preferred Design--
The synchronous formatting-two subcarrier configuration was evaluated for redundancy mechanization to maximize subsystem reliability. Redundancy techniques from a single thread approach (no redundancy) to the subsystem

level was quantatively evaluated. The following discussion describes each approach considered and Figure 4.1-18 illustrates and summarizes the different redundancy configurations.

1) Single Thread

The single thread failure rate was estimated to be 90.66 failures per million hours. Since the reliability of individual components is weighted by the effective mission operational time requirement, the product of failure rate and effective mission time (λ t) is used as the figure of merit for reliability improvement criteria.

The components of the single thread model are ranked as follows in respect to failure rate, λ, and then to λ t product.

Failure Rate	Rank	Component	t Product	Rank
2791	1	Planetary Data Storage	0.0201	3
217	6	Capsule Data Storage Real Time Buffer Mode	0.0112	4
1557	3	Capsule Data Storage Mode	0.00009	7
1557	3	Engineering and Cruise Science Data Storage	0.00009	7
562	4	Data Processor	0.0331	2
2250	2	Engineering Multiplexer	0.1323	1
40		Capsule Data Control	0.0021	6
309	5	Planetary Data Acquisition	0.0032	5

Due to the short mission time, the planetary recorder that is ranked first in failure rate is ranked third in λt. The engineering multiplexer encoder ranked first in the λt ranking.

I. SINGLE THREAD

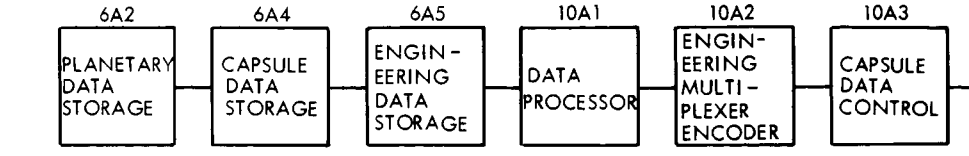

		R.T. STORAGE					
λ	2791	217	1557	1557	562	2250	40
λt	0.0201	0.01120	0.00009	0.00009	0.0331	0.1323	0.0021

II. SUBCOMPONENT

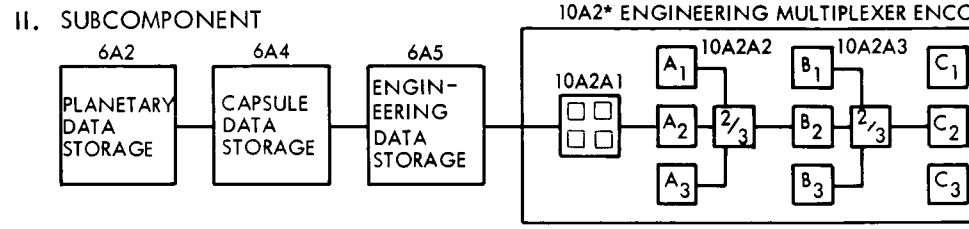

	10A2*	(1015.2)	(202)	(250)	(3
λ	126.6	6.6	10	100	
λt	0.00741	0.00039	0.00059	0.0059	0.0

III. COMPONENT

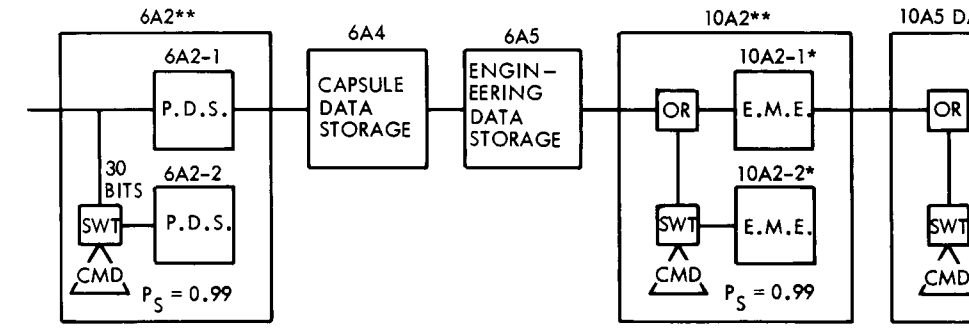

	6A2**
λ	305
λt	0.0022

	OR	SWT	10A2**	OR
λ	30	10	29	30
λt	0.00176	0.00059	0.00171	0.00176

IV. SUBSYSTEM

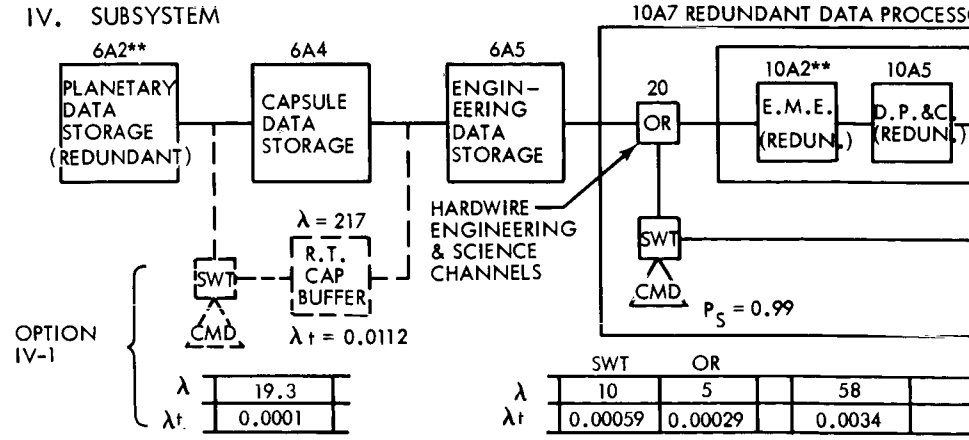

λ	19.3
λt	0.0001

	SWT	OR	
λ	10	5	58
λt	0.00059	0.00029	0.0034

F

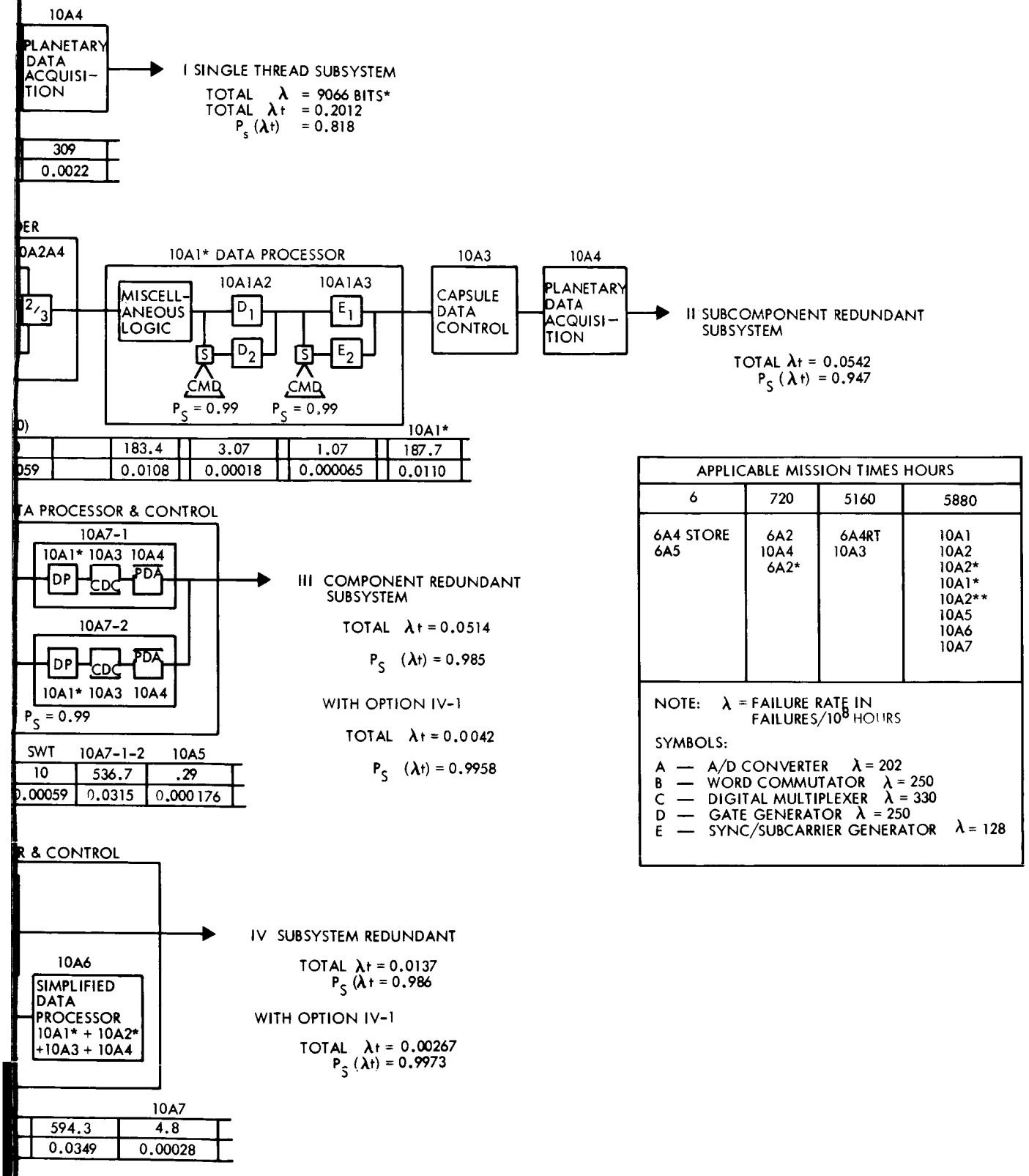

APPLICABLE MISSION TIMES HOURS			
6	720	5160	5880
6A4 STORE 6A5	6A2 10A4 6A2*	6A4RT 10A3	10A1 10A2 10A2* 10A1* 10A2** 10A5 10A6 10A7

NOTE: λ = FAILURE RATE IN FAILURES/10^8 HOURS

SYMBOLS:

A — A/D CONVERTER λ = 202
B — WORD COMMUTATOR λ = 250
C — DIGITAL MULTIPLEXER λ = 330
D — GATE GENERATOR λ = 250
E — SYNC/SUBCARRIER GENERATOR λ = 128

Figure 4.1-18: Telemetry and Data Subsystem Alternate Redundancy Configurations

2) Subcomponent Redundancy

The weakest link, the engineering multiplexer encoder, is delineated to the subcomponent level. The major subcomponents are ranked as follows:

a)	Analog Multiplexer	λ =	1015	Bits
b)	Digital Multiplexer	λ =	330	Bits
c)	Word Commutator	λ =	250	Bits
d)	A/D Converter	λ =	202	Bits
	Total	λ =	1797	Bits

One bit is equal to 1×10^{-8} failures per hour.

It was found that quad redundancy of analog gates and a two-out-of-three majority voting redundancy in the other three subcomponents resulted in the following reliability improvement:

a)	Word Commutator (2/3)	λ =	100	Bits
b)	A/D Converter (2/3)	λ =	10	Bits
c)	Digital Multiplexer (2/3)	λ =	10	Bits
d)	Analog Multiplexer (2/3)	λ =	6.6	Bits
	Total	λ =	126.6	Bits

The λt for engineering multiplexer encoder is now 0.0074 which drops its ranking to fourth. The data processor is now addressed since it is now ranked first. The following are major ranked subcomponents of the data processor:

λ Bits	Nomenclature	Rank
250	Gate Generator	1
183.4	Miscellaneous Logic	2
128.2	Synchronous/Subcarrier Generator	3

The gate generator and synchronous/subcarrier generator can be mechanized with standby redundancy requiring two commands and 153 bits of off-line switching logic each for the following gains:

λ Bits	Nomenclature	Rank
183.4	Miscellaneous Logic	1
3.07	Gate Generator	2
1.07	Synchronous/Subcarrier Generator	3
187.7 Total		

The λt product for the data processor is now 0.0110 which places it below planetary storage at 0.0201. The majority (75 percent) of the planetary storage tape recorder's failure rate results from mechanical parts which are not easily made redundant on the subcomponent level. The next improvements are addressed on the component level.

The subcomponent redundant configuration reliability (Model II) was estimated to have a 0.947 probability of success.

3) Component Redundancy

With subcomponent redundancy, the ranking of components is now:

λ	Nomenclature	λ_t	Rank
2791	Planetary Data Storage	0.0201	1
217	Capsule Data Storage Real Time Mode	0.0112	2
1557	Capsule Data Storage Mode	0.00009	7
1557	Engineering and Cruise Science Data Storage	0.00009	7
187.7	Data Processor	0.0110	3
126.6	Engineering Multiplexer Encoder	0.0074	4
40	Capsule Data Control	0.0021	6
309	Planetary Data Acquisition	0.0022	5

Standby redundancy of the planetary data storage tape recorder requiring one command and 30 bits of off-line switching logic, results in a λ t of 0.0022 which changes its rank to fourth with the planetary data acquisition logic (buffer and modulator).

The capsule data-storage real time mode is ranked first, the data processor is now second and the engineering multiplexer encoder is third. The λ t's are now leveling out and function criticality now dictates the strategy.

The data-processor, capsule-data-control, and planetary-data-acquisition components are grouped into a standby configuration at the cost of one command, 30 bits on a line and 10 bits off-line switching logic. The data processor and control has a λ t of 0.000176.

In the same context, the engineering multiplexer encoder is made standby-redundant at the cost of one command and 45.5 bits of off-line switching logic.

The component redundant Configuration III has a total λt of 0.0154 for a subsystem probability of success of 0.985. Standby redundancy of the capsule storage real time buffer mode (Optim IV-1) would give a total subsystem λt of 0.0042, P_S (Σt) = 0.9958. At this level, alternate configurations of the other interfacing telecommunications subsystems dictates the improvement strategy.

4) Subsystem Redundancy

Complexity of the lower level redundancy forces a backup subsystem approach. This complexity factor in addition to the attractiveness of a backup subsystem to relieve the pressure of the radio subsystem, where subcomponent redundancy is not as easily implemented as in digital circuits, resulted in alternate Configuration IV.

A simplified data processor that has a capability of handling real time science data and 50 percent of the engineering channels is hardwiredin at the appropriate data-input points. This results in a subsystem λt product of .0137 and a probability of success of 0.986.

The simplified data processor backup without standby redundancy of the real time capsule data mode of the memory core storage unit

is not effective. This shows the validity of addressing the weakest link first. On the other hand, failure of the capsule data function will not result in complete subsystem failure from a functional viewpoint but a data processor will cause failure of the total subsystem. Therefore, from a functional viewpoint, backup of the data processing circuits is more critical.

5) Combinations of Redundancy Techniques

Combinations of subsystem implementation employing different percentages of each redundancy level were evaluated. The basis for this evaluation was the single thread analysis that showed the major single-thread weaknesses:

Component	Rank	λt Product
Engineering Multiplexer Encoder	1	0.1323
Data Processor	2	0.0331
Planetary Data Storage	3	0.0201

Other component λt products are a factor of two or better than those listed above.

By addressing the engineering multiplexer encoder on a subcomponent level and using quad redundancy in the analog multiplexer, its λt product was reduced from 0.1323 to 0.0447. By addressing the planetary science recorder on the component level, its λt product was reduced from 0.0201 to 0.0022.

The subsystem reliability using the redundancy described above is then

$$\lambda t = 0.110$$

$$Ps\ (t) = 0.896$$

Other combinations were evaluated and weighted against the weight, volume, power dissipation, and complexity burdens. In particular very poor tradeoffs were realized if redundancy of any level was applied to the data processor. This is primarily due to the extreme complexity of the interface characteristics of this component within itself, other subsystem components and other spacecraft subsystems.

Considering the tradeoff parameters, it was concluded that the optimum redundancy configuration is one in which redundant planetary science recorders are used and quad redundancy is employed in the engineering multiplexer and encoder. This redundancy approach is employed in the preferred subsystem design.

Table 4.1-13 presents a summary of the evaluation of each redundancy technique employed. Reliability improvements over the single-thread approach and required weight, volume, and power dissipation are listed.

4.1.7 Relay Link

Subsystem trades leading to the preferred design of the relay link are principally the selection of operating frequency and the choice of modulation to be used. Over the range of frequency considered for this link,

Table 4.1-13: SUMMARY OF REDUNDANCY TECHNIQUES CONSIDERED FOR THE PREFERRED DESIGN

Redundancy Level	Total λt	Ps (λt) for 5880 hours	λt Improvement over Single Thread Configuration	Required Weight (lbs)	Required Volume (cu. in.)	Power Dissipation (watts)
I Single Thread	0.2012	0.818	———	44	1760	29.2
II Subcomponent	0.0542	0.947	3.7	84	3300	35.6
III Component with Subcomponent Redundancy	0.0514	0.985	3.9	115	3960	41
IV Subsystem	0.0137*	0.986*	14.6	83	3220	34
V Preferred Design	0.110	0.8846	1.8	69	2860	29.3

* Figures are for the Transmission of Real Time Science Data and 50 percent of Real Time Engineering Data.

the frequency and modulation investigations can be treated separately. After a review of subsystem constraints, the operating frequency is selected first and then the trades leading to a choice of modulation technique are presented.

4.1.7.1 Link Constraints

Constraints are imposed on link performance by the spacecraft and capsule trajectories, capsule power limitations, and atmospheric attenuation effects.

The nominal trajectory for the 1971 mission has capsule separation 10 days prior to impact with the separation increasing approximately linearly with time until the capsule and spacecraft are almost 9500 kilometers apart at impact. The capsule look angle at the spacecraft remains at 90 degrees from the flight path until the last 2 hours before impact when the capsule moves ahead because of the increasing planetary attraction. There are no appreciable differences in velocity or acceleration until the last 2 hours before impact. The range, range rate, and radial acceleration between the spacecraft and orbiter in the last minute prior to impact are shown in Figure 4.1-19. After capsule impact, the spacecraft is inserted into orbit--a nominal orbit with 18-hour period, periapsis of 2700 kilometers, and apoapsis of 23,760 kilometers has been used for this development.

Capsule transmitter power capabilities are limited by the allowable weight of power generating equipment (such as batteries, solar cells,

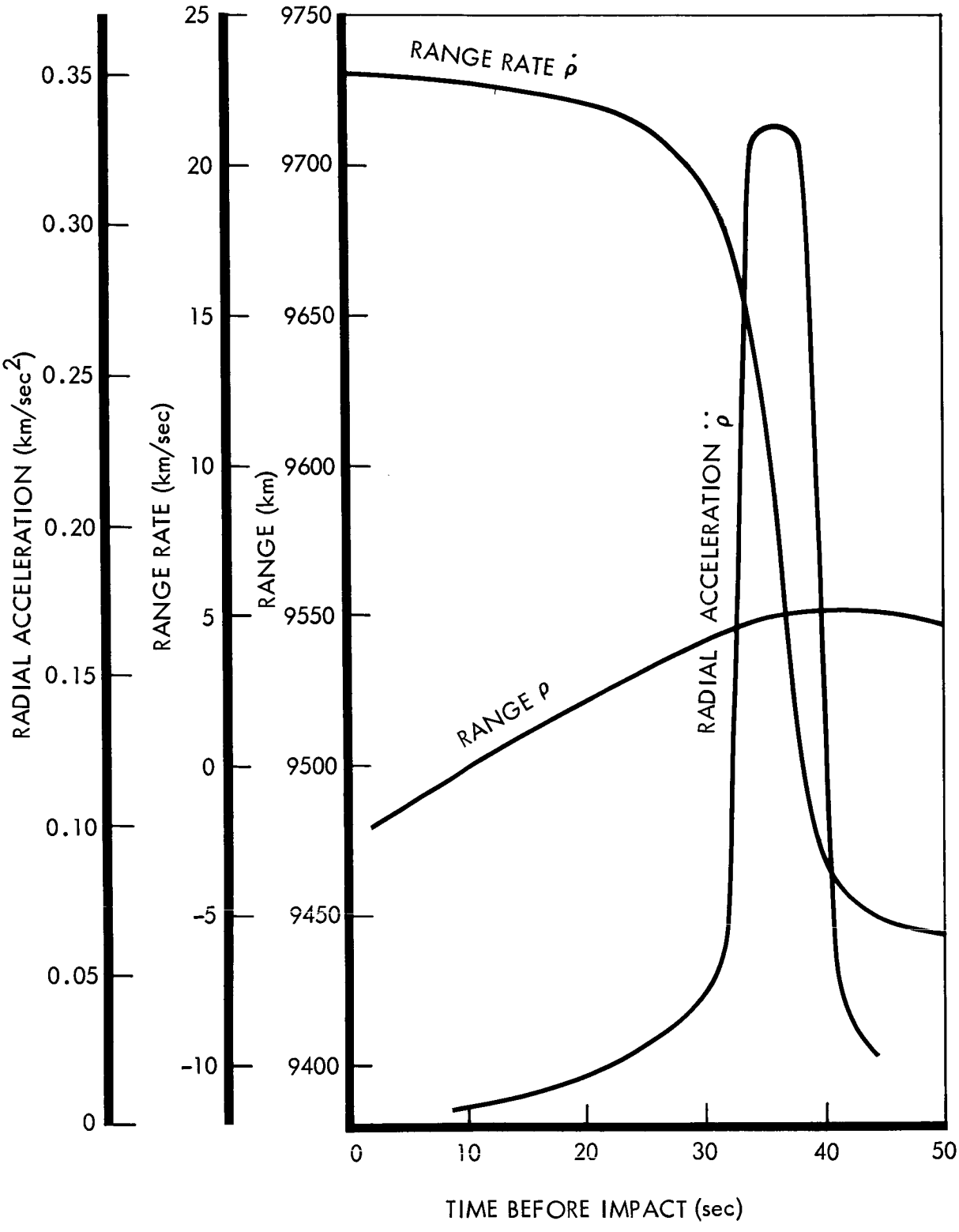

Figure 4.1-19: Spacecraft/Capsule Entry Profile

or radioisotope thermoelectric generators). It is not expected that more than 20 watts of power would be available continuously, although higher power might be supplied for short intervals on an emergency basis. Furthermore, the use of a directional antenna on the capsule to increase radiated power during descent is not advisable unless the attitude of the capsule can be maintained accurately.

Mars atmospheric attenuation is anticipated to be severe for the final few minutes before impact because of plasma formation during entry. Unless extremely high frequencies can be used for this link, some degree of attenuation must be tolerated. If Mars has an appreciable ionosphere, this will limit the minimum frequency for postlanding operation.

4.1.7.2 Frequency Selection

Figure 4.1-20 shows the frequency selection trade study in terms of a normalized S/N ratio that considers the frequency dependence of space loss, transmitter efficiency, and galactic noise temperature and receiver noise figure combined into system noise temperature. The evaluation was performed over the frequency region shown because realizable antenna sizes establish a low-frequency limit, and the increasing magnitude of the space loss fixes an upper bound for consideration. Details of the analysis are in Philco Document WDL-TR-2531, "Mars Mission Communication Analysis." The recommended frequency for operation of the relay link is 100 megacycles.

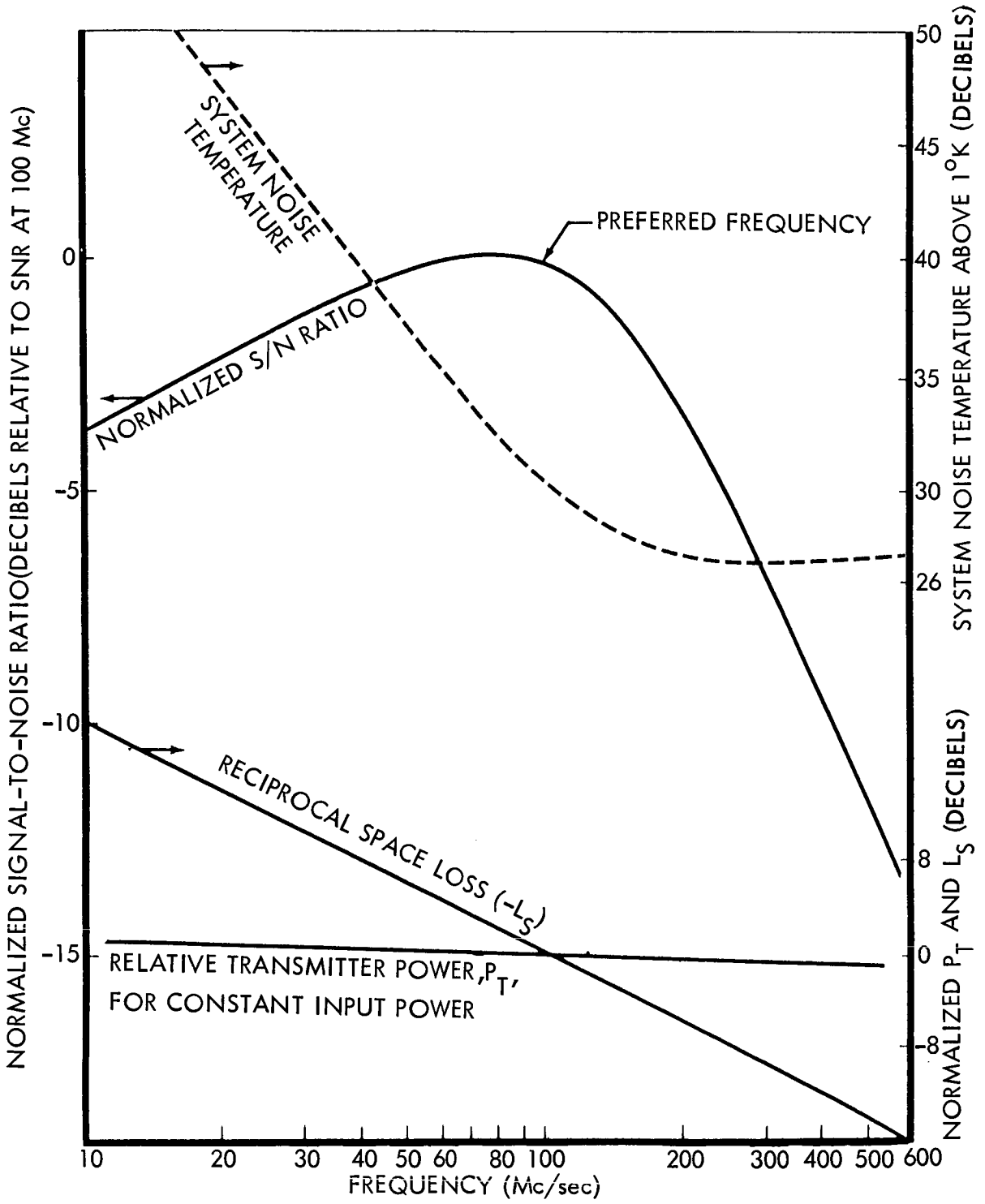

Figure 4.1-20: Frequency-Selection Trade Study

4.1.7.3 Modulation Selection

Configurations using five different modulation techniques have been considered. These configurations are: (1) PSK/PM with a carrier tracking phase lock receiver, (2) PCM/FM with a conventional discriminator, (3) PCM/PM with conventional discriminator, (4) PSK/FM with conventional discriminator, and (5) PSK with phase lock receiver. Performance of the configurations has been compared for the conditions of maximum deceleration within 1 minute of impact, because such conditions represent the worst case encountered during the capsule descent phase.

Link analyses for each configuration are given in Philco Document WDL-TR-2531. Table 4.1-14 compares the five modulation techniques and discusses key advantages and disadvantages of each. In the analysis, the transmitter power was computed that would yield satisfactory performance with the assumed link parameters. Assumptions included spacecraft antenna gain of 7 decibel with 3 decibel polarization loss, line losses of 1.25 decibel for both terminals, and bit rates of 10 bits per second before impact, and 10 and 100 bits per second after impact.

The recommended configuration uses PSK/FM with a conventional discriminator and requires 2 watts for communication at entry. The link requires 10 watts to transmit 10 bits per second to a range of 24,000 kilometer at apoapsis. The increased bandwidth needed to transmit 100 bits per second changes the required power to 14.2 watts with a 0-decibel capsule antenna or 4.5 watts with a 5-decibel capsule antenna. A 5-decibel antenna would provide coverage at elevation angles greater than 30 degrees which is consistent with minimizing multipath effects.

TABLE 4.1-14: COMPARISON OF RELAY-LINK MODULATION TECHNIQUES

MODULATION TECHNIQUE	POWER REQUIRED			DOPPLER-RATE SUSCEPTIBILITY	SIDEBAND LOCK SUSCEPTIBILITY	HARDWARE COMPLEXITY	COMMENTS
	CAPSULE DESCENT 10BITS/SEC	18-hr ORBIT 0 db CAPSULE ANTENNA 10 bps	18-hr ORBIT 5 db CAPSULE ANTENNA, 100 bps				
PSK/PM PHASE-LOCK RECEIVER $2B_{LO}$= 150 cps	16.0 dbm 40 mw	23.1 dbm 205 mw	28.1 dbm 645 mw	NONE, PROVIDED $2B_{LO}$ IS SUFFICIENTLY LARGE	POSSIBLE	COMPLEX	REQUIRES SIDEBAND-LOCK REJECTION CIRCUITRY CARRIER, SUBCARRIER, BIT SYNC LOCK REQUIRED AFTER BLACKOUT ENDS
PSK/FM CONVENTIONAL DISCRIMINATOR B= 0.7 f_{sc} = 200 cps FOR 10 bps OR $666^2/3$ cps FOR 100 bps	32.9 dbm 1.95 w	40.0 dbm 10.0 w	36.6 dbm 4.57 w	NONE BECAUSE PSK DATA IS ON A SUBCARRIER	NO	SIMPLE	SUBCARRIER AND BIT-SYNC LOCK REQUIRED AFTER BLACKOUT ENDS
PCM/PM AND PCM/FM CONVENTIONAL DISCRIMINATOR	31.8 dbm 1.51 w	38.9 dbm 7.76 w	34.3 dbm 2.69 w	SEVERE	NO	COMPLEX	BIT-SYNC LOCK REQUIRED AFTER END OF BLACKOUT
PSK PHASE-LOCK RECEIVER $2B_{LO}$ = 200 cps (FOR AUTOMATIC REACQUISITION)	17.2 dbm 52.5 mw	24.7 dbm 295 mw	29.8 dbm 955 mw	SEVERE	NO	COMPLEX	BIT-SYNC LOCK REQUIRED AFTER END OF BLACKOUT. INCREASED $2B_{LO}$ ALLOWS AUTOMATIC CARRIER REACQUISITION AFTER BLACKOUT

Use of PSK/FM eliminates doppler rate problems and the possibility of sideband lock that could occur with PSK/PM using a phase lock receiver. Operating parameters for the capsule relay system have not been selected as part of the preferred design since this selection will be made by JPL and the capsule contractor.

4.1.8 Antenna Subsystem

The spacecraft antenna subsystem consists of four S-band antennas and one VHF antenna, the control system for the high-gain S-band antenna, and the transmission lines associated with each antenna.

Alternate configurations are considered for the following functional elements:

1) Low-gain antenna (S-band);
2) High-gain antenna (S-band);
3) High-gain antenna control system;
4) Ascent antennas (2-S-band);
5) Relay antenna (VHF);
6) Transmission lines

Low-Gain Antenna--There are several basic factors to be weighed in selecting this antenna system. The first involves linear polarization versus circular polarization; the second involves "omnidirectional" coverage (implying omnidirectional in azimuth only) versus near-spherical coverage, and the effect of the method of orienting the vehicle for maneuvers.

The question of whether to use linear or circular polarization reduces to consideration of the polarization loss that results from operating a linearly polarized antenna with the DSIF. The 3 db polarization loss of the linear antenna over a circularly polarized antenna dictates the circularly polarized antenna, since other trades such as efficiency are fairly even. The linear antenna has a slight weight advantage, and is less complex in construction, but the 3 db disadvantage out weighs all other considerations.

The comparison of near-spherical pattern coverage and omnidirectional coverage is more complicated, since the question of attitude control of the vehicle for a midcourse maneuver needs to be considered. The equivalent of spherical coverage without nulls can be obtained through the use of two hemispherical antennas, each connected to its own receiver with the outputs combined after detection. Combining the two antenna outputs prior to detection causes many interference nulls to appear in the region where the antenna patterns overlap. Since the choice between the omnidirectional antenna and the spherical-coverage antenna would be on the basis of not having any nulls in the pattern coverage, this latter method is precluded. The use of an extra receiver for this spherical antenna, plus the extra transmission lines and added weight of the second hemispherical antenna, indicates that the omnidirectional antenna is more desirable.

The number of microwave antenna configurations capable of generating a circularly polarized omnidirectional pattern is limited. A normal-mode helix is sometimes used at VHF, but dimensional tolerances and small dimensions make it a doubtful choice at S-band. A circularly polarized biconical horn can be regarded as the slot analog of the helix, but with better bandwidth and efficiency because of the larger volume occupied. A photograph and drawing of the preferred right-hand circularly polarized biconical horn, with its dipole-type free-space pattern are shown in Figures 4.1-21, 4.1-22, and 4.1-23. The photograph shows a chem-milled antenna, with white thermal coating.

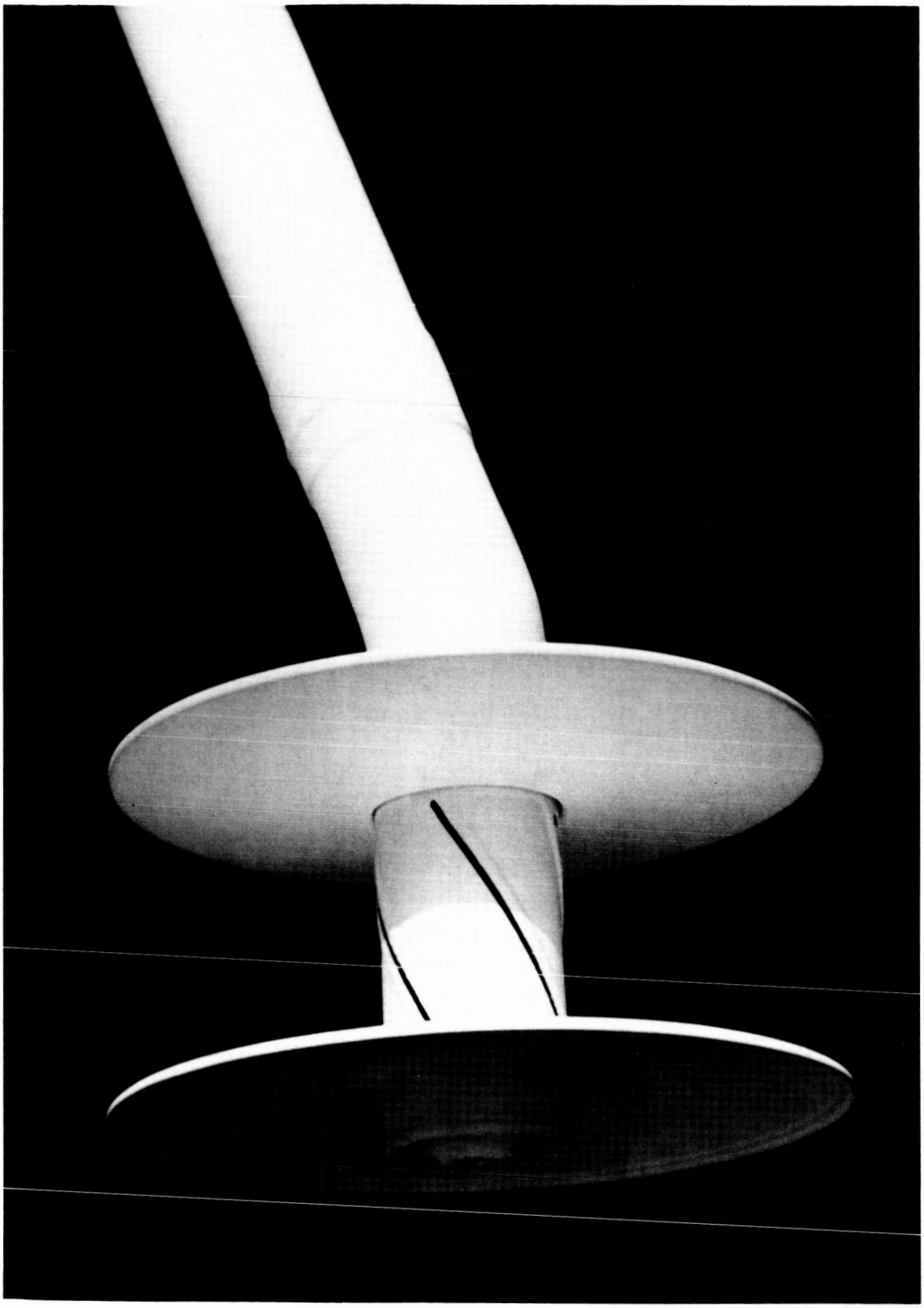

Figure 4.1-21: Low-Gain Antenna

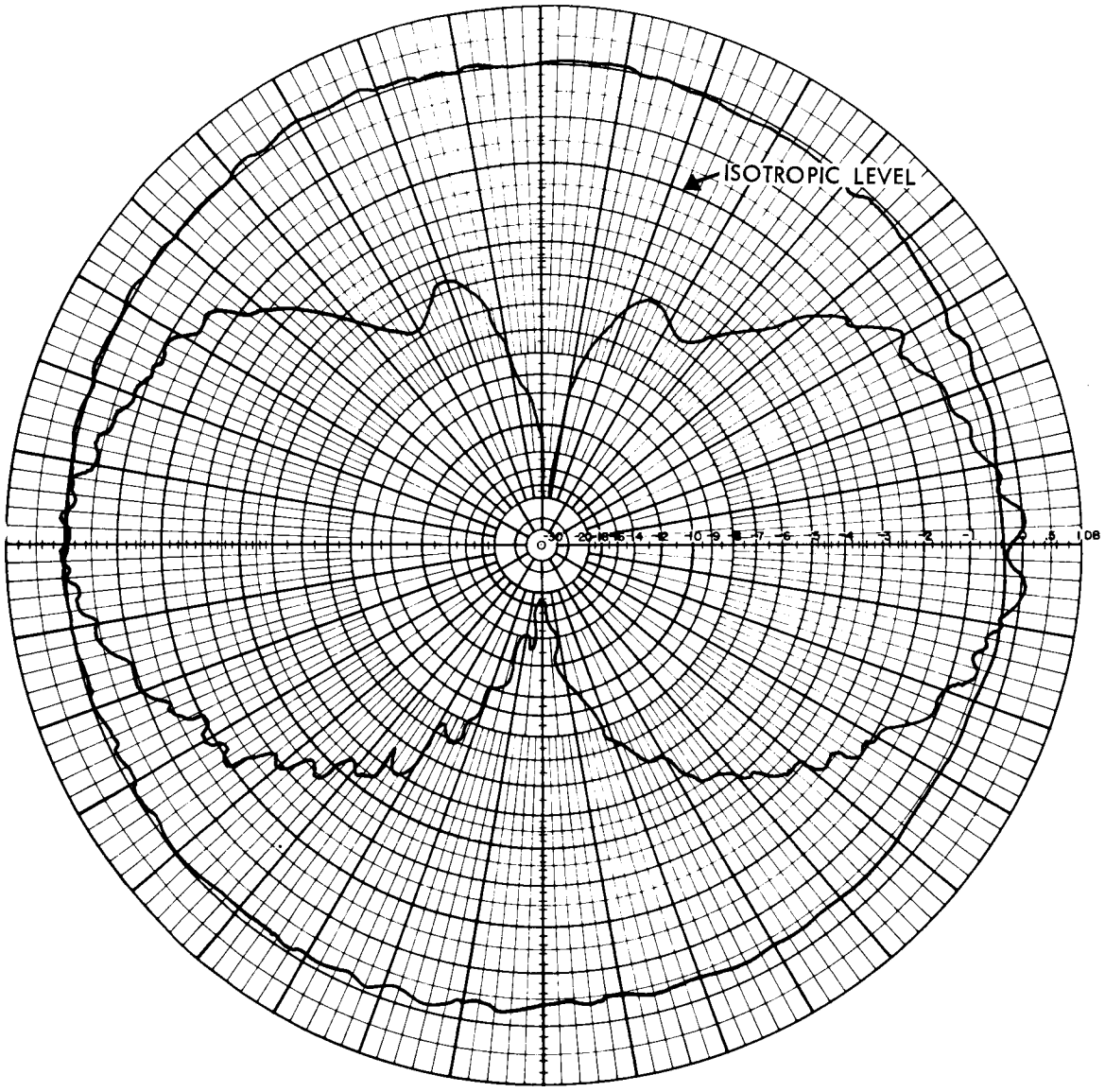

Figure 4.1-23: Radiation Pattern Low-Gain Antenna

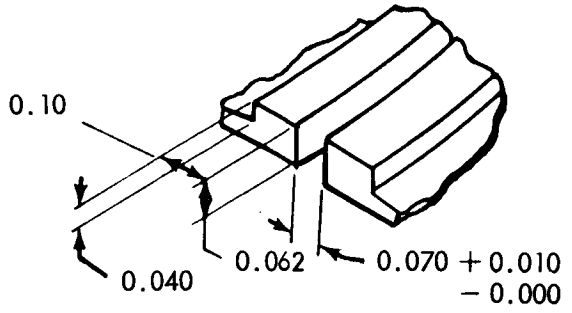

SLOT DETAIL

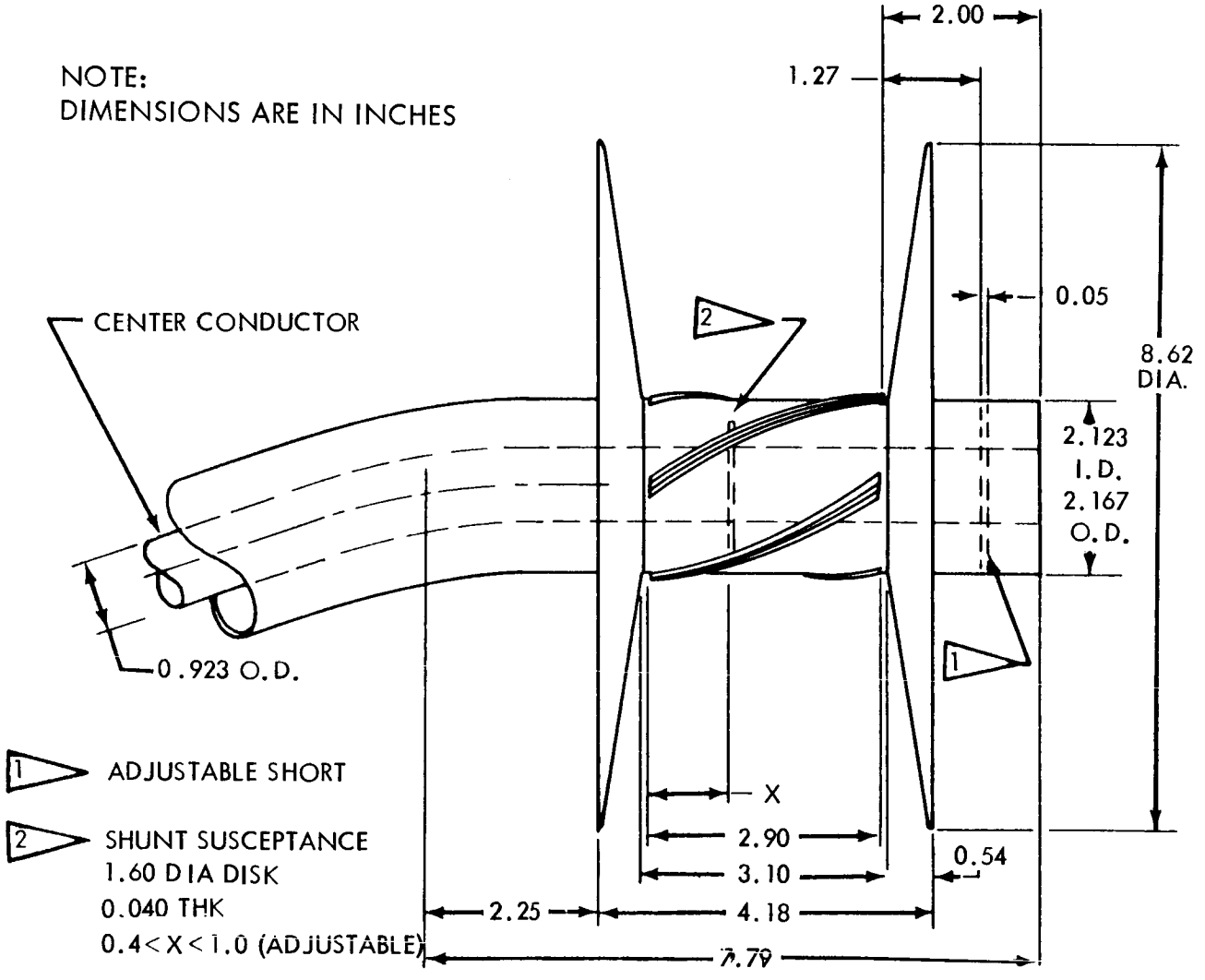

Figure 4.1-22: Low-Gain Antenna

This antenna has a toroidal shaped radiation pattern with the nulls along a normal to the toroid. On a typical spacecraft, it has provided coverage over 95 percent of the sphere at gain levels between +2 db and -6 db. Proper orientation of the antenna on the vehicle allows all earth-look angles to be covered during transit and from orbit, except possibly during a midcourse maneuver, when all directions in space are possible thrust-axis directions. Normally, two rotations about the vehicle axes are required to orient the thrust axis in the chosen direction. With the omni-directional antenna, there are directions of the thrust axis for which the earth is in an undesirably low-gain region of the antenna pattern.

A procedure exists for aligning the thrust axis by using three rotations about the vehicle axis. There is a sequence which allows the earth to remain near the maximum of the radiation pattern while still allowing the thrust axis to point to any direction in space during a midcourse maneuver. This extra rotation requires additional fuel for attitude control, but this weight would be a small addition to the total.

With this method for attitude control, the beamwidth required to cover earth-look angles during the predictable portions of the heliocentric and aerocentric phases is considerably less than provided by a dipole type pattern.

High-Gain Antenna--Several types of high-gain antennas were considered:

1) Paraboloidal Reflectors--with subtypes differing according to the portion of a paraboloidal surface utilized:

   Center-Fed Dishes--With the vertex located at the center of a symmetrical reflector:

Circular Apertures

Unfurlable Reflectors

Rigid Reflectors

Slightly Elliptical Apertures

Elliptical Apertures

Offset-Fed Dishes--With the vertex off the center of the dish

Cassegrainian Feeds

2) Broadside Arrays

3) Endfire Arrays

4) Combinations of Broadside and Endfire Elements

Since high aperture efficiency and low axial ratios are needed in order to maximize data rate, the high degree of symmetry offered by the center-fed circular paraboloidal dish makes it the first choice among paraboloidal reflectors. Offset-fed dishes, although offering favorable impedance-matching characteristics, were rejected because of their poor off-axis polarization properties.

Electrical properties of rigid and unfurlable circular paraboloids are compared in a later paragraph. The space saving offered by the unfurlable reflectors is significant only for reflectors so large that pointing-system problems appear. Weight, relative complexity, and efficiency comparisons also favor the rigid reflector.

Circular apertures do not always make best use of available space. Since gain is approximately proportional to aperture area, a high degree of

symmetry may be retained by the use of an asymmetrically cut paraboloid ("elliptical aperture") with the vertex of the paraboloid still at the reflector center.

Symmetrical feed patterns used for circular dishes may be employed for slightly elliptical dishes (aspect ratios up to about 1.1); for more elliptical apertures a different feed configuration will be necessary. The resulting antenna is expected to have optimum gain and axial ratio at only one frequency; the design would be optimized at the telemetry frequency.

Cassegrainian feeds offer a compact paraboloidal antenna configuration, with the disadvantage of requiring a lengthy experimental design for the feed. For minimum-depth applications a conventionally fed reflector with slightly off-optimum proportions would yield essentially the same performance.

Arrays of individual radiators are alternates to reflector-type antennas. The gain of endfire arrays is proportional to their length which leads to a deep array, difficult to stow; broadside arrays, with gain proportional to area, have the disadvantage of a heavy feed system unless realized in the form of a reflector-type antenna. A combination of the two types, in the form of a broadside array of endfire elements, has been considered. The weight of the feed system is reduced, but estimated weights are still several times weights for comparable reflectors, as shown in Figure 4.1-31. Disadvantages also include the necessity for an experimental feed-network

design, but the versatility of this type, in terms of array depth and aperture proportions, still leaves it a useful alternative for minimum space.

The preferred antenna type is a center-fed paraboloid, with the preferred size and shape of the aperture, proportions of the reflector, and preferred construction to be determined. A discussion of pointing problems precedes the section on the position-control system.

High-Gain Antenna Size--Competing antenna characteristics--gain and coverage--affect the selection of antenna size, and determine control-system requirements. The inverse relationship between gain and coverage is illustrated in Figure 4.1-24, for circular apertures four to ten feet in diameter.

The choice of size is based upon an optimization of factors affecting these competing characteristics, leading to the largest aperture area consistent with weight, volume, and attitude-control constraints.

Since data rate is proportional to the product of antenna gain and power output, the weight penalty associated with an increase in transmitter power to compensate for decreased gain is a part of the trade study; this is shown by the weight versus transmitter output curves of Figure 4.1-25. The corresponding weight penalty for increased antenna gain (but a lower r-f power requirement) is shown in Figure 4.1-26.

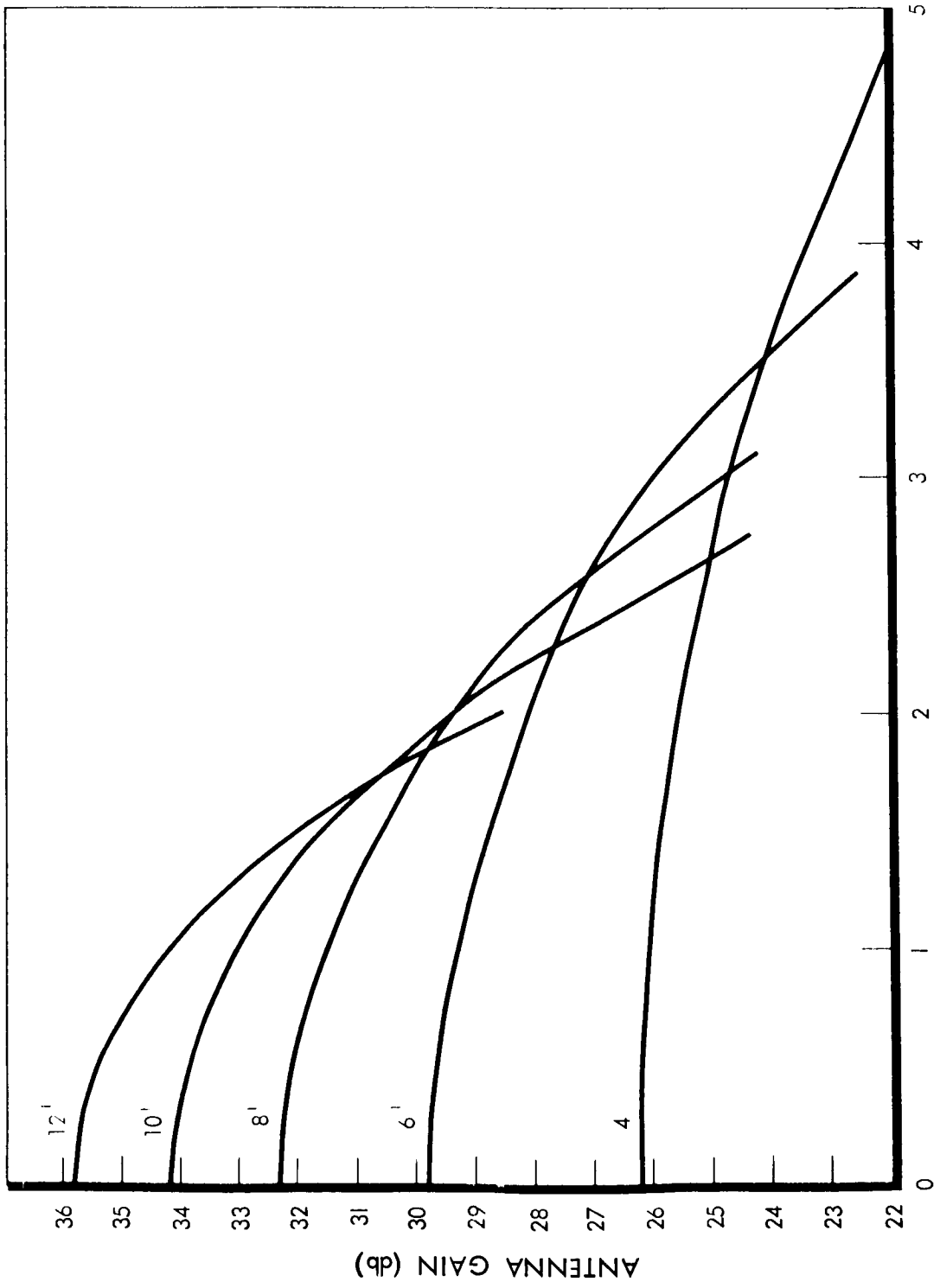

Figure 4.1-24: Antenna Gain Versus Angle-Off Axis

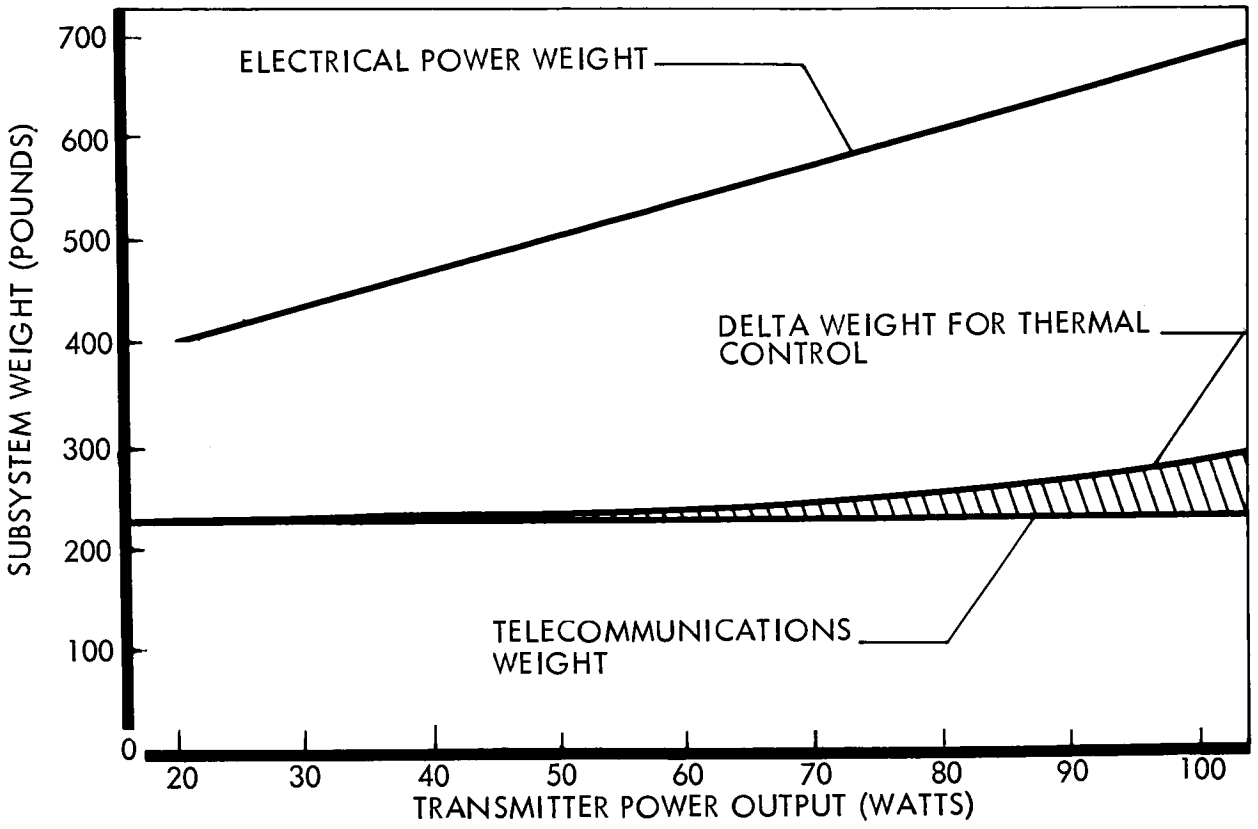

Figure 4.1-25: Subsystem Weight vs Transmitter Power Output

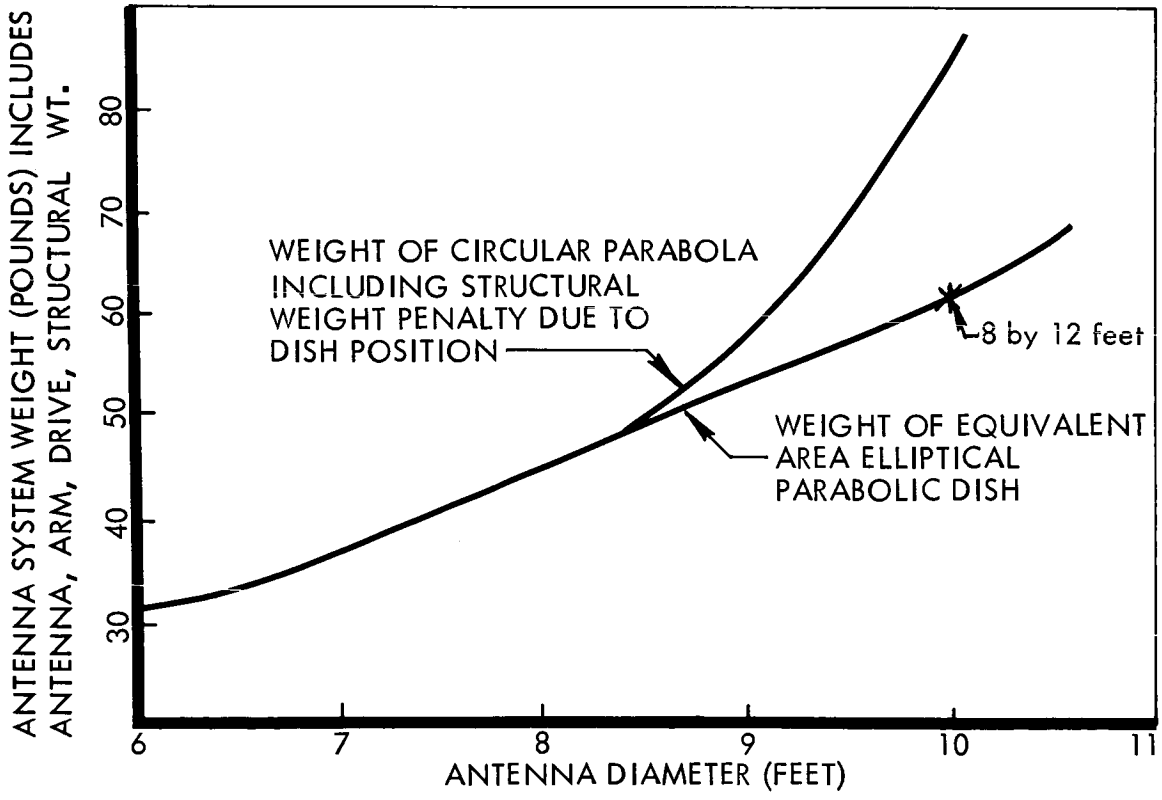

Figure 4.1-26: Antenna Weight Trends — Voyager

A circular reflector (which is preferable from an antenna design standpoint) is acceptable for reflector diameters up to eight feet. At larger diameters, structural weight penalties involved in accommodating a circular aperture favor an elliptical aperture of equal area. An eight-by-twelve-foot antenna makes maximum use of available stowage volume without excessive weight penalties that result from structural cutouts.

A high-gain antenna must be pointed accurately enough so that the effective gain remains close to the maximum. Figure 4.1-27 shows the effective gain for several different values of angular error (the total cone angle from the peak of the beam) as a function of antenna gain.

Antenna Pointing Accuracy--To maintain gain within 1 db of maximum is a design goal for the period after encounter. This means that per-axis angular errors can separately contribute only a half-db. Minimum values for these are estimated as follows:

Attitude-control limit cycle:	$\pm 0.20^{o}$
Antenna Servo Step:	$\pm 0.10^{o}$ (0.20^{o} Step)
Mechanical Alignment:	$\pm 0.20^{o}$
Attitude Sensor Null:	$\pm 0.10^{o}$
	$\pm 0.60^{o}$

From Figure 4.1-27, the largest antenna diameter consistent with a half-db pointing loss at 0.60^{o} off the peak is about eleven feet.

The weight penalty for a tighter attitude-control system is shown in Figure 4.1-28. For the preferred dual-level system, the penalty is seen to increase rapidly below the 0.20^{o} figure used above.

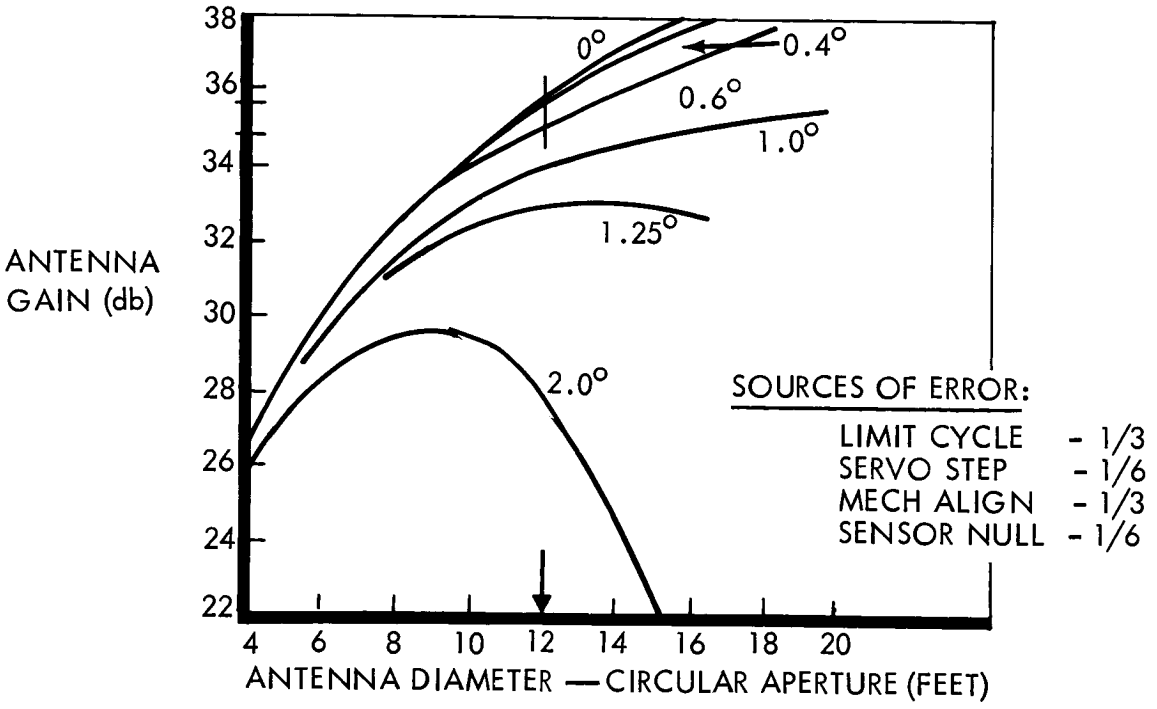

Figure 4.1-27: Gain Versus Pointing Error

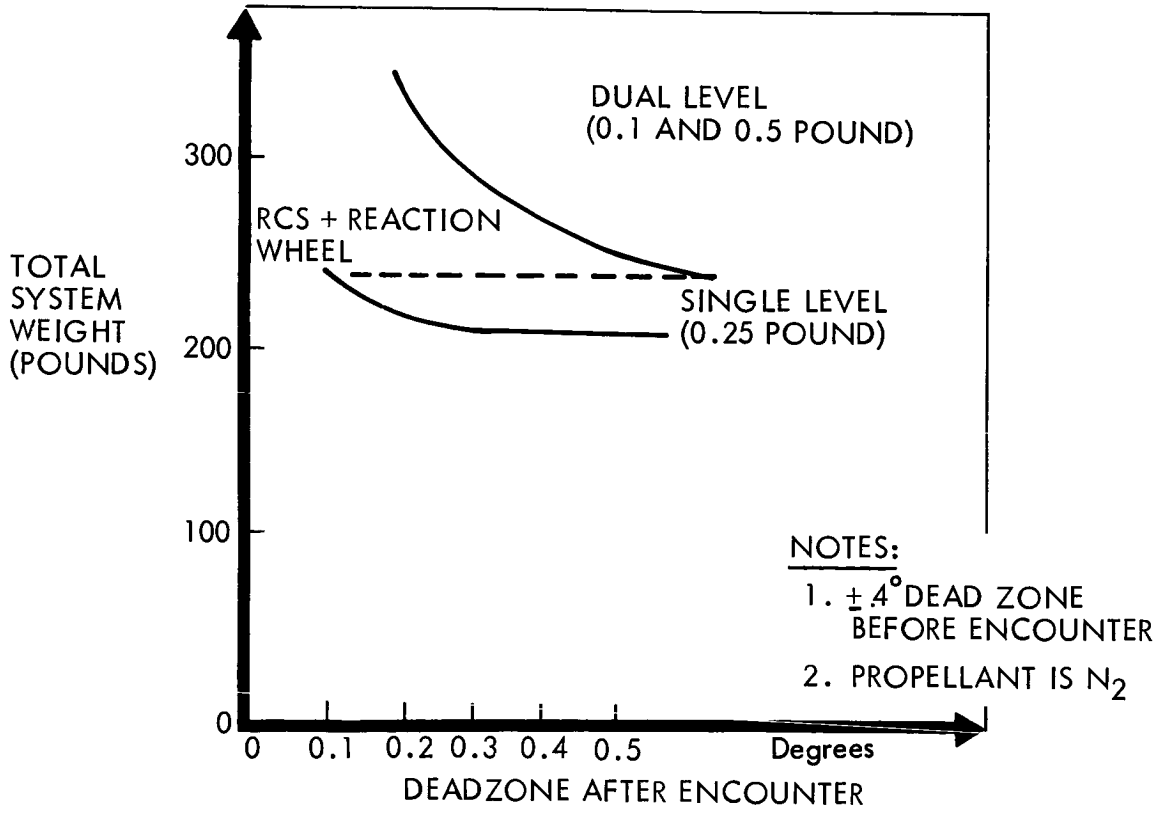

Figure 4.1-28: Effect of Limit Cycle on Reaction Control Weight

Figure 4.1-29 is a summation of weight penalties for constant transmitter power-antenna gain products (effective radiated power) corresponding to:

1)	Effective Radiated Power (ERP):	34 kw	85 kw	170 kw
2)	Data Rate at Encounter:	12,000 bps	30,000 bps	60,000 bps

Contours for constant transmitter power output are also shown. Attitude-control system weights corresponding to maintenance of a one-db pointing loss for the range of antenna diameters are included.

Total system weight has a minimum value as a function of antenna diameter because of electrical-power weight penalties at small antenna diameters and antenna and attitude-control weight penalties for large antenna diameters.

The operating point for the preferred system--135 kw ERP and 48,000 bps, at 50 watts actual transmitter power--appears at an equivalent ten-foot diameter, corresponding to the preferable 8-by-12-foot aperture as indicated by the antenna weight trends curve (Figure 4.1-26). This operating point provides very nearly optimum data-rate performance, while maintaining the transmitter power output within the 50-watt estimated state-of-the-art limit for qualified power amplifiers.

Antenna Proportions--The proportions of a circular paraboloidal reflector are described by the diameter (D), and by the focal length/diameter ratio (f/D). The optimum f/D, for maximum gain, occurs between 0.35 and 0.6; within this range, aperture efficiencies of 65 percent have been achieved. An f/D of 0.35 has been employed in vehicle configurations for which the

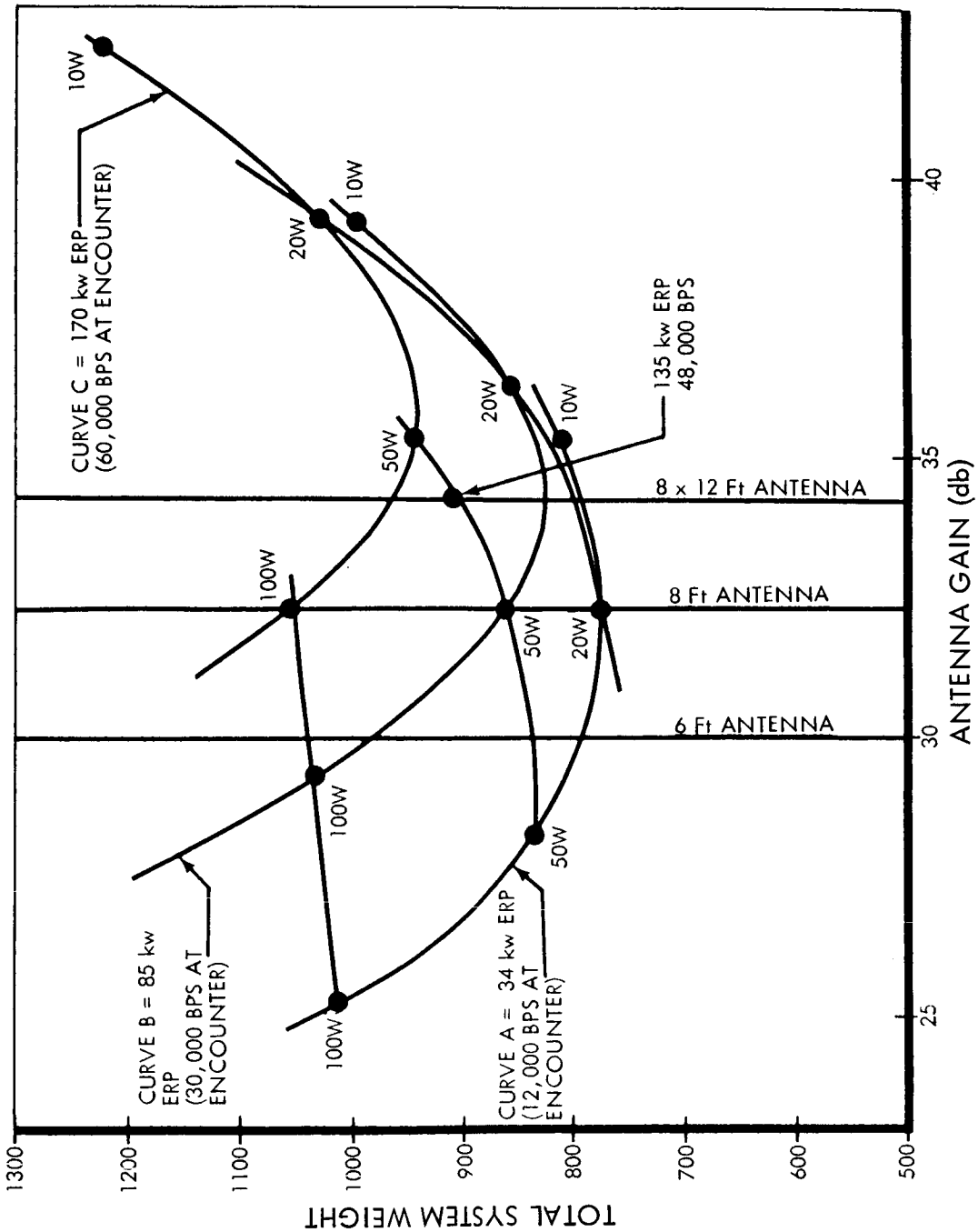
TOTAL SYSTEM WEIGHT
1300
1200
1100
1000
900
800
700
600
500
ANTENNA GAIN (db)
25
30
35
40
8 x 12 Ft ANTENNA
8 Ft ANTENNA
6 Ft ANTENNA
CURVE C = 170 kw ERP
(60,000 BPS AT ENCOUNTER)
CURVE B = 85 kw
ERP
(30,000 BPS AT
ENCOUNTER)
CURVE A = 34 kw ERP
(12,000 BPS AT
ENCOUNTER)
135 kw ERP
48,000 BPS
10W
20W
50W
100W

Figure 4.1 - 29:

minimum overall antenna depth was not required. For minimum-depth applications, f/D = 0.25, with efficiency estimated at 50 percent, was used.

The relationships between f/D and the required feed pattern are illustraded on Figure 4.1-30. Maximum gain is obtained when the edges of the dish are illuminated at a level generally taken as 10-12 db below the level at the vertex.

Selection of a value for f/D and for edge illumination determines the feed-pattern requirement. A suitable choice for an 8-foot, f/D = 0.35 circular paraboloid is illustrated. The effect of slight departures from circularity upon edge illumination by a symmetrical feed pattern is shown. Such design curves serve as a basis for the experimental optimization of the feed-reflector design, for elliptical apertures as well as circular apertures.

Other antenna types examined, in connection with minimum-depth applications, are the Cassegrainian feed system and a planar array of helices. It was concluded that a conventionally fed dish with f/D = 0.25 would be as compact as the Cassegrainian, and would present a more straightforward design problem.

An array of helices half the depth of an 8-foot, f/D = 0.25, paraboloid appears feasible. The principal disadvantage is a weight several times that of a reflector with comparable gain. The increased weight is due to the corporate feed system for the helical elements. Weight estimates for a range of array depths and diameters are shown in Figure 4.1-31.

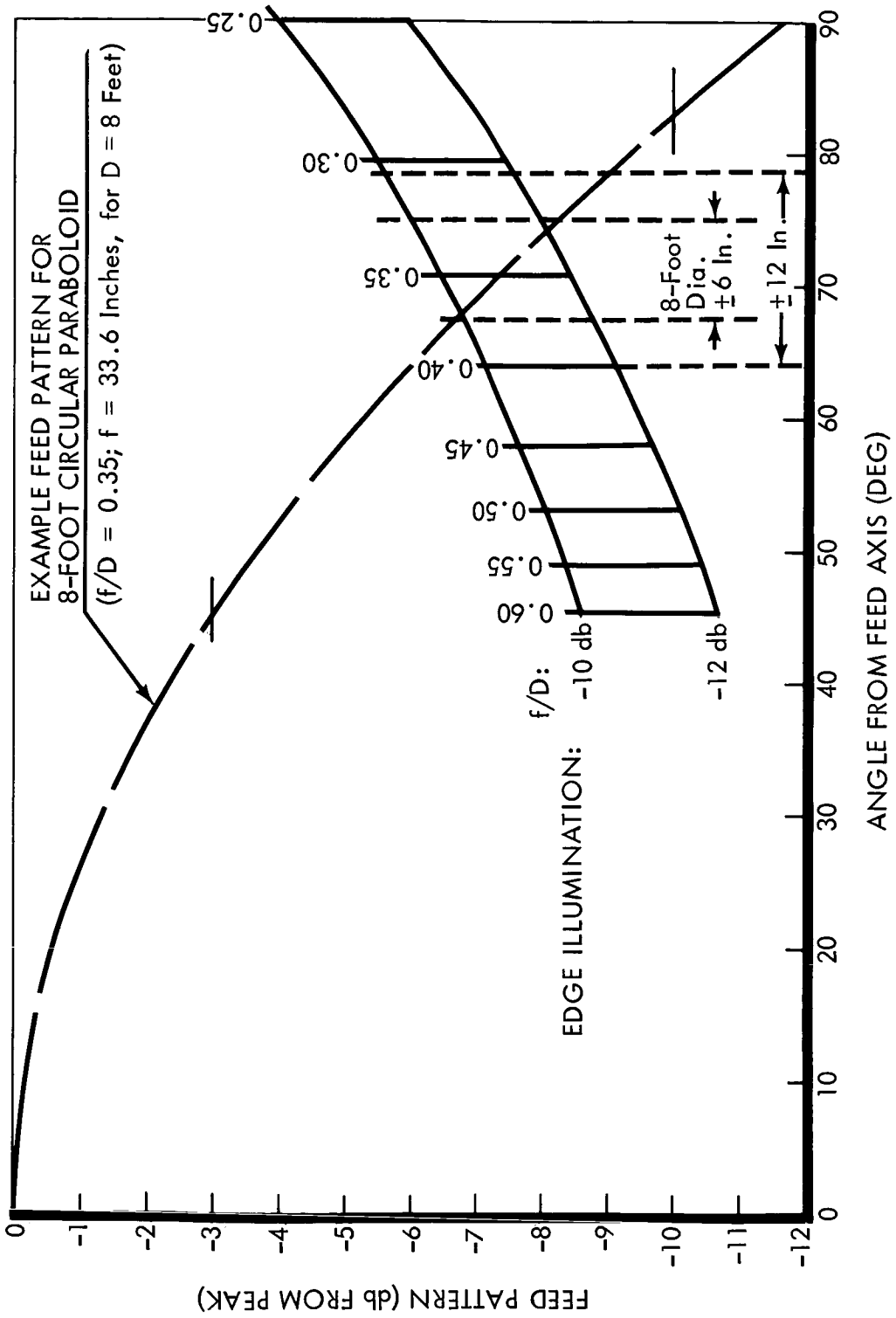

Figure 4.1-30: Feed-Pattern Design Curves

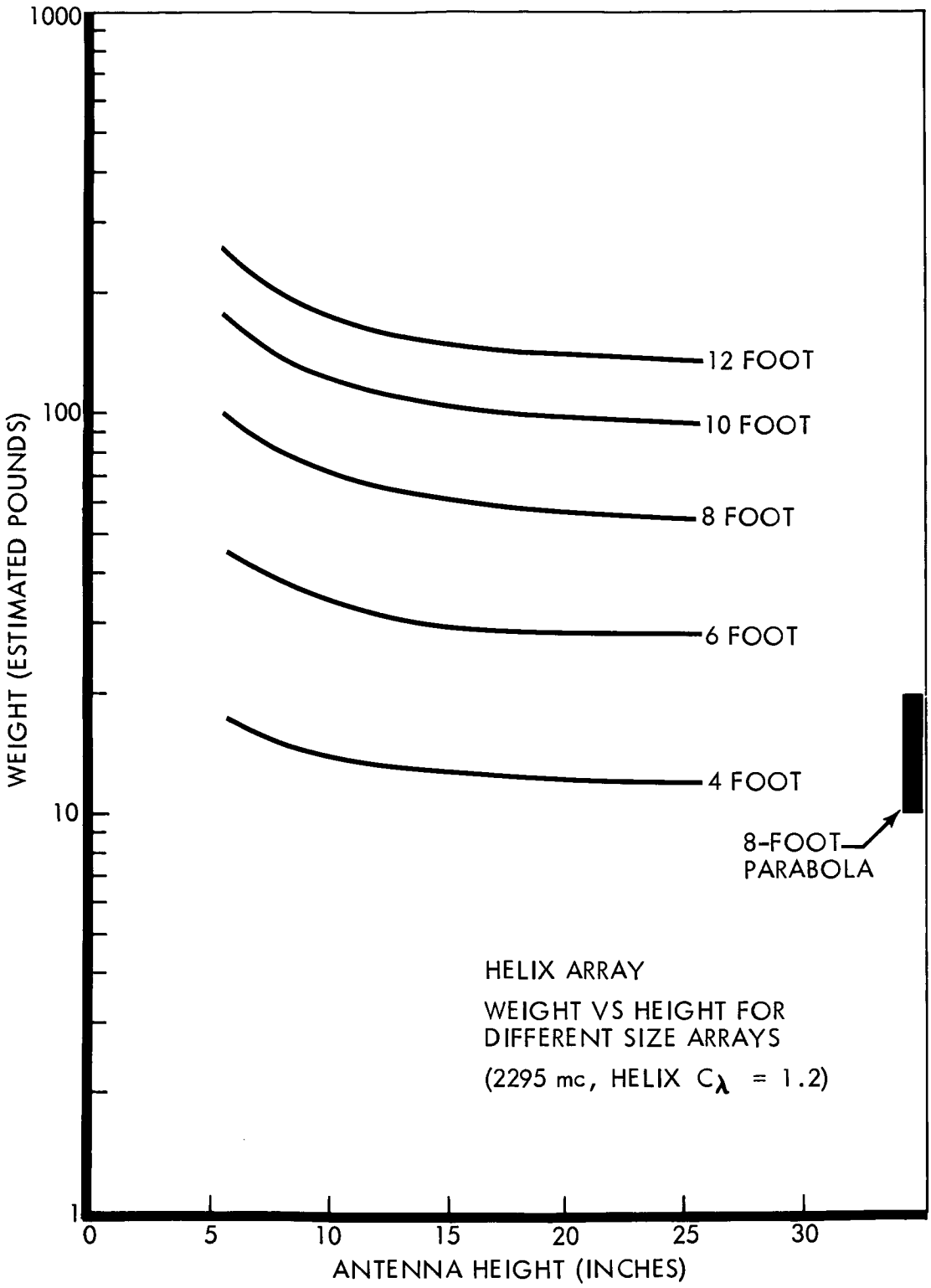

Figure 4.1-31: High Gain Antenna Wt. Comparison

Antenna Construction--Aluminum honeycomb parabolic reflectors have been used successfully on previous spacecraft programs. Some other materials have been examined with interest, in particular an electro-formed nickel material developed by EOS. This material appears to offer the possibility for weights approaching 0.1 pound per square foot, compared to 0.2-0.3 pound per square foot for aluminum honeycomb. Disadvantages for the present application include the use of a magnetic material.

Dish distortion due to solar heating was regarded as a possible problem area. The results of a study of temperature distribution over the surface of an 8-foot aluminum-honeycomb dish, and a worst-case structural analysis, indicate that a nearly negligible beam tilt (of the order of 0.06°) could result, and that gain losses would be negligible. Since the result for beam tilt is from a superposition of worst cases, this estimate is interpreted as indicating a negligible beam tilt in practice. Estimates made by General Electric Co. for a 10-foot dish lead to the same conclusions.

Summarizing, the recommended construction is an aluminum honeycomb paraboloidal reflector. For elliptical apertures with major/minor axis ratios much greater than 1.1, feeds such as dual-mode horns or arrays of turnstiles will be examined.

Antenna Pointing--The selection of an antenna-pointing system is based upon these interrelated characteristics:

1) Antenna size and gain, as shown in Figure 4.1-24.
2) Allowable pointing losses, and hence the allowable errors in antenna pointing.
3) Frequency of operation of antenna drive.

Relationships between these parameters are shown in Figure 4.1-32 for a pointing loss up to 1 db below peak gain. Parameters plotted are attitude-control limit cycle, uncompensated random errors, and peak gain. Gains were calculated for rigid paraboloids with circular apertures 4 feet to 10 feet in diameter, and for unfurlable paraboloids (Goodyear "Swirlabola") 9 feet to 16 feet in diameter.

An 8-by-12-foot aperture is seen to be consistent with the following apportionment of pointing errors, previously described on Page 112.

The 0.10^{o} attitude-reference sensor error and the 0.20^{o} allowance for structure yield an uncompensated error of $\pm 0.30^{o}$, which allows the 12-foot aperture dimension to be utilized with a 1 db pointing loss, at an attitude-control limit-cycle of $\pm 0.20^{o}$.

Utilization of the larger antennas requires increasingly tighter attitude-control. The effect of uncompensated errors becomes more significant with increasing diameter.

The uncompensated error could be reduced by an auto-track error-sensing system operating on the command transmission. Since the command transmission is considered subject to interruption, the antenna control system must provide for steering the antenna to within the acquisition range of the auto-track system. This suggests that a suitable measure of attitude-control requirement for an auto-track system is the 0^{o} curve of Figure 4.1-32.

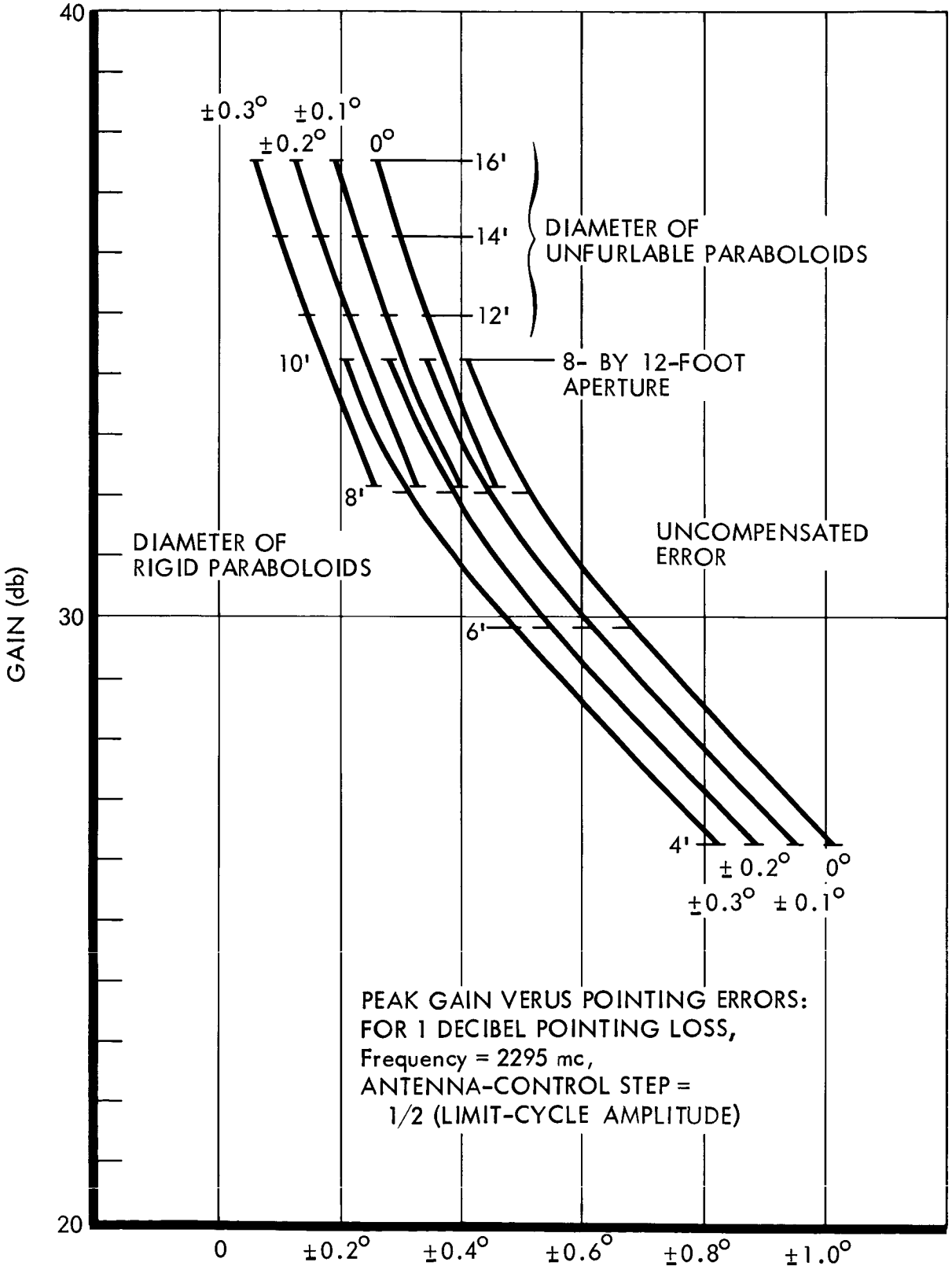

Figure 4.1-32: Attitude Control Limit Cycle

With increasing antenna diameter, there is clearly some point at which use of an auto-track error-sensing system is advantageous. The plotted data indicate that 14-foot to 16-foot antenna diameters might be usable with an auto-track pointing system. Additional factors involved are the angular width of the linear portion of the acquisition region, and random and bias errors in the auto-track system itself.

The large auto-track feed system would decrease aperture efficiency by about 1 db, and also involve at least one additional receiver, associated circuitry, and some considerable complication in the auto-track feed.

Because of the complexity associated with an auto-track pointing system and with an unfurling mechanism, the recommendation has been for a rigid dish with programmed steering. The steering function is discussed in the section following.

High-Gain Antenna Position Control--

Functional Requirements and Design Constraints--The following are operational requirements or constraints which affect the design of the high-gain antenna (HGA) position controller.

1) Periods During which High-Gain Antenna is Required--The high-gain antenna may be required for one or two brief periods early in the mission, for system calibration purposes. Between the 60th and 100th day after launch, the period during which continuous operation is required begins. The design goal is to provide continuous HGA communication in all cruise attitudes from this time until end of the mission.

2) Antenna Pointing Angles--Earth cone and clock angles are shown in Figure 4.1-33. The track of Earth on the celestial sphere as seen from the spacecraft is shown for transits beginning May 9 and July 8, 1971. These lines form the envelope containing all such curves for the two-month period. The Earth track during transit and orbit is shown for a nominal trajectory beginning May 14, 1971. The total angles scanned by the antenna gimbals depend on the orientation of the gimbal axes. For a May 9 launch, X-Y oriented gimbals would require a total excursion of approximately 90 degrees about the Y (yaw) axis and somewhat less than 20 degrees above the X-Z plane if tracking begins on the 60th day.

A much wider range of gimbal angles is required during midcourse maneuvers when the thrust (Z) axis may be pointed in any arbitrary direction. The specific range of antenna gimbal motion required depends on the selection of gimbal axis orientation with respect to the spacecraft.

3) Gimbal Rates--Maximum gimbal rates are determined by maximum vehicle maneuver rates. These latter are 0.2 degree per second and occur in only one maneuver axis at a time. Corresponding gimbal rates depend on orientation of antenna gimbals with respect to spacecraft maneuver axes. During normal tracking of Earth in transit and orbit, gimbal rates will be less than one degree per day in both axes.

4) Pointing Angle Readout--A measure of antenna pointing angles must be available for telemetering back to Earth.

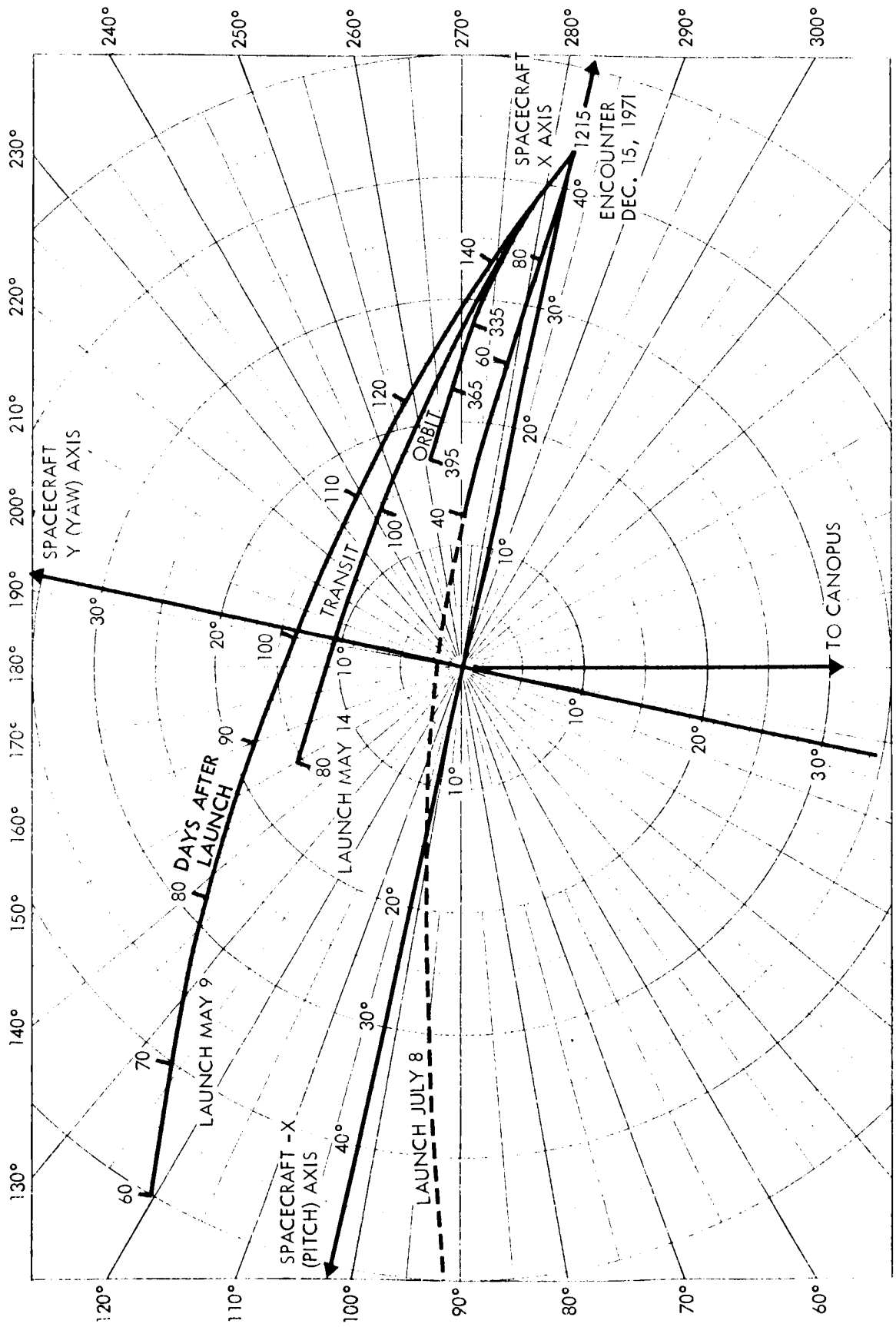

Figure 4.1-33: Earth Cone & Clock Angles

5) Pointing Accuracy--A design goal of one db as maximum loss in antenna gain due to pointing error has been set. This corresponds to pointing errors of ±0.8 degree simultaneously in each of two axes of an 8-foot diameter antenna. An 8-by-12-foot antenna has a somewhat smaller one db contour. The corresponding pointing error allowable simultaneously in each of two axes is ±0.6 degree.

6) Acceleration Loading--The spacecraft will be subjected to maximum acceleration of no more than 4 g. All pre-flight testing must contend with 1-g loading.

7) Alternate Gimbal Configurations--Antenna gimbal orientation can be chosen to conform with spacecraft coordinates, or the choice may be determined by the angular position of the earth track as shown in Figure 4.1-33. An additional choice between one or two axis gimbaling is possible. The implementations of these alternatives and their relative merits are discussed below.

8) Single Axis Antenna Drive--The tracking shown in Figure 4.1-33 for normal cruise attitude during transit and orbit can be accomplished by supplementing a single swivel axis (aligned approximately parallel to vehicle Z axis) with spacecraft roll or pitch motion. Vehicle roll attitude could be controlled by adding a second (roll) gimbal to the Canopus sensor. Pitch freedom can be provided by electronically gimbaling the Sun seeker. The pitch axis would be the better choice for two reasons. Two axis gimbaling of the Canopus sensor is more complicated than adding single axis capability to the Sun seeker.

Moreover total scan motion would be smaller in pitch because that axis is more nearly normal to the Earth line of sight.

During vehicle maneuvers (in one vehicle axis at a time), a single axis antenna drive cannot keep Earth continuously within the antenna field of view. The two rotations required to orient the thrust axis would have to be followed by an additional rotation in roll to bring Earth within the scan range of a single antenna gimbal.

Re-acquisition of the high gain antenna (HGA) link must be accomplished to permit verification of thrust axis orientation and the time the spacecraft remains in an off-scan attitude is correspondingly increased.

9) Two-Axis Drive--A two-axis drive is required to permit continuous tracking of Earth line-of-sight, or to minimize re-acquisition problems if some interruption of the HGA link is allowed during maneuvers. The orientation of the two antenna axes with respect to the spacecraft may be chosen to optimize normal tracking or tracking during maneuvers. To accomplish the former, an orientation of the swivel axis can be chosen which minimizes the angular range required in the hinge axis during transit and orbit periods. For the nominal trajectory shown in Figure 4.1-33, an optimum orientation of the swivel axis (approximately 10 degrees out of the X-Y and Y-Z planes) reduces hinge motion to ± 1 degree. However, because of the range of possible launch dates within the launch window, and the corresponding range of possible Earth trajectories (Figure 4.1-33), it is evident that

no one optimum orientation can be chosen in advance. The optimum for the whole launch period reduces hinge motion only to half the value which results from alignment of the swivel axis parallel to spacecraft yaw axis, a marginal benefit at best.

Tracking during maneuvers is optimized by orienting the swivel axis parallel to yaw and constraining the spacecraft maneuver to the sequence; roll first, then yaw. The roll rotation requires compensating motions simultaneously in both hinge and swivel axis, but the second rotation which carries the vehicle thrust axis off the Sun line can be compensated simply by an equal counter-rotation of the swivel gimbal.

10) Preferred Configuration--A two-axis drive is selected with the swivel axis mounted along the negative Y (yaw) axis of the spacecraft. The hinge gimbal can point the antenna along the negative Z axis and scan to within approximately 10 degrees of the positive Z axis before the flight capsule interferes with the antenna field of view. The swivel gimbal has a scanning range of $\pm$180 degrees. The antenna coverage is therefore approximately the hemisphere centered about the negative Y axis.

With the addition of vehicle roll motion, the antenna can sweep 4 π steradians less the 10-degree cone about the positive Z axis. With this configuration, the HGA can track Earth continuously during cruise and maneuvers subject to acceptance by other subsystems of the following constraints:

Vehicle maneuver away from cruise attitude is executed by a roll rotation first, followed by a yaw rotation and the return is in reverse sequence.

If the normal roll angle command (ϕ) would carry Earth out of the HGA hemisphere of coverage, the roll command must be changed to ($\phi - 180^{\circ}$).

The positive Z axis must not approach the Earth line of sight closer than the 10-degree limit on HGA field of view.

The programmer must generate the appropriate pointing angles in the form of incremental position commands to the gimbal drive mechanisms. During vehicle roll rotation the required hinge and swivel angle commands are arc sin and arc tangent functions, respectively, of vehicle roll attitude (modified by Earth cone angle).

Since continuous tracking during maneuver carries a high penalty in terms of programmer complexity, the programmer will simply command final positions of the hinge and swivel axes, which will place Earth back within the HGA field of view at the completion of the vehicle roll rotation. The HGA link can be re-established while the vehicle is still on the Sun line. The subsequent yaw rotation can be compensated directly by a fixed rate counter rotation of the swivel gimbal and HGA communication will not be interrupted during the off-Sun line portion of the maneuver.

11) Gimbal Drive Mechanization--The functional requirements and mechanical loads on the two axes are sufficiently similar that identical designs are used in both axes. The pointing requirements for the 8- and 12-foot axes are not enough different to cause a change in drive design. The remaining design choices relate to selection of drive components and are described below. The form of the position control system is shown in functional block diagram form in Figure 4.1-34.

12) Motor--A digital motor (Abrams Instrument Corp., Model DMA) is selected that provides antenna motion in discrete steps and positive mechanical detenting of the gimbal axes when not actually stepping. Other types of drive motors considered were:

1) 400-cycle servo motors;
2) DC motors, direct drive or high speed;
3) Conventional stepper motors of permanent magnet or variable reluctance types.

Stepper motors are preferred because a digital motor also serves as an incremental position encoder. A second design requirement is the need for positive locking of gimbals in between stepping periods. Antenna stowing and deployment constraints dictate unbalanced gimbal mounting which in turn results in high torque loads at the gimbals during acceleration loading. The resultant requirement for locking the gimbals can be met by a separate device such as a solenoid-operated brake or ratchet and pawl. Such a device would be heavy and would consume extra power. An even more serious defect would be its inherently low reliability and the catastrophic effect of failure of

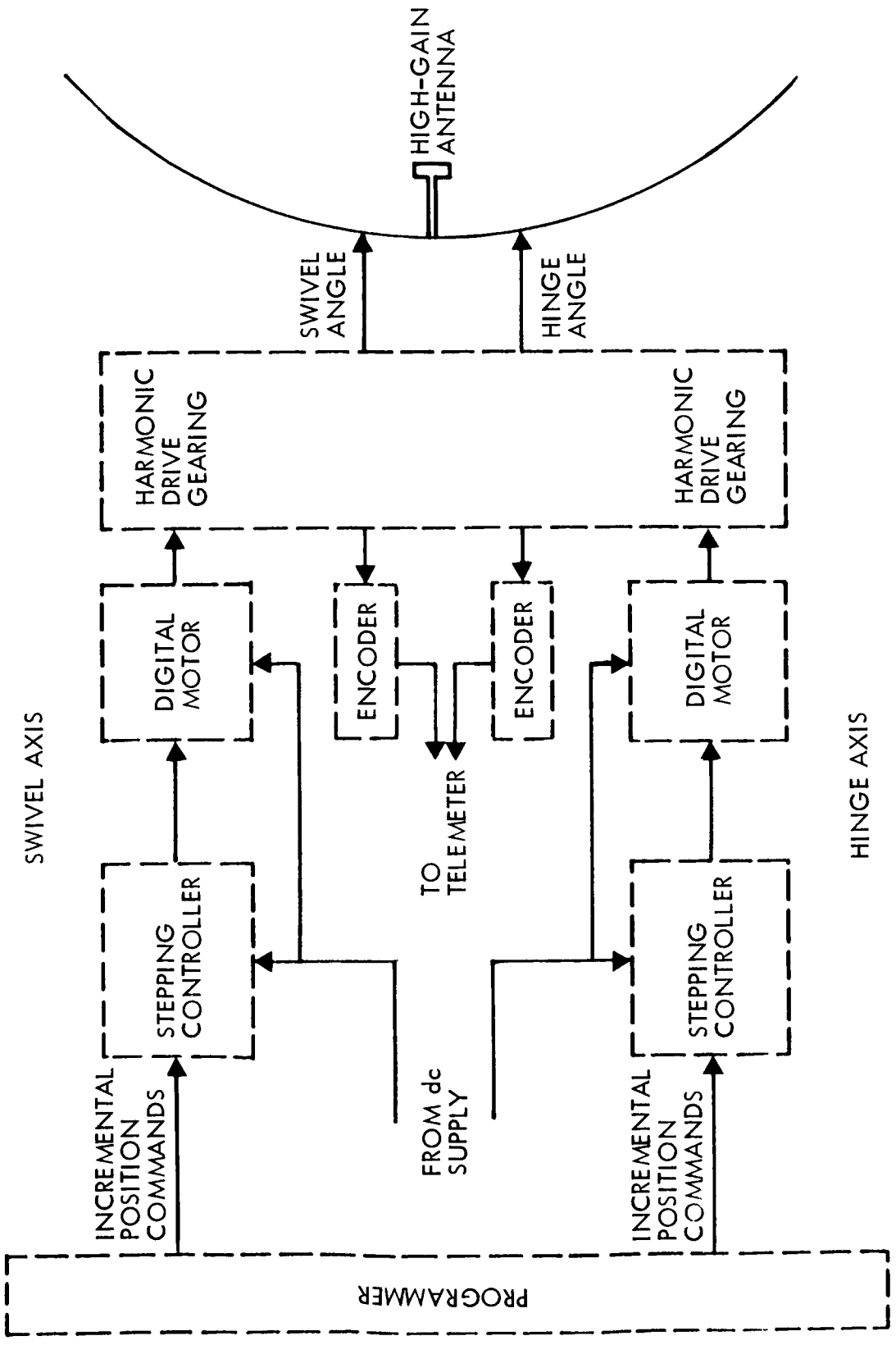

Figure 4.1-34. High-Gain Antenna Position Control

brake release. The motor selected is the only one available which is light weight (9 ounces), digital, and self-detenting without application of electrical power.

The motor has been extensively tested under space conditions by The Boeing Company (and many others) and is being used in a nearly identical application for an HGA drive for the Lunar Orbiter.

13) Gearing--A harmonic drive unit (United Shoe Machinery) is selected with a gear ratio of 205 to 1. This gear ratio reduces the 36-degree steps of the digital motor to 0.175-degree steps at the antenna gimbal. One result of this choice of gear ratio is that motor stepping provides 11-bit incremental encoding of antenna position. With output steps of this size, the uncertainty in antenna position due to actuator granularity need be no greater than $\pm$5.3-arc minutes. This gear ratio provides sufficient torque gain to accomplish antenna drive testing under 1-g loading. The load torque seen by the motor and gearing during preflight test is primarily the bearing friction torque due to bearing radial loads. These loads are orders of magnitude larger than loads occurring during mission maneuvers. The gear ratio is such that the minimum motor torque (at the end of stroke) is sufficient to insure stepping against these 1-g condition friction loads. This results in a very conservative torque to load ratio for all operating conditions during the mission. The gearing is not required to actively step the antenna during Mars orbit insertion, but it must withstand torque loads on unbalanced gimbals that result from

accelerations. The ratio selected reduces the detent torque required of the motor to well within rated values.

A harmonic drive is preferred over spur or planetary types of gearing for several reasons. The harmonic drive is superior from the point of view of size, weight, stiffness and accuracy. As an important additional advantage, its concentric design can provide a hermetically sealed volume, at very little sacrifice in size or weight, which will contain both the drive motor and a shaft transducer. Moreover, the transducer shaft is geared directly at load speed, through a second gear train, thus providing absolute readout of the external shaft position and preserving the hermetic seal. In this drive design the load and transducer rigid spline are driven by a common flexible spline which in turn is connected to the motor through a fixed gear ratio. Thus position indexing between the motor, load and transducer is preserved within the backlash limits of the drive which is $\pm$2-arc minutes or less.

Gimbal Angle Transducer--The choice of a digital motor provides the capability to determine the gimbal angles by accumulating the commanded 0.175 degree increments. A redundant means is provided by a digital shaft encoder driven by the harmonic drive inner gear. Types of transducers considered included potentiometers and digital encoders, incremental or absolute, employing optical, magnetic or brush-type readout. Absolute readout is preferred since incremental is already provided by the motor. Analog measurement is rejected because of the difficulty in providing conversion to digital with an accuracy of 0.1 percent (10 bit).

Optical encoder lamps require standby power and are not highly reliable. Brush-type encoders are smaller and lighter than magnetic types and provide the ultimate in simplicity of readout. Since a hermetically sealed environment is available, the reliability of the brush type is within acceptable limits. The selected encoder is a 10-bit coded drum and brush combination (Northern Precision Laboratories) similar to the unit provided for an identical application on the Lunar Orbiter HGA.

Motor Stepping Controller--The controller receives incremental stepping commands from the programmer. A logic level indicates the desired direction and a pulse is transmitted when each step is required. The controller performs three functions. A one-shot multivibrator establishes the pulsewidth (50 millisec) required to assure completion of the motor step under the most adverse load condition. A gate selects the clockwise or counter-clockwise channel. A solid-state switch in the selected channel energizes the appropriate motor coil for the duration of the one-shot pulsewidth. Power consumed during the ON period is essentially motor power (approximately 50 watts) and power consumption is negligible at all other times. These simple circuits are identical to ones developed for Lunar Orbiter.

Ascent Antennas

Shroud Antenna--A circularly polarized horn antenna in a randome, installed in the envelope of the shroud, will provide maximum gain backward toward the launch site. The cylindrical portion of the shroud is recommended for this location, in order to provide maximum

coverage to Station 71 during the boost phase, and up to shroud separation. The antenna receives RF energy from the launch exciter through an RF coupler in the transmission line leading to the acquisition antennas. At shroud separation, the antenna is disconnected and the RF power is transferred to the acquisition antennas.

RF Coupler--Direct coupling through a separable connector to the launch exciter-launch acquisition antenna transmission line provides a simple means of obtaining almost complete energy transfer to the shroud antenna. The connector is preferable to a loosely coupled probe which would have coupling losses of the order of 20 db. A sketch of the coupler is shown in Figure 4.1-35.

Acquisition Antennas--Two antennas are used to provide nearly spherical coverage after shroud separation; a circularly polarized omnidirectional antenna similar to the low-gain antenna, shown in Figure 4.1-22, and a pyramidal horn. The omnidirectional antenna is mounted on the tip of the capsule so that it has a dipole-type pattern about the roll axis. Pattern coverage is over the major portion of the sphere except for the region behine the vehicle (along the negative Z axis) shadowed by the capsule and vehicle. A horn antenna pointed in this direction provides the required coverage. Since interference lobes in the overlap region are unavoidable, experimental optimization of horn parameters will be necessary. The higher gain of the horn antenna requires a power divider between the two antennas to provide a uniform signal level around the vehicle. Approximately 75 percent of the power is radiated by the omnidirectional antenna.

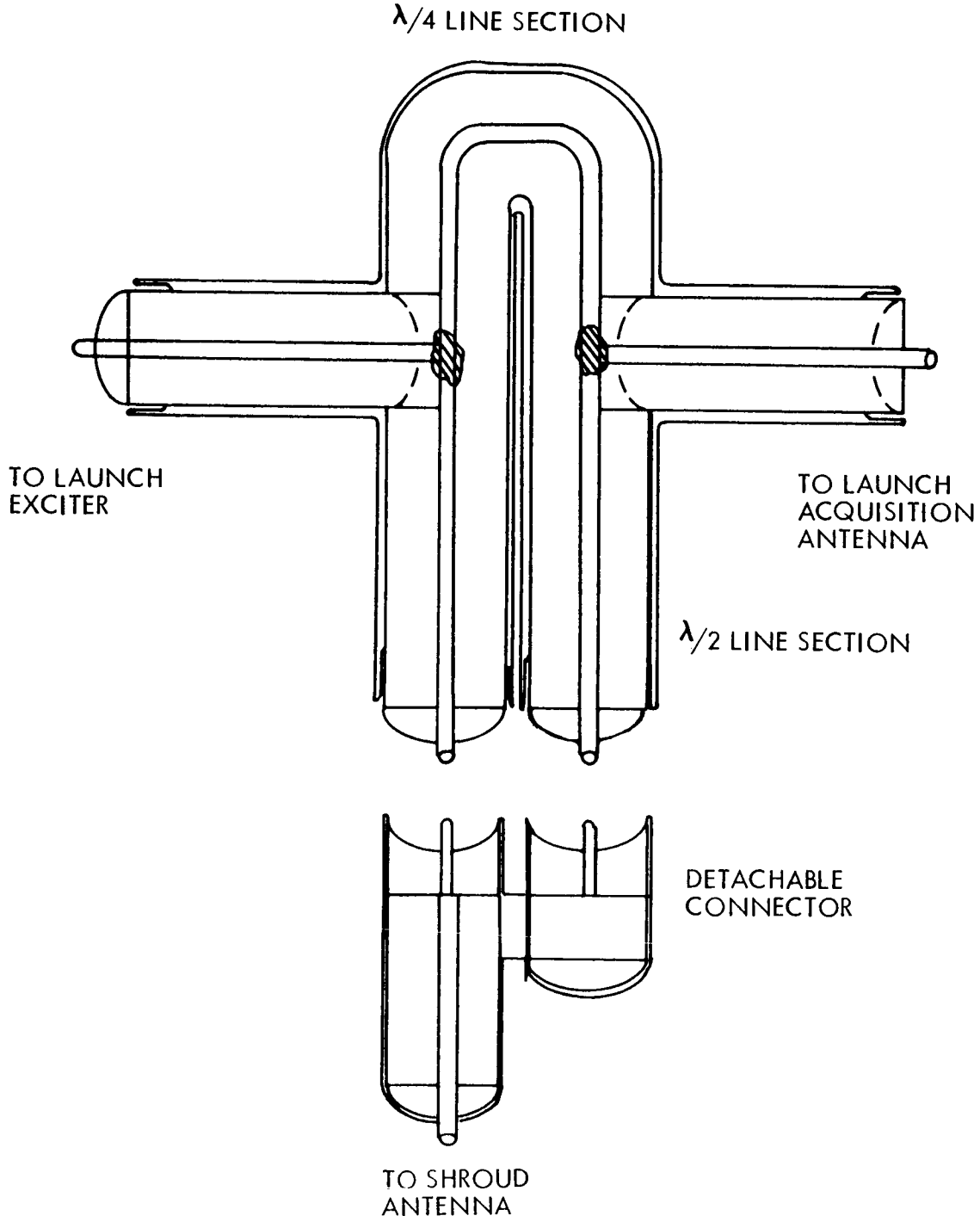

Figure 4.1-35: RF Coupler

Relay (VHF) Antenna--The characteristics of this antenna, used for reception of capsule transmissions from capsule separation to impact and subsequently depend upon the orbital geometry. Coverage requirements were described in Volume A, Section 4.1.3.4. Possible choices resulting from geometrical considerations are:

1) Separate antennas, for separation-to-impact and in-orbit phases;
2) Single antenna;
3) Hemispherical radiation pattern;
4) Unidirectional radiation pattern;
5) Omnidirectional radiation pattern -- with increased directivity perpendicular to the orbital plane.
6) Omnidirectional radiation pattern, with maximum coverage perpendicular to the orbital plane.

Again, the basic conflict is between gain and coverage, with maximum gain obtained by an antenna pattern shaped and oriented for a particular set of orbital characteristics. Maximum coverage for a wide range of orbital properties is provided by a dipole (toroidal) pattern. Antenna volume is minimized by choice of a toroidal pattern.

Specifically, electrical characteristics involve factors which will affect capsule antenna and r-f system design. These are:

1) Radio frequency--100 mc, 135 mc and 260 mc have been considered; system considerations strongly favor the lower frequency range.
2) Polarization

   Circular polarization at capsule and at spacecraft;

   Circular polarization at capsule, linear at spacecraft;

   Linear polarization at capsule, circular at spacecraft.

The geometry of the spacecraft-capsule link, plus the possibility of Faraday rotation in a Martian ionosphere, dictates circular polarization for at least one terminal. A choice between polarizations involves a comparison of polarization losses, antenna efficiency and space requirements, and pointing losses. Antennas compared on the bases outlined include:

1) Two-element turnstile;
2) Normal-mode helix;
3) Linear dipole;
4) Collinear arrays of dipoles or normal-mode helices;
5) Dipole and reflector.

The last antenna can be oriented to provide increased gain at apoapsis, decreasing the variation in received signal intensity over an orbit, and increasing the time available for reception of capsule data in each orbit. The use of higher gain at long range and lower gain at short range makes the dipole/reflector clearly preferable.

This preferred antenna, a two-element array, is shown in Figure 4.1-36. The antenna consists of a radiating element and a reflector, with a simple tuner at the base of the radiator. Gain can be increased by the addition of another element, a director, opposite the reflector. The front-to-back ratio will be increased by this additional element, so that signal variation between apoapsis and periapsis can be decreased even more. The requirement of communication with the capsule after separation places a restriction on the front-to-back ratio of this antenna, since the antenna has to be oriented to provide maximum gain at apoapsis, just opposite to the direction required for reception from the capsule between separation

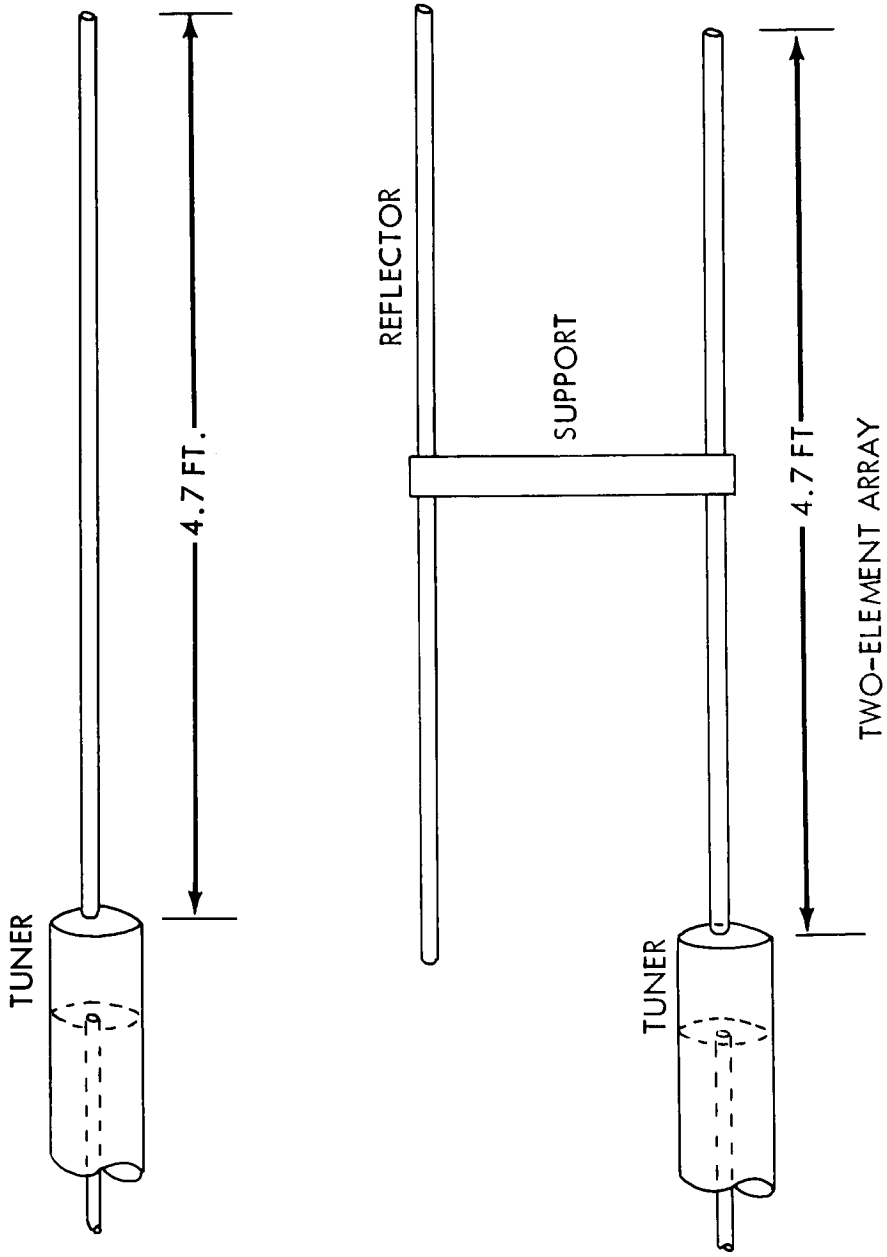

Figure 4.1-36: Linearly-Polarized Antenna For 100 Mc

and impact. A front-to-back ratio greater than 10 db would be undesirable in this respect, as it would put a restraint on the maximum separation distance.

Transmission Lines--Competing characteristics of transmission lines are cross-sectional dimensions, transmission losses and flexibility. The lowest-loss transmission lines are rigid waveguides with large cross sections. The highest-loss transmission lines are light, flexible, small-diameter coaxial cables. There are choices between these extremes.

Bases for selection, besides losses, dimensions, weight and flexibility, include compatibility with structural elements, and the availability of associated components such as connectors, transitions, and rotary joints. Power-handling capacity of flexible cable must be considered in high-power links, as well as losses.

The general types of transmission lines available are:

Waveguide

Circular	Minimum ID 4.3" approx. (TE_{11})
Rectangular	RG-105/U (1.7 - 2.6 gc) 4.3" x 2.15"
	RG-113/U (2.2 - 3.3 gc) 3.4" x 1.7"

Ridged

NOTE: (Flexible, rectangular, and ridged guide is available, but is lossier than rigid types)

Coaxial Lines

Rigid

Standard

Nonstandard (e.g., a coax line with outer conductor integral structural element)

Semirigid

Flexible

The types of line are tabulated in approximate order of increasing losses and also in rough order of decreasing outer dimensions.

Applications include internal cabling, fixed external cabling, cables within deployable booms (as for the VHF and S-band low-gain antennas), and the lines for the articulated supporting structure for the high-gain antenna. Besides line losses, and weight and space constraints, means for transmission of energy through hinge points must be considered in the choice of a transmission-line type.

A rigid open 50-ohm coaxial line has been considered for the low-gain antenna boom. The aluminum outer conductor of this line is the antenna boom.

Comparative attenuation estimates are, for representative transmission-line types:

LINE TYPE	ATTENUATION AT:	
	2200 mc	135 mc
RG-105/U Guide (Rigid)	0.004 db/ft	- - -
RG-113/U Guide (Rigid)	0.0075 db/ft	- - -
Antenna Boom (Typical)	0.008 db/ft	
7/8" Semirigid 50-ohm line:	0.024 db/ft	
1/2" Semirigid 50-ohm line:		
Styroflex	0.044 db/ft	0.01 db/ft
Foamflex	0.055 db/ft	0.0093 db/ft
Flexible 50-Ohm Coax: (Minimum size, maximum Loss):		
RG-142/U	0.22 db/ft	0.045 db/ft
RG-188/U	0.3 db/ft	
Compare quoted figures for coaxial rotary joints:		
Sage Laboratories:		
Types 319, 319W		
320, 320W	0.2 db/max	- - -
340, 340W	- - -	0.2 db/max

Based on the above, initial recommendations are for a construction similar to the low-gain boom, for those S-band transmission lines which are integral with structural elements. For hinge points, a coaxial rotary joint is preferable to a loop of flexible cable at S-band, from the viewpoint of power-handling capacity as well as losses. At VHF, flexible cable is

preferable. The relative reliabilities of the loop and rotary joint do not appear significant, for one-time deployment operations.

For internal spacecraft cabling, the 1/2 or 7/8-inch semirigid types appear suitable. The losses compare favorably with rigid open lines, but the relative suitability of the various types for the space environment calls for detailed investigation.

Rectangular waveguide has been regarded as unsuitable for internal transmission lines, because of its cross-sectional dimensions.

Because of the multiplicity of transmission-line types and the variety of materials and configurations employed, the range of required trades and environmental evaluations is very wide. There are also elements, in particular the high-gain antenna support structure, for which both electrical and mechanical characteristics must be very carefully optimized. The transmission-line trades so far have been for the purposes of: (1) setting reasonable upper and lower limits on line losses, for use in systems calculations; and (2) initial dimensional estimates for the mechanical design.

Exhibit A

NASA-LTR

NATIONAL AERONAUTICS AND SPACE ADMINISTRATION
LANGLEY RESEARCH CENTER
LANGLEY STATION
HAMPTON, VIRGINIA 23365

IN REPLY REFER TO: B/L-97 WTB

October 23, 1964
G-70/0803/1201

The Boeing Company
Lunar Orbiter Program
P. O. Box 3995
Mail Stop 84-80, MPC
Seattle, Washington 98124

Attention: Mr. R. J. Helberg / Mr. N. S. Leach

Gentlemen:

Subject: NASA Contract NAS1-3800 - Lunar Orbiter Project-
Communications Subsystem, DSIF 10 Mc/s IF Characteristics

Reference: (a) NASA Letter D-92 WTB, Dated August 14, 1964
(b) TBC Letter 2-1553-53-091, Dated August 24, 1964

Enclosed are two copies of information provided by JPL describing the amplitude and phase characteristics of the 10 Mc IF output of the DSIF receivers.

NASA believes that this information is sufficient to allow Boeing to complete their analysis to determine whether the 10 Mc or the 50 Mc IF output is technically better for Lunar Orbiter. NASA requests that by November 6, 1964, TBC furnish The Lunar Orbiter Project Office with this analysis and with their recommendation regarding use of the 10 Mc IF.

Sincerely yours,

Thomas N. Bartron
Technical Representative of
the Contracting Officer

Enclosure: JPL Memorandum by M. H. Brockman, Dated October 12, 1964,
Subj: 10 Mc/S Telemetry Output - Fixed Bandwidth

cc: AFPR, TBC w/o encs.
Mr. K. Wadlin, NASA Resident Engineer w/o encs.

Exhibit A

DEEP SPACE NETWORK

OCT 13 1964

Mail to Boyer.

ATTACH TO B/L 97 wt B

JET PROPULSION LABORATORY

INTEROFFICE MEMO

TO: A. S. Sheppard

12 October 1964

FROM: M. H. Brockman

SUBJECT: 10 Mc/S Telemetry Output - Fixed Bandwidth

The fixed bandwidth 10 mc/s telemetry output provides 6.0 ±0.8 mc/s output bandwidth which is set at a 0 (±2) dbm level during non-coherent operation, and at -22 (±2) dbm during coherent operation. The output is linear up to a +7 dbm level (50- ohm load). The attached figures present the output amplitude and phase characteristic of the fixed bandwidth telemetry output. Note that the phase characteristic is linear to ±12° or better across the 6 mc/s bandwidth centered at 10 mc/s. This provides a delay characteristic which is linear to ±3.3 nanoseconds or better in the 6 mc/s bandwidth.

M. H. Brockman

MHB:ggw

Attachments (2)

cc: J. R. Hall
C. W. Johnson
M. S. Johnson ✓
R. K. Mallis
D. J. Mudgway
L. W. Randolph
W. K. Victor

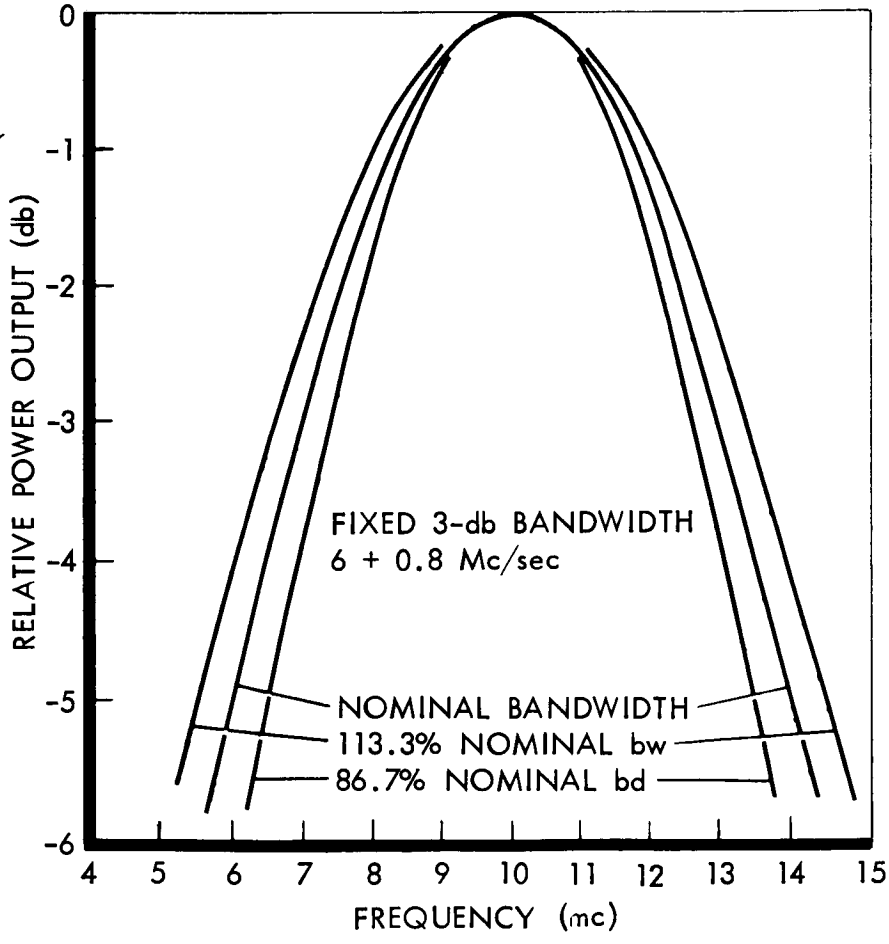

10 Mc/sec Telemetry Output Amplitude Characteristic

4.2 ELECTRICAL POWER

Summary--Electrical power requirements for the 1971 through 1977 Voyager missions were investigated. A solar/photovoltaic/battery subsystem was verified as the optimum choice for the Voyager mission. The subsystem employs N-on-P solar cells to provide 396 watts to the spacecraft loads from 236 square feet of solar panel area. Total subsystem weight is 457 pounds. Wiring of the solar panels is arranged to minimize magnetic interference. A silver-cadmium battery arranged in three identical sections of 38 cells each is used. The battery is rated at 2460-watt hours capacity to support 2.9 hours of occulted operation. Basic power regulation is accomplished by redundant series-switching regulators within the electrical power system, with supplemental power conditioning being accomplished within each using subsystem.

Electrical power for the Voyager missions could be derived from any of three basic sources--solar, chemical, or nuclear. Figure 4.2-1 shows the subsystem trades considered in selecting a preferred configuration. Many lower level trades or design optimizations are presented in Section 4.2, Volume A of this report.

Nuclear power sources are all too heavy (over 1000 pounds) or are not adequately developed to be considered for the 1971 mission. The radioisotope/thermoelectric generator (RTG) offers promise during the latter part of the 1971 to 1977 time period, but generators of the 200- to 500-watt size are not likely to be developed in time for the earlier flights. Thus, for reasons of design conservatism, the RTG system was not further considered.

Top-Level Trades

CANDIDATE CONCEPTS	INTERMEDIATE SELECTION	SELECTED CONCEPT
NUCLEAR SYSTEMS CHEMICAL SYSTEMS SOLAR SYSTEMS	RADIOISOTOPE/THERMOELECTRIC RECHARGEABLE STORAGE BATTERY SOLAR/PHOTOVOLTAIC	SOLAR/PHOTOVOLTAIC AND STORAGE BATTERY

CHARACTERISTICS DETERMINING SELECTION:
- AVAILABILITY
- COST
- RELIABILITY
- WEIGHT

Second-Level Trades

SOLAR ARRAY	FLAT (NONCONCENTRATING) V-RIDGE (CONCENTRATING)	FLAT PANEL
STORAGE BATTERY	NICKEL-CADMIUM SILVER-CADMIUM SILVER-ZINC	SILVER-CADMIUM
CONDITIONING & DISTRIBUTION	CENTRALIZED DECENTRALIZED	DECENTRALIZED
VOLTAGE REGULATOR	SERIES SWITCHING BOOSTER	SERIES SWITCHING REGULATOR

CHARACTERISTICS DETERMINING SELECTION:
- RELIABILITY
- AVAILABILITY
- WEIGHT
- ELECTRICAL EFFICIENCY
- MAGNETICS

Figure 4.2-1: Electrical-Power Trade Studies

Chemical sources of electric power, such as auxiliary power units or fuel cells, capable of fulfilling long-life requirements of the Voyager mission, have not demonstrated such life capability and are excessively heavy (1000 pounds or more).

With respect to solar sources of electrical power, the only concept that has been developed adequately to be considered for Voyager is the solar/photovoltaic concept. This type of subsystem has been successfully operated in many space vehicles (Ranger, Mariner, and others). Solar/photovoltaic subsystems can be designed and fabricated with moderate development and manufacturing costs because of available experience and technology. Thus, the solar/photovoltaic basic source of electrical power was selected, augmented by a battery during periods of off-Sun operation. Within this preferred overall design, the three specific areas examined were (1) solar array, (2) battery, and (3) power regulation, conversion, and distribution.

Solar Array--Several types of array structure were considered. A flat array design similar in concept to the Mariner IV panel was chosen based on flight experience, proven fabrication capability, and confidence in its performance. V-ridge arrays were rejected because of lack of previous flight experience.

Battery--The following battery types were considered:

1) Nickel-cadmium (Ni-Cd);

2) Silver-zinc (AgO-Zn);

3) Silver-cadmium (AgO-Cd).

The three types were compared with respect to magnetic characteristics, weight, life, and cycle life reliability. The Ni-Cd battery was eliminated because it would have a 100-pound weight penalty and would not be able to meet magnetic requirements. Of the two remaining types, an AgO-Cd battery was selected based on its ability to meet reliability, cycling, and life requirements of the mission.

Power Regulation, Conversion, and Distribution--A modified decentralized distribution concept was selected on the basis of trades. The preferred concept shows advantages over others in reliability, weight, electrical interference control, and interface management. Finally, two different methods of accomplishing d.c. voltage regulation were evaluated for effect on total subsystem efficiency, weight, and reliability. A series switching regulator was selected on the basis of savings in solar panel area (6%) and subsystem weight (10%).

4.2.1 Prime Power Source Selection

Studies have been made defining prime power source concepts applicable for Voyager-type missions. The prime requirement to be satisfied in making the power source selection is the average electrical load requirement of 396 watts.

4.2.1.1 Alternates Considered

Suitable power subsystems can be classified by the source from which they derive their energy: solar, chemical, or nuclear. Solar/thermionic, solar/thermoelectric, and solar/dynamic (rotating or reciprocating engines)

conversion systems have not been developed sufficiently to be available for mid-1966 design freeze. Thus, all sources of the solar classification are eliminated except for solar/photovoltaic.

In the chemical class of energy sources, chemically fueled auxiliary power units (APU) and fuel cells can be eliminated because of weight and limited life. Even a 100-percent-efficient system (theoretical) would require at least 1000 pounds of fuel to supply the energy needed for the 13-month mission. The problems of storing cyrogenic fuels for such systems further emphasize their unsuitability. Batteries would be excessively heavy when considered as a sole energy source.

The nuclear classification is divided into two important types. The first type--reactor systems--can be eliminated because weight would be more than 1000 pounds. Radioisotope systems appear to be attractive when combined with appropriate converters. Converters of the rotating or reciprocating engine type must be eliminated because their development status is not compatible with a mid-1966 design freeze, and they would weigh in excess of 500 pounds for the 400 watts required. Radioisotope/thermionic converter systems would be lighter than other radioisotope systems because of their potential high conversion efficiency (10 percent or more) and small radiator area requirements. However, complete systems have not been developed and cannot be considered for the 1971 mission.

Thus, the final choice lies between a radioisotope/thermoelectric generator (RTG) and a solar/photovoltaic system.

Table 4.2-1 evaluates the two alternates against various competing factors. As noted in the table, the RTG offers a number of advantages and for this reason was considered and further evaluated. Specifically, the RTG is insensitive to solar distance and radiation environment. Figure 4.2-2 illustrates the comparison of solar/photovoltaic and RTG systems in a radiation environment.

Important considerations in making this selection are development status, fuel availability, and cost. Consequently, the RTG is not a contender for the 1971 mission. As missions for 1975 and later are considered, the lander capsule will possibly require development of an RTG as the power supply and the development of an RTG for the spacecraft can also be undertaken at the same time. This will permit the consideration of conducting more extensive and sophisticated missions.

4.2.2 Solar Panel Design

The preferred solar panel design concept was selected through a two-step trade study. First, a study was made of basic structural design concepts, then the use of the V-ridge concentrator was compared with the nonconcentrating flat panel.

4.2.2.1 Structural Design Considerations

Three alternate concepts for the design of rigid structural panels were examined.

Alternate 1--A substrate panel supported by an assembly of beams and cross members. This design was successfully used on the Mariner IV spacecraft.

Table 4.2-1: Summary Of Competitive Factors

CONSIDERATION	RTG	SOLAR-PHOTOVOLTAIC
Environments	Interplanetary plus radiation belt — none. Meteoroids — negligible.	28% degradation. Negligible for 1971 Mission.
Mission Life	No limit with suitable isotope	Degradation with time due to environments and mission
Mission Selection	Little effect	Limited to Mars distance
Solar Occultation	No affect	Requires battery plus 25% solar array increment
Weight	1300 - lbs system weight (approx.), including shielding to meet radiation spec. of JPL mission specification	457 lbs
Vehicle Configuration	Adaptable	Stowage and deployment required.
Attitude Control	No dynamic effect No solar orientation required.	Solar orientation required
Effect on Orbit Selection	Very little affect on the drag at Mars. Lower periapsis or decreased orbital period allowed	Significant drag at Mars due to panels. This restricts orbit selection to those high enough to guarantee long life
Sterilization	Sterilized because of operating temperature. Sterilization of battery in system questionable	Sterilizable (battery sterilization questionable)
COST Equipment.	Comparable.	Comparable
COST Fuel For Preferred System Size.	$7,200,000 (approximately) for Pu 238 Dependent on AEC policy.	None
COST Development.	$5,000,000 (estimated)	$500,000 to $2,000,000
Availability	Fuel availability not certain. Dependent on AEC plans for production facilities.	Readily available

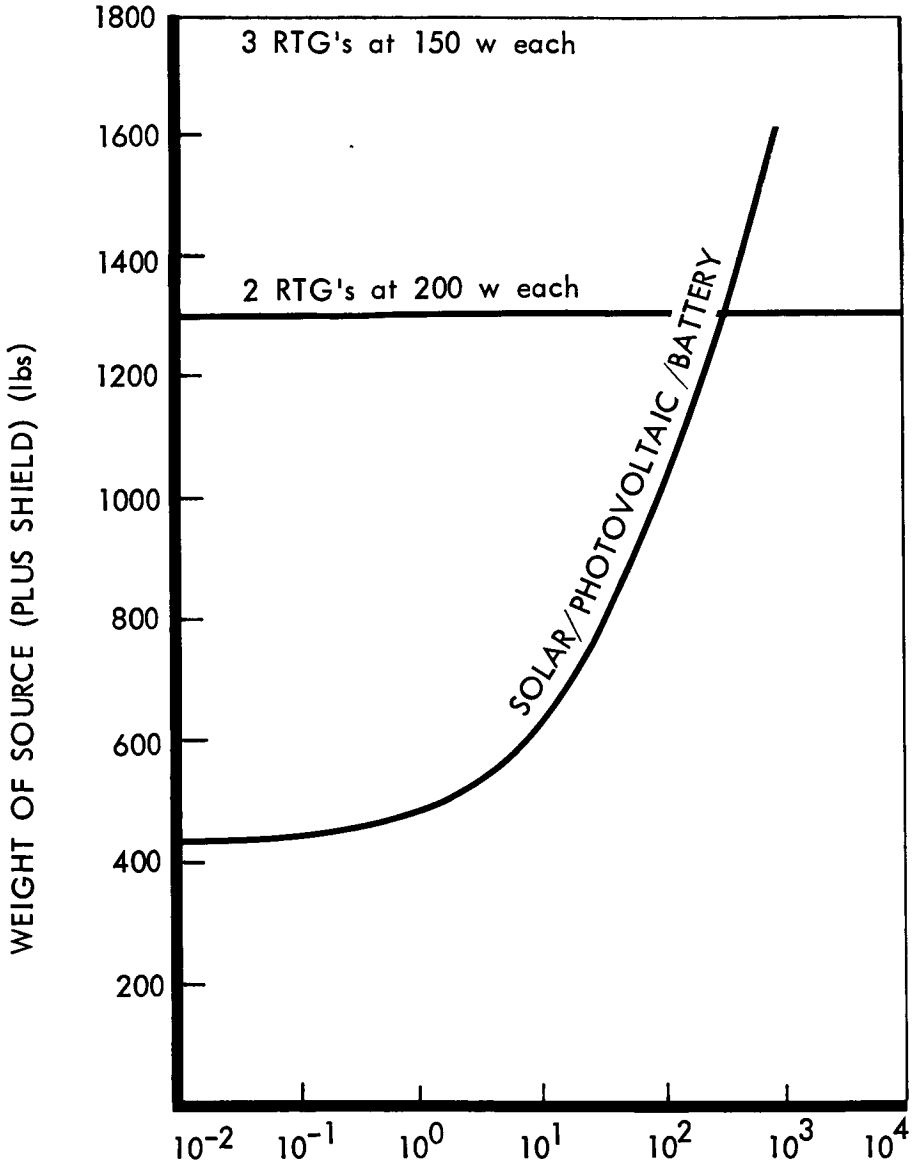

Figure 4.2-2: Effect of Mars Radiation Belt on Power Subsystem Weight

Alternate 2--An integral assembly of substrate and frame. This design concept was used on Mariner II and Ranger 7, 8, and 9.

Alternate 3--Separate small substrate inserts set into a rigid framework (picture-frame-type construction). The OGO Satellite uses this type of panel construction.

Figure 4.2-3 presents a conceptual sketch of each alternate and summarizes the results of detail studies. Alternate 1 was selected as being lightest in weight; adaptable to sectionalizing for ease of manufacturing, handling, and repair; and well supported by previous application experience.

4.2.2.2 Concentrator versus Nonconcentrator Considerations

A V-ridge concentrating panel design was examined and compared to a non-concentrating flat panel design of comparable electrical power output. The two configurations are shown on EOS Drawings D614100A and D614106A, contained in Reference (1). The flat panel construction was selected for use in the preferred spacecraft design because:

1) Considerable operating experience in space exists for flat panels, while the V-ridge concentrator has not been flown.
2) The V-ridge, although 7% less in weight, requires development of cladding processes for high strength aluminum alloys (7075 or 2024) used in order to achieve a satisfactory reflectance.

The data of interest resulting from this study are summarized in the following Table.

	Flat Panel Design (EOS Drawing D614106A)	V-Ridge Concentrator Panel (EOS Drawing D614100A)
Total Array Weight, pounds	284	265
Total Array Area, spuare feet	236	260
Square of Solar Cells	48,708	20,180

4.2.3 Battery

The electrical power subsystem requires the use of an energy storage device for operation during occultation or off-Sun periods and to support peak loads that may occasionally exceed the solar array capacity. Therefore, a battery compatible with the other components of the power subsystem and the total mission must be selected.

The requirements for the Voyager energy storage system are summarized as follows:

1) Minimum voltage--38 volts;
2) Operate during 215 days of transit plus 180 days of orbiting including occultation (no occultation during first 30 days of orbit);
3) Supply loads during maneuvers and Mars insertion--1060 watt-hours;
4) Number of cycles during orbit--200, 18 hours per orbit;
5) Discharge--2.9 hours at 424 watts during orbit occultations (2.7 hours occultation plus 0.2 hours for Sun reacquisition);
6) Charge--15.1 hours during orbit Sun period;
7) Total energy per cycle--1230 watt-hours during occultation.

ALTERNATE 1

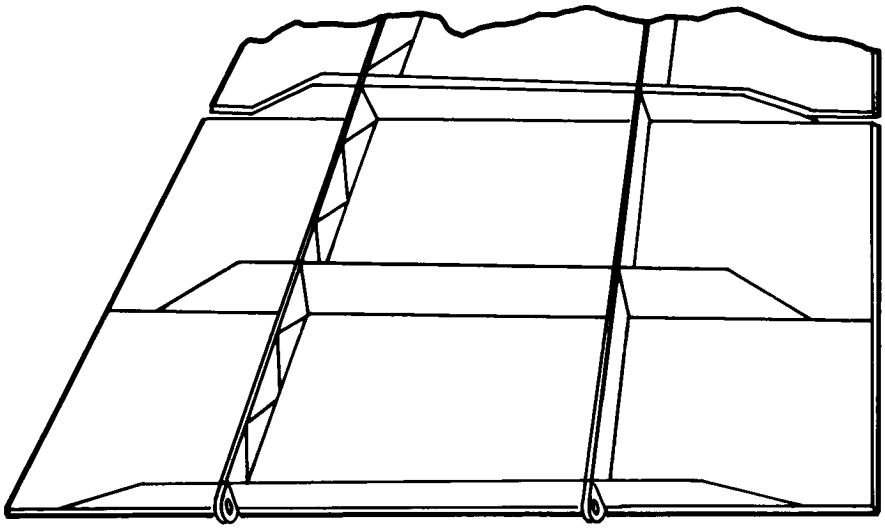

SUBSTRATE PANEL SUPPORTED BY
BEAMS AND CROSS MEMBERS

WEIGHT OF ARRAY:	284 pounds
SPECIFIC WEIGHT:	1.2 psf
BASIC PANEL SIZE:	55 by 103 inches
SMALLEST REASONABLE SUBSTRATE SECTION	27.5 by 103 inches
MANUFACTURING CONSIDERATIONS	PRACTICAL SIZE TO HANDLE
REPAIR CONSIDERATIONS	LARGE BUT STILL PRACTICABLE

ALTERNATE 2

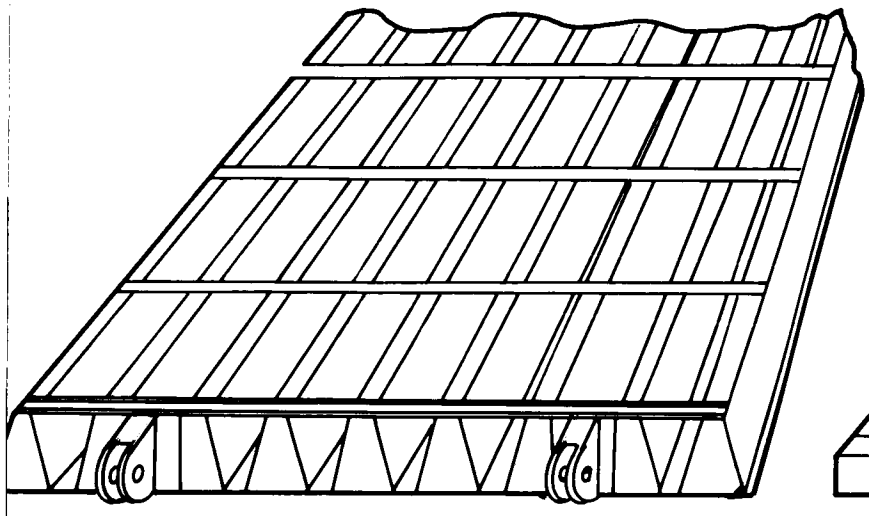

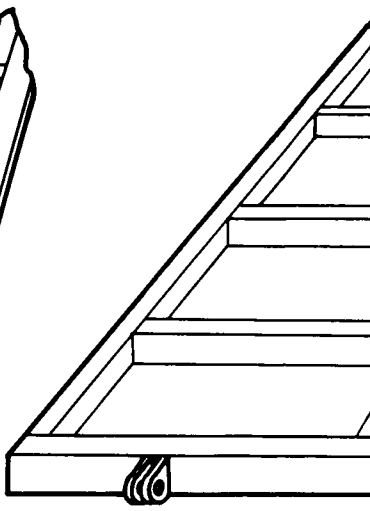

INTEGRAL ASSEMBLY OF SUBSTRATE AND FRAME	SMALL SUBS SET INTO R
398 pounds	366
1.70 psf	1.51
55 by 103 inches	55 b
55 by 103 inches	14 b
TOO LARGE FOR ECONOMICAL HANDLING	MOS M
POSSIBLE BUT NOT ECONOMICAL	MOS

Figur

ALTERNATE 3

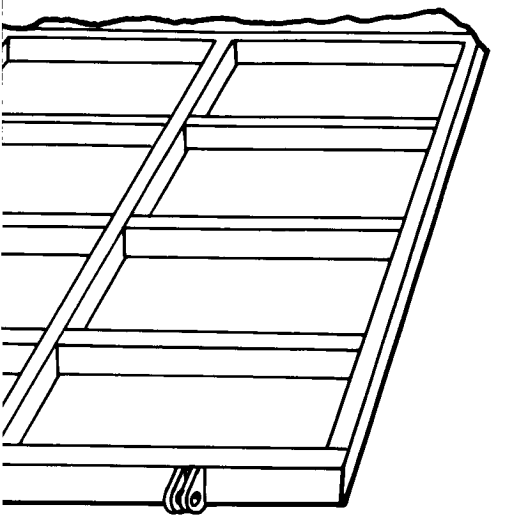

ΓRATE INSERTS
GID FRAME

ounds

psf

103 inches

25 inches

T ADAPTABLE TO
NUFACTURING PROCESSES

T SUITABLE

4.2-3: Solar Panel Structures

Nickel-cadmium (Ni-Cd), silver oxide-cadmium (AgO-Cd), and silver oxide-zinc (AgO-Zn) batteries were compared for use as the energy storage device. The AgO-Cd battery was selected as the best choice to fit the overall requirements of the mission. This selection was made on the basis of cycle life performance, wet life, weight, magnetic properties, and reliability, although other factors, such as safety and sterilization, were also examined.

4.2.3.1 Competing Characteristics and Tradeoffs of Alternates Considered

Cycle Life Performance--Figure 4.2-4 is a compilation of data showing cycle life versus depth of discharge for the batteries under consideration. Sources of this data are listed in Reference (2). Averaged curves are shown that have been developed from a survey of source data as noted in Figure 4.2-4. The standard cycles that have been normally used for evaluation of batteries for space systems are the 100-minute cycle (35-minute discharge, 65-minute charge), and 2-hour cycle (35-minute discharge, 85-minute charge), and a 24-hour cycle (1.2-hour discharge, 22.8-hour charge). For the Voyager mission, the orbit is of an 18-hour duration with 2.9 hours of battery discharge and 15.1 hours of battery charge. The standard 24-hour test cycle is used for the Voyager analysis. The shorter cycle times are shown in Figure 4.2-4 for reference and background only.

In Figure 4.2-4, the AgO-Cd shows a better cycle life at the 24-hour rate than the AgO-Zn battery. No data were found for the 24-hour rate for the Ni-Cd battery.

Figure 4.2-4 shows that, for 200 cycles, the AgO-Cd battery is capable of being discharged at 75-percent depth, based on the 24-hour cycle data, while a AgO-Zn battery is capable of being discharged at 45-percent depth. The Ni-Cd battery is not limited in depth of discharge by battery chemistry; however, cell imbalance considerations limit the discharge to 80-percent depth.

Total Wet Life--The mission requires a total wet life from launch of 395 days. Six additional months of wet life are required for manufacturing of the batteries and delivery to the launching facility. This wet-life requirement presents serious problems for the AgO-Zn battery, since this type of battery deteriorates by silver migration and diffusion of zincate through the separator whether in use or not. Above 90°F, the deterioration becomes irreversible. The AgO-Zn battery life is currently limited to about 1 year. The AgO-Cd battery deterioration rate is less since the negative cadmium plate has negligible solubility; battery lifetimes in excess of 2 years are possible. In the case of the Ni-Cd battery, deterioration rates are less than for AgO-Cd batteries; therefore, this system would be acceptable from a wet-lifetime standpoint.

Weight--In Figure 4.2-5 the watt-hour-per-pound capabilities of the batteries are presented as a function of depth of discharge. These energy-yield capabilities are subject to variation depending on details of construction, size of battery, and rate of charge and discharge at which the energy yield is determined. The levels chosen are approximate values for sealed batteries of the size for the Voyager application.

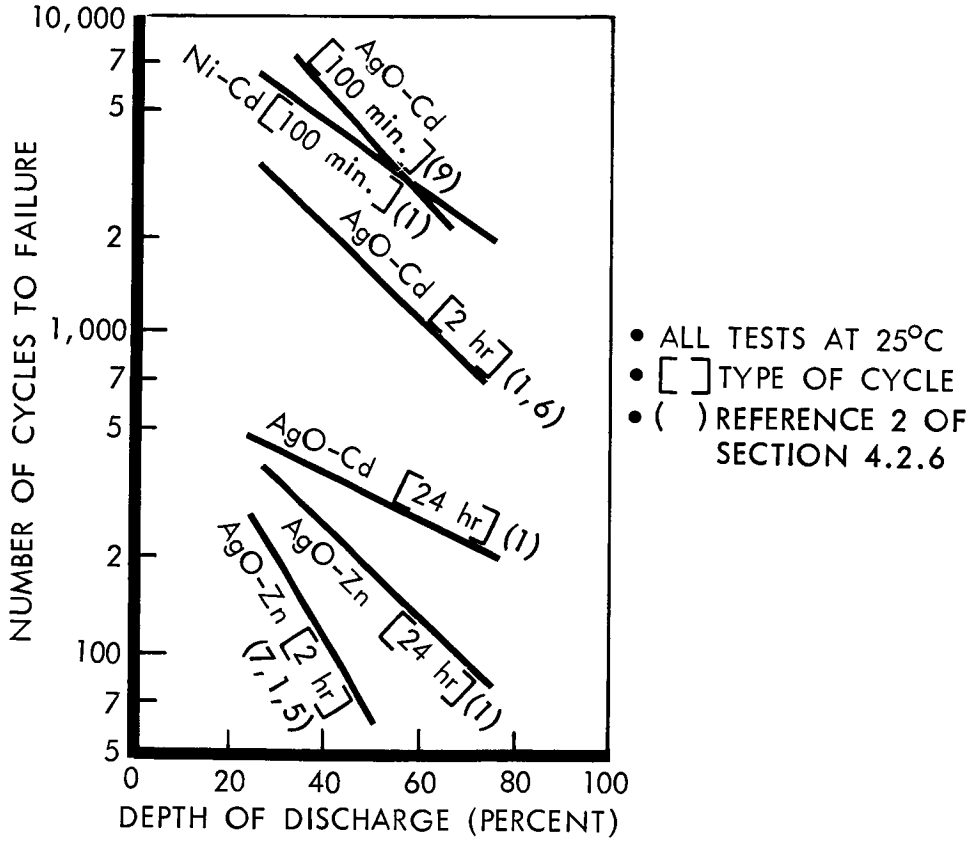

Figure 4.2-4: Cycle Life Performance As A Function of Depth Of Discharge

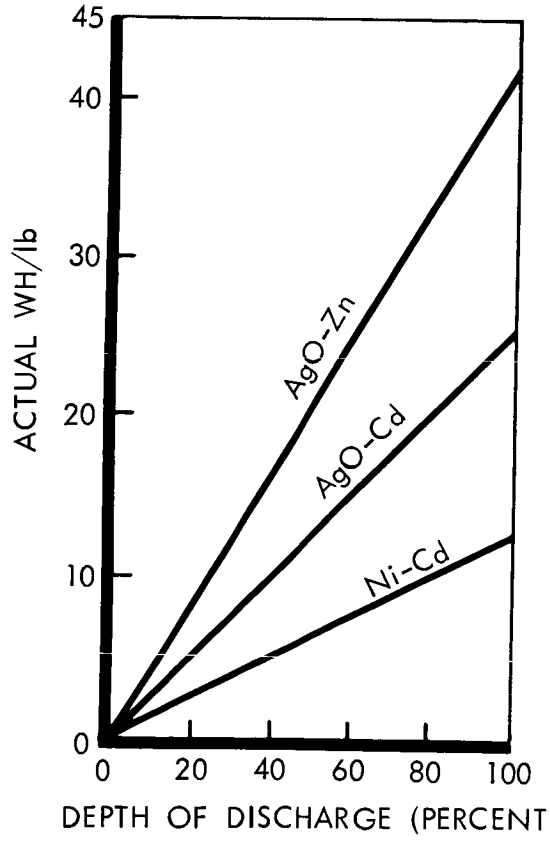

Figure 4.2.-5: Energy Density As A Function Of Depth Of Discharge

For the AgO-Cd battery operating at 75-percent depth of discharge, an energy yield of 18 watt-hours per pound is attainable. The AgO-Zn battery at 45-percent depth yields 19.4 watt-hours per pound, and the Ni-Cd battery at 80-percent depth yields 11.2 watt-hours per pound. Table 4.2-2 summarizes these data and shows weight for the different systems based on the 1230-watt-hour requirement for the orbit cycle, and also shows estimated volumes for all of the systems.

Magnetic Properties--The Ni-Cd battery uses porous nickel plaques as holding matrices for the active material, and nickel oxides or hydroxides (or both) as the cathodic electrode active material. Thus, since nickel is used, the requirement for application of only nonmagnetic materials is violated. Further, the high retentivity of nickel makes corrective action extremely difficult.

AgO-Cd and AgO-Zn batteries can be fabricated using nonmagnetic components and so present no problem with respect to magnetics.

Reliability--As discussed previously, cycle life and depth of discharge are key factors in assessing battery reliability. For the Voyager conditions, test and operating experience indicates that both Ni-Cd and AgO-Cd batteries can meet the individual battery reliability requirement of 0.98 (0.98 is the requirement for an individual battery in the three-battery redundant configuration). The basic construction and material stability of the Ni-Cd battery gives this unit an edge over the AgO-Cd unit. Further specifics are impossible because failure modes are dependent on the exact construction technique and application.

Table 4.2-2: COMPARISON OF SIZE AND WEIGHT OF RECHARGEABLE SYSTEMS (ORBIT APPLICATION)

System	Depth of Discharge (%)	Actual Watt-Hours per pound	Battery Weight at 1230 Watt-Hours	Nominal Cell Voltage	Number of Cells for 40 Volts (Nominal)	Watt-Hours per cubic inch at 100 percent Depth	Actual Watt-Hours per cubic inch	Total Volume for 1230 Watt-Hours	
								Cubic Inches	Cubic Feet
AgO-Zn	45	19.4	63.5	1.45	28	3.0	1.35	915	0.53
AgO-Cd	75	18	68.5	1.05	38	1.8	1.35	915	0.53
Ni-Cd	80	11.2	110	1.22	33	0.9	0.72	1710	0.99

Other Battery Performance Considerations--The following are also performance considerations.

Sterilization--Both silver-oxide-type batteries employ cellulosic-type separator materials that are necessary to reduce silver migration, a potential cause of cell failure. These types of materials are not capable of enduring thermal sterilization at 135°C in the alkaline electrolyte employed within the cells. Other materials still in the research stage may eventually provide sterilizable silver-type batteries that could be used for short-duration and limited-cycling operation. For long-term life and cycling conditions, considerable advances in separator materials will be necessary to provide resistance to sterilization temperatures and the ability to prevent silver migration. The Ni-Cd battery uses separator materials that are essentially electrode spacers and electrolyte holders. The materials currently employed will not withstand the 135°C temperature sterilization. By redesign, the Ni-Cd battery probably could be made to withstand sterilization. (One agency has reported some success with sterilization and cycling , Reference (3).)

Charge Techniques--In the case of the Ni-Cd batteries, the 15.1-hour period allows a low charge rate. Since the cells have an overcharge capability greater than the charging current over the 15.1-hour period, no elaborate controls would be necessary and this unit presents no charging problem.

With present technology, AgO-Cd batteries can be continuously overcharged at a 100-hour rate without damage. At the 15.1-hour charge rate for the Voyager mission, a recombination electrode is required in the battery to facilitate gas recombination.

The AgO-Zn battery is currently limited to overcharging at a rate of 1000 hours. If this unit were selected for Voyager, extensive overcharge controls would be required.

Electrical Characteristics--Figure 4.2-6 shows typical charge and discharge curves for the various battery cells. The following tabulation shows typical storage efficiencies for the different systems, calculated on the basis of the performance shown in the same figure.

TYPICAL STORAGE EFFICIENCY PER CELL OF RECHARGEABLE SYSTEMS

System	Nominal Voltage		Voltage Efficiency (%)	Amphere-Hour Overcharge Required (%)	Power Efficiency (%)
	Discharge	Charge			
AgO-Zn	1.48	1.9	78	5	74
AgO-Cd	1.05	1.48	71	3	69
Ni-Cd	1.22	1.40	87	25	65

From the viewpoint of electrical characteristics, all systems are feasible. The Ni-Cd battery requires overcharge to replace used capacity, but this requirement could be accommodated in the Voyager mission if the Ni-Cd battery were chosen.

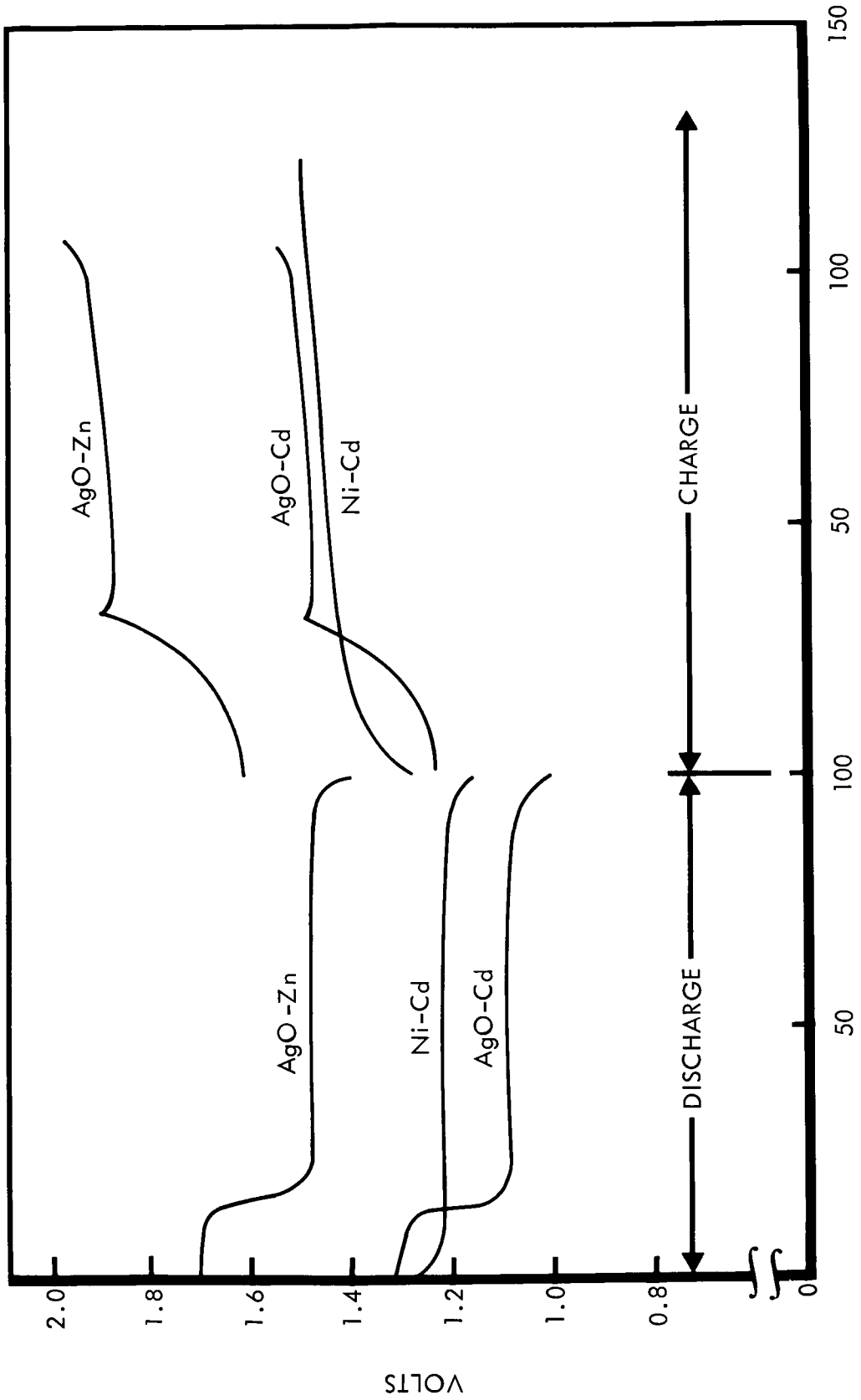

Figure 4.2-6: Typical Charge-Discharge Curves Of Energy Storage Systems

Availability and Experience--Experience with the AgO-Cd battery is not as extensive as Ni-Cd. However, AgO-Cd has been used in the Explorer satellite series. Based on prior work, sufficient information is available for the design of an AgO-Cd battery to meet this application. The design of the recombination electrode will require additional developmental work.

Silver-zinc batteries have been used for some time as primary batteries (nonrechargeable). Only recently has interest been shown in their use as sealed rechargeable batteries. The only space-proven batteries of this type have been used in the Mariner and Ranger applications, and these were in a primary mode of use (essentially not cycled).

The battery that has been used most extensively as an energy storage device for space application in conjunction with solar cells has been the Ni-Cd battery. Sufficient information is available for the design of such a battery.

4.2.4 Power Conditioning and Distribution

The terms conditioning and distribution include all of the many functions of regulation, voltage conversion, filtering, transformation from d.c. to a.c., switching, and ultimate delivery of the electrical energy to the spacecraft subsystems. This section considers both the regulation and conversion functions performed in the power subsystem and those performed in the using subsystems.

For purposes of evaluation, it is possible to define a completely centralized scheme wherein all regulation, d.c.-to-a.c. inversion, and d.c.-to-d.c. conversion are performed by a single assembly and a decentralized approach in which only raw, unregulated d.c. power is supplied to each power user, who then conditions it to his own needs.

The problem has been analyzed for the Voyager spacecraft and a modified decentralized configuration selected to optimize the various trade factors. The selected concept provides from the central electrical power subsystem:

1) Regulated 35 volts d.c.;

2) Regulated 50 volts a.c., 2400 cps;

3) Unregulated 37 to 100 volts d.c.

All other conditioning is accomplished in the using subsystems.

4.2.4.1 Alternate Distribution Concepts Considered

Two types of conditioning and distribution methods are considered:

1) Central conditioning and distribution;

2) Remote conditioning and distribution.

The central conditioning and distribution method provides all of the conversion, inversion, and regulation required for each subsystem. In this case, each user is provided the exact voltage and power levels he requires. The remote conditioning and distribution method provides a common bus voltage that is distributed to each subsystem. Conditioning to convert the common bus voltage to meet the individual user's requirements is performed within the separate subsystems.

Fundamental block diagrams of the alternates are shown in Figures 4.2-7 and 4.2-8.

The following characteristics are the major trade factors:

1) Reliability (interface connections);

2) Weight (interconnect wiring);

3) Versatility;

4) Electrical interference;

5) Magnetics.

Reliability--In terms of reliability, the major difference between the alternates is in the area of interface connections. Based on Ranger and Mariner voltage distribution requirements and estimated requirements of the Voyager spacecraft, the total number of wires required to provide each user's circuitry with his required voltages is 140 wires (not including redundancy). This is the number of wires required between the power subsystem and the other subsystems for the central conversion and distribution method of Figure 4.2-7. In contrast, approximately 30 wires would be required to distribute power in the remote conversion and distribution system (Figure 4.2-8). Considering the number of interconnections, the reliabilities of the distribution types are:

Remote conversion and distribution	0.99984
Central conversion and distribution	0.99916

The difference noted is due to the different number of interconnections. A breakdown of the voltage requirements and the reliability calculations are contained in Table 4.2-3.

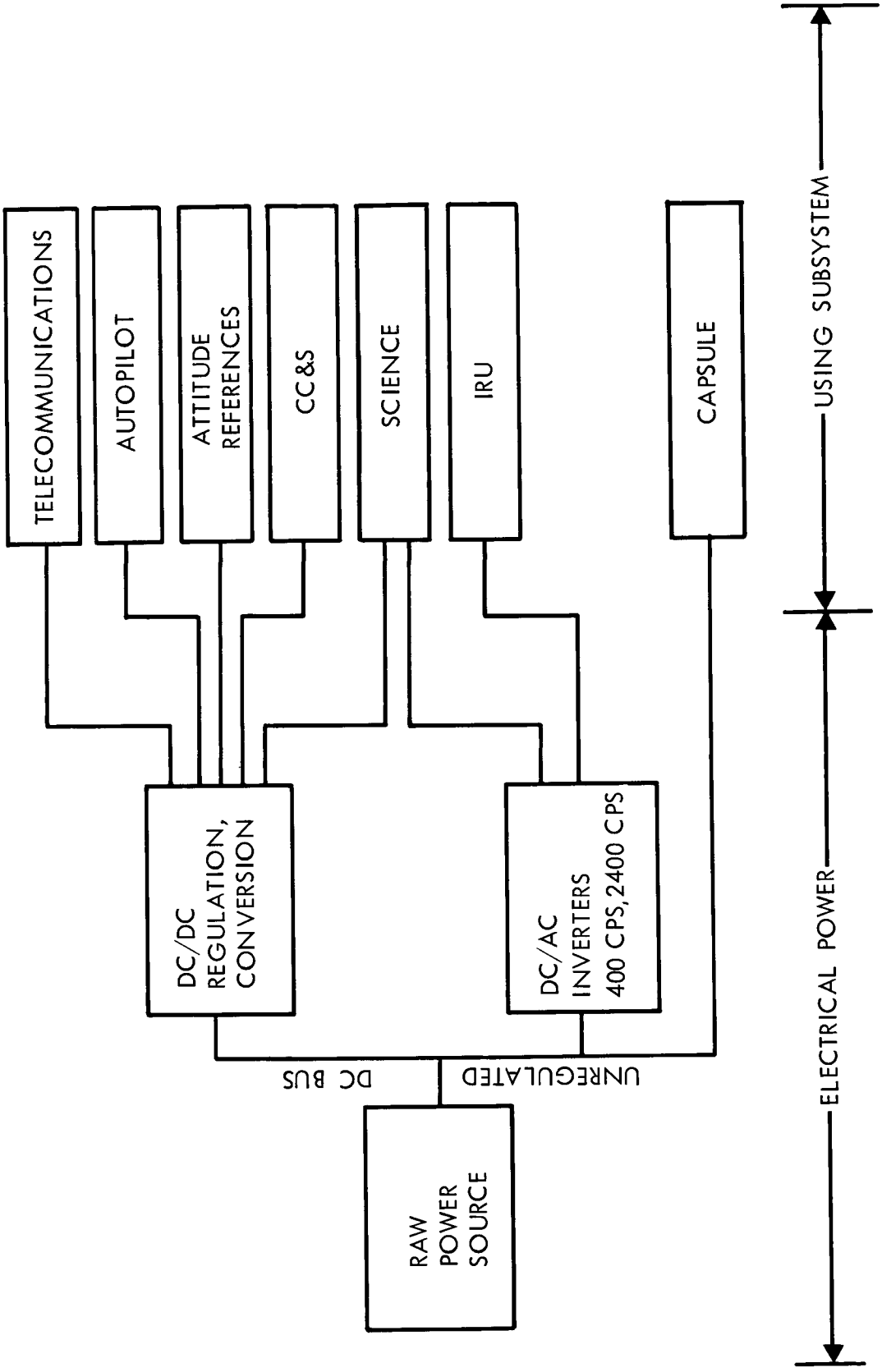

Figure 4.2-7: Centralized Power Conditioning

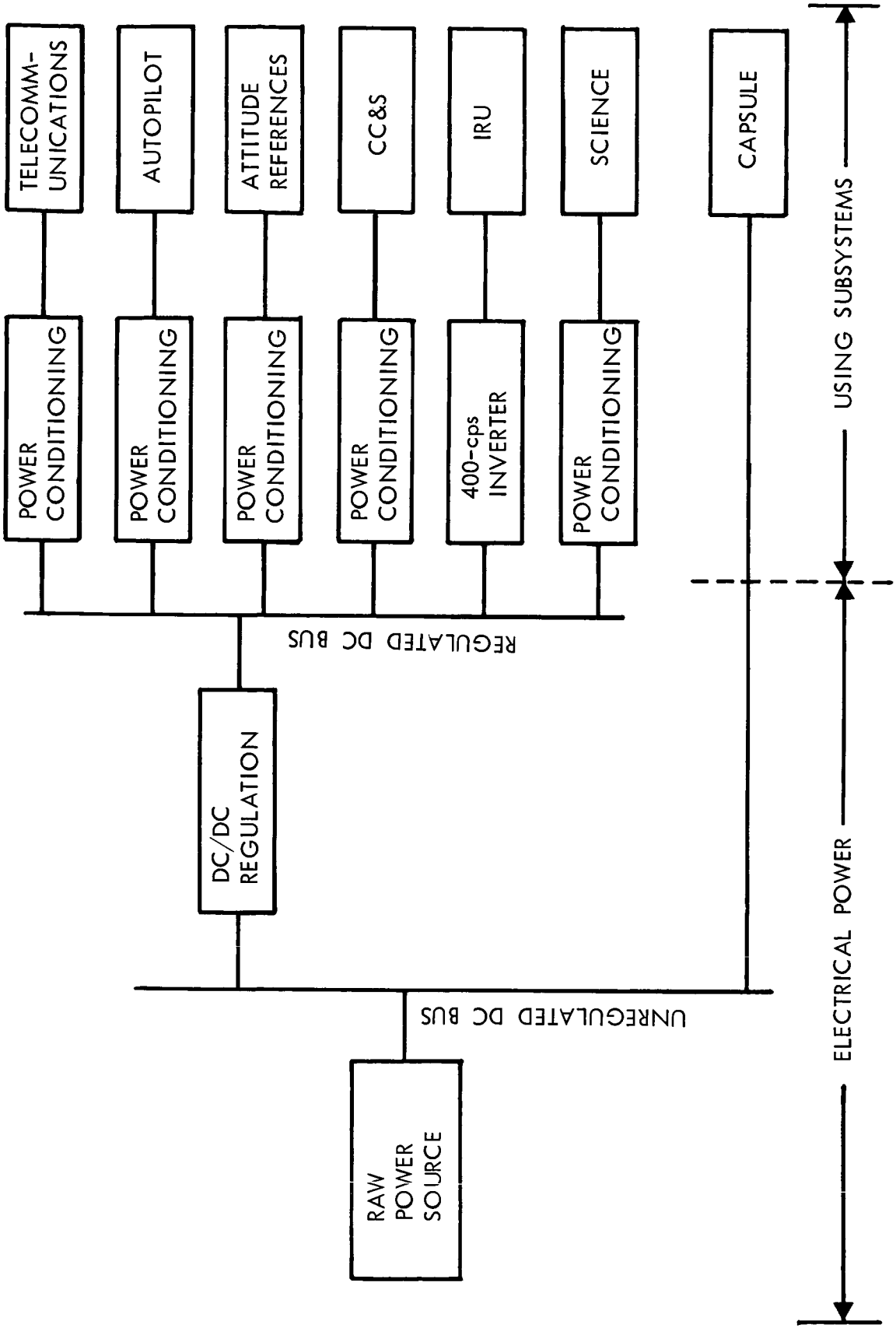

Figure 4.2-8: Decentralized Power Conditioning

Weight--Based on the difference in total interconnect wiring discussed above, weight (in pounds) due to wiring only is estimated to be:

Remote conversion and distribution	5
Central conversion and distribution	14

Versatility--The remote conversion and distribution method is more versatile than the central method because the user can convert the distribution bus voltage to the values required. Subsequent changes in the individual user voltage levels will not require redesign outside of the using subsystem. This independence will minimize intersubsystem coordination during spacecraft design.

Further, interface control and subcontract management are greatly facilitated by adoption of a minimum number of standard distribution voltages.

Interference--Remote conditioning provides greatest protection against electrical interference among subsystems. Low power (comparatively high impedance) circuits will use short leads. The filtering inherent in conditioning apparatus minimizes electrical noise conducted back to the central bus and thereby introduced into other subsystems.

4.2.4.2 Alternate Power Form Concepts

Three alternate forms of distributed electrical power are considered:

1) Regulated a.c.;
2) Regulated d.c.;
3) Unregulated d.c.

TABLE 4.2-3: Subsystem Voltage and Number of Wires Required

Subsystem	Voltages Required	Number of Wires
Autopilot	4	8
400 cps, 1 phase	1	2
400 cps, 3 phase	1	3
Command	4	8
CC & S	1	2
Data Encoder	5	10
Telecommunication	4	8
Science (10 Experiments)	40	80
Data Automation	4	8
Tape Recorder	5	10
TOTAL	—	139

Reliability Analysis

$R = e^{-\lambda t}$

λ = total failure rate (connections)

t = mission time (hours) = 6000

1. 30 pins at 0.001/pin = $\lambda_1 = 0.03 \times 10^{-6}$

2. 140 pins at 0.001/pin = $\lambda_2 = 0.14 \times 10^{-6}$

$R_1 = e^{-\lambda_1 t} = e^{-(0.03 \times 10^{-6})(6000)} = e^{-0.18 \times 10^{-3}} = 0.99984$

$R_2 = e^{-\lambda_2 t} = e^{-(0.14 \times 10^{-6})(6000)} = e^{-0.8 \times 10^{-3}} = 0.99916$

The regulated d.c. distribution system has been selected as the primary system based on its greater efficiency and lower overall weight than a regulated a.c. system. The regulated d.c. distribution system also shows a slightly higher efficiency and less stringent requirements on the user power conditioning equipment when compared to an unregulated d.c. distribution system.

The key competing characteristics of the three alternate concepts are performance (efficiency), weight (overall power subsystem), magnetic field, and ground loops.

Sample calculations were made using representative equipment efficiencies and loads. The results of these calculations are summarized below.

Distribution Form	Efficiency (%)	Weight (pounds)
Regulated a.c.	61.3	480
Regulated d.c.	67.4	447
Unregulated d.c.	67.2	440.5

These weight differences include estimates of the changes in solar array and battery weights because of differences in distribution efficiency.

In terms of the subsystem distribution method selected (a.c. or d.c.) either system is usable. Particular care must be taken with the d.c. system to arrange the wiring to cancel magnetic fields and eliminate ground loops. All distribution will use separate return conductors with twisted-pair techniques.

The remote power conditioning system with d.c. as the prime power form has been selected based on the factors discussed above.

4.2.5 Series-Switching Regulator Versus Booster Regulator

Two types of regulator circuits were considered as suitable for providing the regulated d.c. bus voltage from unregulated raw power:

1) Series-switching regulator;

2) Booster regulator.

The series-switching regulator, selected for the preferred subsystem, can regulate to $\pm$ 1 percent with an overall efficiency range of 90 to 98 percent. The unit regulates without auxiliary equipment over an input voltage range of 37 to 100 volts.

The prime trade factors considered were:

1) Efficiency;

2) Operating range;

3) Weight.

Efficiency--Performance data on an experimental series-switching regulator show that the efficiency will be between 98 and 93 percent over an input voltage range of 35 to 70 volts and a load power range of 150 to 350 watts. The same voltage and power variations with a booster regulator give an efficiency variation of 92 to 87 percent. The series-switching regulator will, therefore, provide an approximate 6 percent increase in efficiency.

Operating Ranges--The input voltage range of the series-switching regulator is determined at the low end by the required regulated output voltage and at the high end by the voltage rating of components. The booster regulator, however, has definite low and high voltage limits set by the basic design of the circuit. This range, for a practical design with the efficiency noted above, is 2 to 1 (e.g., high voltage equals 70 volts, low voltage equals 35 volts). To use a booster regulator in the Voyager system over the 2.7 to 1 voltage range, voltage-limiting zener diodes must be incorporated into the system to limit the maximum array output voltage.

Weight--The weights of the series-switching regulator and booster regulator are approximately equivalent. However, the total subsystem weight is greater when using the booster regulator because of the zener diodes required, the increased solar-array structural weight to provide heat sink and support for the diodes (a box-beam support structure is now required rather than a lighter truss beam), the increased array area (and weight) due to the lower efficiency, and the increased battery weight due to the lower regulator efficiency.

The weight increase (in pounds) caused by using the booster regulator instead of a series-switching regulator is as follows:

Zener diodes	12
Support structure increase	13
Battery weight increase	9
Array weight increase (larger area)	20
Total weight increase	54

The series-switching regulator has been selected for the preferred design because of the subsystem weight saving of 12 percent resulting from the higher efficiency and operating voltage range.

4.2.6 References

1. EOS-V-1041, "Voyager Spacecraft Electrical Power Subsystem Solar Array Structural Drawings"

2. EOS Specification 613847, "Voyager Spacecraft AgO-Cd Battery"

3. U. S. Naval Ammunition Depot, Crane, Indiana; Report QE/C 64-;30 "Effect of Sterilization on Sealed Nickle Cadmium Cells For Use in Space Satellites."

4.3 SPACECRAFT PROPULSION

Summary--The selected spacecraft propulsion module, shown in Figure 4.3-1 consists of a combined solid motor/liquid monopropellant subsystem. The module, which weighs 3500 pounds, satisfies all Voyager mission propulsion requirements through 1977. The liquid monopropellant subsystem utilizes four 50 pound thrust, regulated pressure-fed, radiation cooled, hydrazine engines. These engines, which employ the Shell 405 spontaneous decomposition catalyst, are operated in pairs, thus providing engine redundancy. Thrust vector control is accomplished by jet vanes. A total of 395 pounds of hydrazine is stored in two spherical tanks, with butyl bladders for positive expulsion. Regulated nitrogen gas, drawn from the reaction-control subsystem gas supply, provides for bladder pressurization. Both pressurant and propellant are positively isolated after each firing. The solid motor provides a 5700 fps orbit-insertion velocity increment. The oblate spheroid motor case is fabricated of glass filament and epoxy resin. The nozzle, partially buried, has an exit-to-throat area ratio of 73. The propellant is an aluminized polybutadiene cast in a modified conocyl grain, which provides for regressive burning. Total propellant weight is 2306 pounds. The average nominal thrust is 7,988 pounds, while the maximum acceleration during burn is 2.2 g's. Ignition is provided by an aft-mounted, controlled-pressure, Alclo-iron igniter. Pitch and yaw thrust vector control is supplied by secondary injection, utilizing Freon 114B2 as injectant fluid, with unregulated nitrogen gas as a pressurant. Roll thrust vector control is provided by the reaction control subsystem. The spacecraft propulsion module will be sterilized

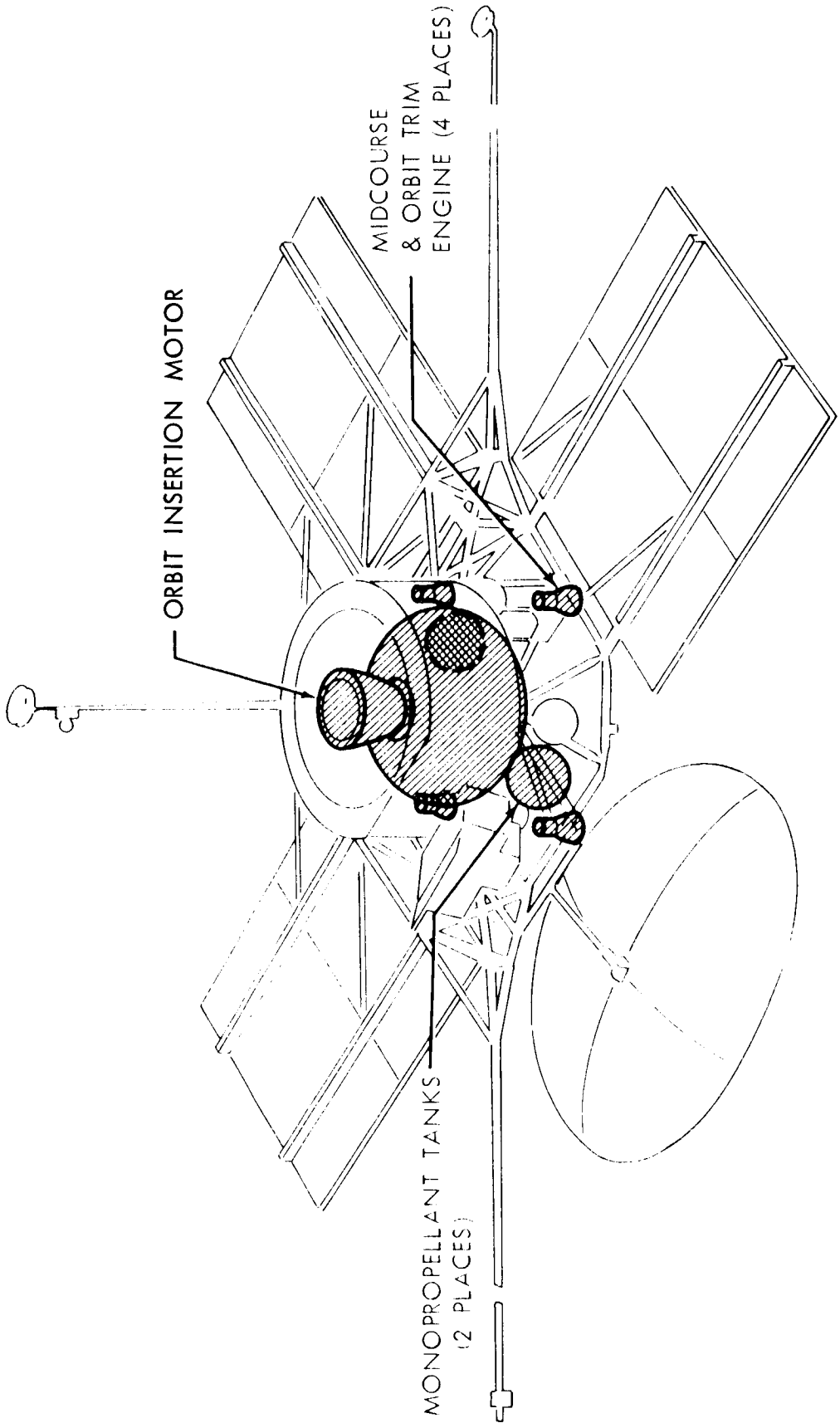

Figure 4.3-1: Propulsion Subsystem

to avoid planetary contamination. The preferred spacecraft propulsion subsystem is described in greater detail in Section 4.3, Volume A.

The selection of the preferred propulsion design concept followed the logic tree shown in Figure 4.3-2. Other spacecraft propulsion designs considered included all-monopropellants, hybrids, and bipropellants. Monopropellants were rejected since they could not provide the ΔV required for the 1971 and 1973 launch opportunities for the specified 3500 pounds. Deep and mild cryogenic bipropellants were rejected because of high development risk, lack of nonpermeable positive displacement expulsion devices, and complexity of handling. Hybrids were rejected because of their early development stage.

An Earth storable bipropellant design utilizing the LEM ascent engine for orbit insertion, coupled with four MA-109 (Apollo & Lunar Orbiter) engines for midcourse and orbit trim was examined. This concept was rejected since it could not fulfill all Voyager energy requirements for the 1971-1973 launch opportunities within the specified 3500 pound limitation. In addition, development status for nonpermeable positive displacement expulsion devices imposes a high risk.

A new bipropellant engine design with a thrust level specifically tailored to Voyager requirements was also considered. Again, within the 3500 pound limitation the ΔV attained by this design was only 5063 fps versus 5700 fps for the preferred design. Moreover, its reliability was inferior since it was a new and as yet unproven design. Finally,

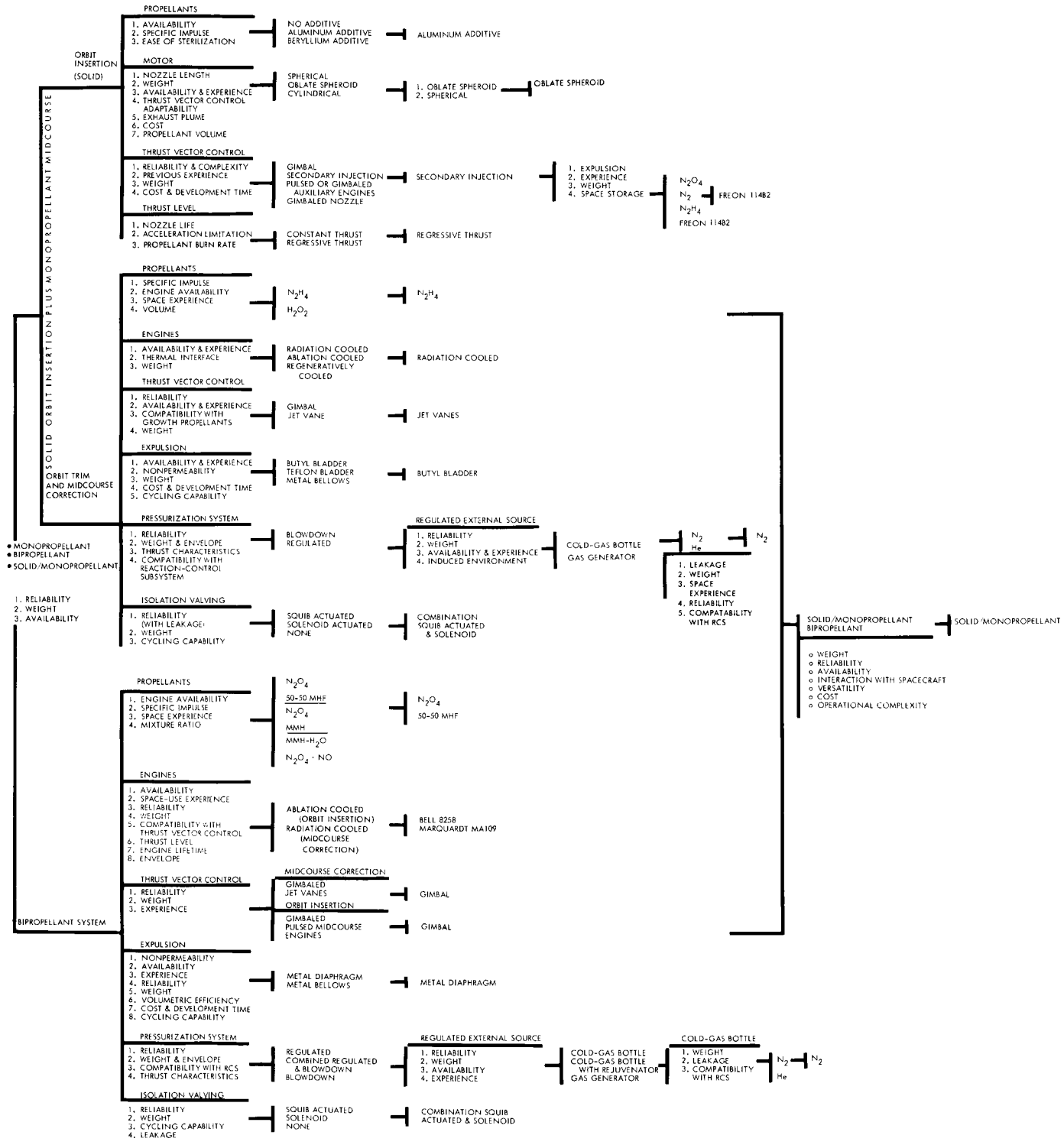

Figure 4.3-2: Alternate Propulsion Mechanizations — Selection Logic Chart

it has the same risk as the previous concept associated with the development of the nonpermeable positive displacement expulsion device.

Preferred Design--Solid Propellant, Orbit Insertion--The preferred solid-motor/monopropellant subsystem can be designed and fabricated at reasonable cost by utilizing materials, components, and concepts that rely on existing experience and technology. In mechanizing the preferred design solid insertion motor, the following areas were examined: motor geometry, motor case material, solid propellant, thrust vector control, thrust level, and thrust termination.

1) Solid Motor Geometry--The oblate spheroid, spherical, and cylindrical motor geometries were considered. The oblate spheroid was selected because it provided maximum propellant volume and high nozzle expansion ratio, resulting in maximum total impulse and minimum thermal interaction with the spacecraft.

2) Motor Case Material--Both glass and titanium cases were considered. The glass case was selected on the basis of weight, fabrication experience, and compatibility with the preferred motor geometry. A weight contingency of 30 pounds which allows for switching to a titanium case, if required, has been allocated.

3) Solid Propellant--Polybutadiene, which is compatible with the preferred motor case geometry, has been considered with and without aluminum and beryllium additives. Aluminum additives have been selected on the basis of highest performance commensurate with minimum risk considerations.

4) Thrust Vector Control--Thrust vector control schemes for pitch and yaw included: (1) gimbaled nozzle, (2) gimbaled motor, (3) secondary injection, and (4) auxiliary engines. Secondary injection, with Freon as the injectant, was selected on the basis of accumulated experience, high reliability, and minimum autopilot complexity. Gimbaled nozzles were rejected since they are in the early development stage. Gimbaled auxiliary engines required unrealistic gimbal angles and rates. The midcourse and orbit trim engines used in the pulsed mode were the strongest contenders to the preferred system and are considered for backup. They have been rejected at the present time due to lack of sufficient data on the performance of pulsed hydrazine engines that employ the Shell spontaneous decomposition catalyst.

5) Thrust Level--Both constant and regressive thrust-time-traces were considered. A regressive thrust trace was chosen since it minimized peak acceleration during burn without exceeding propellant burn and nozzle lifetime limitations.

6) Thrust Termination--Normal depletion, nozzle blowoff, head-end porting, and quenching were considered. Normal depletion was chosen since it was simple and highly reliable, minimized interaction with the spacecraft, and was compatible with orbit-insertion maneuver strategy.

Preferred Design--Monopropellant, Midcourse and Orbit Trim--The mechanization of the monopropellant midcourse and orbit trim subsystem resulted from trades in the following areas: propellants, engines,

thrust vector control, expulsion, pressurization, and isolation valving.

1) Monopropellant--Hydrazine, with and without hydrazinium nitrate, and hydrogen peroxide were considered. Neat hydrazine was selected on the basis of its high specific impulse and previous experience, since the Shell 405 spontaneous decomposition catalyst has been sufficiently developed to be considered ready for flight use.

2) Engines--Radiation-cooled engines were selected on the basis of space-proven experience and minimum weight. A thrust level of 50 pounds was selected using a chamber pressure of 150 psia and an expansion ratio of 50.

3) Thrust Vector Control--Both jet vanes and gimbaled engines were considered. Jet vanes were selected on the basis of reliability and space flight experience.

4) Expulsion--Butyl bladders, teflon bladders, and metal bellows were considered. The butyl bladder was selected on the basis of reliability and space flight experience with hydrazine.

5) Isolation Valving--Both solenoid-actuated and squib-actuated isolation valves were considered. A combination of solenoid and squib-actuated valves was selected because of high reliability (0.999) and versatility.

6) Pressurization--Blow down and regulated pressurization systems were considered. The regulated system was selected because it had higher reliability, 0.999 versus 0.998, occupied less volume, and was lighter. Nitrogen and helium were considered as pressurants. Nitrogen was selected, on the basis of reliability and simplicity, since it could be integrated with the reaction-

control subsystem nitrogen storage tankage. Nitrogen bottle pressure is regulated to 264 ± 2 psia to pressurize the butyl bladders in the preferred design.

4.3.1 Scope

The planetary vehicle requires propulsion capability for midcourse corrections to remove or reduce trajectory dispersions and perform required trajectory biasing. Additional capability is required for inserting the Flight Spacecraft into orbit around Mars and subsequent orbit trimming.

Voyager propulsion trade studies initially considered a wide variety of propulsion concepts, propellant combinations, and attendant components. This section describes the selection process employed in narrowing the design options to a few candidate concepts, and the subsequent identification of the preferred design. Supporting trade studies, problem areas assessment and development status of the preferred design are included. The preferred spacecraft propulsion design is described in detail in Volume A, Section 4.3.

The following are applicable documents.

1) Aerojet General, Proposal SNP 65564B, "Preliminary Design of a Voyager Retropropulsion Motor," Sacramento, California, April 28, 1965 (CONFIDENTIAL).
2) Aerojet General, Proposal SNP 65564, "Voyager Retropropulsion Motor," Sacramento, California, February 10, 1965 (CONFIDENTIAL).

3) Aeroject General Corporation, Proposal SNP 65564-2, "Voyager Retropropulsion Motor Program," Phase IA Report and Confidential Supplement, Sacramento, California, June 1965

4) Bell Aerosystems Company, Report No. D8420-953005, "Planning Proposal, Voyager Spacecraft Rocket Engines--Boeing Propulsion Concepts 1 and 2," July 1965, Buffalo, N.Y. (CONFIDENTIAL).

5) The Boeing Company, D2-82703-2, "Preliminary Specification--Propulsion Engines for Voyager Spacecraft--(Planning Proposal)," June 1965, Seattle, Washington.

6) Thiokol Chemical Corporation, EP631-65, Volume I, Parts I and II, "A Planning Proposal for a Solid Propellant Orbit Insertion Motor for the Voyager Spacecraft," June 25, 1965, Elkton, Maryland (Part II CONFIDENTIAL).

7) Arnold Engineering Development Center, AEDC-TDR-64-211, "Altitude Development Tests of the Bell Model 8258 Liquid Propellant Rocket Engine, Phase I, LEM Ascent Stage Primary Propulsion System," Air Force Systems Command, United States Air Force, November 1964 (CONFIDENTIAL).

8) Arnold Engineering Development Center, AEDC-TDR-64-269, "Result of Testing the Thiokol TE-M-444 Solid Rocket Motor Under the Combined Effects of Simulated Altitude and Rotational Spin," Air Force Systems Command, United States Air Force, December 1964 (CONFIDENTIAL).

9) Bell Aerosystems Corporation, RTD-TDR-63-1048, "Development of Expulsion and Orientation Systems for Advanced Liquid Rocket Propulsion Systems," Division of Bell Aerospace Corp., Buffalo, N.Y., July 1963.

10) General Electric, 635D801, "Voyager Design Study," Missile and Space Division, Philadelphia, Pennsylvania, October 15, 1963.

11) Hughes Aircraft Company, SSD 5118R, "Quality Assurance Testing of Surveyor Main Retro Engine at AEDC" Space Systems Division, February, 1965 (CONFIDENTIAL).

12) Jet Propulsion Laboratory, Spec. No. MC-1-110, "Mariner C Functional Specifications, California Institute of Technology, Pasadena, California, April 1, 1965.

13) Jet Propulsion Laboratory, SPS 37:8-32, "Space Program Summary, Volumes I, II, IV, V, California Institute of Technology, Pasadena, California (Volumes I, II, V CONFIDENTIAL).

14) Lockheed Aircraft Corporation, M-29-64-1, "Final Report, Mariner Mars 1969 Orbiter Study," Lockheed Missiles and Space Company, Sunnyvale, California, October 4, 1964.

15) Shell Development Company, S-13917, "Development of Catalysts for Monopropellant Decomposition of Hydrazine," Division of Shell Oil Company, Emeryville, California, March, 1964 (CONFIDENTIAL).

16) Thiokol Chemical Corporation, EB7-64, "Spherical Rocket Motors," Elkton Division, Elkton, Maryland, January 1965 (CONFIDENTIAL).

17) Thiokol Chemical Corporation, PD 4-65, "Voyager Propulsion Technology," Reaction Motors Division, Denville, New Jersey, March 25, 1965.

18) Thiokol Chemical Corporation, "Voyager Orbit Insertion Motor Presentation," Elkton Division, Elkton, Maryland, June 9, 1965 (CONFIDENTIAL).

19) Thiokol Chemical Corporation, RMD 5052-Q2, "Positive Expulsion Bladders for Storable Propellants," Reaction Motors Division, Denville, New Jersey, November 1, 1964.

20) TRW Space Technology Laboratories, Proposal No. 2985.00, "Proposal for Monopropellant Hydrazine Engine Technology Program," Thompson Ramo Wooldridge Inc., Redondo Beach, California, February, 1964.

21) United Technology Center, Brochure 65-13, "Voyager Propulsion System," Division of United Aircraft Corporation, April, 1965.

22) Rocketdyne, R-3923, "Space Transfer Phase Propulsion System Study," Volumes I-III, Division of North American Aviation, Canoga Park, California, February, 1963 (CONFIDENTIAL).

23) Rocketdyne, R5446, "High Performance Apollo Propulsion System Study," Volumes I-IV, Division of North American Aviation, Canoga Park, California, March, 1964 (CONFIDENTIAL).

24) The Boeing Company, D2-23525-7, "Mars Orbiting Mission-Propulsion, Design Data, Preliminary Information," Seattle, Washington, October, 1964.

4.3.2 Propulsion Concepts Considered

Initial screening of candidate propulsion concepts for the Voyager mission was based on availability and minimum technical risk. As a result, the following four propulsion design concepts were selected for further studies:

1) A pressure-regulated multiple engines all-monopropellant subsystem;

2) A pressure-regulated all-bipropellant subsystem utilizing a new single engine;

3) A pressure-regulated all-bipropellant subsystem, utilizing the LEM ascent and MA-109 Apollo engines;

4) A combined solid and multiple engines pressure-regulated monopropellant subsystem.

Only pressure-fed concepts were considered because of the high weight and low reliability associated with turbopump propellant feed in the thrust range suitable for the Voyager mission.

Cryogenic and hybrid propellants have been rejected because of high risk and lack of applicable space experience. Combined bipropellant-monopropellant and solid-bipropellant concepts have been rejected since they offer no advantage over any of the four concepts delineated above.

Each of the four candidate propulsion design concepts has been mechanized to a sufficient depth to allow for the selection of the preferred design.

4.3.2.1 Subsystem Description

Candidate Propulsion Subsystem Concept 1--Engine, tankage and pressure vessel arrangements for this design concept are shown in Figure 4.3-3. Subsystem component test is given in Table 4.3-1. Subsystem features include five 200-pound thrust hydrazine radiation-cooled engines utilizing the Shell 405 catalyst for spontaneous decomposition. Regulated

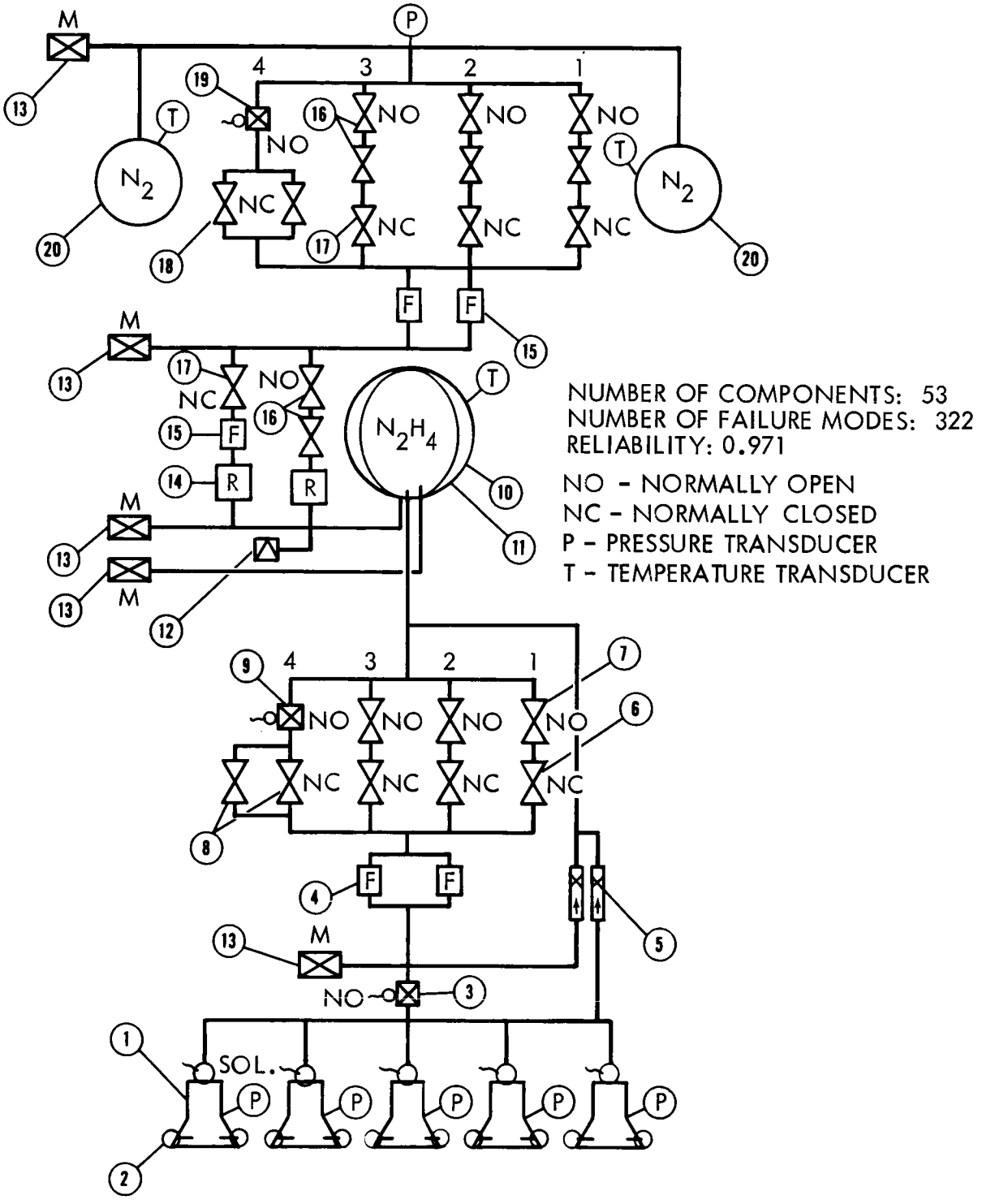

Figure 4.3-3: Monopropellant System, Concept I

Table 4.3-1: COMPONENT LIST - CONCEPT NO. 1

ITEM	QUANTITY	NAME
1	5	Rocket Engine
2	20	Jet Vanes and Actuator Assembly
3	1	Valve, Propellant NO, Solenoid Operated
4	2	Filter, Propellant
5	2	Valve, Propellant, Thermal Relief
6	3	Valve, Propellant NC, Squib Operated
7	3	Valve, Propellant NO, Squib Operated
8	1	Valve, Propellant, NC Dual, Squib Operated
9	1	Valve, Propellant, NO, Solenoid Operated
10	1	Tank, Propellant
11	1	Bladder, Propellant Expulsion
12	1	Valve, Relief
13	5	Valve and Cap, Propellant Fill & Test
14	2	Regulator N_2 Pressure
15	3	Filter, Nitrogen
16	4	Valve, N_2 NO, Dual, Squib Operated
17	4	Valve, N_2 NC, Squib Operated
18	1	Valve, N_2 NC Dual, Squib Operated
19	1	Valve, N_2 NO, Solenoid Operated
20	2	Pressure Vessel, Nitrogen

nitrogen gas pressurization is used for positive expulsion of propellant from a single tank with a butyl bladder. Fuel and pressurant isolation squib valves are provided for each maneuver requiring engine thrust. Thrust vector control is by jet vanes on each engine. All five engines are utilized for orbit insertion. The center engine is used for midcourse and orbit trim in the normal mode. Subsystem and engine performance summaries and advantages are presented in Tables 4.3-2, -3, and -4.

Candidate Propulsion Subsystem Concept 2--This concept, using a newly designed engine, shown in Figure 4.3-4, utilizes hypergolic bipropellants of mixed hydrazine fuels, N_2H_4 and UDMH and nitrogen tetroxide, N_2O_4. Subsystem component list is given in Table 4.3-5. A mixture ratio of 1.6 (O/F) is used to equalize tank volumes. Propellants are contained in two spherical tanks each, for fuel and oxidizer, using convoluted metal diaphragms for positive expulsion. Tank pressurant is provided by a regulated high-pressure nitrogen system using two manifolded pressure vessels. Pressurant and propellant flow are controlled by electric signal to squib-operated isolation valves for each maneuver. Flow circuitry is provided for three midcourse corrections, plus one redundant branch; orbit insertion and orbit trim. Thrust vector control is by engine gimbal, with roll control provided through the reaction control system.

Subsystem and engine performance summaries, and advantages and disadvantages are presented in Tables 4.3-6 through 4.3-8.

Table 4.3-2: CANDIDATE PROPULSION SUBSYSTEM CONCEPT #1

MONOPROPELLANT
SUBSYSTEM PERFORMANCE

SYSTEM PERFORMANCE:	MIDCOURSE CORRECTION	ORBIT INSERTION	ORBIT TRIM
MAXIMUM VELOCITY (FPS)	164	3660	328
MINIMUM VELOCITY (FPS)	0.06	N.A.	0.152
VELOCITY TOLERANCE (FPS)	0.005	0.08	0.016
ACCELERATION, MAX (G'S)	0.0265	0.307	0.064
ACCELERATION, MIN (G'S)	0.0256	0.182	0.057

PROPULSION MODULE PERFORMANCE:		
MANEUVER	MIDCOURSE CORRECTION AND ORBIT TRIM	ORBIT INSERTION
PROPELLANT	HYDRAZINE - N_2H_4	HYDRAZINE - N_2H_4
SPECIFIC IMPULSE (S.S.) (SEC)	235	235
TOTAL IMPULSE (LB-SEC)	73,320	485,980
MINIMUM IMPULSE BIT (LB-SEC)	14	70
SHUTDOWN IMPULSE TOLERANCE (LB-SEC)	1.5	7.5
NUMBER OF ENGINES	1	4 (+1)
THRUST PER ENGINE (LBS)	200	200
ENGINE OPERATING TIME (SEC)	431	486
THRUST VECTOR CONTROL	JET VANES	JET VANES
MODULE INERT WEIGHT (LBS)	1120	
PROPELLANT WEIGHT (LBS)	2380	
TOTAL MODULE WEIGHT (LBS)	3500	
PROPELLANT TANKAGE	COMMON	

Table 4.3-3: CANDIDATE PROPULSION SUBSYSTEM CONCEPT #1
MONOPROPELLANT
ENGINE PERFORMANCE

	ORBIT INSERTION	MIDCOURSE & ORBIT TRIM
MODEL	NEW DESIGN	NEW DESIGN
MANUFACTURER		
NO. USED	5	1
THRUST	200 lb	200 lb
DESIGN BURN TIME	972 sec*	862 sec*
ENGINE BURN TIME	486 sec	431 sec
TOTAL IMPULSE	485,980 lb/sec	73,320 lb/sec
MAX. THRUST/WEIGHT	0.3065	0.0641 (orbit trim)
MAX. % THRUST OVERSHOOT	0	0
ΔV	3660 fps	492 fps

*Estimated

Table 4.3-4: CANDIDATE PROPULSION SUBSYSTEM CONCEPT #1
MONOPROPELLANT
ADVANTAGES AND DISADVANTAGES

ADVANTAGES
. Simple System - High Reliability
. Space Proven Concept
. Low Cost and Short Development Time
. Uses Developed Butyl Bladder
. Uses Developed Jet Vane TVC
. Near-Optimum Thrust Level
. Clean Exhaust
. Spontaneous Start Capability
. Sterilization Feasible
DISADVANTAGES
. Low Performance
. New Catalyst Qualification Program

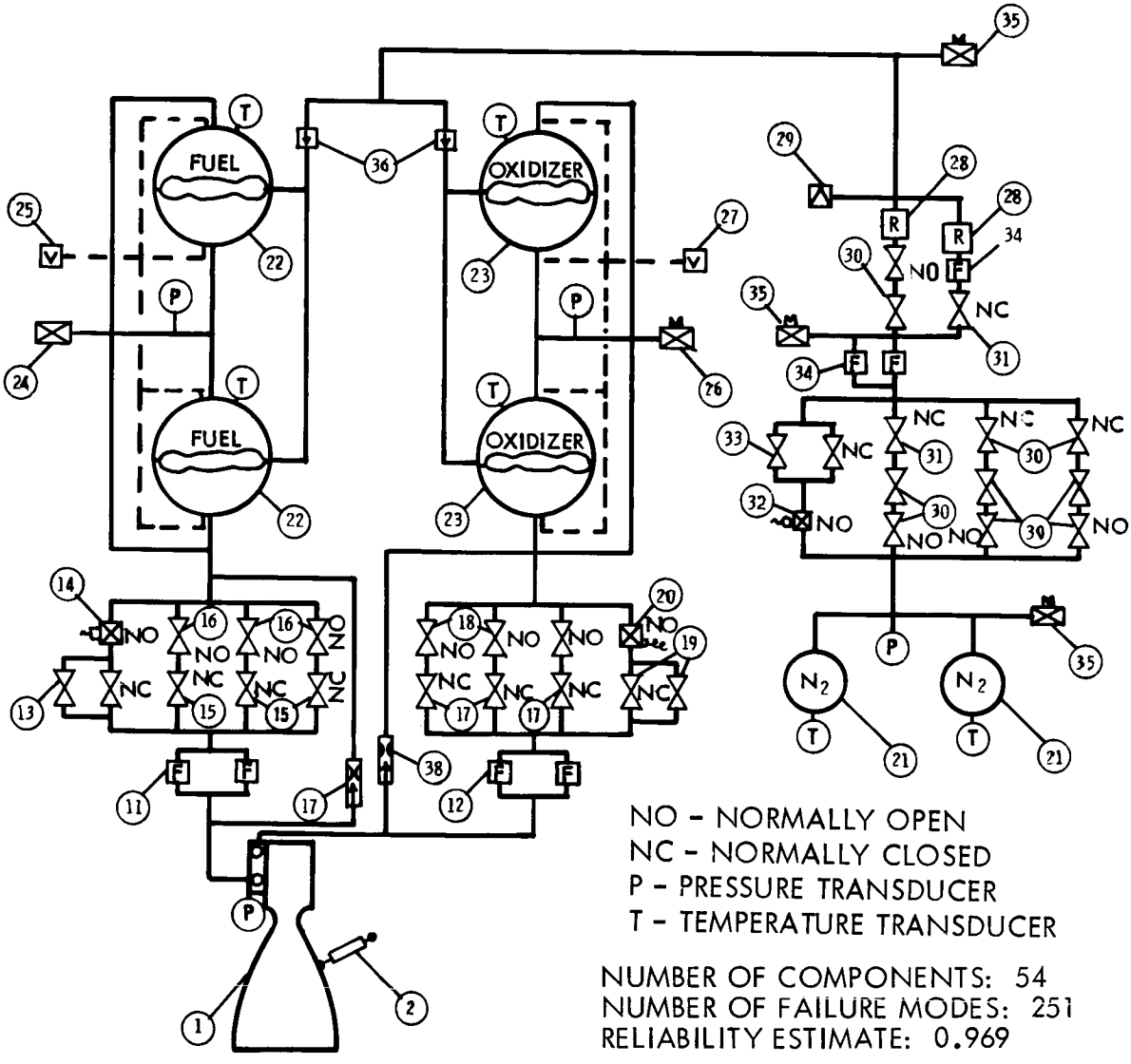

Figure 4.3-4: Midcourse Orbit-Insertion, and Orbit-Trim Engine — Single-Engine, Bipropellant System Concept 2

Table 4.3-5: COMPONENT LIST - CONCEPT NO. 2

ITEM	QUANTITY	NAME
1	1	Rocket Engine
2	2	Gimbal Actuator
11	2	Filter, Fuel
12	2	Filter, Oxidizer
13	1	Valve, Fuel, NC Dual, Squib Operated
14	1	Valve, Fuel, NO, Solenoid Operated
15	3	Valve, Fuel, NC, Squib Operated
16	3	Valve, Fuel, NO, Squib Operated
17	3	Valve, Oxidizer, NC, Squib Operated
18	3	Valve, Oxidizer, NO, Squib Operated
19	1	Valve, Oxidizer, NC Dual, Squib Operated
20	1	Valve, Oxidizer, NO, Solenoid Operated
21	2	Pressure Vessel, Nitrogen
22	2	Tank, Fuel, Including Expulsion Diaphragm
23	2	Tank, Oxidizer, Including Expulsion Diaphragm
24	1	Valve and Cap, Fuel, Fill and Test
25	1	Valve, Fuel Fill Vent
26	1	Valve and Cap, Oxidizer, Fill and Vent
27	1	Valve, Oxidizer Fill Vent
28	2	Regulator, N_2 Pressure
29	1	Valve, Relief
30	4	Valve, N_2, NO, Dual, Squib Operated
31	4	Valve, N_2, NC, Squib Operated
32	1	Valve, N_2, NO, Solenoid Operated

Table 4.3-5 CONTINUED

ITEM	QUANTITY	NAME
33	1	Valve, N_2, NC, Dual, Squib Operated
34	3	Filter, N_2
35	3	Valve and Cap, N_2 Fill and Test
36	2	Valve, N_2 Check
37	1	Valve, Fuel, Thermal Relief
38	1	Valve, Oxidizer, Thermal Relief

Table 4.3-6: CANDIDATE PROPULSION SUBSYSTEM CONCEPT #2

BIPROPELLANT

SYSTEM PERFORMANCE

SYSTEM PERFORMANCE:	MIDCOURSE CORRECTION	ORBIT INSERTION	ORBIT TRIM
MAXIMUM VELOCITY (FPS)	164	5063	328
MINIMUM VELOCITY (FPS)	0.324-0.42	NA	0.804-1.04
VELOCITY TOLERANCE (FPS)	0.046-0.088	NA	0.115-0.219
ACCELERATION, MAX (G'S)	0.0977	0.235	0.243
ACCELERATION, MIN (G'S)	0.0962	0.136	0.226

PROPULSION MODULE PERFORMANCE:	
MANEUVER	MIDCOURSE CORRECTION, ORBIT INSERTION, ORBIT TRIM
PROPELLANT	N_2O_4/(50-50) MHF
SPECIFIC IMPULSE (S.S.)(SEC)	305
TOTAL IMPULSE (LB-SEC)	736,000
MINIMUM IMPULSE BIT (LB-SEC)	77-100
SHUTDOWN IMPULSE TOLERANCE (LB-SEC)	11-21
NUMBER OF ENGINES	1
THRUST PER ENGINE (LBS)	750
ENGINE OPERATING TIME (SEC)	982
THRUST VECTOR CONTROL	GIMBAL
MODULE INERT WEIGHT (LBS)	1085
PROPELLANT WEIGHT (LBS)	2415
TOTAL MODULE WEIGHT (LBS)	3500
PROPELLANT TANKAGE	COMMON

Table 4.3-7: CANDIDATE PROPULSION SUBSYSTEM CONCEPT NO. 2

BIPROPELLANT
ENGINE PERFORMANCE

MODEL	NEW
MANUFACTURER	ROCKETDYNE
NO. USED	1
THRUST	750 LB
DESIGN BURN TIME	
ENGINE BURN TIME	982 SEC
TOTAL IMPULSE	736,000 (LB-SEC)
MAX THRUST/WEIGHT	.243 (ORBIT TRIM)
MAX % THRUST OVERSHOOT	27-73.5% (40 M.S.)
ΔV	5063 FT/SEC

Table 4.3-8: CANDIDATE PROPULSION SUBSYSTEM CONCEPT NO. 2

BIPROPELLANT
ADVANTAGES AND DISADVANTAGES

ADVANTAGES
. Simple System . MultiUse Engine . Near-Optimum Thrust Level . Clean Exhaust . Versatile System
DISADVANTAGES
. New Engine - Development Program Required . Non-Permeable Expulsion Required . Reaction Control Subsystem Must Provide Roll Control

Candidate Propulsion Subsystem Concept 3--Propulsion Concept 3 incorporates similar bipropellants, tankage, expulsion method, pressurization and flow isolation valves as noted for system concept no. 2. Arrangement of major components is shown in Figure 4.3-5; components are shown in Table 4.3-9. The four MA-109 (Lunar Orbiter) engines are capable of either steady-state or pulsing operation. In the Voyager application, these midcourse and orbit trim engines are mounted symmetrically about the orbit-insertion engine, and operated as a pair of opposite engines provide a redundant mode. Thrust is directed parallel to the spacecraft centerline in the direction of the orbit insertion engine thrust. The single model 8258 (LEM Ascent) engine of 3500 pounds thrust for orbit insertion is aligned on the spacecraft centerline. Subsystem and engine performance summaries and advantages and disadvantages are presented in Tables 4.3-10 through 4.3-12.

Candidate Propulsion Subsystem Concept 4--This design concept, shown in Figure 4.3-6, utilizes a single solid-propellant rocket motor for the orbit-insertion maneuver, and four liquid monopropellant hydrazine engines of 50 pounds each to provide impulse for the midcourse correction and orbit trim maneuvers. Components for this design concept are listed in Table 4.3-13. Thrust vector control is supplied by jet vanes installed on the monopropellant engines and a secondary fluid injection TVC system on the solid motor. Roll control is maintained during the midcourse and orbit-trim maneuvers with the jet vanes and by the attitude control subsystem during the orbit insertion.

Nitrogen gas for expulsion purposes is supplied to the N_2H_4 propellant tanks and secondary injection Freon tank from the attitude control subsystem tankage. A series of isolation valves are installed upstream

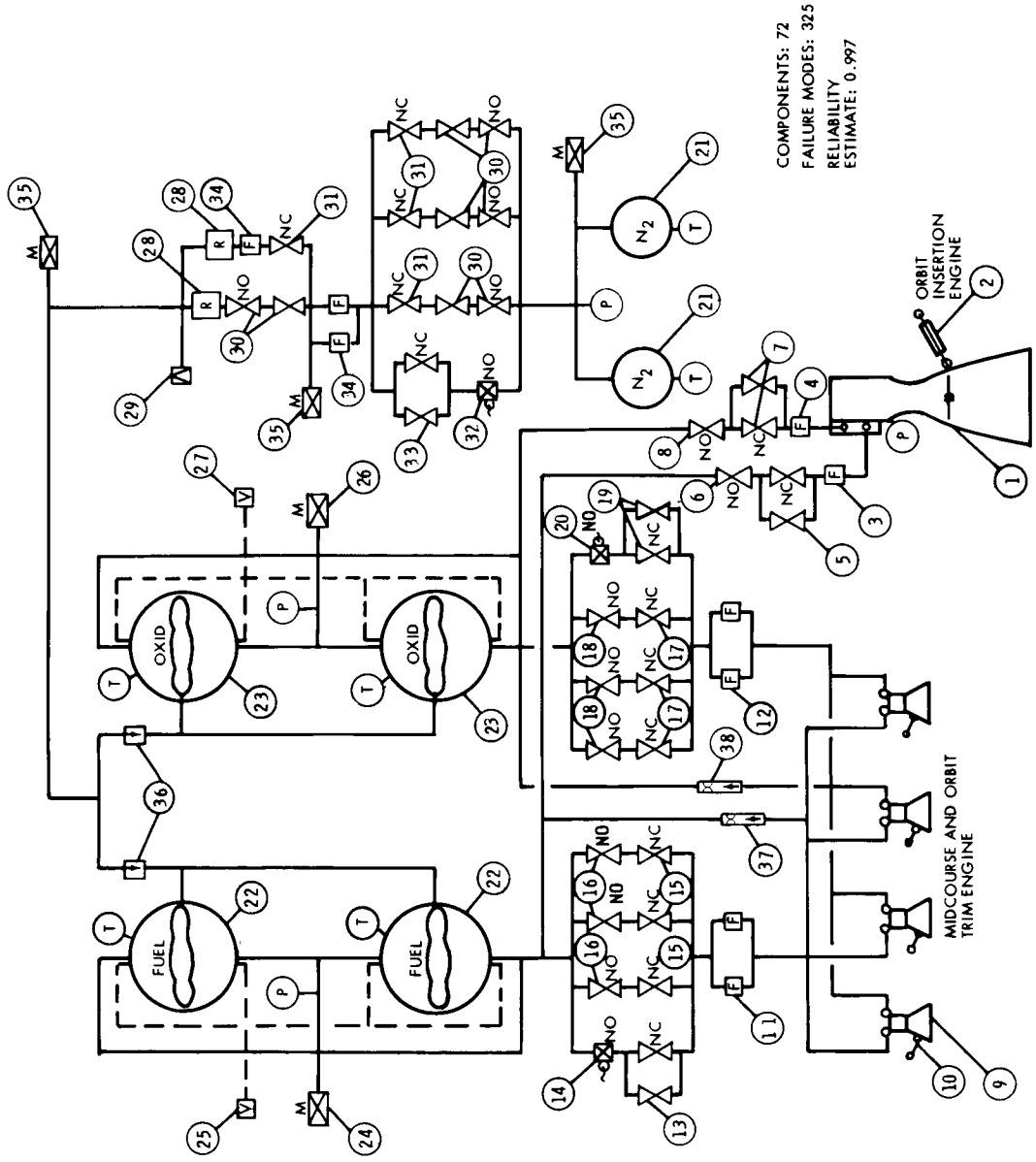

Figure 4.3-5: Bipropellant System Concept No. 3

Table 4.3-9: COMPONENT LIST - CONCEPT NO. 3

Item	Qty	Name
1	1	Rocket Engine
2	2	Gimbal Actuator
3	1	Filter, Fuel
4	1	Filter, Oxidizer
5	1	Valve, Fuel, NC Dual, Squib Operated
6	1	Valve, Fuel, NO, Squib Operated
7	1	Valve, Oxidizer, NC Dual Squib Operated
8	1	Valve, Oxidizer NO, Squib Operated
9	4	Rocket Engine--Midcourse
10	8	Gimbal Actuator
11	2	Filter, Fuel
12	2	Filter, Oxidizer
13	1	Valve, Fuel, NC Dual, Squib Operated
14	1	Valve, Fuel, NO Solenoid Operated
15	3	Valve, Fuel, NC, Squib Operated
16	3	Valve, Fuel NO, Squib Operated
17	3	Valve, Oxidizer, NC, Squib Operated
18	3	Valve, Oxidizer, NO, Squib Operated
19	1	Valve, Oxidizer, NC Dual, Squib Operated
20	1	Valve, Oxidizer, NO, Solenoid Operated
21	2	Pressure Vessel, Nitrogen
22	2	Tank, Fuel, Including Expulsion Diaphragm
23	2	Tank, Oxidizer, Including Expulsion Diaphragm

Table 4.3-9 (Continued)

Item	Qty	Name
24	1	Valve and Cap. Fuel, Fill and Test
25	1	Valve, Fuel Fill Vent
26	1	Valve and Cap. Oxidizer, Fill and Vent
27	1	Valve, Oxidizer Fill Vent
28	2	Regulator, N_2 Pressure
29	1	Valve, Relief
30	4	Valve, N_2, NO dual, Squib Operated
31	4	Valve, N_2, NC, Squib Operated
32	1	Valve, N_2, NC, Solenoid Operated
33	1	Valve, N_2, NC Dual, Squib Operated
34	3	Filter, N_2
35	3	Valve and Cap. N_2 Fill and Test
36	2	Valve, N_2 Check
37	1	Valve, Fuel, Thermal Relief
38	1	Valve, Oxidizer, Thermal Relief

Table 4.3-10: CANDIDATE PROPULSION SUBSYSTEM CONCEPT #3
BIPROPELLANT
SYSTEM PERFORMANCE

SYSTEM PERFORMANCE:	MIDCOURSE CORRECTION	ORBIT INSERTION	ORBIT CHANGE
MAXIMUM VELOCITY (FPS)	164	4550	328
MINIMUM VELOCITY (FPS)	0.004	5.81	0.004
VELOCITY TOLERANCE (FPS)	0.002	4.03	0.002
ACCELERATION, MAX. (G'S)	0.0261	1.04	0.062
ACCELERATION, MIN. (G'S)	0.0256	0.637	0.057

PROPULSION MODULE PERFORMANCE:		
MANEUVER	MIDCOURSE CORRECTION, ORBIT TRIM	ORBIT INSERTION
PROPELLANT	N_2O_4/(50-50) MHF	N_2O_4/(50-50)MHF
SPECIFIC IMPULSE (S.S.) (SEC)	290 (assumed)	305 (assumed)
TOTAL IMPULSE (LB-SEC)	74,000	611,500
MINIMUM IMPULSE BIT (LB-SEC)	0.4	580 ± 125
SHUTDOWN IMPULSE TOLERANCE (LB-SEC)	0.2 (EST)	360 ± 60
NUMBER OF ENGINES	2	1
THRUST PER ENGINE (LBS)	100	3500
ENGINE OPERATING TIME (SEC)	370	175
THRUST VECTOR CONTROL	GIMBAL	GIMBAL
MODULE INERT WEIGHT (LBS)	1240	
PROPELLANT WEIGHT (LBS)	2260	
TOTAL MODULE WEIGHT (LBS)	3500	
PROPELLANT TANKAGE	COMMON	

Table 4.3-11: CANDIDATE PROPULSION SUBSYSTEM CONCEPT #3
BIPROPELLANT
SYSTEM PERFORMANCE

	ORBIT INSERTION ENGINE	MID-COURSE ENGINES
MODEL	8258 (LEM ASCENT)	MA 109
MFG	BELL AEROSYSTEMS	MARQUARDT
NO. USED	1	4
THRUST	3500 lb	100 lb
DESIGN BURN TIME	525 sec	4800 sec
ENGINE BURN TIME	175 sec	450
TOTAL IMPULSE	611,500 lb-sec	74,000 lb-sec
MAX. THRUST/WEIGHT	1.04	0.062*
MAX. % THRUST OVERSHOOT	38% (30 M.S.)	200%-400% (5 M.S.)
ΔV	4550 fps	492 fps (M.C. + O.T.)

* 2 engines at orbit trim.

Table 4.3-12: CANDIDATE PROPULSION SUBSYSTEM CONCEPT NO. 3
BIPROPELLANT
ADVANTAGES AND DISADVANTAGES

ADVANTAGES
• Near-Existing Funded Components • Redundant System (With Complex Autopilot) • Clean Exhaust • Low Cost and Short Development Time • Engines Space Proven by '69 • Fully Ablative Engine (Orbit Insertion)--Low Thermal Load • Versatile System
DISADVANTAGES
• Complex Subsystem • High Thrust Level (Orbit Insertion) • High Inert Weight • Non-Permeable Expulsion Required

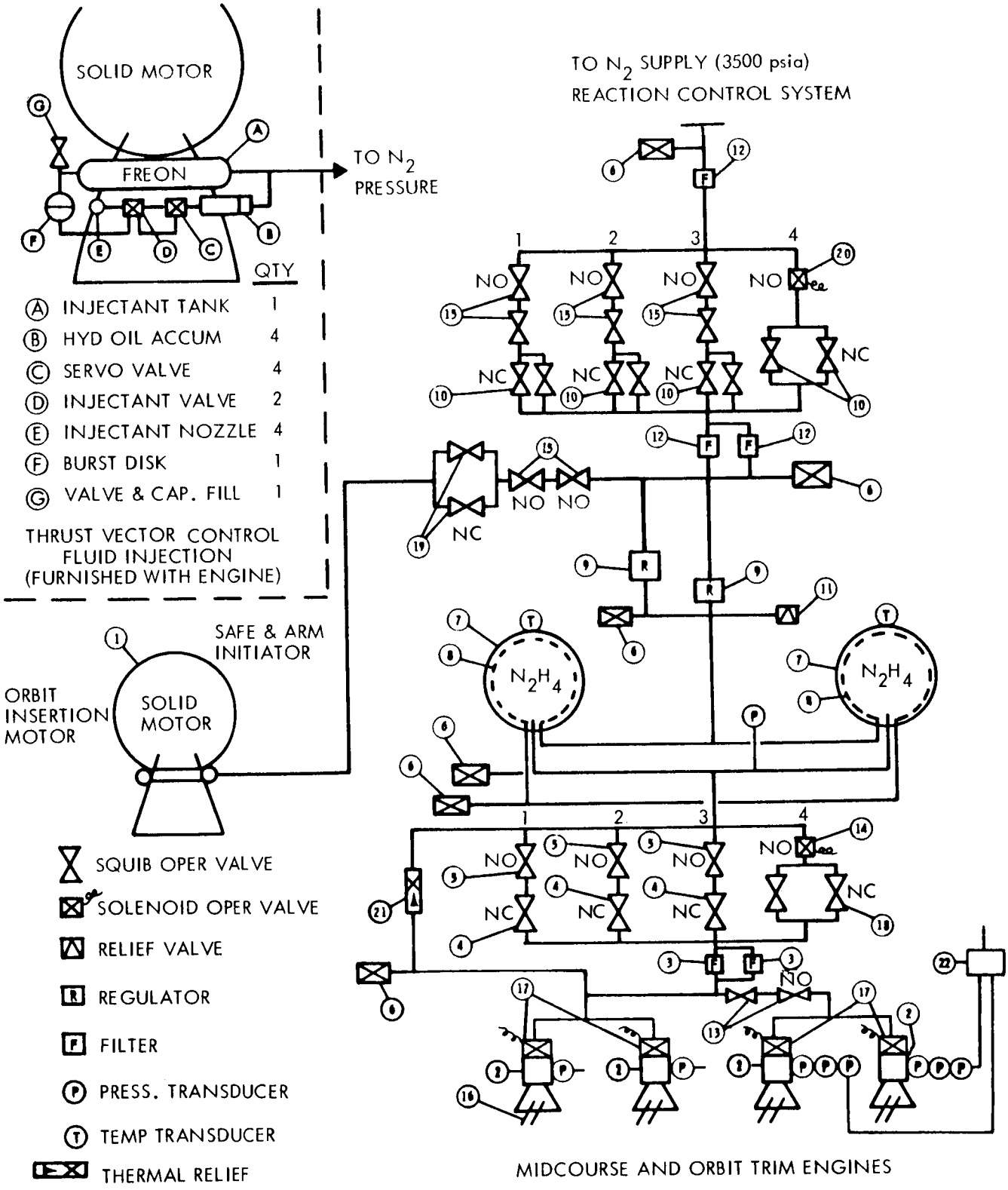

Figure 4.3-6: Solid/Monopropellant System — Concept No. 4

Table 4.3-13: COMPONENT LIST - CONCEPT NO. 4

ITEM	QTY	NAME
1	1	Rocket Motor (TVC)
2	4	Rocket Engine
3	2	Propellant Filter
4	3	N.C. Propellant Squib Valve
5	3	N.O. Propellant Squib Valve
6	6	Propellant Fill and Test Valve and Cap
7	2	Propellant Tank
8	2	Propellant Tank Bladder
9	2	N_2 Pressure Regulator
10	8	N.C. N_2 Squib Valve
11	1	N_2 Relief Valve
12	3	N_2 Filter
13	1	N.O. Squib Valve (Dual)
14	1	N.O. Latching Solenoid
15	4	N.O. Squib Valve (Dual)
16	16	Jet Vanes and Actuators
17	4	N.C. Solenoid Valve
18	1	N.C. Propellant Squib Valves (Dual)
19	1	N.C. TVC Isolation Squib Valves (Dual)
20	1	N.O. Latching Solenoid
21	1	Thermal Relief Valve
22	1	Malfunction Detection Signal Conditioner

of redundant regulators to minimize the leakage during the long coast periods. Regulated gas pressurizes the butyl bladders in the N_2H_4 tanks for midcourse and orbit trim maneuvers. Another series of isolation valves are installed downstream of the propellant tanks to minimize N_2H_4 leakage. The radiation-cooled engines are operated in pairs with a solenoid valve for each engine. By use of a switching logic circuit, a failure in one pair of engines will result in shutdown and subsequent switchover to the alternate pair. The engines contain the Shell 405 catalyst, which assures spontaneous decomposition at all temperatures down to the propellant freezing point.

The solid-motor secondary-injection Freon tank is pressurized by unregulated N_2 obtained from a tap-off just downstream of the N_2 isolation valve bank. A butyl bladder is utilized as a positive expulsion device. Four servo-operated modulating valves supply Freon 114B2 liquid to the four quadrant ports on the solid-motor exhaust nozzle as changes in thrust vector angle are required. The Freon tank is isolated from the gas supply by redundant squib valves to minimize the time that the system is under high pressure. Redundant gas shut-off squibs are fired at the conclusion of the solid motor firing to minimize N_2 leakage.

The solid motor is protected by a safe-and-arm device to prevent premature operation. An Alclo-iron igniter is activated on command from the CC&S to initiate the orbit insertion maneuver. Solid-motor thrust termination is by natural depletion. The monopropellant orbit trim subsystem compensates for ΔV errors caused by the small (about 0.6%) total impulse tolerance.

Subsystem and engine performance summaries and advantages and disadvantages are presented in Table 4.3-14 through -16.

Table 4.3-14: CONDIDATE PROPULSION SUBSYSTEM #4
SOLID & MONOPROPELLANT SYSTEM PERFORMANCE

SYSTEM PERFORMANCE:	MIDCOURSE CORRECTION	ORBIT INSERTION	ORBIT TRIM
MAXIMUM VELOCITY (FPS)	246	5700	328
MINIMUM VELOCITY (FPS)	0.00427	N.A.	0.0119
VELOCITY TOLERANCE (FPS)	0.00043		0.00119
ACCELERATION, MAX. (G'S)	0.0132	2.2	0.36
ACCELERATION, MIN. (G'S)	0.0128	2.2	0.34

PROPULSION MODULE PERFORMANCE:		
MANEUVER	MIDCOURSE CORRECTION AND ORBIT TRIM	ORBIT INSERTION
PROPELLANT	HYDRAZINE -- N_2H_4	SOLID PROPELLANT
SPECIFIC IMPULSE (SS) (SEC)	235	300(assumed)
TOTAL IMPULSE (LB-SEC)	92,825	694,106
MINIMUM IMPULSE BIT (LB-SEC)	1.0	N.A.
SHUTDOWN IMPULSE TOLERANCE (LB-SEC)	0.1	
NUMEER OF ENGINES	4	1
THRUST PER ENGINE (LBS)	50	7988
ENGINE OPERATING TIME (SEC)	928	90
THRUST VECTOR CONTROL		
MODULE INERT WEIGHT (LBS)		799
PROPELLANT WEIGHT (LBS)	395	2306
TOTAL MODULE WEIGHT (LBS)		3500
PROPELLANT TANKAGE	SEPARATE	SEPARATE (IN MOTOR)

Table 4.3-15: CANDIDATE PROPULSION SUBSYSTEM CONCEPT #4
SOLID AND MONOPROPELLANT
ENGINE PERFORMANCE

	SOLID PROPELLANT	MONOPROPELLANT
MODEL	NEW	NEW
MFG		
NO. USED	1	4
THRUST	7988 lb average	50 ± 1 lb
ENGINE BURN TIME	90 sec	928 sec
TOTAL IMPULSE	694,106 lb-sec	92,825 lb-sec
MAXIMUM THRUST/WEIGHT	2.2	0.36 (ORBIT TRIM)
ΔV	5700 fps (ORBIT INSERTION)	574 fps (MIDCOURSE AND ORBIT TRIM)

Table 4.3-16: CANDIDATE PROPULSION SUBSYSTEM CONCEPT NO. 4
SOLID AND MONOPROPELLANT
ADVANTAGES AND DISADVANTAGES

ADVANTAGES
• Simple System - High Reliability • Low Inert Weight - Good Performance • High System Density • Simple Autopilot--Short Burn Times • Minimum Prelaunch Operations • Sterilization Feasible
DISADVANTAGES
• Fluid Injection Thrust Vector Control Required • "Dirty" Exhaust

4.3.2.2 Completing Characteristics

Competing characteristics established for selection of the preferred propulsion design concept are:

1) Reliability;

2) Velocity increment capability;

3) Availability;

4) Interaction with the spacecraft (thermal, mechanical, electrical);

5) Versatility;

6) Cost;

7) Operational Complexity (service, checkout, number of ground-originated commands).

These provide the basis for a preliminary selection of the preferred design concepts as discussed below.

4.3.2.3 Selection Rationale

The velocity increment requirements for the spacecraft include a mid-course correction ΔV of 75 m/sec (246 fps) and an orbit trim ΔV capability of 100 m/sec (328 ft/sec). The 1971 orbit insertion ΔV requirements are indicated in Figures 4.3-7 and 4.3-8. With a fixed arrival date of 15 December 71, Figure 4.3-7 shows that the ΔV required to insert the spacecraft into an 18-hour orbit about Mars varies from 4075 to 4970 fps. This allows for a 50-day launch opportunity starting 7 May 71 and ending 26 June 71, and accommodates periapsis altitude variations about the nominal 2700 km (see D2-82709-1, Section 3.1). Launch dates prior to 7 May 71 are restricted because of launch azimuth and launch window limitations. Launches after 27 June 71 are restricted because of C_3 limitations. The orbit insertion engine capabilities

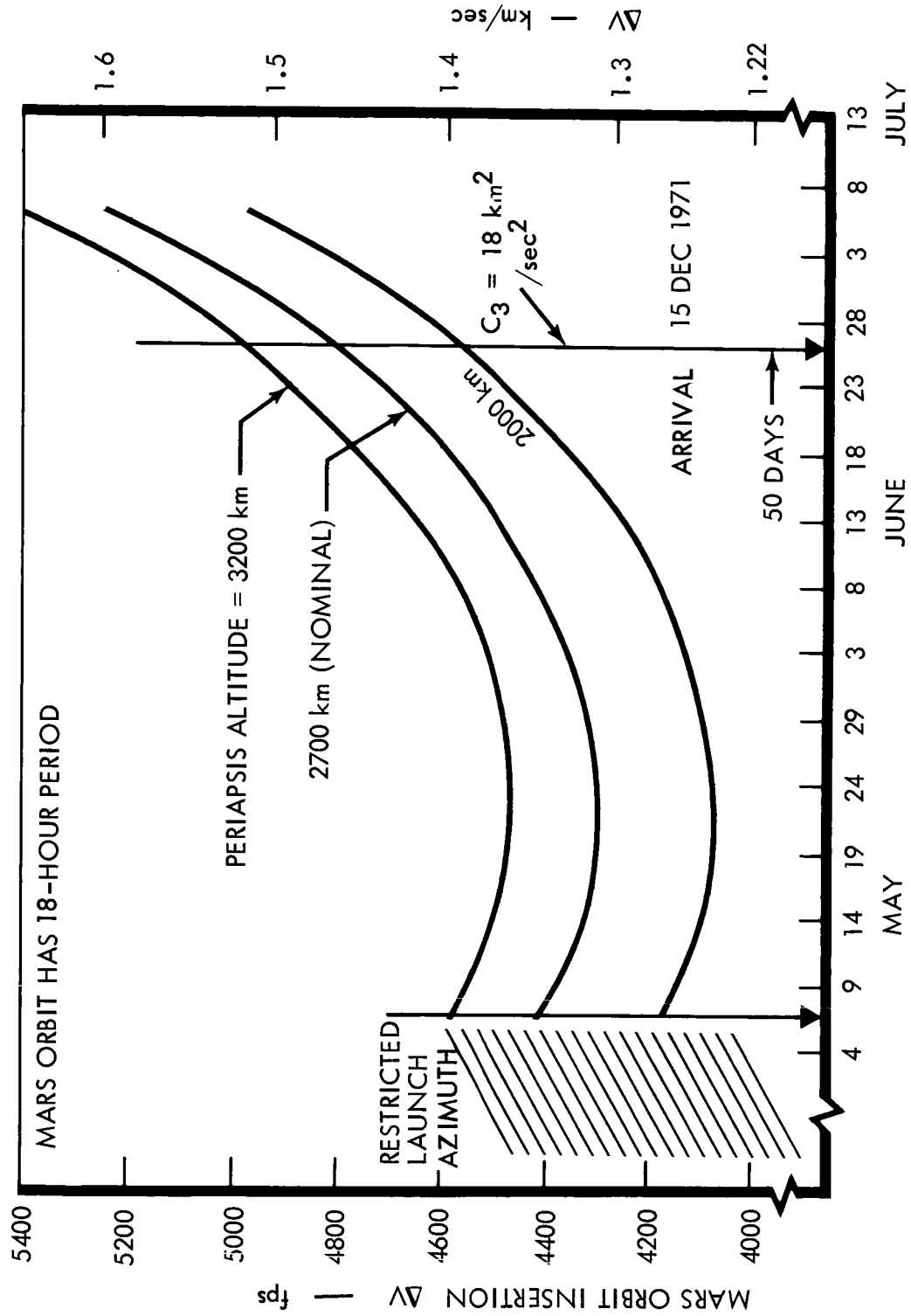

Figure 4.3-7: Orbit-Insertion Velocity Requirements — Fixed Arrival Date

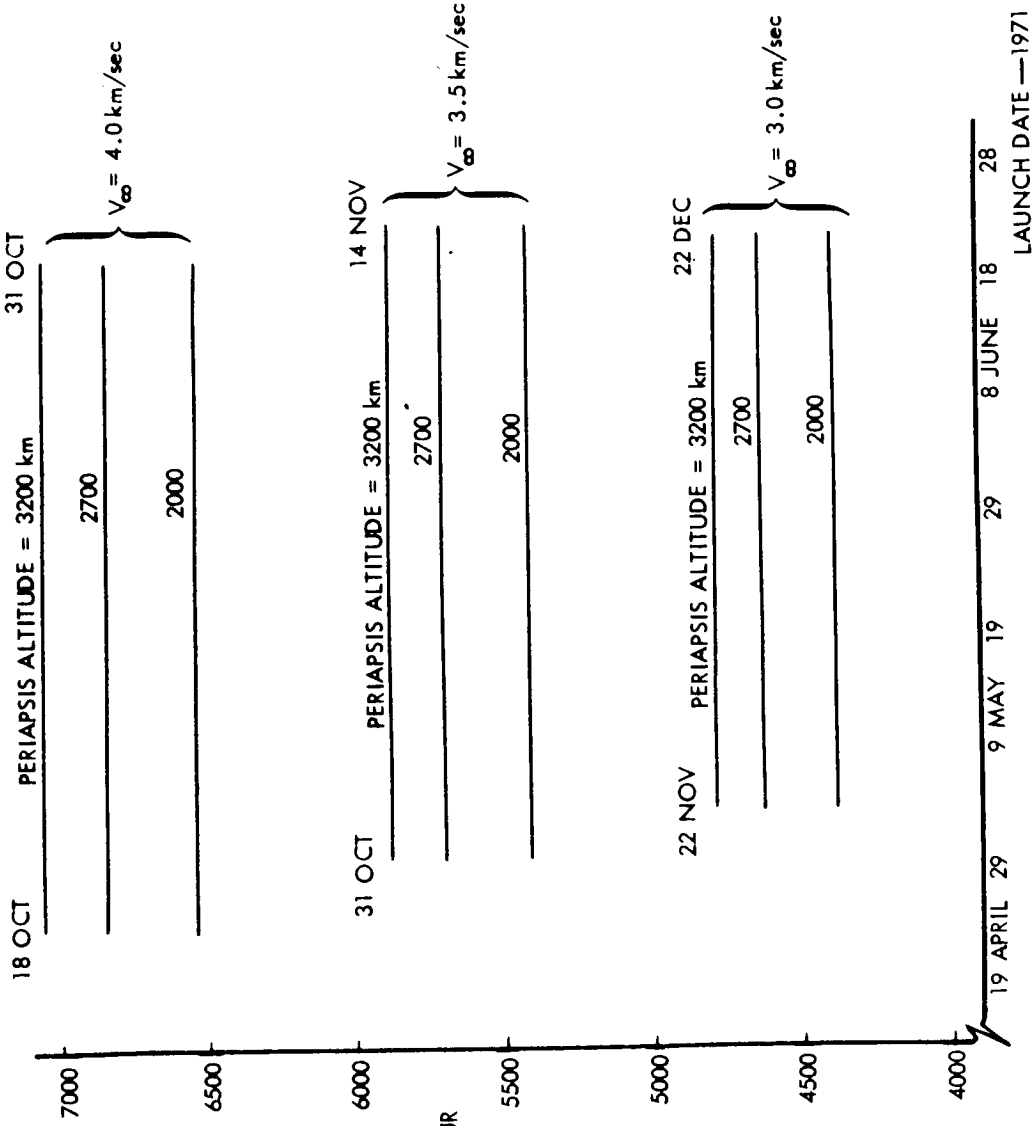

Figure 4.3-8: Orbit-Insertion Velocity Requirements — Fixed V_∞

must cover that required for the nominal periapsis altitude, 4300 to 4800 fps. The orbit-trim propulsion will provide the additional ΔV required by the off-nominal periapsis altitudes.

The orbit-insertion ΔV requirements for a variable arrival date are shown on Figure 4.3-8 for V_∞ of 3.0, 3.5 and 4.0 km/sec. A constant ΔV of 5700 fps, corresponding to a V_∞ of 3.5 km/sec, will provide an 18-hour orbit about Mars with an arrival date variation of 15 days over a launch opportunity of 55 days. Again, the orbit trim capability is adequate for periapsis altitude variations.

The 1973 orbit insertion ΔV requirements are shown on Table 4.3-17 and Figure 4.3-9. As shown, the ΔV required varies from a minimum of 4600 to a maximum of 5700 fps depending on the selected arrival date. The variable arrival date ΔV requirements are shown on Figure 4.3-9. A ΔV of 5700 fps allows an arrival date variation of 9 days for a 38-day launch opportunity with a V_∞ of 3.5 km/sec.

Orbit insertion velocity increment capability for all four candidate design concepts is shown and compared with requirements in Figure 4.3-10. Attendant reliability numbers are also indicated.

The weight data shown include allocations for a 100-m/sec orbit-trim-maneuver velocity increment and a midcourse maneuver velocity increment of 50 m/sec for the all-liquid bipropellant subsystems. (75 m/sec midcourse for the combination solid-liquid subsystem). The all-monopropellant hydrazine concept, No. 1, proved to have inadequate velocity

Table 4.3-17

1973					
Constant Arrival Date Missions					
Periapsis Altitude =2700 km			18-hour Period		
Arrival Date	First Launch Date	Last Launch Date	Max. ΔV (fps)	Min. ΔV (fps)	Launch Opportunity Days
26 Jan 74	10 Jul 73	13 Aug 73	5700	5300	35*
8 Feb 74	27 Jul 73	15 Aug 73	4700	4600	26

* Increasing the launch opportunity by 2 days requires 200 fps additional ΔV.

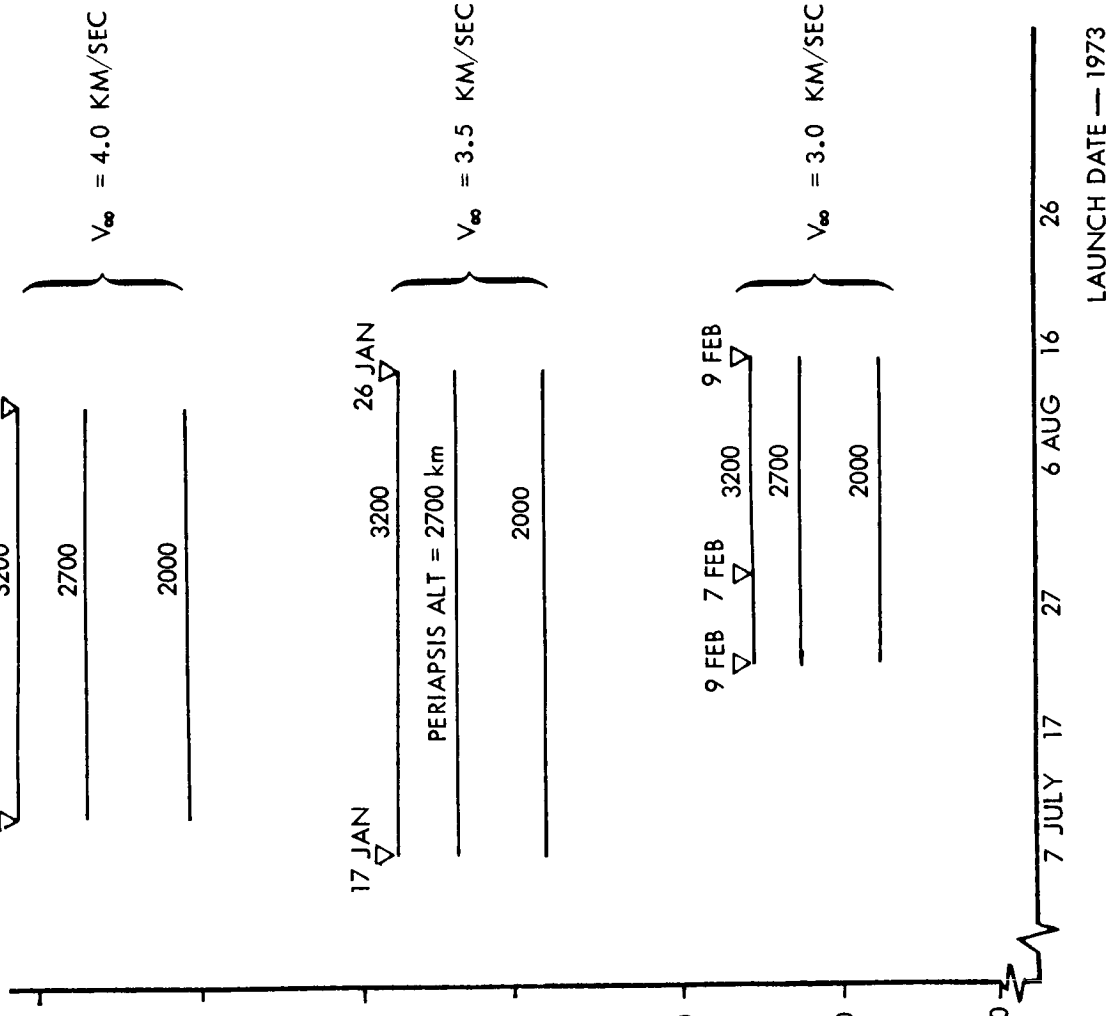

Figure 4.3-9: Orbit Insertion Velocity Requirements — Fixed V_∞

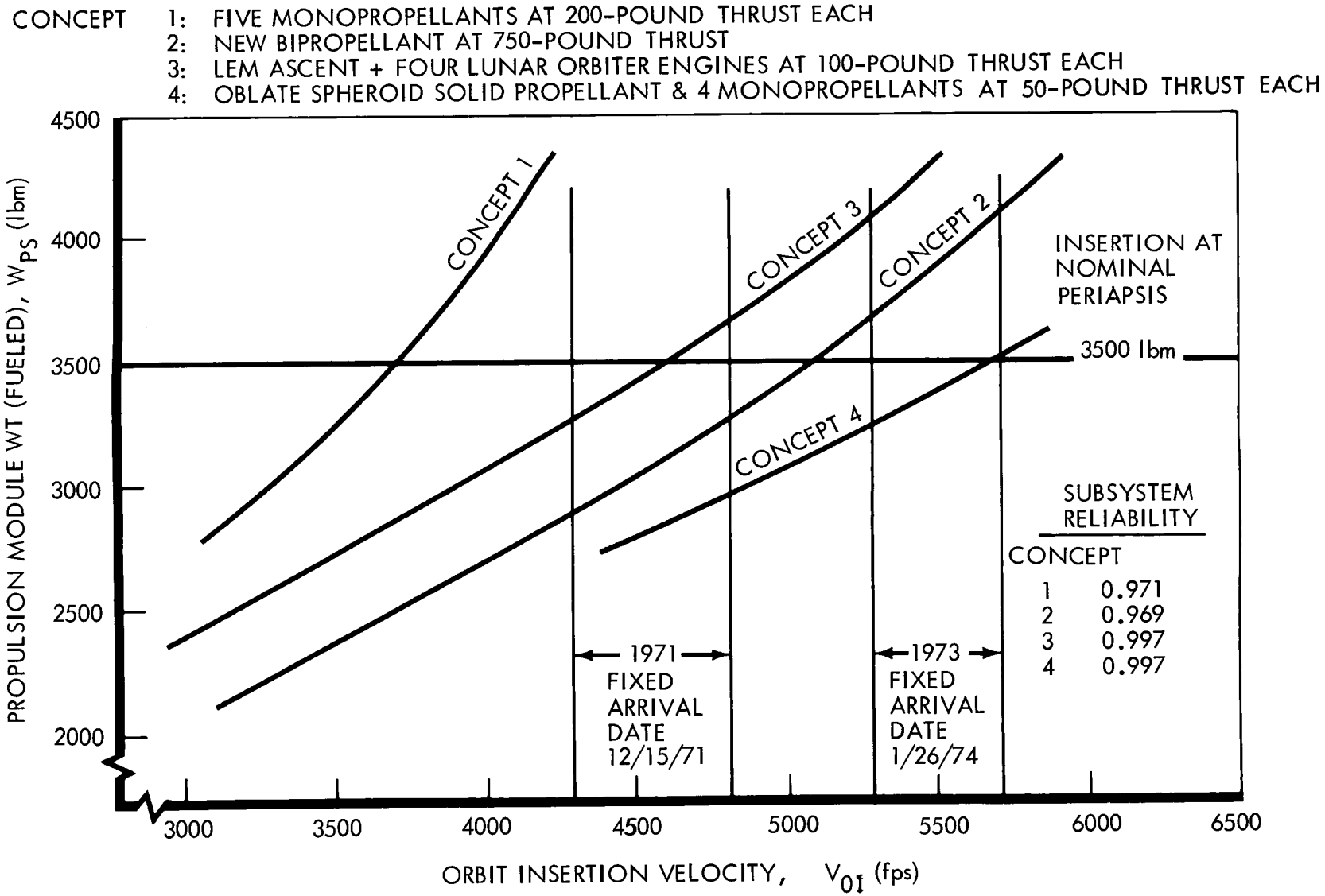

Figure 4.3-10: Orbit Insertion Velocity Capability: Candidate Concepts

performance, yielding only a 3,660 fps orbit insertion capability. This was due to the relatively large inert weight (1,120 pounds) and low specific impulse of 235 seconds. The all-bipropellant, concept No. 2 and the combination solid-liquid propellant concept were shown to have sufficient performance potential for 1971. The all-bipropellant concept No. 2 could provide a 5,063 fps orbit-insertion velocity due to its specific impulse capability of up to 315 seconds, though module inert weights were still relatively large (1,085 pounds). The combined system No. 4, yielded an orbit insertion velocity capability of 5,700 fps due to the lower inert weights (799 lbs) and in spite of the slightly lower specific impulse value of 300 (assumed) seconds.

The solid/monopropellant concept was the one capable of meeting the velocity requirements for both 1971 and 1973 opportunities.

The solid-monopropellant concept No. 4 was selected as the preferred design on the basis of being the only concept able to perform the 1971 and 1973 missions within the 3500 pound propulsion system weight restriction. However, in subsequent sections both the preferred high performance solid-monopropellant, No. 4, and the more available all-bipropellant concept, No. 3, will be discussed.

4.3.3 Solid-Monopropellant Concept

The solid motor and monopropellant subsystem components analyses and trade studies are described below:

4.3.3.1 Solid Motor Components

Propellants--

Candidates--The following general solid propellant formulation types were considered: polyurethane, polysulfide, double base, polybutadiene and several experimental propellants. Fuel additives included aluminum and beryllium.

Competing Characteristics--The primary solid propellant selection competing characteristics are:

1) Demonstrated reliability;
2) Availability;
3) High performance (specific impulse);
4) Usefulness over a fairly wide temperature range;
5) Space storability;
6) Ease of heat sterilization.

Selection Rationale and Discussion--The polyurethane, polysulfide, double base and the experimental propellants were rejected for the following reasons:

1) Polyurethane - Susceptible to binder crystallization at low temperatures and exhibits plasticizer volatility at high temperatures. (30^{o} to 100^{o}F. maximum operational limits);
2) Polysulfide - Low performance characteristics (Isp std~215 $\frac{\text{lbf - sec}}{\text{lbm}}$);
3) Double Base - Class 9 propellant. Also tends to degrade under space storage conditions;
4) Experimental Propellants - All rejected because they have not demonstrated their reliability.

Thus the only propellants left for further consideration were the polybutadiene with and without additives.

Nonmetallized solid propellants have in tests to date demonstrated a better heat cycle sterilization capability than propellants containing aluminum. For this reason, and because of their low plume radiosity characteristics, they were considered. However, calculations indicate that, because of their low specific impulse, the propulsion system weight penalty would be 750 pounds. This was considered excessive and nonmetallized propellants were discarded.

Accounting for both the increased specific impulse and reduced density of beryllium-containing propellants, a propulsion system weight saving of 140 pounds can be made. Beryllium propellants have been demonstrated in many subscale and full scale tests and are generally considered state of the art. The primary disadvantages to beryllium are its toxic exhaust, which complicates handling and static test requirements; high nozzle throat erosions have characterized many tests, heat-cycle sterilization has not been demonstrated; and plume radiation is high. Beryllium propellants are considered to be an excellent backup and offer the propulsion system good growth potential for post-1971 missions; however, the use of beryllium propellants at this time would lower the system reliability.

In summarizing, the nonmetallized propellants were eliminated because of their poor performance. The beryllium propellants were rejected because the high reliability required of the solid motor has not yet been

demonstrated with beryllium. The double-base, polysulfide and polyurethane classes of propellant were rejected for poor space storage capability, low performance and limited operational temperature limits, respectively.

The preferred aluminized polybutadiene propellant, ANB-3066, was developed by Aerojet for the Minuteman program and is used in both development and production motors. To date, no failures have been attributed to this propellant. Over 4,000,000 pounds of polybutadiene propellants have been produced for Minuteman, Polaris, Sparrow, Genie, and Sprint motors. This propellant was selected because it has demonstrated high reliability, is safe to handle, has a wide operational temperature range, has demonstrated good space storage capability, and delivers a high specific impulse.

Heat cycle sterilization of a full-scale motor containing aluminized propellants, followed by a successful firing, has not yet been demonstrated. Subscale motors and propellant samples indicate that heat-cycle sterilization is feasible in a solid propellant motor. Both Aerojet and Thiokol have successfully sterilized and fired subscale motors. The propellant selected is especially formulated for wide temperature cycling and is therefore considered a candidate with the basic characteristics suitable for demonstrating sterilization capability. However, it is anticipated that some propellant binder reformulations will be required. These modifications are not considered sufficiently significant to modify the motor design.

Motor Case--

Description--The three general configurations considered were cylindrical, spherical, and ellipsoidal (oblate spheroid).

Competing Characteristics--The following competing characteristics have been considered in the selection of the preferred motor case geometry and case material:

1) High total impulse (total propellant volume and nozzle expansion ratio);
2) Availability and experience;
3) Inert weight;
4) Exhaust Plume (radiation and particulate contamination);
5) Adaptability to thrust vector control;
6) Cost.

Selection Rationale and Discussion--Because of the length limitations, the cylindrical shape was eliminated immediately. The spherical and ellipsoidal motors (Figure 4.3-11 and -12) initially appeared competitive. However, careful evaluation with regard to spacecraft compatibility indicates there are several important advantages associated with the ellipsoidal design. This design with its naturally smaller minor axis, in a length-limited rocket, results in a longer nozzle with a higher expansion ratio. As a result the ellipsoidal motor delivers a higher total impulse with a smaller propellant loading, as shown in the following.

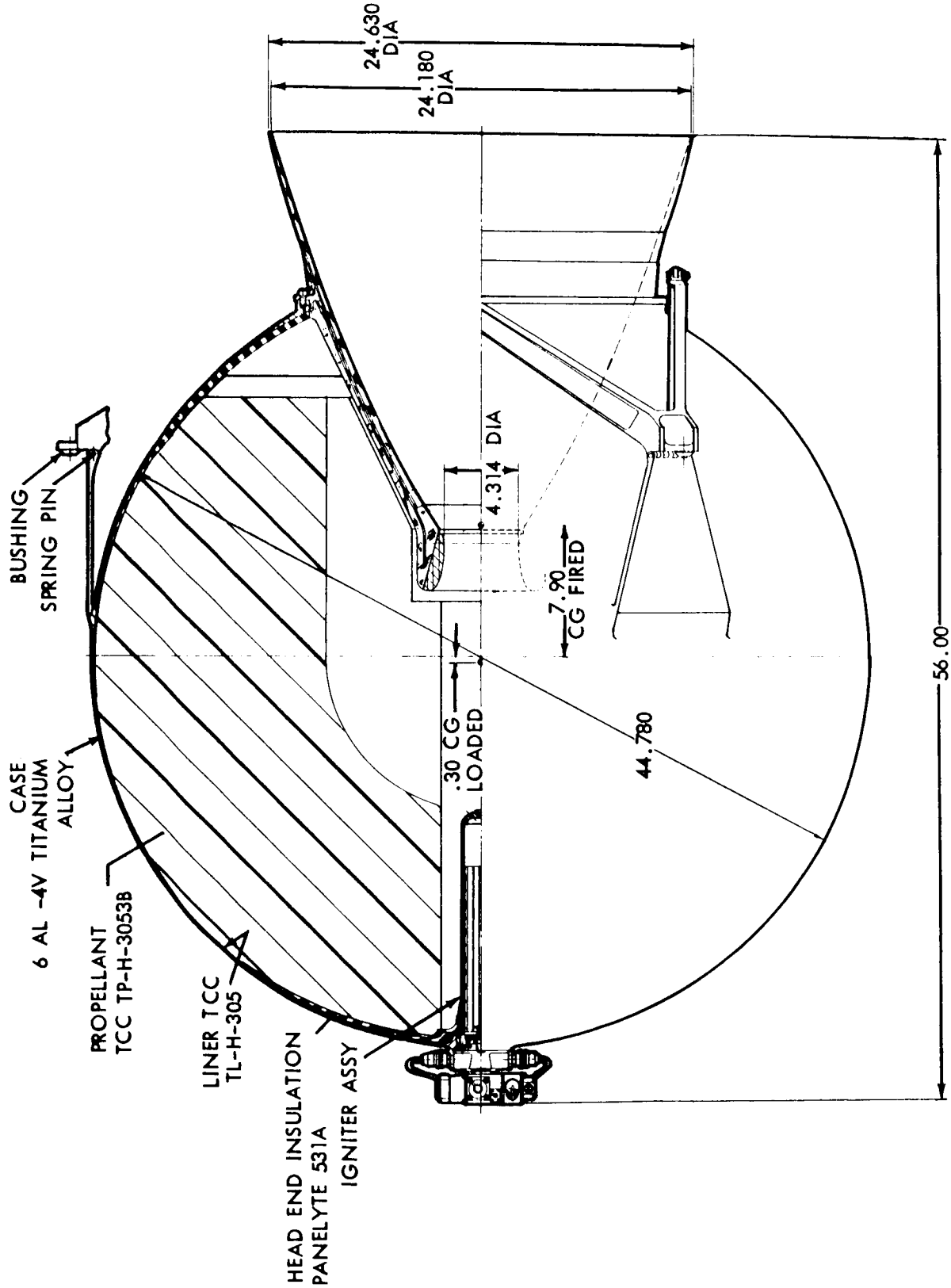

Figure 4.3-11 : Voyager Orbit Insertion Motor — Spherical Concept

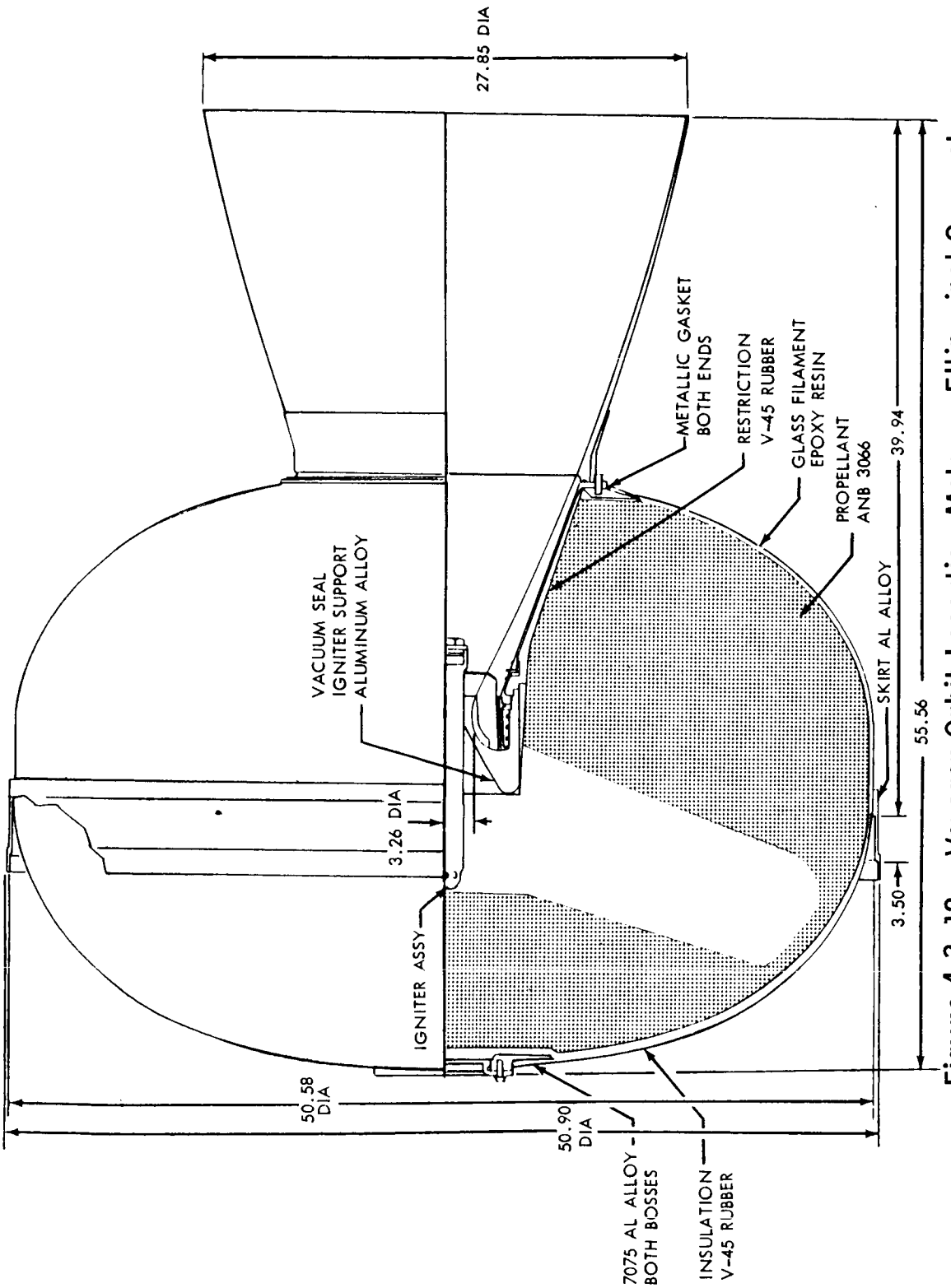

Figure 4.3-12: Voyager Orbit Insertion Motor — Ellipsoipal Concept

	Spherical	Ellipsoidal
Total Impulse (lbf-sec)	706,260	725,440
Nozzle Length (in.)	23.78	35
Nozzle Expansion Ratio	31	73
Wp (lbm)	2511	2378

Another advantage of the longer nozzle with the higher expansion ratio is the cooler exhaust products. Calculations have been made considering two-phase flow, utilizing radiosity readings recorded on Surveyor and Minuteman second-stage tests in an altitude chamber. The results indicate the maximum solar panel heating rate from the longer nozzle's plume is about one-third of that from the plume of the nozzle on the spherical motor (see D2-82709-2, Section 4.4.1). Hence, the heat-shield weight (about 240 pounds) required to protect the spacecraft and the solar panels during a spherical-motor firing can be reduced to 107 pound (spacecraft heat protection only) when the ellipsoidal motor is used. One additional disadvantage resulting from use of the spherical motor is associated with exhaust product deposition on the spacecraft. With the Prandtl-Meyer expansion angle approximately 11 degrees greater than this angle for the spheroidal motor, the probability of exhaust product deposition on the spacecraft is higher.

Figure 4.3-13 compares the delivered velocity performance of the spherical and spheroidal motors. The reduced heat shield weight, combined with the ellipsoidal motor's 21-lbf-sec/lbm specific impulse advantage, results in a propulsion subsystem weight for the ellipsoidal motor which is 300 pounds lighter than the spherical in the region of interest.

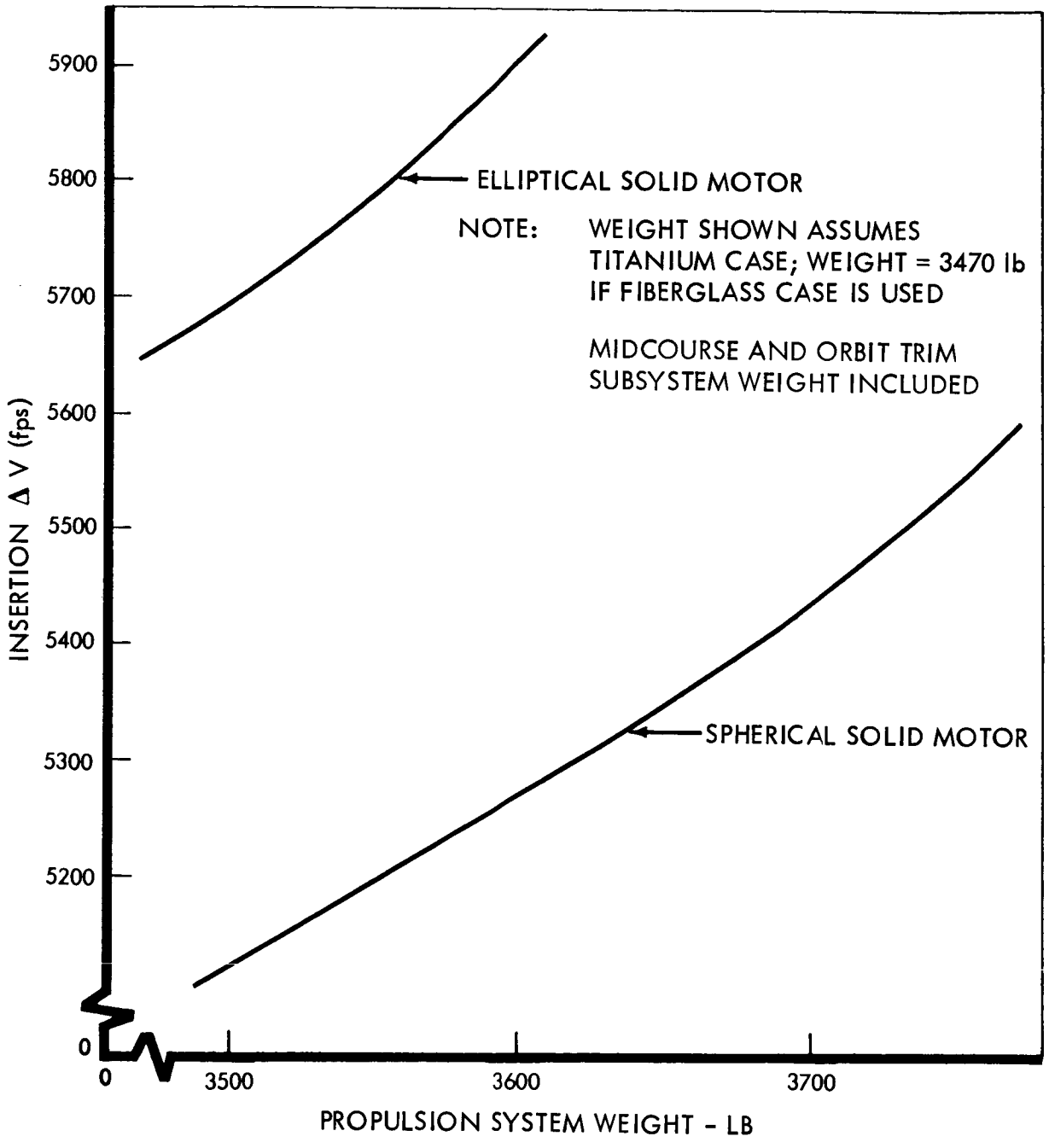

Figure 4.3-13: Solid Motor Velocity Performance Comparison

The deep submergence of the nozzle on the spherical motor would compromise the use of a secondary-injection TVC system. Injection would have to occur at the 60 percent nozzle expansion ratio section. This results in a 45 percent injection fluid weight penalty. The nozzle on the elliptical motor, on the other hand, was found compatible with injection at the optimum 40 percent nozzle expansion ratio section.

The elliptical motor incorporates a short cylindrical section between the domes, permitting 532 pounds of additional propellant-loading capability without shortening the nozzle. The spherical motor cannot carry more propellant without reducing nozzle length.

In summary, evaluation of the two primary motor shapes indicates that either can be adopted. However, the ellipsoidal motor velocity has performance and vehicle compatibility characteristics superior to the spherical one. The ellipsoidal motor has been selected for the Voyager mission.

Confidence in the successful development and reliable operation of this motor is based on the proven reliability of each element of design as follows:

1) Propellant - The ANB-3066 propellant is a fully developed and qualified propellant in use on the operational Wing VI Minuteman.
2) Nozzle - The materials and submerged nozzle concept are identical to that used on the Minuteman.
3) Elliptical Case Sections - Elliptical forward and aft fiberglass domes of identical shape are used on both the Polaris and Minuteman. (Titanium can be substituted for fiberglass for a 30-pound weight penalty.)

4) Grain Design - The conocyl grain design has been successfully demonstrated on Skybolt.

5) Igniter - The Alclo-iron igniter is used in the Polaris missile.

Thrust Vector Control--

Description--Thrust vector control is required during the solid retro operation to compensate for thrust misalignment and center-of-gravity offset. Six systems were considered: 1) gimbal the monopropellant motors, 2) jet vanes in the monopropellant exhaust, 3) pulse the small monopropellant motors, 4) gimbal the whole solid motor, 5) gimbal the nozzle, and 6) liquid secondary injection.

Competing Characteristics--The criteria used for selection were:

1) Demonstrated reliability;

2) Sterilizability;

3) Compatibility with spacecraft dynamics;

4) Space Storage Capability;

5) Weight;

6) Safety.

Selection Rationale and Discussion--Gimbaling the monopropellant motors or inserting jet vanes into the monopropellant exhaust were studied and found deficient in control authority.

Attitude control during the main retrofiring can be achieved by pulsing the monopropellant midcourse-orbit trim engines. This system was found

to be one of the lightest studied. For a typical duty cycle, the weight chargeable to TVC on the pulse monopropellant system is approximately 25 pounds for the engines operated in the normally-off mode and 90 pounds for the normally-on mode. A functional block diagram of an autopilot employing these engines operated in the normally-on mode is shown in Figure 4.3-14. Of concern is the effect of the response characteristics of the monopropellant engines on control-system limit cycle stability. The range of expected obtainable response characteristics for the engines considered is shown in Figure 4.3-14. An analog simulation of this system, using the maximum delay times of the engine response, indicates that this system is stable for a maximum lateral center of gravity offset of 0.35 inch and thrust angular misalignment of 0.25 degrees. An example of the system performance is shown in Figure 4.3-15 for the 3σ tolerances on center of gravity offset (Volume A, Section 3.1) and thrust misalignment. The thrust vector pointing error of 0.4 degrees is well within the allocation given in Volume A, Section 3.8.

Using the monopropellant engines for orbit insertion TVC results in additional heating loads to the solar panels. Moreover, this concept has not been flight proven to date. Consequently, this concept has been discarded as the primary control mode, but is considered as an adequate backup method.

Gimbaled Motor--Gimbaled motor designs are relatively heavy and impose severe design constraints on the thrust vector autopilot. Maximum thrust vector rate and position limits are severely limited because of the large size and mass of the engine. Actuator load requirements are high. During

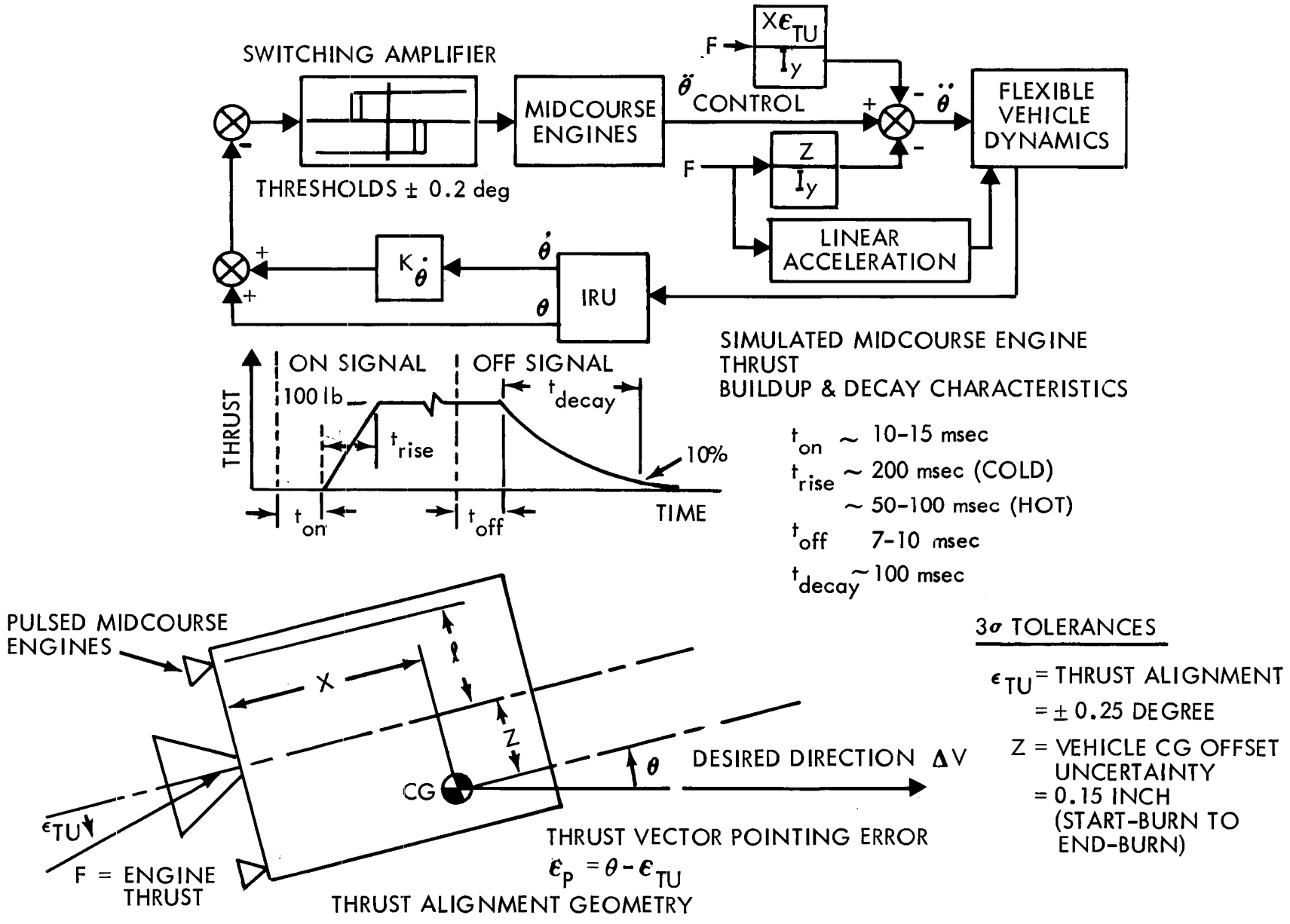

Figure 4.3-14: Pulsed Midcourse Engine TVC Autopilot — Orbit Insertion

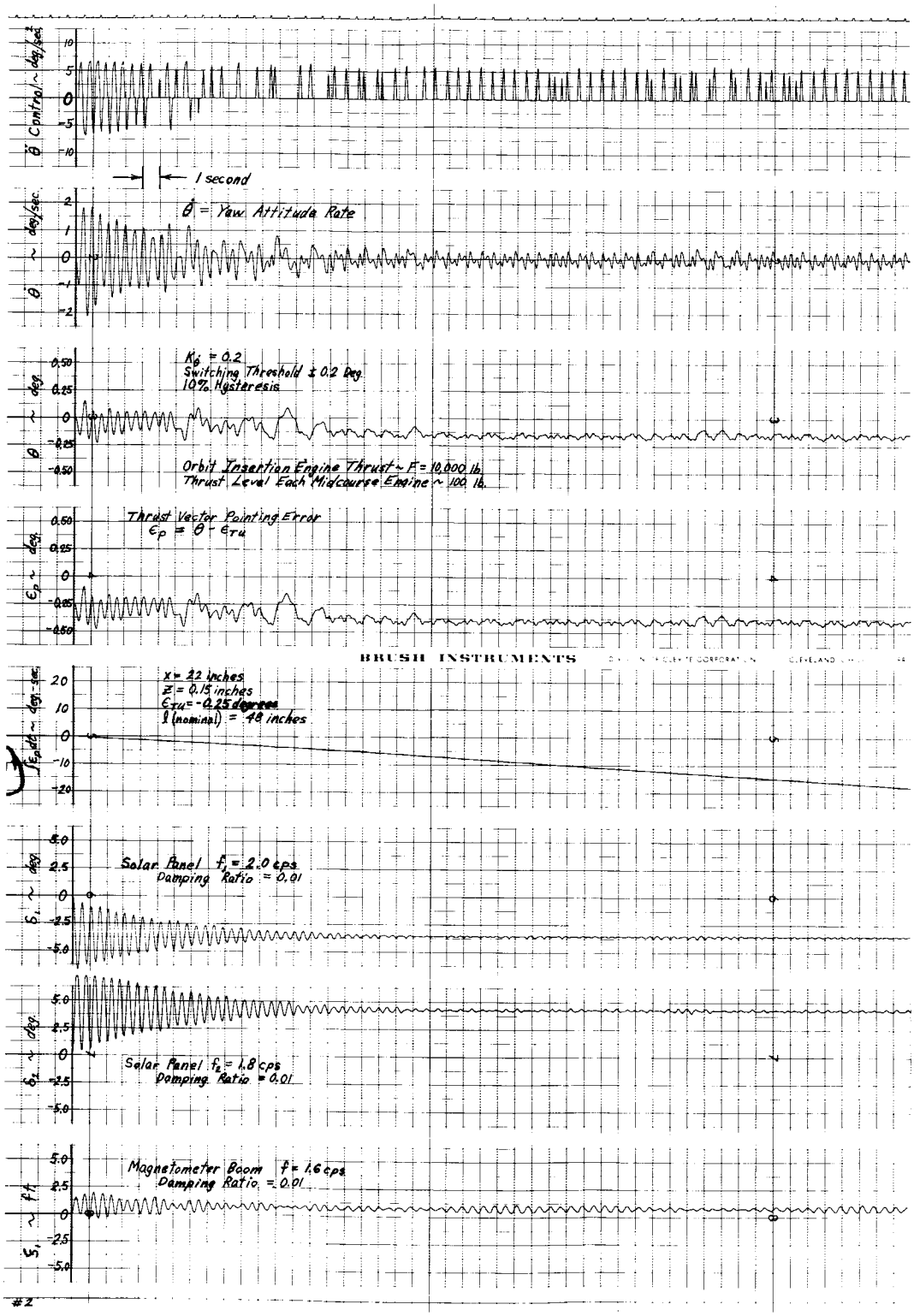

Figure 4.3-15: Start-Burn Time Response Pulsed Midcourse Engine TVC — Orbit Insertion

engine burning, the frequency of control reversal (tail-wags-dog frequency) sweeps through the range of natural frequencies of the solar panels. Complex filter networks are therefore required to prevent autopilot instability in this frequency range. This concept was rejected.

Gimbaled Nozzles--Submerged nozzles with dual axis gimbal capability have been demonstrated on experimental programs. To date, no operational system uses this technique. For this reason, gimbaled nozzles were rejected.

Liquid Secondary Injection--LITVC systems are currently being used on Polaris A2, Minuteman Wing VI second stage, HiBEX, Sprint first stage, Lance, and Titan III-C Solid. The primary performance advantages of secondary injection are high valve response rate and ability to modulate the thrust vector. Disadvantages are thrust vector angle limitations and moderate inert weight penalty. Analyses indicate, however, that large angles are not required. The reliability of such a system has been proven in all the above programs. Three injectant fluids were considered in mechanizing this concept:

1) N_2O_4;

2) Hydrazine;

3) Freon 114B2.

Reactive liquids such as N_2O_4 and N_2H_4 offer higher amplification factors (side force per unit mass). Freon, however, has been more widely used to date. N_2O_4 is used on the booster stage of the Titan III-C, while hydrazine has been adopted for Lance.

N_2O_4 possesses a high bulk density, as well as a high amplification factor. In addition, it can be stored in standard steel tanks. However, an acceptable expulsion device capable of long-term space storage and compatible with N_2O_4 has not yet been fully developed. Also N_2O_4 delivers an oxygen-rich mixture, which reacts with fuel-rich exhaust and increases nozzle erosion rates.

Hydrazine is an attractive monopropellant injectant because it is highly exothermic. Erosion problems are less severe than with N_2O_4 because of its fuel-rich products. It has a lower bulk density, requiring larger tankage.

Freon 114B2 exhibits the following characteristics:

1) Sterilization -- Freon may be heat-cycle sterilized in a heavy-weight ground-based system. Similarly, the dry secondary injection system may be heat-soak sterilized and loaded aseptically with Freon.
2) Reliability -- The reliability of the Freon liquid injection system has been flight demonstrated.
3) Safety -- Freon 114B2 is a dense, inert liquid at normal temperature conditions ($< 117^{\circ}$ F). Upon decomposition, approximately 800° C, the maximum allowable toxicity concentration is 0.1 parts/million.

Weight and performance data for a typical LITVC duty cycle, using Freon 114B2 hydrazine and N_2O_4 are shown in Table 4.3-18.

Table 4.3-18: SECONDARY INJECTION TVC SUMMARY

INJECTANT	FREON 114B2		N_2O_4		HYDRAZINE
Pressurization System	Gas Generator	GN_2 Blow-Down	Gas Generator	GN_2 Blow-Down	GN_2 Blow-Down
Injector Pressure	750 psi	1300 to 1500 psi	750 psi	3000 psi	3000 psi
Injectant Weight (lb.)					
Useable	56	56	31	31	28
Residual	5	5	4	4	4
TVC System Wt. (lb.)	100	108	77	82	81
Side I_{sp} (sec.)					
at 3^o	107	107	204	204	224
at $.8^o$	153	153	244	244	268
Space Storable	Yes		Yes		Yes
Toxicity (Max. Allowable Conc)	If decomposes .1 part/million		5 parts/million		1 part/million

In summary, gimbaled motors and nozzles were eliminated because of weight and dynamic cross-coupling, and unproven reliability, respectively. Pulsed midcourse monopropellant engines are considered as an acceptable alternate to the preferred scheme. Hydrazine and N_2O_4 secondary injection systems were rejected because of their limited demonstrated capability. Freon 114B2 secondary injection was selected as the preferred design for the following reasons:

1) Demonstrated reliability (Minuteman second stage, Polaris A2, HiBEX and Sprint);
2) Space storability and sterilizability;
3) High frequency response characteristics required for quickly stabilizing vehicle during ignition;
4) Safety;
5) Moderate weight penalty.

The duty cycle used in the TVC sizing analyses is shown in Figure 4.3-16. This curve is based on calculations that indicate that the maximum lateral center-of-gravity offset will not exceed 0.15 inches and that the nominal thrust vector angularity will be less than .25 degree. The minimum distance between the thrust vector trunnion point during secondary injection and the spacecraft center-of-gravity during burning will range from 18 to 22 inches. For preliminary calculations, 20 inches was used in the design. (see Figure 4.3-17) The valves are sized for a maximum deflection angle of 3 degrees, which was found adequate for quickly stabilizing the vehicle following retro ignition. The secondary injection system will operate between 1300 and 1500 psi. Between 3 and 4 pounds of nitrogen from the main nitrogen supply (60 pounds total) will be required for secondary injection pressurization. The injectant weight

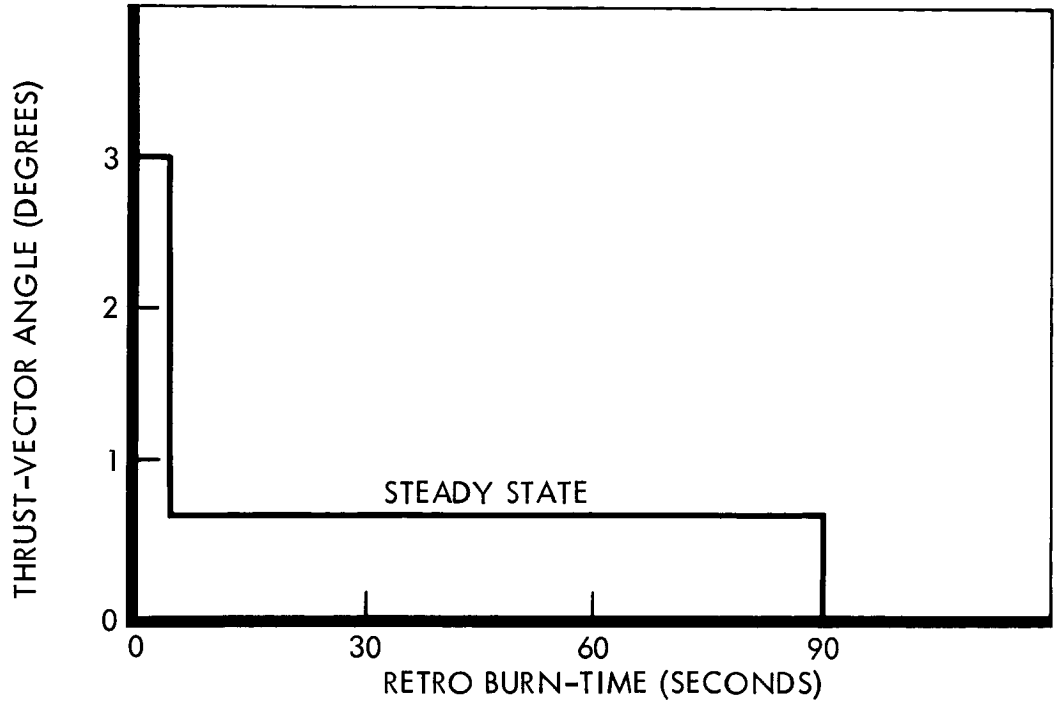

Figure 4.3-16: Solid Retro Secondary-Injection Duty Cycle

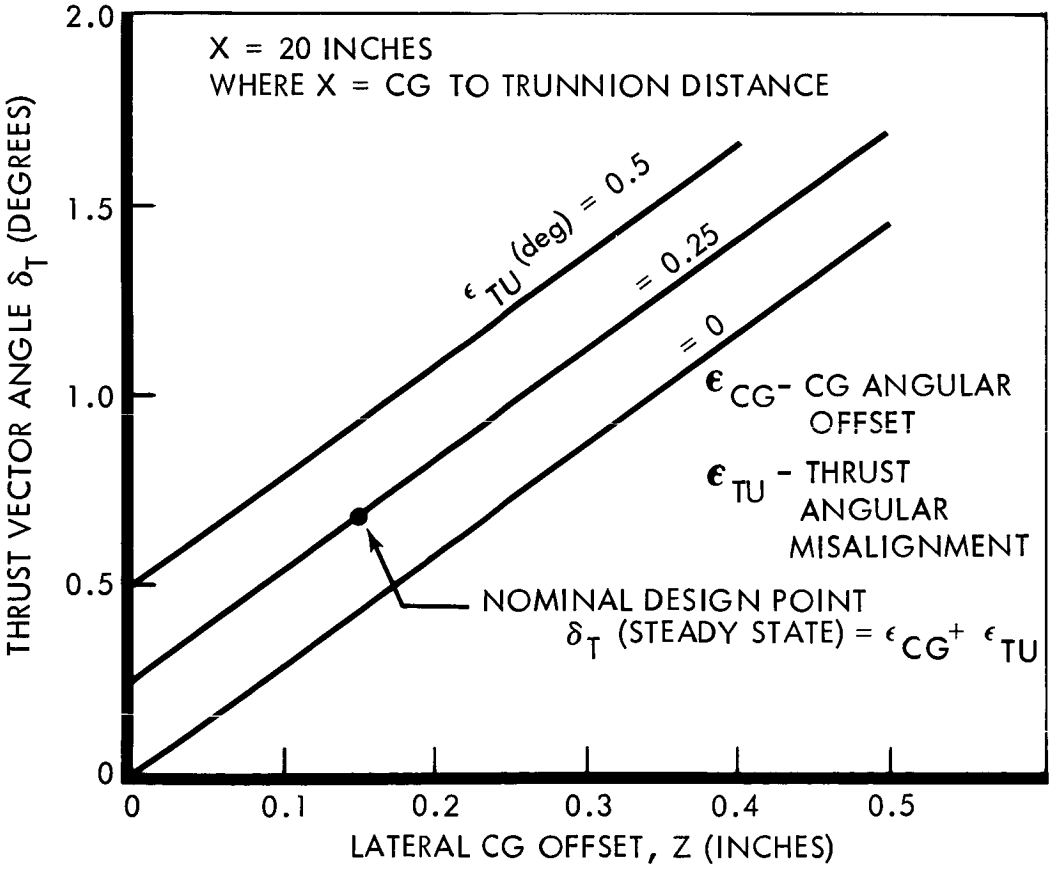

Figure 4.3-17: Secondary-Injection Steady-State Duty Cycle

flow required to satisfy the duty cycle was derived from Figure 4.3-18. This curve is a compilation of test data, reduced to parametric form, from the following sources:

1) Aerojet second stage Minuteman;

2) Thiokol research tests;

3) Lockheed Polaris;

4) Boeing HiBEX.

With a 10 percent safety factor assumed, the total loaded Freon 114B 2 required is 61 pounds. Total system weight is 108 pounds.

A functional block diagram of the autopilot considered is shown in Figure 4.3-19. Shown in Figure 4.3-20 is an example of the transient following engine ignition, corresponding to the 3σ tolerances on center-of-gravity offset and thrust misalignment (start burn to end burn). The high response rate of this system provides high damping of the solar panel motion. Due to the axial motion of the center of gravity during engine burning, the thrust vector pointing error will vary from 0.52 to 0.62 degrees, well within the previously-noted allocation. The effect of blow-down on the secondary injection Δp will not significantly alter the autopilot loop gain during engine burning (see Figure 4.3-18).

Thrust Level

Description--The following two thrust time traces were considered; neutral and regressive.

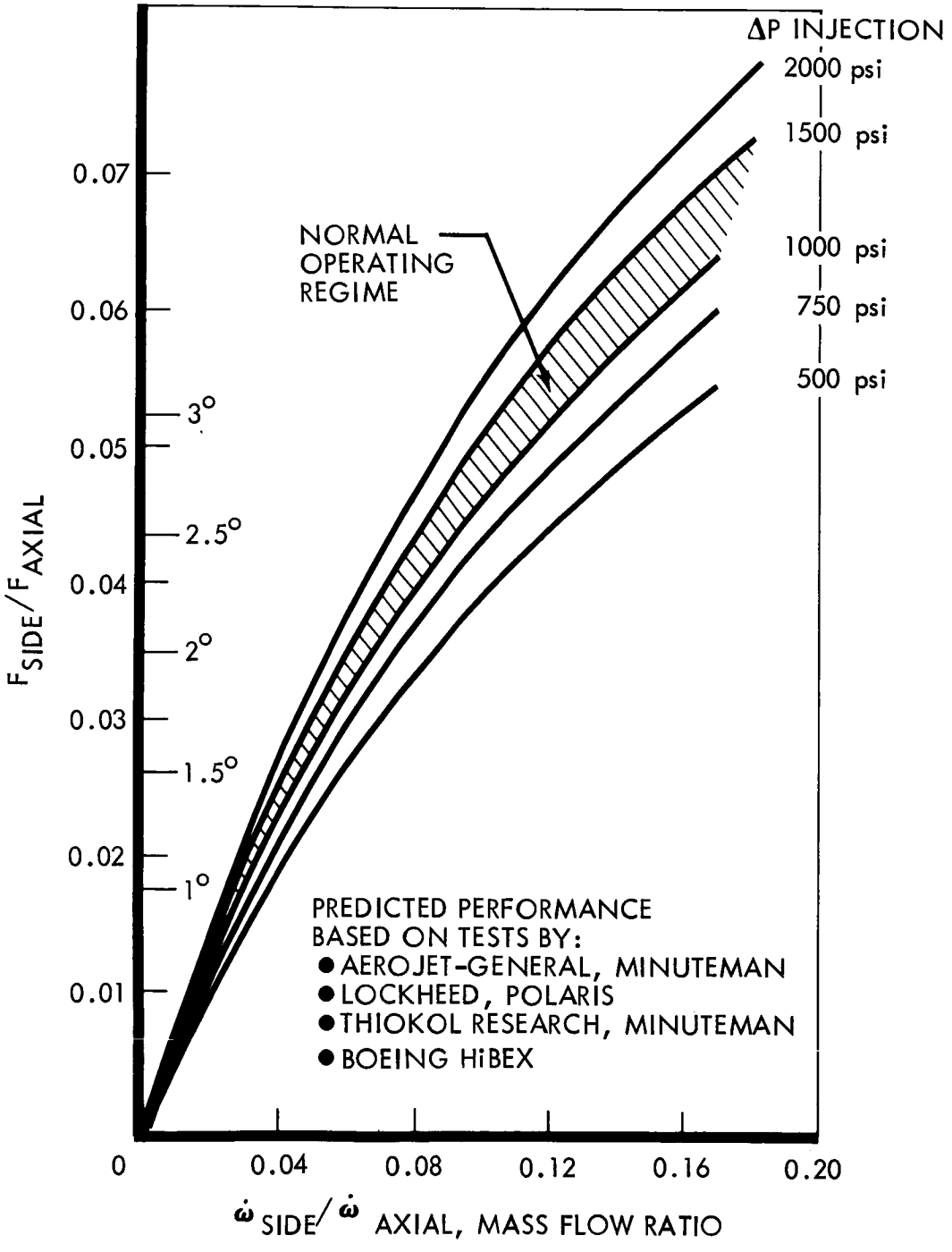

Figure 4.3-18: TVC Performance — Freon 114 B2

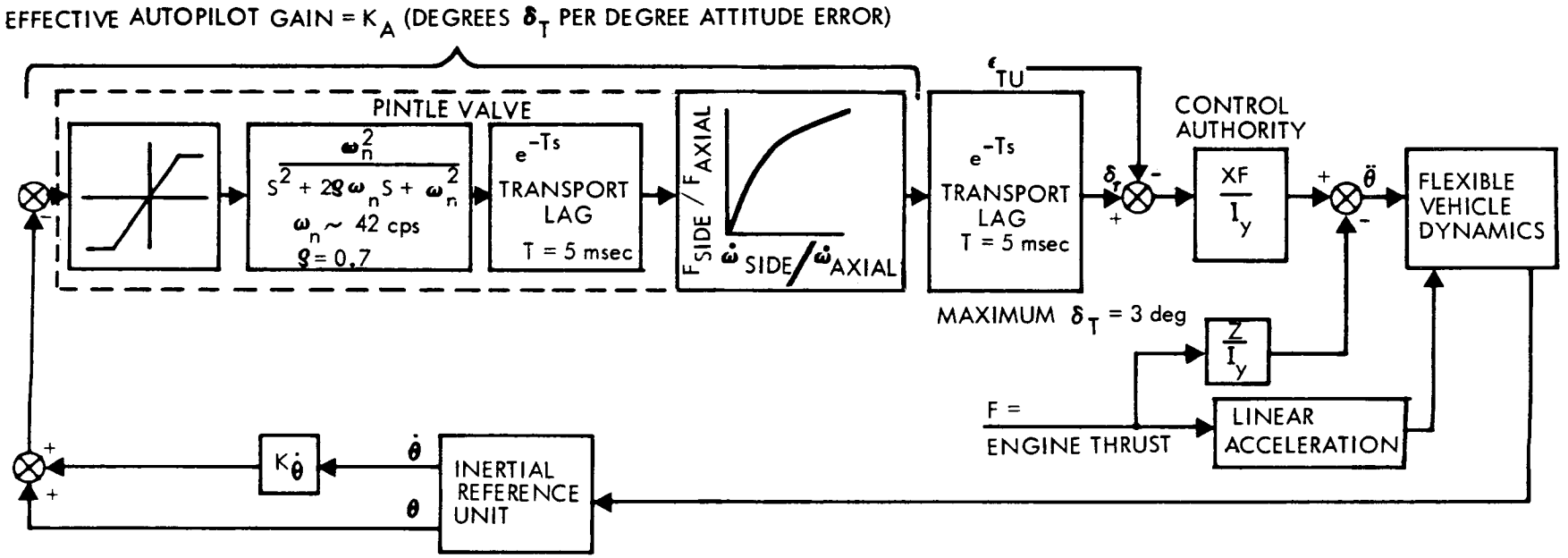

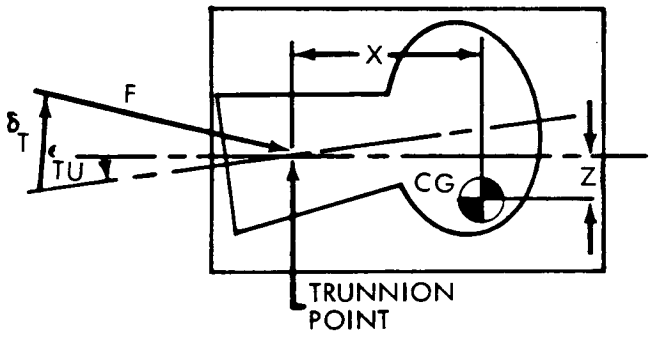

THRUST-ALIGNMENT GEOMETRY

3 σ TOLERANCES

ϵ_{TU} = THRUST-ALIGNMENT UNCERTAINTY
= $\pm$ 0.25 DEGREE

Z = VEHICLE CG OFFSET UNCERTAINTY
= $\pm$ 0.15 INCH (START-BURN THROUGH END-BURN)

Figure 4.3-19: Secondary-Injection TVC Autopilot — Orbit Insertion

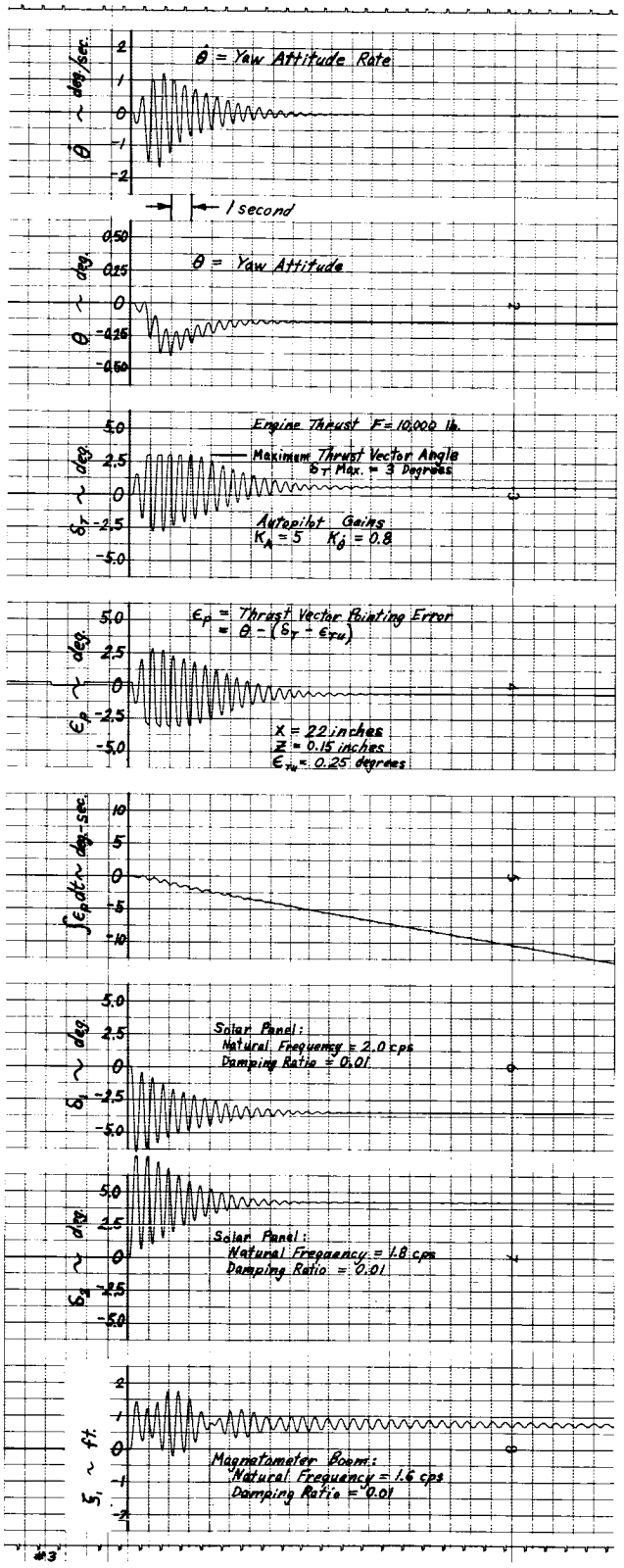

Figure 4.3-20: Start-Burn Time Response — Secondary Injection TVC:Orbit Insertion

Competing Characteristics--Selection of the preferred thrust trace was based on trading the following competing characteristics:

1) Vehicle "g" limits;

2) Motor burn time limitations;

3) Propellent burn rate limitations.

Selection Rationale and Discussion--A neutral thrust trace which does not exceed the required 2.2 Earth "g" limits, results in a 3 minute burn time. This implies burning rates on the order of 0.11 inches/second at 500 psia. An operational high performance propellant with demonstrated reliability is not available to meet this requirement. Therefore, a regressive trace which is characterized by a constant "g" level was selected.

Thrust Termination--Several methods suitable for solid rocket impulse control were analyzed. None of the systems proved satisfactory for the 1971-1973 missions; however, with further development, one of the methods might be considered for later applications. The three thrust termination-neutralization techniques are compared schematically with the normal burnout termination motor on Figure 4.3-21. The three systems analyzed were nozzle release, head-end porting and liquid quench.

Nozzle Release--Upon command, explosive bolts holding the nozzle to the motor are activated and the nozzle is ejected. In the elliptical design, the hole left in the case is about thirty times bigger than the throat.

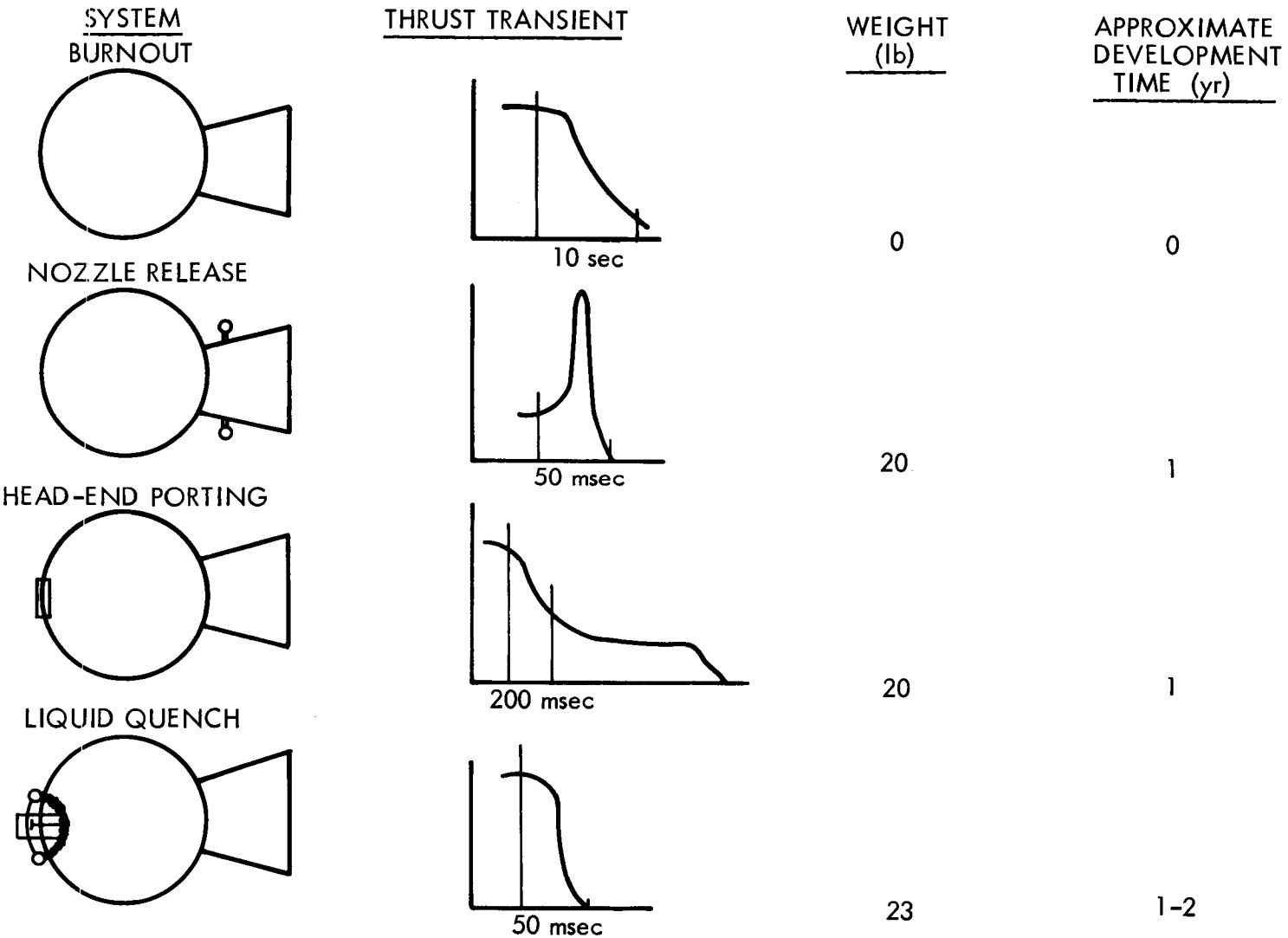

Figure 4.3-21: Thrust Termination Concepts

Tests at Thiokol have shown that such a change results in a near-instantaneous flame extinguishment. The most serious system deficiency is that upon ejection a sharp thrust spike is generated. (See Figure 4.3-22) Analyses indicated that spikes similar to those shown may damage some of the spacecraft components. In addition, there is no data available showing the magnitude of any pitching moments which may be incurred. For these reasons, and because the method is still considered to be in a state of development, this technique was eliminated.

Head-End Porting--Thrust neutralization by porting the head end offers a possible means of terminating thrust without an attendant thrust spike. Such a technique is used on the third-stage Minuteman for impulse control. However, for the Voyager, venting from the forward end through a low-expansion-ratio port results in a high-energy-plume emitting from both ends of the spacecraft. Also, with venting on the sun side, the possibility of contaminating the solar panels and optical equipment with exhaust products is increased. Therefore, considering the additional heat shielding required and vehicle deposition hazards, this technique was discarded.

Liquid Quench--The liquid quench system shown on Figure 4.3-23 has the capability of controlling incremental velocity while eliminating detrimental hot gas plumes without ejecting hardware. This system would only be operational from forward web burnout which occurs at 40 seconds after ignition through to motor tailoff. Actuation involves only firing of explosive valves. Based on extinguishing tests on motors ranging from

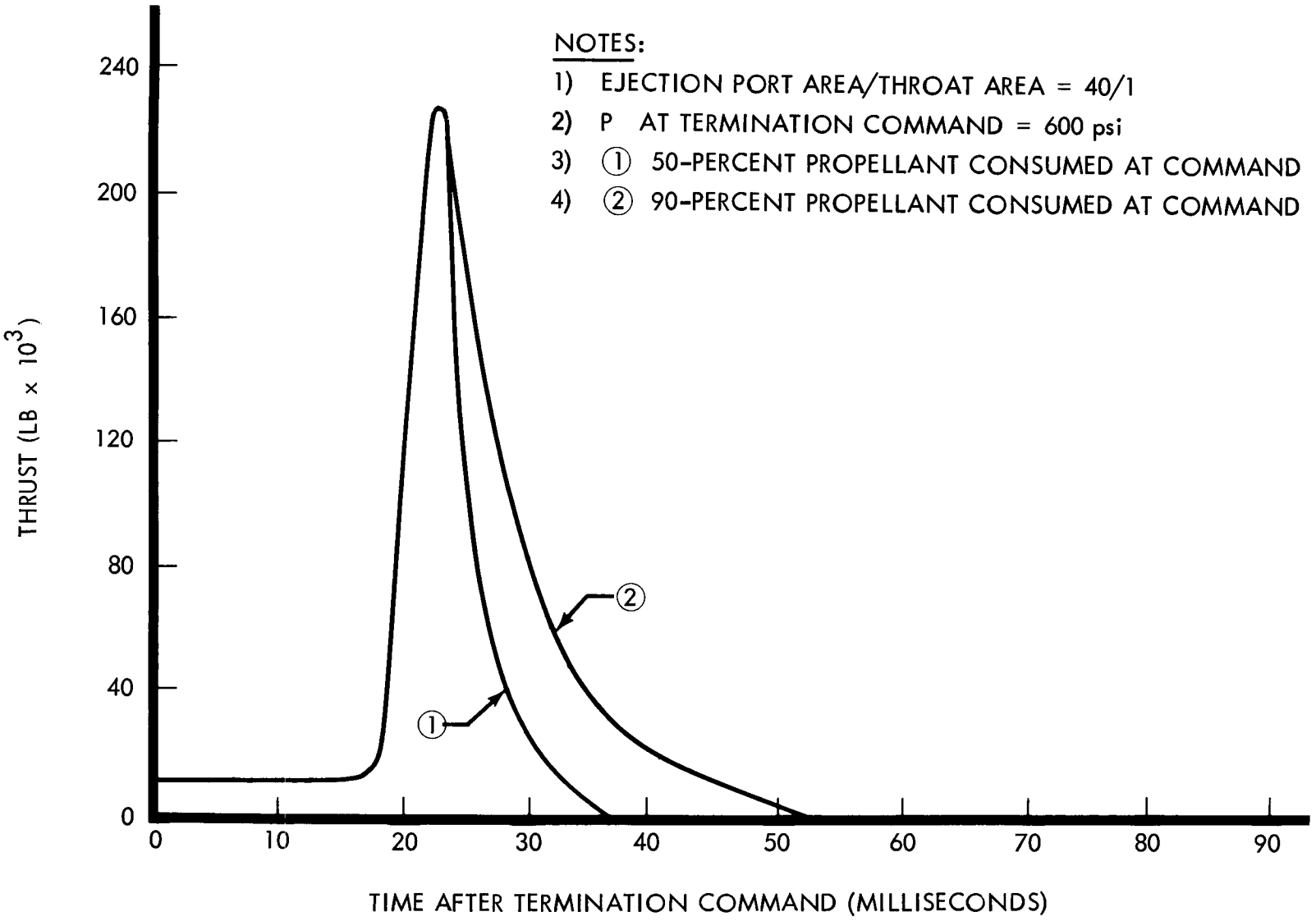

Figure 4.3-22: Nozzle Ejection Thrust Spike

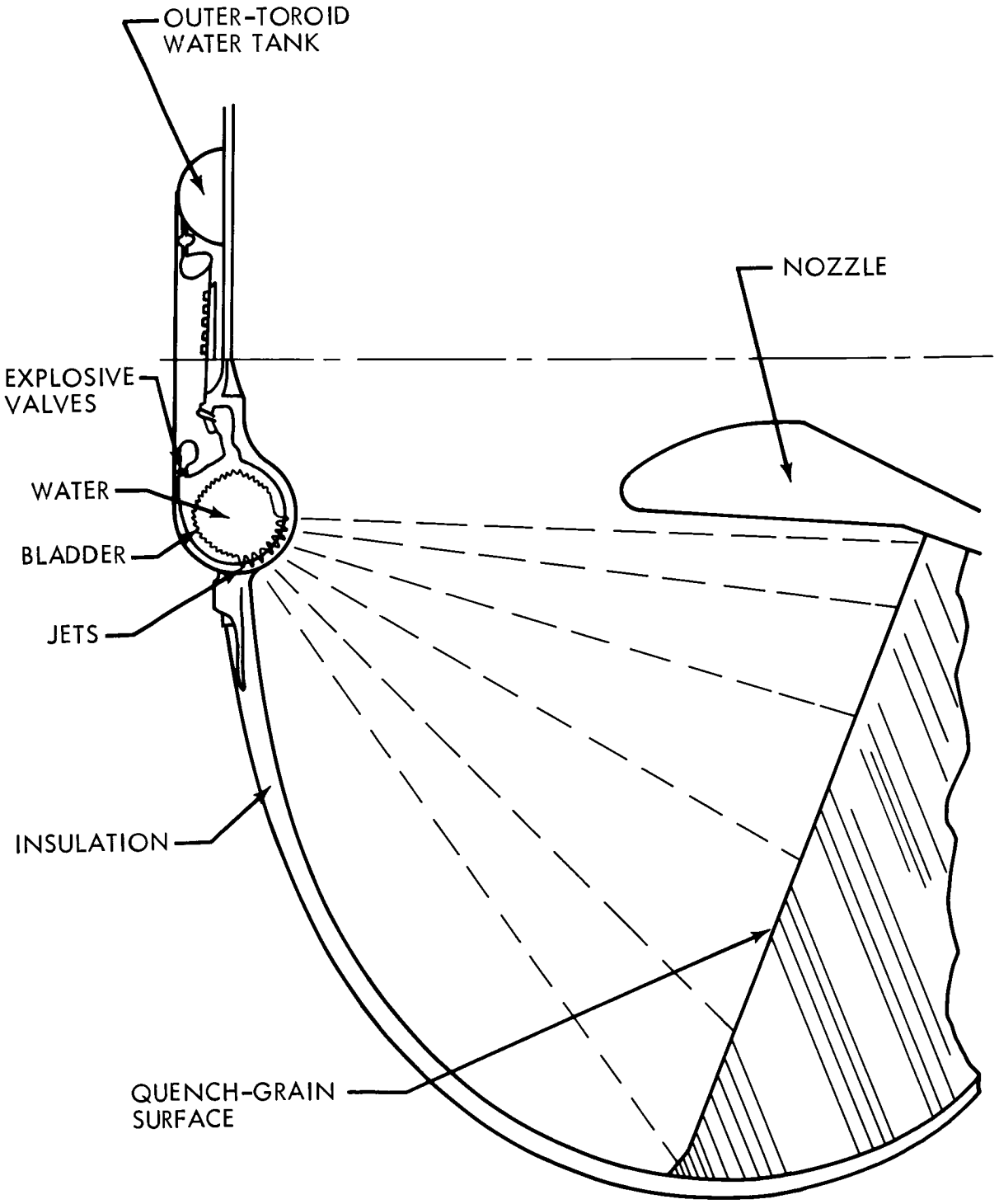

Figure 4.3-23: Quench-Thrust Termination

8 to 20,000 pounds, the time to zero chamber pressure for the proposed retro motor is about 50 milliseconds.

The main component of the quench system is a toroidal titanium tank having 1.65 inch radius and a 10-inch major diameter. The interior face is drilled to form the required injector. Streams are directed to interrupt burning and cool the surface. This device contains 10 pounds of water, and tankage and insulation weighs an additional 13.6 pounds for a total weight of 23.3 pounds. This system has been test demonstrated; however, definition of the quench transients and associated impulse and velocity errors require more effort before acceptance for this program. This system has been set aside for possible consideration on post-1973 growth missions.

Normal depletion has been selected for the preferred design. The fixed total impulse associated with this technique is compatible with all Mars approach geometries. Variations in hyperbolic excess velocity and aim point B-vector are accommodated by thrusting at a position different from approach hyperbola periapsis and, if required, in a direction not collinear with the flight path. (See Volume A, Section 3.1).

4.3.3.2 Monopropellant Midcourse and Orbit Trim Subsystem Components

Propellants--

Description--Table 4.3-19 presents a list of the candidate monopropellants and their characteristics. A brief discussion of candidate monopropellants is given below:

1) Hydrogen Peroxide (H_2O_2)--Hydrogen peroxide has had numerous attitude control applications such as Mercury, X-15, and Syncom. Its performance is inversely proportioned to the amount of water

Table 4.3-19: CANDIDATE MONOPROPELLANTS

Hydrogen Peroxide	Freezing Point °F	Boiling Point (1.)°F	Specific Gravity (2.)	Shock Sensitivity Kg-cm (3.)	Flame Temp. °R	Specific Impulse LBF Sec/LBM (4.)
90%	11.1	286	1.392		1832	148
95%	21.0	294	1.42		2098	155
98%	27.5	299	1.437		2203	161
100%	31.2	309	1.448		2315	163
Hydrazine	34	236	1.0	>120	2260	186 (235)[5]
Ethylene Oxide	-167	51.3	0.87	>120	2220	189
Ethyl Nitrate	-152	192	1.11	1.9	3499	224
Nitromethane	-20.2	214	1.13	67.4	4462	244
Methyl Nitrate	-4.0	149	1.21		5789	259
Hydrazine/ Hydrazinium nitrate/H_2O (.75, .24, .01)	2		1.10		2660	(256)[5]

(1.) At 14.7 psia
(2.) At 68° F
(3.) Impact energy for 50% probability of explosion. 1.6 for nitroglycerin
(4.) 1000 psia to 14.7 psia. Optimum expansion, frozen equilibrium
(5.) Vacuum Performance, Ammonia dissociation = 50%

in the solution. The most common used concentration is 90 percent H_2O_2. Peroxide solutions are insensitive to the initiation and propagation of detonation. The flame temperatures are low enough to preclude materials compatibility problems even though the exhaust products are oxidizing in nature. Decomposition is initiated by proven catalysts such as permanganate salts or activated silver screens. Long-term storage is usually a problem because of a concentration loss rate of approximately 1 percent per year. Storage and handling problems require cleaned and chemically-treated materials to prevent accidental catalytic decomposition.

2) Hydrazine (N_2H_4)-- Hydrazine is a toxic, flammable liquid that possesses moderate performance. It was used in space-proven propulsion systems (Mariner, Ranger). It is not shock sensitive and is compatible with metals and nonmetals used in rocket systems. Metals include stainless steels, aluminum and titanium tankage and stainless steels, Inconel and Haynes Alloy No. 25 for thrust chambers. Nonmetals include butyl rubber, teflon, polyethylene and ethylene propylene. Its thermal stability is good up to the rapid-decomposition temperature of 500°F. Decomposition has been started by use of hypergolic start slug. The recent development of a truly spontaneous catalyst by the Shell Development Company (Shell 405) has eliminated the hypergolic start slug. Specific performance is a function of the percentage of ammonia dissociation which is an endothermic process that decreases the performance as dissociation percentage increases.

3) Hydrazine/Hydrazinium Nitrate/Water--Mixtures of hydrazine, hydrazinium nitrate, and water are alternate monopropellants. This mixture results in a freezing point temperature as low as -65° F. Proper selection of mixtures can raise the performance of neat hydrazine. However, propellant stability reduces as the percentage of hydrazinium nitrate increases. If evaporation of water occurs, shock-sensitive hydrazinium nitrate crystals are liable to form. This higher combustion temperature requires further catalyst development. The Shell 405 will not stand the higher temperature. All other monopropellants listed in Table 4.3-19 are either highly toxic or unstable and have not been considered despite their high specific impulse.

Competing Characteristics--The monopropellant selection was based on the following competing characteristics:

1) Specific Impulse;
2) Engine Availability;
3) Space Experience;
4) Propellant Volume;
5) Compatibility with Spacecraft Materials.

Selection Rationale--The hydrazine-hydrazinium nitrate mixture has been rejected because it is not yet fully developed. The two most applicable monopropellants, hydrogen peroxide and hydrazine, have been considered.

Figure 4.3-24 compares the total propulsion system weight versus total impulse requirements for a typical midcourse and orbit trim propulsion subsystem.

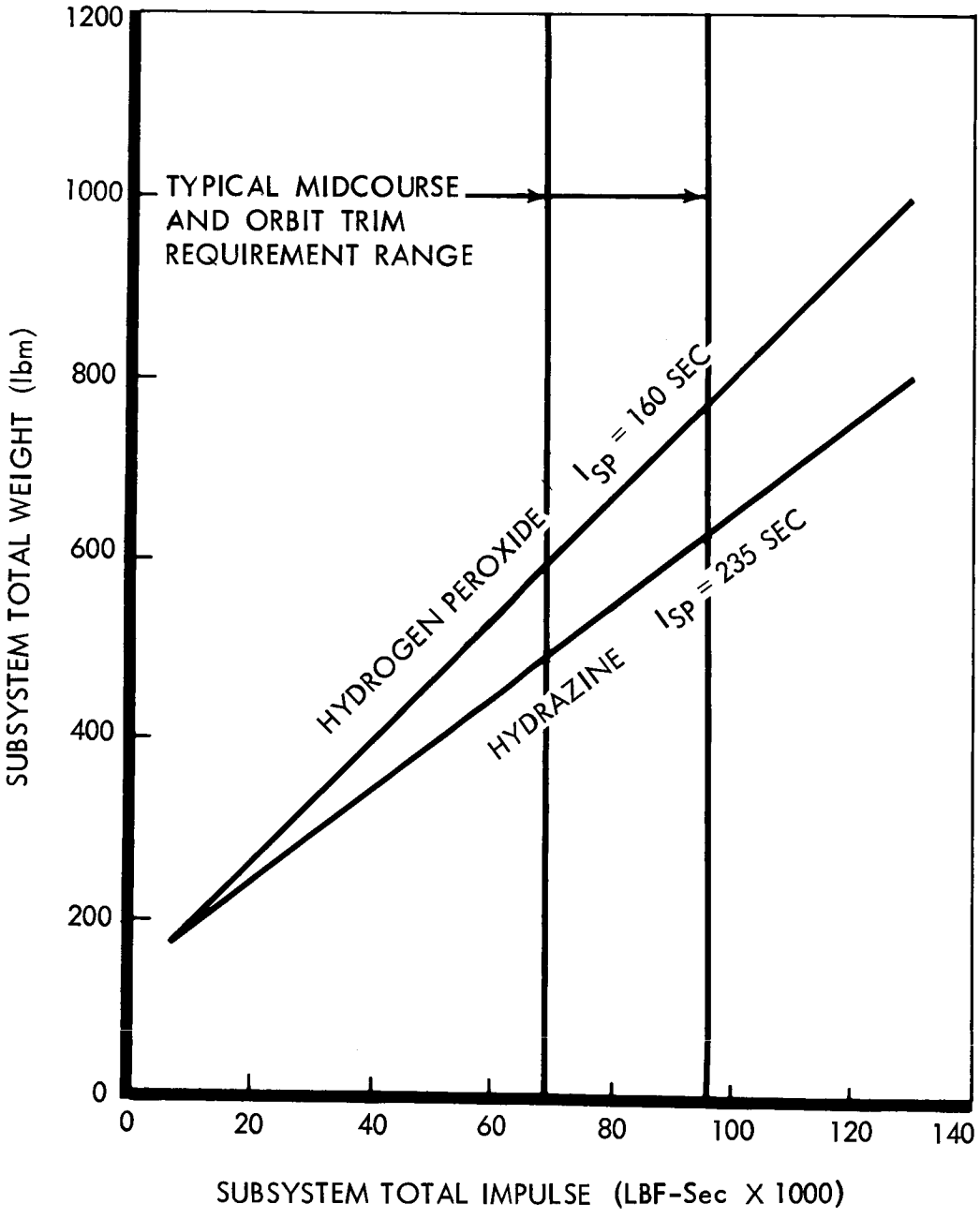

Figure 4.3-24: Monopropellant-Propulsion Subsystem Comparison

On the basis of the current monopropellant propulsion development programs including the Shell catalyst development, space application experience, propellant stability, storability, reliability, confidence, and specific impulse, hydrazine was selected as the most applicable monopropellant for the Voyager design studies.

Engines (Selection Rationale)--Radiation-cooled monopropellant engines have been selected on the basis of availability, space experience and relatively low decomposition temperatures.

Ignition--

Description--The following two ignition concepts were considered:

1) N_2O_4 Start Slug;

2) Shell 405 Spontaneous Catalyst.

Competing Characteristics--Ignition mode selection was based on trading the following competing characteristics:

1) Reliability;

2) Availability.

Selection Rationale--The spontaneous catalyst is more reliable. It has been sufficiently developed to be considered ready for flight use and has therefore been selected.

Thrust Level--

Description--Thrust levels ranging from 50 - 200 pounds were considered.

Competing Characteristics--The following were considered in trading thrust levels:

1) Minimum velocity increment and increment tolerance requirements;
2) Engine availability;
3) Gravity losses during orbit trim;
4) Engine Weight;
5) Burn time.

Selection Rationale--Velocity increment penalties for orbit trimming at both periapsis and apoapsis, for a typical Mars-bound orbit are shown in Figure 4.3-25 as a function of initial thrust-to-weight ratio. The effect of engine thrust level on engine weight is shown in Figure 4.3-26. For engine thrust levels between 50 and 200 pounds the effects of increased engine weight with thrust for two engines nearly balance propellant weight savings resulting from reduced velocity increment penalties. A thrust level of 50 pounds has been selected on the basis of engine availability and previous experience in this thrust range. The minimum velocity increment and tolerances can be easily met. Maximum engine burn time for both midcourse and orbit trim maneuvers is on the order of 1000 seconds as shown in Figure 4.3-27. This is considered acceptable from solar power and thermal control considerations.

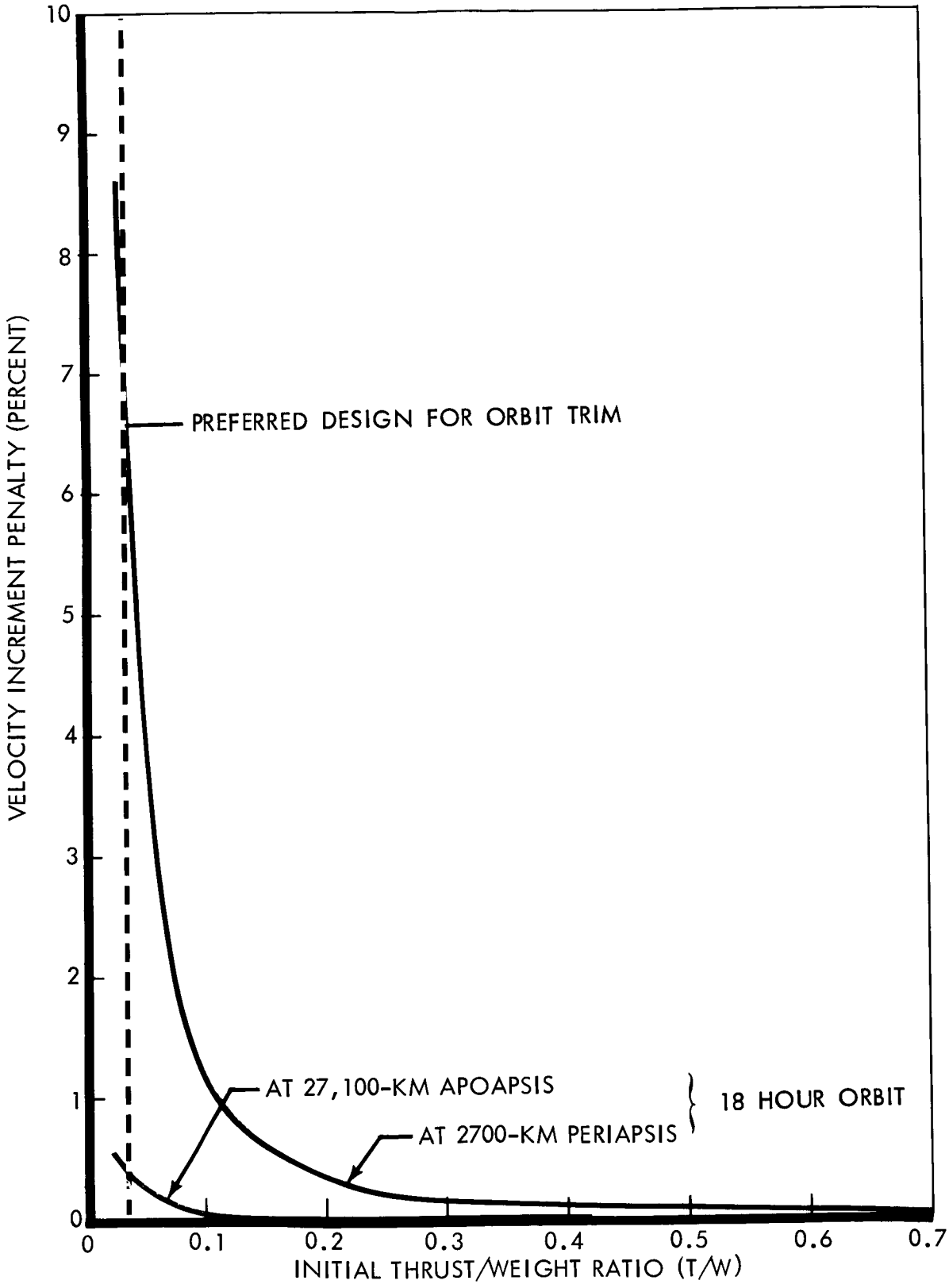

Figure 4.3-25: Finite Thrust Velocity Increment Penalty

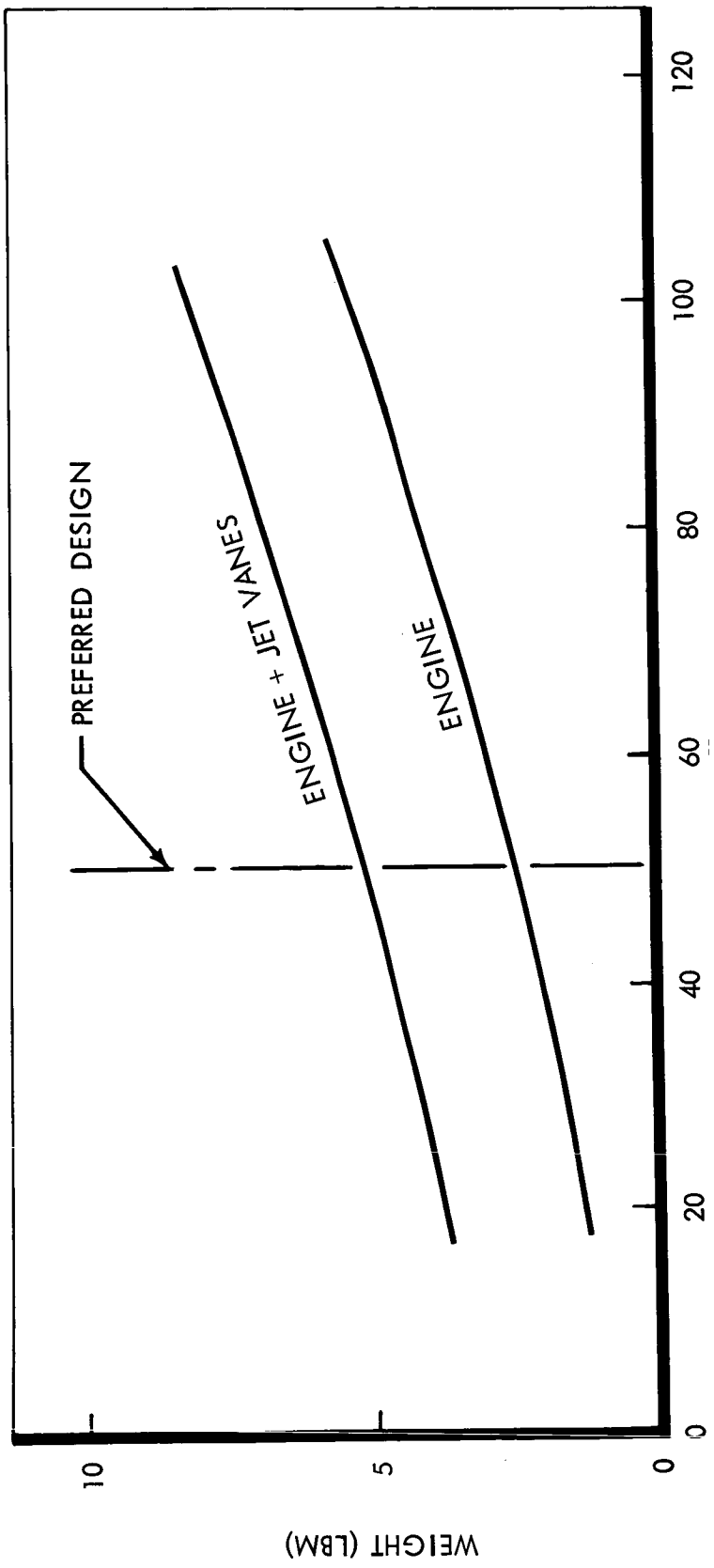

Figure 4.3-26: Hydrazine-Engine and Jet-Vanes Weight

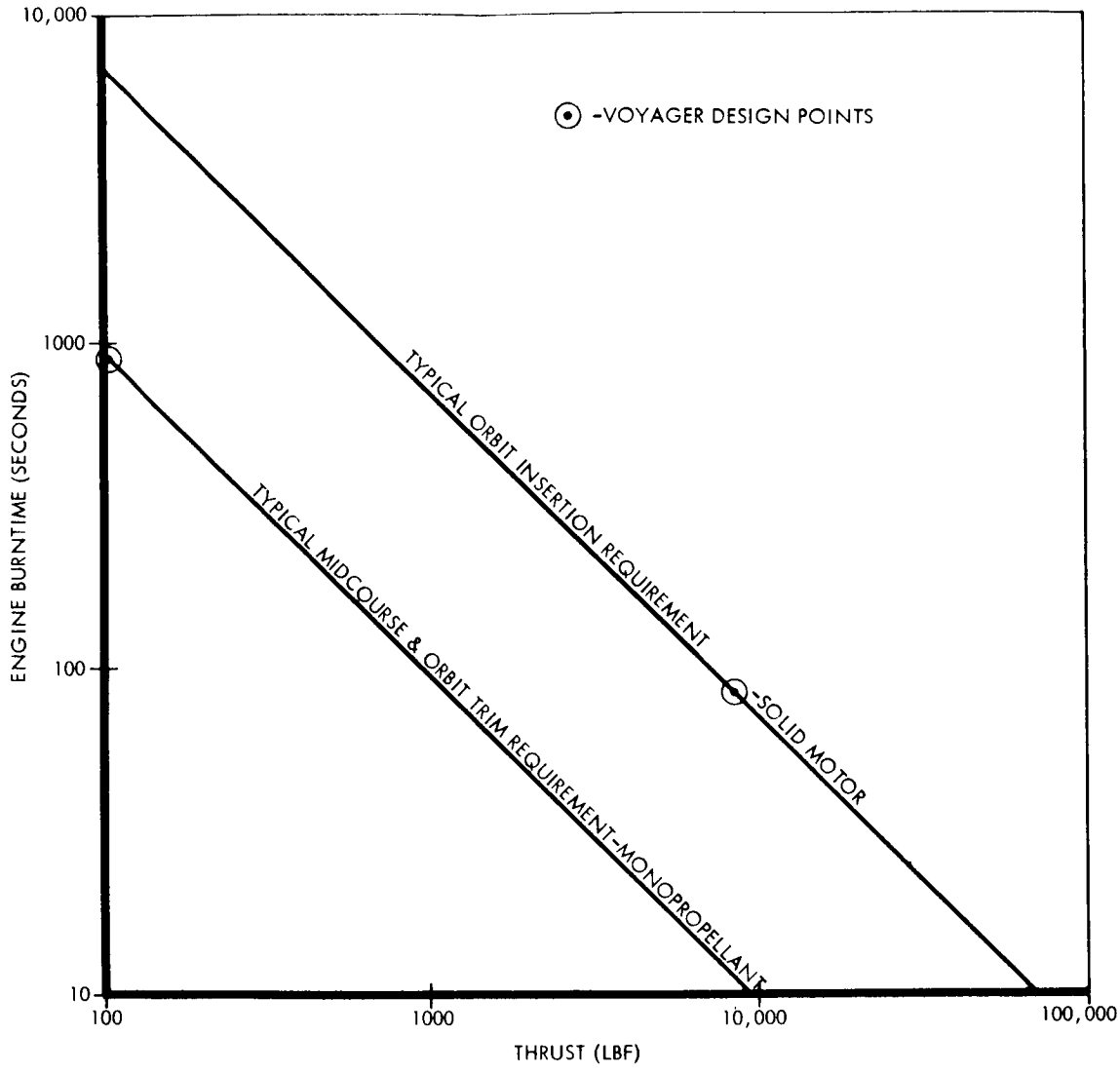

Figure 4.3-27: Thrust vs Burn Time

Thrust Vector Control--

Description--A midcourse propulsion subsystem thrust vector control is required to provide adequate attitude control authority during engine firing to adjust for dispersion of thrust vector alignments, and to accommodate for shifts of the total vehicle center-of-gravity. The methods considered for obtaining thrust vector control were pulsed engines, gimbals, and jet vanes.

The midcourse thrust vector control autopilot must be capable of providing the minimum ΔV required, while at the same time satisfying the thrust vector pointing requirements. The residual attitude and attitude rate following shutdown of the midcourse engines must be such that gyro limitations are not exceeded during recovery with the low-level nitrogen reaction control subsystem. If required, the burn time must therefore be long enough to allow sufficient time for settling of the transients resulting from engine ignition and shutdown.

Competing Characteristics--Selection of the preferred thrust vector control concept was based on the following competing characteristics:

1) Reliability;
2) Availability;
3) Weight;
4) Adequate response.

Pulsed Engines--This system employes two engines operated in the normally-on mode and the engines are pulsed off to provide attitude control torques. A functional block diagram of the autopilot is shown in Figure 4.3-28.

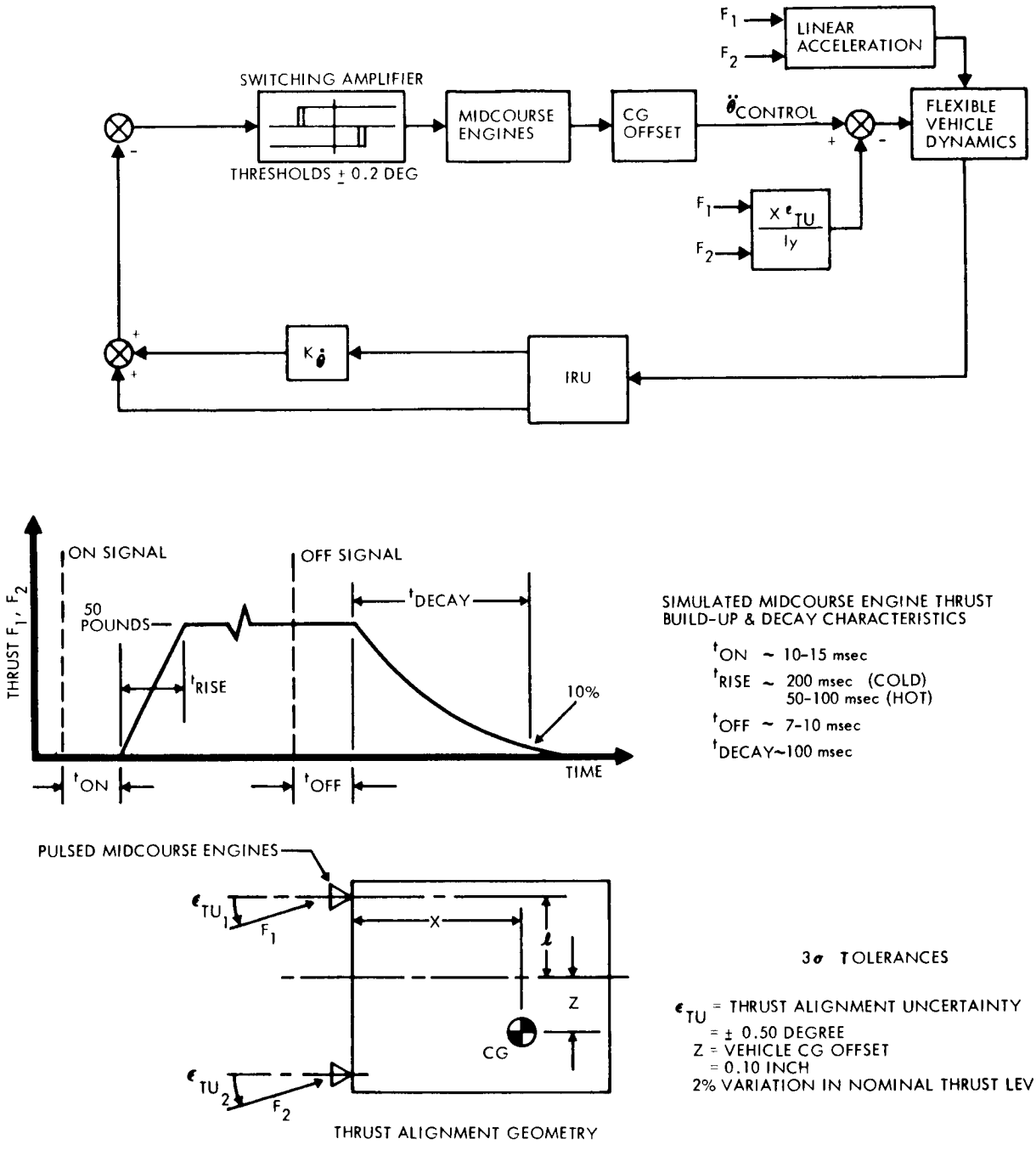

Figure 4.3-28: Pulsed Midcourse Engine TVC Autopilot — Midcourse Correction

An example of the start-burn transient is shown in Figure 4.3-29 for the worst case tolerances as indicated. This system is somewhat insensitive to the normal tolerances in nominal thrust level and cg offset. The maximum pointing error at any time during the transient is limited to 0.7 degrees for the tolerances assumed. This is well within the TVC autopilot allocation (Volume A, Section

Jet Vanes and Gimballed Engines--These systems are similar except for thrust vector actuation dynamics. The thrust vector maximum rate is limited for gimballed engines while the jet vane actuators offer relatively fast response. Maximum thrust vector capability for both systems is limited to 3 to 5 degrees. A functional block diagram of the autopilot appears in Figure 4.3-30. Examples of the performance for these two systems appear in Figures 4.3-31 and 4.3-32. The sensitivity of both systems to tolerances in nominal thrust levels is increased with the offset distance of the engines from the vehicle roll axis. With these engines offset 48 inches from the roll axis the 3σ steady-state pointing error is 1.4 degrees for jet-vane TVC, which is just within the TVC allocation. As shown in the response curves, the transient pointing error is in excess of this value and the burn time must be long enough to allow the time integral of the pointing error to be within the requirement. Lagged feedback of the gimbal position or jet vane position to provide trim compensation of the pointing error is practical here only if the trim time constant is about 25 seconds or greater.

Selection Rationale--Jet vanes have been selected because they are highly reliable, light in weight, and have been successfully space-flown on Ranger and Mariner vehicles.

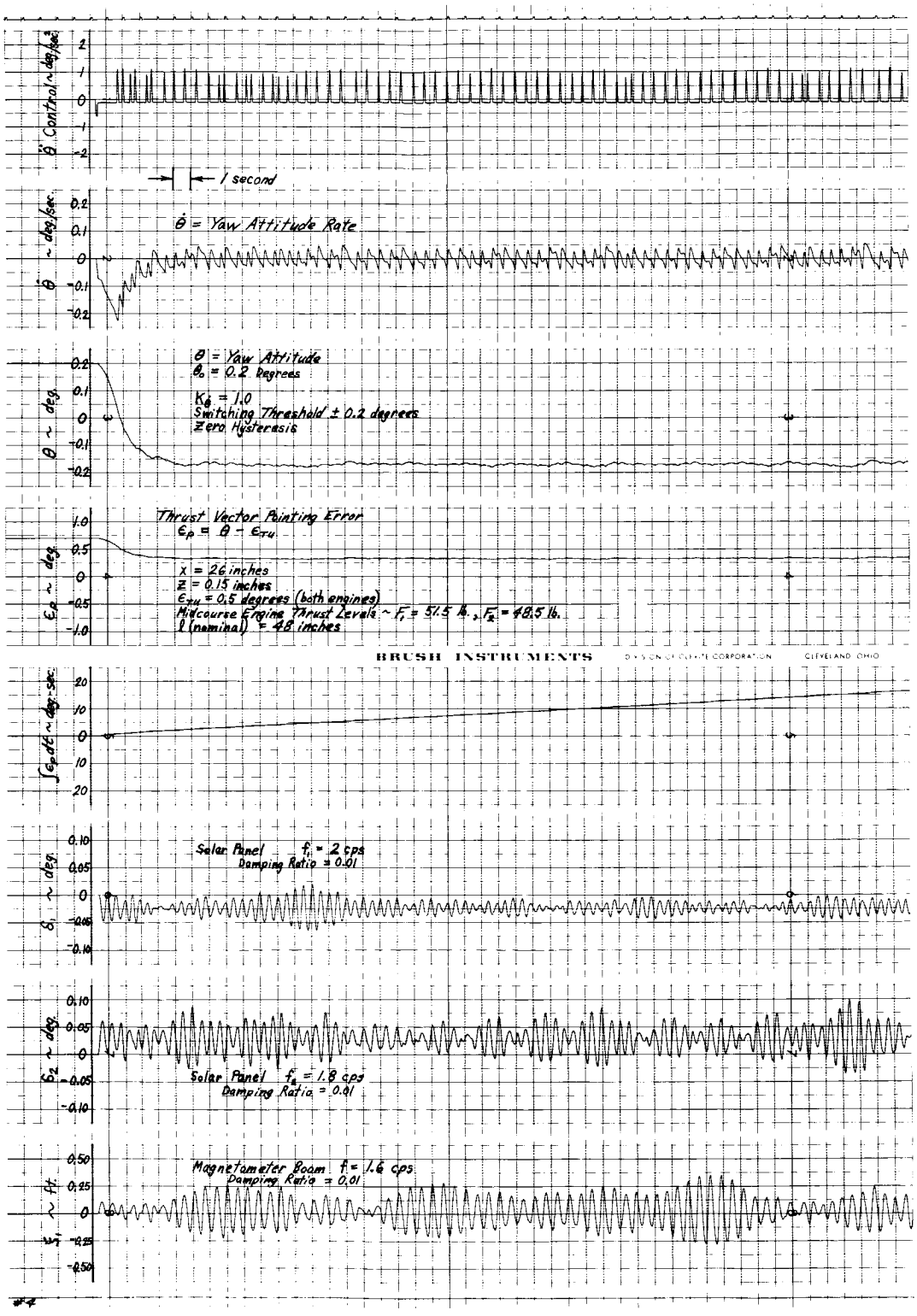

Figure 4.3-29: Start-Burn Time Response Pulsed Engines TVC — Midcourse Correction

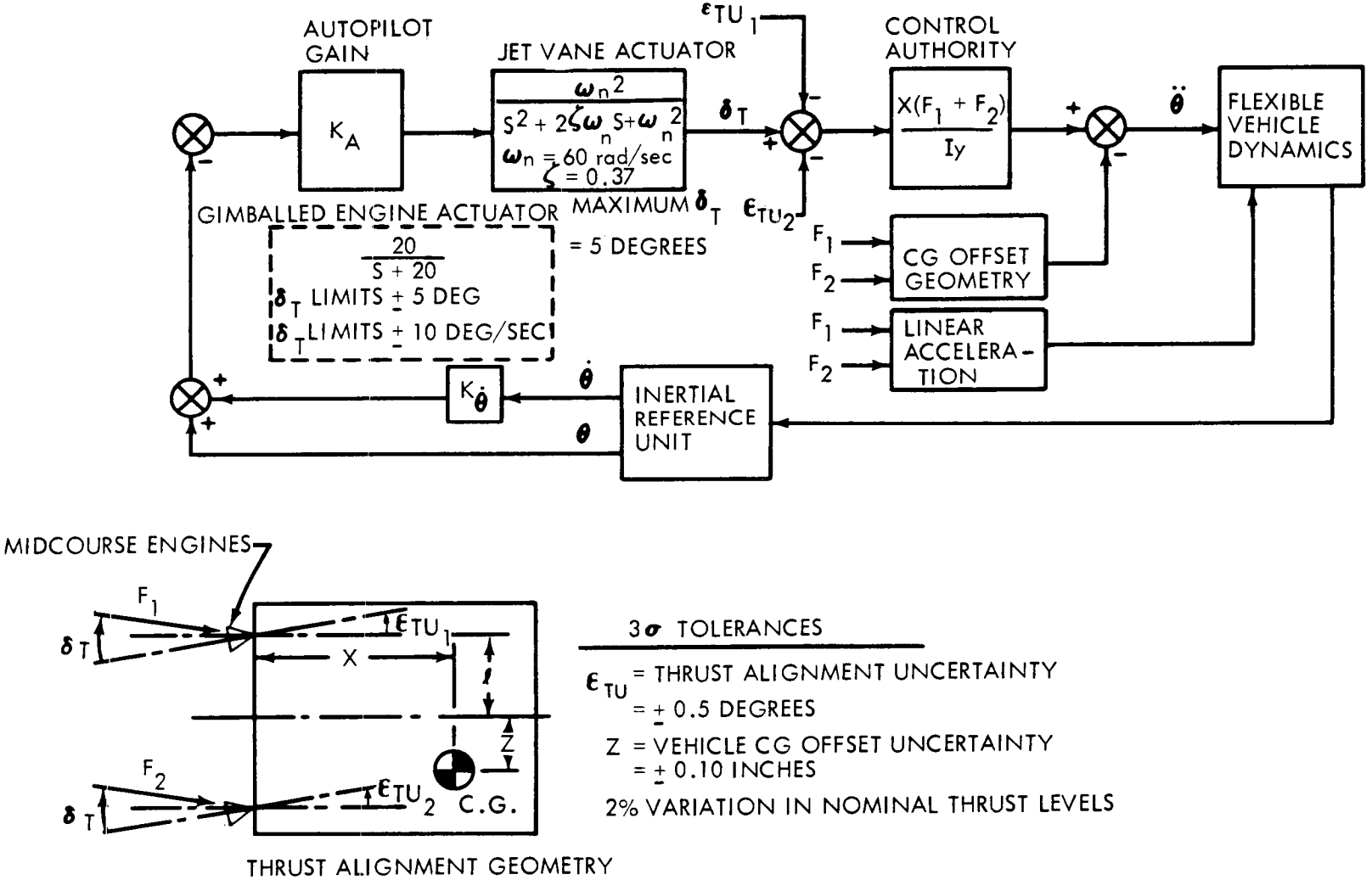

Figure 4.3-30: Jet Vanes or Gimbaled Engines TVC - Midcourse Correction

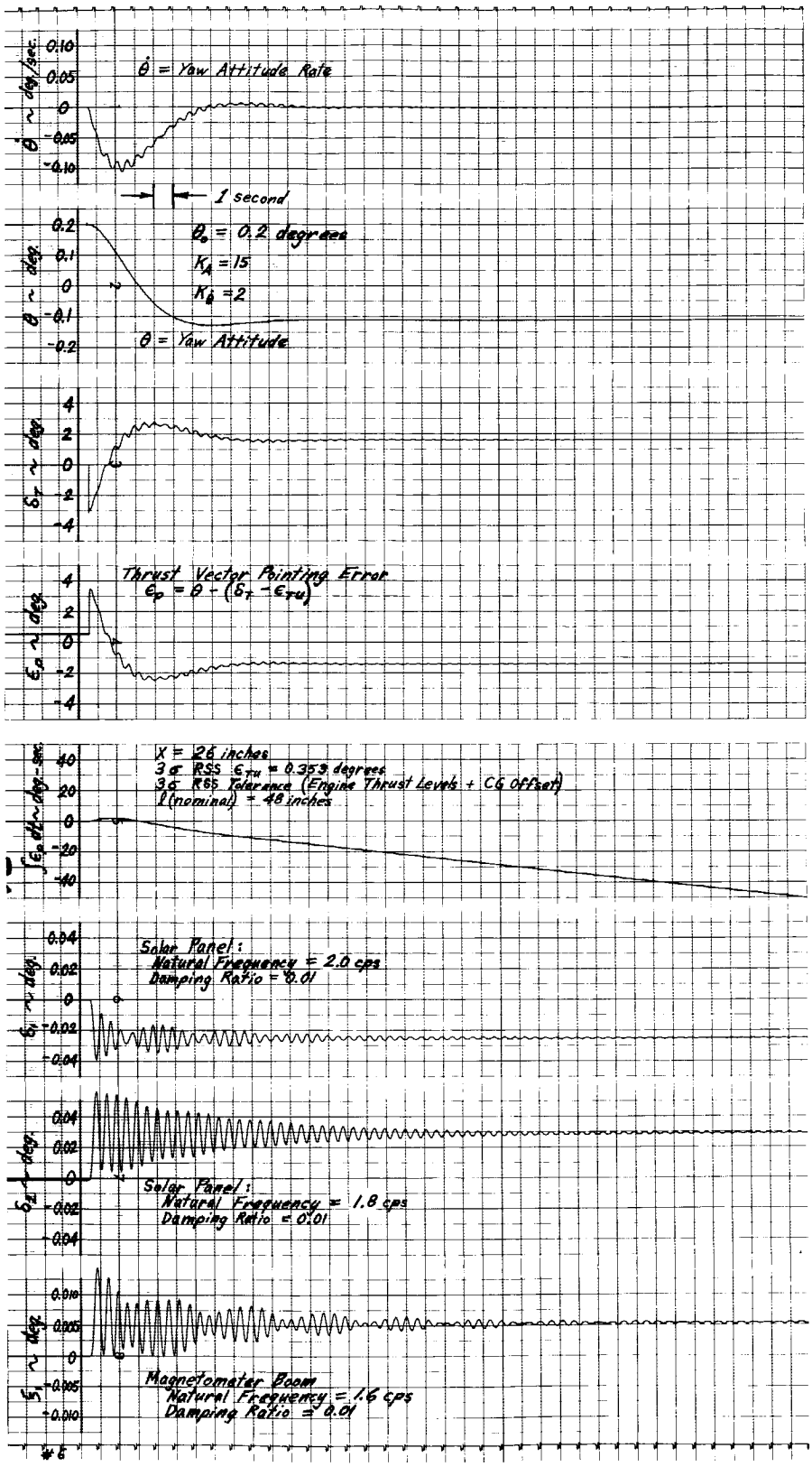

Figure 4.3-31: Start-Burn Time Response Jet-Vane TVC — Midcourse Correction

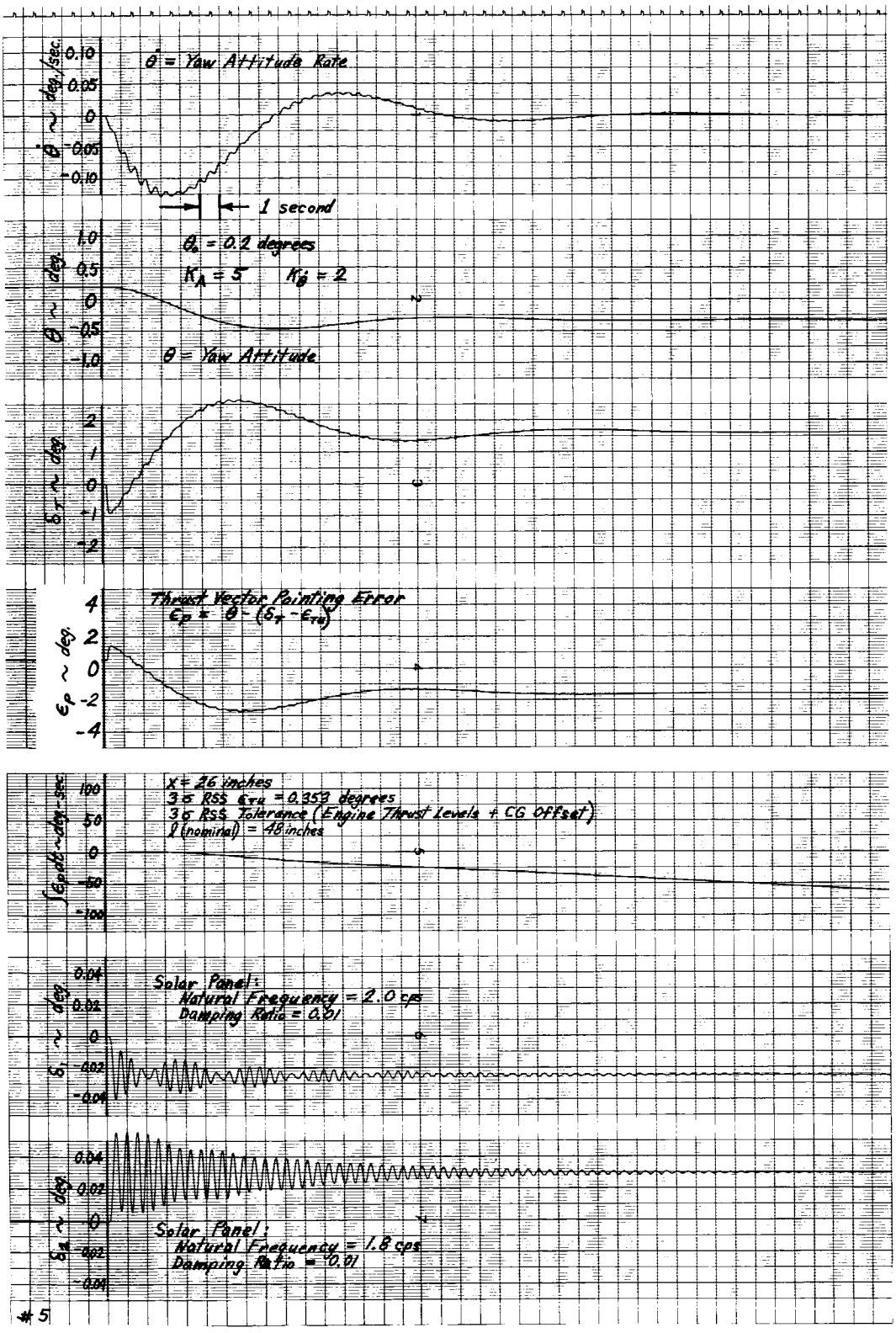

Figure 4.3-32: Start-Burn Time Response Gimbaled Engines TVC — Midcourse Correction

Expulsion--

Description--For space applications, only positive-expulsion methods are considered. The mission specification limits positive-expulsion methods to those of positive displacement. Positive expulsion methods considered are:

1) Bladders;

2) Diaphragms, metal or non-metal;

3) Mechanical (e.g. piston);

4) Bellows.

Competing Characteristics--Competing characteristics used for evaluation and selection of the preferred expulsion system for monopropellants are:

1) Reliability;

2) Availability;

3) Life cycle;

4) Weight;

5) Permeability;

6) Expulsion and volumetric efficiencies;

7) Dynamics.

Selection Rationale--Metal diaphragms were rejected because of poor reliability and critical dynamics. Mechanical (e.g., piston expulsion) device were rejected because of their high weight. Metal bellows were rejected because of their high weight and poor volumetric efficiency. Butyl bladders were selected, despite their high permeability, on the basis of good reliability, excellent life cycle, low weight, and previous space experience.

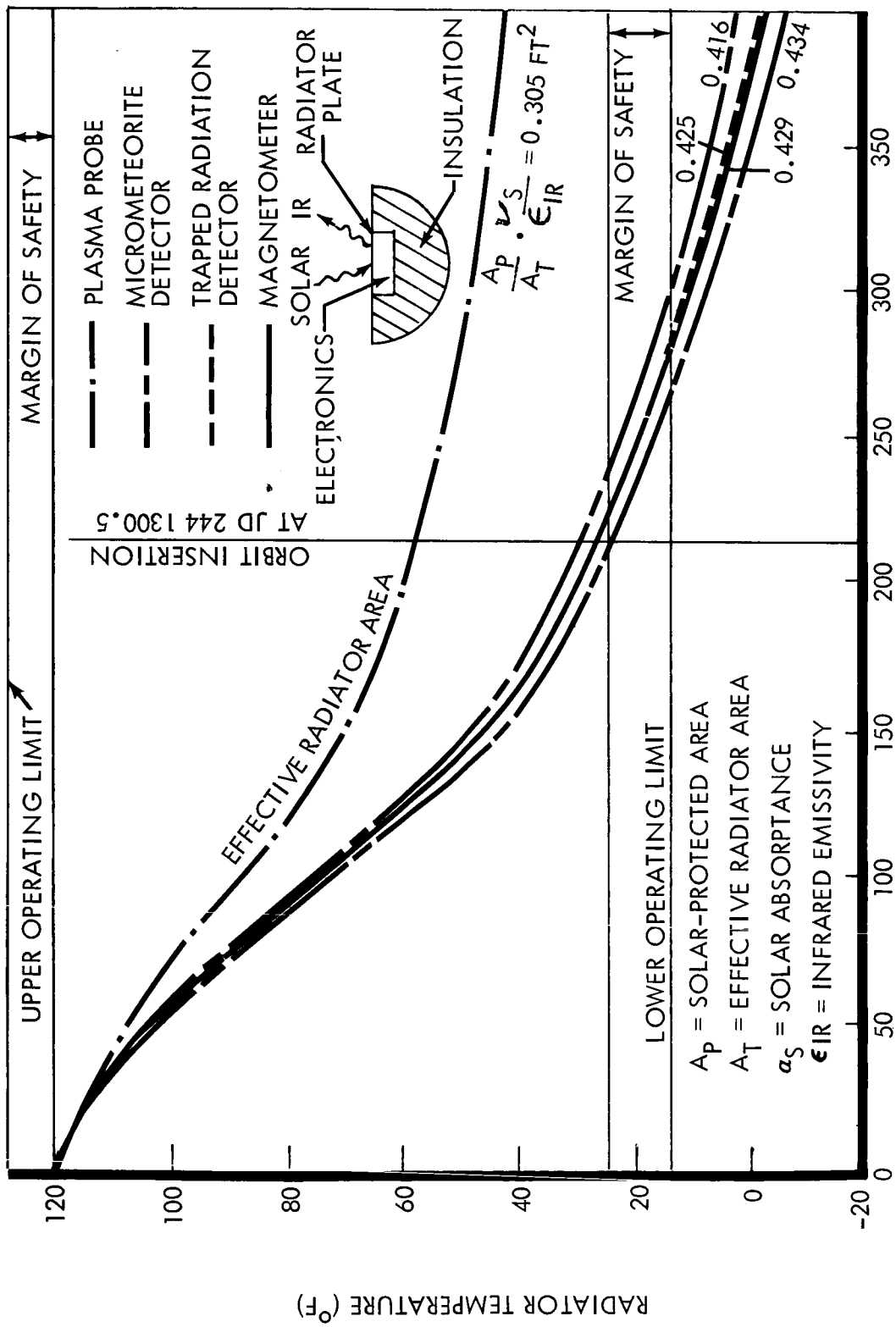

Figure 4.4-14: Temperature Profiles of Externally Mounted Instruments Surface Coating Concept

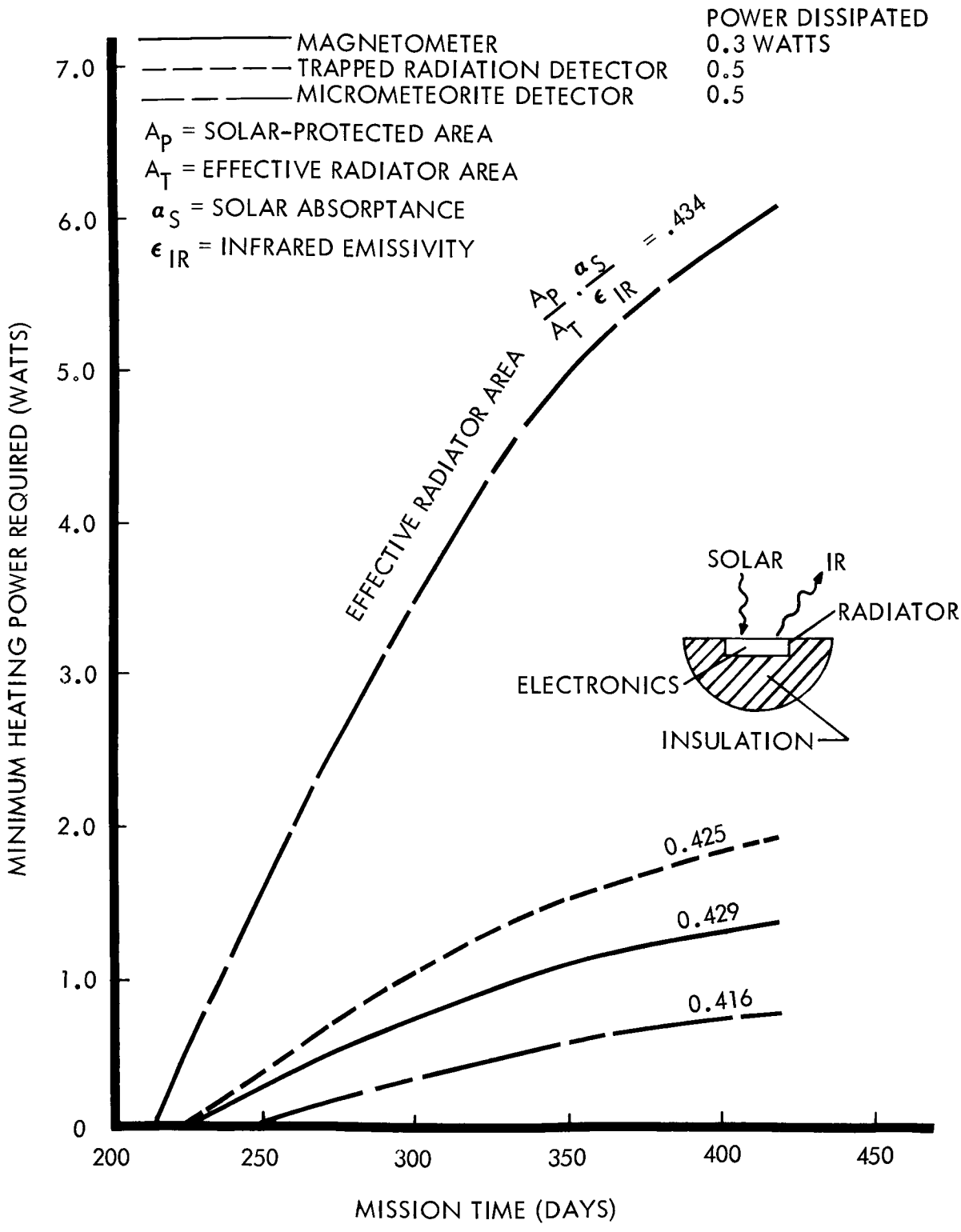

Figure 4.4-15: Power Requirements for Externally Mounted Instruments Surface Coating Concept

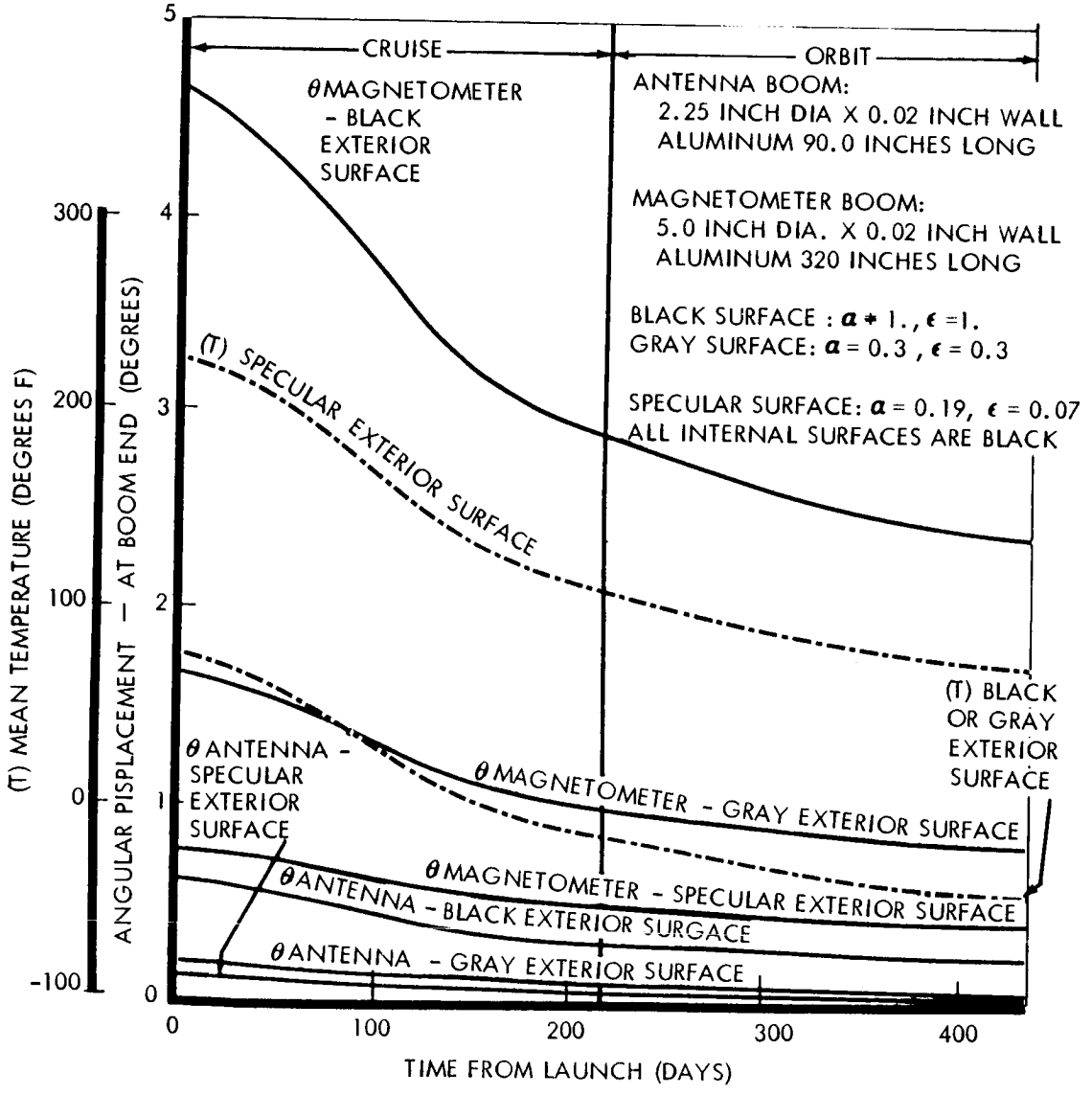

Figure 4.4-16: Temperature and Deflection of Exterior Booms

nozzle facing the capsule during the transit period. The attitude control thrusters and the midcourse correction engines are projecting through the Sun face of the spacecraft. The surface is covered with a solar shield to reduce the heat flow into the propulsion bay. The capsule face or cold face is covered with a heat shield to reduce the heat loss during transit and orbit periods. In addition, this shield reduces the heat flow into the propulsion bay and internal equipment compartment during firing of the orbit insertion engine. Heat shields are also provided around the midcourse engines. The sides of the propulsion bay which interface with the internal equipment bays are insulated to prevent heat flow into or out of the propulsion bay. This makes these two groups of equipment thermally independent for analysis and test verification of the subsystem performance. High-temperature insulation surrounds the orbit insertion engine to reduce the effects of soak-back after firing.

The temperature limits for the various portions of the propulsion module are shown in Table 4.4-7. These temperature limits establish the design criteria for the various phases of the mission. The temperatures are maintained from launch to orbit insertion between +40°F and +90°F, from orbit insertion to orbit trim at +40°F to +110°F, and from orbit trim to mission end between -30°F to +150°F. Since the heat rejection rate of the propulsion module is zero except during rocket firings, an active control system must be provided to control the temperature of the module.

Table 4.4-7: PROPULSION MODULE TEMPERATURE LIMITS

Item	Operating Temperature (°F) Min	Max	Storage Temperature (°F) Min	Max
Orbit Injection Rocket	+30°	+90°	+30°	90
Midcourse Correction Propellant Tanks	+40	+110	+35	+125
Attitude Control Gas	-30	+150	-30	+150
Squibs	+40	+110	+28	+125

Three concepts were investigated for thermal control of the propulsion module. These are electric heat, solar louvers and conventional louvers. Schematics of all concepts are shown on Figure 4.4-17. The criteria for selecting a preferred design are reliability and weight.

The electric-heat concept is designed to passively maintain temperatures within the desired limits near Earth. As the spacecraft nears Mars, the temperature within the bay reduces, and electric heaters located in the module are turned on to maintain temperature.

The solar louver concept is similar to the electric heat concept except that solar louvers are used to provide the heating rather than electric heaters. The heat is distributed generally through the propulsion module by radiation coupling to the solar louvers and is directed to critical areas by reflectors.

The conventional louver concept uses a space-facing radiator covered with louvers to control the outflow of heat from the bay. The solar

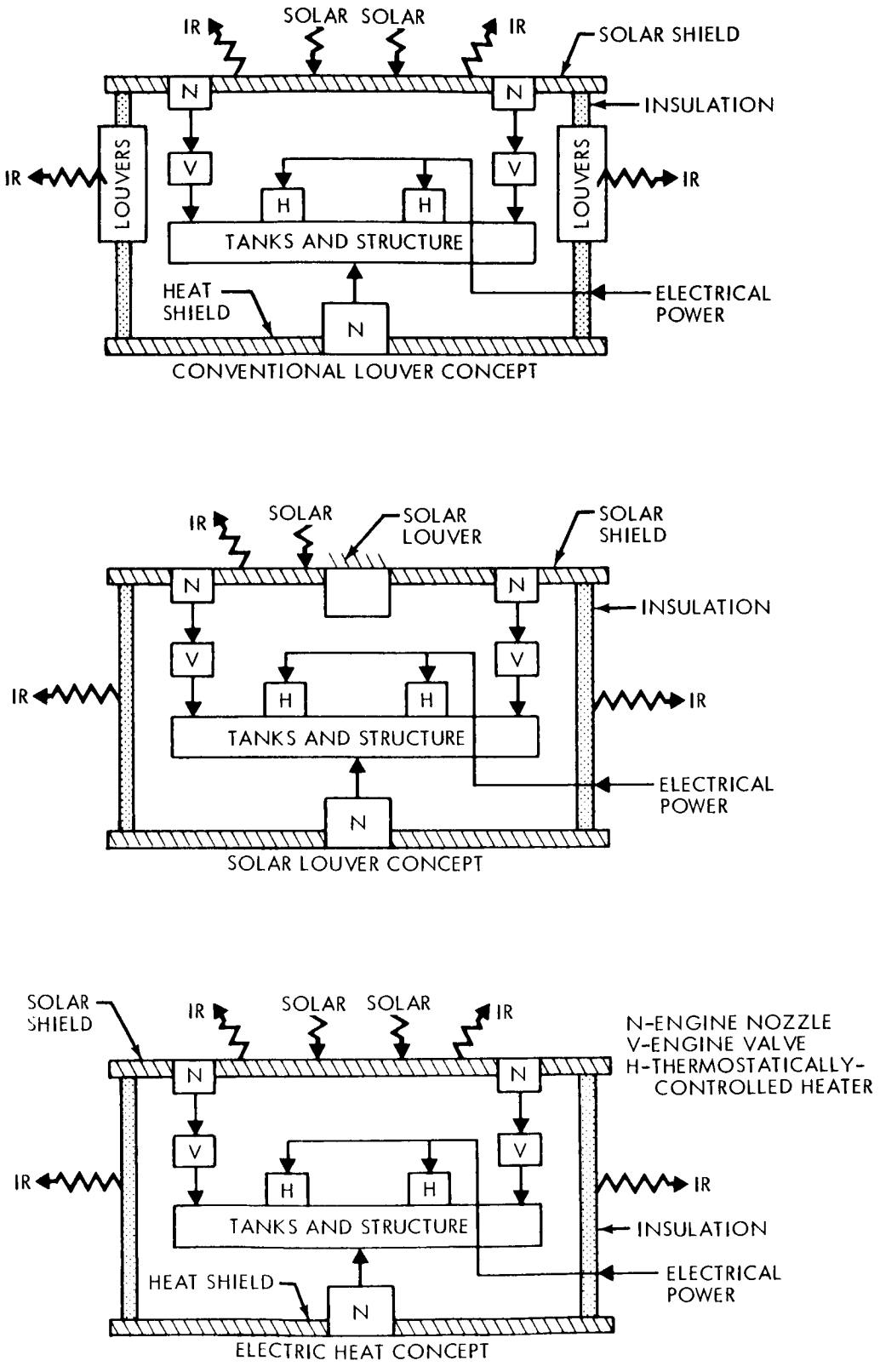

Figure 4.4-17: Propulsion Module Temperature Control Concepts

shield in conjunction with the exposed nozzles, is designed to allow heat to flow into the compartment at a rate which will maintain the proper bay temperature with the minimum loss through the louvers for the Mars solar flux. The heat is distributed through the propulsion bay by radiation coupling to the solar shield. Reflectors and absorbers are provided for local temperature control.

Weight--To establish weight trades, it was necessary to perform some preparatory analysis. First, to determine the heat leak through the midcourse engine nozzles, a parametric study was conducted to determine the effective radiating nozzle area to be used to achieve an optimum temperature at Earth and Mars. Figure 4.4-18 shows nozzle temperature and heat leak into the tank and plumbing systems versus the effective nozzle radiating area. With an effective radiating area of 0.60 square feet, the nozzle temperature will be 28^{o}F at Mars and 96^{o}F at Earth. This corresponds to a loss of 19 Btu/hour at Mars and a gain of 6.6 Btu/hour at Earth.

With an established heat flow into the propulsion bay through the nozzles, a parametric study was conducted to determine the performance of each concept considered. Preliminary analysis revealed that the heat lost from the sides of the bay that interfaces with the internal equipment compartments and deep space is the same for each concept. A study was conducted with assumed heat leaks through the interfaces to determine the solar-shield conductance, radiator areas, louver areas, and electric heater power required to maintain the propulsion bay

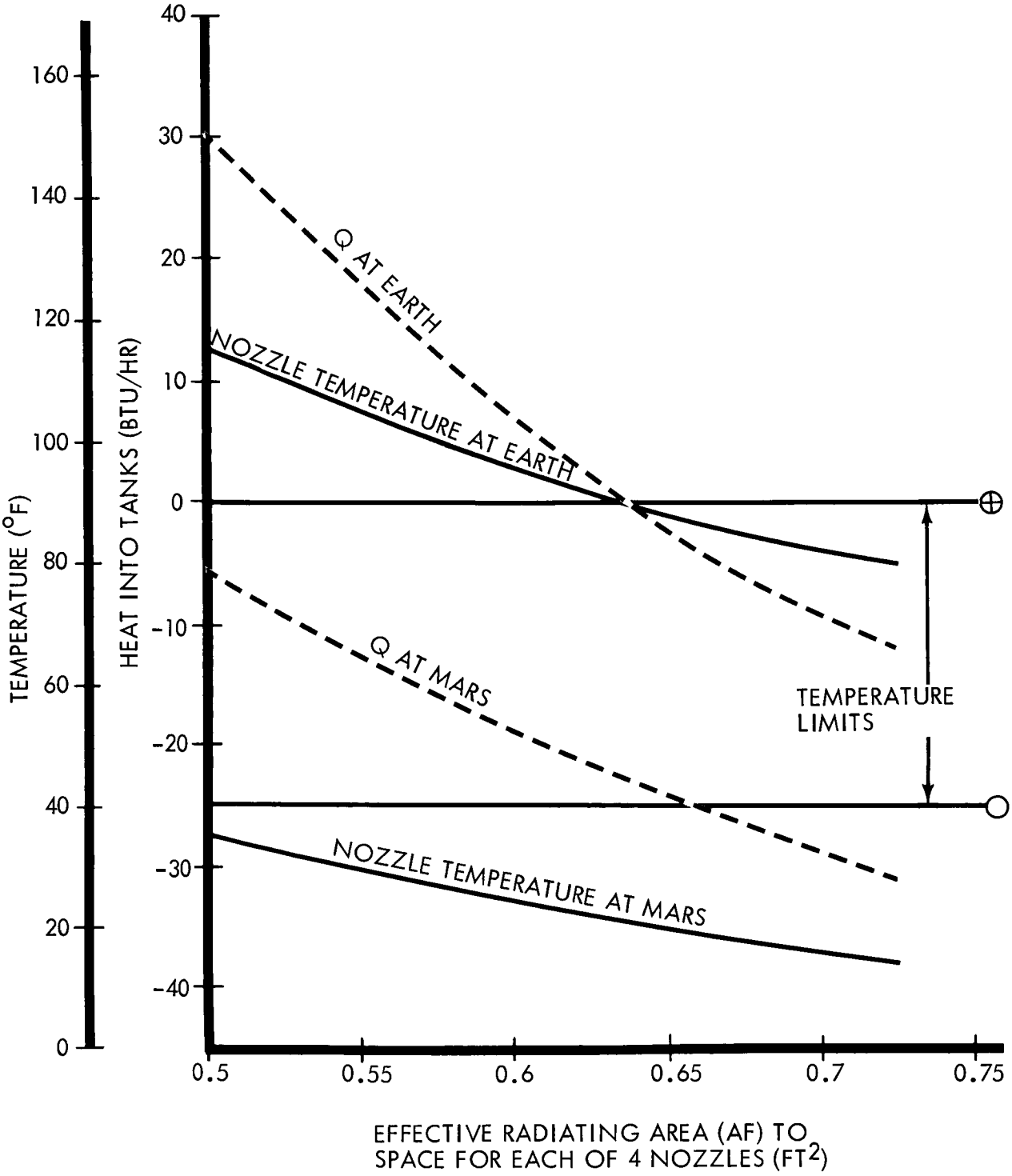

Figure 4.4-18: Midcourse Engine Heat Leak

temperature between 40°F and 90°F. The results are shown on Figure 4.4-19. Assuming a total heat leak of 150 Btu/hr at Earth through all the module surfaces except the solar shield, the thermal conductance through the solar shield is 0.66 Btu/hr-°F and requires 36 watts of electric heat to maintain bay temperature at 40°F at Mars. The solar louver concept requires a solar shield conductance of 1.05 Btu/hr-°F and a solar louver area of 0.72 square feet, while the conventional louver area would require a solar shield conductance of 1.48 Btu/hr-°F assuming no reduction in performance due to space blocking by solar panels and high-gain antenna. With the requirements for radiator and louver areas, electric heater power and solar shield conductance requirements, the concept subsystem weight penalties were calculated. Figure 4.4-20 shows the weight penalty versus variable heat losses through the back faces of the bay. With a heat loss of 100 Btu/hr at Earth, the weight penalties are as follows: Conventional louver concept -- 1.9 pounds; Solar louver concept -- 0.9 pounds; Electric heater concept -- 16.0 pounds.

Reliability--Based on the complexity of the concepts, the reliability of each was computed. The reliability of the propulsion module temperature control subsystem concepts are 0.9982 for the conventional louver concept, including louver actuators and reflectors, 0.9986 for the solar-louver concept, including louver actuators and reflectors, and 0.9986 for the electric-heater concept, including the heaters and switches.

Justification of the Preferred Design--The conventional louvers were chosen as the preferred concept. The reliability and weight of the

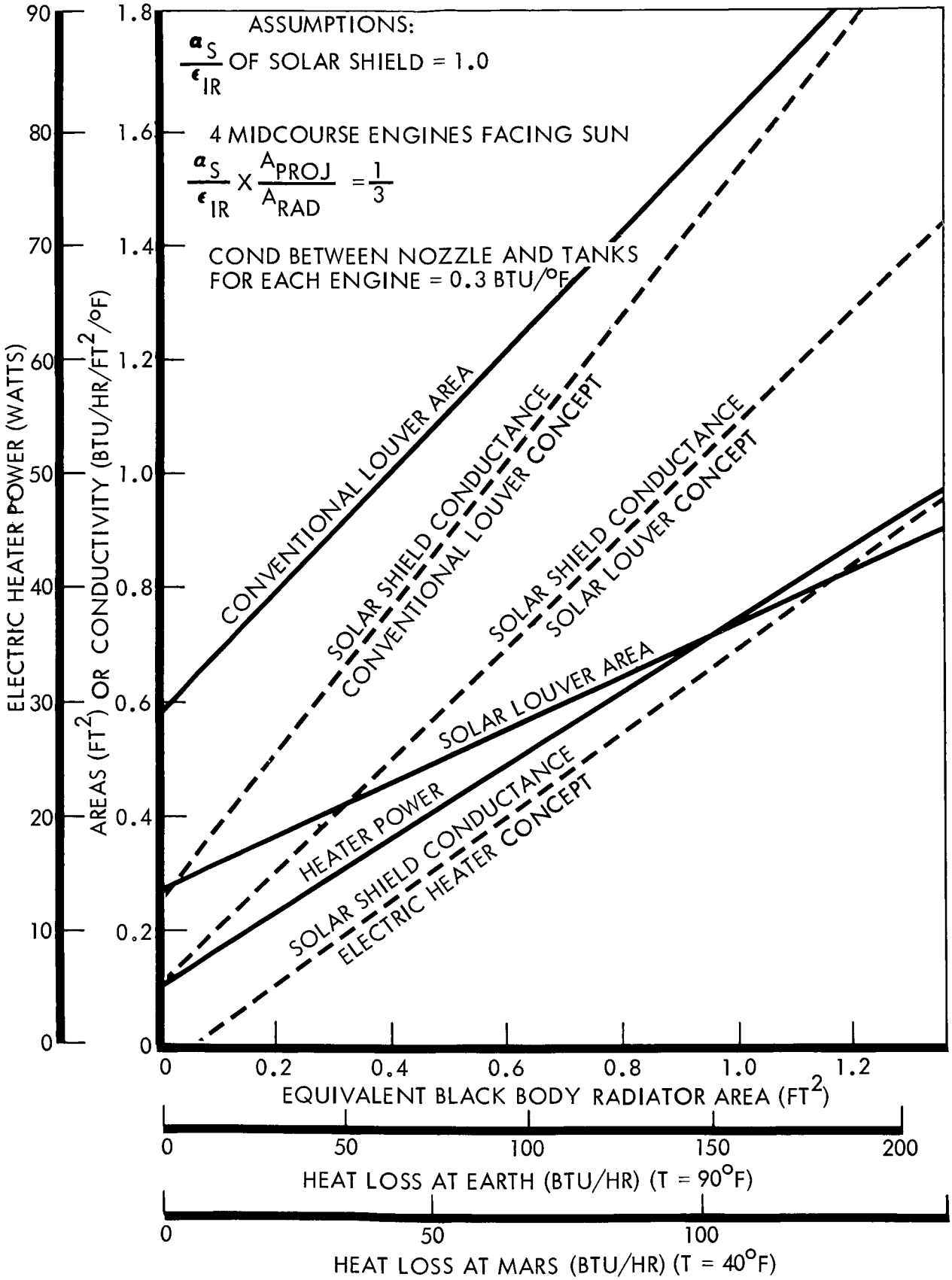

Figure 4.4-19: Propulsion Module Temperature Control Performance

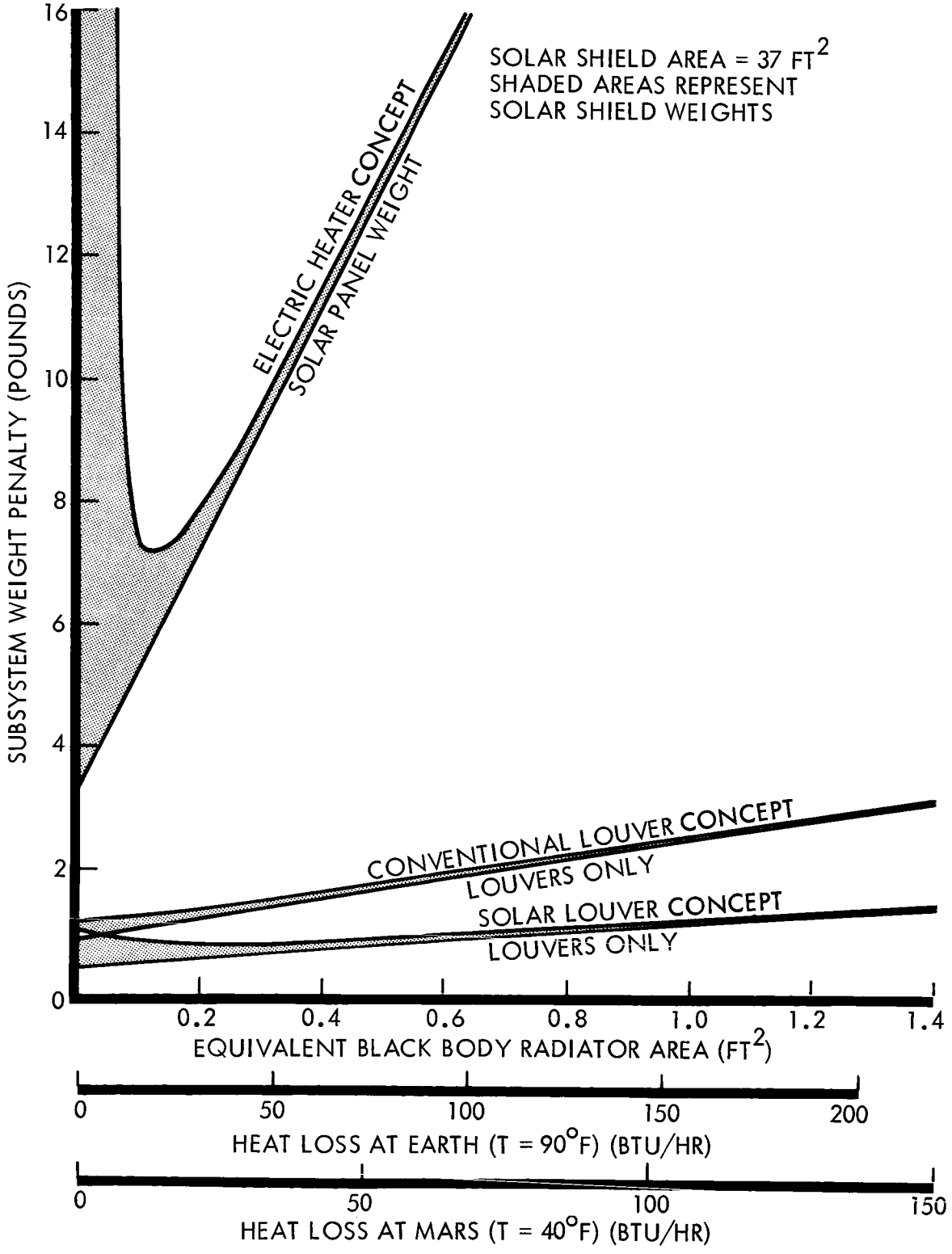

Figure 4.4-20: Concept Weight Penalties

conventional and solar louvers were essentially the same. Therefore, the decision was made on the basis of the space-proven experience of the conventional louvers.

4.4.1.4 Planet-Scan Platform

The planet-scan platform includes the planetary sensors, housing and articulation gear to observe Mars during the orbiting phase. The platform rotates during the orbit, changing its position in relation to the Sun and deep space. This rotation represents the major temperature-control problem.

The thermal-control concepts considered are space radiators, conventional louvers, and control of platform orientation. These three concepts are shown in Figure 4.4-21. Each concept is judged on the basis of reliability and weight.

The temperature requirements and heat dissipated for the scan platform components are shown in Table 4.4-8.

TABLE 4.4-8

Item	No. Req'd	Heat Dissipated (Watts)	Operating Temperature Limits (°F) Min	Max	Dormant Temperature Limits (°F) Min	Max	Wt.
T. V. Camera	2	1.0 Ea.	+15	+131	-22	+176	43
Mars Scanner	1	4.4	-40	- 4	-58	+158	20
IR Spectrometer	1	2.5	-125	+ 50	-125	+140	27
Support Structure and Actuating Equipment	1	5.0					45
TOTAL		13.9					135

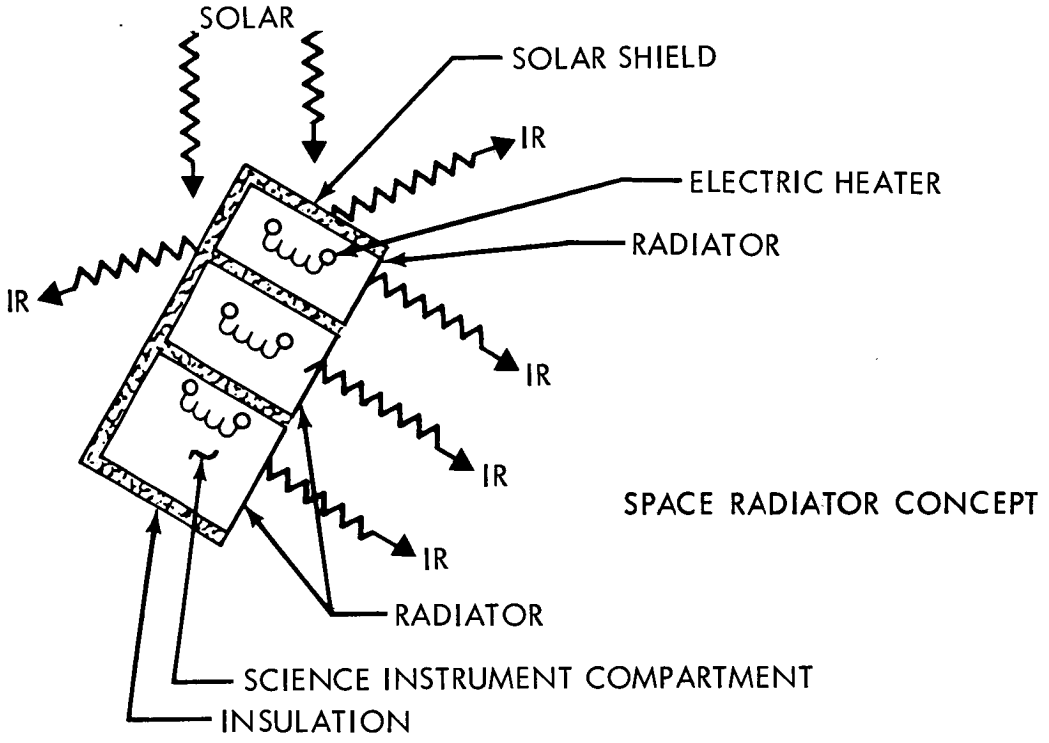

SPACE RADIATOR CONCEPT

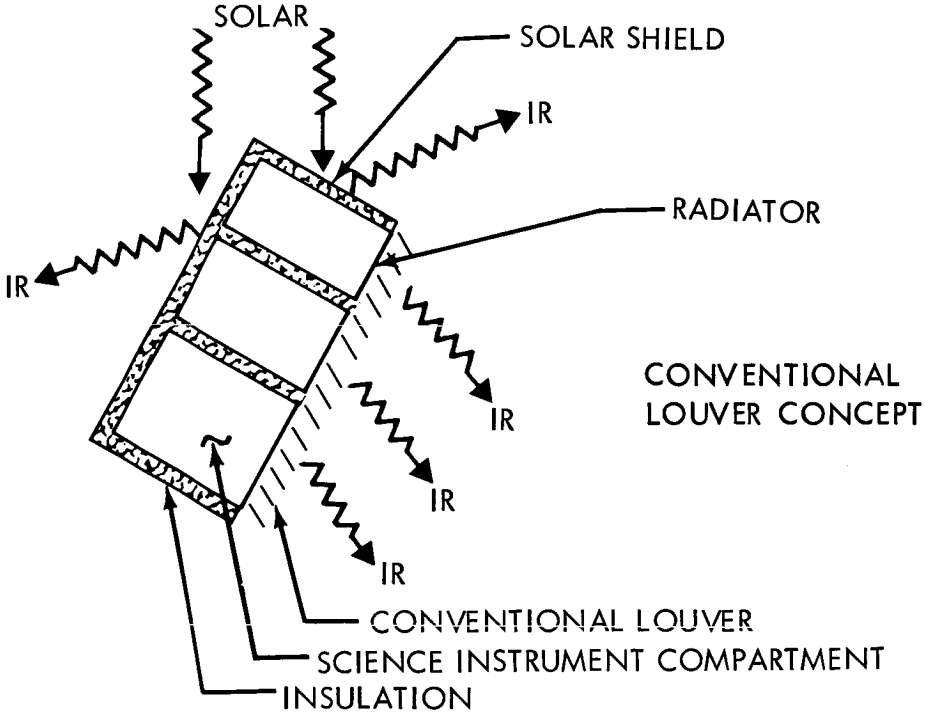

CONVENTIONAL LOUVER CONCEPT

45

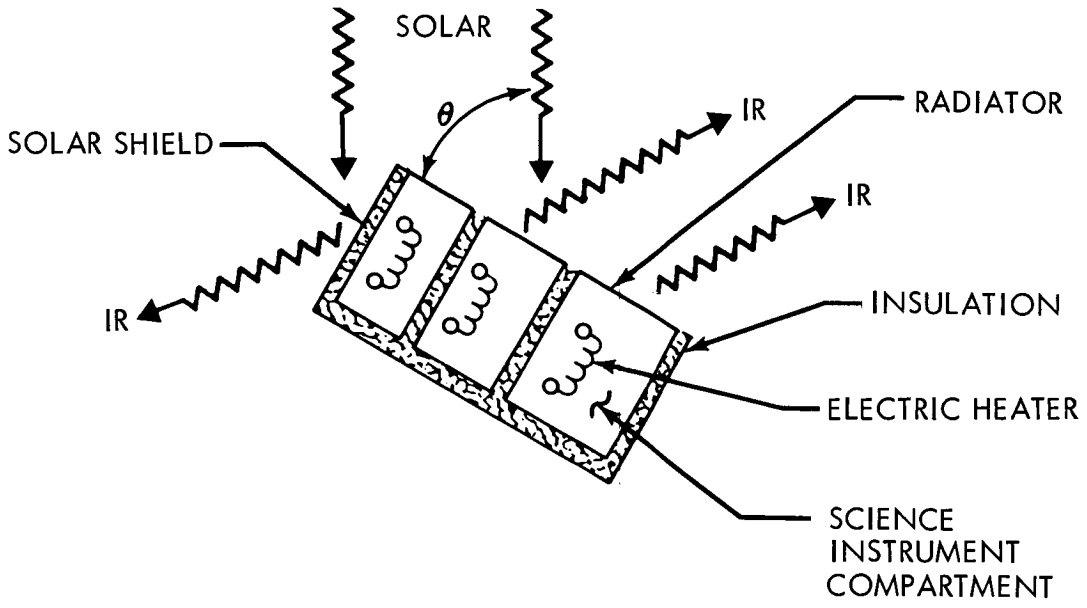

ORIENTATION CONCEPT

Figure 4.4-21: Planet Scan Platform Functional Block Diagram

The space-radiator concept uses a radiator plate facing deep space to reject the heat produced by the components. An insulated black solar shield with an $\alpha_s/\epsilon_{IR} \cong 1.0$ is provided to reduce the heat flow into and out of the platform except as controlled by the space radiator. The black solar shield is provided on all sides of the platform except the radiator face and the viewing ports since the Sun strikes all surfaces except the viewing port during the mission. A black radiator with an $\alpha_s/\epsilon_{IR} = 1.0$ is provided for heat rejection since it is not subject to degradation from the Mars environment. The scan platform will be stowed with the radiator facing the spacecraft to maintain component temperatures during transit. Automatically controlled electric heaters will be required within each science experiment to maintain temperatures during dormant and occultation periods in orbit.

The conventional louver concept uses space radiators covered with conventional louvers to provide variable heat rejection for the scan platform equipment. During the transit time, the louvers are rotated toward the spacecraft allowing heat from the spacecraft structure to maintain component temperature without the addition of electric heat. A solar shield and radiator plate identical to the space radiator concept are provided for temperature control. Highly specular louver blades are provided for an overall evittance of 0.70 in the open position and an ϵ =0.10 in the closed position. Electric heaters with automatic temperature controls within the components are provided for emergency heating in case of component failure.

The orientation concept uses a radiator plate that is oriented toward space for heat rejection or toward the Sun to add heat during the dormant periods of the mission. A heater is included to provide for periods of solar occultation. The radiator is sized for no heat dissipation at Mars with $\theta \sim 90^{o}$. During the transit period, the radiator will be rotated into the spacecraft to maintain proper temperature control without the use of electric heaters. A solar shield and radiator identical to the space radiator concept are provided. Temperature control is achieved during the orbit dormant period by rotating the radiator face with respect to the Sun. Automatic electric heaters within the components will be required to maintain proper temperature control in case of component failure and periods of occultation.

Weight--Concept weights were established on the basis of operation for an 18-hour orbit with a maximum solar occultation of 2.5 hours. The scan platform scientific equipment was assumed to operate from 15 degrees before morning terminator to 15 degrees past evening terminator.

The total subsystem weight penalties for the three concepts considered, including the power penalty for electric heaters, are:

Space radiator concept--6.6 pounds

Platform orientation concept--5.8 pounds

Conventional louver concept--5.2 pounds

Reliability--Reliability was computed on the basis of concept complexity. No major differences were found. The reliability for the planet scan

platform temperature control concepts are 0.99998 for the conventional louver concept, including louver actuators, 0.99900 for the platform orientation concept, including electric heaters and orientation drive motors, 0.99991 for the space radiator concept, including the electric heaters.

Justification of Preferred Design--The conventional louver concept was chosen because there appeared to be no weight nor reliability advantage in selecting the other concepts. The conventional louver has proven experience and is capable of operating with varying science payloads.

4.4.2 Packaging and Cabling

Summary--Investigation was made of spacecraft packaging and cabling requirements for the 1971 Voyager mission. The packaging concept selected provides for placement of the 19 assemblies around a cylindrical shell as shown in Figure 4.4-22. Each package is bolted to a structural stiffener on the shell by standard-spaced bolts at the back side (i.e., the side toward the spacecraft centerline). Each package has a standard 8-inch radial dimension, 8-inch or 16-inch circumferential dimension, and variable dimension along the spacecraft centerline to suit volume and temperature control requirements. Cabling is connected to the spacecraft packages at the side, top, or bottom by NAS 1599 circular connectors manually assemblied. Packages are shielded by insulation and meteoroid bumpers. A louver assembly is located at the front side (i.e., facing space) of those packages requiring modulated temperature control. Spacecraft cabling is in tray harnesses.

Packaging and cabling trades have been limited to the spacecraft system level. Selection of detail packaging methods within the assemblies will be discussed as part of the subsystem design descriptions in Section 4.0, Volume A. Electronic packaging standardization including control of parts through a preferred parts document is described in Section 5.0, Volume A.

As indicated in the logic chart (Figure 4.4-23), package installation methods considered were flush mounted and back mounted. The flush-mounted assembly is similar to the Mariner IV, utilizing the structure

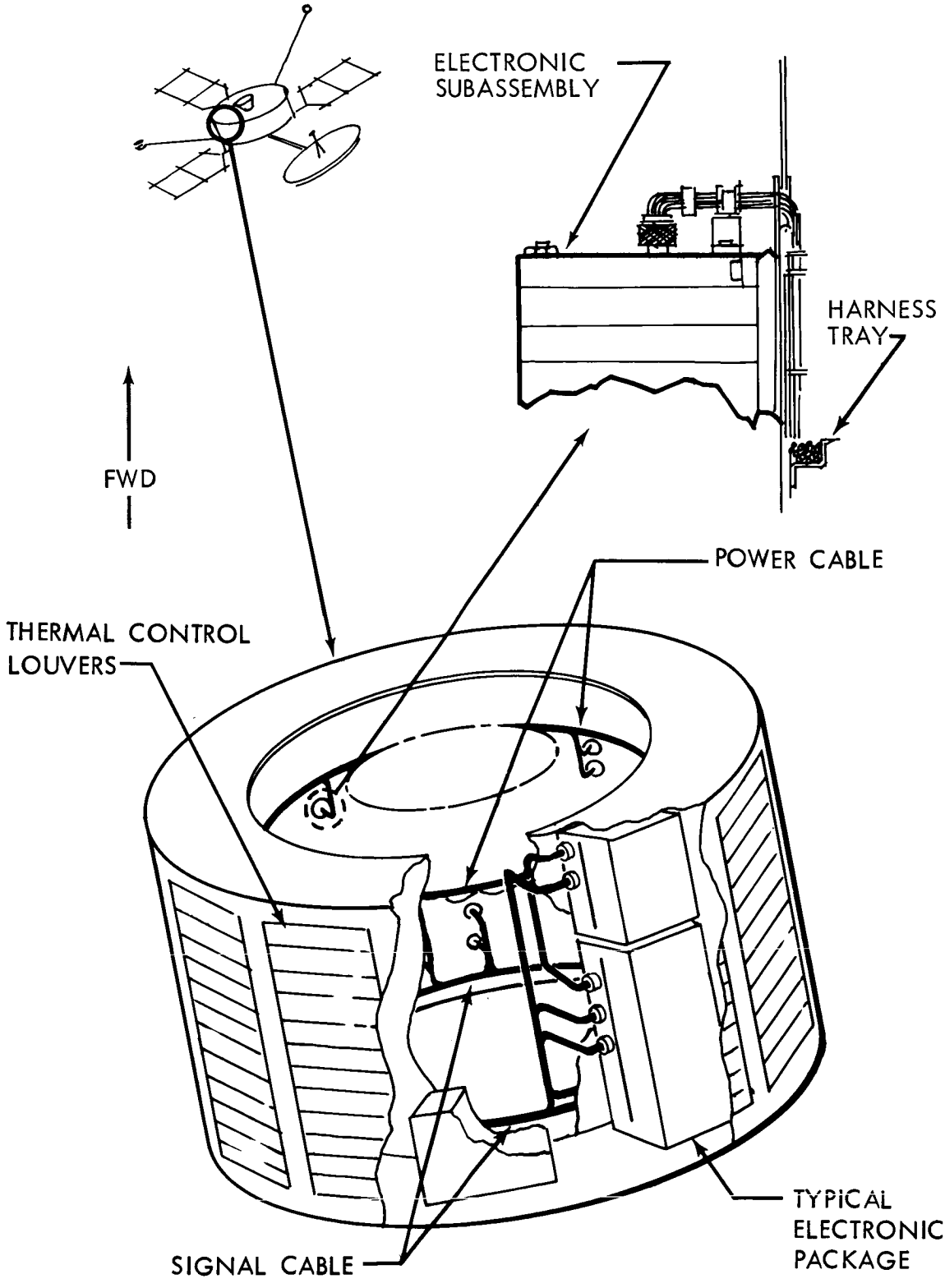

Figure 4.4-22: Spacecraft Packaging and Cabling

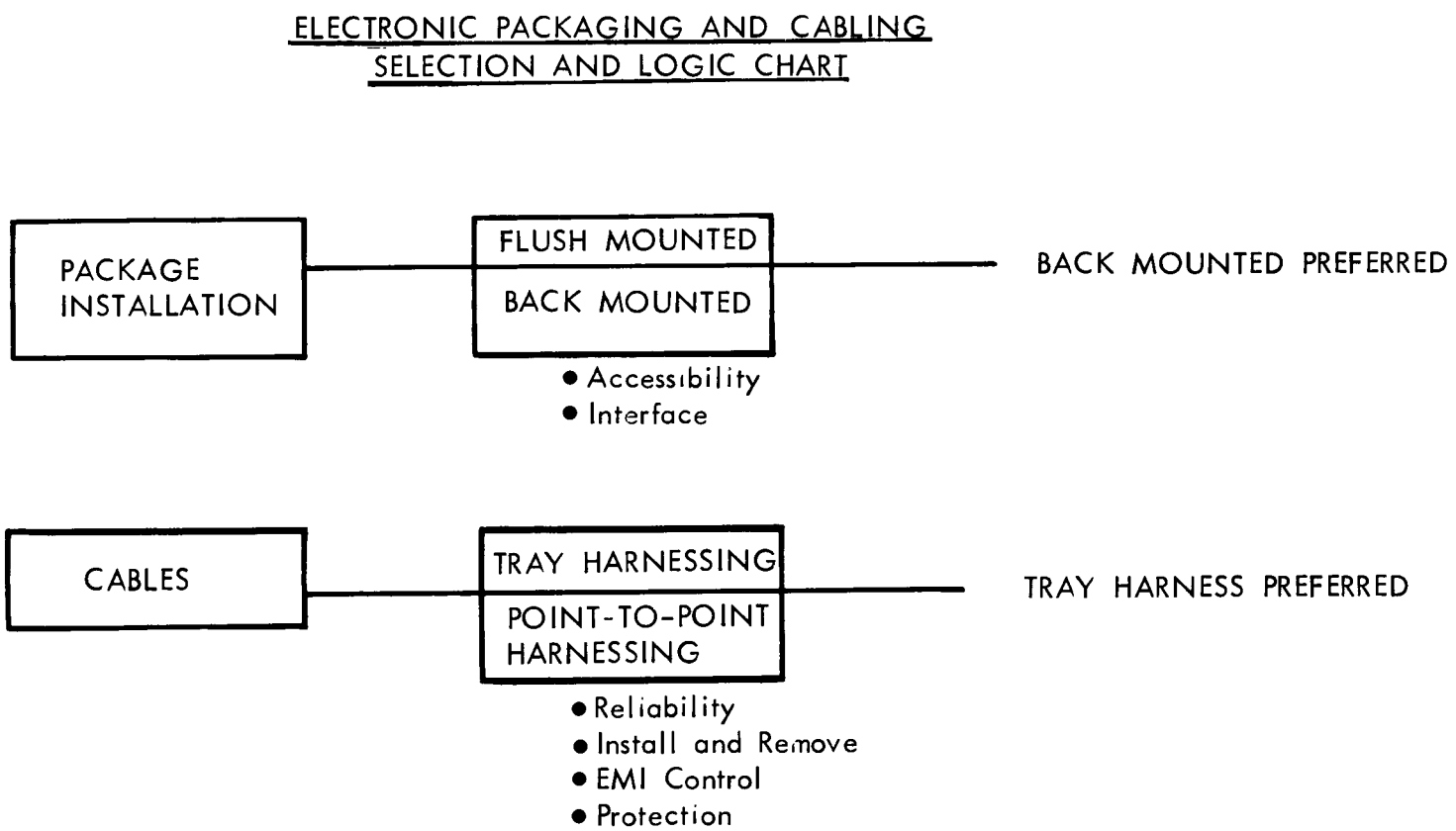

Figure 4.4-23: Installation Of Packages And Cables

shear wall as the radiating face. This method provides good lateral thermal distribution and meteoroid protection. The back-mounted installation is attached to the structure with the package completely exposed, providing good accessibility, handling, temperature control, adaptability to change, and interface simplicity. The back-mounted installation is preferred because its features result in inherently better reliability.

The study on cabling considered two conventional cable and harness runs, one with cable runs around the periphery of the structure utilizing harness trays, the other direct point-to-point routing using the structure for mounting support. The peripheral tray arrangement was preferred because it improves reliability through easier installation and removal, provides better electro-magnetic interference control, and is better protected.

Packaging

Back Mounted--The back-mounted package, or "corn cob" type mounting, is attached to the structure by standard-spaced bolts at the back side (i.e., the side toward the spacecraft centerline). The package radiating surface faces space. Meteoroid protection is provided by a bumper on the package space-facing surface. Temperature control is obtained by louvers attached to the spacecraft equipment compartment bulkheads.

Flush Mounted--The flush mounted package is attached to a shear carrying-radiator plate on the exterior of the spacecraft. Meteoroid protection is provided by either the thickness of the radiator plate or a bumper

on the outside of the plate. Access to connectors is limited unless provisions are made to reach the inner portion of the package through the top or bottom of the spacecraft.

The two concepts have been evaluated on the basis of interface complexity and accessibility.

Interface Complexity--The flush-mounted unit employs the front side to carry spacecraft structural loads. This requires numerous mounting bolts to be installed in close-tolerance holes. Since the mounting structure serves as a thermal junction, adjacent packages are thermally dependent.

The back-mounted unit is not required to carry spacecraft primary structural loads. As a result, units can be positioned as required to meet thermal balance, weight and balance requirements. The thermal interaction between adjacent units can be controlled by the design of the mounting interface.

Accessibility--The spacecraft and test connectors of the flush-mounted unit are not readily accessible when the unit is installed. Special supports for the spacecraft package harness are required to protect the cable from damage during installation and launch vibration. Inspection of the installed connectors is difficult.

The back-mounted concept is arranged for cable and test connector manual installation on the sides. Spacecraft and test connectors are accessible

for inspection and test by removal of the insulation strip. Structure, louvers, and cabling are not disturbed for this procedure. Installation of the package is easily accomplished, using readily available attachment points. As a result of the foregoing, the back-mounted package installation is preferred.

Cabling--The conventional cabling and harness technique employed on Mariner IV was selected for interconnecting electronics for the spacecraft. Flat cables (round wire) harnesses and flat ribbon wire harnesses were evaluated and rejected because of their incomplete development status.

Two conventional cable and harness arrangements were considered:

1) Routing of a harness in a tray around the periphery of the spacecraft equipment support structure as shown in Figure 4.4-2. This arrangement consists of two harness trays, one for signals and the other for electrical power distribution.
2) Direct routing of cables through the structure using the shortest route possible (point-to-point). This arrangement would rely on fastening cable clamps directly to the structure, minimizing additional support.

The two concepts were evaluated on the basis of weight and reliability. The tray-routed harness was selected on the basis of improved reliability and conservative design practice. The positive attachment, protection against handling damage, and ease of cable fabrication of the cable tray concept more than compensated for the pounds weight penalty over the direct routing concept.

4.4.3 Spacecraft Structure

Summary--The primary structure of the spacecraft, is shown in Figure 4.4-24. The equipment-support structure consists of a 0.095-inch-thick AZ31B-H24 magnesium cylindrical shell, 60 inches in diameter and 32 inches long. This cylindrical shell is stiffened by vertical Z-section stiffeners, 4.75 inches apart. The stiffeners also act as equipment support beams. The structure is supported at top and bottom by an 80-inch-diameter magnesium ring frame. The upper frame consists of a 0.070-inch-thick AZ31B-H24 web with ZK60A-T5 extruded chords and stiffeners. The lower-frame web is 0.15-inch thick. Flight-Capsule vertical loads are introduced at four points into machined 7075-T6 truss-type longerons. These longerons are equally spaced around the periphery of the cylinder oetween the upper and lower frames. The lower-support structure consists of a welded 6Al-4V annealed titanium tubular space truss. This truss attaches to the equipment-support structure at each longeron and to the Centaru adapter at eight points. A truss-type bulkhead is located at the separation plane. Vertical members are 3.00 inches in diameter with 0.047-inch-thick walls. Diagonals are 3.00 inches in diameter with 0.034-inch-thick walls. The diameters of lower bulkhead members range from 2.0 to 2.5 inches. The primary-load-carrying structure weighs 250 pounds and is capable of supporting a 2300-pound capsule with a 3500-pound propulsion subsystem or a 4500-pound capsule and a 500-pound propulsion subsystem. The structure also supports a 250-pound science payload and 1500 pounds of nonstructure Spacecraft-Bus weight.

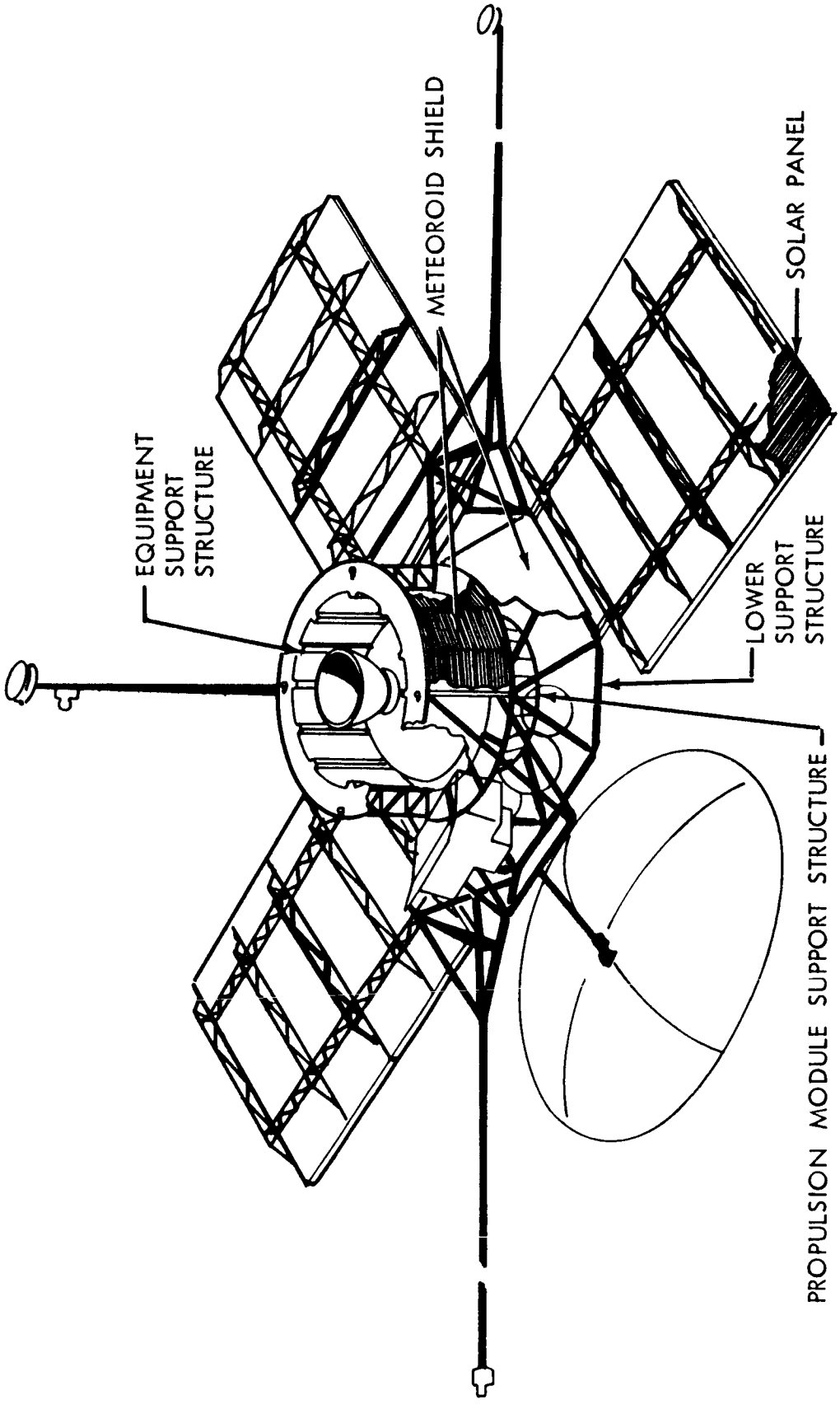

Figure 4.4-24: Structure Subsystem

The spacecraft structural concepts and arrangements discussed in this section comply with the specified general arrangement of the Planetary Vehicle. Structural design criteria and loading conditions specified in Section 2.1 of Volume A are used for preliminary sizing of the structures considered. The resulting design ultimate load factors, as developed in Boeing Document D2-82729-1, are summarized in Figure 4.4-25 and form the basis for structural trade studies.

The analysis of the primary structure is shown diagrammatically in Figure 4.4-26. The analysis included consideration of truss and semimonocoque-shell structural arrangements. Further, four-, six-, and eight-sided trusses were investigated. Aluminum, magnesium, and titanium were considered as structural materials for each arrangement. The study results show that for minimum weight a semimonocoque magnesium shell should be used for the equipment-support structure and a titanium truss for the lower-support structure.

Although the ideal structural-weight-optimization trades indicate that six-sided truss arrangements are lighter, this arrangement is not advantageous for mounting and temperature control of equipment within the equipment-support area. A four-longeron equipment-support structure using a magnesium shell and aluminum longerons was selected. With the upper structure arranged in this manner, a six-sided lower truss is impractical; therefore, a lower truss having eight attachment points at the Centaur adapter and four attachments at the bottom of the equipment-support structure was selected. This lower-truss arrangement re-

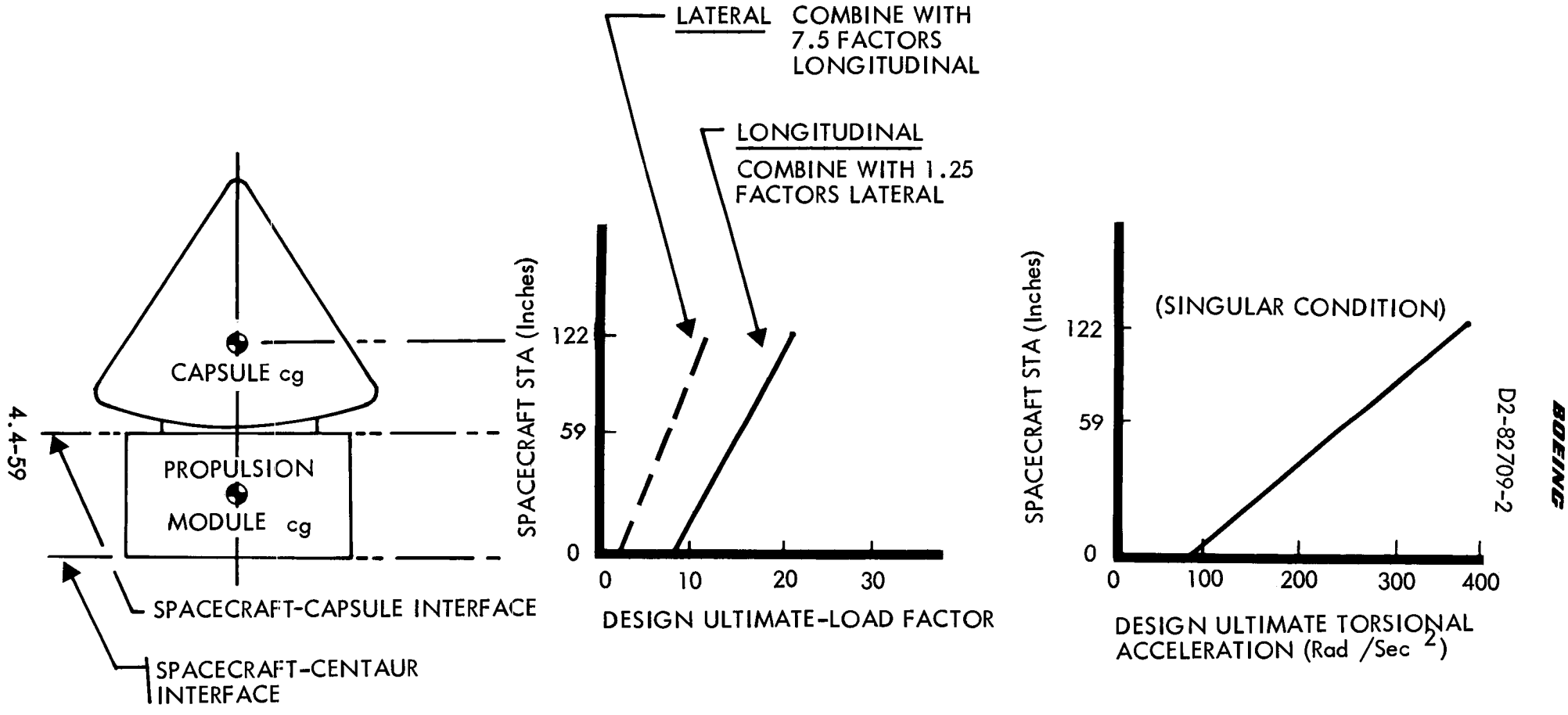

Figure 4.4-25: Design Ultimate — Load Factors

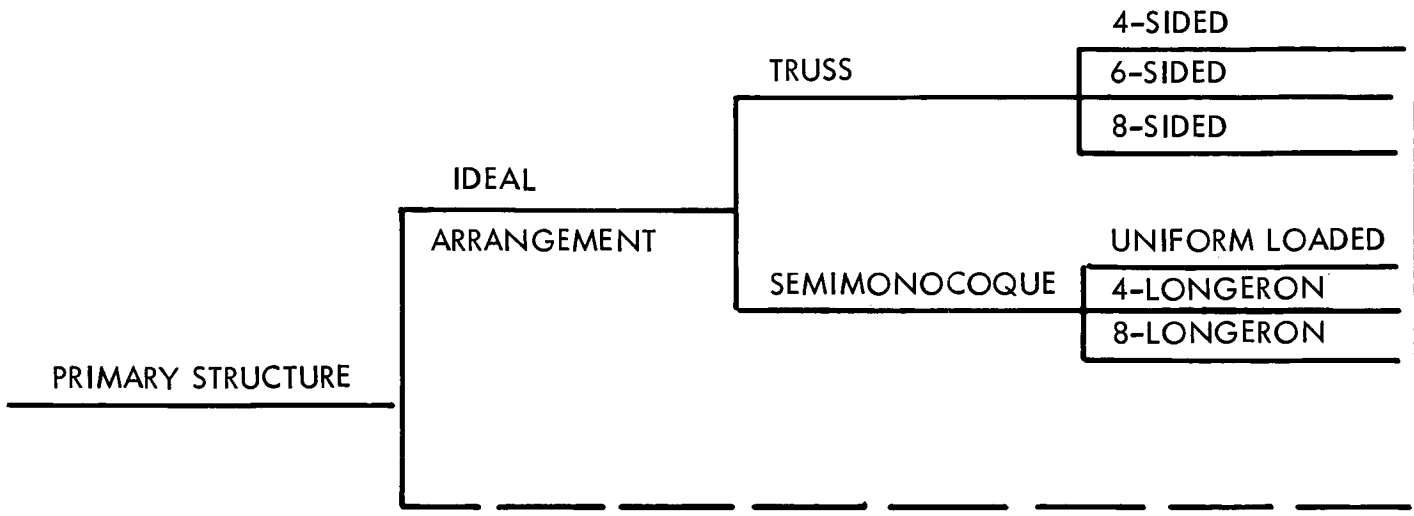

(SEE SECTION 4.2)

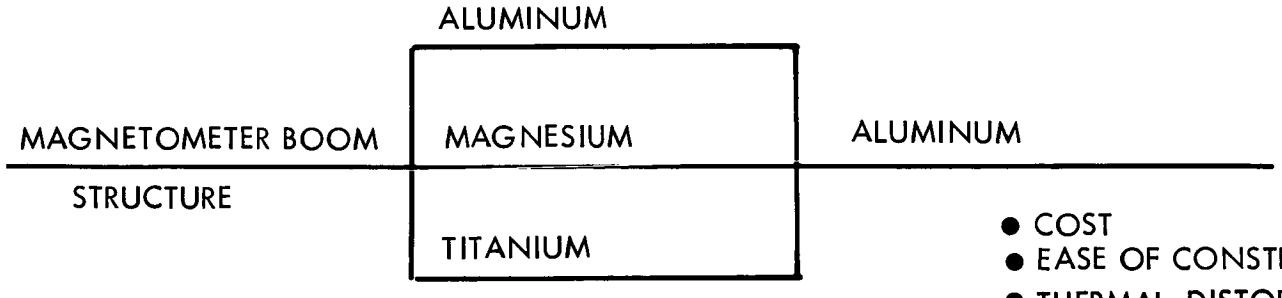

- COST
- EASE OF CONSTRUCTION
- THERMAL DISTORTION

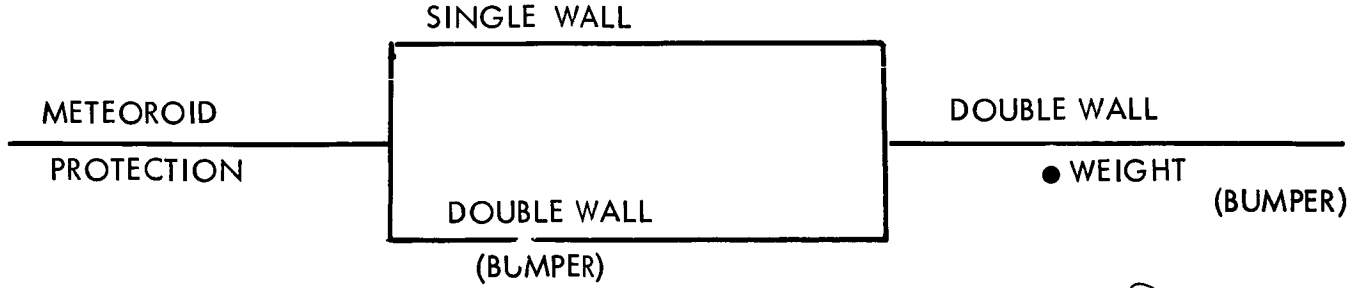

- WEIGHT

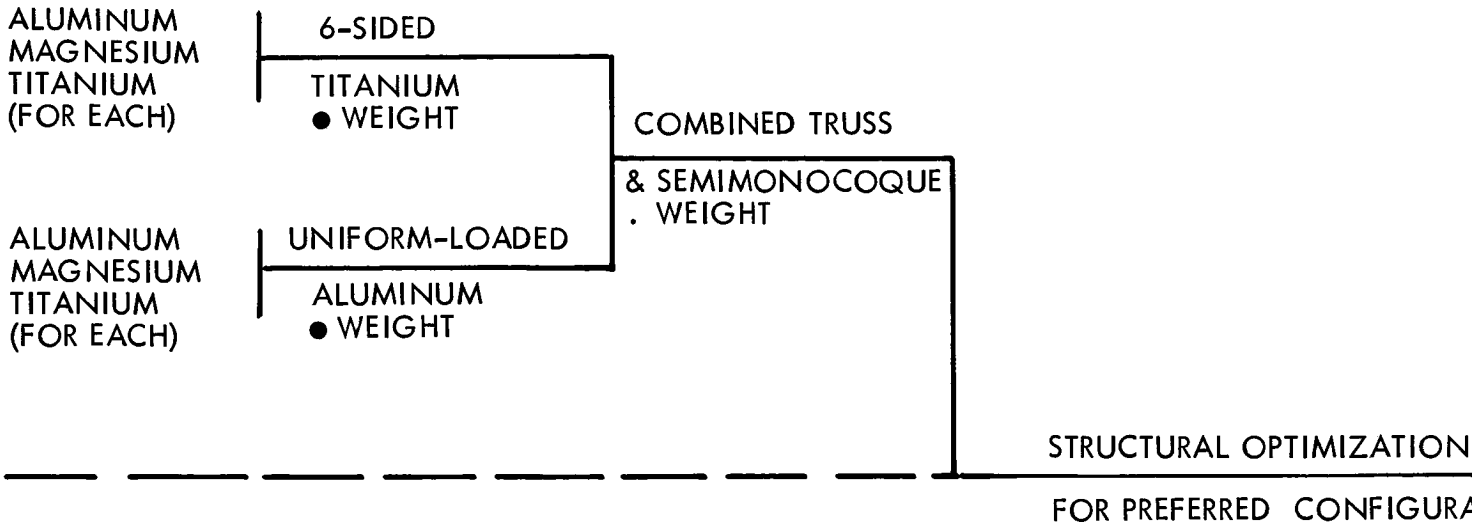
ALUMINUM
MAGNESIUM
TITANIUM
(FOR EACH)
6-SIDED
TITANIUM
● WEIGHT
ALUMINUM
MAGNESIUM
TITANIUM
(FOR EACH)
UNIFORM-LOADED
ALUMINUM
● WEIGHT
COMBINED TRUSS
& SEMIMONOCOQUE
. WEIGHT
STRUCTURAL OPTIMIZATION
FOR PREFERRED CONFIGURA

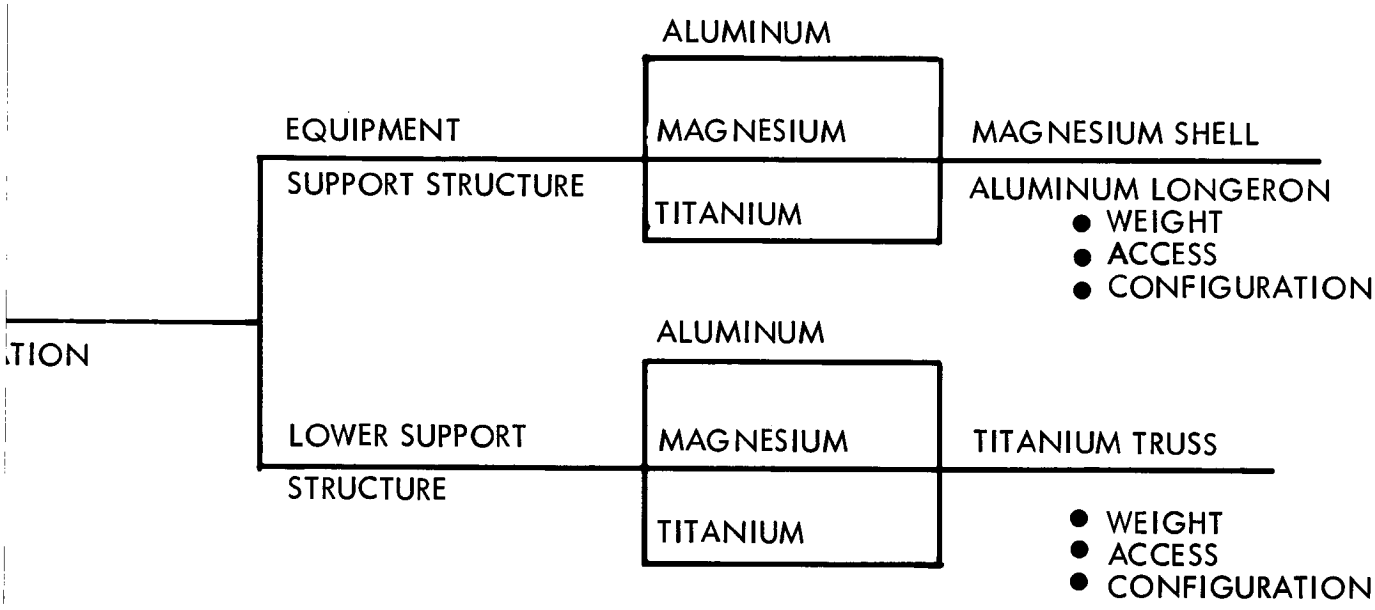

Figure 4.4-26: Structures — Selection Logic Diagram

duces the concentration of loads in the adapter and facilitates solar-panel and appendage support.

Solar-panel structural trades are presented in Section 4.2 of this document. Studies leading to selection of the lightest magnetometer boom were based on strength requirements imposed by the 7.5-g design ultimate load experienced in the stowed condition during boost. A 606-T6 Aluminum tube linearly tapered from 6- to 2-inch diameter along its length was selected. Meteoroid protection is provided by a single-sheet bumper of 0.006-inch minimum-gage aluminum spaced approximately 1 inch from the surface being protected. This bumper in conjunction with the 0.06 inch or thicker shell fulfills protection requirements. The thermal barrier around the lower truss serves as a bumper to protect the propellant and nitrogen tanks from meteoroid damage.

4.4.3.1 Primary Structure

The primary structure design is based largely on the requirement to support the capsule and the propulsion module as stated in Volume A, Section 1.5 of this report. Major design loads for the structure are determined by these massive components and the appropriate load factors defined in Figure 4.4-25. A summary of the design loads for each condition is presented in Figure 4.4-27.

For the ideal arrangement of the primary structure, two basic concepts have been considered for the Model 945-6026 preferred spacecraft configuration described in Section 3.0. These two concepts are the space-truss and semimonocoque type structures.

MISSION WEIGHTS

	1971 & 1973	1975 & 1977
PROPULSION MODULE	3500	500
CAPSULE	2300	4500

DESIGN LOADS [1]

LOAD CONDITION	STATION 5.0	STATION 27.0	STATION 59.0
1—LONGITUDINAL (COMBINE WITH LATERAL OF 1.25 FACTORS)	SHEAR (LB) A. 9750 B. 8750 AXIAL (LB) A. 107,120 B. 118,020 MOMENT (10^6 IN.-LB) A. 0.549 B. 0.73	SHEAR (LB) A. 7250 B. 6250 AXIAL (LB) A. 89,500 B. 100,400 MOMENT (10^6 IN.-LB) A. 0.302 B. 0.512	SHEAR (LB) A. 2875 B. 5640 AXIAL (LB) A. 48,300 B. 94,500 MOMENT (10^6 IN.-LB) A. 0.181 B. 0.354
2—LATERAL (COMBINE WITH LONGITUDINAL OF 7.5 FACTOR)	SHEAR (LB) A. 48,300 B. 60,810 AXIAL (LB) A. 58,500 B. 52,500 MOMENT (10^6 IN.-LB) A. 3.98x B. 6.58	SHEAR (LB) A. 43,800 B. 56,310 AXIAL (LB) A. 43,500 B. 37,500 MOMENT (10^6 IN.-LB) A. 2.65 B. 4.88	SHEAR (LB) A. 27,600 B. 54,000 AXIAL (LB) A. 17,300 B. 33,800 MOMENT (10^6 IN.-LB) A. 1.74 B. 3.41
3—TORSIONAL (SINGULAR)	TORQUE (10^6 IN.-LB) 7.2	TORQUE (10^6 IN.-LB) 7.2	TORQUE (10^6 IN.-LB) 7.2

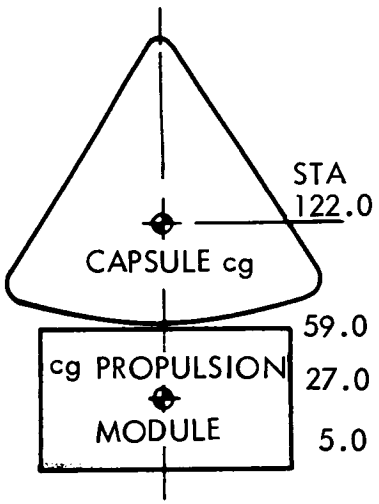

[1] A. LOADS REFER TO 1971 & 1973 CONFIGURATION
B. LOADS REFER TO 1975 & 1977 CONFIGURATION

Figure 4.4-27: Design Loads

The upper 32 inches of the space-truss arrangement were designed with vertical sides coinciding with the 40-inch radius of capsule-attachment points. The lower 22 inches were designed as a frustrum of a right-angle pyramid with the longitudinal members matching the upper-truss longitudinals and the 60-inch radius of the Centaur adapter. Preliminary structural designs were developed with four-, six-, and eight-sided truss arrangements typical of those shown in Figure 4.4-28 to determine the minimum-weight geometry for this concept. Weight estimates were calculated for each geometry based on 2219-T851 aluminum, AZ80A-T5 magnesium, and 6Al-4V titanium.

All truss members have been designed in compression to fail simultaneously in lateral and local buckling. All end fittings and joints have been included in these weight estimates. As shown in Figure 4.4-29, the six-sided configuration is the minimum weight arrangement. From a materials standpoint, the titanium truss is clearly the lightest due primarily to the members being designed in the short-column (inelastic buckling) range. In this range, member weight is a function of compression yield strength of the material and results in minimum cross-sectional area requirements.

The semimonocoque configurations consist of cone-cylinder combinations. The upper 32 inches were designed as a cylinder with a radius matching the 40-inch radius of the capsule-attachment points. The lower 22 inches were designed as a frustrum of a right angle cone with an upper surface radius matching the 40-inch radius of the cylinder and lower radius matching the 60-inch radius of the Centaur adapter. The following

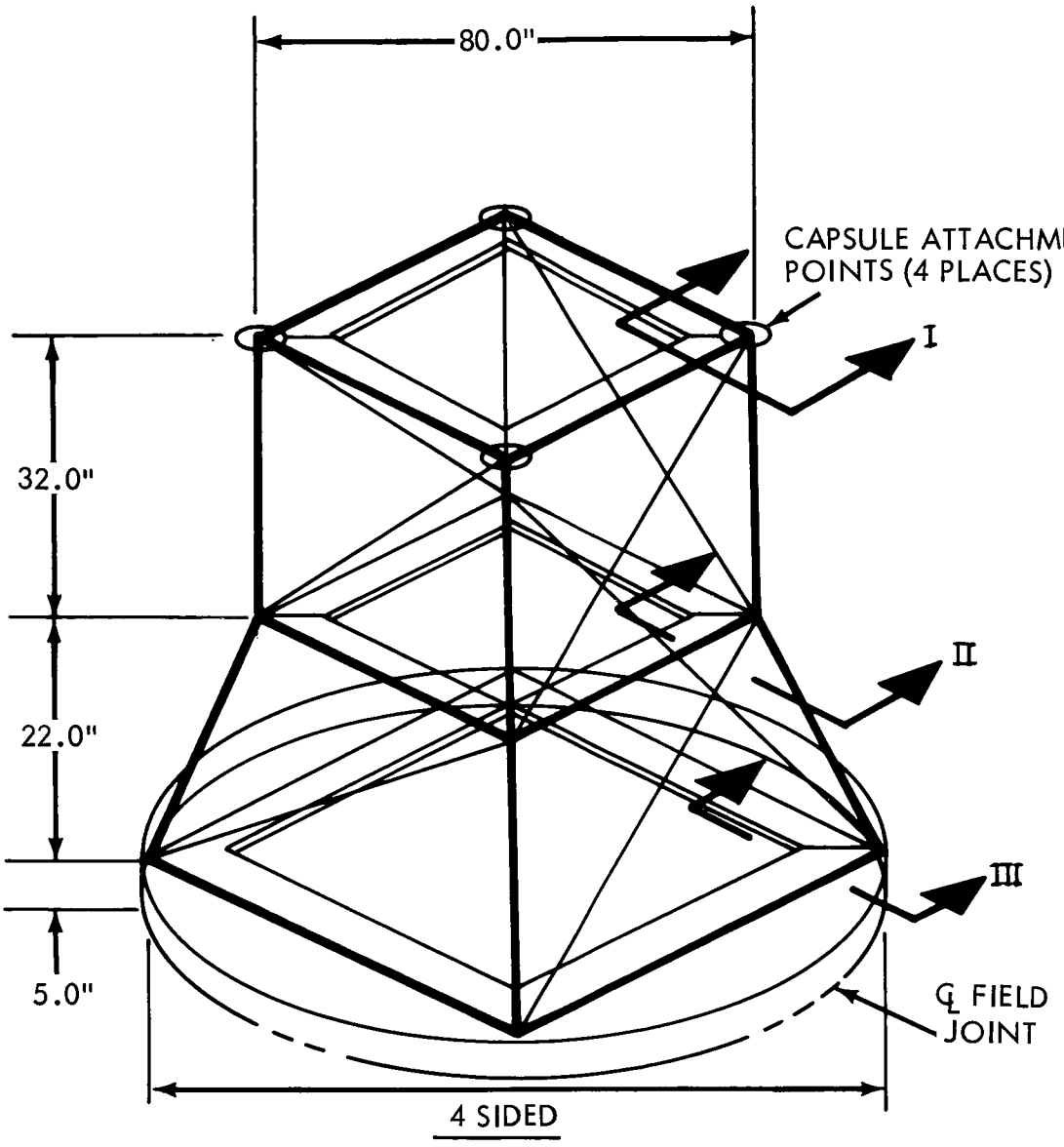
80.0"
CAPSULE ATTACHMEN
POINTS (4 PLACES)
I
32.0"
II
22.0"
III
5.0"
℄ FIELD
JOINT
4 SIDED

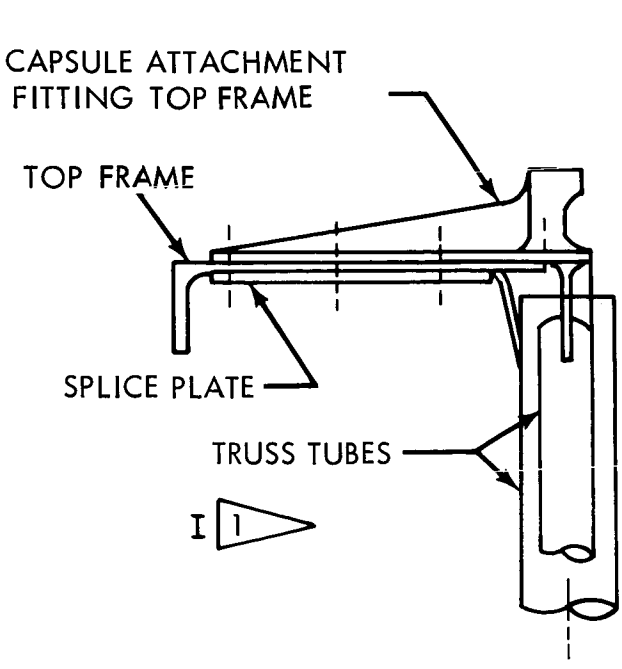
CAPSULE ATTACHMENT
FITTING TOP FRAME
TOP FRAME
SPLICE PLATE
TRUSS TUBES
I
1

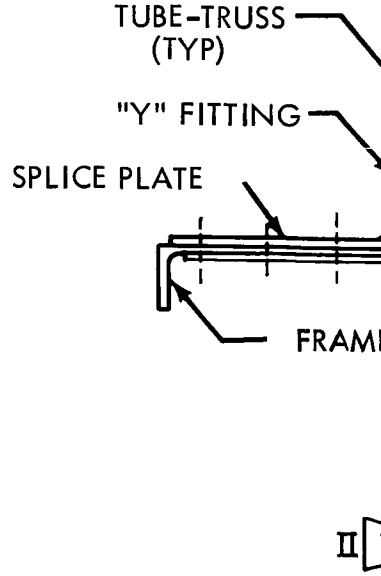
TUBE-TRUSS
(TYP)
"Y" FITTING
SPLICE PLATE
FRAM
II

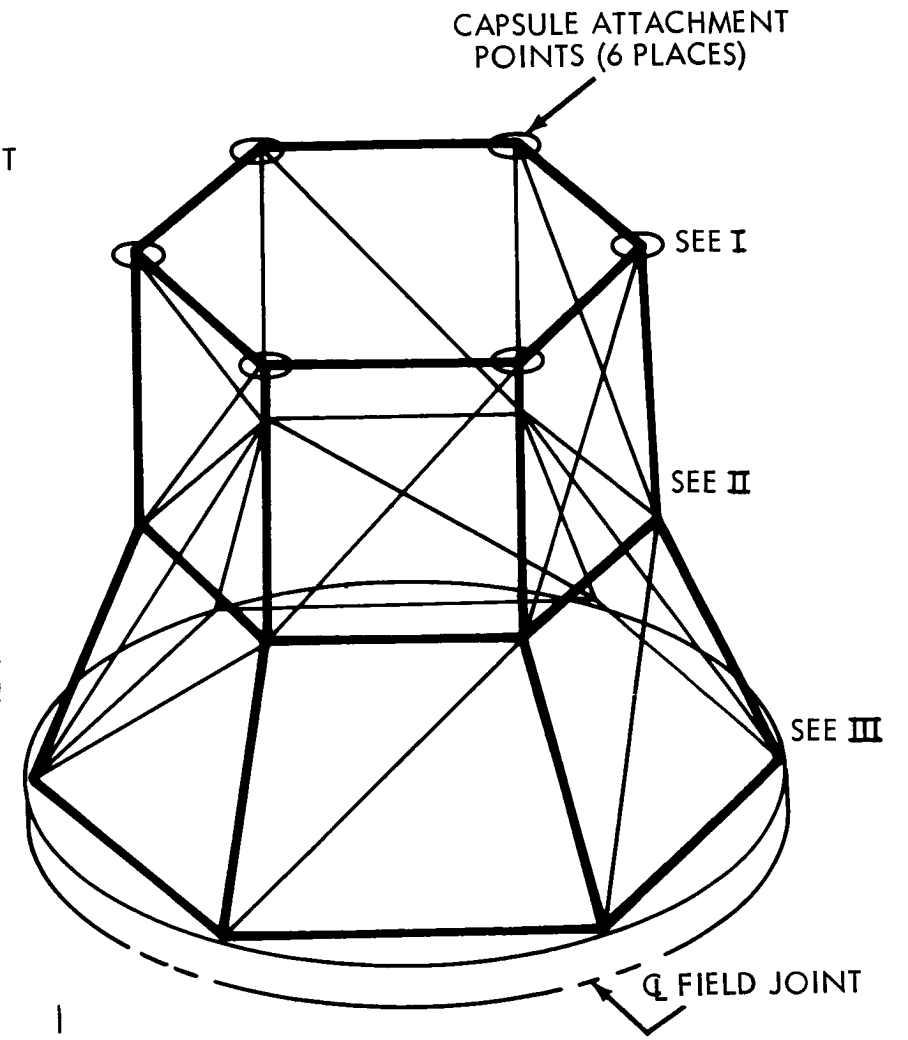
CAPSULE ATTACHMENT
POINTS (6 PLACES)
SEE I
SEE II
SEE III
℄ FIELD JOINT

6 SIDED

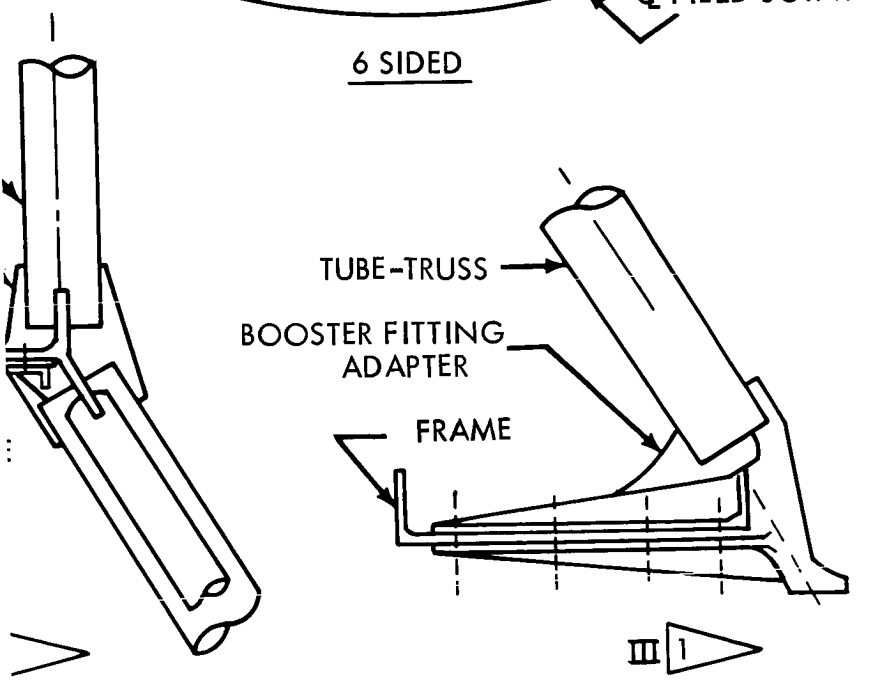
TUBE-TRUSS
BOOSTER FITTING
ADAPTER
FRAME
III 1

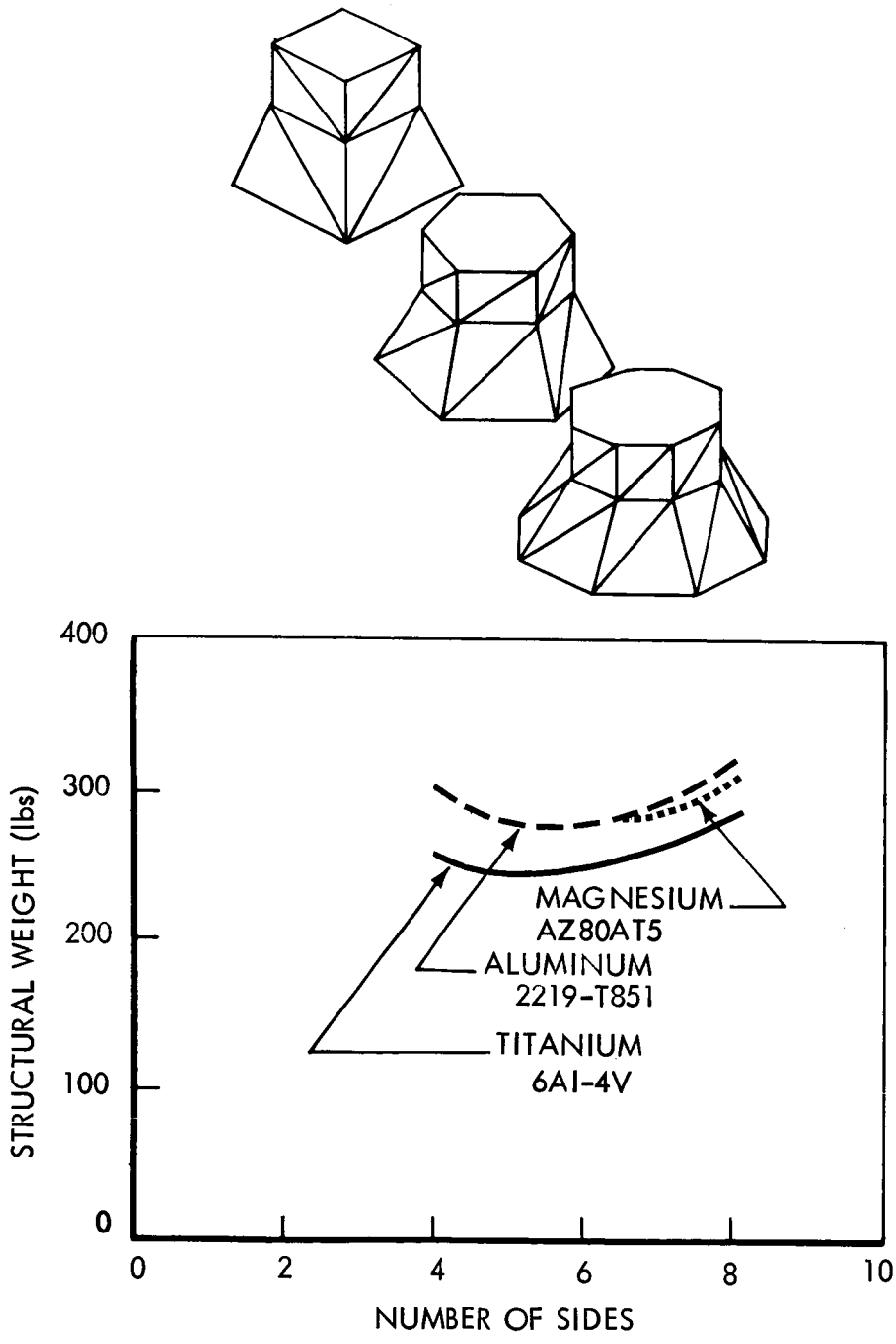

Figure 4.4-29: Truss Weight

preliminary structural designs of two shear-resistent-web semimonocoque structural arrangements were conducted:

1) A longitudinally stiffened shell with ring frames at the top and bottom of the cone-cylinder shell and a ring frame at the junction of the cone-cylinder sections--all loads were introduced uniformly into the shell structure by these frames (Figure 4.4-30).
2) A semimonocoque structure identical to 1) except that the longitudinal loads are carried by eight longerons (Figure 4.4-31).

Weight estimates, calculated for each design based on 2219-T851 aluminum, AZ31BH24 magnesium, and 6Al-4V titanium, are summarized in Table 4.4-9. Included in this figure for comparison are the truss weights. In addition, an estimated weight for a four-longeron semimonocoque structure is shown for comparison with the four-sided truss arrangement.

As shown, the uniformly loaded semimonocoque structure is the lowest-weight configuration--it weighs least when made of aluminum and is only 2 pounds heavier when made of magnesium. The titanium six-sided truss is the lightest configuration of all the structures considered--52 pounds lighter than the minimum weight shell. The lightest structural arrangement, however, results from a combination of a magnesium, semimonocoque uniformly loaded equipment-support structure and a six-sided titanium truss. This combination weighs 226 pounds. Six stiffeners in the shell must be increased in area at a penalty of 20 pounds to accept the concentrated loads induced by the truss.

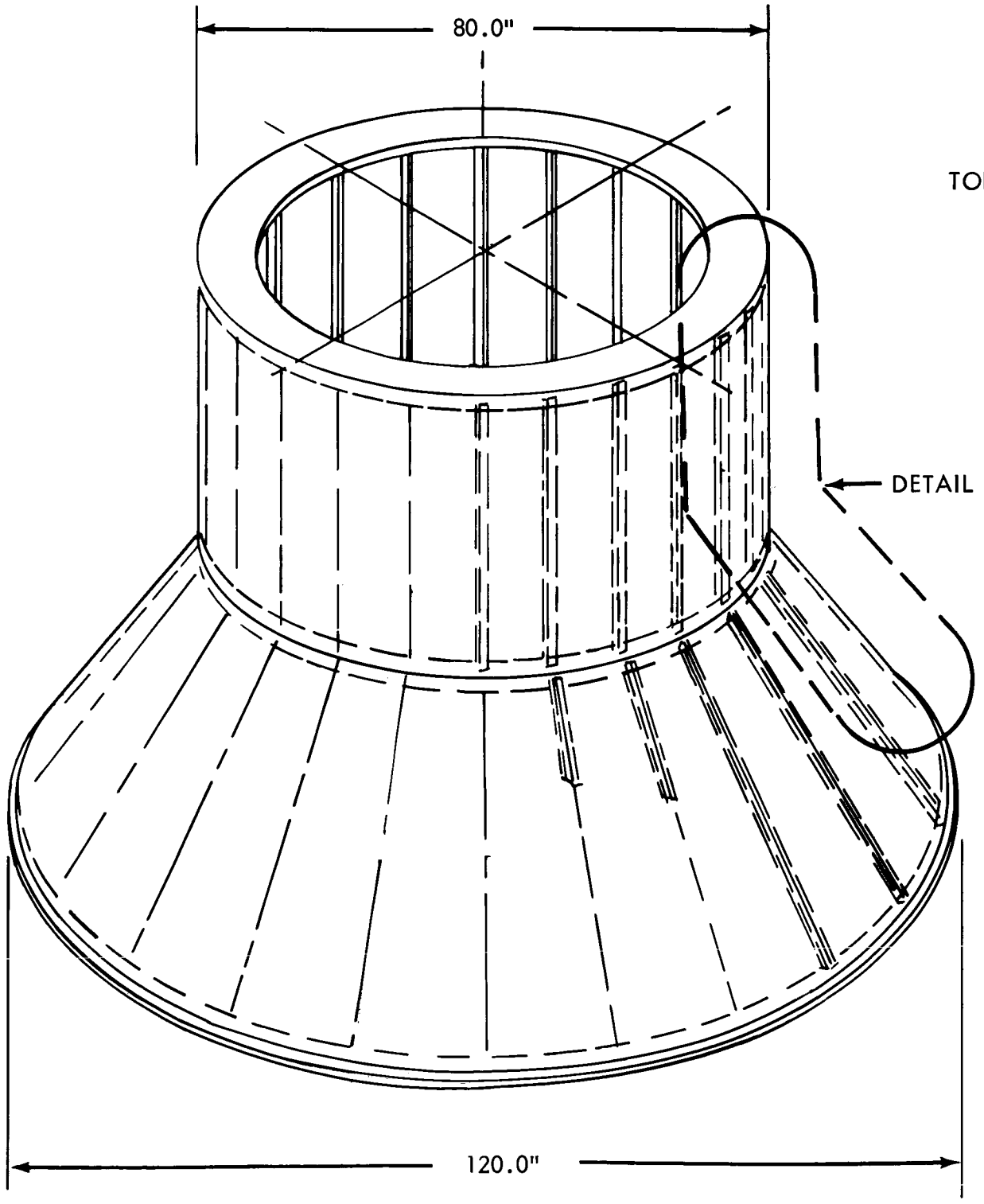

710

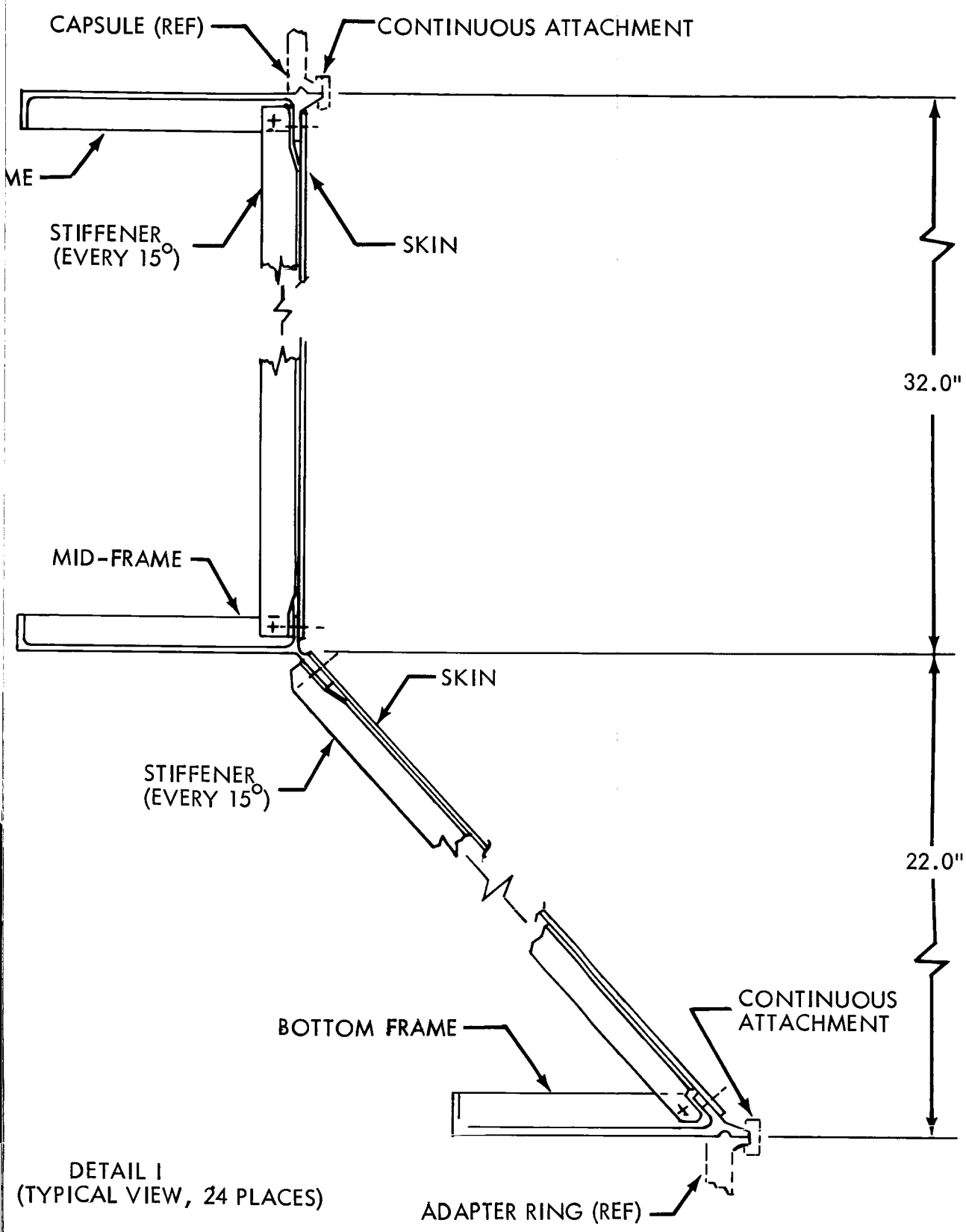

Figure 4.4-30: Semimonocoque Design

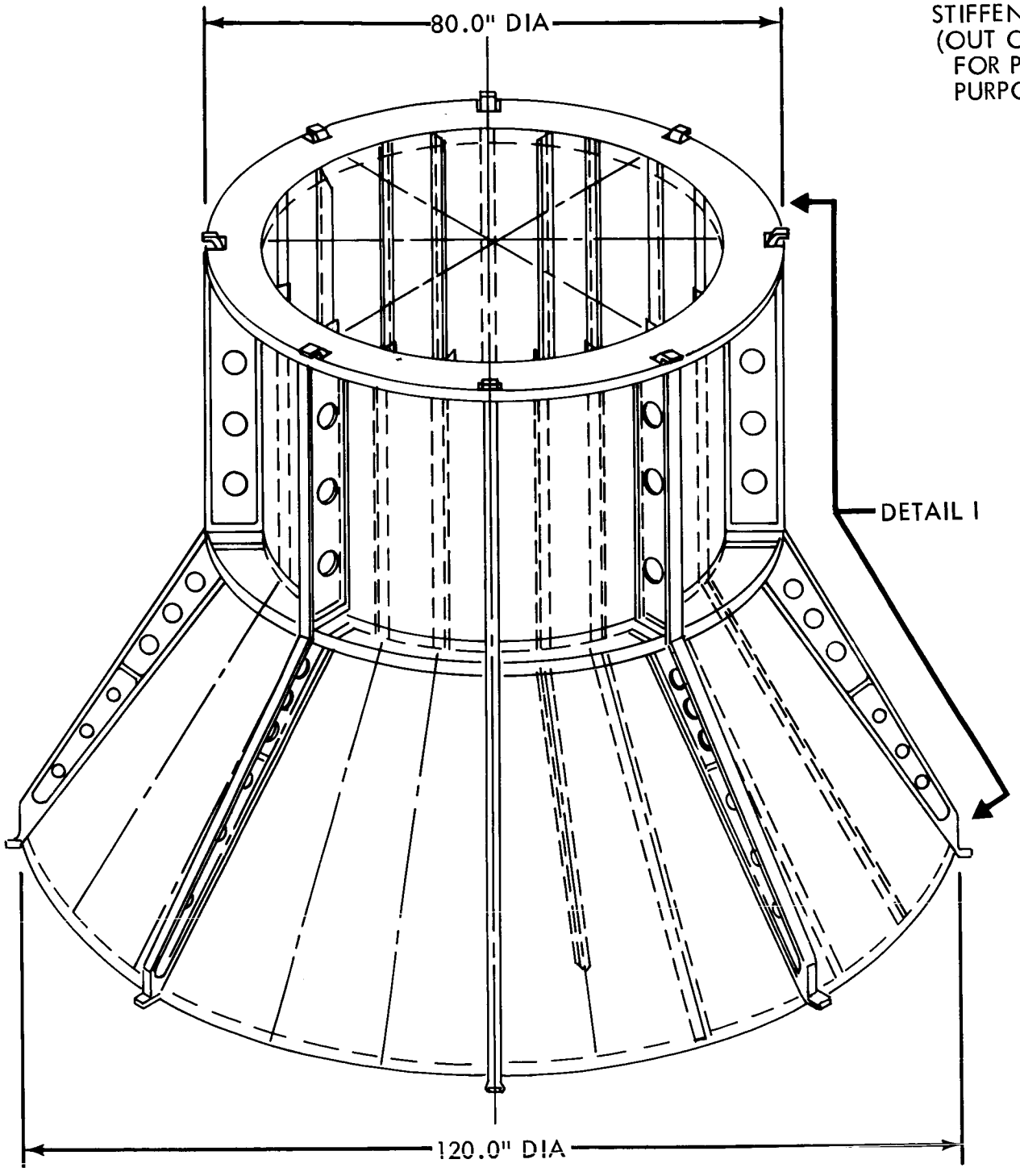

STIFFENER (
(OUT OF PO
FOR PICTO
PURPOSES)

730

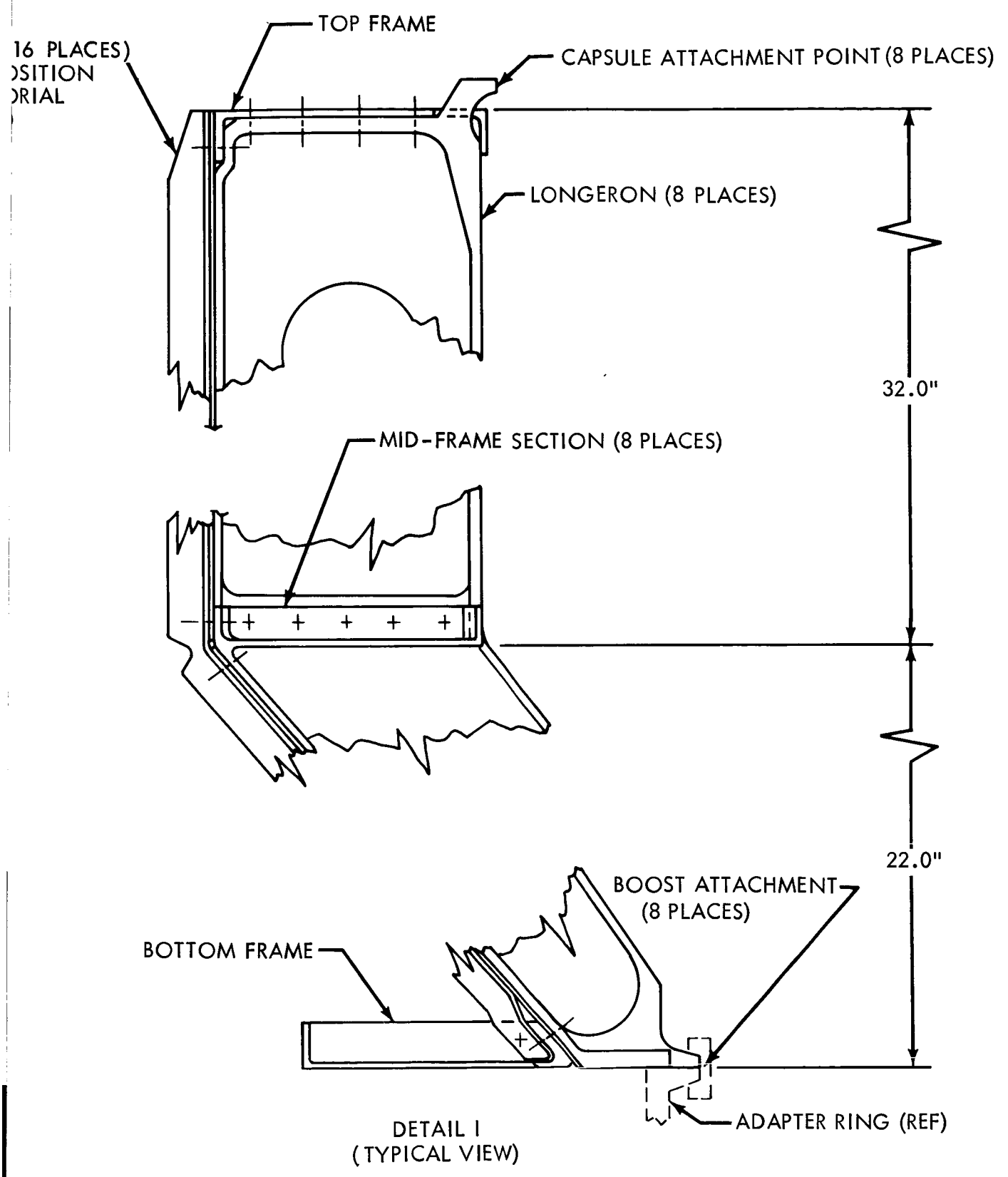

Figure 4.4-31: Semimonocoque Design

Table 4.4-9: STRUCTURAL CONCEPT WEIGHTS

STRUCTURAL CONCEPT	Lwr. Support Struct.			Equip. Support Struct.			Total Struct.		
	Mg	Al	Ti	Mg	Al	Ti	Mg	Al	Ti
	(lb.)	(lb.)	(lb.)	(lb.)	(lb.)	(lb.)	(lb.)	(lb.)	(lb.)
SEMIMONOCOQUE									
1. Semimonocoque (uniform load)	180	175	176	125	128	145	305	303	320
2. Semimonocoque (8 Longerons)	211	204	196	145	149	161	356	353	357
3. Semimonocoque (4 Longerons)	213	205	197	147	151	161	360	356	358
TRUSS									
1. 4 sides	151	144	127	155	163	131	306	307	258
2. 6 sides	138	126	101	144	155	150	282	281	251
3. 8 sides	154	154	133	158	167	155	312	321	288

Having established the weight trends of the ideal structural arrangement, additional factors were considered before a final selection of the primary structural concept was made. Foremost among these factors was the accessibility for installation, servicing, and maintenance of the functioning components in the spacecraft. Truss structures provide the maximum accessibility. Semimonocoque structural arrangements completely block access to the interior of the spacecraft unless access doors or openings are provided. Such doors and openings, in turn, increase the complexity and weight of the structural system. However, by reducing the diameter of the semimonocoque shell and providing external truss longerons, equipment packages can be mounted on the shell exterior for excellent accessibility.

Based on these modifications to the ideal structural arrangement, the preferred configuration discussed in Section 3.0 of this document is shown in Figure 4.4-32. A detailed structural-weight analysis was conducted using the three candidate materials.

COMPONENT	Magnesium (pounds)	Aluminum (pounds)	Titanium (pounds)
Truss Longeron	30.3	20.4	18.2
Lower Truss	75.6	74.6	55.4
Lower Bulkhead	63.2	62.0	45.9
Upper Frame	15.3	28.2	32.2
Middle Frame	46.1	58.9	65.2
Shell & Stiffeners	68.7	81.6	95.6
TOTAL	299.2	325.7	312.5

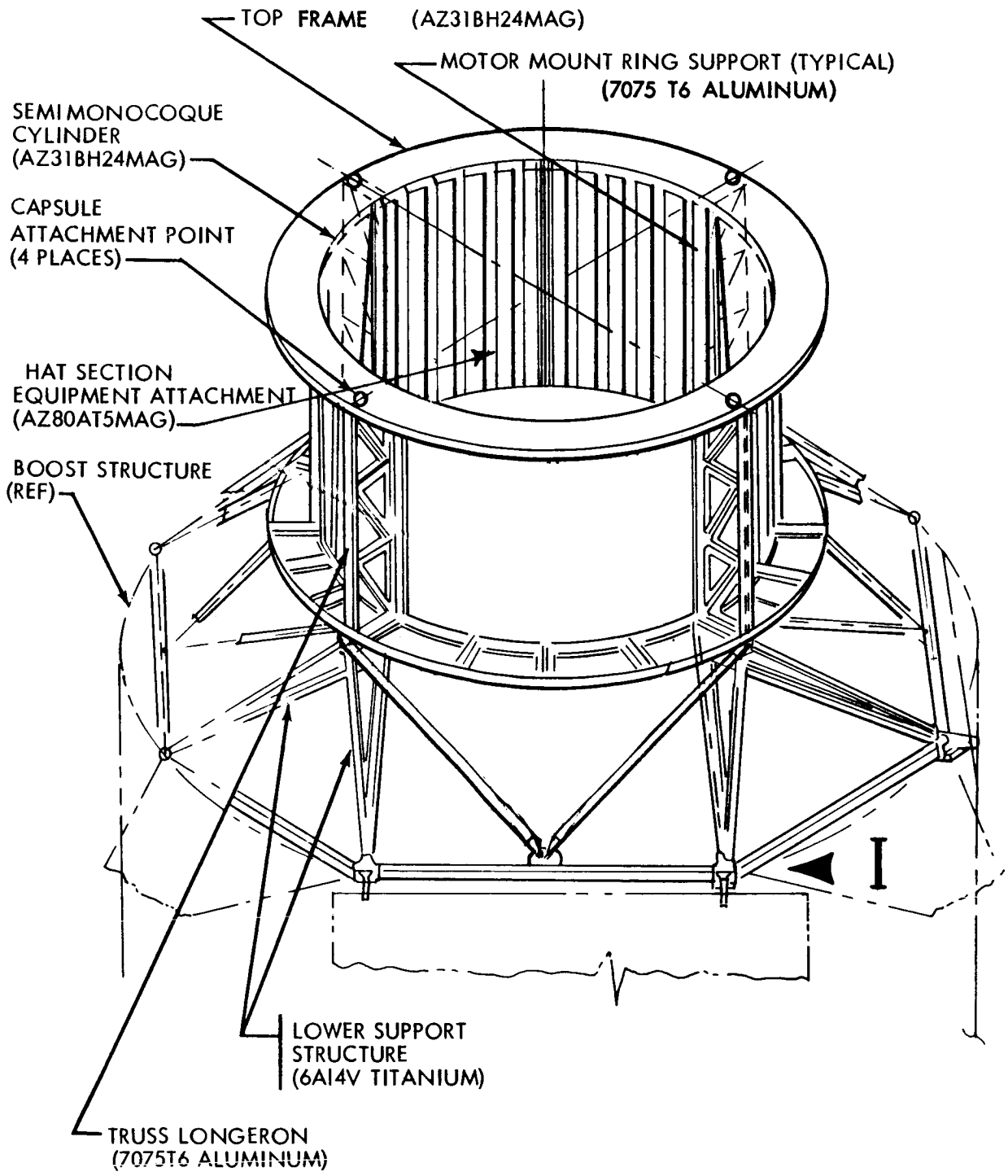

Figure 4.4-32: Selected Structural Arrangement

As can be seen from the weight tabulation above, a magnesium semimonocoque equipment-support structure combined with a titanium-truss longeron and lower-truss-support structure is the optimum structural combination and weighs 250 pounds. Substitutions of 7075-T6 aluminum for the titanium-truss longeron results in only a 2-pound increase. This substitution provides improved thermal compatibility to reduce stresses and deformations resulting from longeron attachment to the magnesium semimonocoque shell.

Magnesium in contact with titanium or aluminum creates a corrosion condition that can be overcome by separating the magnesium from the titanium and aluminum by anodizing (Dow 17) and using zinc-chromate primer or by separating with Mylar film. In addition, the following techniques apply:

1) Riveted joints
   a) Use 5056-aluminum alloy rivets only;
   b) Install with manufactured head (preferably universal type) on the titanium side;
   c) Install rivets with wet zinc-chromate primer;
2) Bolted joints
   a) Install 6061-aluminum bolts with wet primer--the manufactured head should be on the titanium or aluminum side and a NAS-1197 washer should be on the magnesium side;
   b) Install titanium bolts in either direction but with a wet primer; a NAS-1197 washer must be placed between the magnesium and titanium nut or bolt head. A flush installation may be obtained on the magnesium side by using a shaped washer under the bolt head.

The selected structural system, then, consists of a 6Al-4V titanium lower-truss support, 7075-T6 aluminum truss longerons, and AZ31BH24 magnesium equipment-support structure.

4.4.3.2 Solar Panel Structure

The structural trades on solar panels are presented in Section 4.2 of this document.

4.4.3.3 Magnetometer Boom Structure

The magnetometer boom structural arrangement is primarily determined by three factors:

1) The boom must support 1.0 pound located 400 inches from the spacecraft Z axis. The boom is designed to withstand a 7.5g ultimate load factor.
2) Vibration of the boom at its natural frequency must not degrade the ability of the autopilot and reaction-control subsystem to maintain desired spacecraft attitude.
3) Thermal deflections of the boom will not cause a magnetometer misalignment of more than 1 degree during periods when magnetometer readings are being taken. Tapered round tubes fabricated of magnesium, aluminum, or titanium were found to be comparable in weight. Therefore, the 6061-T6 aluminum was selected on the basis of cost and ease of fabrication.

4.4.3.4 Meteoroid Protection

The preliminary-design meteoroid environment used for analysis of shielding requirements is shown in Boeing Document D2-82709-1, Section

1.0. For establishing the meteoroid-shield design, it is assumed that there must be at least a 99 percent probability that no vital component will be penetrated by a meteoroid during the 215-day transit phase and the minimum 30-day Mars-orbit mission. The probability of no penetration for the 180-day-orbit mission was also determined. Both single- and double-wall meteoroid-shielding designs were evaluated.

Most of the spacecraft components are provided with some inherent meteoroid protection. Equipment package containers provide some protection depending on the metal thickness between the component and the environment. Thermal-control louvers shade a portion of the equipment module, but provide only minor protection when open. Pressure tanks have inherent meteoroid resistance.

Increased meteoroid protection can be provided for the equipment module by increasing the outside skin thickness of the electronic packages or by adding a meteoroid bumper that is properly spaced away from the equipment-package faces. Effective shielding of the propulsion module can be accomplished by adding aluminum face sheets on the surfaces of the thermal insulation.

A comparison showing relative efficiency of two-wall and single-sheet meteoroid barriers is shown in Figure 4.4-33. This data is based on transit asteroidal particles (ρ = 4.37 g/cc, V = 30 km/sec). The curves are quite conservative for cometary particles (ρ = 0.4 g/cc) but roughly the same thickness-spread occurs between single- and multiple-sheet designs. As shown, a two-wall barrier will stop particles two to three orders of magnitude greater in mass than will a single-wall barrier.

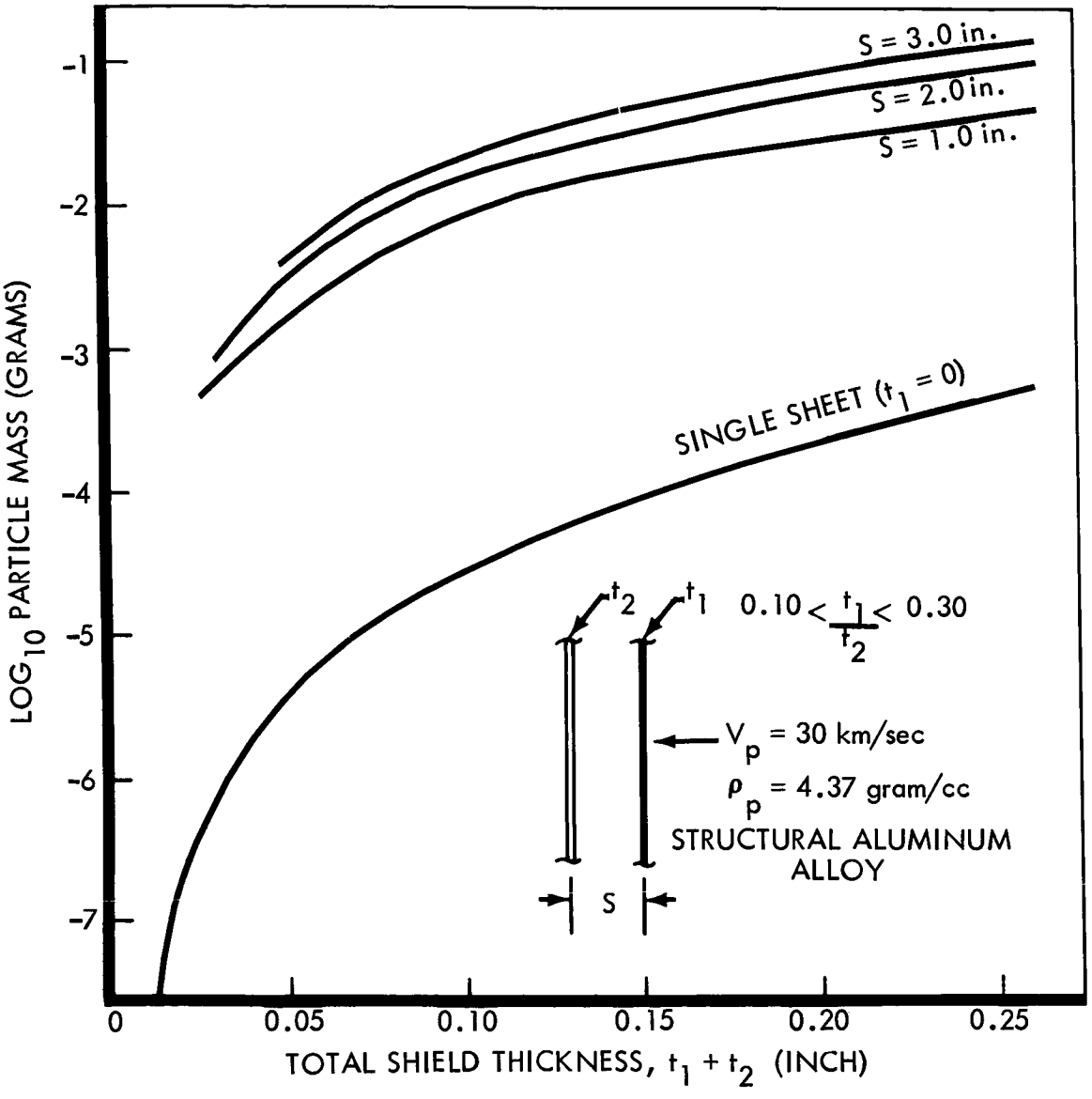

Figure 4.4-33: Meteoroid Shield Thickness Versus Particle Mass

Table 4.4-10 summarizes the meteoroid-shielding weight required to achieve the 99 percent probability of no penetration of the equipment module during the 30-day Mars-orbit mission. Also, the probability of no penetration of the equipment module during 180 days in orbit is given. These weights are based on shielding thickness in excess of the electronic-package wall thickness of 0.060 inch. A total exposed surface area of 50 square feet is assumed.

Table 4.4-10: SHIELDING WEIGHTS

SHIELD DESIGN	SHIELD THICKNESS (inches)		SHIELD SPACING (inches)	SHIELD WEIGHT (lbs.)	P(o) Mission (orbit)	
	Outer	Inner			30 days	180 days
Single wall	0	0.347*	0	.248	0.990	0.9475
Double wall	0.006**	0 *	1	5	0.9914	0.9600

* Thickness in excess of 0.060-inch package wall

** Minimum practical gage = 0.006-inch aluminum

As shown in Table 4.4-10, the addition of a 0.006-inch minimum gage aluminum bumper spaced 1.0 inch from the equipment module provides the same protection as an increase of .295 inch in the package wall thickness. The bumper design is 207 pounds lighter. A 99.14 percent probability of no penetration is achieved with this minimum gage bumper.

The addition of a 0.006-inch minimum gage exterior face sheet and an 0.018-inch gage interior backup sheet, spaced 1.0 inch from the exterior sheet on the insulation surrounding the propulsion module, provides higher than 99 percent probability of no penetration of this component

for the 215-day transit phase. The probability of no penetration of one of these tanks exceeds 99.99 percent.

Single-wall-shield thickness required to stop a meteoroid having a volicity greater than 10 Kilometers per second was determined by Bjork's penetration equation. For particles with velocities less than 10 Kilometers per second, the equation of Summers and Charters was used. Appropriate spalling factors were used in each case. The design method for the double-wall shields was developed at Boeing under NASA Contract NAS3-2570 (NASA Report CR-54201, "Meteoroid Protection for Spacecraft Structures" by Lundeberg, Stern, and Bristow).

4.4.4 Spacecraft Mechanisms

Summary--Spring-actuated folding mechanisms are used for the deployment of booms; d.c. digital motors actuating harmonic drives articulate the planet-scan platform and high-gain antenna; bimetallic springs actuate the thermal louvers; a motor drive actuates the science optics cover; and a squib-fired V-band release separates the capsule and its biological barrier from the spacecraft. (See section 4.2, volume A, for discussion of solar panel deployment.)

The logic by which these preferred designs were determined is diagrammed in Figure 4.4-34. On this chart, it can be seen that mechanisms are divided in two categories--those involving a single operation, and those involving intermittent or continuous operation. In the single-operation category are the deployment mechanisms for the booms carrying the VHF antenna, the S-band low-gain antenna, and the magnetometer. Two deployment mechanisms were considered--folding booms and the DeHavilland extensible mechanisms. Folding booms were selected because of their lower weight and higher reliability. The lower reliability of the DeHavilland mechanism is due to complexity of feeding coaxial cables and instrumentation wiring into the extending boom. Also in the single-operation category are the mechanisms for separation of the capsule and its biological barrier. For this purpose, the V-band release and collet release methods were considered. The V-band release was selected because of the higher reliability resulting from a simpler pyrotechnic system.

For the intermittent operation of the high-gain antenna and the planet-scan platform, planetary gear trains and the harmonic gear drive were considered. The harmonic gear drive was selected because of low friction loss, essentially zero backlash, and high reliability resulting from concentric gearing and low bearing loads on the gear teeth. Study of means for activating these drive mechanisms included consideration of d.c. torque motors, d.c. digital motors, and a.c. servo motors, with the d.c. digital motor being selected because of high reliability, low power requirement, and inherent braking capability.

For actuation of the planet-scan-platform optics cover, both spring devices and electric motor drives were considered. The requirements for repeated actuation and high reliability led to selection of a motor drive mechanism.

4.4.4.1 Boom Deployment Mechanisms

Mechanisms considered for deployment of booms carrying the VHF antenna, the low-gain S-band antenna, and the magnetometer were spring actuation and DeHavilland extensible actuation.

Spring Actuation--Analyses considered both one-piece and two-piece booms. The booms were deployed by Vinson actuators, which combine a compression spring with an oil damper to control the deployment velocity. Spring-loaded taper pins are employed to lock the boom elements in their deployed positions upon completion of the deployment cycle.

SINGLE OPERATION

4.4.4.1 VHF ANTENNA DEPLOYMENT
LOW-GAIN ANTENNA DEPLOYMENT
MAGNETOMETER BOOM DEPLOYMENT → EXTENDABLE
FOLDED

4.4.4.2 CAPSULE AND BARRIER SEPARATION → COLLET RELEA
V-BAND RELE

SOLAR-PANEL DEPLOYMENT → SEE SECTION

INTERMITTENT OR CONTINUOUS OPERATION

4.4.4.3 HIGH-GAIN ANTENNA POINTING → GEAR TRAIN
HARMONIC D
d.c.TORQUE M
d.c.DIGITAL M
a.c.SERVOMO

4.4.4.4 PLANET SCAN PLATFORM POINTING → ONE AXIS
TWO AXES

4.4.4.5 SCAN PLATFORM SCIENCE OPTICS COVER → SPRING
MOTOR

4.4.4.6 TEMPERATURE CONTROL LOUVERS → THERMISTORS
BOURDON TU
BIMETAL SPRI

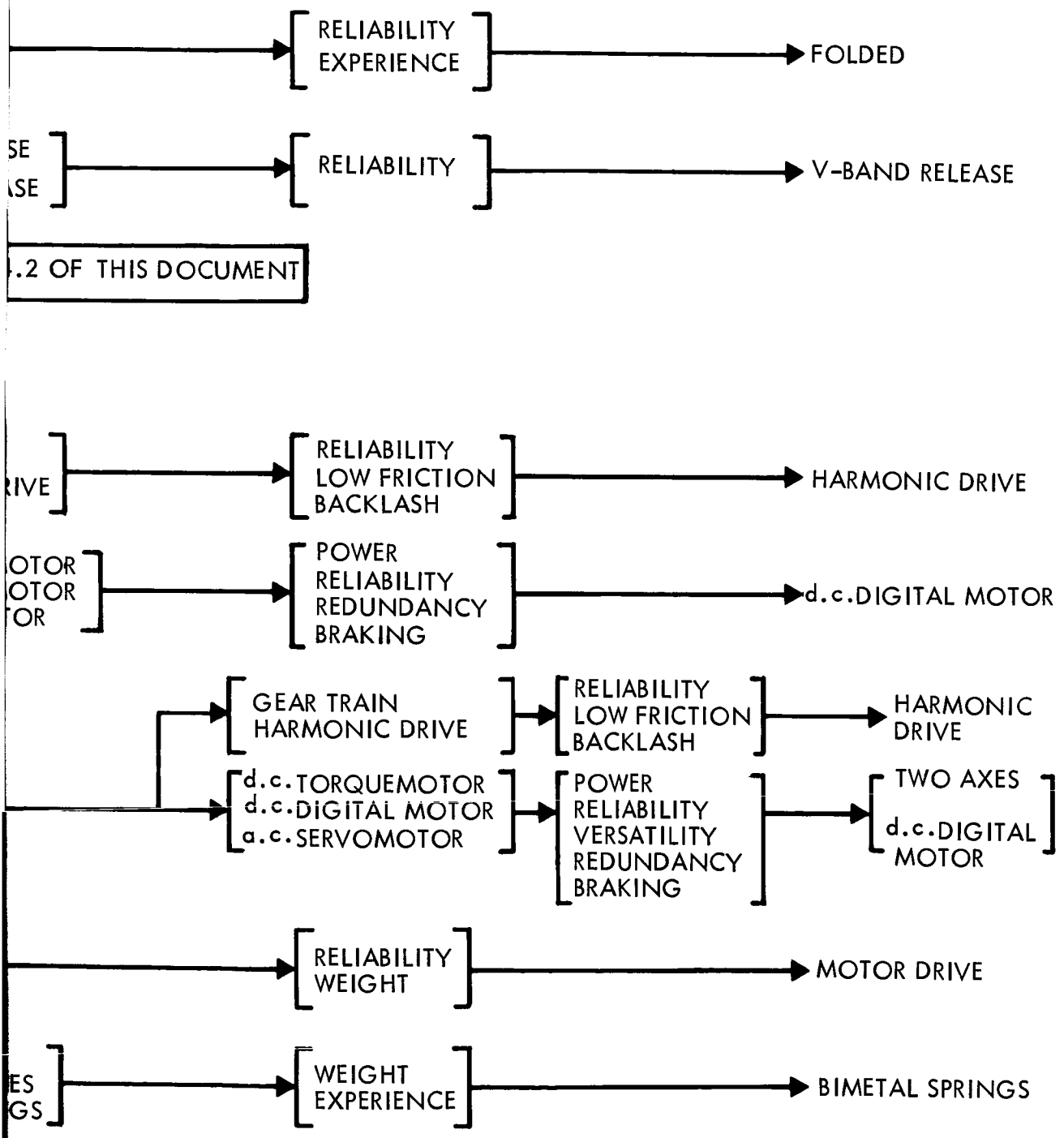

Figure 4.4-34: Alternate Mechanism Subsystem Selection Logic Chart

DeHavilland Extensible Actuation--As shown in Figure 4.4-35, this design uses preformed metal ribbons to form a structural tube that deploys the antenna or magnetometer and houses the coaxial line or instrumentation cables. The curved metal ribbons are rolled on a reel prior to deployment and the coaxial line or instrumentation cable is fed into the tube from a second reel as the boom is formed and deployed.

The primary competing characteristics were reliability, simplicity, and weight. The complexity associated with feeding coaxial cables or instrumentation wiring from a reel into the formed tube detracts from the reliability of this concept. On this basis Vinson actuators were selected. An additional factor favoring the Vinson actuator is its proven performance on Mariner IV.

4.4.4.2 Capsule and Barrier Separation

The designs considered for separation of the capsule and barrier from the spacecraft were a pyrotechnically released collet and a pyrotechnically released V-band.

Pyrotechnically Released Collet--The collet-type release mechanism was evaluated because of its successful use on the Hound Dog air-to-ground missile. The mechanism consists of a conical piston retained by the segments forming a collet. An extension of the piston forms the tension member, bolting the capsule to the spacecraft. Firing an explosive charge behind the piston opens the collet, releasing the bolting member. Four collet release mechanisms are required to adequately support the

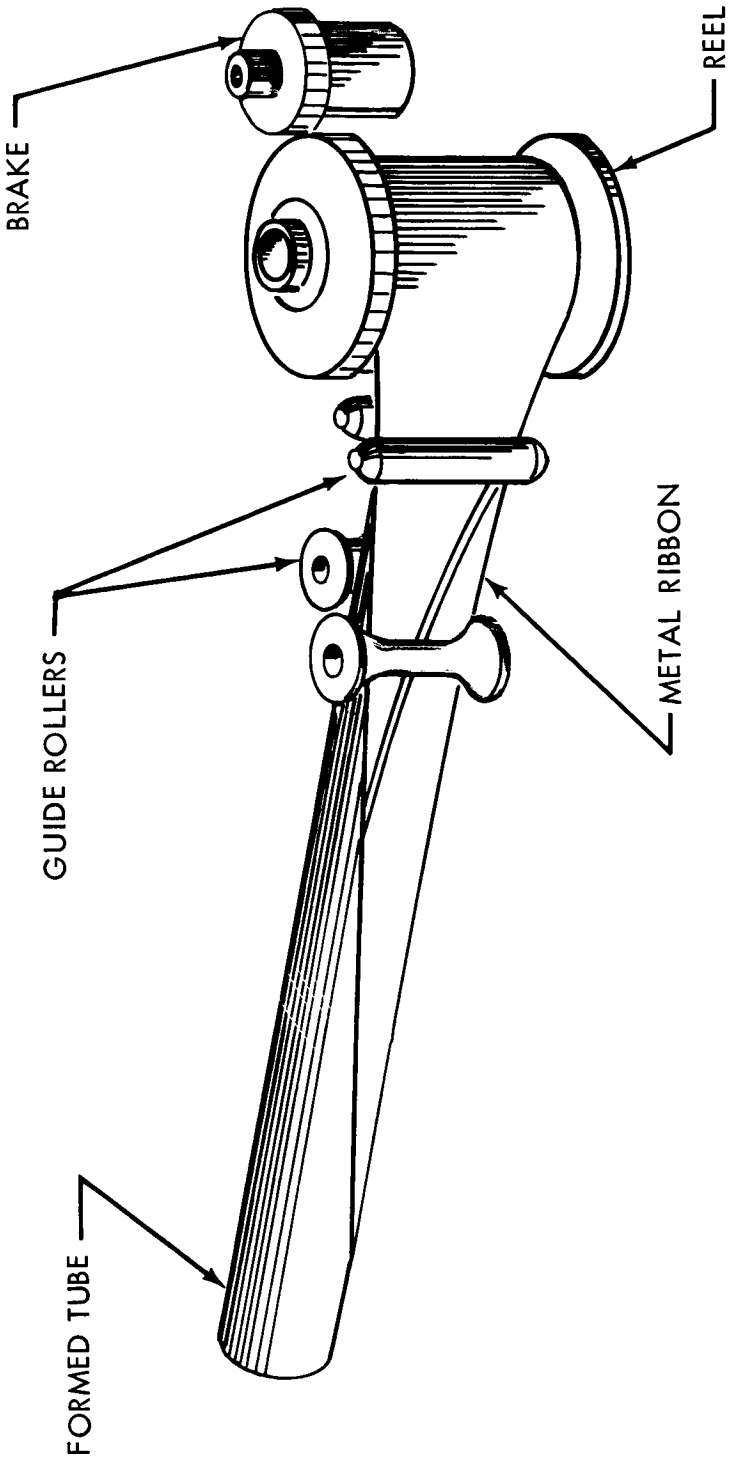

Figure 4.4-35: DeHavilland Extensible Boom Principal

flight capsule. Dual-squib firing from separate circuits is employed. The collet is the only nonredundant item in this design.

Pyrotechnically Released V-Band--The V-band evaluated was a conventional type. Two cutters are fired simultaneously by pyrotechnics to cut the band. Since either cutter will release the band, full redundancy is achieved.

The primary criterion for selection was reliability. Capsule release is not only essential to complete its own portion of the mission, but also is necessary to expose the science package on the planet-scan platform. The V-band release was selected because it has a significantly lower probability of failure owing to its having two independent separating devices either of which will separate the capsule.

4.4.4.3 High-Gain-Antenna Deployment and Positioning Mechanism Because of limited space the antenna is stowed in a near-inverted position which complicates design of the deployment linkage. The selected linkage is shown in Figure 4.4-36.

In selecting a drive unit for the antenna pointing mechanism, the following operational requirements and constraints were considered.

1) Pointing error during cruise must not exceed ± 0.2 degree.
2) Pointing error during midcourse maneuvers (when data rates are reduced) must not exceed ± 2 degrees.

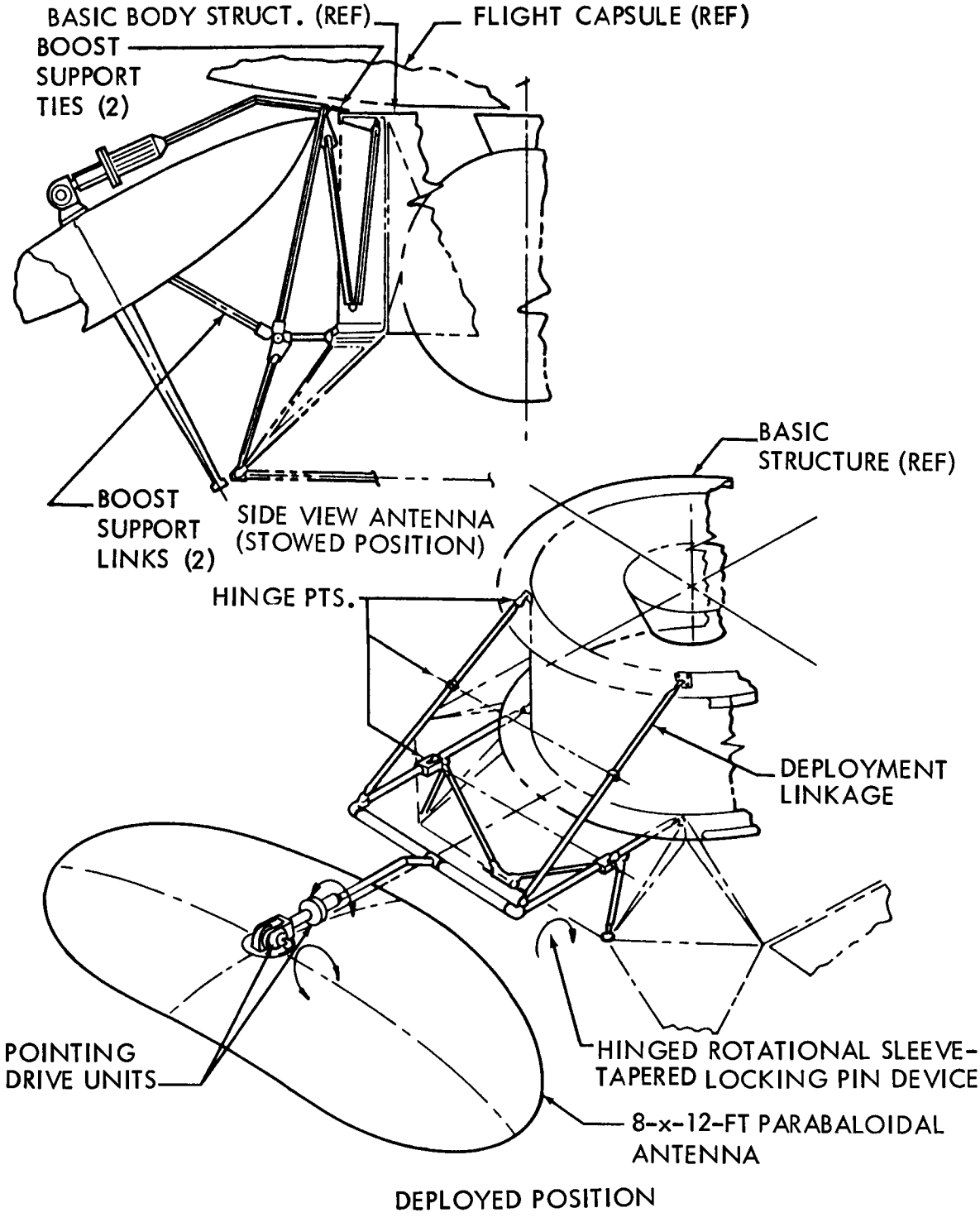

Figure 4.4-36: High-Gain Antenna Deployment and Pointing Mechanism

3) Gimbal rates must be at least 0.2 degree per second about each axis to counter the maneuvering rate of 0.2 degree per second.

4) Antenna pointing angles must be monitored.

The constraints imposed on the pointing accuracies dictate a high drive ratio combined with a gear drive of essentially zero backlash. The harmonic drive was selected because it meets these requirements and provides the additional advantages of low volume, minimal gearing, low friction loss, and capability for hermetic sealing.

Candidate drive motors were: (1) a.c. servomotor, (2) d.c. torque motor, and (3) d.c. digital motor. On the basis of the analysis of these three candidates appearing in Section 4.1.8 of this document, the digital motor was selected for further evaluation. A comparison of the three candidate motors is shown in Table 4.4-11.

On the basis of the characteristics considered in the evaluation, the digital motor was selected for the following reasons: (1) higher reliability, (2) positive locking inherent in motor design, (3) holding power not required in the off-duty cycle, and (4) redundant position indication readout capability inherent in the motor design. The fact that this unit will be space proven on the Lunar Orbiter spacecraft also contributed to its selection.

Table 4.4-11: DRIVE MOTOR CHARACTERISTICS

	Parameter	Servo-motor	Torque Motor	Digital Motor	Comments
1.	Position Accuracy	2	2	1	
2.	Braking	2	2	1	
3.	Reliability	0.99985	0.99947	0.99998	1
4.	Weight	-	-	-	2
5.	Power	3	2	1	3
6.	Adaptability	3	2	1	4

LEGEND: 1 = best, 3 = poorest

1 This reliability rating is based on one month's orbital operation for the motor only.

2 The difference in weight was negligible, varying somewhat between motor manufacturers.

3 The torque motor has a higher torque and power capability, but the digital motor requires no standby power.

4 The digital can accept data bits directly from a programmer such as has been selected for the spacecraft.

4.4.4.4 Planet-Scan-Platform Positioning Mechanism

To achieve the high reliability inherent in design simplicity, the planet-scan-platform design study was restricted to concepts that either performed no deployment operation or incorporated this function with one of the pointing operations. Four design concepts were evaluated. A minimum case providing rotation of the scan platform about one axis only was selected as one extreme, and a maximum case providing independent

rotation about two separate axes plus orientation of the stowed position of the platform in the plane of initial orbit was selected as the other extreme.

The effect of providing redundant drive mechanisms was also investigated, but only to the extent of determining that parallel redundant drive units with the necessary switching circuit and unclutching devices produced a reduction in overall reliability. The feasibility of using drive units in series to improve the pointing reliability is recognized, but needs further investigation.

The effect of the designs on the selection of a suitable cover for the scan platform instruments was considered concurrently to ensure maximum compatibility. The actual design of the mechanism is covered in Section 4.4.4.5.

The four concepts are shown in Figure 4.4-37, and are discussed in the following paragraphs.

Concept 1--This is the minimum case having a single axis of rotation and a moveable optics cover. The axis is oriented normal to the initial orbit plane, permitting the scan platform to point along local vertical in the plane of the orbit. Since the platform cannot be pivoted about an orthogonal axis, it is not possible to scan to either side of local vertical nor is it possible to maintain pointing along local vertical as the orbit plane angle changes with respect to the spacecraft axes.

Since the resolution of camera or television optics systems varies as the cosine of the angle for small off-point angles, very little degradation would occur up to about 6 degrees. The drift of the platform pointing axis out of the orbit plane could thus be tolerated for a limited period. The effect of this drift could be countered to some extent by offsetting the pointing axis in the direction of drift.

The fact that no deployment is required to put the scan platform in operation contributes to the simplicity and reliability of this concept; however, the simplicity and reliability are achieved at the expense of the ability to correct for orbit perturbations and a reduction in the quantity and quality of data acquired.

Concept 2--This concept employs two axes of rotation, one normal to the initial orbit plane and the other orthogonal to it. A moveable optics cover is installed. With two axes of rotation, the scan platform may be pointed along the local vertical throughout the mission as well as pointed to either side of the orbit plane. Continuous updating of the orbit plane pointing angle is thus possible.

The second axis of rotation adds to the complexity of the system since two drive units must be employed and wire bundles must be routed through two rotating joints to reach the scan platform instruments.

The quality and quantity of data that can be acquired is greatly increased by the addition of the second degree of freedom since continuous pointing along the local vertical, plus side scanning, is possible. No

CONCEPT		DEPLOYMENT			
	CONCEPT	FIXED POSITION	DEPLOYABLE	SEPARATE REDUNDANCY PROVIDED	CONSTANT RATE TRACKING
1 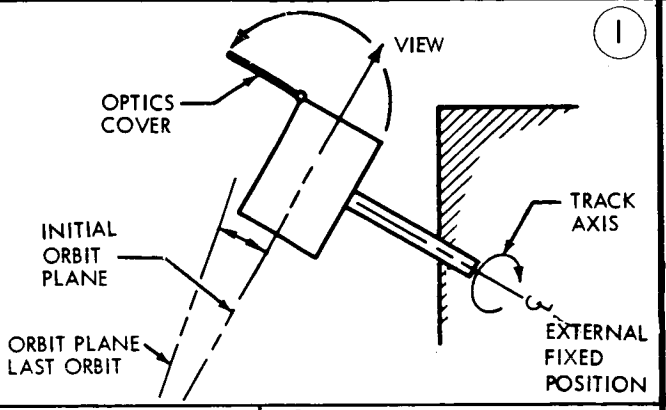 	1	✓	NO	NO	✓
2 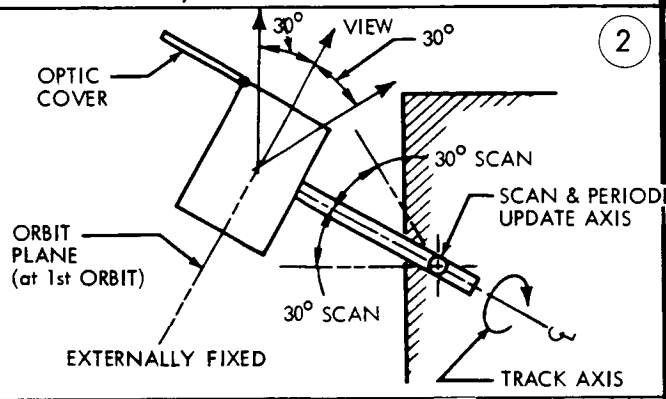 	2	✓	NO	NO	NO
	3	NO	✓	NO	NO
3 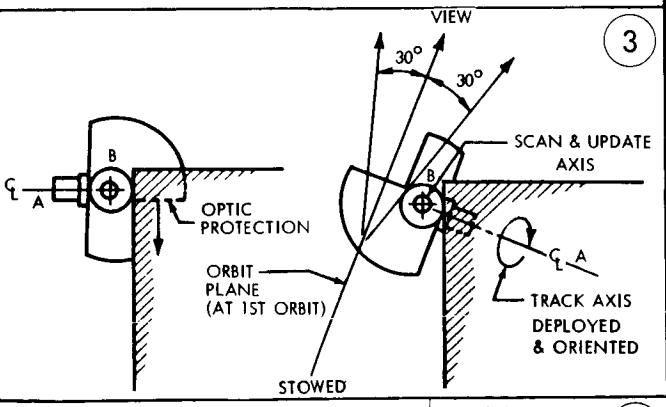 	4	NO	✓	*** ✓	NO
4 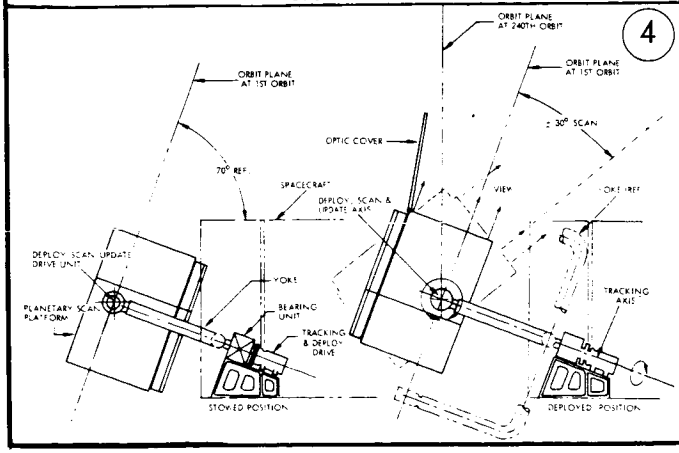 					

570

TRACKING			SCANNING		ORBIT UPDATING		OPTICS COVER		
LOCAL VERTICAL TRACKING	PREPOSITIONING REQUIRED	ORBIT CORRECTION PROVIDED	NO CAPABILITY	$\pm 30^{\circ}$ SCAN	NO CAPABILITY	STEPPED PERIODIC UPDATE	FIXED	POSITIONABLE	TOTAL RELIABILITY
NO	✓	NO	✓	NO	✓	NO	NO	✓	0.999942
✓	✓	** ✓	NO	✓	NO	** ✓	NO	✓	0.99929
✓	NO	* ✓	NO	* ✓	NO	* ✓	✓	NO	0.999926
✓	✓	* ✓	NO	* ✓	NO	* ✓	NO	✓	0.999929

*Provided by Deployment Drive
**Provided by Scan Drive
***Limited Deployment Provided by Track Drive for Emergency Operation

Figure 4.4-37: Scan Platform Evaluation

rotation of the platform is required to point the platform axis along the local vertical in the initial orbit plane.

Concept 3--In this concept, the scan platform has two axes of rotation, one of which is also normal to the initial plane. No separate cover for the scan platform instruments is provided. Protection of these optics is achieved by rotating the scan platform into a fixed housing rigidly attached to the spacecraft. Rotation of the platform about its scanning axis is necessary before the instrument optics are exposed.

This concept has the same advantages provided by the two orthogonal axes used in Concept 2. It has the disadvantage of requiring rotation about the scan axis to put the unit in operation. Its countering advantage is that no cover positioning mechanism is required. The shorter support yoke is also an advantage.

Concept 4--This concept is basically the same as Concept 2. It differs in that the scan platform must be rotated 180 degrees from the deployed position to point the scan platform instruments toward the Martian surface. Normal rotation for initial pointing is about the scanning axis; however, rotation about the tracking axis will also accomplish the initial pointing function. A moveable optics cover is installed.

The advantages of this concept are the same as those cited for Concept 2 except that this concept has the further advantage of bringing the center of mass of the scan platform and the science instruments closer to the supporting structure of the spacecraft, thereby lessening the loads

imposed on the platform mount during boost. The rotation of the platform during deployment moves the platform away from the spacecraft structure, thereby allowing for either improving the field of view of the platform-mounted instruments or shortening the platform support mount.

Competing characteristics used in the evaluation of the concepts were reliability, adaptability, and failure mode operation. The factors used to assess the reliability of each concept appear in Figure 4.4-37 and include the operation of the moveable optics cover when employed. The drive unit considered in the assessment was a d.c. digital motor coupled to a harmonic drive in a hermetically sealed unit. The harmonic drive was selected because it possesses the advantages of high reliability, low friction loss, essentially zero backlash, and a high reduction ratio with minimal gearing. The digital motor was selected for its high reliability, low power requirement, and integral braking capability, as discussed earlier in the summary of Section 4.4.4.

The reliability assessment showed little difference between the four concepts, being principally a function of the motor and drive unit reliability. From the standpoint of adaptability, Concept 4 was selected for the following reasons:

1) The scan platform can be placed in the viewing position by rotation about either of the two axes.
2) Two degrees of freedom of the scan platform permit local vertical tracking, scanning to both sides of the orbit plane, and updating of the orbit plane pointing.

3) The unit can be brought closer to the spacecraft in its stowed position, thereby utilizing less spacecraft envelope in the boost configuration.

4) Deployment away from the spacecraft for viewing makes larger view angles possible.

5) The closer proximity of the platform to the spacecraft during boost should allow use of lighter support structure.

4.4.4.5 Planetary-Scan-Optics Cover Mechanism

With reference to the four scan platform positioning concepts shown in Figure 4.4-37, two methods of protecting the science system optics on the scan platform are possible: (1) rotating the scan platform into a cover mounted on the spacecraft body, or (2) providing a moveable cover. Since Concept 4 in Figure 4.4-37 has been selected as the preferred design, considerations for cover design have been focused on this concept.

Two cover actuation designs were considered for evaluation: (1) an electric drive motor, and (2) a torsion spring drive. Descriptions of each design follow and are shown in Figures 4.4-38 and 4.4-39, respectively.

Electric Motor Drive--This design consists of a one-piece cover that is rotated 100 degrees or more against a stop to fully expose the science system optics. Rotation of the cover is accomplished by a d.c. digital motor coupled to a harmonic-drive-type gearhead, both housed in a single hermetically sealed unit. Initially, the cover is locked in the closed

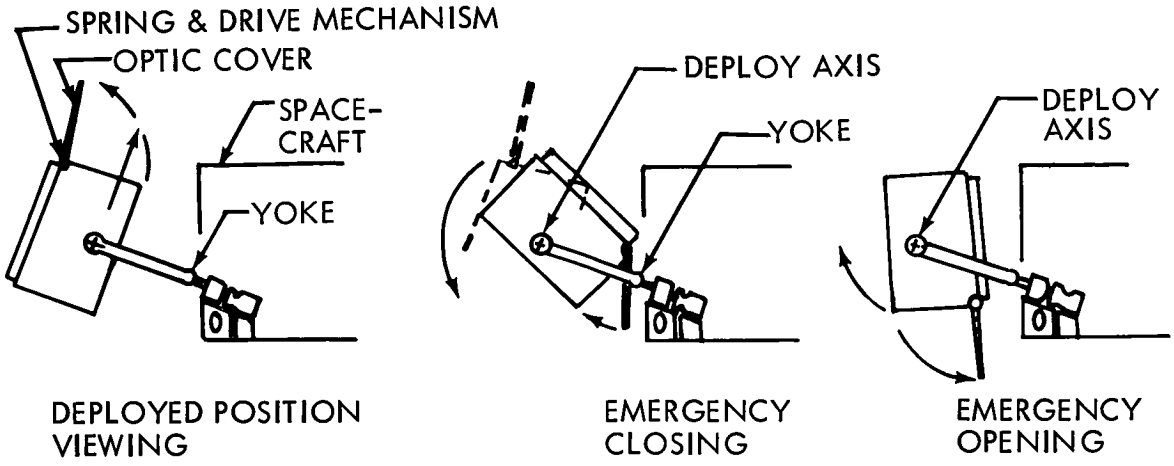

Figure 4.4-38: Motor Actuated Cover

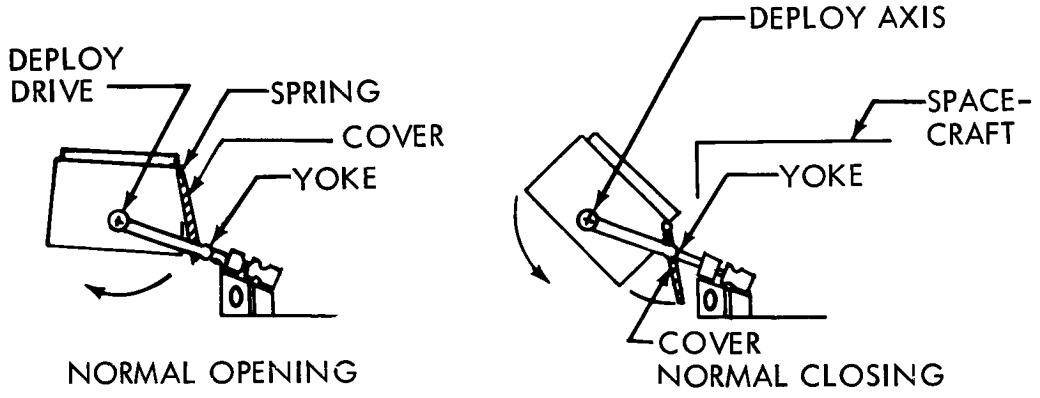

Figure 4.4-39: Spring Actuated Cover

CONCEPT	HARMONIC DRIVE UNIT	SQUIB PIN PULLER	SPRING	YOKE CLOSURE	DEPLOYMENT HARMONIC DRIVE	HINGE BEARINGS	TOTAL RELIABILITY
MOTOR ACTUATED	×	×	(1)	×	–	×	0.999996
SPRING ACTUATED	–	–	(2)	×	×	×	0.999965

Table 4.4-12: Reliability Evaluation

position by a mechanical detent integral with the stepper motor. Activation by the spacecraft programmer causes the motor to rotate the cover to the open position. Positioning of the cover is accomplished by having the programmer send the required number of pulses to the digital motor. The mechanical detent then retains this cover position.

A redundant mode of operation for opening the cover is incorporated by inclusion of a torsion spring and pyrotechnic pin puller. The torsion spring is wound as the motor drives the cover closed. The pin puller permits disconnecting the drive motor from the cover shaft, allowing the torsion spring to drive the cover to the open position. With the cover opened in this manner it cannot be operated again by the motor; however, this feature does permit using the science package instruments even though the optics remain unprotected.

Torsion Spring Drive--This design incorporates a torsion spring that drives the cover to the open position. No drive motor or pin puller is employed. The cover is opened and closed by rotating the scan platform about the scanning axis so that the yoke of the platform mount either forces the cover closed or permits the torsion spring to open the cover as it is released by the yoke. There is no backup feature and the scanning axis drive motor must be functioning to accomplish cover actuation. Failure of the scanning drive unit prior to initial orbit precludes viewing with the instruments mounted on the scan platform.

The two design concepts were evaluated on the basis of reliability and weight. The concept employing the motor is heavier by the weight of

the drive unit, 2.5 pounds. The motor-driven cover is more reliable, as reflected in Table 4.4-12. This higher reliability results from the fact that the cover can be operated even if the scanning drive unit fails. This is not true of the spring-actuated cover.

The motor-driven cover was selected on the basis of its higher reliability even though it is heavier. When the mission reaches the point of scanning the Martian surface, high reliability in cover actuation becomes paramount.

4.4.5 Pyrotechnic Subsystem

Summary--The preferred design for fulfilling pyrotechnic requirements involves equipment in the switching assembly of the central computer and sequencer as shown in Figure 4.4-40. Referring to the diagram of Figure 4.4-41, two typical circuits are shown. Both employ a 50 millisecond amplified control signal from the CC&S to drive two silicon power transistor switches in order to initiate the two pyrotechnic devices shown. An arming switch is located next to the battery to permit arming all circuits at the appropriate time. An inhibit switch (actuated by command through the CC&S) is also placed in one of the two circuits. The circuit including the inhibit switch is typical for the capsule separation, propulsion and scan platform devices. The circuit without the inhibit switch is typical for the devices which deploy the booms for the VHF antenna, low-gain S-band antenna and magnetometer, and for the device for deploying the high-gain antenna.

A total of 108 pyrotechnic circuits is provided, each circuit redundant. Fifty-six of the circuits initiate propulsion subsystem pyrotechnic devices, 14 initiate capsule and capsule cannister separation devices, and 38 initiate mechanisms for deployment and actuation of booms, solar panels, the high-gain antenna and the planet scan platform. Total weight of the Central Computer and Sequencer Switching Assembly, including the Pyrotechnic subsystem, is 29 pounds. Less than one watt of continuous power is required. Subsystem reliability has been assessed at 0.9997. It occupies approximately one-half cubic foot volume. This design is similar to that used on the Lunar Orbiter spacecraft.

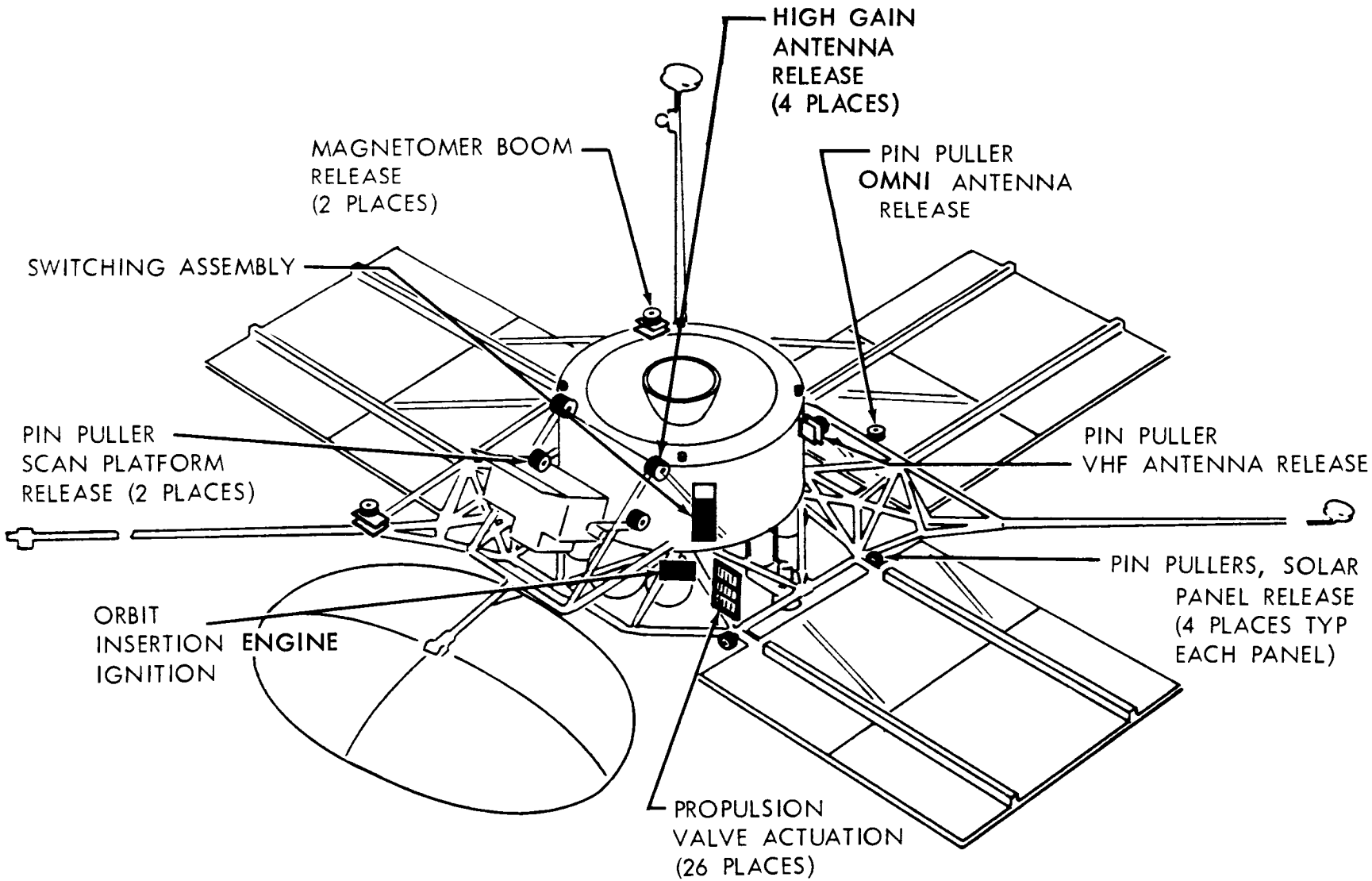

Figure 4.4-40: Pyrotechnics Subsystem

4.4.5.1 Discussion of Alternate Approaches

In selecting the preferred design, three approaches were considered as shown in the logic chart, Figure 4.4-44. Approach number one is similar to the Lunar Orbiter concept as summarized above and shown diagramatically in Figure 4.4-41. Approach number two, shown diagramatically in Figure 4.4-42, is similar to the Mariner IV concept wherein the battery power supply is replaced by a power supply which draws from a 2.4-kc bus through a transformer rectifier and capacitor bank. This power then is supplied to a silicon controlled rectifier, directly or via inhibit switches. From the silicon controlled rectifier the pulse is supplied to the pyrotechnic device. Approach number three, shown diagramatically in Figure 4.4-43, is the same as approach number one, except it draws power from a separate battery instead of drawing power from the normal spacecraft battery.

During evaluation of the three alternate approaches, it was apparent that the design selection was dependent on determination of whether or not approach number one would cause normal battery power to other electrical loads to suffer undesirable transients when pyrotechnic circuits were fired. An analysis was conducted, which indicated that 12 bridge wires could be fired simultaneously from the large battery to be supplied on the Voyager Spacecraft, with no ill effects on spacecraft power regulation, if the battery charge level was greater than 60 percent and other electrical loads did not exceed 200 watts. Analysis of the Voyager mission requirements disclosed no instances when electrical

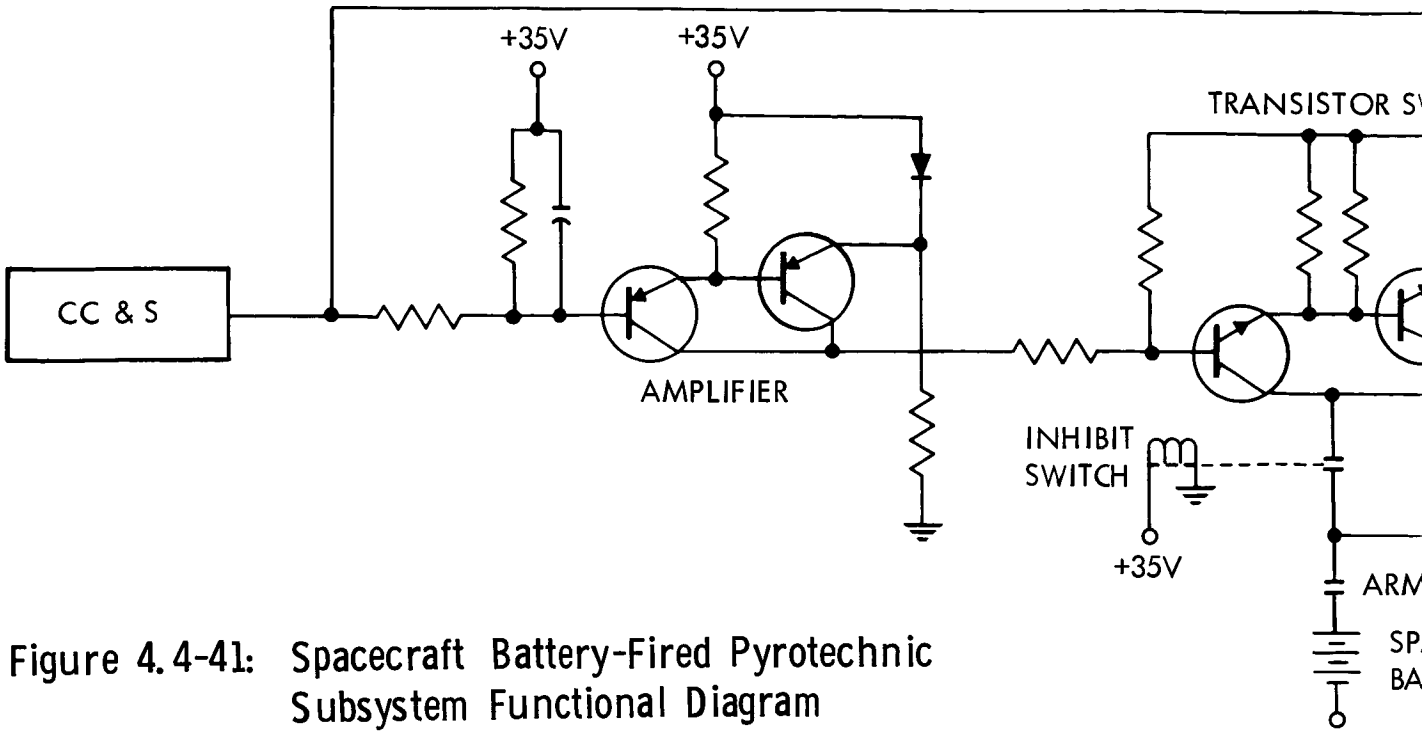

Figure 4.4-41: Spacecraft Battery-Fired Pyrotechnic Subsystem Functional Diagram

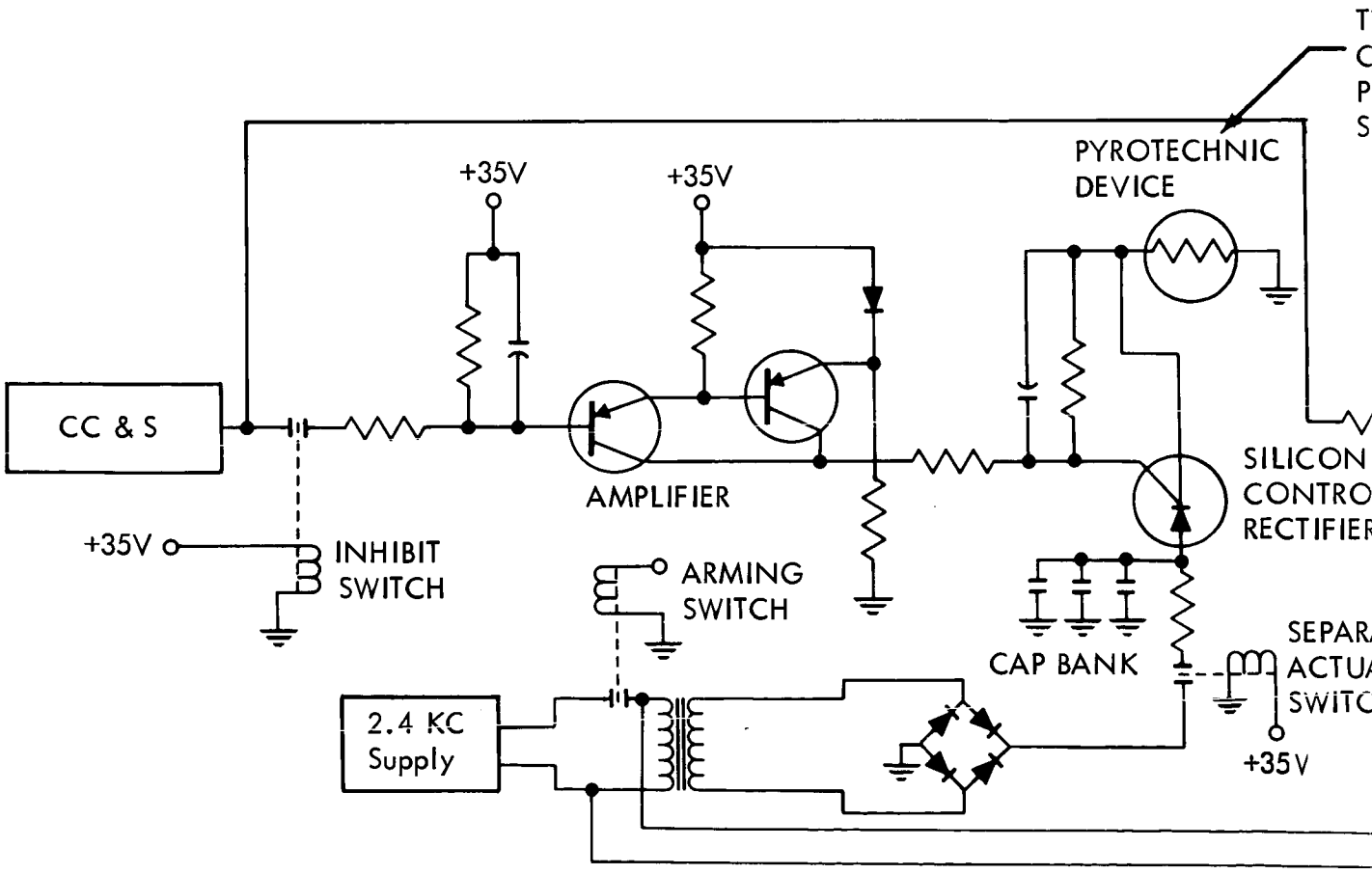

Figure 4.4-42: Capacitor Fired Pyrotechnic Subsystem Functional Diagram

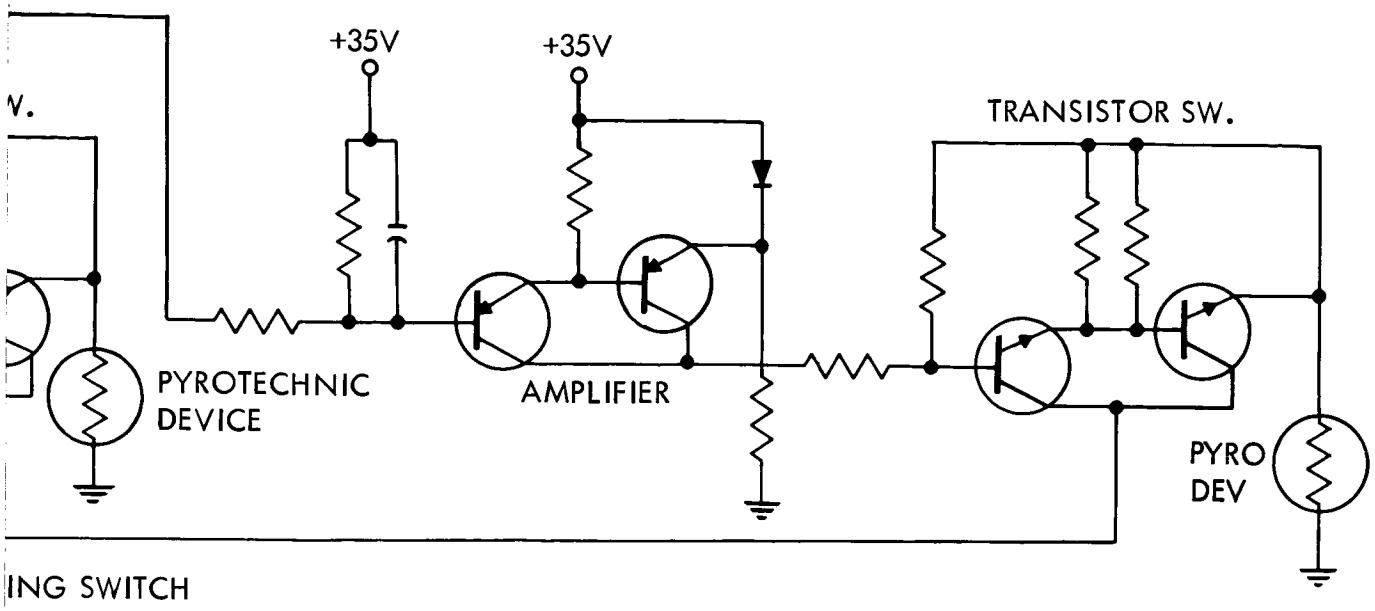

ING SWITCH

ACECRAFT
TTERY

YPICAL FOR:
APSULE SEPARATION
ROPULSION SUBSYSTEM
CAN PLATFORM

TYPICAL FOR
VHF ANTENNA
LG ANTENNA
MAGNETOMETER BOOM
SOLAR PANELS
HIGH GAIN ANTENNA

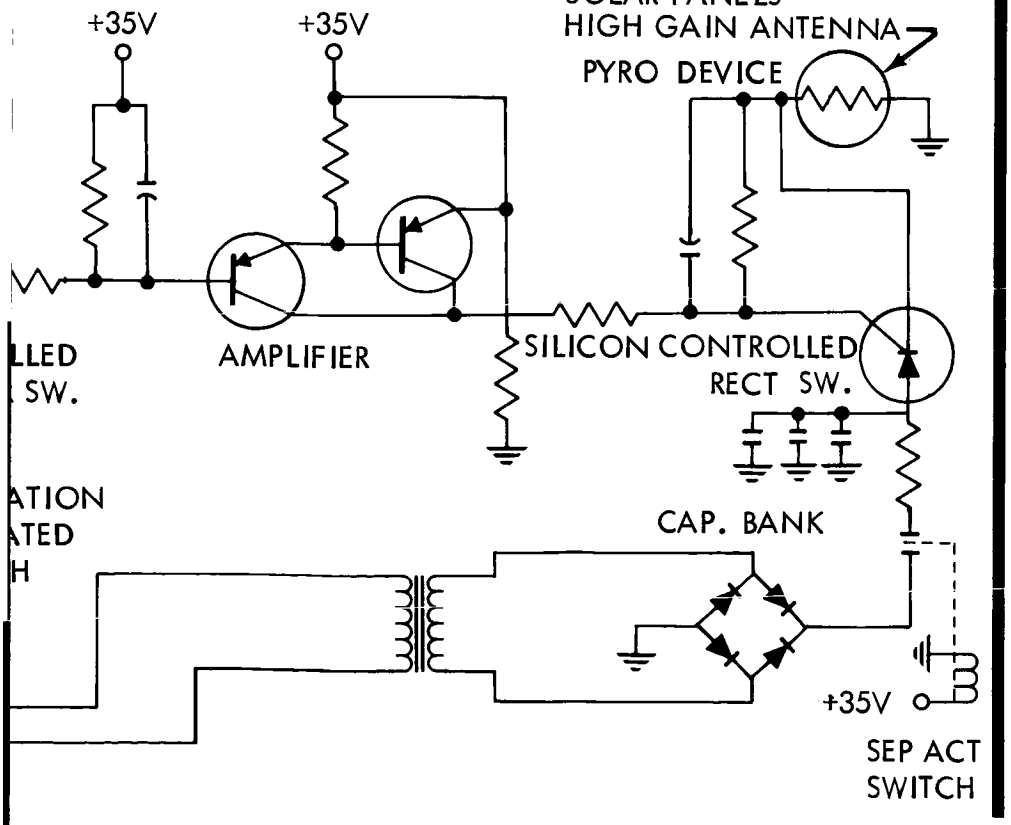

LLED
SW.

ATION
ATED
H

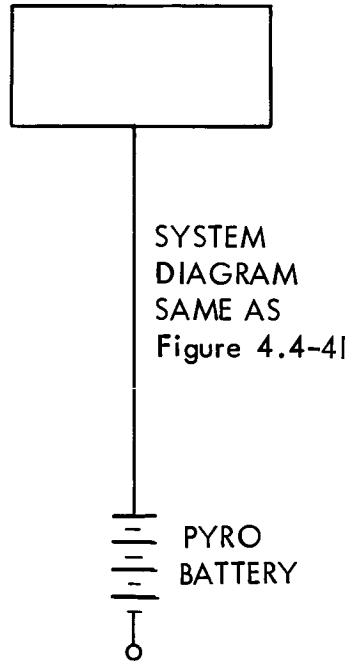

Figure 4.4-43:

Separate Battery-Fixed Pyrometric Subsystem Functional Diagram

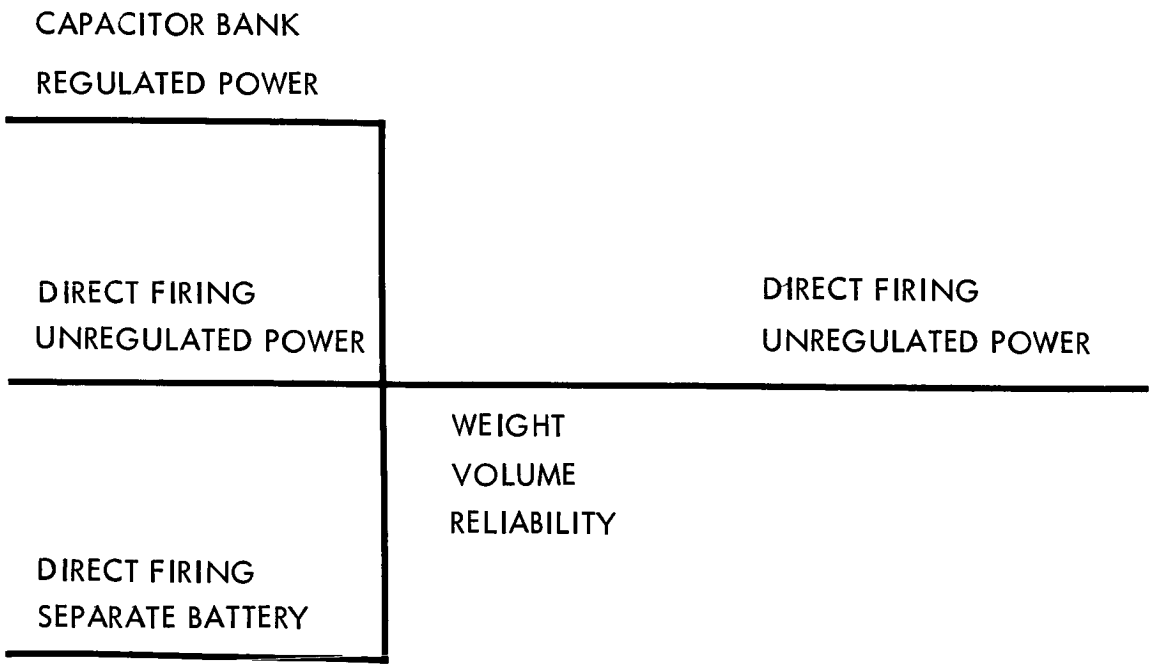

Figure 4.4-44: Pyrotechnics — Selection Logic Diagram

power subsystem ill effects would accrue. A full report supporting the above analysis is included as support data in D2-82724-1, Voyager Reliability, submitted as part of the Voyager Phase IA final report.

Based on the above, the extra battery required in approach number three, and capacitor bank and attendant weight required in approach number two were considered unnecessary. Consideration of complexity of approach number one and approach number two as tabulated in Figure 4.4-45 showed roughly the same total number of electronic parts but a substantially higher failure rate for approach number two. This higher rate is caused primarily by the silicon controlled rectifier switches tending to become conductive even though no control signal has been applied. Additional comparison of the two approaches showed a distanct benefit in favor of number one with respect to its reduced weight and freedom from generation of radiated interference. The data presented in the upper portion of Figure 4.4-45 reflects an 18 firing circuit study conducted on the Lunar Orbiter. Voyager requires 108 firing circuits. The total weight and volume for 108 firing circuits is shown in the lower portion of the figure. By comparison, a pyrotechnic subsystem weight of 17 pounds is shown in JPL document EPD 250 for a total of approximately 22 firing circuits.

The circuitry used in the preferred design is treated further in Section 4.7.2.4 as part of the CC&S discussion and is considered in additional detail in Section 4.8 of Volume A.

Figure 4.4-45: SQUIB FIRING CIRCUIT COMPARISON SUMMARY (LUNAR ORBITER STUDY RESULTS)

Comparison of Factors	Approach Number 1 (Lunar Orbiter)	Approach Number 2 (Mariner IV)
Weight of Components (18 firing circuits)	1.1 pounds	8.5 pounds
Power - Off State	0.900 watts	0.990 watts
- On State (No current limiting or switch drop.)	0.145 watts	0.106 watts
Complexity (total electronic parts)	348	304
Total Failure Rate (1×10^{-6} failure/ hour.)	1.9	6.8
Failure Rate, Single Thread (1×10^{-6} failure/hour)	0.26	0.64
Reliability, Inadvertent Firing (all circuits)	0.9997	0.9994
Volume (Module Basis for 18 Firing Circuits)	23 cu. in.	71 cu. in.
Generated Radiated Interference	Less	More
Generated Conducted Interference	More	Less
Peak Battery Drain	5 amps	Very small

TOTAL PACKAGED WEIGHT AND VOLUME ESTIMATES

Subsystem	Weight	Volume
Approach Number 1 (108 Firing Circuits)	29 pounds	888 in^3
Approach Number 2 (108 Firing Circuits)	61 pounds	1799 in^3
EPD 250 Similar to Approach Number 2 (Approximately 22 Firing Circuits)	17 pounds	-

4.5 ATTITUDE REFERENCES AND AUTOPILOT SUBSYSTEM

Summary--The function of the Attitude Reference and Autopilot Subsystem is to provide input signals to the reaction-control thruster valves, jet-vane actuators of the midcourse engines, and secondary injection valves of the orbit-insertion engine such that the spacecraft attitude, attitude rate, thrust vector alignment, and velocity are controlled within specified limits. The subsystems depend on the central computer and sequencer for commands, integration, comparison, and switching functions.

By a series of system trades, and hardware trades, as illustrated in Figure 4.5-1, a preferred attitude reference and autopilot subsystems have been defined. This preferred subsystems are composed of celestial reference sensors, inertial reference unit, and an autopilot, which controls both powered and unpowered flight. Celestial reference sensors are fully redundant. Two Barnes/JPL instruments are preferred for Canopus sensing. Sun sensors are Nortronics (primary) and Ball Brothers (backup). The inertial reference unit has three Autonetics G1OB two-axis free-rotor gyros in a caged strapdown configuration. Any two of the three gyros can supply all axis rate and position signals. The two accelerometers of the IRU (Bell III-B primary, Autonetics EMA back-up) are aligned with the thrust axis, operated in parallel to measure velocity maneuvers.

The autopilot is basically an analog device with d.c. amplifiers. It can be switched to operate with the various sensors in rate or limit cycle modes to drive the spacecraft attitude and ΔV thrusters.

System trades summarized in the following pages defined the most reliable subsystem configuration that could meet all other requirements. Further trades select design approach, or the most suitable hardware item.

System-level trades described in this section were necessary to assess the value of gimballing the Sun sensor (Trade 1, Figure 4.5-1), and to select the means of velocity control (Trade 4). Related system trades, described in other sections, which had impact on the subsystem concept were: propulsion control techniques, reaction-control mechanization, and navigation concepts for Mars approach and Mars orbit determination. No trade was conducted to select celestial references since Canopus and the Sun were specified in the "Voyager Mission Guidelines".

Following these system studies, intrasubsystem trades were performed to determine gyro and accelerometer configuration and control laws for cruise, maneuver, and thrust vector control. Finally, design trades and evaluations of existing instruments were used to select the preferred subsystem design. In selecting redundant components, preference was given to dissimilar components to lessen the chances of systematic failures. In other cases, the degree of dissimilarity, state-of-development, and other factors caused the selection of identical redundancy to be more suitable.

The following paragraphs have been organized to illustrate the processes and logic used to select the preferred subsystem design. Summaries of the data and analysis supporting these paragraphs have been included in

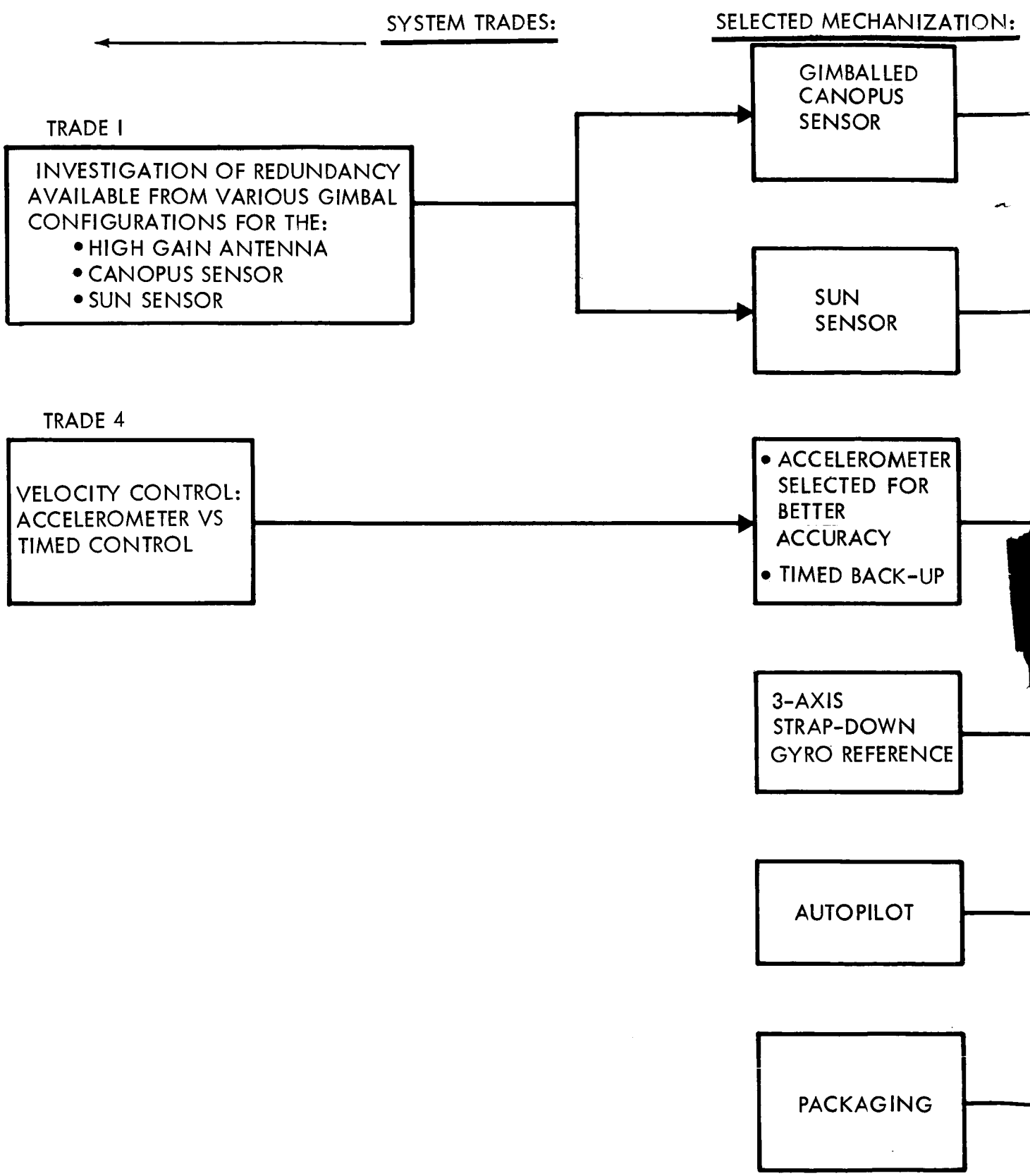
SYSTEM TRADES:
SELECTED MECHANIZATION:
TRADE 1
INVESTIGATION OF REDUNDANCY AVAILABLE FROM VARIOUS GIMBAL CONFIGURATIONS FOR THE:
• HIGH GAIN ANTENNA
• CANOPUS SENSOR
• SUN SENSOR
GIMBALLED CANOPUS SENSOR
SUN SENSOR
TRADE 4
VELOCITY CONTROL: ACCELEROMETER VS TIMED CONTROL
• ACCELEROMETER SELECTED FOR BETTER ACCURACY
• TIMED BACK-UP
3-AXIS STRAP-DOWN GYRO REFERENCE
AUTOPILOT
PACKAGING

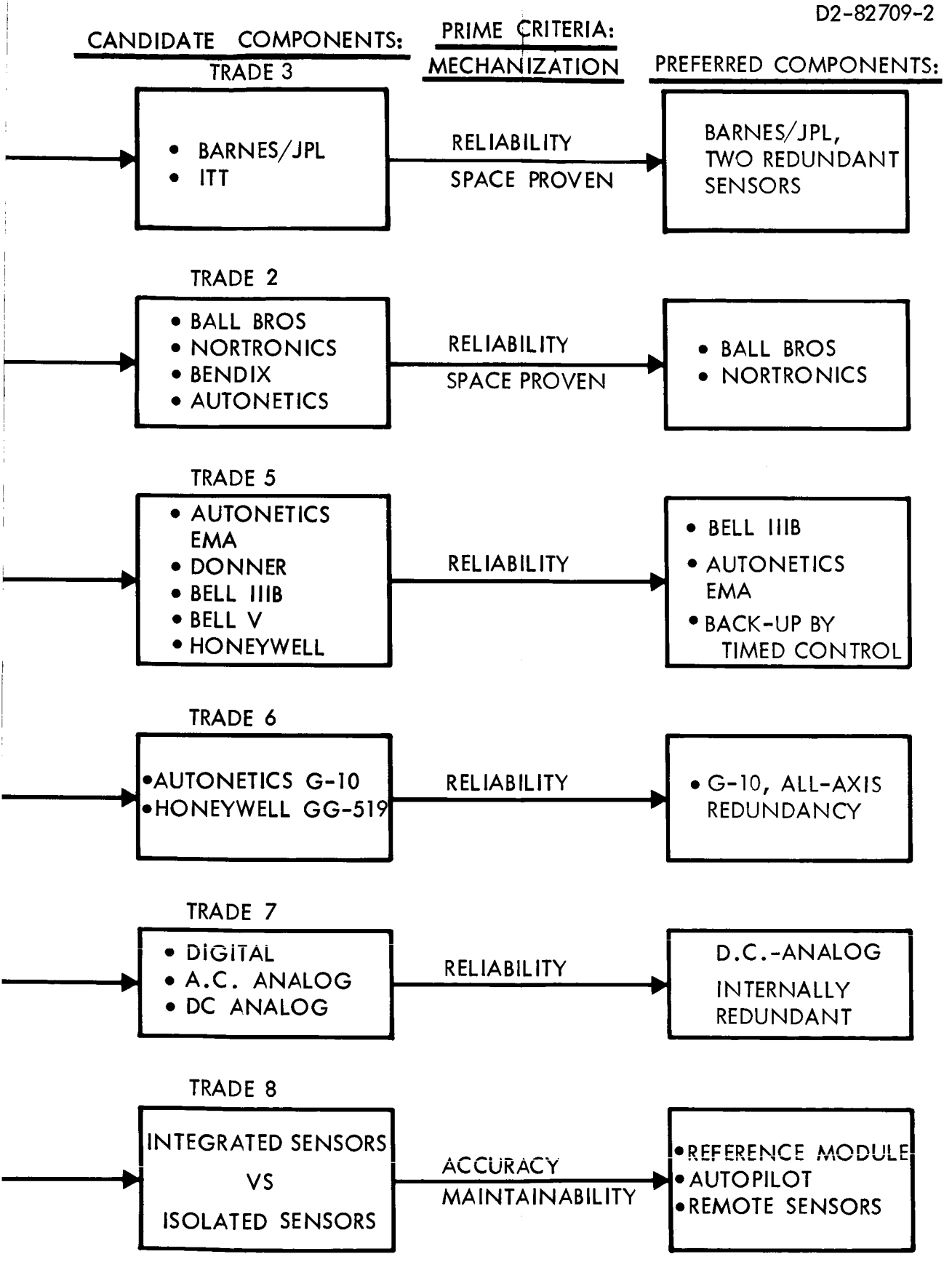

Figure 4.5-1: Trade Flow Diagram — Attitude Reference and Autopilot

this report; greater detail is contained within applicable documentation, such as the "Voyager-Attitude Reference and Autopilot Subsystems Investigation" document, Autonetics Report T5-1161.1/3061B

4.5.1 Optical Reference Sensors

The trades associated with the optical attitude references are discussed in this section. The first trade presented considers the possible advantages of electronically gimballing the Sun and Canopus sensors as backup to mechanical gimbals of the high-gain antenna. Next, trades that were performed to select the best of avaiable instruments are summarized. Barnes/JPL Canopus sensors, and Nortronics (primary), Ball Brothers (backup) Sun sensors were selected for the preferred design.

4.5.1.1 Spacecraft Gimballing Considerations

The use of the Sun and Canopus as attitude references is specified in the "Voyager Mission Guidelines". The selection of sensor, gimbal and field-of-view configurations is primarily dependent on two requirements. The first is that the sensors must accommodate the potential $\pm 16^{\circ}$ variation in the Sun-vehicle-Canopus angle and the second is that the high-gain antenna must be pointed at the Earth during both the cruise and the insertion attitudes.

The narrow beam width of the high-gain antenna precludes it from being fixed to the spacecraft frame. Therefore, at least one antenna gimbal is required. There are space-proven Canopus trackers that can be

gimballed electronically about one axis with relay switching. While one-axis gimballing of the Canopus tracker will satisfy the Sun-vehicle-Canopus angle variation requirement, using such a tracker with a one-gimbal antenna will not satisfy Earth-pointing requirements. Modifications that would satisfy both requirements are: (1) adding a second gimbal to the antenna (2) adding a second gimbal to the Canopus tracker, or, (3) adding a gimbal to the Sun sensor. Gimballing the Sun sensor is limited by the requirement of solar-cell orientation.

The gimbal freedom required can be estimated by recognizing that the motion of the Earth about the vehicle lies close to the plane of the roll-yaw axes. Hence, one antenna gimbal will be nearly parallel to the pitch axis. One of the antenna gimbals could be eliminated if the optical sensors could be gimballed around either the roll axis, using the Canopus tracker, or around the yaw axis, using the Sun sensor. Trajectory analyses showed that the angular degree of freedom requirements were significantly smaller for yaw gimballing and that a freedom of $\pm 5^{o}$ was sufficient at all times except for the early portions of missions launched late in the window, as shown in Figure 4.5-2.

Two antenna gimbals were selected as the preferred approach because of their capability of pointing during maneuvers and because gimballing the Sun sensor is a new and untried technique. Gimballing the Sun sensor about yaw, in addition to the two antenna gimbals, is to be considered as an alternate as it can be implemented with a minimum change to the system and the Sun sensor gimbal can serve as a backup to both the Canopus gimbal and the antenna trim gimbal.

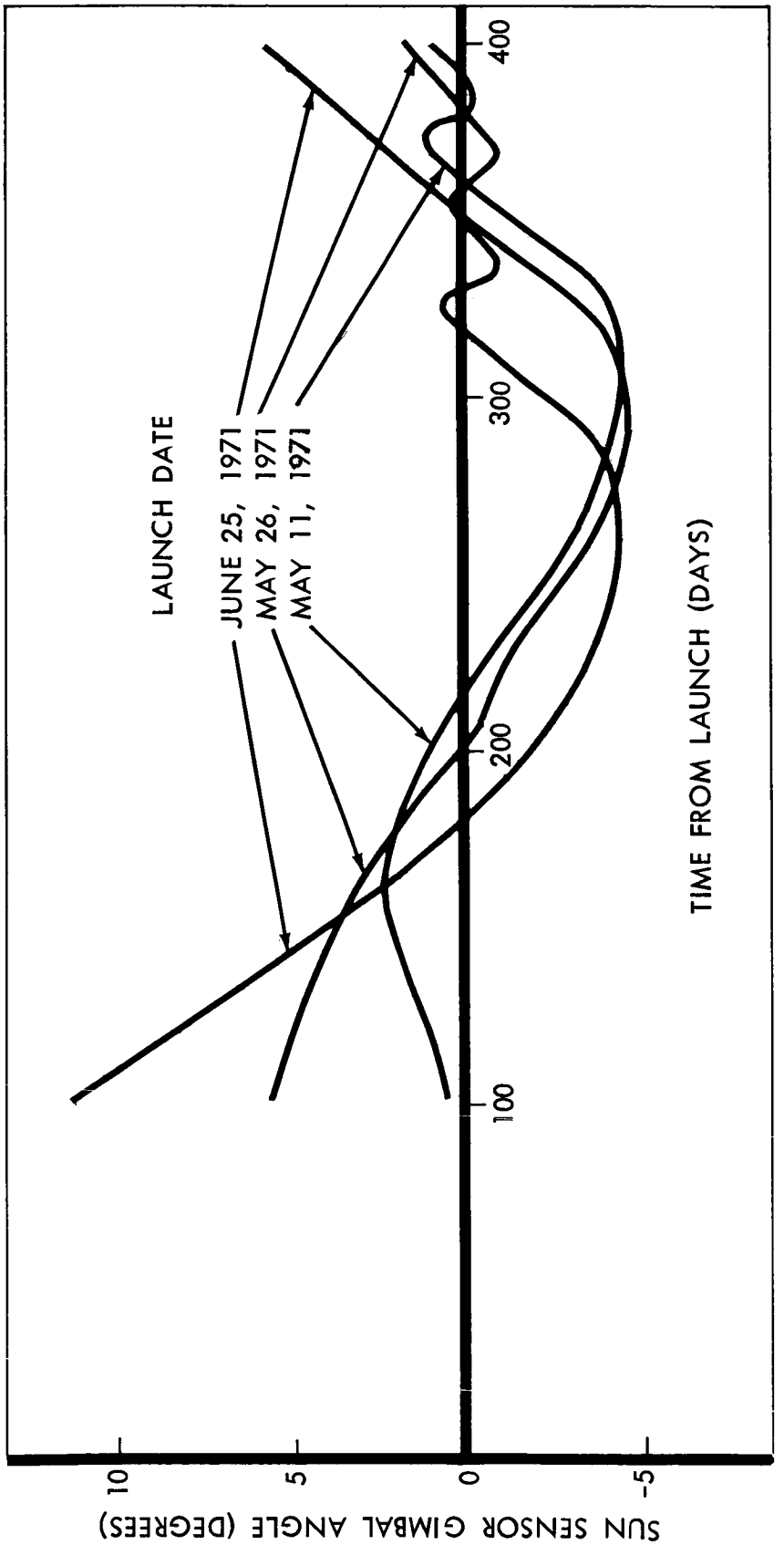

Figure 4.5-2: Sun Sensor Gimbal Requirements

4.5.1.2 Canopus Sensor Selection

The Canopus tracker is used to define the direction of the line of sight from the spacecraft to Canopus. This line is used for attitude reference about the roll axis. The tracker has an optical system to collect radiation from Canopus and focus it onto an image plane, a photodetector for sensing the position of the image, and the necessary electronic circuitry to derive attitude-error information from the position of the star image.

The Canopus tracker must have a total field of view of 32 degrees in pitch to cover the range of possible Canopus positions relative to the Sun-oriented spacecraft. The position is a known function of time and trajectory. This allows reduction of the instantaneous field of view, and programmed cone angle changes (electronic gimbaling) to increase signal-to-noise ratio. The desired field of view in roll is at least ± 2 degrees to permit rapid reacquisition of the star after maneuvers. The tracking accuracy required is 0.1 degree. This error is a share of the total $\pm 0.2^{\circ}$ error allowed to spacecraft orientation as derived from high-gain antenna pointing requirements in Mars orbit. The tracker must also be capable of providing a signal to the telemetry subsystem, indicating the magnitude of the star signal.

The preference for electronic gimbaling limits the applicable tracking techniques to image dissectors. These include internal scanning mechanism and solid state detectors found in mosaic and limit-cycle mechanizations which do not require star image scanning. Only the mosaic technique is significantly developed at the present time. The image dissector trackers described in this section employ this principle.

Present solid-state photodetector technology limits the sensing materials to cadmium sulfide and silicon. Neither material is available in an existing tracker, but the potential advantage in higher reliability, lower power, smaller size, weight, etc., suggest that they be considered in the present study. The preferred Canopus tracker selected as a result of this study is the Mariner IV tracker. This tracker was made by Barnes Engineering Company and modified by JPL.

Description of Alternates Considered--

Barnes Canopus Tracker--The Canopus tracker proposed by Barnes Engineering Company is based on an image-dissector tube manufactured by CBS Laboratories. The optical portion of the tracker consists of a semi-solid Schmidt-Cassegrain telescope with a 1-inch aperture, a system of baffles to mask the tracker from reflected sunlight, and a Sun shutter assembly to protect the image dissector from direct Sunlight. The electronics package includes power supplies, deflection signal generators, and signal processing electronics. The tracker recommended for Voyager is essentially identical to the one used on Mariner IV. The performance figures available, however, are based on the Mariner tracker delivered by Barnes Engineering Company. The total field of view is 32 degrees by 4 degrees; the instantaneous field is 10 degrees by 4 degrees, gimballed in 4.6-degree steps by applying d.c. voltages to the pitch axis of the image dissector. The tracking accuracy of the device is better than 0.1 degree. Canopus identification is provided by bracketing the image-dissector photocurrent between two preset thresholds.

ITT Canopus Tracker--The Canopus tracker proposed by ITT is very similar in concept to the Barnes unit except that it has an image-dissector tube made by ITT.

The ITT Canopus tracker is now part of the Lunar Orbiter System; successful operation of this tracker will prove space performance and reliability for the basic ITT design. The Voyager tracker proposed by ITT, however, includes a redesigned optical system to achieve a 32-degree field of view and the introduction of electronic switching of the instantaneous field of view. Considering the space proven status of the Barnes/JPL unit, and modifications required in the ITT unit, the Barnes/JPL unit is preferred.

Autonetics Canopus Tracker--Star trackers using cadmium-sulfide photodetector material are currently under development by Autonetics. Due to its present development status, the Autonetics star tracker will not be considered further. In the event that heat sterilization becomes necessary, the CdS device may be reconsidered.

Other Canopus Trackers Considered--A number of alternate Canopus trackers were considered, including the following:

1) Nortronics Canopus tracker proposed for Lunar Orbiter;
2) Honeywell Canopus tracker proposed for Lunar Orbiter;
3) Honeywell QMP star tracker; and
4) Santa Barbara Research Surveyor Canopus tracker.

Mechanical choppers are used in the proposed Nortronics and Santa Barbara Research Surveyor trackers. The Santa Barbara Research Surveyor tracker has a fixed ±2.3-degree cone angle and could not be used without modification. The two Honeywell trackers and the Nortronics unit are not developed to an extent where they are competitive with the Mariner IV and Lunar Orbiter trackers and were therefore eliminated from further consideration. Pertinent characteristics of these rejected devices are summarized in Table 4.5-1.

Competing Characteristics--Table 4.5-2 shows the major characteristics upon which the selection was based. The higher MTBF for the ITT sensor cannot be considered as firm as that of the much used Barnes unit. For future reference, it may be noted that photocathodes of the image dissectors begin to deteroirate at about 75°C, and are completely destroyed at 100°C, thus prohibiting sterilization by heat.

Logic of Selection--The Barnes Canopus tracker was chosen as the primary tracker because of its present space-proven status. The ITT tracker does not provide significant advantages over the Barnes unit and would require modifications of its optics. The ITT tracker was considered for use as a backup. However, the differences between the Barnes and ITT units are not significant. Consequently, the failure modes of the two units are considered to be similar. The costs in terms of (1) the non-space-proven status after adding optics modifications and (2) The logistics and integration required for two different units, are considered to outweigh the potential advantages of nonsimilar redundant units.

Table 4.5-1: SALIENT FEATURES OF ALTERNATE CANOPUS TRACKERS

Proposed Nortronics	Santa Barbara Surveyor	Honeywell QMP	Honeywell Lunar Orbiter (Proposed)
Modification of Mariner II long-range Earth sensor Photomultiplier detector not developed; mechanical chopper	Photomultiplier detector Cone angle coverage only $\pm 2.3^{\circ}$ Mechanical chopper	Uses quadrant photomultiplier Stepper motor drives mirror to change cone angle. This lowers space environment reliability	Similar to Mariner with different optics; not developed

Table 4.5-2: CANOPUS SENSOR COMPARATIVE CHARACTERISTICS

	Barnes	ITT
Field of View (32°) Mod. Required	No	Yes (16°)
Sensor Space-proven	Now	Soon
Reliability	137,000 Hours	167,000 Hours*
Transfer Function	Linear	Linear
Power	2 Watts	3.5 Watts
High Voltage	Yes	Yes
Weight	6.25 lb	6 lb
Size	11 x 5 x 4.5	12 x 5 x 4
Sterilization by Heat	No	No

* ITT estimates 500,000 hr. for space environment by use of a 0.3 uprating factor. For uniformity, however, a factor of 1.0 has been used in this table.

4.5.1.3 Sun Sensors

This section contains descriptions of the candidates considered for the spacecraft Sun sensors. The candidate sensors are similar in principle of operation, relying on the position of a shadow or image on a pair of bridged photocells to determine the attitude of the sensors relative to the Sun.

The primary differences are in the photodetectors used and in the mechanical structure which holds the detectors and provides the shadows or images. These differences result in different sizes and performance capabilities for the various sensors considered.

The selection of the two sensors for Voyager was based on space-proven development status and proven performance. The Nortronics sensor was selected as the primary sensor, and the Ball Brothers sensor as a parallel redundant unit.

The Sun sensor units must provide a 4 π steradian field-of-view to generate Sun acquisition control signals. The tracking accuracy must be 0.1 degree and the pointing error signal should be a linear function of pointing error within a range of several degrees to be compatible with the present autopilot concept. Alternate Sun sensors considered are described below.

Ball Brothers Sun Sensor--The photodecectors used in the Ball Brothers unit are silicon cells used in the photovoltaic mode. Two of these cells mounted in parallel and connected to a common 50-ohm load resistor, produce a positive or negative current through the

resistor that is an approximately linear function of the positive or negative pointing error. Another pair of cells provides a similar error signal about the other sensing axis. The four cells are mounted in a common casting, which also houses appropriate lenses for illuminating the cells. One group of sensors has a linear field of view of ± 2.5 degrees and provides the accurate Sun line sense. Another group of four sensors, the coarse sensor set, has a field of view of approximately 2π steradians. An additional unit with four coarse sensors mounted on the shaded side of the spacecraft completes the spherical coverage required for initial acquisition. The casting also contains a fifth cell that is exposed to a conical field of view about the nominal pointing axis, which indicates the presence or absence of the Sun in the field.

The output of the sensor is 12 mv/degree. Therefore, preamplifiers are used to boost the signal level prior to routing to the autopilot.

The Ball Brothers Sun tracker is a fully developed device, with the principal components space-proven on the Starfish and OSO and a similar Sun tracker developed for the Lunar Orbiter. Because of radiation effects encountered in the Starfish program, a hardened configuration has been developed which includes radiation filters for all the cells, cerium-doped lenses, and a hardened cell structure. One unit used on the OSO has been operating for 3 years in space.

Nortronics Sun Sensor--The photodetectors used in the Nortronics unit are made of sintered cadmium sulfide, fabricated by Clairex Company. The photosensors are contained within three specially designed shadow

blocks. One block contains four cells for performing fine error sensing about the pitch and yaw axis, and a fifth cell for Sun acquisition indication. Two of these cells, mounted under partial shades so that the illumination reaching each cell is a function of the Sun position, are connected in a bridge whose output is approximately a linear function of the angle of the Sun from the nominal pointing direction.

Another pair of cells indicates the pointing error in the other axis. A fifth cell sees a conical field-of-view of a few degrees centered about the nominal pointed axis, and merely indicates the presence or absence of the Sun in this field. Two other blocks contain a total of eight cells which provide coarse sensing over 4 π steradians.

The unit includes regulated positive and negative d.c. supplies for biasing the photoconductive cells. The predicted MTBF of the Nortronics sensor subsystem includes these components.

The basic Northrop Nortronics Sun Tracker is fully developed and space-proven, and is currently operating successfully on Mariner IV. However, a minor change affecting scale factor and linear range is desirable for the Voyager program. The change necessary is to move the light shade with relation to the sensing element so that light variation over the sensing surface is linear for up to 4 degrees of angular error rather than the present 1/2 degree.

Bendix--The Bendix model (1818787) Sun sensor consists of 12 silicon photovoltaic cells, providing 2 π steradian, two-axis coverage. Two

of these units can be used to cover the full 4π steradian field of view. In each unit, there are four cells (the "quad" cells) for fine control. These are mounted on a casting behind a square-aperture plate which acts as a shadow mask. Each pair of diametrically opposed cells is interconnected, one pair for each channel. Eight cells mounted on the periphery of the casting, at right angles to the quad cell structure provide coarse ontrol. The whole structure is hermetically sealed by a glass dome. The cells are N on P silicon used in the low-impedance mode, with the null error causing a proportional current output. Control of switching from coarse to fine modes can be enhanced by the addition of one more photocell, aligned to the fine sensor field-of-view.

The Bendix model (1818787) Sun sensor is fully developed, has been qualified to Atlas-Agena D specifications, and has been tested by Sandia Corporation, and in the EROS experiment.

Autonetics Sun Tracker--The Autonetics Sun tracker consists of 13 vacuum-evaporated CdS-CdSe photoconductive strips, providing 4 steradian, two-axis coverage. Two bridge pairs of detectors, one pair in each axis, provide fine error readout over a small field-of-view. Four bridge pairs, two pairs in each axis, provide coarse control over the remainder of the 4π steradians. One detector acts as a fine acquisition sensor. The fine sensing unit and a two-pair unit of the coarse sensors face opposite directions. These two units are aligned under shadow masks. As the Sun direction varies, the relative illumination on the two detectors of a bridge pair varies, and the ratio of

their electrical resistance change proportionally with the pointing error.

The Autonetics Sun tracker is in the development stage. Autonetics is currently under contract to JPL to fabricate the vacuum-evaporated photoconductors for evaluation.

Competing Characteristics--The competing characteristics of the four candidate Sun sensors are tabulated in Table 4.5-3. As shown on the table, the accuracy, size, weight, and power of the three candidate sensors are not significantly different. The MTBF of 10^5 hours for the Nortronics sensor versus 10^6 hours for the Ball Brothers appears at first to be significant. However, there is no apparent reason why the reliabilities should be different and the given differences are assumed to be a result of different reliability criteria. The shift of scale factor as a function of distance from the Sun displayed by the Ball Brothers sensor is undesirable because it affects the limit cycle range of the autopilot control.

Logic of Selection--The selection of the Nortronics and the Ball Brothers Sun sensors was made on the basis of their development status and the fact that they are both space-proven. The choice of the Nortronics unit as the primary sensor was based on its higher sensitivity, and the fact that its null sensitivity is not dependent upon the distance from the Sun. The use of dissimilar redundancy provides two fundamentaly different fully developed and proven Sun sensors to reduce the likelihood of systematic failure.

Table 4.5-3: Sun Sensor Competing Characteristics

Characteristic	Nortronics	Ball Brothers	Bendix	Autonetics
Status	Space Proven	Space Proven	Fully Developed	In Development
Type of Detector	Sintered CdS	Silicon	Silicon	Vacuum-deposited CdS-CdSe
Accuracy	0.1 deg	0.0_2 deg	0.1 deg	.01 deg
Null Sensitivity	1 v/deg	15mv/deg (Earth) 7.5mv/deg (Mars)	10 mv/deg	1 v/deg
Linear Range	$\pm$3 deg	$\pm$5 deg (Earth) $\pm$3.5 deg (Mars)	$\pm$10 deg	$\pm$3 deg
Fine Sensor Field	160 x 45 deg	$\pm$15 deg	$\pm$30 deg	$\pm$15 deg
Size	21.5 in^3	18 in^3	4.3 in^3	2 in^3
Weight	11 oz.	6 oz.	3 oz.	4 oz.
MTBF	10^5 hr	10^6 hr	4.5 x 10^5 hr	10^6 hr
Operating Temp. Range	-16° to +66°C	-12°C to +85°C	-40°C to +70°C	-55°C to +100°C
Thermal Sterilization Allowed	No	Yes	Yes	Yes
Power	300 mw	200 mw	200 mw	200 mw
Constant Scale Factor	Yes	No	No	Yes

The Autonetics device was eliminated because of its early development status. The Bendix Sun sensor, although fully developed, is not space-proven to the same degree as either the Ball Brothers or Nortronics instruments.

4.5.2 Velocity Control

The magnitude of velocity changes at midcourse correction, and Mars orbit insertion can be controlled in two basic ways:

1) By timed operation of engines which have precisely-known thrust.
2) By integration of accelerometer outputs, and engine cut-off when commanded ΔV is reached.

The first trade therefore determines whether or not an accelerometer is required.

Following discussion concerns the number of accelerometers and their configuration, and the selection of preferred instruments from those available.

4.5.2.1 Accelerometer or Timer Control of Midcourse Velocity Change

As stated in its "Voyager Mission Guidelines", it is desired that midcourse velocity changes be performed to an accuracy of about 1 percent (1σ) of the thrust.

Timed Engine Operation--The preferred midcourse engines described in Section 4.3 of Volume A may have a midcourse thrust tolerance as high as 1 percent. Other uncertainties such as variations in the exact mass of the spacecraft at midcourse, and thrust axis misalignment contribute

small fractions of a percent of error. Timed engine shutoff was considered therefore to be marginal to achieve the desired accuracy.

Accelerometer Controlled Engines--Accelerometer control as described in detail in Section 4.6 of Volume A is capable of controlling midcourse ΔV to approximately $\frac{1}{2}$ percent. Higher thrust levels would improve the margin of accuracy which the accelerometer has over the timed thrust mode.

Preferred Velocity Control Mode--Based on the margin of accuracy provided by accelerometer control of velocity changes, this method is preferred. Timed control is a desirable backup mode, and will be incorporated as such.

Cross-axis accelerometer usage was briefly considered, but based on the specified accuracy of thrust axis alignment with the vehicle center of gravity (0.25°, per Volume A, Section 3.8), the less complex roll axis-only instrumentation was selected. The more simple mechanization of the two parallel, redundant accelerometers caused this arrangement to have the greater reliability even though the other configurations offered slightly more accuracy. Greater accuracy was not required, so reliability was the factor responsible for choosing the two-accelerometer configuration. Weight and power requirements were secondary considerations in favor of the two-accelerometer parallel-redundant configuration.

4.5.2.2 Accelerometer Selection

The preferred accelerometer configuration consists of two instruments aligned along the roll axis, both operating simultaneously. The CC&S accumulates the two pulse trains independently and terminates thrust based on either accelerometer. Minimum and maximum allowable thrust times are used for failure detection and backup thrust termination, respectively. The following discussion describes the process which led to the selection of one each of the Bell IIIB and Autonetics EMA.

Description of Alternates Considered--Preliminary instrument screening resulted in the selection of the following instruments for evaluation:

1) Systron-Donner model 4318 pulse rebalance accelerometer;
2) Autonetics model A40 EMA digitized electromagnetic accelerometer;
3) Bell Aerosystems model DVM IIIB digital velocity meter;
4) Bell Aerosystems model DVM V digital velocity meter; and
5) Minneapolis-Honeywell pulse-digitized CG 177 accelerometer.

Donner 4318--The Donner 4318 accelerometer is a pulse-rebalanced accelerometer for use in digital systems. The basic sensor used in the accelerometer is the Model 4810, a redesigned version of the Model 4310, of which 15,000 units have been built. About 40 Model 4810 accelerometers have been built. Two prototypes of the 4318 are under construction.

EMA Accelerometer--A cutaway view of the Autonetics electromagnetic accelerometer is shown in Figure 4.5-3. The acceleration-sensing

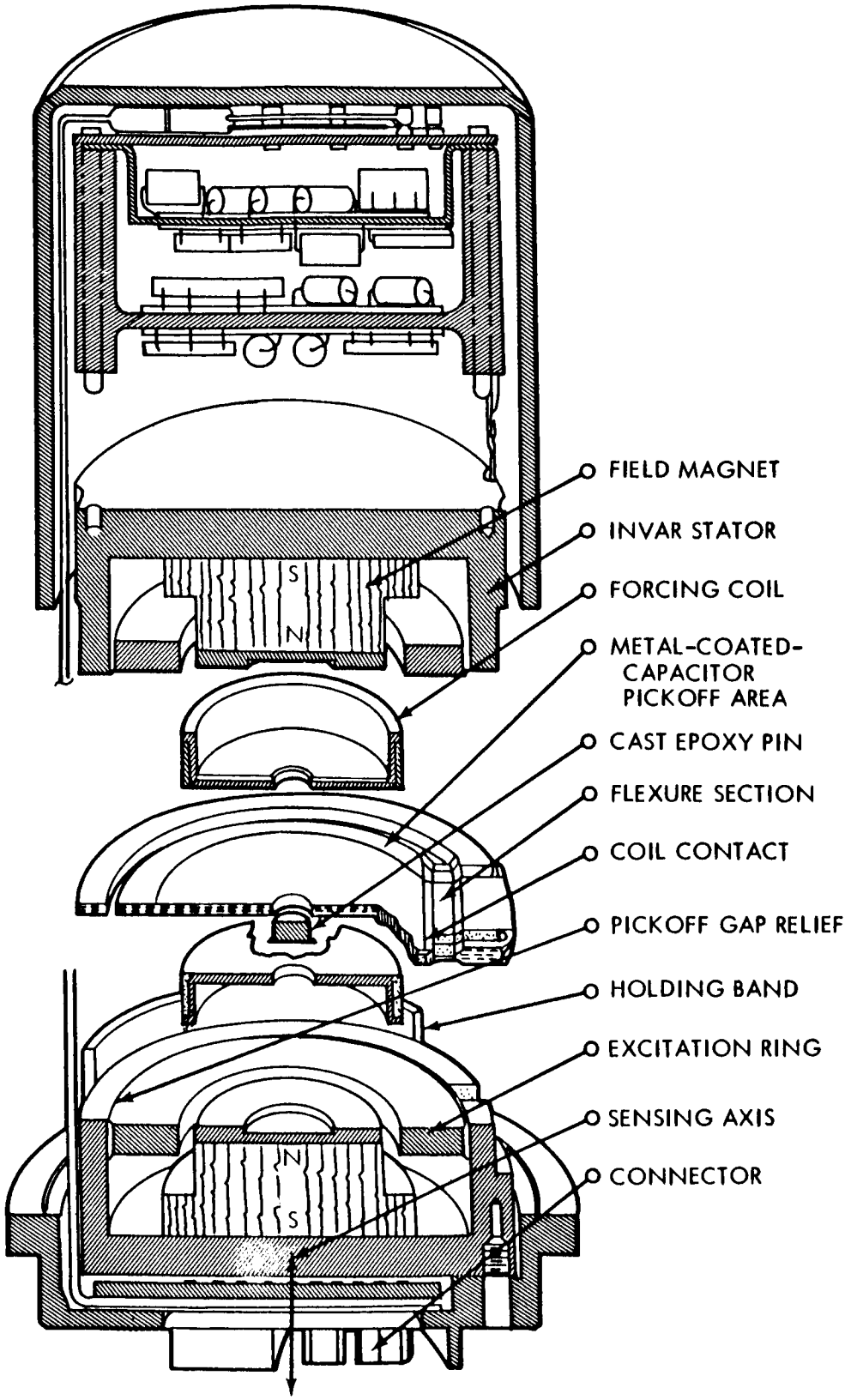

Figure 4.5-3: EMA Cross Section

member shown in the figure is a fused, silicon-proof mass that is attached to the accelerometer stator members by means of an integral flexure section. The pickoff, which generates an electrical signal in response to the proof mass displacement, is a capacitance bridge. The forcing coils are located in the radial magnetic field of the Invar stator permanent magnet circuits. The force servo loop uses pulse currents to obtain a digital output. About 27 EMA accelerometers have been built. A test program on two accelerometers has recently been completed at Holloman AFB and two are a part of the prototype Autonetics N16 inertial navigation system. The others have been radiation and laboratory tested.

Bell IIIB--The Bell IIIB accelerometer is a high-accuracy unit which has been proven in many space applications, including Agena, Ranger, and Mariner. It uses a metal flexure suspension of the proof mass and is a 'dry' instrument, i.e., not fluid filled. The weight of the accelerometer is relatively high, at four pounds, including the digitized electronics. A cutaway view of the sensor is shown in Figure 4.5-4. The sensor unit shown in the figure is combined with a digitizing electronic unit to form a self-contained assembly.

Bell DVM V--The DVM V sensor is basically a flexure spring-suspended pendulum accelerometer mechanized in a manner similar to the DVM IIIB sensor. The sensor is packaged with its servo electronics in a self-contained accelerometer assembly. When coupled with its pulse rate converter unit, it is designated as the Bell Model DVM V.

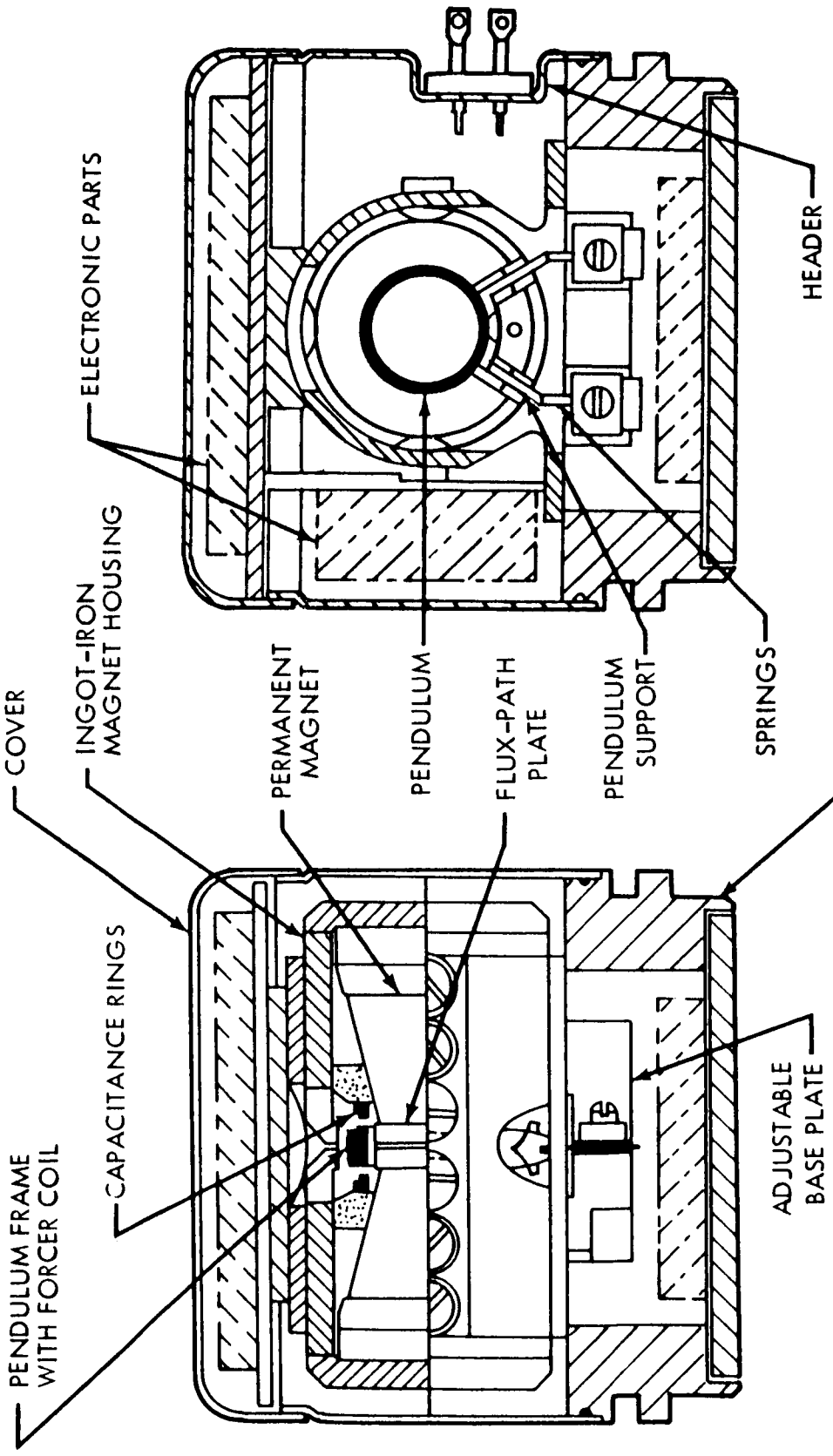

CROSS SECTION THROUGH ACCELEROMETER

Figure 4.5-4: Bell DVM-111B Sensor

Performance characteristics comparable to the Model DVM IIIB are reported by the manufacturer, but only limited data appears to be available. Approximately 80 sensor units have been delivered to date. However, instruments complete with digitizer will not be in production until January, 1966.

Honeywell GG 177--The Honeywell GG 177 uses a flexure hinge-supported pendulum as the sensing element, a differential transformer pickoff, a permanent magnet torquer. The instrument is fluid-filled to provide viscous damping. Accelerometer torquing uses a pulse-on-demand system. From 200 to 300 of these instruments have been built, with major applications being in the Centaur guidance system and the Apollo stabilization and control system.

Competing Characteristics--Table 4.5-4 summarizes the trade data for each of the accelerometers considered.

Logic of Selection--The five accelerometers listed in Table 4.5-4 will perform within the required system limits; thus the tradeoffs will not depend upon performance characteristics. The problem is then reduced to one of choosing the best accelerometer (or accelerometers) on the basis of reliability, volume, weight, power, and proven capability.

The Autonetics EMA has many desirable characteristics for space application, such as low weight, small volume, low power, and high reliability; it will easily meet the performance objectives for this mission. Therefore, the Autonetics EMA has been selected as one of the

accelerometers for the inertial reference unit. The EMA represents the mating of a new generation of miniaturized, highly reliable accelerometers with low power and microminiaturized, integrated circuit control electronics. The EMA has not yet been used in a space application and is in an early production status.

The Bell DVM IIIB is recommended to provide parallel redundancy with the EMA. The DVM IIIB has a considerable background of production experience and has been used in many space applications. Redundancy is thus assured by using two dissimilar instrument designs; one appears ideal for the intended application but has not been proven, and the other has had extensive space experience but is large, power-consuming, and not as reliable.

4.5.3 Inertial Attitude References

System trades briefly described in the following section identify the three-axis, strap-down gyroscope concept as the means of providing references for maneuver or acquistion. The following paragraphs summarize trades and analyses which form the basis for selection of the preferred design.

As a part of the gyro selection, consideration was given to the various single-thread and redundant mechanization methods. The prime candidates, each mechanized in its optimum configuration, were:

Three Autonetics G1OB two-Axis free-rotor gyros; and

Six Honeywell GG159 MIG rate-integrating gyros.

	Donner 4318	Autonetics EMA
Size Sensor: Servo & Digitizer:	1.41 by 1.53 by 3.01 inches 2.97 by 3.00 by 1.41 inches	1-inch dia. x 1-3/8 in. (Including Servo & Digitizer)
Weight Sensor: Servo & Digitizer:	7 oz. 8-1/2 oz.	2-1/2 oz. Total
Accel. Range (As Desired Up to Indicated Level)	±10g	±20g
Suspension Type	Jewel & Pivot	Quartz Flexure
Power Required	* +28v d.c. ± 10%	** +28v d.c. ± 10%
Power Consumption	2.8 Watts	0.5 Watts
Accel. Threshold	< 20 µg	< 2 µg
Linearity	±250 µg to 1g ±.02% of Input to 6g	< 50 µg/g
Cross Axis Sensitivity	< 0.001g/g	-
Cross Coupling	100 ppm/g	30 ppm/g
Scale Factor (Pos. to Neg.)		< 50 ppm
Scale Factor	0.3 to 1 ft/sec/pulse	0.05 to 0.2 ft/sec/pulse
Scale Factor Stab.	0.01%/mo.	0.01%/mo.
Scale Factor Temp. Sens.	50 ppm/°F	50 ppm/°F

270

Table 4.

Bell DVM IIIB	Bell DVM V
4.0-inch dia. by 3.0 inches (Sensor & Servo) 3.5 by 4.94 by 3.0 inches (Digitizer)	1-3/4-inch dia. by 1-3/4 inches (Sensor & Servo) 1-3/8 by 2-1/2 by 2-1/2 inches (Digitizer)
35-1/2 oz (Sensor & Servo) 33-1/2 oz (Digitizer)	16 oz. Total
±100g	±150g
Metal Flexure	Metal Flexure
+28v d.c. ± 10%	+28v d.c. ± 10%
8 Watts 12 Watts (Digitizer Temp. Control)	6 Watts
< 1 μg	1 μg
30 μg to 0.3g 0.01% of Input to Max. Range	30 μg to 0.3g 0.01% of Input to Max. Range
5 μg/g	Not Available
10 ppm/g	50 ppm/g
< 10 ppm	< 10 ppm
0.04 to 1.0 ft/sec/pulse (variable)	0.04 to 1 ft/sec/pulse (variable)
0.006%/mo.	0.004%/mo.
1 ppm/°F (with Compensation)	30 ppm/°F (Compensated) op. in ±10° w/o Temp. Control

5-4: Accelerometer Trade Summary

Min-Hon GG177
1-3/4-inch dia. by 1-3/4 inches (Sensor) 1-1/8-inch by 2-3/4 by 6 inches (Balance Loop) 1-1/8 by 2-3/4 by 6 inches (Prec. Pulse Supply) 1 by 1-3/8 by 2-1/4 inches (Pulse Ref. Excl. Oven)
8 oz. (Sensor) 48 oz. (Electronics Excl. Oven)
±15g
Metal Flexure
+28v d.c. ± 10%
8 Watts + 20 Watt Heater
10 μg or Less
60 μg max, 20 μg RMS to 1g (Data on Higher Range is Classified)
1 μg/g
-
< 100 ppm
0.01 to 1 ft/sec/pulse
0.005%/mo.
3.0 ppm/°F (Over ± 5° Range.) Approaches 1500 ppm at 30° off Comp. Temp.

	Donner 4318	Autonetics EMA
Bias	< 300 μg (Zero Output)	< 300 μg (Can be Adjusted Out)
Bias Hysteresis	± 50 μg	± 10 μg
Bias Stabilized from Turn-On to Turn-On	± 100 μg	± 10 μg
Fluid-Filled	Yes	No
Bias Temp. Sens.	3 μg/°F	< 10 g/°F
Bias Stab. (Short Term)	-	20 μg (Per Day)
Bias Stab. (Long Term)	100 μg (1 Year)	50 μg (90 Days)
Vibration Sensitivity	100 $\mu g/g^2$	< 50 $\mu g/g^2$ (20 cps) 20 $\mu g/g^2$ (Above 20 cps)
Input Axis Alignment w.r.t. Ref Surface	15 $\widehat{Min}$	1 $\widehat{Min}$
Input Axis Stability (Long Term)	20 $\widehat{Sec}$ (1 Month) 50 $\widehat{Sec}$ (1 Year)	5 $\widehat{Sec}$ (90 Days)
Input Axis Temp. Sensitivity	Remain within Initial 15 $\widehat{Min}$ from -40F to +200F	< 0.1 $\widehat{Sec}$/°F
Reliability, Operating	116,000 Hours MTBF for Electronics Only. 58,000 Hours MTBF for Complete Instrument (Calculated)	1,000,000 Hours MTBF (Calculated)
No. of Units Built (Approx)	50 Sensors and 2 Complete Instruments. Sensor is Modification of 4310 Sensor of which 15,000 Have Been Built	27
Applications on Specific Programs	X-15, SIGS	SLAM, Autonetics N16, SIGS

*Requires a separate supply approximately the size of the servo and digitizer electronics to provide inversion and 0.1% regulation.

Table 4.5-4: Accel

Bell DVM IIIB	Bell DVM V
Can be Adjusted to ± 50 ug	Can be Adjusted to
± 20 ug (Repeatability)	± 20 μg (Repeatabili
± 20 ug	± 20 μg
No	No
10 μg/°F	5 μg/°F
1 μg (Per Day)	1 μg (Per Day)
50 μg (30 Days)	50 μg (30 Days)
3 $\mu g/g^2$	3 $\mu g/g^2$
1 $\widehat{\text{Min}}$	40 $\widehat{\text{Sec}}$
-	-
-	-
10,000 Hrs MTBF (Calculated) 16,000 Hrs Life Demonstrated on Sensor	20,000 Hrs MTBF (Calculated)
50 DVM IIIB and 400 Sensors	80 (Sensors Only) N Complete Instrumer Production Starting Jan. 1966
Agena Ranger Mariner MM Re-Entry	Sensors Only: LEM Guid. System. Sp SGN10 Platform Skyscraper Program

**The accelerometer operates from the gyro supply whi

±10V, 1%	Each matched to 5%
±20V, 1%	20 kc, 6V
	2 kc, clock

erometer Trade Summary (Cont.)

	Honeywell GG177
= 50 μg	50 μg
ty)	5 μg
	± 40 μg
	Yes
	20 μg/°F
	-
	80 μg/mo
	Not Available
	40 Sec
	4 Sec (47 Days)
	1.0 Sec/°F
	50,000 Hrs MTBF (Calculated)
lo its.	200 to 300
l Abort erry	Apollo Stability Control Centaur

ch provides:

The G1OB gyro was selected as the preferred component based primarily on the proven reliability of the free-rotor gyro. Other favorable factors were: power requirements, state of development, and the provision of all-axis redundancy by the addition of only one gyro.

4.5.3.1 Gyro Configuration

Considering the limited life and reliability of mechanically-gimballed platforms, only strapdown-gyro configurations were considered for Voyager. Two basic approaches to strapdown-gyro usage were examined. These are:

1) Use of an uncaged gyro, and maneuver by torquing of the gyro by a precision torquing current for a precise length of time. The reaction-control thrusters then act to drive the spacecraft to align it with the new gyro rotor position.
2) Use of a caged gyro which has an output proportional to angular rate at all times. In this mode, slew commands enter the attitude control loop until the desired rate, or integrated rate (position), is achieved.

Mechanization and response of these two schemes are shown in Figures 4.5-5 and 4.5-6. Both maneuver schemes have been used in space. Accuracies are comparable. The choice of maneuver scheme is thus dependent on the gyro to be selected; and gyro selection need not be compromised to accommodate a preferred maneuver scheme.

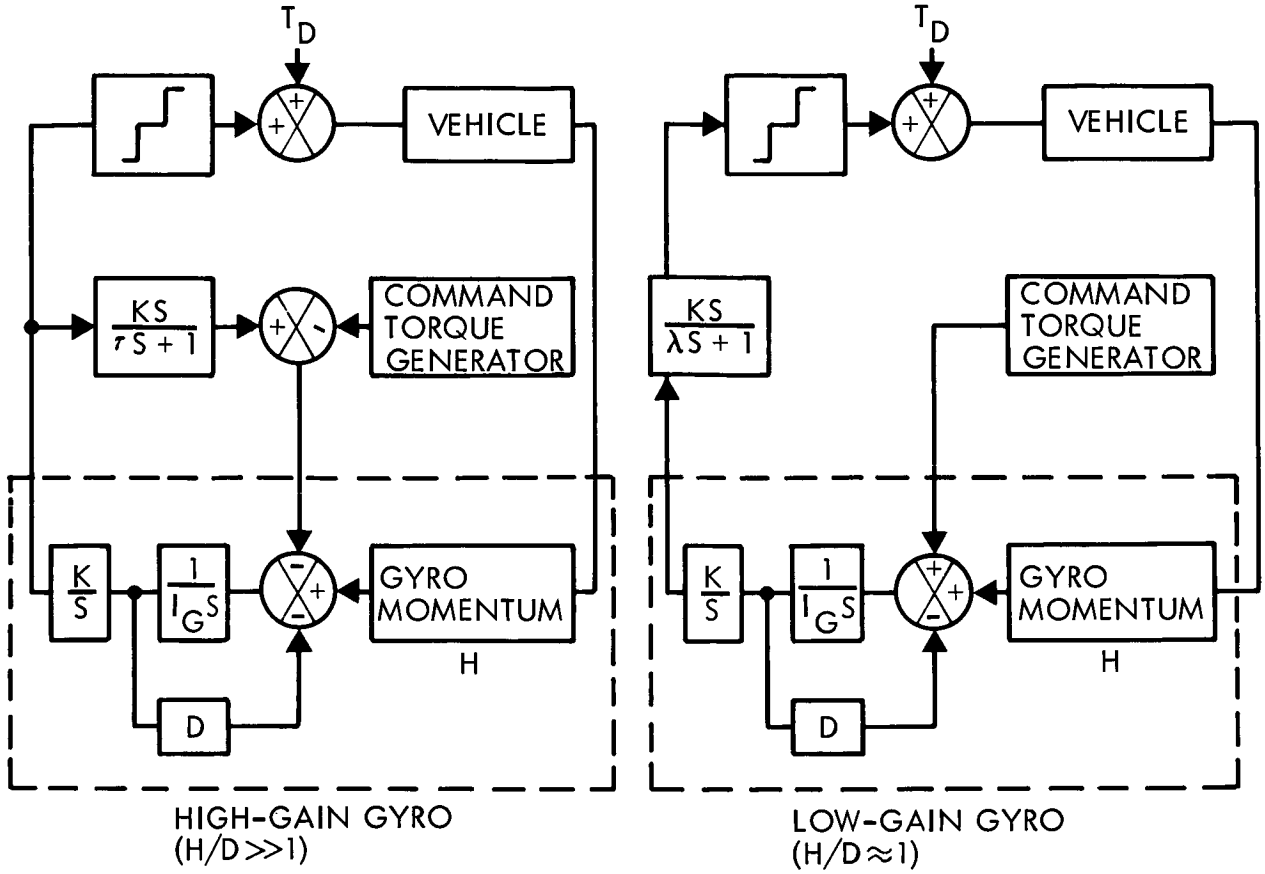

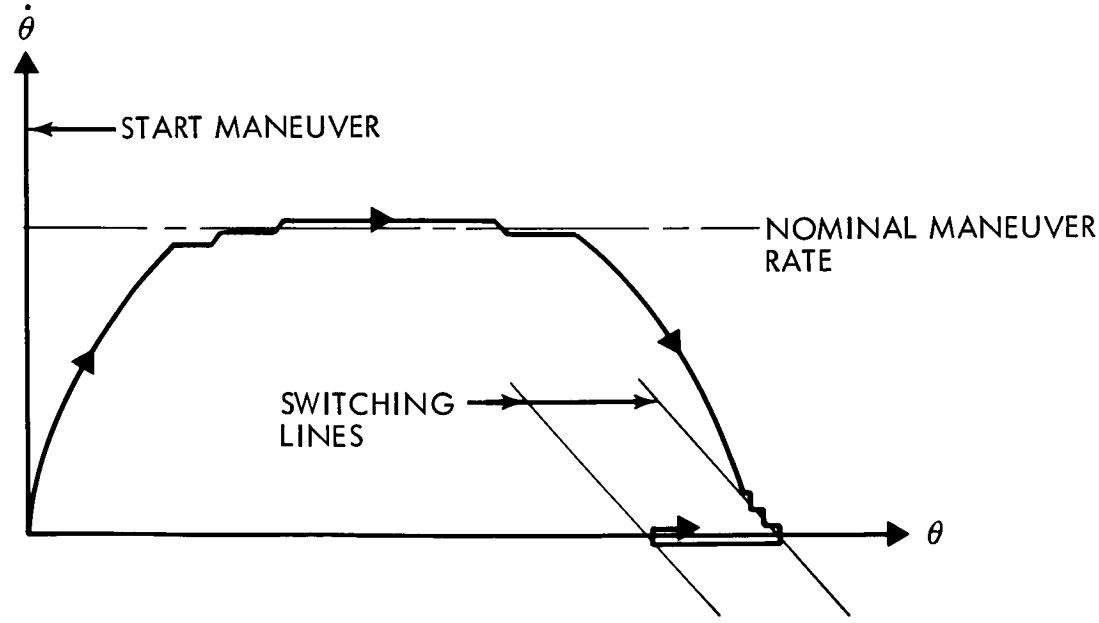

Figure 4.5-5: Maneuvers with High- and Low-Gain Gyros

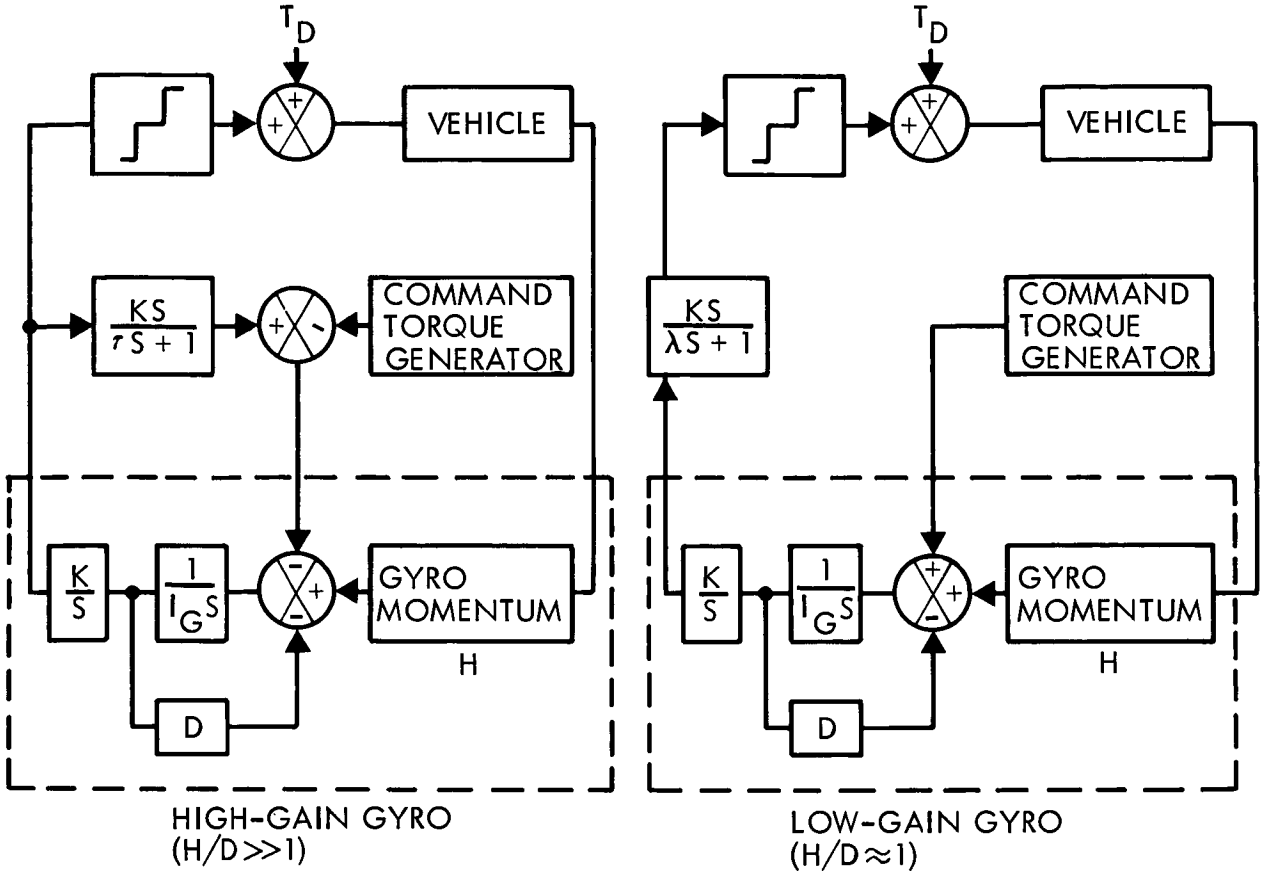

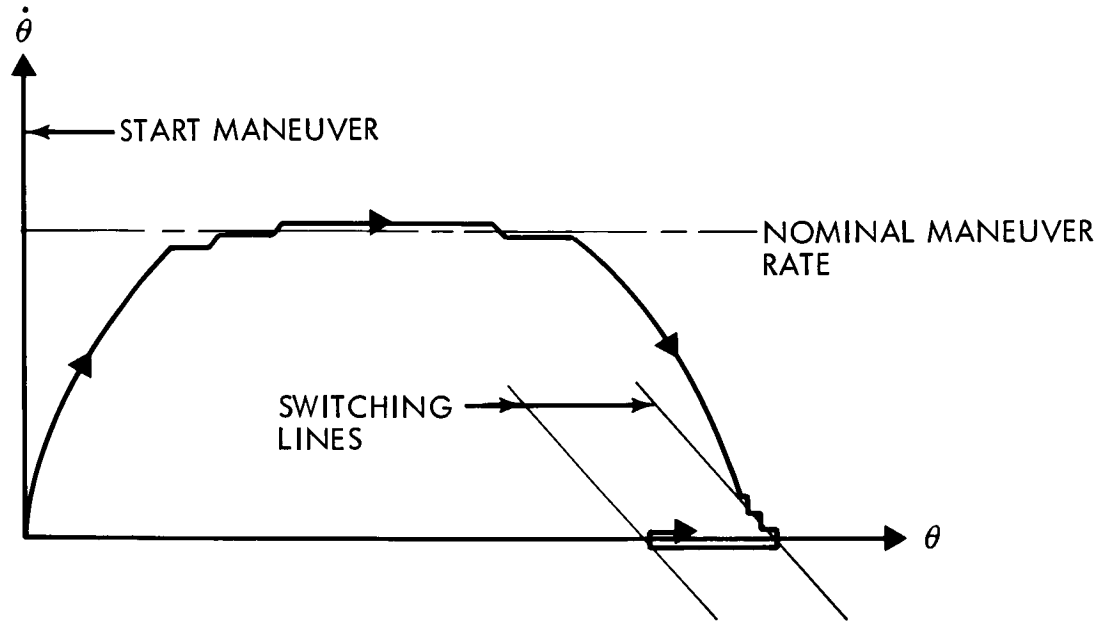

Figure 4.5-5: Maneuvers with High- and Low-Gain Gyros

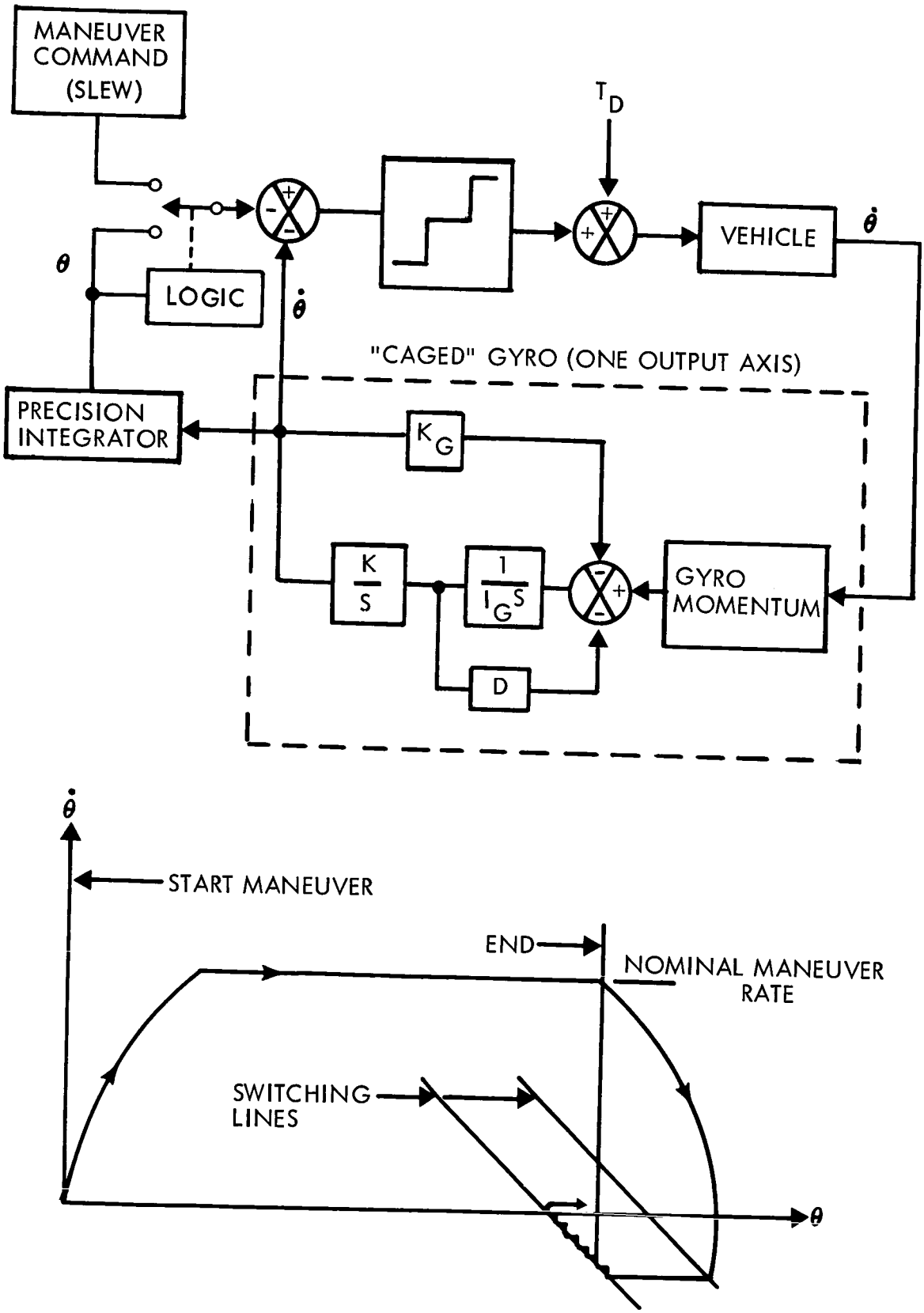

Figure 4.5-6: Maneuvers with Caged Gyros

4.5.3.2 Gyros Considered

The most widely used gyro in space vehicles is the floated single degree of freedom ball bearing spin motor gyro. These gyros have well known performance and reliability capabilities and have been proven in many space missions. Depending on the failure criterion, the MTBF of ball bearing gyros can be 20,000 hours or more. The wearout life, determined by bearing life, is in the neighborhood of 6,000 hours. A basic trade between gas bearing single degree of freedom and ball bearing single degree of freedom gyros is reliability. The gas bearing gyro, while not proven to the same degree as ball bearing gyros, have accumulated more than 17 million hours of operating time (eg., Minuteman G-6 free-rotor gyro) and have exhibited much high reliability because of their simpler design. The gas bearing gyro also has better performance, but both gyros will meet Voyager performance requirements. The consideration thus involves confidence. Here the space-proven status of the ball bearing single degree of freedom gyro must be traded against the advantages of the more reliable gas bearing gyro. Also included is the consideration of gyro life. The gas bearing gyro has no wearout mechanism, and therefore, throretically unlimited wearout life. Should there be a requirement for running time in excess of 6,000 hours (for optical sensor backup, for example), the gas bearing gyro is the better choice. However, a series redundant ball bearing gyro could also accomplish the mission with a high degree of confidence. This confidence is based on its space proven performance. The gyro trade studies involved consideration of the gas bearing free rotor gyro and the gas bearing single degree of freedom gyro. The Autonetics GLOB was chosen as the most promising free rotor gyro, and the Honeywell GG159 was

chosen as the best suited single degree of freedom gyro. The Kearfott C702590 KING II gas bearing gyro was not traded because of its incomplete development status.

Autonetics G1OB--The Autonetics G1OB (Figure 4.5-7) is a high-reliability, two-axis displacement gyro capable of torquing rates of up to 5 deg/sec. Except for the electrical components and mu-metal shield, the G1OB gyro is constructed entirely of aluminum. The sensitive or gyroscopic element consists of a simple flywheel rotor. The rotor is spun by an induction-drive motor supported by a self-lubricated gas bearing. This spherical gas bearing affords the rotor three degrees of angular freedom and permits definition of a spin axis and two displacement axes. Relative displacement between the rotor and case structure is sensed by a two-axis capacitor pickoff. A four-pole torquer produces forces on a metallic sleeve attached to the rotor, resulting in controlled gyroscopic precession. This method of torquing, coupled with a slow-speed rotor operation, permits extremely high torquing capability with a low input power and inertial-grade instrument performance for space guidance application. Approximately 100 G-10 gyros are currently in production.

Honeywell GG159 Advances Gas Bearing (MIG) Gyro--The single-degree-of-freedom GG159 advanced miniature integrating gyro design combines a hydrodynamic gas spin-bearing, a hydrostatic gimbal suspension, a moving-coil signal torque generator, a micro-vernier balance pan, and a thermal shield. These developments provide long life and high reliability, low null torque uncertainties, improved gimbal mass stability and low

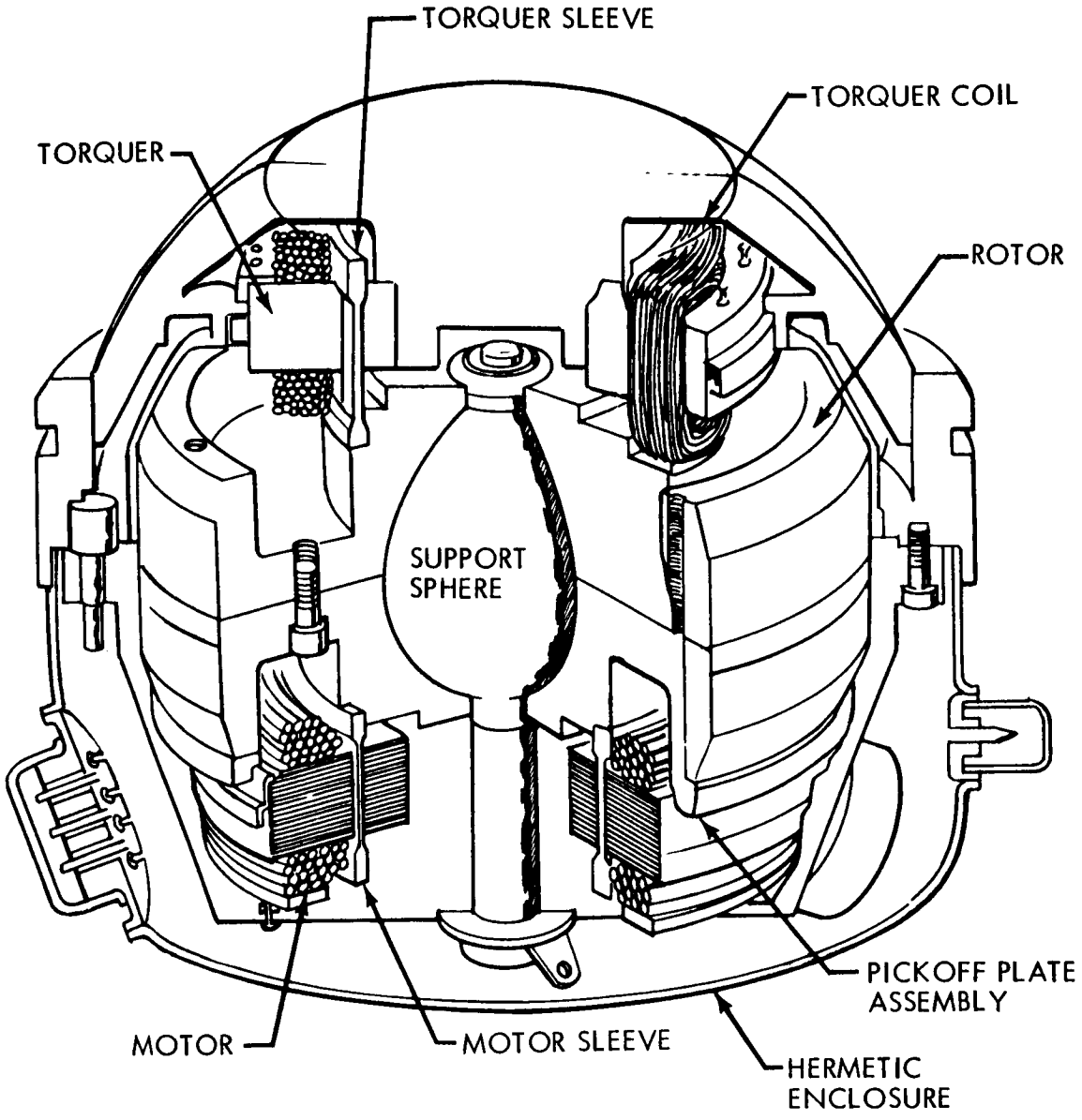

Figure 4.5-7: Autonetics G10 Gyro

g-and non-g-sensitive drift rates.

The hydrodynamic gas spin bearing is a self-acting device in which the rotor is supported on a microthin gas film. The mechanization for thrust support is supplied by a spiral-grooved thrust plate which is an integral portion of the spin motor. The hydrostatic gimbal suspension provides a non-contact feature which eliminates alignment uncertainties associated with pivot and jewels. Required pressure and flow characteristics are provided by a miniature positive-displacement pump integral with the gyro case. Filtering inserted into the fluid flow lines provides a continuous self-cleaning feature. A moving-coil torque generator provides the torque necessary for gyroscopic precession.

These instruments are being used on a classified space mission. Over 120 gyros have been built.

Competing Charteristics--The outstanding feature of the free rotor gyro is simplicity in design. The instrument contains only one moving part and permits no metal-to-metal contact when operating. The start-stop wear characteristics of the gas bearing is the only mechanism where metal-to-metal contact is made and is, thus, the only failure mode to prevent a theoretically infinite operation life. This unique design is supported by the remarkable proven reliability record that the G6B4 Minuteman gyro has accumulated over the past several years. The G6B4 has accrued 17,107,708 operational hours (at a current rate of 36,690 hours per day) as of 12 June 1965. Because the G10B is basically a

scaled-down version of the G6B4 gyro, equivalent reliability is expected.

Extensive experimental testing has shown that the G6B4 gas bearing can withstand over 20,000 starts and stops before failure. Comparable performance may be expected of the G10B.

The MH-GG159 (MIG) gyro will have a high-reliability gas bearing. Literature indicates that the MH-GG159 gyro is capable of 10,000 start-stops with no detectable wear damage or degradation of performance. An aluminum ceramic gas bearing spin motor is used.

The free-rotor gyro does offer several advantages over liquid-filled gyros such as the GG159. The absence of a flotation fluid eliminates the problems of buoyancy balance and convection torques. There are no lead-in wires to produce coercion on the rotor. The gyroscopic element may be completely non-magnetic, eliminating drift due to magnetic fields. The rigid, sensitive element with no motor laminations, stator windings, or ball bearings has an extremely stable mass center. Self-induced vibration is reduced to virtually zero with a spherical gas bearing; hence, long life and high reliability are assured.

Fluid contamination, pump hysteresis effects, and the added reliability degradation due to the additional moving parts give a floated instrument an inherent disadvantage when compared with the free-rotor concept. In

Table 4.5-5 shows the G10 and GG159 subsystem reliability prediction. As can be seen, the electronics reliability for the two subsystems is roughly the same. The G10 failure rate of 1 x 10-6 failures per hour is based on G6B experience. The GG159 failure rate is estimated by the manufacturer to be 20 x 10-6 failures per hour. The GG159 gyros have not accumulated enough operating hours to establish a failure rate having a high degree of confidence.

Either gyro subsystem has two possible operational modes. In the first mode, the gyros are run during the entire mission, providing for continuous bias updating and optical sensor checking. In the second mode, gyros are run only when absolutely necessary, such as immediately before midcourse maneuvers, during Mars orbit injection and Sun occultation, and are shut-down immediately after each event. The first mode obviously offers more advantages, provided the required reliability can be achieved. A comparison of the mission reliabilities achievable by the two systems in both the single-thread and fully redundant cases is presented in Table 4.5-6, which shows the following:

1) Neither system can meet the apportioned reliability of 0.9965 percent in the single-thread configuration, although the G10 system achieves 0.9937.
2) Either redundant system can exceed the apportionment if operated only when required.
3) The G10 is the only one which can meet the apportionment during continuous operation.

Table 4.5-5

G10 and GG159 Gyro Subsystem Reliability Predictions			
G10 System		GG159 System	
	X10-6 Failure/hr		X10-6 Failure/hr
1. G10 Gyro	1.0000	1. Gyro Assembly	
2. PWM Servo	0.5595	GG159 Gyro	20.000
3. Speed Controller	0.5356	Relay	0.2360
4. Electronics Circuit Breaker	0.1392	Current Supply	0.5385
5. Motor Supply	0.6221	Preamp and Demod	0.0455
6. Temperature Compensation	0.0406	2. Inverter	0.8908
7. Field Current Supply	0.2068	3. Countdown Circuit	0.5476
8. Up/down Count, D/A Convertor Detect/select	0.4075	4. Gyro Pump Supply	0.1508
9. Countdown plus 19.5 Kc Amp	0.5476	5. Gyro Heater Supply	0.5562
10. Inverter	0.4504	6. PIM Electronics	0.6057
		7. D R Electronics	1.0752

Table 4.5-6

G10 Vs GG159 Gyro System Reliability		
Single-Thread System		Fully-Redundant System
G10	0.9937	0.9999+
GG159	0.9432	0.9990
Operating Continuously		
G10	0.9574	0.9994
GG159	0.6637	0.9581

Radiation Hardening--Because of the simple design (one moving part), inert gas bearing (hydrogen gas), and absence of O-ring seals, the G10 is expected to withstand much higher levels of radiation than the floated gyros. In radiation tests of two G6B4 Minuteman gyros, the gyros were subjected to 3×10^{16} nvt neutron bombardments and 4×10^{10} ergs/cm gamma radiation for 105 hours. Post-radiation tests showed satisfactory gyro operation.

Power Requirements--Table 4.5-7 shows the power requirements for the different gyro configurations considered. Power consumption using the GG159 system is based on half-speed (12,000 rpm) operation of the gyros. Tests run at Honeywell during the study showed adequate performance with half-speed operation with a reduction in spin motor power from 6.3 to 2.1 watts. The estimated power dissipated by a completely redundant free-rotor gyro system is about 25 watts. A completely redundant GG159 system required 44 watts. A GG159 system with three gyros in standby redundancy required 29 watts.

Table 4.5-7

GYRO UNIT POWER REQUIREMENTS

GYRO TYPE	G10B	G10B	GG159	GG159
NUMBER ASSUMED IN SIMULTANEOUS OPERATION	(2)	(3)	(3)	(6)
Motor Excitation (Max. 16,000°/hr)	1.3	2.0	6.3	12.6
(Max. 1,000°/hr)	1.3	2.0	6.3	12.6
Pickoff Excitation		-	-	-
Torquer (Max. 16,000°/hr)	3.6	5.4	8.4 (3°/sec)	16.8(3°/sec)
(Max. 1,000°/hr)	.2	0.3	0.7	1.4
Heater		-	10.0(est)	15.0(est)
Temperature Controller		-	0.3	0.6
PWM Servos	4.0	6.0	4.2	7.2
Speed Controller	4.0	6.0	-	-
Pump Power		-	2.1	4.2
Frequency Standard	1.2	1.2	0.8	0.8
Gyro Selection		3.0	1.0	2.0
Inverter (75% Efficient) High Rate	4.0	7.9	6.0	11.0
Low Rate	3.0	6.6	4.0	7.0
TOTALS High Rate	19.4	31.5	39.1	70.0
Low Rate	15.0	25.1	28.7	43.6

Logic of Selection--Table 4.5-8 summarizes parameters considered in selecting the preferred subsystem. Three G-10 Free-rotor Gyros are preferred because of the higher reliability, and because of the reduced power required (particularly at the time of orbit insertion.)

Although the floated instruments exhibit somewhat better performance in random drift and in the acceleration sensitivity coefficents, in a zero-g environment these advantages are not significant. Autonetics has fabricated floated gas bearing instruments as well as free-rotor gas bearing gyros for 10 years. The complexity of design of floated instruments coupled with the problems of fluid contamination make the single-degree-of-freedom gyro less reliable and thus less desirable than the G10B free-rotor gyros. The effect of these differences on reliability can be seen in the 50,000 hr.-versus 1,000,000 hr.-MTBF comparison.

Table 4.5-8: COMPARISON MATRIX

Requirements	G10	GG159
Martian Planetary Quarantine	Can be sterilized	Can be sterilized
Reliability		
a) MTBF Operating	10^6 hours	5×10^4 hours
b) Based upon Mission Profile	0.99937	0.99617
c) Radiation Hardened	Yes	Partial*
d) No. Instruments Required For Redundancy	3	6
Development Status		
a) Operational	In production	In production
b) Space Proven	Aircraft Proven	Yes
Safety Problems	None	None
Performance		
a) Torquing Capability	5°/sec	3°/sec
b) Torque Linearity	0.01%	0.01%
c) Drift Rate °/hr rms	0.005	0.003
d) Start Stop Capability	20,000	10,000
Versatility	Operating throughout mission	On only during maneuvers
Weight lbs (all gyros) Power Watts	6.1	5.5
a) Excluding Electronics	2.3	7.3**
b) Including Electronics	25.1	28.7**
Magnetic Fields Meets Requirements	Yes	Yes

*Component parts have been tested but there is no gyro test data available.
**Operation at half rotor speed.

4.5.4 Autopilot Mechanization

This section contains the results of the trade-off studies performed to define the optimum autopilot for the Voyager mission. The autopilot functions to control the spacecraft attitude during both powered and unpowered flight. Preliminary studies were performed to select the best means of passive rate generation. Subsequent trades were performed to select a preferred mechanization from possible digital and analog alternates. As a result of these studies, a d.c. analog autopilot with alternate rate inputs is the preferred design. Rate information during acquisition and maneuver is obtained from the gyro system. During limit-cycle operation, rate is derived by a lag circuit around the switching amplifier.

4.5.4.1 Rate Feedback Trades

During the cruise phase, attitude position information is obtained directly from the celestial sensors. The generation of rate information in addition to position is essential for damping and minimum-impulse limit cycle operation. Alternate means of generating rate information are shown in Figure 4.5-8 and are considered below.

On-Off System/Measured Rate and Position ("1" of Figure 4.5-8)--This method has a wide dynamic range of control and is useful for damping large disturbances to an efficient limit cycle. Limit cycle rates of 1^{o}/hour have been achieved in tests on an air bearing simulator. In closely controlled tests, rates as low as 0.02^{o}/hr. were recorded.

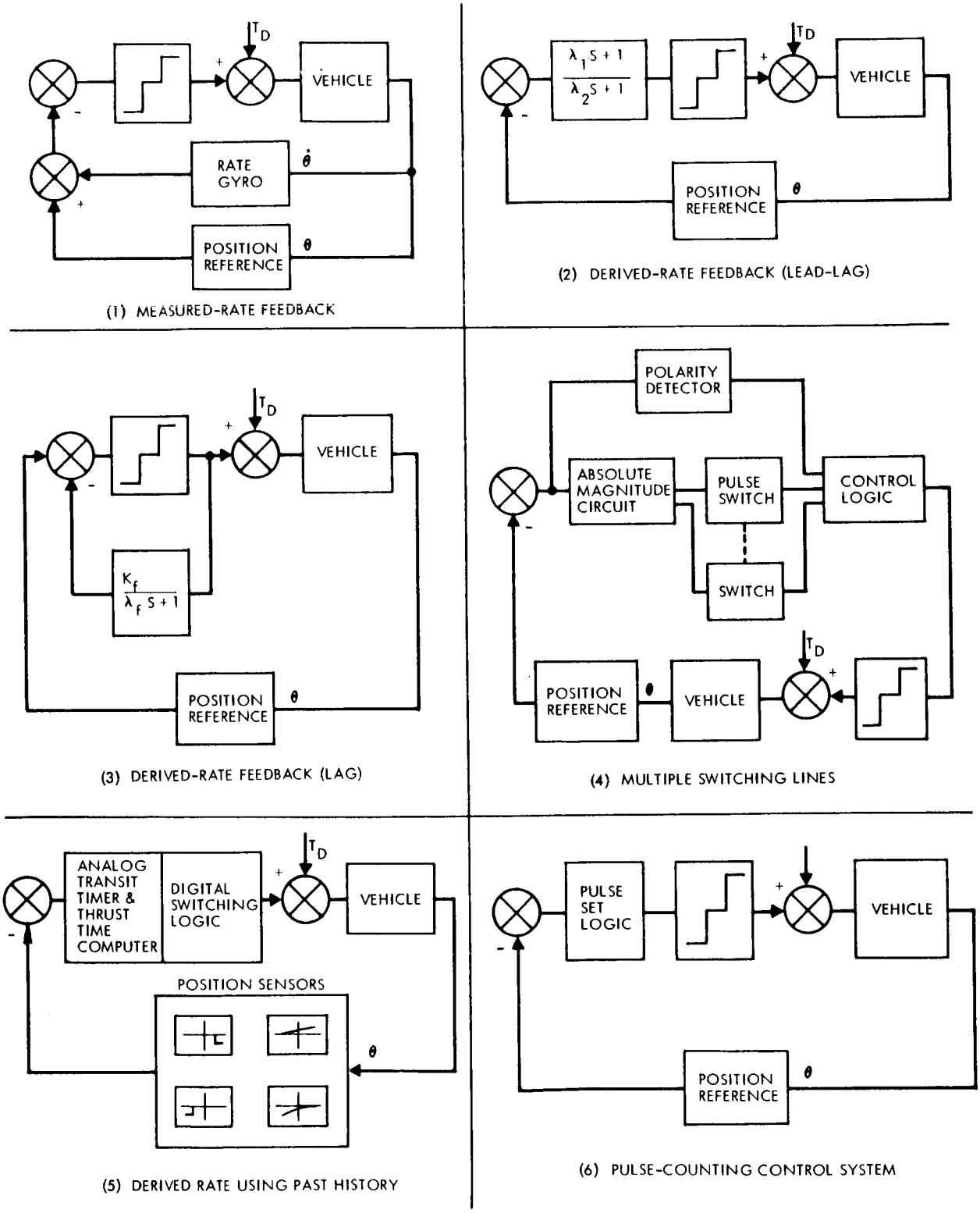

Figure 4.5-8: Alternate Attitude Control Systems

On-Off System/Derived Rate/Lead-Lag Compensation (2)-- This method is being used in the Lunar Orbiter. It has good dynamic range, but is sensitive to system noise.

On-Off System/Derived Rate/Lag-Compensation (3)--In this method lag compensation is fed back around the switching amplifier. This method has been extensively developed. It does not display good characteristics over a wide dynamic range but has excellent limit-cycle characteristics. It can be adjusted through passive R-C elements to produce the minimum capability of the reaction jets.

On-Off System/Derived Rate/Multiple Switching Lines (4)--This system provides stability by limiting the on-time of jet pulses as the vehicle attitude error passes successive switching lines. An extreme limit actuates a backup switch and assures rate reversal.

On-Off System/Derived Rate/Predictive Logic (5)--This system is one form of many techniques using past history. It has been analysed and tested on an air bearing simulator. It has good dynamic control range (0.5^{o}/sec to 5^{o}/hr. have been achieved in test) but requires an on-board computer.

On-Off System/Derived Rate/Pulse Counting (6)--In this method (described in Reference 6), a vehicle rate is reduced by applying a series of jet pulses at the attitude dead-zone limit. The vehicle rate is reversed and damped by applying half the number of counted pulses (to an

even integer) in the opposite direction.

Attitude Stabilization System Selection--The various systems described above have been compared on the basis of several system considerations as shown in Table 4.5-9. Primarily with regard to performance, long-life reliability, and development, Systems 1 and 3 have been selected for the various mission phases. These choices are in accordance with the "Voyager Mission Specifications" for acquisition and interplanetary cruise.

4.5.4.2 Autopilot Design

This section contains the results of the trades performed in defining the optimum autopilot subsystem for the Voyager mission. Six alternate electronic configurations ranging from all-digital to all-analog designs were investigated to optimize the autopilot subsystem on a single thread basis. Then, redundancy techniques of different forms were applied to achieve the autopilot probability of mission success of 0.9996.

Basic parameters considered were reliability, power, weight, volume, and versatility. The result of the studies was the selection of the d.c. analog autopilot, herein identified as analog alternate no. 2, as the preferred system. Though most of the alternates considered, when made redundant, can satisfy mission reliability requirements, the analog alternate no. 2, d.c. analog subsystem was selected on the basis of minimum power and weight.

Table 4.5-9: ALTERNATIVE ATTITUDE CONTROL SYSTEMS

System Number	System Description	Acquisition Maneuver Capability	Limit Cycle Perf.	Sensitivity to System Noise	Dynamic Control Range	Sim-plicity	Long-Life Reliability	State of Development
1	On-Off System Using Measured Rate Feed-back (Gyros)	Good	Fair	Fair	Good	Good	Poor	Good
2	Derived Rate On-Off System Using Series Lead-Lag Compen-sation	Fair	Fair	Poor	Good	Good	Good	Good
3	Derived Rate On-Off System Using Feed-back Lag Compen-sation	Poor	Good	Good	Poor	Good	Good	Good
4	On-Off System Using Multiple Switching Lines	Fair	Good	Fair	Fair	Fair	Fair	Fair
5	Derived Rate On-Off System Using Past History	Good	Good	Good	Good	Poor	Fair	oor
6	Pulse Counting On-Off System	Poor	Good	Good	Poor	Fair	Fair	Fair

Basic Considerations--To meet the apportioned probability of mission success of 0.9996, the paramount consideration was to maximize reliability with due consideration given to the aspects of weight, power, and volume.

The reliability of most of the autopilot configurations considered is sufficient that two complete autopilots in a redundant configuration with reasonably high probability of fault sensing and switching would be adequate. However, it would be extremely difficult to determine, in the case of noncastrophic failure, which channel to select. In addition, this mechanization would require switching of a large number of input and output signals at once. For these reasons, internal redundancy was investigated in several forms, which are described below. The selected system used all of these types of redundancy the particular application being dictated by the type of problem encountered in each case.

A functional block diagram of the autopilot subsystem is shown in Figure 4.5-9. Input (attitude reference) and output (propulsion) subsystems are included in the diagram to clarify the operation of the autopilot during the various modes. The various control modes provided by the autopilot subsystem are keyed to the demands of these flight phases. It can be seen by the functional block diagram that the autopilot subsystem consists of the following subfunctions:

1) The autopilot electronics, which includes the signal amplifiers, variable dead-band generators, derived-rate networks, single-shot

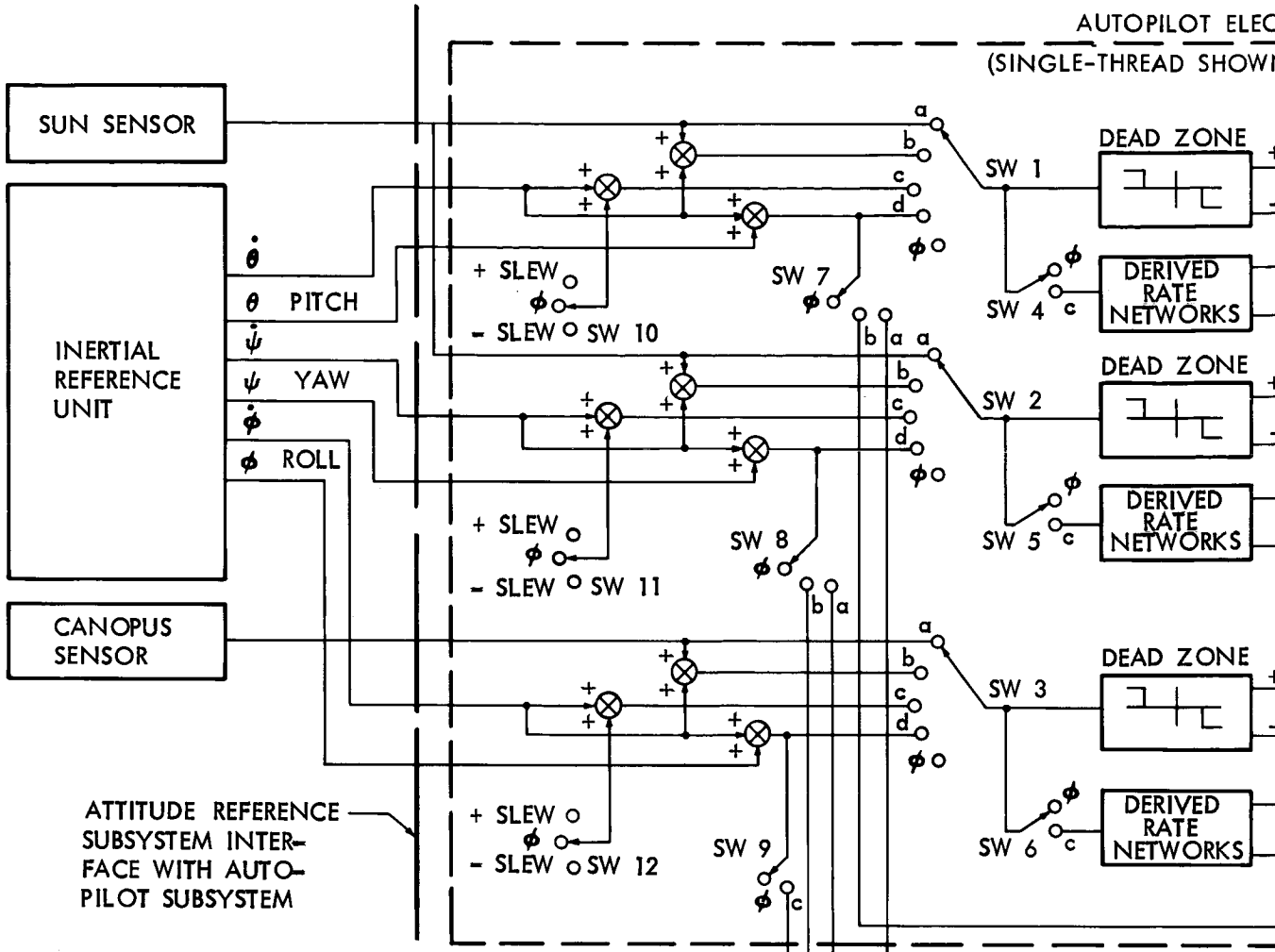

MODE	SW 1 & 2	SW 3	SW 4–6	SW 7 & 8	SW 9	SW 10–12
SUN/CANOPUS ACQUISTION	b	b	φ	φ	φ	φ
SLEW	c	c	φ	φ	φ	+or −
INERTIAL HOLD	d	d	φ	φ	φ	φ
MIDCOURSE TVC	φ	φ	φ	a	c	φ
ORBIT INSERTION TVC	φ	d	φ	b	φ	φ
CRUISE	a	a	c	φ	φ	φ

510

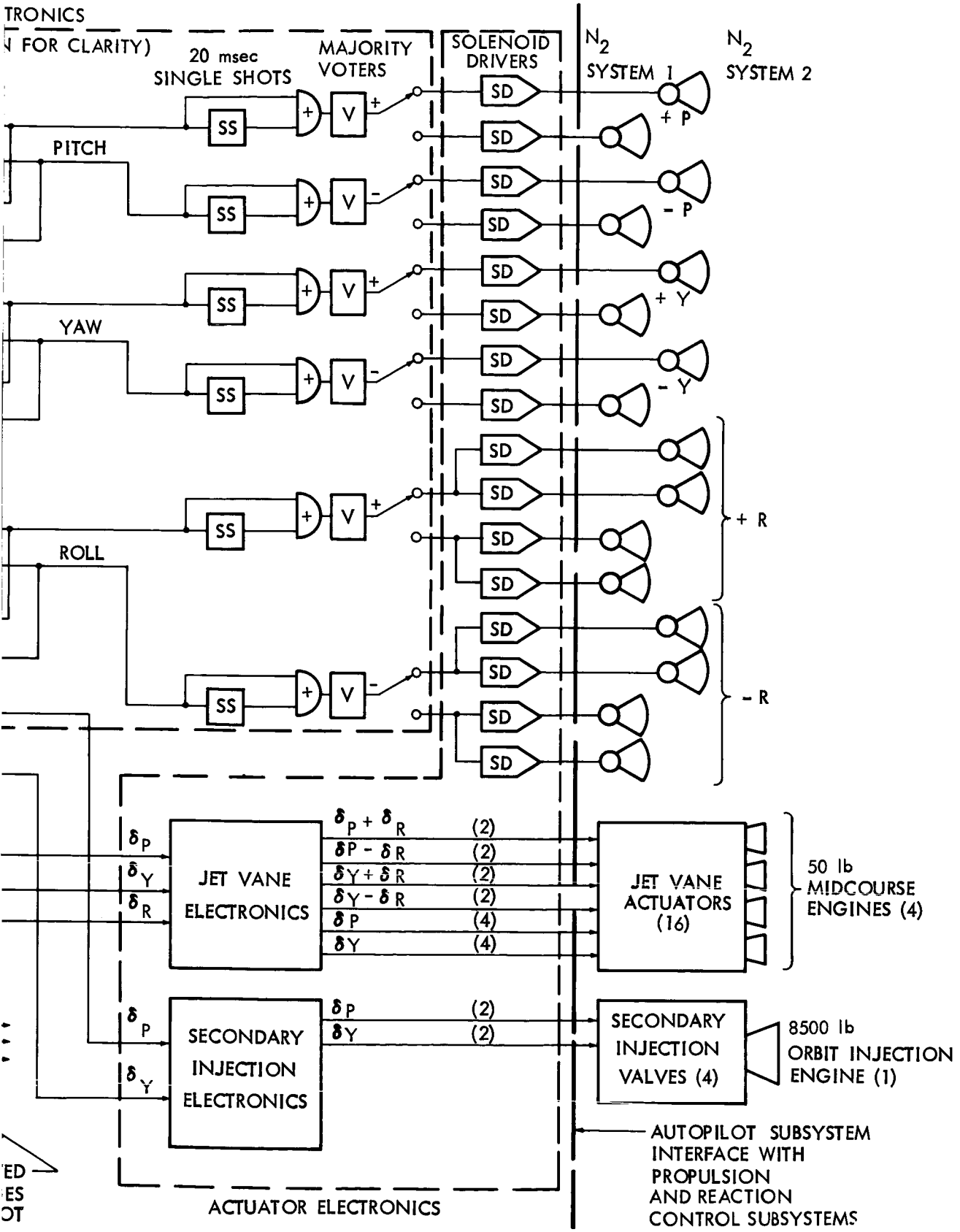

Figure 4.5-9: Autopilot Functional Block Diagram

delays, and the majority voters;

2) The actuator electronics, which includes the power switches for the solenoid drivers, jet vane electronics for the midcourse propulsion jet vane control, and the secondary injection electronics for the orbit injection engine thrust vector control;

3) The power supplies to furnish power at appropriate voltages and regulated conditions to the electronics listed above.

Redundancy Considerations--Consider now the application of redundancy techniques at the subsystem level to achieve high reliability. The dual standby system, the first method considered requires two full systems with a reliable means of fault detection and switching to the standby system. The probability of success for this configuration is given by:

$$P_s = 1 - (P_{F_a} P_{F_b} + P_{F_{mon}})$$

where

P_{F_a} = probability of failure of system a

P_{F_b} = probability of failure of system b

$P_{F_{mon}}$ = probability of failure of the monitor

Ps = probability of mission success

It can be seen from the equation that the monitor scheme is of utmost importance in the dual standby concept.

The second redundancy method is the nonmonitored scheme which is essentially self-healing. This is primarily a triple system with either majority vote techniques, or predetermined gain and scaling factors

in which failures are essentially compensated for by an adaptive technique. The probability of success for either of these techniques is approximated by the following equation:

$$Ps = 1 - (3 P_F^2 + P_{F_{mon}})$$

where P_F = a single channel probability failure

P_{Fmon} = probability of failure of monitor.

The monitor is far simpler in this method than for the dual system, the first method discussed. The drawback is the weight and power increase to accommodate three systems which must operate at all times.

Finally, a composite of redundancy techniques which combines the different methods of redundancy in an optimum manner to achieve a high probability of mission success may be applied.

Constraints--In examining a dual-redundant scheme whereby monitoring and switching is done at the input and output of the autopilot, it was found necessary to switch d.c. analog inputs and high-power, two-level outputs. Both switching techniques examined in the subfunction trade-off section were found to be unsatisfactory.

Because the number 1 and 2 nitrogen reaction-control jets perform in a backup mode to one another, they may be assumed to be in a dual redundant configuration. With the failure rate of the valve drive electronics (power switch) a factor of 156 less than the thrusting solenoid valve, the power switch and jet valve may be taken in series as a unit. This allows valve switching by the CC&S to be done at the signal level.

Similar assumptions may be made at the jet vane electronics and the secondary injection electronics. Failure rate of these amplifiers is on the order of 30 times less than the jet vane assembly and 32 times less than the injector. These devices may also perform in a backup mode or in a dual redundant setup.

The area of the autopilot electronics consisting of the signal amplifiers, deadzone generation, derived rate equipment and single-shot remains. These electronics may be connected in a dual standby mode utilizing a monitoring scheme, or connected in a triple redundant fashion. Both schemes were investigated, and are discussed in the paragraph entitled, "Subfunction Trade-off Studies."

Now consider the application of redundancy techniques at the subfunction level. Here, three major configurations that may be used are (a) the single switch, (b) two switches connected in parallel or series, and (c) a series parallel arrangement. The choice, and, for that matter, the very use of this type of redundancy depends largely on the reliability achieved at the switching assembly. Thus, this particular area will be discussed later where specific mechanizations are presented.

Alternate Designs Considered--Several trades were conducted as illustrated by the discussion that follows and summarized in Table 4.5-10. Such trade studies led to the adoption of the composite redundancy approach which uses redundancy techniques of majority voting, TRISAFE, dual-standby redundancy, and parallel redundancy. A prime motive for adopting the majority boting and TRISAFE mechanizations is their

inherent ability to detect and correct automatically and predominate modes of failure that may occur. Figure 4.5-10 shows a block diagram of the essential features of the digital alternate designs while Figure 4.5-11 shows the analog alternate designs. The majority voter mechanization is essentially identical for all of the alternate designs considered. The actuator electronics are, in essence, identical in operation. A breakdown of the actuator electronics is shown in Figure 4.5-12.

As shown by Figure 4.5-10 the basic feature of the digital alternate is the time-sharing process. Triple redundancy is applied using the majority voting techniques of automatically detecting and correcting failures. The analog alternates, shown in Figure 4.5-11, applies the TRISAFE and majority voting mechanizations for automatically detecting and correcting failures. The redundant mechanization applied at the actuator electronics group to some degree depended upon the jet control requirements.

TRISAFE--Autonetics has developed an analog triple redundant circuit technique called TRISAFE (Triple Redundancy, Incorporating Self-Adaptive Failure Exclusion). This type of redundancy is applied on a unit level to such items as signal amplifiers, inertial sensors, valve drivers, shaping units, and other analog signal devices. This method of automatic failure correction has been termed self-adaptive failure exclusion because no measuring device outside of the triple unit, such as a majority voter, is required.

Design Identification	Basic Characteristics, Autopilot Electronics	Att Gyro Position
Digital Alternate No. 1	1. Signal Level Electronics Time Shared, Pitch, Yaw and Roll 2. Rate Derived from Gyro Position 3. No Gyro Bias Removal Capability 4. Stabilization by Optical Sensors	Pulses
Digital Alternate No. 2	1. Same as Digital Alternate No. 1 (D/A1) Except Analog Derived Rate Provided During Cruise Mode.	Pulses
Digital Alternate No. 3	1. Same as D/A1 Except Derived Rate During Cruise Mode Provided by Digital Computation	Pulses
Digital Alternate No. 4	1. Fully Digital with Near-Computer Capabilities. 2. Performs Gyro Bias Update and Gyro Signal Conditioning.	Pulses
Analog Alternate No. 1	1. AC Amplification and AC Operation Up to Actuator Electronics Interface	Small Ar (Limited DC
Analog Alternate No. 2*	1. DC Amplification and DC Operation Throughout	Same as A/A 1

*Selected for Preferred System

Table 4.5-10

itude Reference Interface Assumptions			Cruise Derived Rate	Other External Requirements Assumed	Actuator Electronics Interface Assumptions	Redundancy Mechanization
	Gyro Rate	Optical Sensors				
	None	DC Voltage with Threshold Detection	1. Two-Level Altitude Threshold Switch	CC&S Required for Mode Control Only	1. Analog Position Command to Midcourse Jet Vane Electronics. 2. Analog Position Command to Secondary Injection Electronics	1. Autopilotelectroni Redundant with Mc 2. Power Switches an Standby Dual Redu 3. Secondary Electror
	None	Same as D/A 1	1. Analog Derived Rate from Output of Jet Commands	1. Same as D/A 1	1. Same as D/A 1	1. Same as Digital Al (D/A 1)
	None	Same as D/A 1	1. By Digital Computation	1. Same as D/A 1	1. Same as D/A 1	1. Same as D/A 1
	None	Same as D/A 1	1. Same as D/A 1	1. Same as D/A 1	1. Same as D/A 1	1. Same as D/A 1
gle	Direct from Gyro	Same as D/A 1	1. Same as D/A 2	1. Requires CC&S Computation of Gyro Position θ θ Error and Slew Command	1. Same as D/A 1	1. Autopilot Electror Redundant, Major 2. Power Switches & Standby, Dual Re 3. Secondary Electro
	Same as A/A 1	Same as D/A 1	1. Same as D/A 2	1. Same as A/A 1	1. Same as D/A 1	1. Same as A/A 1

57 (2)

Summary of Basic Characteristics, Advantages, and Disadvantages of Alternate Designs Evaluated

	Major Advantages	Major Disadvantages
:s is Time Shared, Triple ijority Voting Scheme d Jet Vane Electronics, ndant ics, No Redundancy	1. Slow Rate & Dead Zone Easily Changed by Radio Command 2. Generate Rate Internally	1. Less Reliable 2. Relatively Slow Convergence to Minimum Impulse Limit Cycle
ternate No. 1	1. Less Power Required Than Digital Alternate No. 1 (D/A 1)	1. Lacks Versatility in Changing Derived Rate Characteristics
	1. Versatile (Dead Zone and Derived Rate Time Constant Readily Changed by Radio Command)	1. Low Reliability 2. High Weight & Power 3. Complexity
	1. Most Versatile System 2. Potential for Optimum Convergence to Minimum Impulse Limit Cycle 3. Minimum Fuel Orientation Possible	1. Very Complex, Possibly, Twice as Many Parts as D/A 1 2. Low Reliability
ics TRISAFE, Triple ity Voting Scheme Jet Vane Electronics dundant Mode nics, No Redundancy		1. More Power than A/A 2 2. Requires External Gyro Conditioning
		1. Subject to Drift

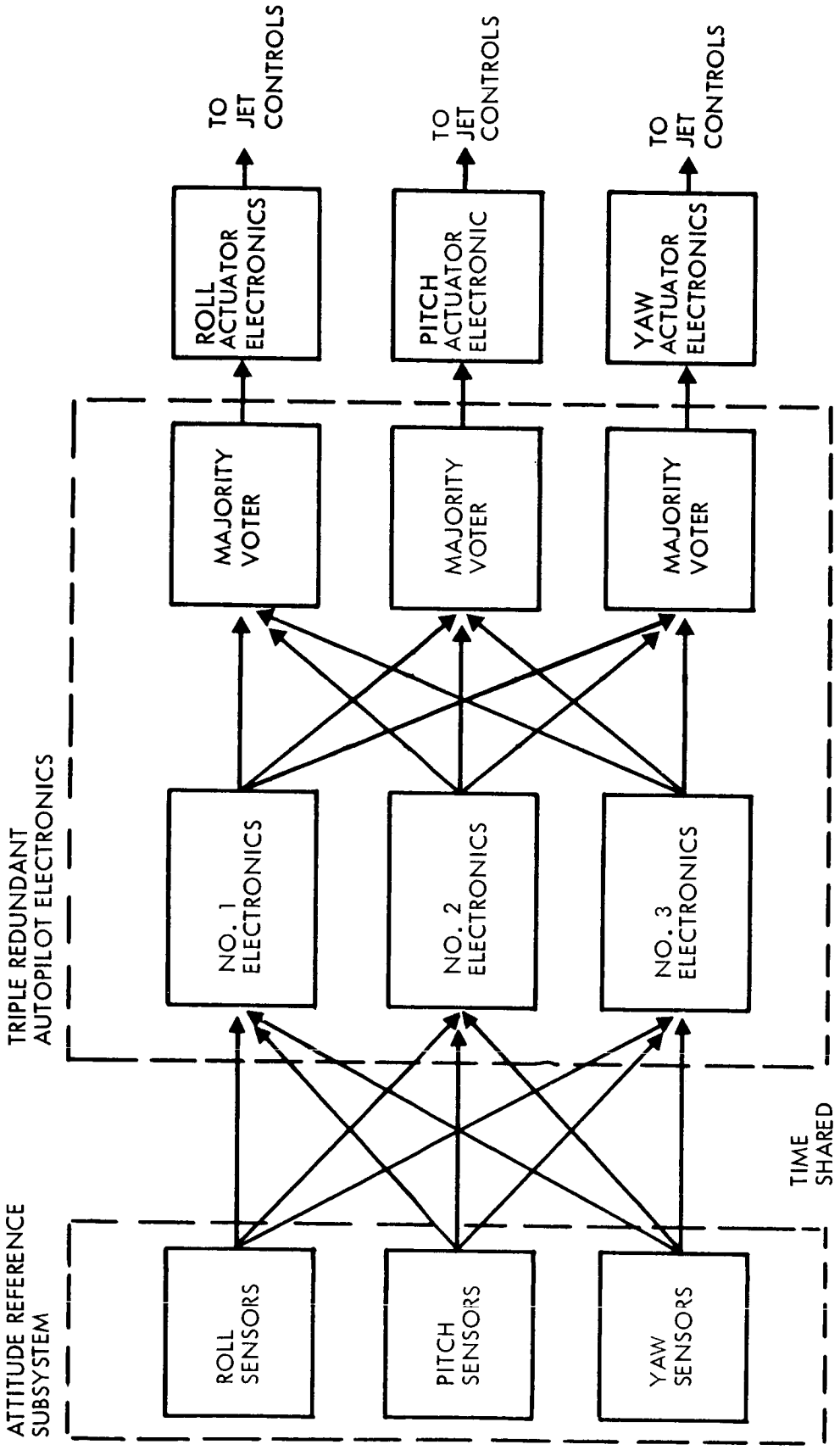

Figure 4.5-10. Mechanization Block Diagram of the Digital Alternate Design

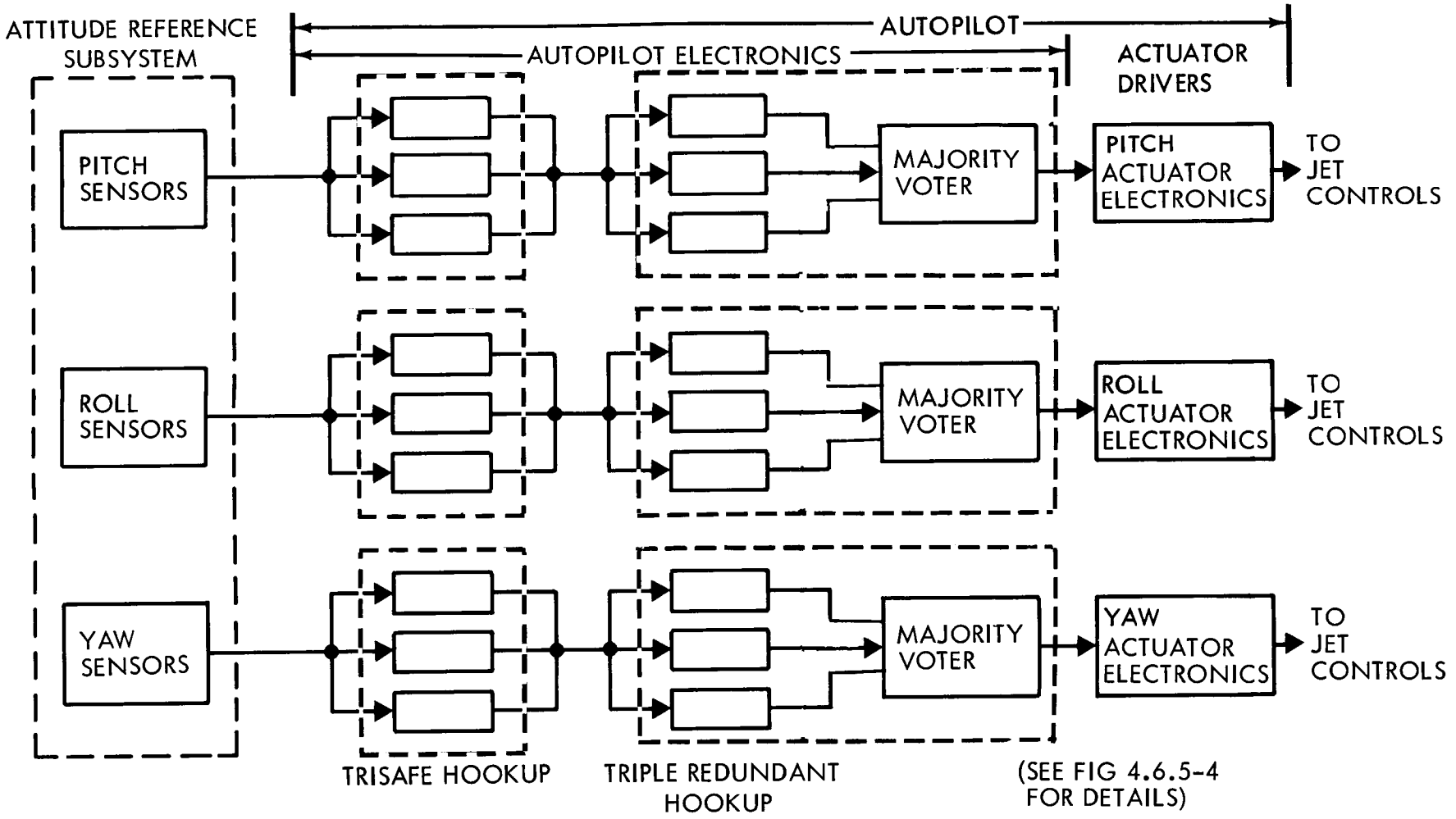

Figure 4.5-11: Mechanization Block Diagram of the Analog Alternate Design

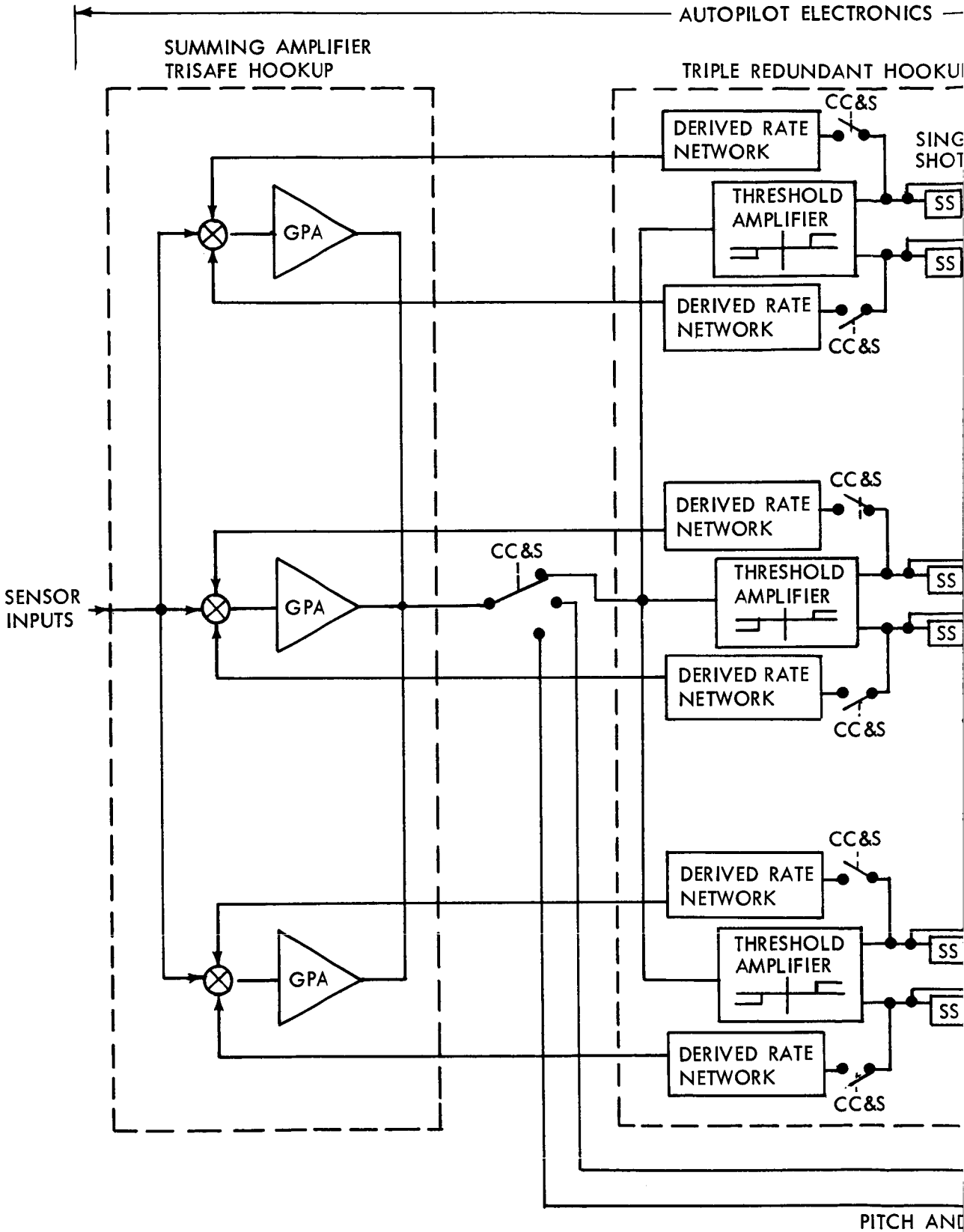
AUTOPILOT ELECTRONICS
SUMMING AMPLIFIER
TRISAFE HOOKUP
TRIPLE REDUNDANT HOOKU
SENSOR
INPUTS
GPA
GPA
GPA
CC&S
CC&S
CC&S
CC&S
CC&S
CC&S
DERIVED RATE
NETWORK
DERIVED RATE
NETWORK
DERIVED RATE
NETWORK
DERIVED RATE
NETWORK
DERIVED RATE
NETWORK
DERIVED RATE
NETWORK
THRESHOLD
AMPLIFIER
THRESHOLD
AMPLIFIER
THRESHOLD
AMPLIFIER
SS
SS
SS
SS
SS
SS
SING
SHOT
PITCH AND

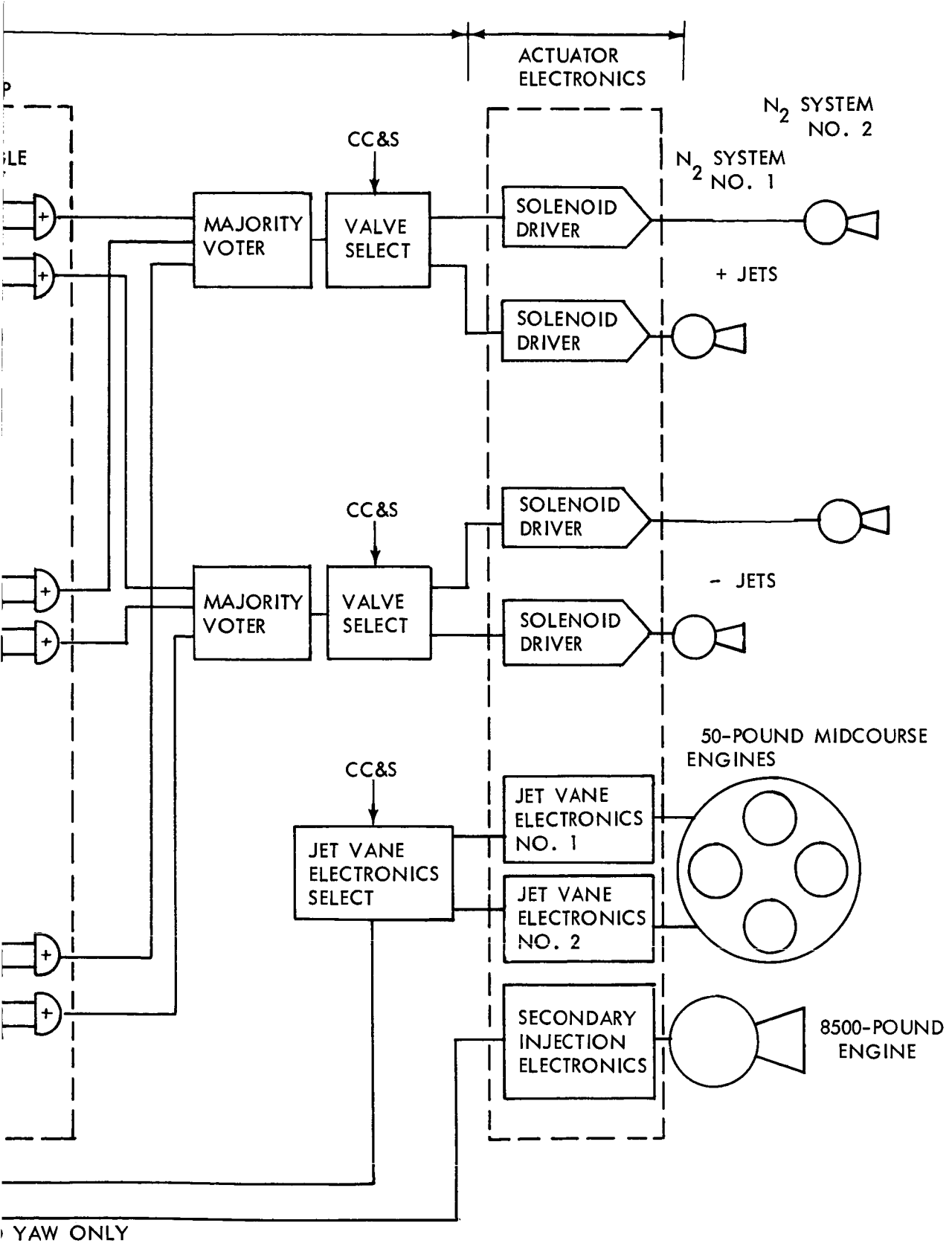

Figure 4.5-12: Voyager Autopilot Redundant Single-Axis Block Diagram

Majority Voting--In some cases, such as digital signals, it is not feasible to mechanize the TRISAFE feature. At the same time, no simple method of checking a dual redundant system accurately is available for the autopilot. Therefore, a triple redundancy with majority voting also was considered in detail as a method of redundancy.

To prevent the reliability gain accomplished by redundancy from being lost in the voting circuit, the voter has been mechanized with diodes in a "quad" redundant scheme. This is a parallel-series arrangement that is redundant with respect to both open-circuit and short-circuit failures. By use of this technique, the standard voting circuit is predicted to have an extremely low failure probability over the mission of 26×10^{-9}.

Dual Redundancy--The jet vanes and nitrogen valves have been mechanized in a dual redundant system with the CC&S selecting the primary or standby units. Since these units have a much higher failure rate than the valve power switches and the jet vane electronics which interface with them, and since a triple redundancy scheme would be required to mechanize these items if they were attached alone, it has been considered advisable to mechanize these systems in a series-parallel arrangement with the jet vanes and valves. This not only simplifies the equipment, but also allows the CC&S to switch the valves and jet vanes at the signal level rather than at the power level.

Digital Alternate No. 1--The digital subsystem utilizes its inherent time share capabilities, which causes the subsystem operation to be

sampled data in nature. Past experience with performance calculations and simulations have shown that sample times on the order of 0.1 second or less are necessary.

Standard digital mechanizations have been used throughout and separate arithmetic functions have been kept at a minimum. No dependence on the CC&S is required except for position, rate, dead zone commands, and mode switching direct signals. However, a more efficient system could be obtained if the necessary arithmetic functions are present in the CC&S and could be time shared with the autopilot.

Digital Alternate No. 2--The major hardware items remain the same in this mechanization with the exception of the optical sensor interface electronics. Here, an analog-derived rate scheme is employed. It has an operational advantage as opposed to a fixed impulse, in that the limit cycle conditions will be approached more rapidly.

Digital Alternate No. 3--Again, the basic hardware remains the same, and the optical sensor interface equipment is replaced. In this case, the derived rate and dead zone functions are obtained by a completely digital computation approach. The primary advantage in this scheme is versatility and accuracy, since a programmed word may be used to modify any of the performance characteristics. Considering the duplicate autopilot redundancy, and assuming identical active autopilots, the failure of one autopilot has no effect on the operation of the other autopilot.

Digital Alternate No. 4--In this proposed mechanization, all functions including redundant gyro selection, bias corrections, and autopilot computations are done digitally. The major reason for consideration of a system of this type is its versatility. Examples follow:

1) The autopilot is capable of both measuring and computing gyro bias errors, and then correcting all actual gyro information based on the computed values.

2) All gyro readings are continuously and automatically compared in a gyro select unit of the autopilot and non-catastrophic gyro failures, represented by both axis readings of a malfunctioning gyro differing by some predetermined amount from properly operating gyro information is produced as output information.

3) An extremely broad attitude control capability is included in this autopilot. The technique makes use of the fact that the cold-gas jets, actuated by one-shot multivibrators, act analoguously to digital stepping motors except that each actuation of a jet incrementally changes its rotational velocity rather than position. By observing this fundamental relationship, it is possible to program the spacecraft attitude to oscillate between any desired limits, at any particular rate and to stop at any particular angular position. The numbers required for digital comparater employed to match angular velocities and positions may come from the CC&S, from the ground via the communication links, or they may be stored in additional registers not specifically included in the autopilot design.

The difficulty for this autopilot to meet reliability requirements, as well as the decision to place the majority of the gyro processing electronics in the inertial reference unit resulted in the elimination of this approach or an appropriate alternate for this study.

Preliminary investigations showed that mechanizing the autopilot would require in excess of 400 integrated circuits. Therefore, this approach is not recommended.

Analog Alternate No. 1--The basic reasoning behind an ac mechanization involves the effects of long-term operating conditions on circuit stability and accuracy. This is particularly important if integrated circuits of the Minuteman type are used. These circuits have a substantially higher drift rate than newer circuits; however, they have an extremely long record of reliability data.

In this mechanization, various signal frequencies or dc inputs may be used without significant differences in reliability. The inputs--gyro rate, gyro position, optical sensor position--are switched to the summing junction of an ac amplifier by a transistor switch. The optical sensor signals are summed with a derived rate signal which permits a 0.006°/sec by a 0.2-degree deadband in the phase plane. The output of the a.c. amplifier is full wave demodulated and fed to two level sensors. These level sensors switch on +0.2 degree and -0.2 degree and may be switched to activate on +0.4 degree and -0.4 degree. These trigger

circuits then provide the valve power switch command, and input to the derived rate network. Also tied to the trigger circuit through an or gate is a monostable multivibrator delay circuit to assure a minimum power pulse of 20-millisecond duration.

Analog Alternate No. 2--This is the preferred system mechanization completely described in Volume A, including block diagrams and schematics of the detailed functional blocks.

This system assumes all d.c. inputs from the sensors, and utilizes dc linear integrated circuits as the basic system building blocks. Figure 4.5-12 is a block diagram of the autopilot subsystem. Its prime disadvantage is its susceptibility to bias changes and drift with fluctuating temperatures. However, preliminary analysis conducted shows that the affect error introduced is expected to be negligible relative to the autopilot performance desired. The prime advantages of this system are simplicity and very high predicted reliability using the least amount of power and space relative to all other designs evaluated.

Subfunction Tradeoff Studies--

Valve Driver Power Switch--Three major configurations that could be used here are:

1) The single switch;

2) Two switches connected in parallel or series; and

3) A series parallel arrangement.

The basic switch configuration has a discrete part failure rate of 0.0296 $F/10^6$ hours, which gives $P_f = 0.0001746$ for a 5,900 hour mission.

The figure assumes that the probability of failing open (Pf_o) is equal to the probability of failing short (Pf_s).

For a parallel connection, the probabilities of failure from the path A to B are:

$Pf_o = Pf_1 \times Pf_2 = 3.045 \times 10^{-8}$ and

$Pf_s = Pf_1 \times Pf_2 = .000349.$

For a series parallel configuration, the probabilities of failure are:

$Pf_o = 2\ (Pf)^2 = 6.09 \times 10^{-8}$ and

$Pf_s = 4\ (Pf)^2 = 12.18 \times 10^{-8}.$

The parallel configuration results in a failure mode which is worse than a single switch; that is, with a shorted mode. A series connection would provide the same results, only in the open mode. The series-parallel configuration provides at least an improvement by a factor of 2400 in the worst failure mode.

This gain would entail approximately 2.5 watts additional power drain, plus the addition of another mounting board. It is felt, however, that unless dual valve coils are used, the gain in the switch is unwarranted.

A redundant switch in the autopilot would increase the probability of success of maneuver about either pitch or yaw axis by only 0.000008.

This is not worth the price of the 2.5 watts increased power dissipation, the configuration of all systems studied has a single non-redundant power switch for each thruster valve output and results in a probability of failure of 3.045×10^{-8}.

Jet Vane Servo Electronics--Since the jet vanes are operating in a dual backup mode in a manner similar to the thruster valves, and since the probability of failure of the electronics is approximately 30 times less than that of a jet vane assembly, a single servo amplifier for each vane actuator seems to offer the most satisfactory scheme.

If the amplifiers are made monitorless and triple redundant, and if they are switched to the appropriate valve, 24 single-channel amplifiers would be necessary. These in turn would be in series with the selector switches. The resulting probability of failure becomes $P_f = 0.00012$ which is essentially that of the switch. If the channels are assumed dual redundant with a single driver amplifier per vane than $P_f = 0.03765 \times 10^{-5}$. Consequently, the system tradeoff studies all assumed that the vanes operate in a dual-backup mode, requiring 16 single-channel servo amplifiers.

In the case of the secondary injection electronics, there is only one main engine and it has no backup thrust vector injection. Since the electronics is already more reliable than the injection (0.9999 vs. 0.9995) and since if redundancy were employed, triple redundancy would be required to isolate the failure, the single channel of injector electronics is considered sufficient.

Competing Characteristics--The results of the system mechanization comparisons, both on a nonredundant and redundant basis, are shown in Table 4.5-11. The redundancy techniques used were those described in a previous paragraph. The volume and weight figures are based on two-layer printed circuits on both sides of an 8 x 8 x 0.6 inch magnesium board. The mission time was taken as 5,900 hours.

Reliability--Reliability tradeoffs for the autopilot electronics subsystem were performed in conjunction with engineering and system level tradeoffs. Specifically, design work was directed toward mechanizing both digital and analog autopilots, and comparing the performance parameters including reliability on an overall system basis. As far as was practical, each system was considered in single-thread and dual and triple redundancy arrangements. The range of reliability predictions resulting from these mechanizations was from .99548 for a single-thread system to .999676 for the preferred system. Reliability predictions for a number of systems are presented in Table 4.5-11. It may be noted that a number of system mechanizations met the mission reliability apportionment of 0.9996. Although the preferred system did achieve the highest predicted reliability, reasons other than reliability also supported its selection; namely, it had the least increase in weight, size, and power requirements per unit increase in reliability. The reliability block diagram for the preferred system is shown in Volume A. Mission reliability was summarized per subsystem in Table 4.5-11.

Logic of Selection--The results of the various system studies and subfunction tradeoff studies indicate that a number of schemes will satisfy

Table 4.5-11: TABLE OF COMPETING CHARACTERISTICS

	Digital 1	Digital 2	Digital 3	Digital 4	Analog 1	Analog 2**
Non-Redundant						
Probability of Success	0.98548	.98579	.97673	0.9763	.99650	.99694
Power (watts)	15.3	12.3	18.2	20.0	10.1	8.9
Volume (in^3*)	192	192	230	269	230	192
Weight (pounds)	4	4	5	6	4	4
Composite Redundant						
Probability of Success	0.99908	0.99911	0.99810	0.9993	0.99959	0.99968
Power (watts)	36.7	27.6	45.3	50	18.6	15.0
Volume (in^3*)	269	269	307	500	269	269
Weight (pounds)	6	6	7	10	6	6

*Minimum requirement for electronics **Preferred systems

redundant. Examination of other system parameters such as power and weight shows the d.c. analog system to be somewhat superior. While it is not as versatile as some of the digital schemes, it is felt that adequate versatility can be implemented through CC&S switching modes to satisfy the mission requirements. In addition, the d.c. system proves to be the least complex of those studied. This is reflected in its lower weight and power, and in the reliability estimates. This system is made practical by the establishment of the d.c. sensor interfaces. With this assumption, the conditioning of the digital gyro outputs and the low level optical sensor outputs fall to those respective instruments, consequently increasing their power and weight and reducing their reliability totals. There are difinite advantages in having each instrument to do its own signal processing and mode selection. One of these is in the area of subsystem functional test. Each item is an autonomous function and does not rely on outside equipment to prove its operation. Secondly, this interface and system interconnections become simpler. Certainly, high-level d.c. inputs to the autopilot simplify not only its internal hardware by its checkout, functional test, and failure isolation techniques as well.

In addition, the most efficient digital mechanization appears to be one in which a portion of the CC&S computational and memory capability could be time-shared with the autopilot. Since this capability is extremely limited, some of the advantages of a digital system are not realized. Secondly, the extreme simplicity of the system, based on the possible d.c. interfaces is most favorable to the analog mechanization.

In the event autopilot failures could be detected with an ultrareliable system external to the autopilot, savings in power and weight would be realized by employing two separate systems, one of which would be turned off until a failure was detected. Different types of systems could be used to reduce systematic failures. Since the ultrareliable sensing system does not exist, this approach must be abandoned.

The one major area of doubt with the d.c. system is its susceptibility to long-term drift. New integrated-circuit general-purpose amplifiers, now readily available on the market, have much improved drift rate characteristics. All design approximations indicate that these drift estimates are well within the required value for the mission.

Consequently, the d.c. system when compared to other system approaches, and considering the subsystem interfaces defined, seems to be the most logical system choice.

4.5.5 Packaging Design

Standard Voyager packaging techniques as described in Section 4.4.2 will be used for the Autopilot subsystem. This will result in an unsealed radiation cooled autopilot module of 8 x 8 x 10 inches that can be mounted on one of the equipment faces of the spacecraft. The attitude references however, must be carefully aligned with the spacecraft, and will be assembled into a special attitude reference module as defined by the following trades.

Alternate Designs Considered--The following were considered.

Integrated Attitude Reference Module--This concept is to locate all instruments which must be accurately aligned to the spacecraft into one precision module. Layouts have been prepared in which the Inertial Reference unit (and electronics) Canopus trackers (and electronics) and fine Sun sensors assembled and aligned to .01 degree, are in one module, which in turn is aligned to spacecraft to within 0.1 degree.

Individual Sensor Mount--This approach is to mount individual reference sensors, or the redundant pairs on the spacecraft. Alignment to within .01 degree is then accomplished by means of a large optical alignment fixture, and optical cubes on each small package.

Module Conecpt Selected--The integrated attitude reference module concept is preferred since it provides the best assurance of adequate inter-axis alignment among the attitude reference sensors. It also eases fabrication assembly, and maintenance problems by accomplishing alignment before integration with the spacecraft. Precision mount points ($\pm$ 0.001") will allow removal and replacement of the reference module without spacecraft reference realignment. Bending or distortion effects are also reduced by use of a single rigid mount frame.

Intermodule Design--The sensor units can be assembled into the reference module in a number of alternate arrangements. These are determined by the need to provide an adequate field of view, prevent reflections into the Canopus sensor and to simplify structure and cabling. The arrangement selected has the fine Sun sensors on the Sun side, inertial reference

in the middle, and Canopus sensor on the shade side of the module. Sketches of this arrangement are in Section 4.6 of Volume A.

Card Packaging--The circuit cards will be packaged as standard metal substrate circuit boards in an open module assembly. This construction is preferred to the sealed module for the following reasons: The heat radiation capability of an unhermetically sealed module is higher since the heat radiator flange can be attached directly to the electronic card. The repairability is superior since cards can be easily removed and replaced. However, open module construction is more susceptible to contamination prior to launch unless a sterilization shield is used. It is also free of the deflections and stresses caused by pressure differences in sealed modules.

Thermal Considerations--Each card will normally radiate its own excess heat through the wide card flange. During either peak or low-power operation however, heat will be shared by conduction through the mounting structure.

Integration with the Spacecraft--The autopilot and attitude reference module are mounted adjacent to each other on the cylindrical support structure of the spacecraft as shown in Figure 4.5-13. The reference module location is carefully selected to provide Sun and Canopus views, and to orient the spacecraft properly in space. The cylindrical support structure is appropriate since minimum angular vibration is desired at

Figure 4.5-13: Attitude Reference And Autopilot

the insertion engine burn period. Vibration amplitudes and frequencies above reasonable limit could allow gyros to hit their stops, and cause output errors.

The coarse Sun sensors are separated into two shade side remote Sun sensors each of which observes a quadrant of the sphere. Two redundant coarse Sun sensors on the Sun side observe the other half of the sphere, and provide complete coverage of Sun angle without need for a search maneuver.

4.5.6 References

1. 2-5722-5, "1964 Flight Technology Research Results," A. D. Jacot, 5/21/65

2. D2-100330-1, "Analysis of Lunar Orbiter Attitude Control System," 1/8/65

3. TR 32-663, "Ranger Block III Attitude Control System," Will Turk, 11/15/64

4. 2-5782-CS-02 "Reaction Control for Space Vehicles," R. Piller, G. Burmeister, 4/8/63

5. D2-90336, "Dual Mode Predictive Logic Gas Jet ACS," L. Leistrikow, D. Fosth, 10/11/63

6. D2-22035, "Survey of Space Vehicle Attitude Control," J. P. C. Clark, 1/22/63

7. D2-23254, "Comparison of Spacecraft Maneuvering Systems Employing Strap-Down Gyros," C. Henrikson, G. Price, 4/9/64

8. 2-5410-5045/CS, "Selection of Gyros for Voyager," T. Savoy, 5/28/65

9. T5-1161.1/3061B, "Voyager Attitude Reference and Autopilot Subsystems Investigation" (Autonetics)

4.6 REACTION CONTROL MECHANIZATIONS

Summary--The selected spacecraft reaction control subsystem is a cold gas (nitrogen) mass expulsion system. The nitrogen thrusters produce a force of 0.25 pounds and are mounted at the periphery of the spacecraft body. Either of two completely redundant sets of eight thrusters can be used. Thrusters operate singly in yaw and pitch, and in pairs in roll. Sixty pounds of sterilized nitrogen, of which 15 are reserved for use by the propulsion subsystem as presurrant, are stored at 3500 psia in four tanks. The 45 pounds of reaction control propellant is twice as much as required for a nominal mission. The pressure is reduced by regulators to 50 psia for use by the thrusters. Total subsystem weight is 212 pounds and reliability is 0.9996. The preferred configuration is discussed in greater detail in D2-82709-1, Paragraph 4.7.

Many trade-offs were involved in arriving at the preferred mechanization. A diagramatic representation of the selection logic is shown in Figure 4.6-1.

The control concepts considered ranged from momentum exchange devices, which proved too heavy, to solar vanes which were inadequate by themselves and required a supplementary mass expulsion system. A mass expulsion system operating alone was selected as being best able to meet both maneuver and limit cycle requirements.

Propellant selection involved study of five competing subsystems. Subliming solids were rejected as being unable to meet initial acquisition

requirements. A bipropellant reaction control subsystem is too complex, and metal diaphragms for positive expulsion are not adequately developed to be considered competitive for the 1971 mission. Both the monopropellant catalyst thruster and the monopropellant plenum chamber reaction control subsystems offer promise during the latter part of the 1971-1977 time period, but cannot be recommended at this time because of incomplete development. Longevity and low duty cycle operational characteristics of the plenum chamber have not been fully determined.

A cold gas reaction control subsystem employing nitrogen is the only concept which has been developed adequately to be considered for Voyager. It is selected, in spite of relative low I_{sp} (68sec) and relatively heavy weight, due to its reliability, simplicity, hardware availability, thruster response characteristics, and space-proven status. This concept has been successfully used or is scheduled to be used on many spacecraft (OSO, OAO, Ranger, Mariner, Syncom, Surveyor, Lunar Orbiter, Nimbus, and advanced Pioneer). Cold gas reaction control subsystems can be fabricated at low development and manufacturing costs because of available experience and technology.

Redundancy--On the basis of reliability, a requirement for redundant thrusters was established. A subsystem consisting of two completely separate arrangements of tanks and thrusters was rejected, however, because of the large weight penalty. A lighter configuration employing common tankage, dual selectable thruster sets, and malfunction detection was selected.

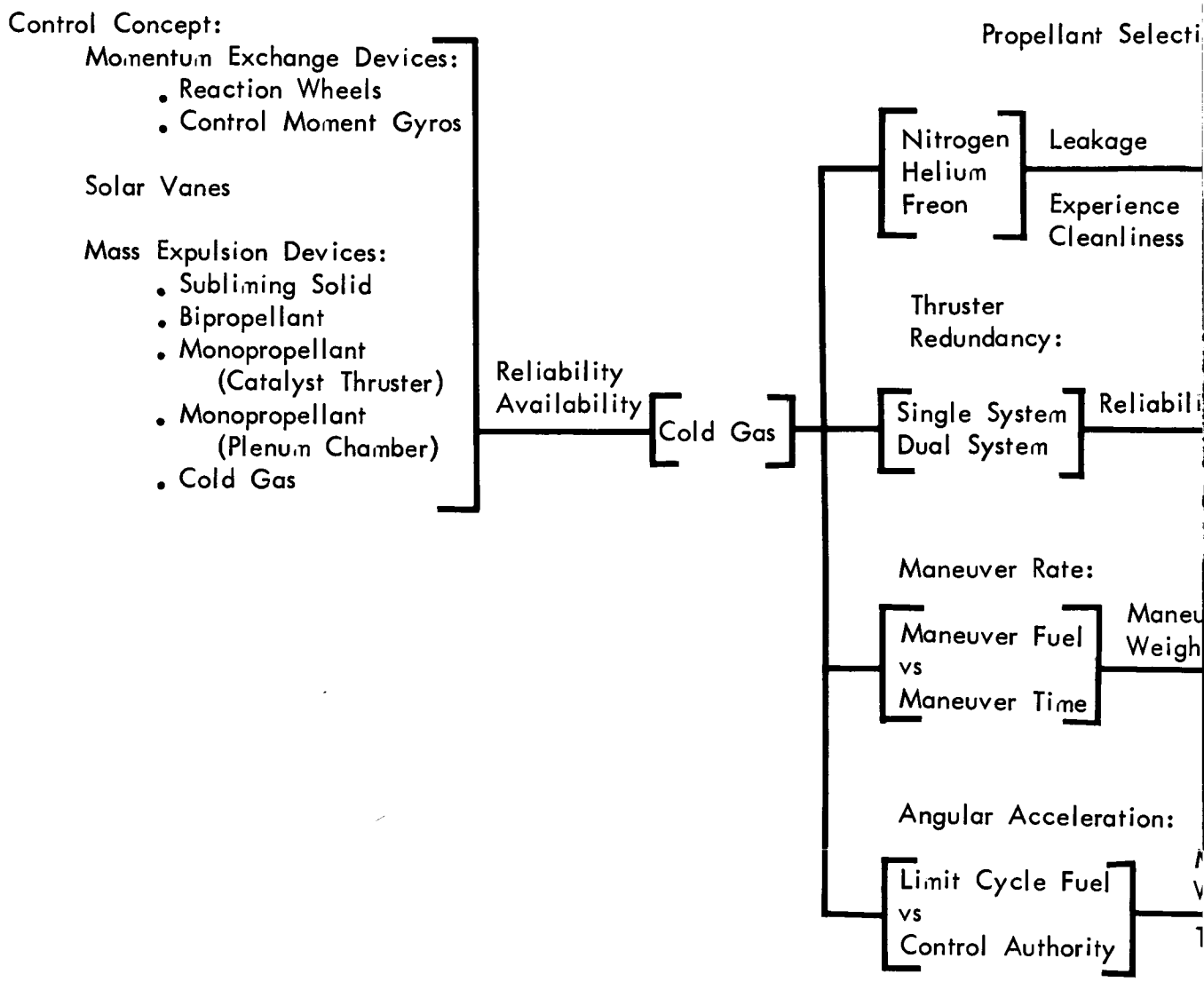
Control Concept:
Momentum Exchange Devices:
• Reaction Wheels
• Control Moment Gyros
Solar Vanes
Mass Expulsion Devices:
• Subliming Solid
• Bipropellant
• Monopropellant (Catalyst Thruster)
• Monopropellant (Plenum Chamber)
• Cold Gas
Reliability
Availability
Cold Gas
Propellant Selecti
Nitrogen
Helium
Freon
Leakage
Experience
Cleanliness
Thruster
Redundancy:
Single System
Dual System
Reliabili
Maneuver Rate:
Maneuver Fuel
vs
Maneuver Time
Maneu
Weigh
Angular Acceleration:
Limit Cycle Fuel
vs
Control Authority

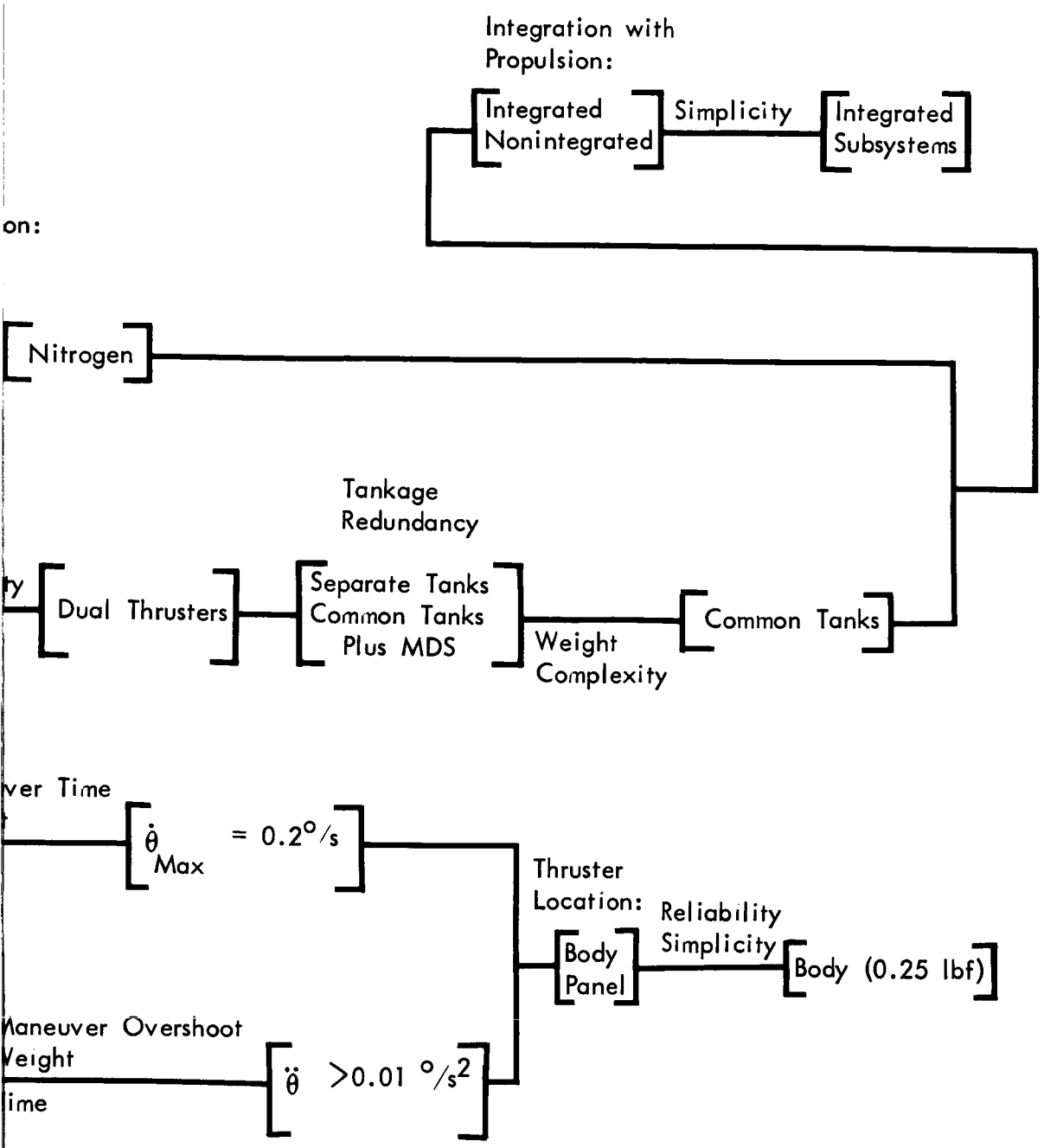

Figure 4.6-1: Alternate Reaction Control Mechanization

Thrust Levels--Control authority was determined by trade-offs of maneuver rate and angular acceleration versus nitrogen weight. The resultant compromise was a maneuver rate of 0.2 degrees per second and a control authority equal to or greater than 0.01 degrees per second squared. From these values a thrust level of 0.25 pounds was chosen for each nozzle.

Thruster Location--Panel mounting and body mounting were considered. The potential fuel savings made possible by panel mounting could not overcome the simplicity and reliability that could be achieved by body mounting.

4.6.1 Alternate Mechanizations Considered

Reaction-control subsystem studies included those concepts summarized in Table 4.6-1. These concepts are discussed below.

4.6.1.1 Reaction Wheel Concept

The reaction torque from an accelerating flywheel can be used to provide spacecraft control. Each axis of the spacecraft would incorporate a wheel system consisting of a flywheel, drive motor, revolution counter, braking mechanism and housing. A reaction wheel subsystem for Voyager which provides for limit-cycle and maneuver control torques would weigh over 100 pounds and require up to 500 watts peak power. Moreover, reaction wheels cannot provide large amounts of angular momentum without overspeeding. Thus, supplementary reaction controls would be required to desaturate the rotors during initial acquisition and after long periods of solar torque. Total system weight would be about 250 pounds.

CONTROL CONCEPTS CONSIDERED

REACTION WHEELS

ADVANTAGES:

(1) PROVIDES FINE CONTROL;
(2) PROVIDES CONVENIENT DAMPING.

DISADVANTAGES:

(1) EXCESSIVE WEIGHT;
(2) REQUIRES EXPULSIVE DEVICES FOR DESATURATION;
(3) REQUIRES LARGE ELECTRICAL POWER FOR OPERATION;
(4) INADEQUATE TO DAMP SEPARATION RATES;
(5) LIMITED APPLICATION TO DATE.

CONTROL MOMENT GYROS

ADVANTAGES:

(1) PROVIDES LARGE OUTPUT TORQUES FOR SMALL INPUT TORQUES;
(2) PROVIDES FINE CONTROL.

DISADVANTAGES:

(1) RELATIVELY HEAVY;
(2) REQUIRES EXPULSIVE DEVICES FOR DESATURATION;
(3) INADEQUATE TO DAMP SEPARATION RATES;
(4) LARGE ELECTRICAL POWER REQUIREMENT;
(5) LIMITED ANGULAR IMPULSE AVAILABLE;
(6) COMPLEX COUPLING INTER-RELATIONSHIPS.

BIPROPELLANT

ADVANTAGES:

(1) FEASIBLE FOR LARGE TOTAL IMPULSE;
(2) HIGH SPECIFIC IMPULSE;
(3) GOOD RESPONSE CHARACTERISTICS.

DISADVANTAGES:

(1) COMPLEXITY;
(2) FRACTIONAL THRUST LEVELS NOT FULLY DEVELOPED;
(3) HIGH COMBUSTION TEMPERATURES;
(4) I_{sp} DEGRADATION WITH SHORT PULSES;
(5) CHAMBER COOLING NECESSARY;
(6) POSITIVE EXPULSION METAL DIAPHRAGM CANNOT MEET JULY 1966 FREEZE DATE.

MONOPROPELLANT

ADVANTAGES:

(1) HIGHER RELIABILITY THAN BIPROP;
(2) LOWER COST THAN BIPROP;
(3) SHORTER LEAD TIME THAN BIPROP;
(4) HIGHER I_{sp} THAN COLD GAS;
(5) MORE ADVANCED THAN BIPROP;
(6) GREATER SAFETY, STORABILITY, AND DURABILITY ADVANTAGES THAN BIPROP.

DISADVANTAGES:

(1) REQUIRES POSITIVE EXPULSION;
(2) MINIMUM PULSE WIDTH LIMITATIONS;
(3) I_{sp} DEGRADATION WITH SHORT PULSES;
(4) FRACTIONAL THRUST LEVELS NOT FULLY DEVELOPED;
(5) PULSE PERFORMANCE DEPENDENT UPON DUTY CYCLE.

Table 4.6-1: Control Concepts

SOLAR VANES

ADVANTAGES:

(1) PROVIDES MEANS OF BALANCING BIAS TORQUES;
(2) REDUCES JET ACTUATION CYCLES DURING CRUISE.

DISADVANTAGES:

(1) TORQUE LEVELS VERY LOW;
(2) SYSTEM EFFECTIVENESS DEGRADES AS DISTANCE FROM SUN INCREASES;
(3) SPACECRAFT RESPONSE VERY LOW;
(4) NO OVERALL WEIGHT REDUCTION ACHIEVED;
(5) STOWING VANES IN SHROUD INCREASES COMPLEXITY OF CONFIGURATING;
(6) INCREASES NUMBER OF COMPONENTS AND OPERATIONS SUBJECT TO MALFUNCTION.

SUBLIMING SOLIDS

ADVANTAGES:

(1) LOW WEIGHT;
(2) NO COMBUSTION OR IGNITION;
(3) MINIMIZED VALVE LEAKAGE;
(4) NO PRESSURE REGULATOR REQUIRED;
(5) LIGHTWEIGHT TANKS;
(6) LOW PRESSURE SYSTEM.

DISADVANTAGES:

(1) THRUST LEVELS INADEQUATE;
(2) LIMITED APPLICATION TO DATE;
(3) LIMITED BY RATE OF SUBLIMATION;
(4) REQUIRES 10 THERMAL WATTS OF HEAT PER MILLIPOUND OF THRUST FOR SUBLIMATION;
(5) VARIABLE TEMPERATURE ENVIRONMENT RESULTS IN VARIABLE THRUST;
(6) REQUIRES CONTINUOUS SUPPLY OF HEAT FOR SUBLIMATION.

MONOPROPELLANT PLENUM CHAMBER

ADVANTAGES:

(1) FAST RESPONSE CHARACTERISTICS;
(2) LOW PRESSURE SYSTEM;
(3) POSSIBLE INTEGRATION WITH PROPULSION FEED SYSTEM;
(4) UTILIZES COLD GAS THRUSTERS;
(5) HIGHER I_{sp} THAN COLD GAS;
(6) THRUSTERS INDEPENDENT OF REACTOR DECOMPOSITION KINETICS;
(7) LIGHTER WEIGHT THAN COLD GAS;

DISADVANTAGES:

(1) PLENUM CHAMBER NOT SPACE PROVEN;
(2) REQUIRES FURTHER DEVELOPMENT WORK;
(3) IMPOSES ADDITIONAL THERMAL CONTROL REQUIREMENTS.

COLD GAS

ADVANTAGES:

(1) SIMPLICITY;
(2) HIGH RELIABILITY;
(3) SHORT LEAD TIME;
(4) COMPONENTS WELL DEVELOPED AND SPACE-PROVEN;
(5) FRACTIONAL THRUST LEVELS AVAILABLE;
(6) EXCELLENT VALVE PERFORMANCE;
(7) MINIMUM DEGRADATION OF I_{sp} WITH SHORT PULSES;
(8) LOWER COST THAN BI/MONO SYSTEMS;
(9) EASE OF HANDLING.

DISADVANTAGES:

(1) LOW SPECIFIC IMPULSE;
(2) TANK-TO-FUEL WEIGHT RATIO IS 2.17 to 1.0 (NITROGEN).

Reaction wheel subsystems did not receive further consideration because of their excessive weight and power requirements.

4.6.1.2 Control Moment Gyro Concept

A control moment gyro (CMG) generates a reaction torque in a manner somewhat similar to the reaction wheel. A CMG consists of a gyro rotor, drive motor, gyro housing, torque module, sensor module, outer gimbal, frame, and covers. A CMG subsystem would require continuous electrical power and a supplementary reaction jet subsystem as does the reaction wheel. The total weight of a control moment gyro subsystem sized for Voyager would exceed that of a reaction wheel subsystem. Control-moment gyro subsystems were therefore not considered suitable for Voyager.

4.6.1.3 Solar Vane Concept

Solar vanes are an entirely passive means of maintaining solar orientation during cruise flight. They operate easily in conjunction with reaction controls by reducing the vehicle motions to values inside the reaction control thresholds. Solar vanes are desirable for vehicles which do little maneuvering and hence can save a large fraction of their propellant by eliminating limit-cycle operation. Moreover, solar vanes can back up the normal control subsystem if mission requirements can be met without maneuvering. The Voyager mission, however, requires many maneuvers--some relatively late in the flight. Any small weight-savings made possible by solar vanes is more than offset by their additional complexity. Moreover, if fuel is provided for solar vane malfunction, no weight-saving is possible at all. Solar vanes are not recommended for Voyager.

4.6.1.4 Subliming Solid Concept

The subliming solid control rocket is an attitude control reaction jet device in which a solid propellant sublimes directly into a low molecular weight vapor. Vacuum specific impulse is approximately 60 seconds. The propellant is stored as a solid crystalline mass in the propellant tank. Vapor equilibrium maintains vapor pressure in the tank. When a propellant valve is opened the vapor escapes through a nozzle to produce thrust. The vapor pressure is a function of temperature with ten watts required per millipound of thrust to provide continuous sublimation. Subliming solids could be used only for supplementary cruise control. Their low I_{sp} puts them in the same class as cold gas reaction controls but without their simplicity, thermal insensitivity, and capability of performing the entire mission. Subliming solids are not recommended for Voyager.

4.6.1.5 Bipropellant Reaction Control Concept

A bipropellant reaction control subsystem consists of thrust chamber assemblies, propellant tanks, expulsion metal diaphragms, propellant controls, pressurization tanks, pressurant controls, and instrumentation. This concept requires a complete set of propellant storage and controls for both the oxidizer and fuel. Oxidizers have a notoriously deleterious effect on materials. A bipropellant concept implemented for Voyager utilizes about 60 components. The large number of components increases the possible modes of failure and thus decreases the subsystem reliability. Theoretical specific impulses of up to 280 seconds are obtainable.

The high energy release of bipropellants occurs with a thrust chamber temperature of about 5,000° Fahrenheit. Bipropellant engines have good response characteristics. Pulse widths of 20 milliseconds are achievable. The development and application of bipropellant systems has been directed primarily toward large, sophisticated, manned spacecraft requiring long-term applications, moderate thrust levels, and large total impulse requirements. Thrusters of less than one pound thrust are only in the developmental stage. Metal diaphragms for positive expulsion cannot be developed with sufficient certainty to meet the July 1966 freeze date. Expulsion bladders are unsatisfactory because of possible diffusion through the bladder. Characteristics of a bipropellant reaction subsystem are summarized in Figure 4.6-2.

The bipropellant concept should not be used for Voyager because the concept is too complex, metal diaphragms for positive expulsion are not adequately developed to be considered competitive for the 1971 mission, and fractional-pound-thrust nozzles have not been developed.

4.6.1.6 Monopropellant Concept

A monopropellant reaction control subsystem consists of thrust chamber assemblies, spontaneous-combustion catalyst, propellant tank and bladder, propellant controls, pressurization tank, pressurant controls, and instrumentation. A diagram and summary of characteristics of a monopropellant subsystem is shown in Figure 4.6-3.

The performance of a monopropellant subsystem is lower than a bipropellant system, while complexity is decreased by a factor of approximately

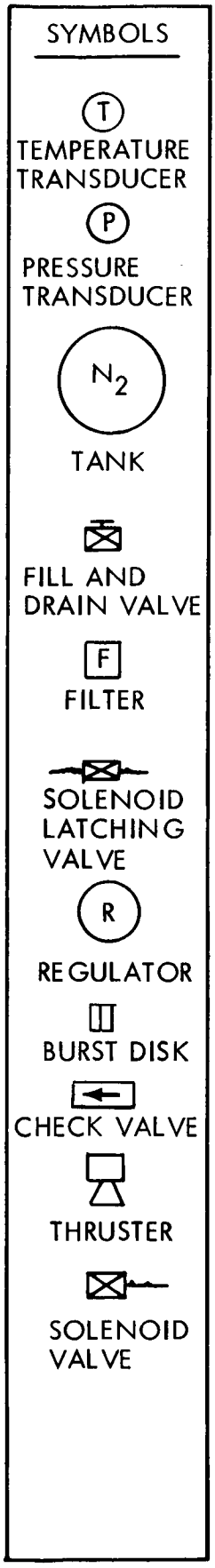

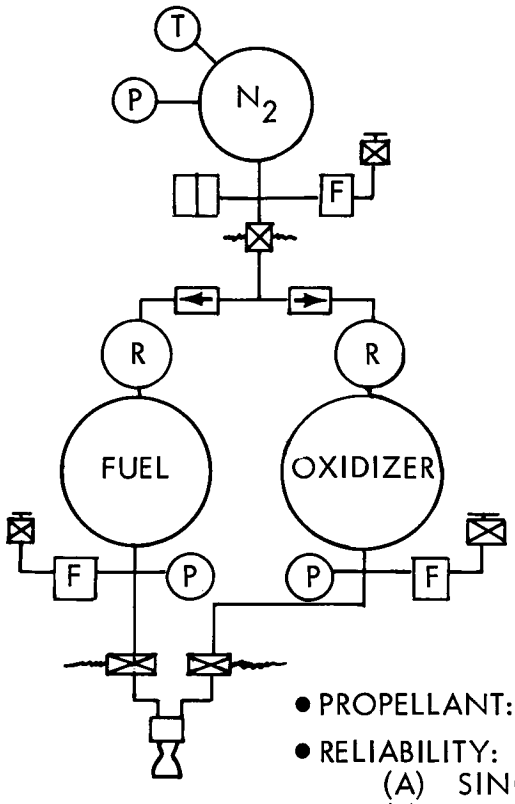

- PROPELLANT: N_2O_4/MHF
- RELIABILITY:
  - (A) SINGLE — 0.972
  - (B) REDUNDANT — 0.999
- NUMBER OF COMPONENTS: 44 PER SYSTEM
- WEIGHT
  - (A) SINGLE — 45.88 POUNDS
  - (B) REDUNDANT — 91.76 POUNDS
- SPECIFIC IMPULSE:
  - (A) STEADY STATE — 280 SECONDS
  - (B) 20-m sec PULSES — 165 SECONDS
- DEVELOPMENT STATUS: QUALIFICATION BY JULY 1966 FREEZE DATE NOT POSSIBLE
- COST: HIGH
- FRACTIONAL THRUST LEVELS: 0.2 POUND AND 0.5 POUND UNDER DEVELOPMENT

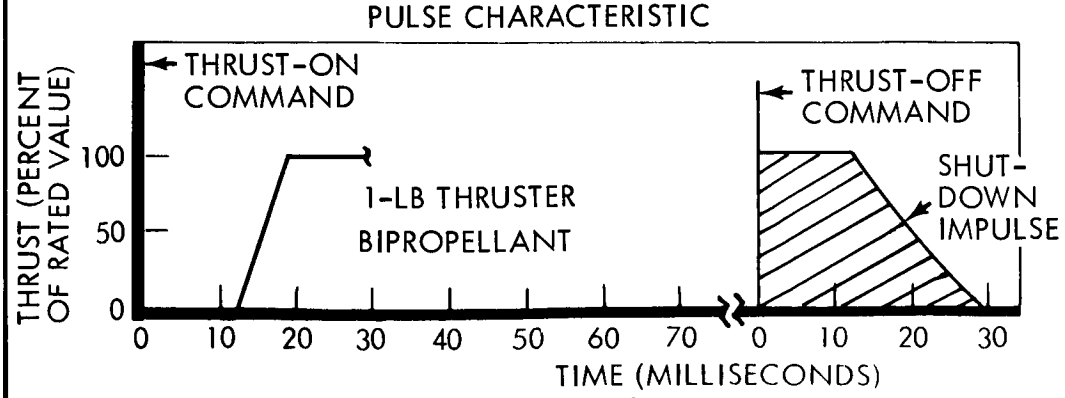

Figure 4.6-2: Bipropellant Reaction Control Concept

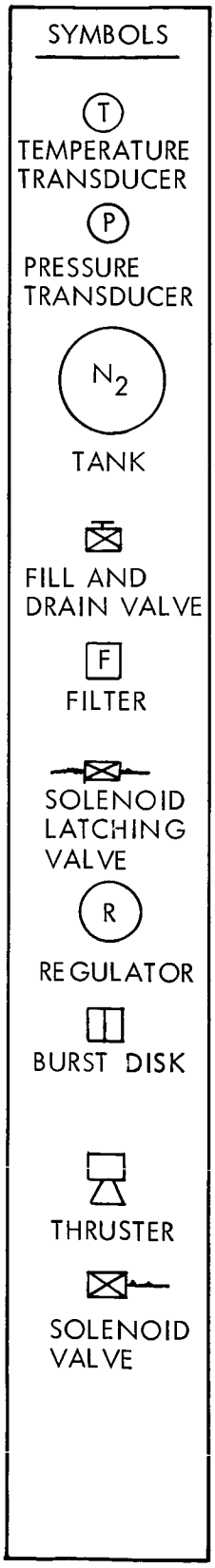

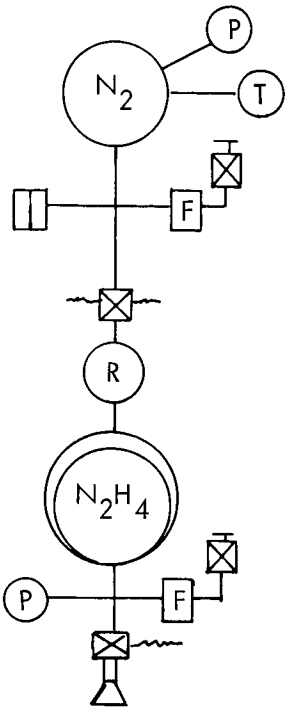

- PROPELLANT: N_2H_4
- RELIABILITY
  - (A) SINGLE — 0.985
  - (B) REDUNDANT — 0.999
- NUMBER OF COMPONENTS: 21 PER SYSTEM
- WEIGHT:
  - (A) SINGLE — 33.62 lbs
  - (B) REDUNDANT — 67.24 lb
- SPECIFIC IMPULSE:
  - (A) STEADY STATE — 240 SECONDS
  - (B) 20-m sec PULSES — 175 SECONDS
- DEVELOPMENT STATUS: QUALIFICATION BY JULY 1966 FREEZE DATE POSSIBLE
- COST: MEDIUM
- FRACTIONAL THRUST LEVELS: 0.05 POUND AND 0.5 POUND UNDER DEVELOPMENT

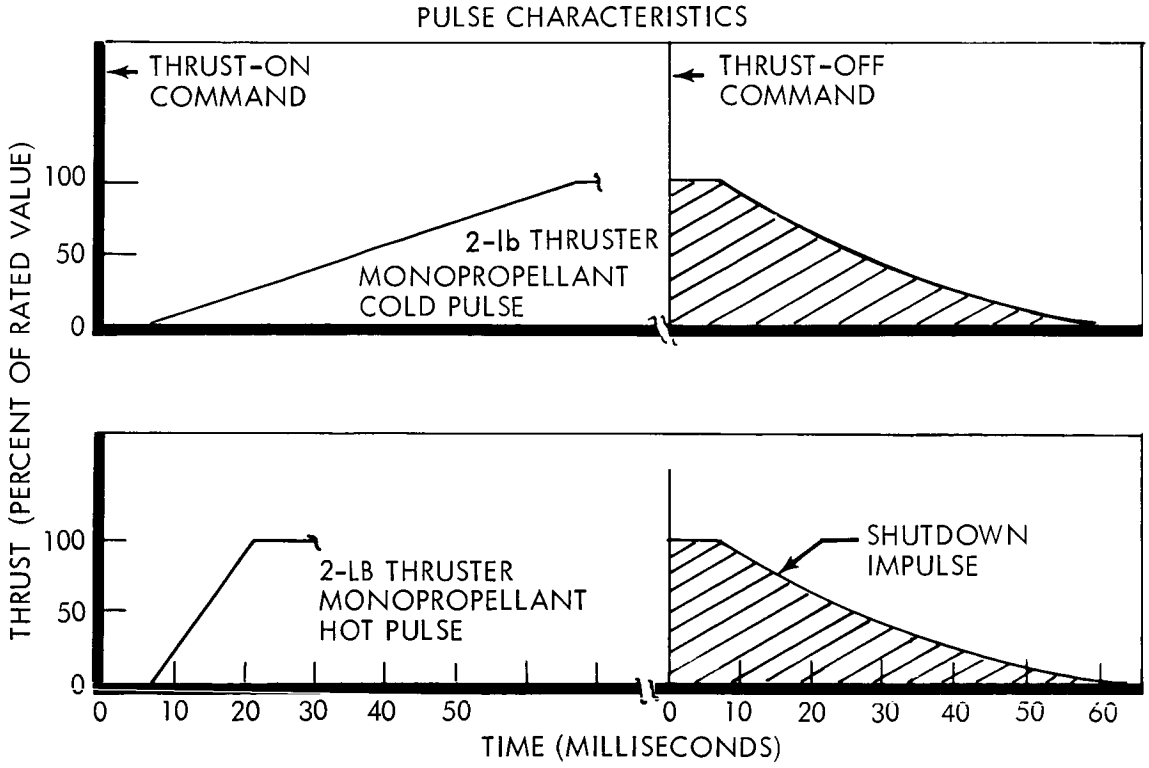

Figure 4.6-3: Monopropellant Reaction Control Concept

two. Since the system represents a simplification from the bipropellant system, it is inherently more reliable.

Hydrazine chambers operate at temperatures of only 2000° Fahrenheit, with nozzle temperatures even lower. This permits monopropellant designs which do not require special cooling since suitable materials are available to operate in this range.

The most common monopropellant in past applications has been 90% hydrogen peroxide with a specific impulse in the range of 160 to 170 seconds. Engine thrusts were one pound or greater. Most recently, the development of the Shell 405 spontaneous catalyst for the decomposition of hydrazine-based fuels has increased the attractiveness of monopropellant hydrazine rocket engines. Deliverable specific impulse above 240 seconds is indicated and current tests include engines with thrusts of less than one pound. Several problems remain, however. One in particular is the low I_{sp} that results during short pulse, low-duty cycle operation.

It is possible that current development work could resolve all conceptual monopropellant problems by July 1966; however, a monopropellant subsystem cannot be recommended at this time. Development work on this concept should be watched since it could result in substantial weight savings on later missions.

4.6.1.7 Monopropellant Plenum Chamber Concept

A monopropellant plenum chamber reaction control subsystem consists of thruster assemblies, propellant tank and bladder, propellant controls, pressurization tanks, pressure controls, plenum chamber and reactor, and instrumentation.

In the past, monopropellants have had limited use in low total-impulse attitude control systems because of minimum impulse-bit limitations and lack of fractional-thrust nozzles. However, the hydrazine plenum concept permits using monopropellant fuel with its high specific impulse with the advantages of cold gas minimum impulse widths.

The hydrazine plenum system consists of a plenum chamber which contains the gaseous hydrazine decomposition products. The plenum system gases are relatively cool and may be routed to the same type of thrusters which are employed with cold nitrogen gas attitude-control systems. The response and pulse characteristics are thus determined solely by the valve and are independent of the reactor decomposition kinetics. Pressure in the plenum chamber is automatically controlled. Specific impulse for this fuel is specified as 135 seconds at a plenum temperature of 300°F. Typical plenum pressure is about 20 psia.

The major design constraint is control of gas temperatures in order to avoid overheating the thruster valves. The probable mode of heat rejection is radiation. The high surface-to-volume plenum chamber required might be achieved by configurating the chamber from two tubes which are

located on the circumference of the spacecraft as shown in Figure 4.6-4. The gases from the reactor pass completely around the spacecraft in the first, or cooling, tube before entering the distribution tube. The cooling must be sized for the time of greatest propellant flow, initial acquisition. The thrust nozzles are located on the circumference of the second tube, which, together with the first tube, form the total plenum volume. Characteristics of the monopropellant plenum chamber concept are summarized in Figure 4.6-5.

The plenum chamber concept, though promising, is not recommended because of incomplete development work and the problem of heat dissipation.

4.6.1.8 Cold Gas Concept

The simplest type of mass expulsion system is the cold gas system. It has the highest reliability, is essentially off-the-shelf, and is the lowest in cost. Cold gas systems are capable of fractional-pound thrust levels that are unattainable with bipropellant systems and only recently have reached the developmental stage for monopropellant systems. The components in a cold gas system are well developed, all having been space-proven. The major disadvantage of a cold gas system is weight. Characteristics of a cold gas reaction control subsystem employing nitrogen are summarized in Figure 4.6-6. This control concept is selected as the preferred subsystem.

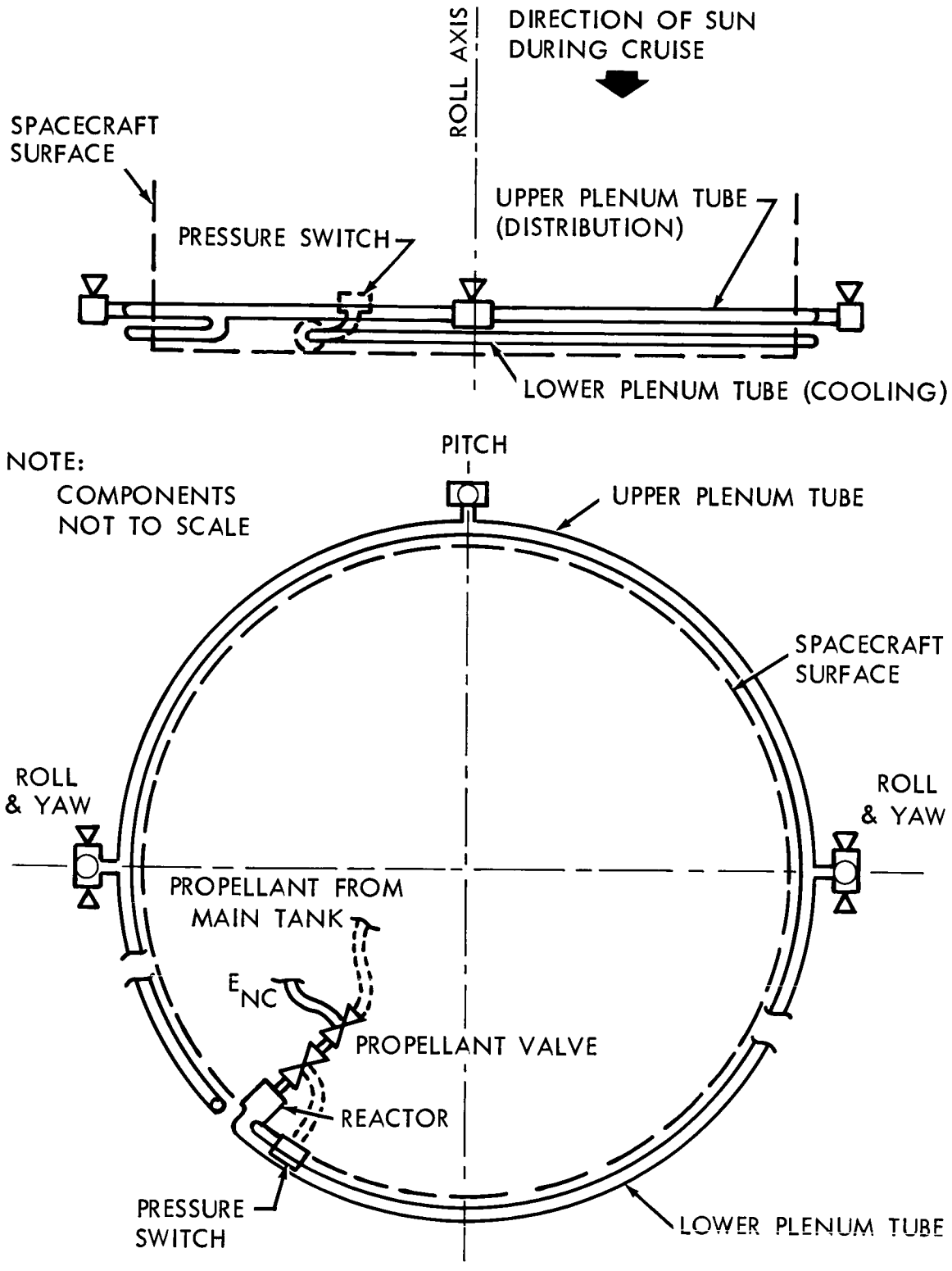

Figure 4.6-4: Monopropellant Hydrazine Plenum Schematic

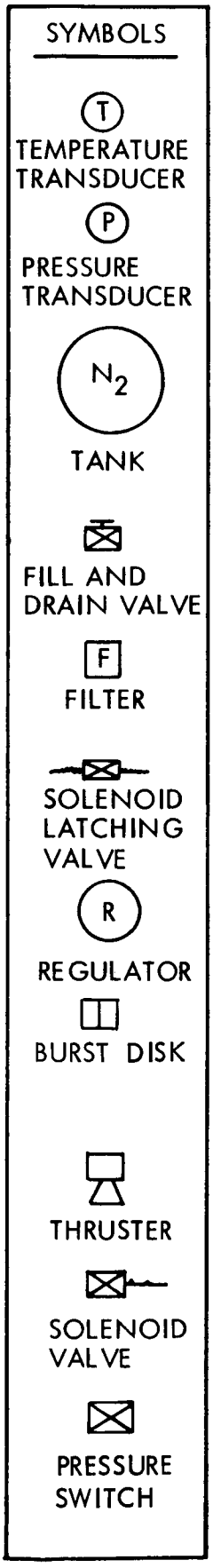

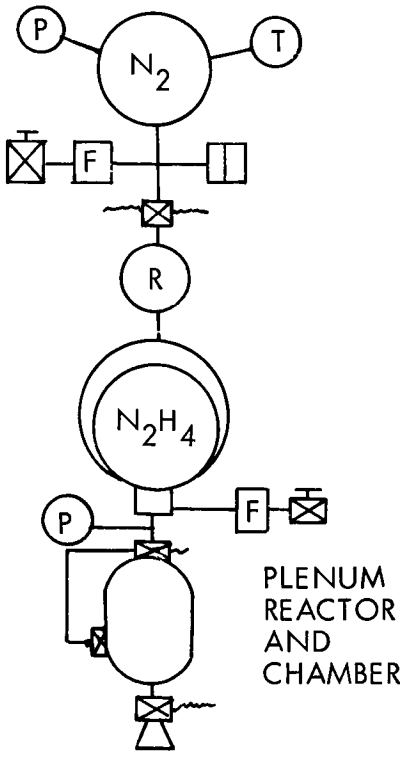

- PROPELLANT: N_2H_4
- RELIABILITY:
  - (A) SINGLE — 0.927
  - (B) REDUNDANT — 0.997
- NUMBER OF COMPONENTS: 33 PER SYSTEM
- WEIGHT:
  - (A) SINGLE — 40.87 POUNDS
  - (B) REDUNDANT — 81.74 POUNDS
- SPECIFIC IMPULSE:
  - (A) STEADY STATE — 135 SECONDS
  - (B) 20 MSEC PULSES — 135 SECONDS
- DEVELOPMENT STATUS: QUALIFICATION BY JULY 1966 FREEZE DATA POSSIBLE
- COST: MEDIUM HIGH
- FRACTIONAL THRUST LEVELS: USES SAME THRUSTERS AS COLD-GAS SYSTEM

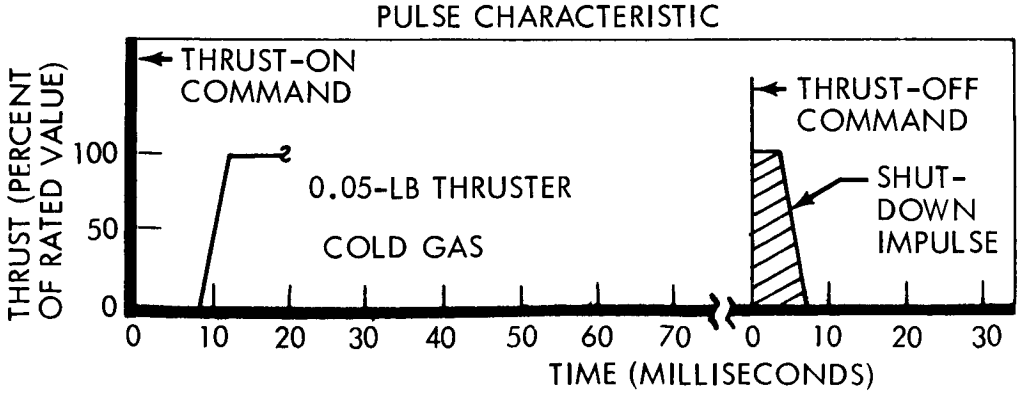

Figure 4.6-5: Monopropellant Plenum Chamber Concept

SYMBOLS

- (T) TEMPERATURE TRANSDUCER
- (P) PRESSURE TRANSDUCER
- (N_2) TANK
- FILL AND DRAIN VALVE
- [F] FILTER
- SOLENOID LATCHING VALVE
- (R) REGULATOR
- THRUSTER
- SOLENOID VALVE

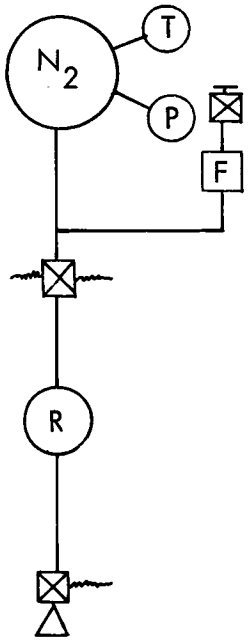

- PROPELLANT: N_2
- RELIABILITY:
  - (A) SINGLE - 0.985
  - (B) REDUNDANT - 0.999
- NUMBER OF COMPONENTS: 15 PER SYSTEM
- WEIGHT:
  - (A) SINGLE - 83.33 LB
  - (B) REDUNDANT - 166.66 LB
- SPECIFIC IMPULSE:
  - (A) STEADY STATE - 68 SEC
  - (B) 20 MSEC PULSES - 68 SEC
- DEVELOPMENT STATUS: SPACE-PROVEN HARDWARE
- COST: LOW
- FRACTIONAL THRUST LEVEL: 0.05 TO 1.0 SPACE-PROVEN

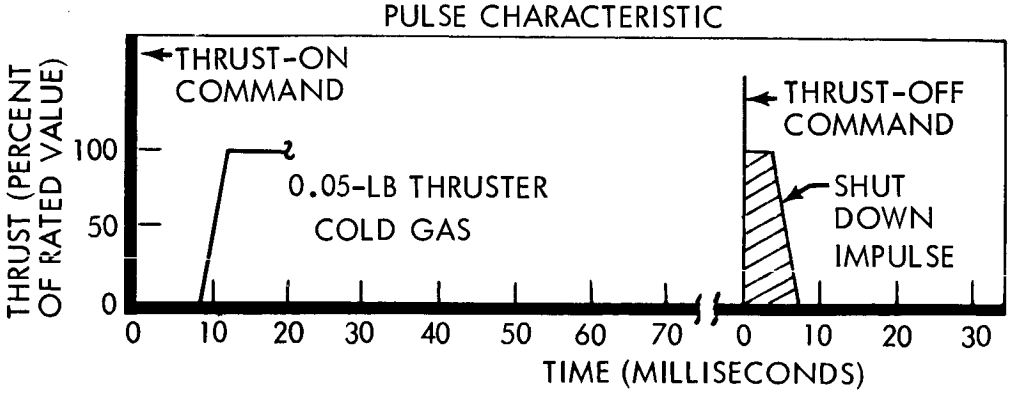

Figure 4.6-6: Cold Gas Reaction Control Concept

4.6.2 Alternate Mechanizations of the Selected Concept

4.6.2.1 Propellant Selection

Nitrogen, helium, and Freon were considered as cold gas propellants. A weight comparison of the three propellants is shown below for a non-redundant subsystem designed to meet Voyager impulse requirements.

Propellants	I_{sp} (sec)	Tank Weight / Fuel Weight	Total Subsystem Weight (pounds)
Nitrogen	68	2.12	152
Helium	175	11	219
Freon 14	33	0.25	127

Helium produces the heaviest system, is hard to contain, and hence is rejected. Freon 14 yields the lightest system but is a relative unknown. It has been used in space only in a Freon-nitrogen mixture in Agena. The use of Freon as a Voyager propellant would entail a study of contamination of solar panels and optical sensors under long-term exposure to Freon 14 exhaust plumes. Freon 14 is hence rejected.

Nitrogen is selected as the cold gas propellant.

4.6.2.2 Thruster Redundancy

Considering the state-of-the-art limitations on the reliability of the electromechanical solenoid-operated thruster valves, the long mission

time, and the importance of attitude control to mission success, a redundant thruster system is recommended. The higher required reliability is achieved in this manner at the cost of only twelve pounds of additional weight.

4.6.2.3 Tankage Redundancy

Separate tanks vs. common tankage: Pertinent features are shown and discussed in Figure 4.6-7. The principal trade is between the higher weight of the separate system (which requires three times the calculated fuel quantity) and the added complexity of the combined system (which requires malfunction detection sensors). Reliability is about comparable because the failure rate of the malfunction sensors is balanced by the increased failure rate of operating two thruster sets at a time. For this reason, the lighter common tankage system was chosen. The required malfunction detection is reasonable and not overly complex as is shown in the next section. The simplicity of the separate tank system remains desirable, however. Its use in space in the Ranger and Mariner programs is encouraging. The separate system will remain a strong alternative.

4.6.2.4 Tankage Integration

Separate tanks vs. integration with propulsion subsystem: The integrated arrangement was selected because of the following advantages:

1) Four tanks are required instead of six (simplifies mechanical design and assembly).
2) All tanks operate at reduced pressure earlier in the mission, lowering the probability of tank failure.
3) Common reserves are available to all subsystems.

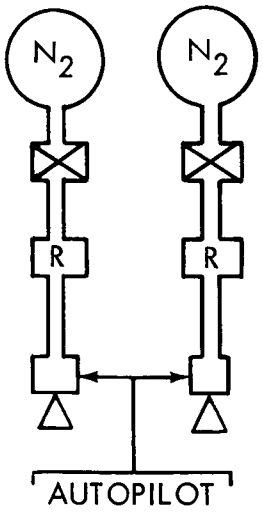

SEPARATE SYSTEMS

ADVANTAGES:
- SIMPLICITY (REQUIRES NO MALFUNCTION DETECTION OR SWITCHING);
- WILL TOLERATE AN UNDETECTED OPEN JET FAILURE

DISADVANTAGES:
- REQUIRES N_2 SUPPLY 3 TIMES THAT FOR THE NO FAILURE CASE;
- HALF SYSTEM (AFTER MALFUNCTION) HAS BELOW OPTIMUM THRUST;
- BACKUP SYSTEM IS IN THE OPERATIVE MODE, REDUCING ITS RELIABILITY;
- SAFETY FACTOR OF 3 DECLINES TO 1 IN THE EVENT OF AN EARLY OPEN-VALVE FAILURE.

REMARKS:
- WEIGHT = 227 LBS
- RELIABILITY = 0.999

COMMON TANKAGE WITH MALFUNCTION DETECTION

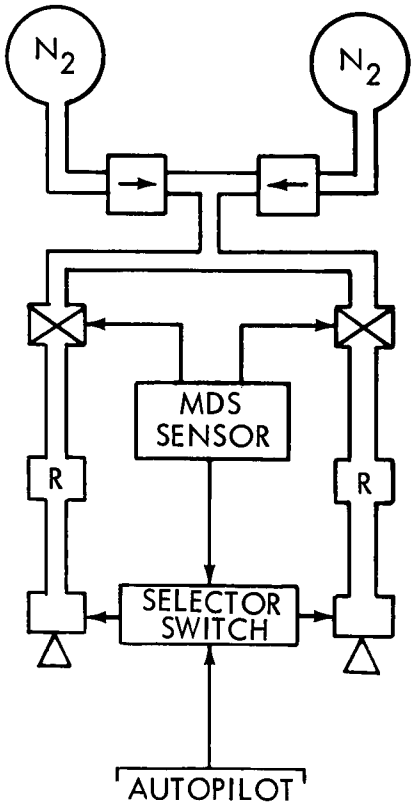

ADVANTAGES:
- BACKUP SYSTEM IN STANDBY MODE UNTIL NEEDED, RESULTS IN HIGHER RELIABILITY;
- THRUST LEVEL CAN BE OPTIMIZED FOR EACH SYSTEM;
- SAFETY FACTOR OF 2 IS MAINTAINED AFTER MALFUNCTION SWITCHING;
- MAKES POSSIBLE INTEGRATION OF N_2 SUPPLY WITH PROPULSION SUBSYSTEM.

DISADVANTAGES:
- HIGHER COMPLEXITY (MALFUNCTION DETECTION AND SWITCHING REQUIRED).

REMARKS:
- WEIGHT = 157 LBS
- RELIABILITY = 0.999

Figure 4.6-7: Redundant Propellant Storage Concepts

The principal disadvantage is that an undetected leak or open failure could deplete the entire nitrogen supply. For this reason, check valves divide the gas storage so that a tank leak in one side will not affect the other half. Weight and calculated reliability are not significantly different for the two alternatives. A schematic diagram of the selected reaction control subsystem is shown in Figure 4.6-8.

4.6.2.5 Malfunction Detection and Switching Alternatives

Thruster Malfunction Sensors--The first malfunction detection system considered consists of a device which will give an indication of the mechanical condition of the valve (open or closed). This can be a simple electrical switch, an inductive pickoff or a chamber pressure transducer. A disagreement between the switch indication and the electrical input to the valve is evidence of one of the following failures: mechanically stuck open or closed valve, or a defective solenoid. If the condition persists for some minimum time, the comparison logic causes the standby-reaction jet system to be activated by switching the attitude error signals to the standby drivers and by causing the solenoid latching-valve in the cold gas line to be opened. The failed system is isolated by closing its latching valve at the same time. The advantages of this method are the simplicity of the logic and the speed of reaction due to the directness of the failure detection. The method, however, will not detect leaks which are too small to result in actuation of the valve switch. This failure mode, however, is not catastrophic, and ground detection and switching is acceptable.

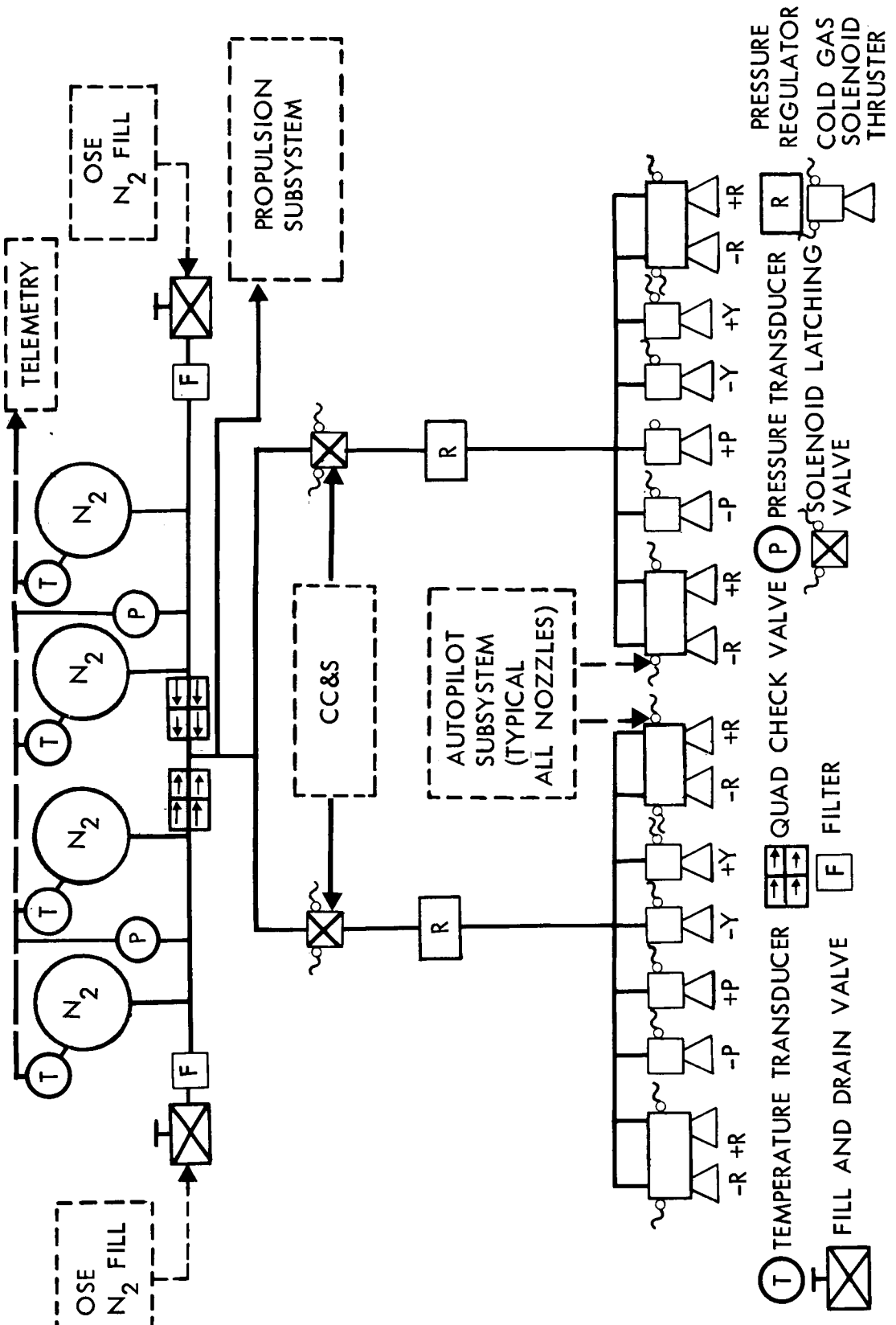

Figure 4.6-8: Reaction Control Subsystem

On-Time Integration--An alternate malfunction-detection scheme makes use of the fact that a failure is evidenced by excessive (greater than normal) jet electrical on-time for either a failed-closed valve or the valve opposite a failed-open jet. The electrical on-times of all of the valves are time-integrated, and a value which exceeds a previously-determined normal time will cause the standby system to be switched in. The integrators are reset to zero every telemeter sampling period. This method has the advantage of providing useful information, as well as malfunction detection. Disadvantages are: circuit complexity, required deactivation during attitude maneuver, and susceptibility to false signaling, i.e., excessive jet on-time can result from attitude reference subsystem or autopilot failures and also from large disturbances.

Series Valves--The use of a series-redundant valve in the cold gas line to each thruster was considered as a protection against open-jet failures. This concept was discarded because of the following disadvantages: (1) it protects against one type of failure only, (2) the probability of a closed failure is increased, (3) matching of dynamic characteristics of the series valves is required to ensure reliable minimum-impulse operation, and (4) a 100% increase in driver power is required.

The selected malfunction detection method employs the thruster malfunction sensors. If unforeseen difficulties are encountered in mechanization of the thrust valve switch, the integrated on-time method is quite acceptable. The detection of failures by monitoring telemetered data is

available as a backup for the onboard system. The communication transit time delay, however, makes this alternative unacceptable as a primary means of malfunction detection and correction. Ground control override of all malfunction switching is provided.

4.6.2.6 Angular Acceleration and Maneuver Rate Alternatives

Angular acceleration and maneuver rate must be carefully selected so as to minimize reaction control fuel consumption and yet meet mission requirements. Figure 4.6-9 depicts the trades involved.

Maneuver rate must be kept low to conserve fuel, but must be high enough to assure reasonable total times for midcourse, orbit insertion, and capsule separation sequences. A value of 0.2 degrees per second is the compromise selected, and the slewing voltage in the autopilot is selected to give this value.

Angular acceleration must be kept low to minimize reaction control limit-cycle fuel consumption. If it is too low, however, the angular overshoot at the end of a maneuver can become excessive and the time to achieve maneuver rate becomes long. Both of these effects are shown on Figure 4.6-9. The overshoot is particularly important if the strapdown gyro is to be operated open-loop at the end of maneuvers. Normal low-gain gyros have only a few degrees of input angle capability. Overshoot in the Voyager is not as critical because of use of the Autonetics G10 gyro. The gyro always operates caged and the position output appears in a digital register that can be easily expanded.

The variations in spacecraft moments of inertia can cause a variation in angular accelerations. For operational simplicity, one thrust level for all thrusters is selected. The resultant range of accelerations for Voyager are shown in Figure 4.6-9. These accelerations represent 0.25-pound thrusters mounted on the spacecraft body.

4.6.2.7 Thruster Location

From the standpoint of fuel consumption, the reaction control thrusters should be located as far from the spacecraft centerline as possible. Figure 4.6-10 shows the effect on total Voyager nitrogen weight of variations in thruster moment-arm. The panel tips appear to be the best location.

On the other hand, many disadvantages exist if thrusters are moved off the spacecraft body. These and other mounting considerations are summarized in Table 4.6-2.

Voyager thrusters are located on the spacecraft body in spite of the potential fuel savings which might be realized through use of more remote mounting locations. Thruster placement on the end of the first section of the solar panels is attractive and could be adopted with little sacrifice in reliability if the weight reduction is required.

A schematic diagram of the spacecraft showing the location of thruster clusters as well as other major reaction control components is shown in Figure 4.6-11.

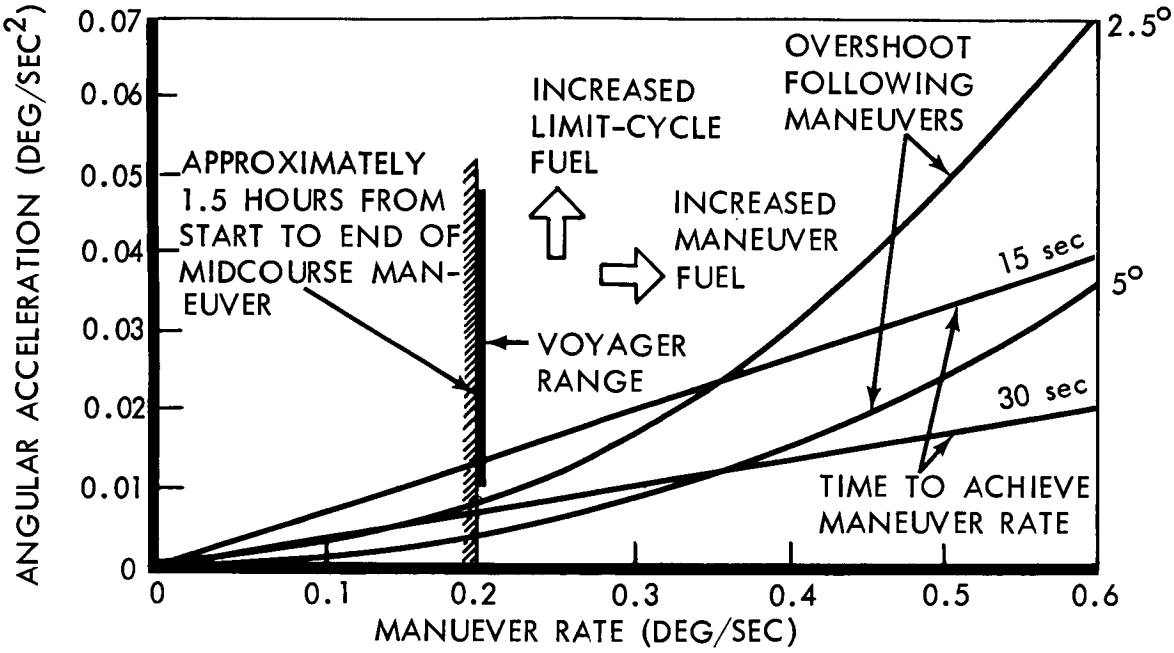

Figure 4.6-9: Angular Acceleration And Maneuver Rate Trade

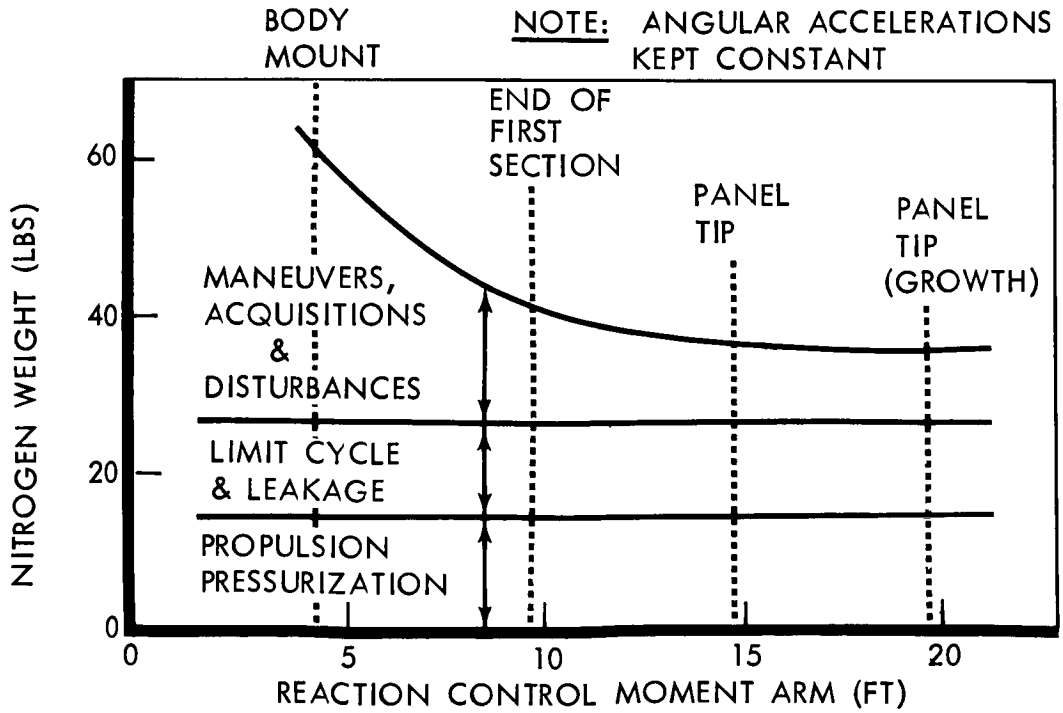

Figure 4.6-10: Thruster Location Trade

TABLE 4.6-2

THRUSTER LOCATION

Solar Panel Tip Mounted	Body Mounted
Advantages: • Larger moment arm • Decreases fuel requirement • Lower thrust levels • Reduces possibility of plume impingement on surfaces Disadvantages: • Increased plumbing problems • Requires flexible joints (2 per panel section) • More susceptible to leakage • Larger supply line size required to compensate for pressure drop • Does not permit complete modular concept	Advantages: • Reduces plumbing line lengths • No flexible tubing required • Eliminates cross coupling due to panel flexibility • Reduces thermal control requirements • Modular concept possible • Assures more consistent and reliable valve performance • Reduces interface constraints • Higher thrust levels permit consideration of monopropellant and bipropellant systems Disadvantages: • Small moment arm • Requires more fuel • Higher thrust levels • Increases the likelihood of plume impingement

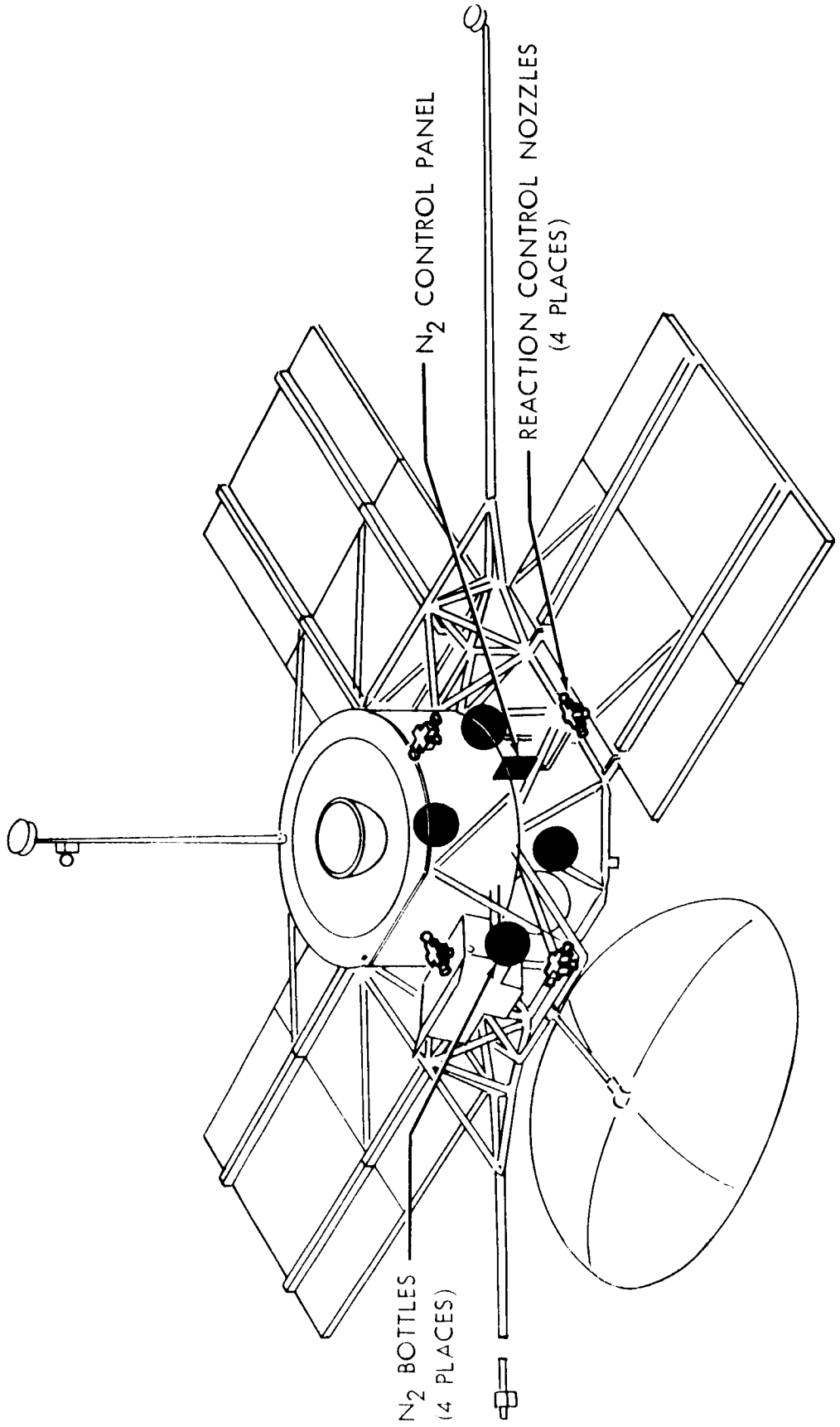

Figure 4.6-11: Reaction Control Subystem

4.7 CENTRAL COMPUTER AND SEQUENCER SUBSYSTEM

Summary--The central computer and sequencer (CC&S) provides event timing, sequencing, synchronization, and switching signals for spacecraft control and operation during prelaunch and all mission operations. To meet these requirements, the CC&S must incorporate both data processing and power-switching circuitry. The design selected utilizes a modified NASA Lunar Orbiter programmer, which is a special-purpose, memory-oriented (digital) computer. The equipment consists of two separate functional assemblies; the control assembly containing redundant data processors; and the switching assembly providing complete redundancy in all power switching. Switching of all CC&S functions may be accomplished by either ground or onboard command. The CC&S design provides the following: a reliability of 0.9941 over the mission period of 5880 hours (245 days); a random-access storage capacity of 256 words at 21 bits per word; a timing accuracy for mission control of one part in 10^6 over a period of 16 hours; plus, the capability to execute up to 333 different commands. The system weighs 58 pounds, occupies a volume of 2600 cubic inches, and requires 40 watts of power. The system block diagram is shown in Figure 4.7-1 and the system is discussed in detail in Section 4.8 of Volume A.

The method used to arrive at the selected CC&S design first considered the general computer mechanizations that appear capable of performing the Voyager tasks and, second, examined each mechanization in detail to see if functional requirements, reliability, and availability could be met. The mechanizations are:

1) Timer-oriented (fixed-wired);

2) Special-purpose, memory-oriented;

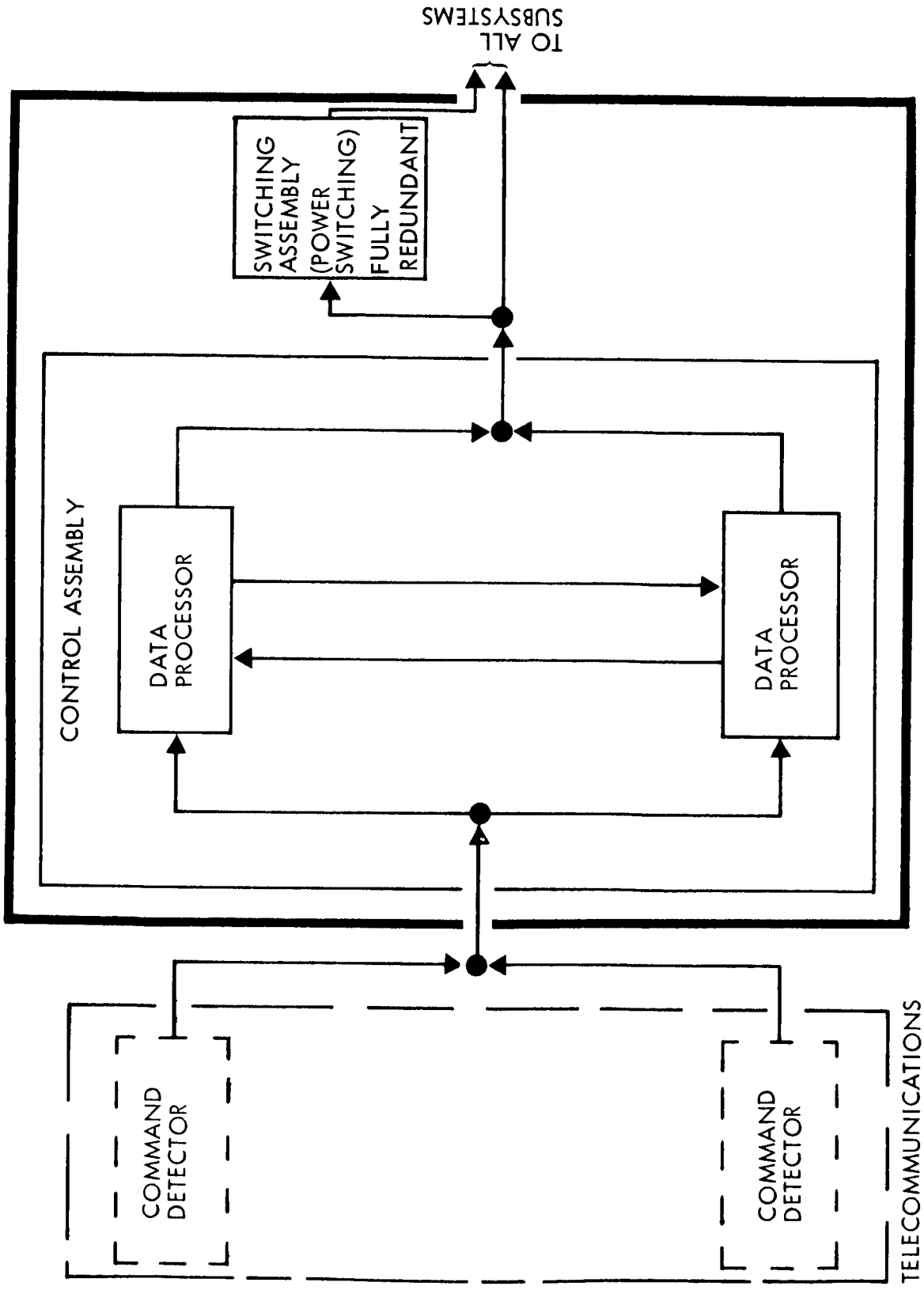

Figure 4.7-1: Central Computer and Sequencer System Block Diagram

3) General-purpose, memory-oriented.

Equipment representing each of the three general mechanizations was then considered in terms of development status as follows:

1) Off-the-shelf;

2) Off-the-shelf with modifications;

3) New design.

Emphasis was placed on use of equipment in either Development Status 1 or 2 in the interest of technical and program conservatism.

An evaluation of the Mariner C switching assembly design versus a modified Lunar Orbiter switching assembly was also conducted.

The study approach is illustrated in Figure 4.7-2, and the results of the CC&S investigation are summarized in Table 4.7-1.

4.7.1 Subsystem Identification and Intended Usage

The central computer and sequencer (CC&S) is the major control element with which man will direct the Voyager mission. The CC&S will execute a preplanned sequence of events stored internally and supplemented by the insertion of mission variables from mission operations. Specifically, the CC&S provides sequencing and timing command signals to spacecraft subsystems as directed by the stored flight program or as directed from ground control for the entire period from Earth launch through Mars orbit: it provides the logic implementation to control the magnitude and direction of spacecraft maneuvers; it provides timing signals and

CONTROL ASSEMBLY
MECHANIZATIONS CONSIDERED

TIMER ORIENTED
(FIXED WIRED) COMPUTER

REQUIREMENTS

CENTRAL COMPUTER &
SEQUENCER PROVIDES:

EVENT TIMING;
SEQUENCING,
SYNCHRONIZATION &
SWITCHING SIGNALS
FOR SPACECRAFT CONTROL
AND OPERATION DURING:

1969 TEST FLIGHT;
1971 MARS ORBIT;
1973 MARS ORBIT;
1975 MARS FLYBY;
1977 MARS FLYBY.

SPECIAL PURPOSE
(MEMORY ORIENTED) COMPUTER

SYSTEM DESIGN CONSIDERATIONS

FUNCTIONAL REQUIREMENTS;
AVAILABILITY;
RELIABILITY;
MISSION INDEPENDENCE;
WEIGHT.

GENERAL PURPOSE
(MEMORY ORIENTED) COMPUTER

SWITCHING ASSEMBLY

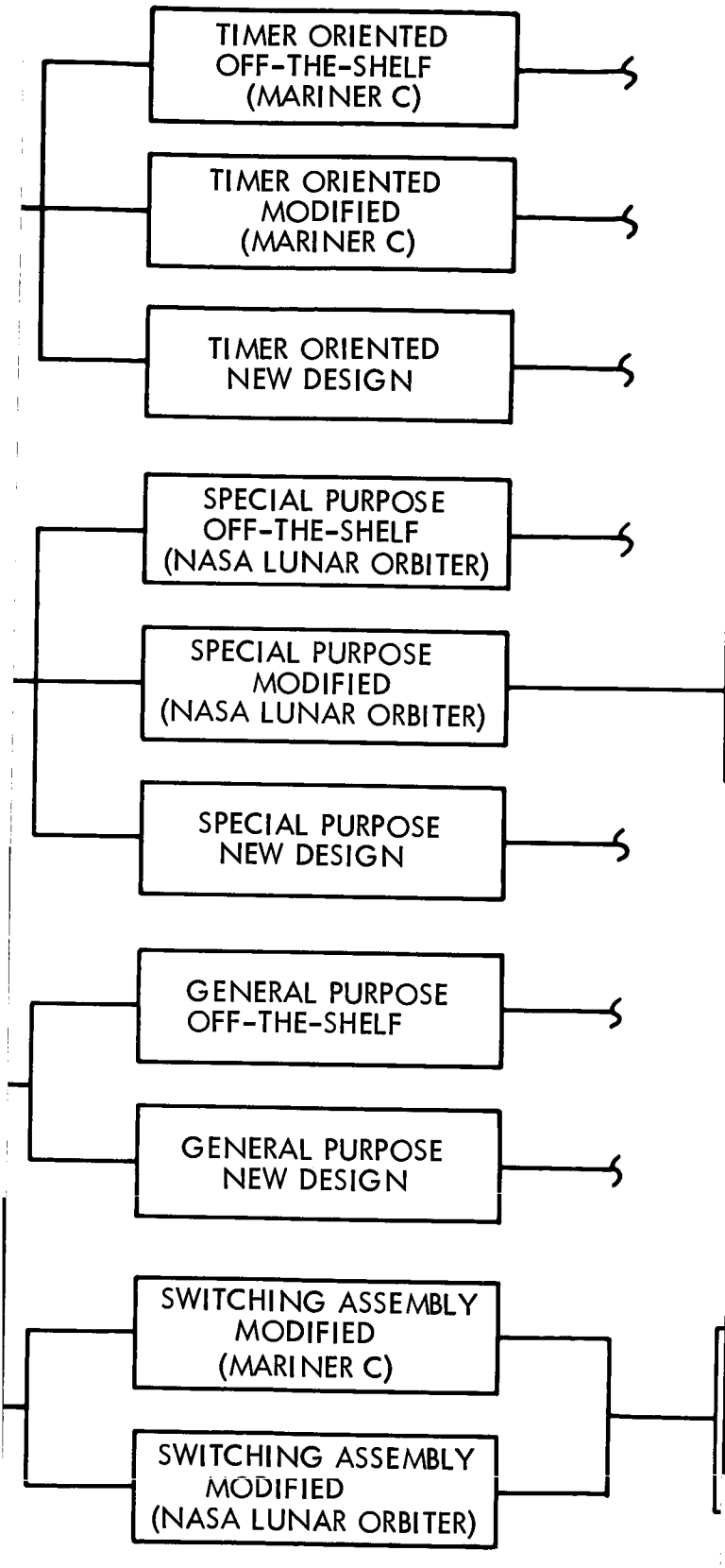
TIMER ORIENTED
OFF-THE-SHELF
(MARINER C)
TIMER ORIENTED
MODIFIED
(MARINER C)
TIMER ORIENTED
NEW DESIGN
SPECIAL PURPOSE
OFF-THE-SHELF
(NASA LUNAR ORBITER)
SPECIAL PURPOSE
MODIFIED
(NASA LUNAR ORBITER)
SPECIAL PURPOSE
NEW DESIGN
GENERAL PURPOSE
OFF-THE-SHELF
GENERAL PURPOSE
NEW DESIGN
SWITCHING ASSEMBLY
MODIFIED
(MARINER C)
SWITCHING ASSEMBLY
MODIFIED
(NASA LUNAR ORBITER)

CONTROL AND SWITCHING ASSEMBLY PREFERRED MECHANIZATION

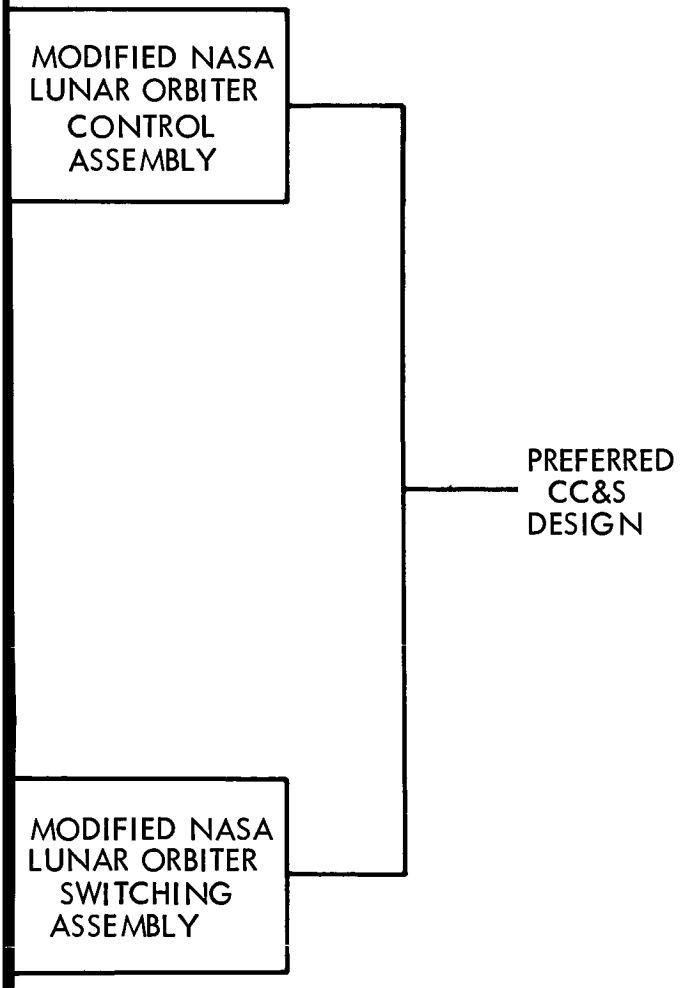

Figure 4.7-2: Central Computer & Sequencer Mechanizations Considered

Table 4.7-1 Central Computer and Sequencer Study Results

	MECHANIZATION		
DEVELOPMENT STATUS	TIMER-ORIENTED (FIXED-WIRED)	SPECIAL-PURPOSE, MEMORY-ORIENTED	GENERAL-PURPOSE, MEMORY-ORIENTED
Off-the-Shelf	Does not meet mission functional or reliability requirement.	Does not meet mission functional or reliability requirement.	Does not meet mission functional or reliability requirement.
Off-the-Shelf Modified	Extensive modification. Not mission independent. Too heavy.	Will meet all mission functional and reliability requirements.	Extensive Modification. Too heavy. Excessive power. High cost.
New Design	High development risk. Not mission independent	Will meet all mission functional requirements. High development risk.	Will meet all mission functional requirements. High cost. High development risk.

pulse trains to other spacecraft subsystems.

4.7.2 Mechanizations Considered

Summaries of available mechanizations considered and of their competing characteristics are shown in Table 4.7-2.

4.7.2.1 Timer-Oriented (Fixed-Wire) Computer

Timer-oriented computers contain sequential-time-decoding logic that produces events in a fixed order defined by the hardware configuration. Several characteristic features that affect the reliability and operation of a timer-oriented computer are:

1) The operational reliability will be high because of the slow internal data-transfer rate (25 cycles/sec in the case of Mariner C). This slow data rate reduces the probability of error over a prolonged period of time because error rate is related to the design noise margin, and noise is a function of computer speed.
2) The timer-oriented system will issue commands in relation to clock time, and with a clock timer malfunction (due to noise or transient radiation effects), it is possible that this type of system would issue many random commands.
3) In order to change the timer-oriented (fixed-wired) computer to issue commands for a different sequence of events, either the wiring must be changed (through a pre-set patch panel) or commands must be issued from ground control to supplant the patch panel commands. The latter method does not meet the JPL requirement for minimum ground-to-air transmission.

	TIMER ORIENTED (FIXED WIRED)	
CHARACTERISTICS	TIMER-ORIENTED MARINER C (FIXED WIRED)	NO. 1 (TAPE PROGRAMMER)
OPERATIONS	SERIAL/BINARY	SERIAL/BINARY
MEMORY	FLIP FLOPS (SIX 25-BIT REGISTERS)	35 MM PUNCHED TAPE (4 108,000 WORDS /TAPE
DATA WORD	-18 BITS (8 BASIC WORDS)	49 BITS
INSTRUCTIONS	—	49 BITS
NUMBER OF LEVELS OF PRIORITY INTERRUPT	1	—
BASIC INSTRUCTIONS	—	21 BITS
INPUT/OUTPUT CAPABLE OF ADDRESS UP TO	ANY NUMBER TO MEET THE SYSTEM REQUIRE-MENTS	2500 BITS/IN^2 63 OUTPUTS CHANNELS
PERIPHERAL DEVICES	—	—
ADD	—	—
MULTIPLY	—	—
POWER	6 WATTS	13 WATTS, 28 VOLTS
WEIGHT	14 POUNDS	25 POUNDS (INCLUDING MOD. SW. ASSEMBLY)
VOLUME	—	990 CUBIC INCHES
MTBF (RELIABILITY BETWEEN FAILURE)	-12,700 HOURS (SINGLE THREAD SYSTEM)	22,800 HOURS
CLOCK	—	1.0 m.c.

*EXCLUSIVE OF I

TABLE 4.7-2 OFF-THE-SHELF CONSIDERED COMPUTERS

SPECIAL PURPOSE	GENERAL PURPOSE	
LUNAR ORBITER (MEMORY ORIENTED)	AIRBORNE DIGITAL COMPUTER NO. 1	AIRBORNE DIGITAL COMPUTER
SERIAL/BINARY	PARALLEL/BINARY	PARALLEL/BINARY
MAGNETIC CORE 128 (21 BIT WORD)	MAGNETIC CORE 4,096 (32 BIT WORD)	MAGNETIC CORE 4,096 (25 BIT WORD)
21 BITS	16 BITS (INCLUDING SIGN)	25 BITS (1 PRIORITY 1 SIGN INCLUDED)
26 BITS	32 BITS	24 BITS
1	6	8
32	62	64
ANY NUMBER TO MEET THE SYSTEM REQUIRE-MENTS	64 DISCRETE SIGNALS	64 DISCRETE SIGNALS
—	8 CHANNELS	8 CHANNELS
10 MILLI-SECONDS	5.6 MICROSEC.	2 MICROSEC.
—	17 SEC.	9 SEC.
34 WATTS, AT 27 VOLTS	140 WATTS	60 WATTS
24.6 POUNDS (INCLUDING SW. ASSEMBLY)	27 POUNDS	35 POUNDS
1000 CUBIC INCHES	487 CUBIC INCHES	*.67 CUBIC FEET
14,300 HOURS (SINGLE THREAD SYSTEM)	8500 HOURS	6718 HOURS
2.4 k.c.	8.3 m.c.	1.0 m.c.

IPUT/OUTPUT CIRCUITS.

Several off-the-shelf computers were evaluated. All of them were eliminated from further study due to their failure to meet mission functional and reliability requirements.

Off-the-shelf computers, modified to meet Voyager requirements, were also evaluated. The Mariner C CC&S was the best. This computer would, however, require extensive modification, such as an increase in logic decoding and output amplifiers to enable it to execute the commands required for Voyager. In addition, a timer-oriented (fixed-wired) computer system is designed for specific mission profiles and is not mission independent without rewiring. This system, therefore, is not considered acceptable as stated in a study by JPL, reference EPD 250, Pages 11-25 through 11-33. A modified Mariner C would also be heavier and less reliable than an available modified special-purpose computer.

A timer-oriented (fixed-wired) computer of new design could meet all mission functional and reliability requirements. Being a new design, however, and requiring development and qualification testing, the new system would result in a high degree of risk involved in meeting required schedules. In addition, such a computer would still not be mission independent without rewiring.

4.7.2.2 Special-Purpose, Memory-Oriented Computer

Memory-oriented computers contain arrays of information-retention devices in which data is inserted, modified, and retrieved to produce events in sequences as ordered by the mission constraints and requirements. The special-purpose computer, using limited arithmetic capability,

is designed specifically to provide subsystem functional control. This computer has the additional capability to accept changes in event sequencing at any time by reprogramming. The NASA Lunar Orbiter programmer is an example of this design. Pertinent operational features that affect the reliability and operation of the special-purpose computer are:

1) Special-purpose computers are specifically designed to meet system functional requirements and, therefore, the data-transfer rates are not made higher than necessary (2.4 Kilocycles/sec for the NASA Lunar Orbiter programmer; refer to the timer-oriented computer section for comparison);
2) Internal data transfer is checked to verify functional operation providing increased operational reliability;
3) Decoding functions are minimized to meet system requirements, thus improving reliability by reduction of internal wiring;
4) A clock failure will prevent the issuance of random commands, thus reliability in mission execution may be improved through work-around modes.

The only special-purpose, off-the-shelf computer available for study was the NASA Lunar Orbiter programmer. Mission functional and reliability requirements cannot be met by this computer as it exists.

The NASA Lunar Orbiter programmer with modifications will meet all Voyager mission functional and reliability requirements. Two modifications necessary to meet these requirements are: (1) an expansion of its output commands from 116 to 333 and (2) incorporation of two redundant data processors and the control to switch between them. Since the

programmer is reprogrammable, mission variations both inflight and between missions are easily handled.

A newly designed special-purpose computer could meet all mission functional requirements and could have a slightly higher reliability than the modified NASA Lunar Orbiter programmer. Availability of such a new computer to meet program schedules is questionable because of the complete development and qualification testing required.

4.7.2.3 General-Purpose, Memory-Oriented Computer

The general-purpose computer incorporates an array of information-retention devices as in the special-purpose, memory-oriented computer, except that the general-purpose computer logic organization is designed to perform a general class of arithmetic and data-processing functions. The system is not designed for a specific mission and some capability is generally wasted when it is used for a specific mission. Some of the important characteristics of the general-purpose computer that affect the reliability and operational performance are:

1) The data-transfer rate in a general-purpose computer is chosen to meet the data-processing requirements for a general system. The data-transfer rate, therefore, is made very high (megacycle range). Refer to the timer-oriented computer section for comparison.
2) Because of the general information flow exhibited by the general-purpose computer, only a single path exists for execution of both real-time and stored-program commands. A separate path for each type of command provides a more reliable system.

3) A clock failure will prevent the issuance of random commands, but work-around modes are only available through redundant processors.

Off-the-shelf general-purpose computers do not meet mission functional and reliability requirements and therefore were not considered for the Voyager CC&S.

A modified general-purpose computer would require an expansion of its output functions plus a complete packaging redesign to meet mission functional and space environmental requirements. It would be about 30 pounds heavier, its power consumption two times greater, its cost 2.5 to 3 times greater, and it would be less reliable than a modified timer oriented or special-purpose computer.

A general-purpose computer could be designed to meet Voyager requirements; however, it would be heavier and would cost more than either a timer-oriented or the special-purpose new design. Its availability is also in the high-risk category due to the requirement for complete development and qualification testing.

4.7.2.4 Switching Assembly

The switching assembly is made up of a few basic types of circuits that are used to switch power to high-current loads such as squibs, relays, valves, and motors. With each circuit type required, there is a trade involved in the best way to implement these functions. Some of the basic circuit requirements for the switching assembly are: squib, valve, relay, and motor drivers; +35-v.d.c.-power switches; and input-interface circuits.

Of the basic circuits listed, only one (the squib driver) required a trade study. This circuit was the most heavily used and was the most critical from a circuit standpoint (because of safety considerations). The basic trade on the squib driver has been the use of a silicon-controlled rectifier versus a silicon power transistor to fire the squib. An extensive trade study on this subject has been made on the NASA Lunar-Orbiter program. The results of this study, shown in Table 4.7-3, demonstrate that power consumption for both is about equal. Complexity considerations favor the Mariner C circuit but weight, reliability, and failure modes favor the Lunar-Orbiter circuit. Schematics are shown in Figures 4.7-3 and 4.7-4.

4.7.3 Preferred Design and Justification for Its Selection

Four major factors that are prominent in establishing the justification for the preferred CC&S design are: mission reliability; mission functional requirements; equipment availability; and equipment weight.

The preferred central-computer-and-sequencer design is a redundant NASA Lunar Orbiter programmer with outputs added to meet functions required by the Voyager mission. The design exceeds the assessed reliability requirement and meets mission functional requirements of timing, sequencing, synchronization, and signal switching for spacecraft control and operation. It also satisfies allocated physical parameters and imposed environmental requirements and will be available to meet Voyager schedules. For a detailed discussion of the preferred design, refer to Boeing Section 4.8, in Volume A.

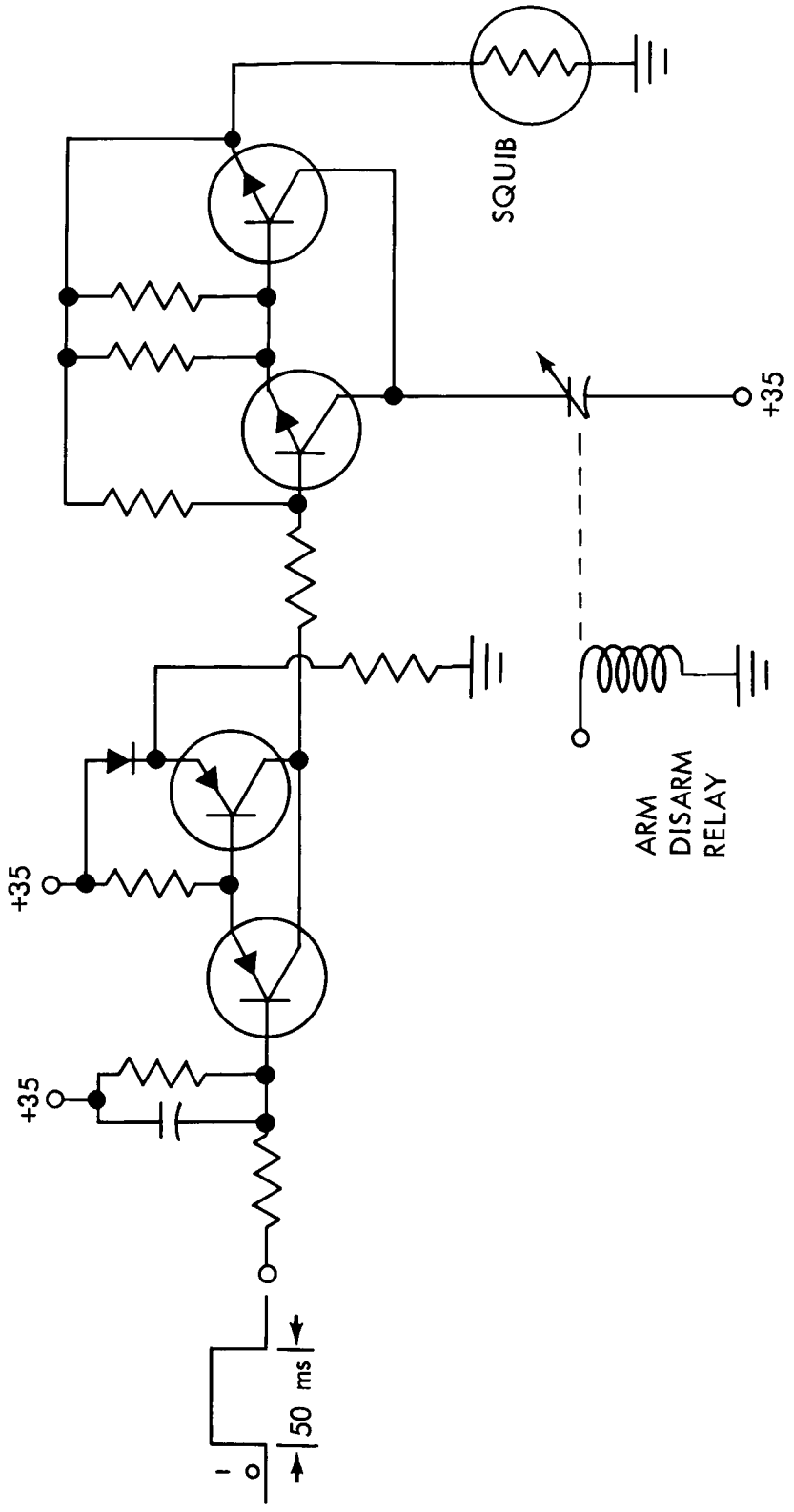

Figure 4.7-3: Silicon Power Transistor Squib Driver

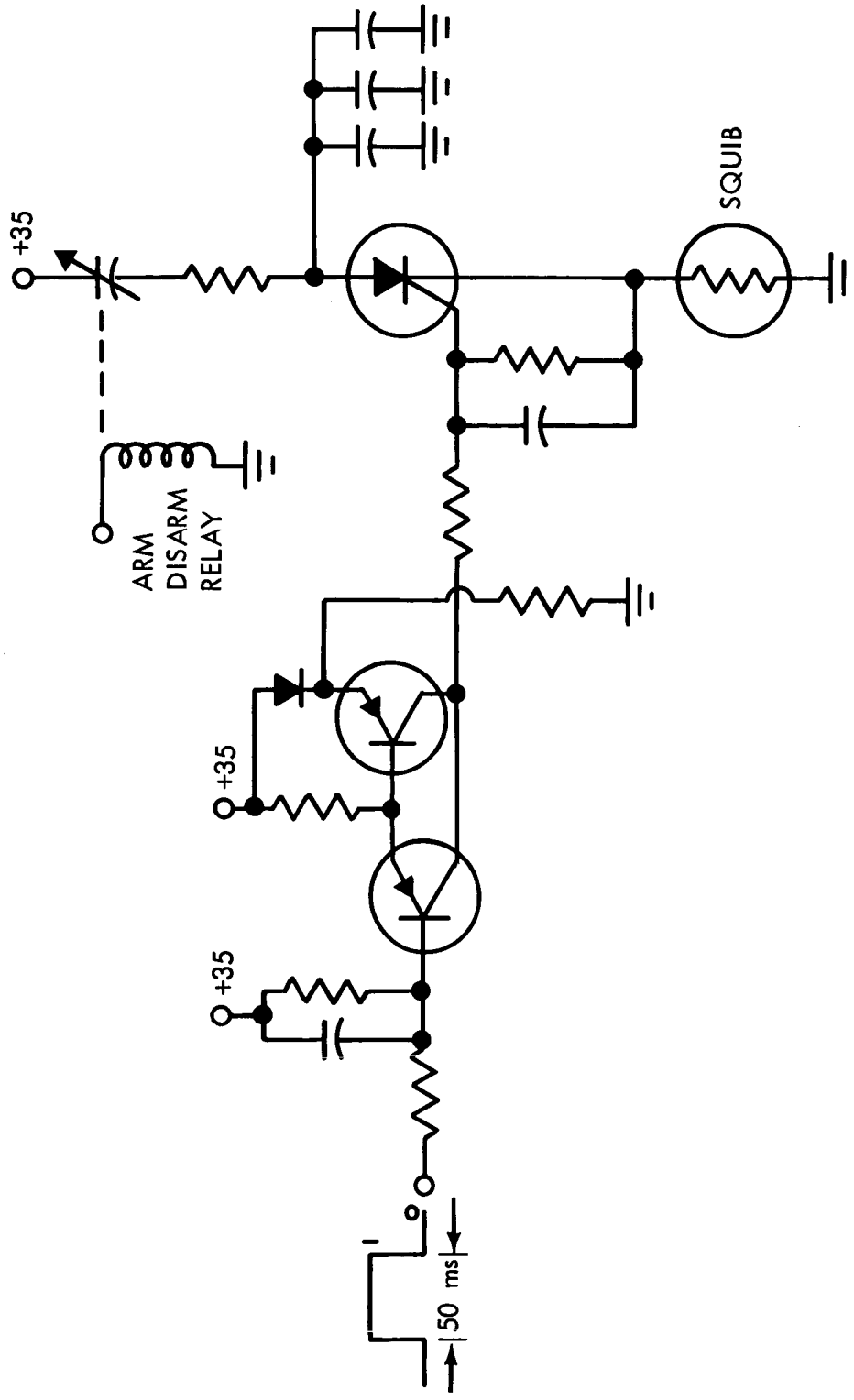

Figure 4.7-4: Silicon Controlled Rectifier Squib Driver

5.0 SCHEDULE AND IMPLEMENTATION PLAN

5.0 SCHEDULE AND IMPLEMENTATION PLAN

Detailed analysis and comprehensive trade studies of the alternate spacecraft designs discussed in this volume indicate that the adoption of any one of these alternates will have no significant effects or implications on the schedules and implementation plans discussed in relation to the preferred spacecraft design in Volume A. Moreover, the schedules presented in Volume A are sufficiently flexible to accommodate any combination of the features of the alternate spacecraft designs discussed in this volume without significant impact on such schedules.

Propellant Storage--

Description--Both spherical and cylindrical tanks were considered.

Competing Characteristics--The following were considered:

1) Available installation volume;

2) Propellant expulsion method;

3) Weight;

4) Tankage availability.

Selection Rationale--Spherical tanks were selected on the basis of available installation volume. A survey of existing tankage indicated that a cluster of either Apollo LEM attitude control system or Centaur reaction-control cluster tankage could meet Voyager tankage requirements. Both use bladders for expulsion.

Pressurization--

Selection Rationale--Basic pressurization concepts considered are separate gas storage and combined gas storage for the reaction control subsystem and the midcourse propulsion subsystem. Both helium and nitrogen are considered for the combined gas storage concept. The results of the weight trades of the variable weights, namely gas and storage tank, are as shown on the following page.

Even though the separate storage concept is the lightest, volume constraints and the number of gas storage tanks required dictates the use of a combined gas storage concept.

	Combined Gas Storage		Separate Gas Storage
	Nitrogen	Helium	Nitrogen RCS plus Helium for Propulsion
Storage tank weight (lb)			
Reaction control system	130	290	97
Midcourse and orbit trim Propulsion system	none	none	33
Gas weight (lb)			
Reaction control system	45	17	45
Midcourse and orbit trim propulsion system	15	2	2
Total	190	309	177

Isolation Valves and Plumbing--

Description--Valve arrangements considered included all squib-operated valves, all solenoid-operated valves, and combinations of squib- and solenoid-operated valves. Both the pressurization and propellant feed subsystems were considered. Plumbing considerations were restricted to tubing materials and tubing fitting selections.

Competing Characteristics--Primary competing characteristics are:

1) Reliability;

2) Compatibility with pressurant and propellant;

3) Contamination;

4) Leakage.

Selection Rationale--Squib valves are more reliable than solenoid valves. Squib valves, however, are single use, or one-shot, items. For multiple

operations, may valves are required. Squib valves lend themselves well to redundancy. Solenoid valves, however, are excellent multiple-use valves. Leakage is greater with solenoid valves than with squib valves. The preferred design is one of combined usage of squib valves and solenoid valves to maximize reliability. Solenoid valves are used only in instances where there are relatively short time periods between operations.

Stainless tubing with brazed fittings are utilized. The brazing material is compatible with N_2H_4 and N_2O_4. Brazed joints were selected over standard tubing fittings to minimize leakage.

Selection Rationale--Malfunction detection and attendant switching to a redundant mode can be accomplished either onboard the spacecraft or via ground command. Ground detection requires excessive time for operations near or at Mars. Onboard detection complicates the CC&S. In the preferred design, the system was provided with sufficient redundancy in order to minimize CC&S complexity. Malfunction detection is accomplished by mounting triply redundant pressure transducers on each of the pair of midcourse and orbit trim engines used for normal operations. The resultant interface with the CC&S is discussed in Volume A, Section 4.3.4.

4.3.4 Multiengine All-Bipropellant Concept

This concept is based upon available engines and is included for information only. Component analyses and trade studies which led to the mechanization of the all-bipropellant multiengine concept are described below.

4.3.4.1 Engines, Propellants, and Thrust Level

Candidates--Engines considered included both radiation-cooled and ablation-cooled hardware. Candidate engines for both midcourse, orbit trim and orbit insertion are shown in Table 4.3-20.

Table 4.3-20: CANDIDATE BIPROPELLANT ENGINES

Designation	Application	Thrust	Manufacturer
SE-9	Transtage ACS	25 lb	Rocketdyne
MA-109	Lunar Orbiter	100 lb	Marquardt
TD-339	Surveyor	104 lb	Thiokol-RMD
MIRA-180	Surveyor	180 lb	STL
MA-118	S-IVB Ullage	(1750 lb)	Marquardt
AJ10-131	Apollo Subscale	(2200 lb)	Aerojet
	Apollo Subscale	(2200 lb)	UTC
		(1500 lb)	Rocketdyne
8258	LEM Ascent	3500 lb	Bell

Note: ( ) indicates not currently available

Competing Characteristics--The following competing characteristics were considered in the final selection of preferred engines:

1) Availability;

2) Space use experiences;

3) Reliability;

4) Weight;

5) Thrust level;

6) Envelope;

7) Engine lifetime;

8) Compatibility with spacecraft (TVC and exhaust plume).

Selection Rationale--No single available engine could perform all Voyager propulsion maneuvers within the mission constraints. The high-thrust-level engines could not perform the minimum midcourse maneuver to the required accuracy. The low-thrust-level engines could not provide the required orbit-insertion total impulse within engine life-time limitations. Recourse was therefore made to a multiple-engine concept utilizing a high thrust engine for orbit insertion coupled with a low thrust engine(s) for midcourse and orbit trim.

Orbit Insertion--The only available (currently funded) high-thrust engine suitable for Voyager application is the Bell Model 8258 LEM ascent engine utilizing N_2O_4-MHF propellants. Performance data for this engine is shown in Table 4.3-21. This engine will be space proven prior to the first Voyager mission. Its thrust level is compatible with maximum spacecraft acceleration limitations. It fits within the spacecraft dynamic envelope and has sufficient lifetime to meet all Voyager orbit requirements. Its only disadvantage is its relatively high dry weight. Its exhaust plume is gaseous with low radiosity and hence considerably cooler than that of a solid motor with metal particles in the exhaust. This, coupled with the fact that the engine is fully ablative cooled, will reduce engine thermal shielding requirements. The rocket exhaust plume, shown in Figure 4.3-33, indicates the probable impingement of very-low-density exhaust gases on spacecraft and appendages.

TABLE 4.3-21

ENGINE DATA SHEET

Designation	Model 8258
Manufacturer	Bell Aerosystems
Status	Development
Propellants Fuel	Aerozine 50 (MHF)
Oxidizer	Nitrogen Tetroxide
Engine Thrust	3500 lb
Engine Specific Impulse	(Classified)
Mixture Ratio O/F	1.6 ± 0.016 1%
Expansion Ratio A_e/A_t	45.6
Exit Area	750.6 sq in.
Chamber Pressure	120 psia
Start Time and Impulse	0.355 $\pm$ 0.016 sec; 91^{+15}_{-25} lb-sec
Shutdown Time and Impulse	0.14 sec; $360\ ^{+55}_{-60}$ lb-sec
Minimum Total Impulse Bit	476 $\pm$75 shutdown @90% thrust 580 $\pm$125 lb-sec with 0.375 sec Elec. command pulse width to ensure 100% thrust
Throttle Ratio	None
Restart Capability	35 maximum
Service Life	525 sec
Ignition	Hypergolic
Cooling	Ablative
Weight, Dry	218.54 lb
Size Length	51 in.
Diameter	31 in.
Thrust Vector Type	None
Angle	
Rate	
Acceleration	
Fuel Inlet Pressure	165 psi
Oxidizer Inlet Pressure	165 psi

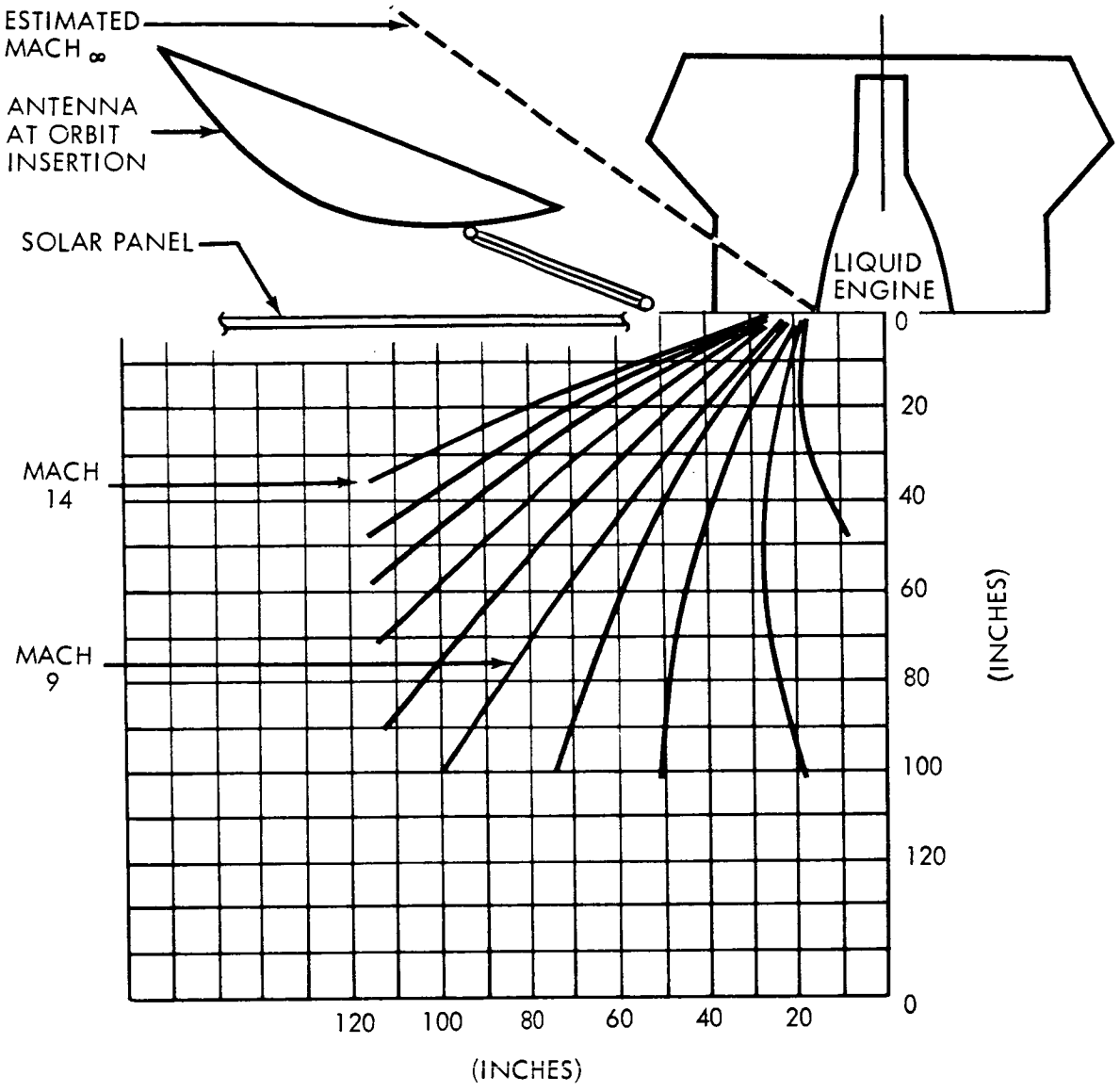

Figure 4.3-33: Exhaust Plume Definition — Lem Ascent Engine

Midcourse and Orbit Trim--Only three engines are currently available in the 25-to-500-pound thrust range as shown in Table 4.3-20. These are the MA-109 Lunar Orbiter engine, the Surveyor TD-339, and MIRA-180 engines. The TD-339 engine has been rejected because its propellants, MON-MMH + water, are not compatible with the LEM engine. The MIRA-180 engine was also incompatible with the LEM engine propellants and was burntime limited. Midcourse engine lifetime is of particular significance for the all-bipropellant concept since the midcourse engines provide backup to the orbit-insertion engines. The MA-109 engine was consequently selected as the preferred design. Engine data summary is provided in Table 4.3-22. A total of four midcourse and orbit-trim engines were selected. With length restrictions necessitating the mounting of the midcourse engine off the centerline, a single engine could not be utilized due to large center-of-gravity shifts along the spacecraft longitudinal axis during the mission. Two engines were required as a minimum and had to be mounted with their thrust line parallel to that of the orbit insertion engine. Four engines were selected to provide redundancy for midcourse and orbit trim. Moreover, four of these engines could provide backup for orbit-insertion, or for thrust-vector-control when utilized in their pulsing mode. The above engine selection rationale has automatically established subsystem propellants and thrust levels.

4.3.4.2 Expulsion

Candidates--The following expulsion candidates were considered:

1) Nonmetal diaphragms or bladder;

2) Metal diaphragms or bladder;

3) Piston;

4) Metal bellows.

Table 4.3-22: ENGINE DATA SHEET

Designation		MA 109
Manufacturer		Marquardt
Status		Production
Propellants	Fuel Oxidizer	Aerozine 50 Nitrogen Tetroxide
Engine Thrust		100 lb
Engine Specific Impulse		(Classified)
Mixture Ratio O/F		2.0 ± 0.025
Expansion Ratio A_e/A_t		40
Exit Area		
Chamber Pressure		96 psia
Start Time and Impulse		
Shutdown Time and Impulse		
Minimum Total Impulse Bit		0.5 lb-sec
Throttle Ratio		None
Restart Capability		Multiple
Burn Time/Service Life		Classified/4800 sec
Ignition		Hypergolic
Cooling		Radiation
Weight, Dry		4.42 lb
Size	Length Diameter	12.9 in. 6.3 in.
Thrust Vector	Type Angle Rate Acceleration	None
Fuel Inlet Pressure		170 psia
Oxidizer Inlet Pressure		170 psia

Competing Characteristics--The following major competing characteristics were considered in trading expulsion concepts:

1) Reliability;

2) Life cycle;

3) Weight;

4) Permeation;

5) Volumetric efficiency;

6) Dynamics;

7) Availability;

8) Compatibility with tankage.

Selection Rationale--A relative evaluation of expulsion methods according to the above competing characteristics is shown in Table 4.3-23. A convoluted metal diaphragm has been selected on the basis of minimum permeation, moderate weight, and fair volumetric efficiency. The positive expulsion device (convoluted metal diaphragm) requires considerable development.

4.3.4.3 Propellant Storage

On the basis of packaging requirement and compatibility with the preferred expulsion method, spherical tankage was selected. A survey of available tankage revealed that no existing tankage could satisfy the concept requirements.

4.3.4.4 Thrust Vector Control

Candidates--Three candidate concepts considered were:

1) Gimbaled main engine with roll attitude control;

TABLE 4.3-23 RELATIVE EVALUATION OF EXPULSION METHODS

Evaluation Criteria	Expulsion Concept			
	Non-Metal Diaphragm or Bladder	Metal Diaphragm or Bladder	Piston	Metal Bellows
Reliability	Good	Poor	Excellent	Good
Life Cycle	Excellent	Poor	Excellent	Good
Weight	Low	Moderate	High	High
Diffusion	High	Very Low	-	Very Low
Leakage	High	Very Low	High	Very Low
Permeation	High	Very Low	-	Very Low
Expulsion Efficiency	98%	97%	98+%	98+%
Volumetric Efficiency	Good	Fair	Poor	Poor
ΔP Variation	Low	Moderate	High	Low
Storage	Poor	Good	Poor	Good
Dynamics	Critical	Critical	Good	Questionable
Status	In use for space applications	Requires Development	In use for non-space applications	In use for space applications

2) Gimbaled midcourse engines with fixed main engine;

3) Pulsed midcourse engines with fixed main engine.

Competing Characteristics--Major competing characteristics considered were:

1) Reliability;

2) Weight;

3) Compatibility with spacecraft dynamics;

4) Previous experience.

As opposed to the gimbaling of solid motors, gimbaling of the liquid propellant engine is much more practical because of the reduced weight and size of the engine. Thrust levels are characteristically lower and hence the disturbance torques due to center-of-gravity offset and thrust misalignment are less severe. Position and rate limiting and the steady limit cycle behavior due to Coulomb friction of the actuator are factors to be considered in the autopilot design. The maintenance of center-of-gravity location is more difficult for liquid propellant engines because of uneven fuel runout from tanks. However, since orbit insertion will always involve a relatively long burn time, this effect can be compensated with lagged feedback of the gimbal position to bias the attitude error. The steady-state thrust vector pointing error can be held to no larger than the thrust alignment angular error (about $\pm$ 0.5 degrees) with this type of compensation. Large liquid engines do have the one further disadvantage that fuel slosh may produce undesired dynamic coupling. An example of an autopilot employing derived-rate compensation is shown in Figure 4.3-34. An example of the transient following engine ignition is shown in Figure 4.3-35.

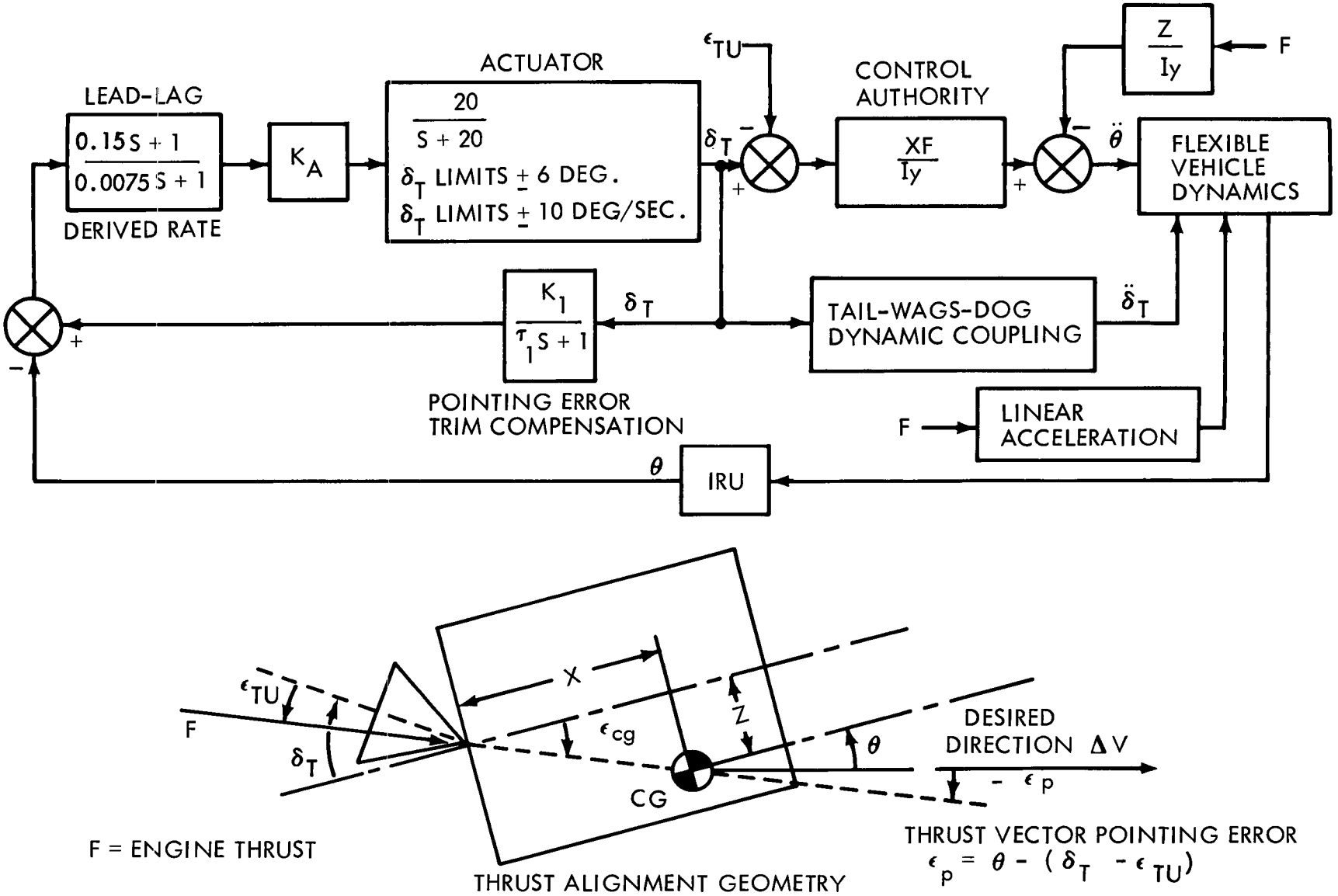

Figure 4.3-34: Gimbaled Engine TVC Autopilot—Orbit Insertion

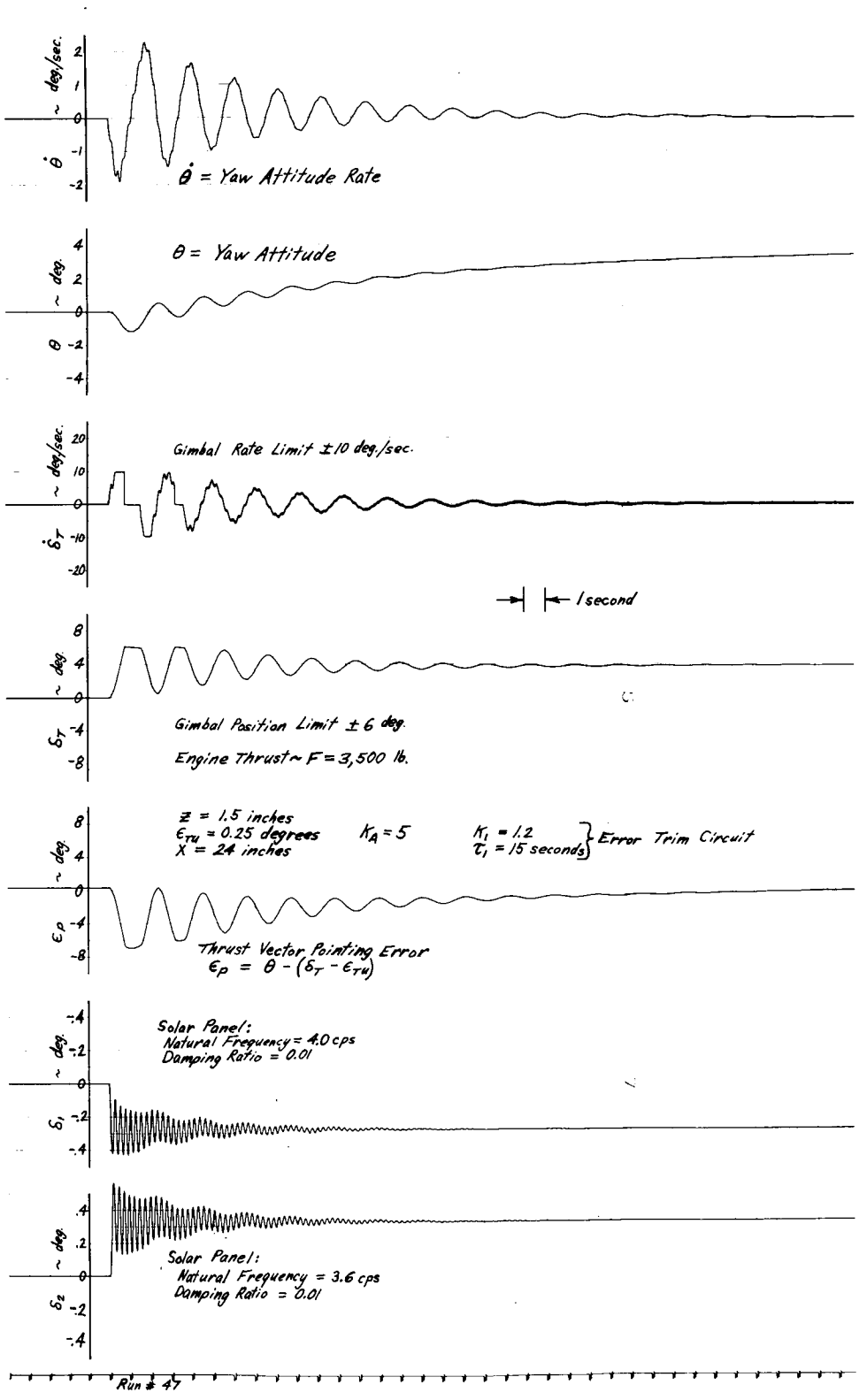

Figure 4.3-35: Start Burn Time Response Gimbaled Engine TVC — Orbit Insertion

Selection Rationale--Because spacecraft center-of-gravity was located within the engine envelope, the implementation of thrust vector control was difficult. The pulsed midcourse engine concept was rejected on the basis of reliability degradation associated with pulsing the MA-109 engines. Gimbaling the midcourse engines was rejected because of inadequate control authority.

The gimbaled main engine concept was selected on the basis of high reliability, adequate control authority, and moderate weight penalty.

4.3.4.5 Pressurization

Pressurization and pressurant concepts are similar to those considered for the monopropellant concept discussed previously in Section 4.3.3.2. The only exception is the introduction of a combination regulated-blowdown system. This latter concept utilizes propellant tank pressurant storage for midcourse and regulated pressurant for orbit insertion. Results of the pressurization trade study are shown in Figure 4.3-36. The regulated system was selected on the basis of reliability, previous experience, and constant midcourse thrust-time trace.

Pressurant trade studies considered nitrogen and helium. Although study results showed nitrogen to be 80 pounds heavier, it was selected because it provided a backup reservoir for the attitude control subsystem.

4.3.4.6 Isolation Valves

The combined squib-actuated and solenoid-actuated valve system, previously discussed for the monopropellant concept in Section 4.3.3.2, was selected.

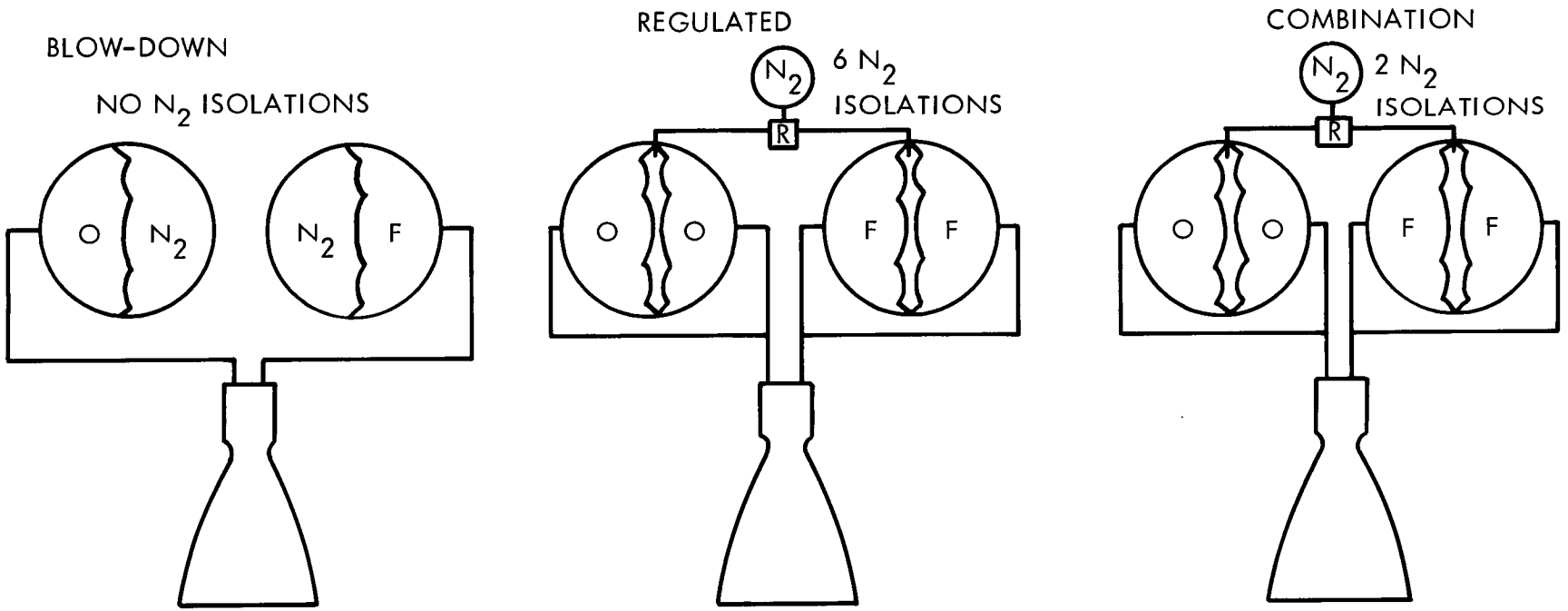

RELIABILITY	0.998	0.9992	0.9992
△WEIGHT	330 LB	0	0
VOLUME: TANK	73.5	45.8	45.8
N_2 BOTTLE	0	5.2	4.3
THRUST	DECREASING	CONSTANT	DECREASING (MIDCOURSE) CONSTANT (ORBIT INSERTION)

Figure 4.3-36: Pressurization System Trades

Because of the large number of bipropellant engines, this resulted in a large number of components and increased system complexity. Nevertheless, overall system reliability was high because of redundancy.

4.3.5 Preferred Design Selection Rationale and Problem Area Evaluation

The preliminary selection of the preferred propulsion concept was based on three key competing characteristics: reliability, velocity increment capability, and availability. The solid monopropellant concept was retained since it was the only concept that could meet the 1971 and 1973 insertion velocity requirements. Its selection as the preferred design required a careful evaluation of several potential problem areas. These can be overcome through early recognition and careful planning. These are discussed below.

In considering the selection of a solid rocket for the primary retro motor, five potential problem areas had to be evaluated:

1) The inherent inflexibility of a solid-propellant motor;
2) Two-phase flow plume with high radiosity;
3) Sterilization;
4) Swirl torques;
5) Space storability.

Inflexibility--The solid rocket motor, as proposed for the preferred concept, is a fixed-impulse device. Even with batch-to-batch variations and conditioning temperatures ranging between 30 to 100°F, in a vacuum, its total ΔV variation is not expected to exceed $\pm$ 10 meters per second. It would thus appear that only those heliocentric transfer trajectories

that provide a constant hyperbolic speed at Mars can be accommodated.

It can be shown, however, that even trajectories that result in a variable hyperbolic excess speed at Mars over the launch opportunity can also be accommodated. This is accomplished by inserting into orbit at a point different from the periapsis of the approach hyperbola and, if necessary, by thrusting in a direction not collinear with the flight path. (See Volume A, Section 3.1.4). This results in some variations in the Mars-bound orbit periapsis position, which in many cases is favorable.

Exhaust Plume--To achieve high performance from the solid motor, metal additives are cast into the propellant matrix. Therefore, during burning, metal-oxide particles are carried in the exhaust. The temperature of these particles at the nozzle exit exceeds that of the gas due to thermal lag. The radiation from the solid motor plume greatly exceeds that from the semiclear, clean exhaust of a liquid engine. Semi-empirical calculations based on characteristics derived in successfully predicting the exit-plane heating rates from the Minuteman second stage in altitude tests were used to predict the heating rates from the proposed solid motors. These analyses indicated that with the long, high-expansion-ratio nozzle proposed, the maximum solar panel temperature rise rate in the motor exist plane would not exceed 150°F per minute. This was found to be an acceptable level. However, as a safety feature the solid motor was oriented in the spacecraft with the exhaust nozzle pointed away from the Sun side of the panels. When additional data becomes available on exhaust radiation, the orientation of solid motor will be reconsidered. Reorienting the solid motor will provide for several advantages. Paramount among them is the

feasibility of using the monopropellant midcourse engine in a pulsing mode for backup thrust vector control in a manner which augments orbit insertion total impulse. To ensure the adequacy of the thermal shielding, tests should be conducted to:

1) Measure plume radiation with radiometers and thermocouples;
2) Verify their capability to predict heating rates with size effect accounted for;
3) Determine plume radiation effects.

The Prandl-Meyer expansion angle plus the nozzle half angle for the proposed motor is about 115 degrees. Therefore, some of the very low pressure exhaust products can be expected to impinge on the spacecraft. The alumina particles in the exhaust tend to follow a straight line but are subjected to trajectory variations caused by the expanding gases. The smaller particles are more easily forced to follow the gases. Figure 4.3-37 -- which is based partly on a JPL study and partly on particle limit streamlines established by a Boeing two-phase flow program -- indicates only about 0.5 percent of the particles can be expected to fall outside of a 17-degree cone emanating from the nozzle exit. Extrapolation of the data shown indicates particle sizes capable of being turned over 90 degrees might approach molecular size and the total weight of alumina will be minimal. However, to ensure against impingement of any particles on the solar panels, antenna face, or optical equipment, the solid motor was oriented away from the Sun side of the vehicle.

Sterilization--Work on sterilization of solid-propellant motors began at at the time the Surveyor program was initiated. At that time, it was

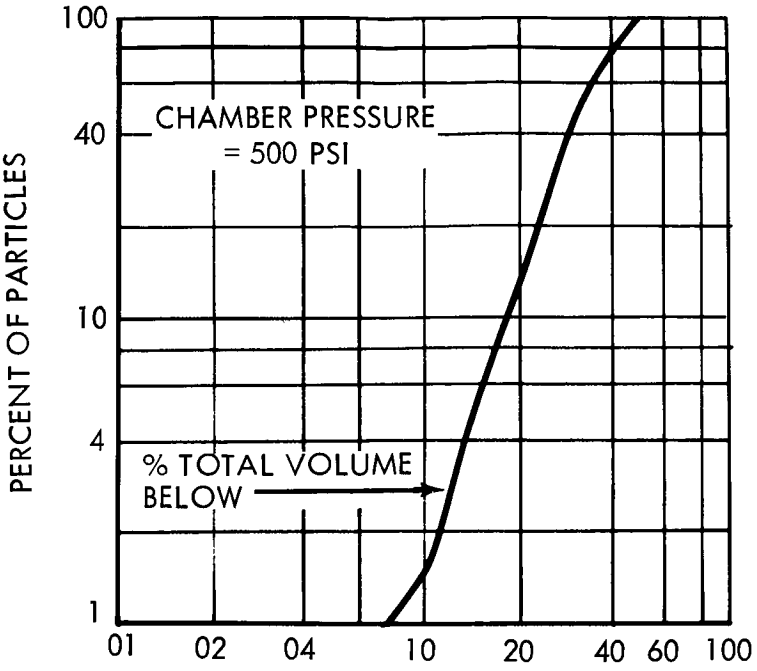

PARTICLE SIZE RANGE OF ALUMINUM OXIDE SAMPLE OBTAINED FROM MOTOR FIRINGS AT 500 psi.

NOTE: FROM ABOVE ONLY 7% OF PARTICLES HAVE RADII LESS THAN 79 μ. ALSO ONLY 7% OF MASS FLOW IS OUTSIDE STREAMLINE SHOWN BELOW. THEREFORE TOTAL PARTICLE FLOW OUTSIDE STREAMLINE = .07 X .07 X 100 = 0.49% OF THE PARTICLE MASS.

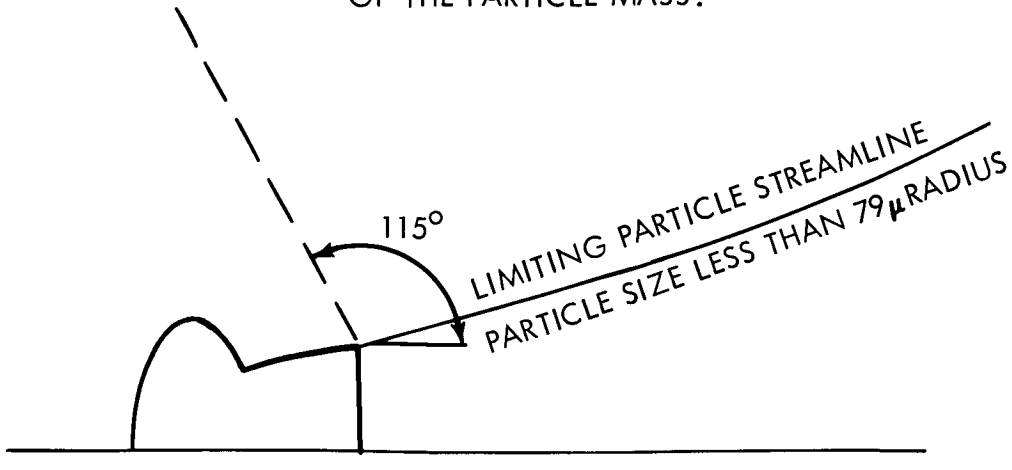

Figure 4.3-37:

intended to send a sterile package to the Moon. Although this requirement was later rescinded, work at Thiokol, Elkton, and Aerojet (Sacramento) continued. At Thiokol, the propellant type proved superior in all investigations, utilized an HA-hydrocarbon binder and an imine (MAPO) curing agent. Aerojet found a polybutadiene propellant had the thermal resistance characteristics required for heat sterilization. Also, a nonaluminized polystyrene formulation has demonstrated sterilizable characteristics. To demonstrate the effects of sterilization on the ballistic properties, Thiokol temperature aged (293^{o}F) in a nitrogen atmosphere eight TE-240 motors having a six-point star configuration and containing about 70 grams of nonaluminized propellant each. Four of these were controls and were fired unaged. The four aged motors (one at 40 hours, one at 72 hours and two at 114 hours) were then fired at 500 psi. The data from the aged motors fell exactly on the curves established for the unaged motors and indicated that aging had not affected the ballistic properties.

The primary effect of the heat cycle sterilization is a hardening of the propellant. Particularly in an oxidizing atmosphere, density changes, increased elasticity modulus, and decreased strain capability were noted. By heating in a nitrogen environment, these effects are greatly reduced. In the proposed motor bore strain is the critical structural restraint. Using the proposed propellant unsterilized, a safety factor of 2 exists between the propellant strain capability of 30^{o}F and that required. Assuming that the proposed propellant strain characteristics deteriorate in a manner proportional to that recorded on the samples, the safety factor will still exceed 1.5.

To verify the fact that thermal sterilization is effective, dry spores of bacillus subtillis var niger (B. globigii) obtained from the Wilmot Castle Company of Rochester, New York, were used to innoculate a batch of Surveyor propellant during mixing. The propellant was innoculated to a level of 0.5×10^6 spores per gram of propellant. As can be seen in Table 4.3-24, the $250^{\circ}F$ heating cycle effectively limited bacteria growth.

Table 4.3-24: VIABLE MICRO-ORGANISM ASSAY OF INNOCULATED SURVEYOR PROPELLANT

Heat ($250^{\circ}F$) Treatment	Sterility	Result*
Time	Direct	Subculture
Control	2/2	-
24 hours	4/4	-
48 hours	0/4	0/4
72 hours	0/4	0/4

*The results are recorded as the number of samples with growth per the number of samples assayed.

Three 5-inch CP test motors containing Surveyor aluminized propellant were aged for 3, 5, and 7 days at $260^{\circ}F$ and then static tested. The recorded data show the motors operated normally and reproducibly. Encouraged by these results, two full-scale motors were heated for 121 hours at $260^{\circ}F$. The first slumped, purportedly because of moisture allowed to accumulate in the chamber during previous curing. Although second appeared to have no physical defects when fired, the motor liner malfunctioned causing failure at 120 milliseconds.

Considering additional work, Aerojet is presently heat-cycle sterilizing Janaf specimens of their proposed, aluminized, polybutadiene propellant. The results of the physical properties tests will be reported during the oral presentation. Boeing is working on a company-funded program to determine the effect of chamber environment on the survivability of various organisms. Samples of propellant will be innoculated with live spores of various specii, cast into a scale motor and fired. Small samples of the exhaust will be captured aseptically and the contents analyzed.

In conclusion, although the only static firing of a heat-aged aluminized full-scale motor was a failure, the following indicate that heat cycle sterilization can be accomplished:

1) Nonaluminized propellants have been heat cycled and static tested with no apparent ballistic property changes;
2) Physical property changes can be minimized by sterilizing in an inert atmosphere;
3) Scale motors with aluminized propellant have been heat aged at 260°F for several days and successfully tested;
4) Aerojet has recently heat cycled (3 cycles to 294°F) samples of an aluminized polybutadiene propellant with little apparent effect on the propellant. (However, it has not yet been static tested.)

Early in the program a vigorous effort should be made to demonstrate the sterilization capabilities of an aluminized propellant solid motor. Following subscale demonstration, several of the full-scale PFRT motors should be sterilized before static firing.

Swirl Torques--Large roll moments were reported on one of the Surveyor motor tests. However, analyses of the data by the Surveyor contractor indicated these forces may have been caused by instrumentation anomalies. Future Surveyor tests will be monitored for further swirl torque information. At least one of the Voyager motors should be instrumented to determine the value of any swirl torques.

Space Storage--The flight of the Voyager vehicle from initial Earth orbit to ignition of the propulsion system will constitute a storage period in space of 7 to 8 months. The potential hazards known to exist in outer space include ionizing radiation of all types, micrometeoroids, solar thermal radiation, and hard vacuum. The motor is shielded by the spacecraft from micrometeoroids and intense thermal radiation protection is provided. Therefore, only hard vacuum and radiation are considered.

Radiation--The principal sources of ionizing radiation which the Voyager will encounter in space include solar flares, primary cosmic rays, Van Allen belt and similar radiation belts around Mars. Two series of experiments were conducted at the Jet Propulsion Laboratory and Battelle Memorial Institute to determine the effects of radiation on propellants with various binder systems. These data show that all of the propellants tested were able to absorb a dose of 10^6 rad with negligible change in mechanical or ballistic properties. A 1-year exposure in the Van Allen belts would be required to accumulate this dosage. Therefore, this is a strong indication that radiation problems will not be severe.

Hard Vacuum--The most notable effect of vacuum storage is a hardening of the propellant due to loss of volatiles. The propellant will be

hermetically sealed from space by a diaphragm at the throat. Inside the propellant bore molecules are emitted until an equilibrium number are present. At this condition, some molecules are emitted from the surface and at the same time other molecules are striking and condensing. Therefore, a pressure equal to the vapor pressure of the species will be established in the motor. In the case of a semi-sealed system in which the mean free path of a molecule is large in relation to the size of the opening, escape of molecules from the system will be minimized and the system weight loss will be negligible.

On the basis of tests, Battelle concluded, "The effects of vacuum on mechanical and burning properties of the PBAA propellant after ten months are great enough to be statistically significant and instructive, but not great enough to represent appreciable degradation of the propellant."

It is recommended that additional research combining the radiation and hard vacuum effects on propellant properties be conducted on samples.

4.4 ALTERNATE ENGINEERING MECHANICS

Alternate design methods and designs were evaluated for the following engineering mechanics subsystems and disciplines:

1) Temperature control subsystem;

2) Packaging and cabling,

3) Structure subsystem;

4) Mechanisms subsystems; and

5) Pyrotechnics subsystem.

These designs and methods are discussed in detail in each of the following sections and the rationale leading to selection of the preferred design is indicated.

Materials applicable to the studies conducted are summarized in document D2-82734-1, "Materials and Processes for Voyager--Phase IA".

4.4.1 Temperature Control Subsystem

Summary--Temperature control is handled by treating separately the following four categories of equipment: internal equipment, external equipment, propulsion module, and planet scan platform. The preferred system uses conventional louvers to maintain the internal equipment within a 30°F band while dissipating electronic heat loads from 238 to 377 watts. The propulsion module and the planet scan platform also use conventional louvers to maintain control. Limits of 40° to 90°F are maintained in the propulsion module during early mission phases. The scan platform has varying requirements, depending on the science load and position in orbit. Small external equipment has solar shields and insulation. Equipment support booms use low emittance polished surfaces ($\epsilon \cong .05$).

Trades were made for each of the four categories of equipment. The logic for evaluating the concepts is shown in Figure 4.4-1. The criteria by which specific concepts were selected are:

1) Reliability;
2) Development status;
3) Weight; and
4) Off-design performance

Internal Equipment--Completely passive concepts would not provide adequate temperature control for internal equipment because of:

1) Inefficient adiabatic interfaces (inflight configuration changes);
2) Programmed heat load changes (238 to 377 watts);
3) Spacecraft maneuvers (off Sun for 50 minutes near Earth); and

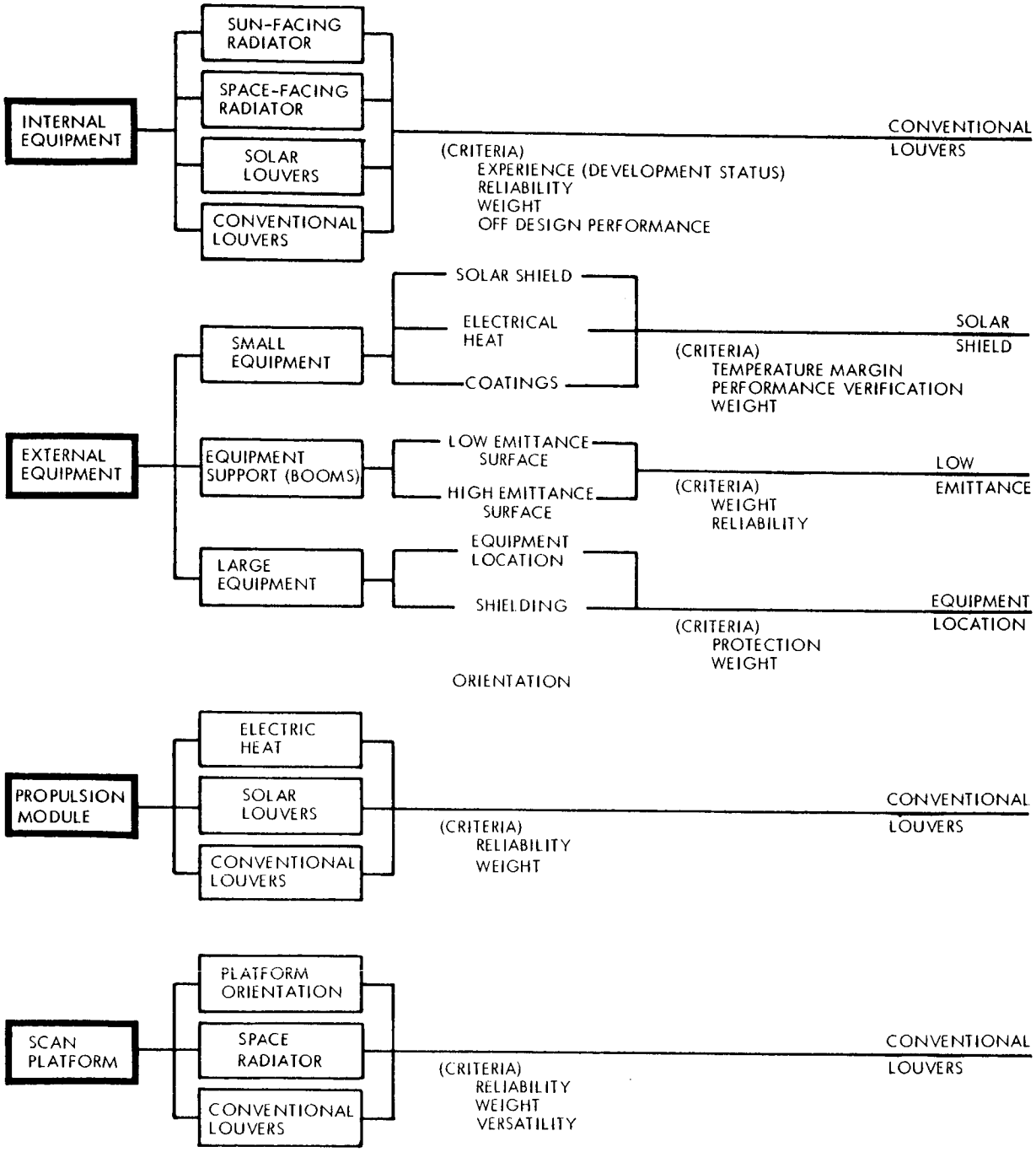

Figure 4.4-1: Temperature Control Subsystem: Logic Diagram

4) Variable solar intensity (130 to 47 watts per square foot).

Therefore, only semiactive and active concepts were evaluated.

The candidate approaches were Sun-facing radiator, space-facing radiator, solar louvers, and conventional louvers. The conventional louver concept was selected because:

1) Components have been flight proven on spacecraft such as Nimbus, Pegasus, Mariner II, Mariner IV, and Ranger.
2) The reliability of 0.996 meets the allocation (0.996)
3) Its off-design performance is equal or superior to the other concepts.

Solar louvers were eliminated because they have not been developed adequately at this time.

External Equipment--This category is composed of several unrelated equipment items. It was, therefore, divided into groups based on common thermal requirements.

Small Equipment (Independently-Mounted Sensors)--From the candidate temperature control approaches of solar shield, electric heat, and coating, the solar-shield approach was selected. This approach generally offers the highest reliability (0.999938) at a comparable weight.

Equipment Support (Booms)--A polished surface with emittance $\epsilon \tilde{=} 0.05$ was preferred over a black coating for the magnetometer and low-gain

and high-gain antenna booms because deflections are held to a minimum. With an α/ϵ of 2.7 for polished aluminum equilibrium temperatures of the booms are approximately 120°F higher than with a gray or black surface.

Large Equipment (Solar Panels and High-Gain Antenna) -- The exhaust plume of the solid orbit-insertion engine places a thermal load on the solar panels and high-gain antenna. Of the two approaches considered for reducing this load, shielding and direction of the exhaust plume, the latter was selected. By directing the thrust of the solid motor in the direction away from the Sun, the maximum heat rate at the solar panel was reduced approximately 73 percent over than encountered with the engine exhausting in the opposite direction. Shielding was rejected on the basis of a 100-pound weight penalty.

Propulsion Module--Temperature control based on solar louvers, electric heaters, or conventional louvers were the candidates considered. Since the other approaches provided no reliability or weight advantage, space-proven conventional louvers were selected.

Planet Scan Platform--Temperature control was investigated with respect to platform orientation, electric heater, and conventional louvers. Space-proven conventional louvers are preferred because of experience and versatility.

4.4.1.1 Internal Equipment

Internal equipment includes the package assemblies for telecommunications, attitude control, guidance and navigation, power and science payload (except for scan platform). Design temperature limits are established in Section 3.0 of Volume A for the individual components. However, to ensure adequate margins for thermal control during large variations in equipment heat loads (238 to 377 watts), a narrower control range was established. Table 4.4-1 is a partial list of the critical components in the internal equipment category. On the basis of the design temperature limits shown, a temperature control range of 50^{o} to 80^{o}F was selected. These temperature limits are used in a later section as a criterion against which the performance of alternate thermal control concepts can be judged.

The concepts considered for temperature control of internal equipment, identified by the dominant component, are:

1) Space-facing radiator;
2) Sun-facing radiator;
3) Solar louvers; and
4) Conventional louvers.

Schematics and functional flow diagrams are shown for each concept in Figure 4.4-2. The specific techniques used with each concept are shown in Table 4.4-2.

Table 4.4-1: PARTIAL LIST OF INTERNAL COMPONENTS TEMPERATURE LIMITS

Subsystem	Component	Operating Temperature Limits Min. °F	Max. °F	Max. Rate °F/min.	Dormant Temperature Limits Min. °F	Max. °F
Telecommunication	Telemetry	40	85	2	-13	167
	Data Storage	40	85	2	-13	122
	TWT	40	113	2	-13	185
	Transmitter	40	113	2		
	Receiver	40	113	2		
Science	UV Spectrometer	14	104	3.6	-22	140
	Electronics	40	85	10	-15	167
Power	Battery	40	110		14	110
	DC/DC Regulator	40	113		-13	185
Guidance	IRU	30	131		30	131
	Gyros	178	182			
	Canopus Sensor	-30	100		-30	125
	CC&S	40	113		0	185

Table 4.4-2: COMPONENT BREAKDOWN

Space-Facing Radiator	Sun-Facing Radiator	Solar Louver	Conventional Louver
Radiator Plate	Radiator Plate	Radiator Plate	Radiator Plate
Thermal Shield	Thermal Shield	Thermal Shield	Thermal Shield
Insulation	Insulation	Insulation	Insulation
Joint Filler	Joint Filler	Joint Filler	Joint Filler
Environmentally Insensitive Coatings	Low α/ε Coating	Lower α/ε Coating	Environmentally Insensitive Coatings
Solar Shield		Solar Shield	Solar Shield
		Solar Louver Assemblies	Conventional Louver Assemblies

In the space-facing radiator concept, heat dissipated in electronic assemblies is rejected directly to space from the radiator. A coating with high emittance is used on the surface. The efficiency of the radiator is dependent on its view factors to space. Solar panels, high-gain antenna or the capsule in the proximity of the radiator plate can decrease the efficiency by as much as 30 percent. The heat gain and heat loss from the system are controlled with insulation. In this concept, equilibrium temperatures are primarily a function of power level, whereas transient temperatures depend on the thermal inertia. Thermal inertia is a function of the equipment mass and the thermal coupling between other equipment packages.

In the Sun-facing radiator concept, advantage is taken of the external heat loads to establish equilibrium temperatures at the desired value.

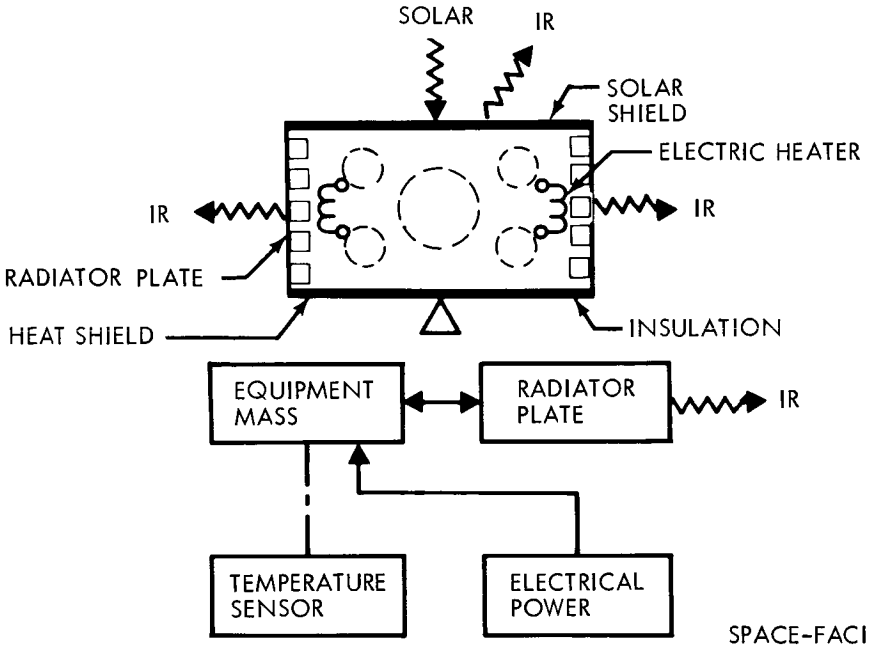

SPACE-FACIN

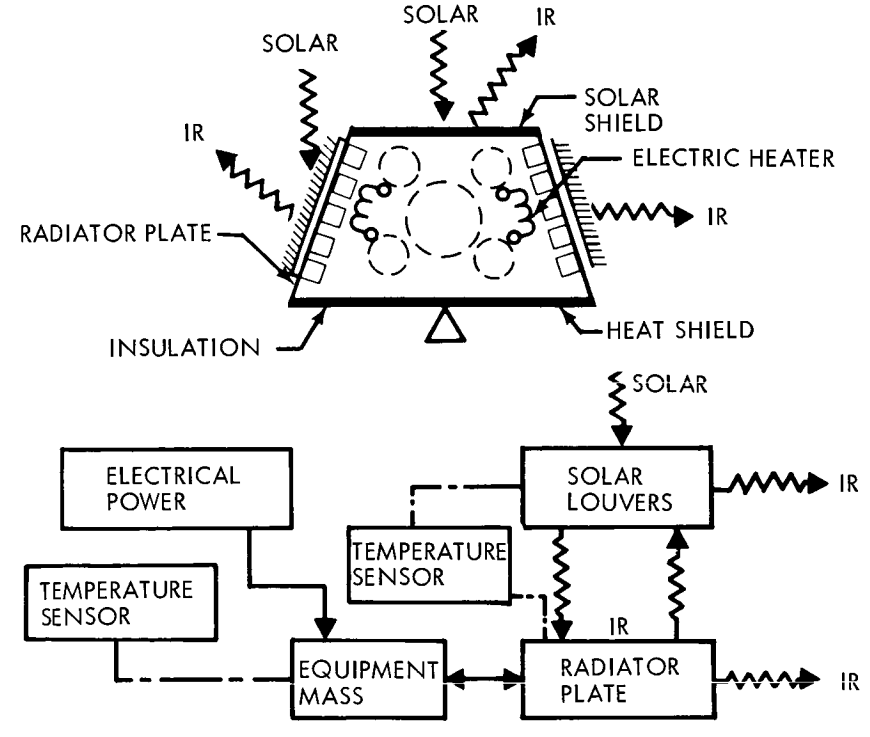

SOL

Figu

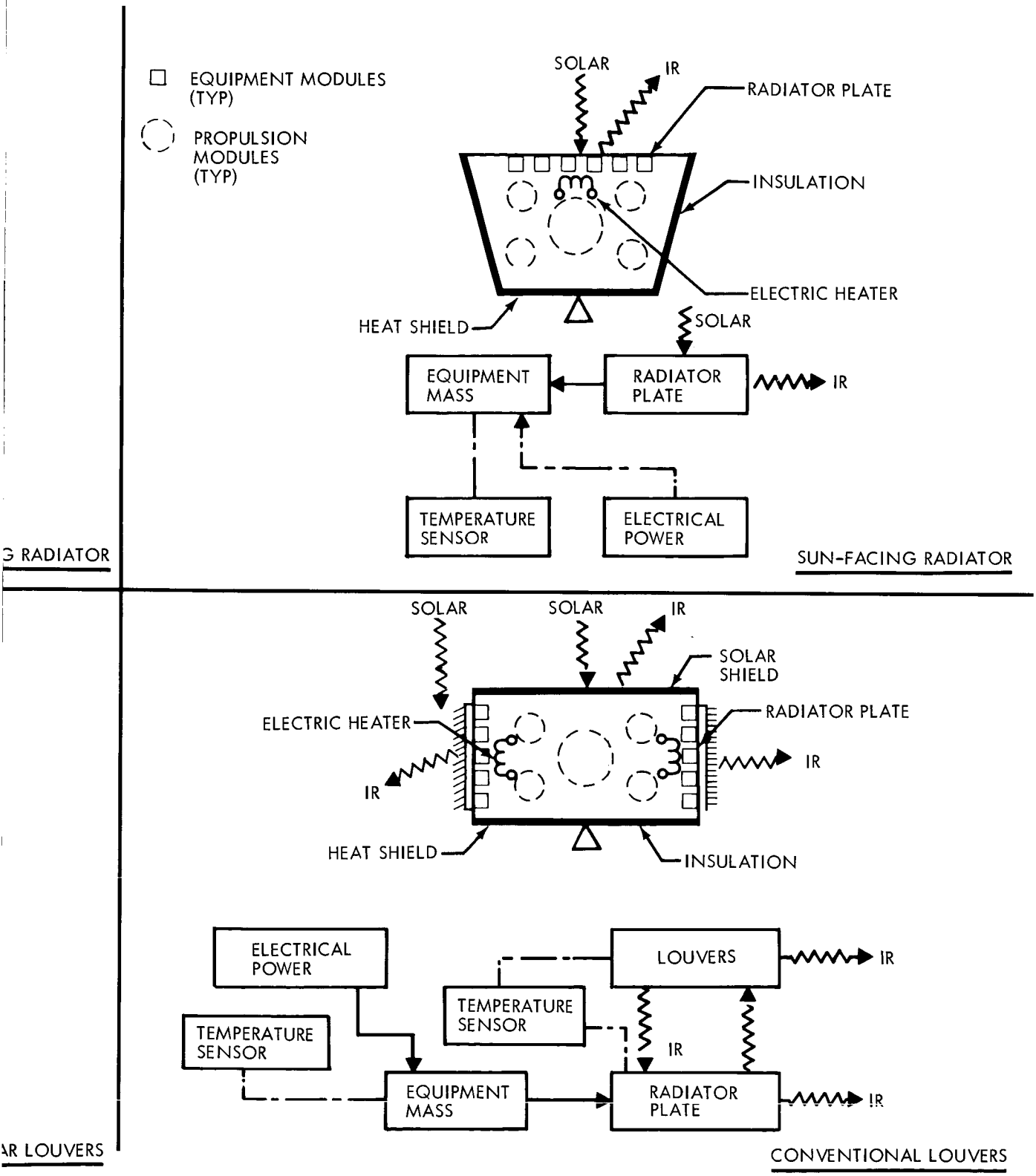

e 4.4-2: Schematic and Functional Block Diagram Internal Equipment Concepts

Consequently, internal power fluctuations become secondary. This is the approach that was used on Lunar Orbiter. The desired temperature is established by a selected thermal-control coating on the radiator plate. Extraneous heat leaks are limited by enveloping the remainder of the spacecraft in a thermal shroud. In this concept, the transient temperature response is also entirely dependent upon the thermal inertia achieved by close coupling between equipment packages.

In the solar-louver concept, the principle of external-heat-load temperature stabilization is combined with the modulation provided by louvers. Louver assemblies, mounted on the equipment radiator inclined to the Sun-line, are set to absorb solar energy inversely proportional to the internal power level. To obtain favorable response characteristics, the louver blades are limited in movement so that the angle of solar incidence is between 0 and 90 degrees.

In the conventional-louver concept, the equipment temperatures are dependent on the internal power levels. The louvers act as a variable-emittance control compensating for changing internal and external heat loads. The louver assembly consists of a number of blades individually actuated by spirally wound, bimetallic elements that sense (by radiation) the temperature of the radiator plate directly beneath them. Surface coatings and coupling of internal equipment packages are used to obtain temperature performance during transient conditions.

The temperature control concepts described above are compared on the basis of experience, reliability, weight, and off-design performance.

Experience--The confidence associated with any of the concepts can be related to the development status of the component parts. Table 4.4-3 lists the development status, in decreasing order, of each concept.

Table 4.4-3: DEVELOPMENT STATUS OF THE TEMPERATURE CONTROL CONCEPTS

Rank	Concept	Development Status	Program
1	Conventional Louvers	Operational	Nimbus, Pegasus, Mariner II, Mariner IV, Ranger (Pioneer, OGO)
2	Space-Facing Radiator	Operational	Mariner, Explorers, OSO
3	Sun-Facing Radiator	Test	Lunar Orbiter
4	Solar Louvers	Conceptual	--

Reliability--The alternate concepts can be characterized on the basis of reliability in two ways:

1) Reliability of temperature control function with respect to design temperature limits;

2) Reliability of temperature control function with respect to desired temperature control range (50° to 80°F).

Table 4.4-4 presents the results of a reliability appraisal of the alternate temperature control concepts with respect to 1) and 2), above. To meet the requirement of 2), the space-facing radiator concept must add automatic electric heat control and the Sun-facing radiator concept depends on attitude control of the spacecraft.

Table 4.4-4: RELIABILITY APPRAISAL OF ALTERNATE INTERNAL EQUIPMENT TEMPERATURE CONTROL CONCEPTS

Concept	Reliability Appraisal	
	Design Limits	50° to 80° F Limits
Space-facing radiator	0.9999	0.9977
Sun-facing radiator	0.9999	0.9950
Conventional Louvers	0.9960	0.9960
Solar Louvers	0.9921	0.9921

Figure 4.4-3 shows the comparison of the temperature profiles versus time for all concepts. The solar and conventional louver concepts easily meet the desired temperature performance (50° to 80°F) during the majority of the mission. However, without augmentation the space-facing and Sun-facing radiator concepts are only able to meet the extreme limits of the equipment.

Weight--The desired temperature control range of 50°F to 80°F was used as a basis to obtain an overall weight comparison between the concepts. The weight is a function of radiator area, louver area, and the heater power penalty. Figure 4.4-4 is a comparison of radiator and louver area (weight) versus internal power, assuming a mean temperature of 65°F.

To keep temperatures within the 50° to 80°F control range stipulated for maximum reliability and margin, electric heat must be added to the space radiator concept. The heater power penalty weight for this concept is 47 pounds. This value is based on the maximum power dissipated of 1350

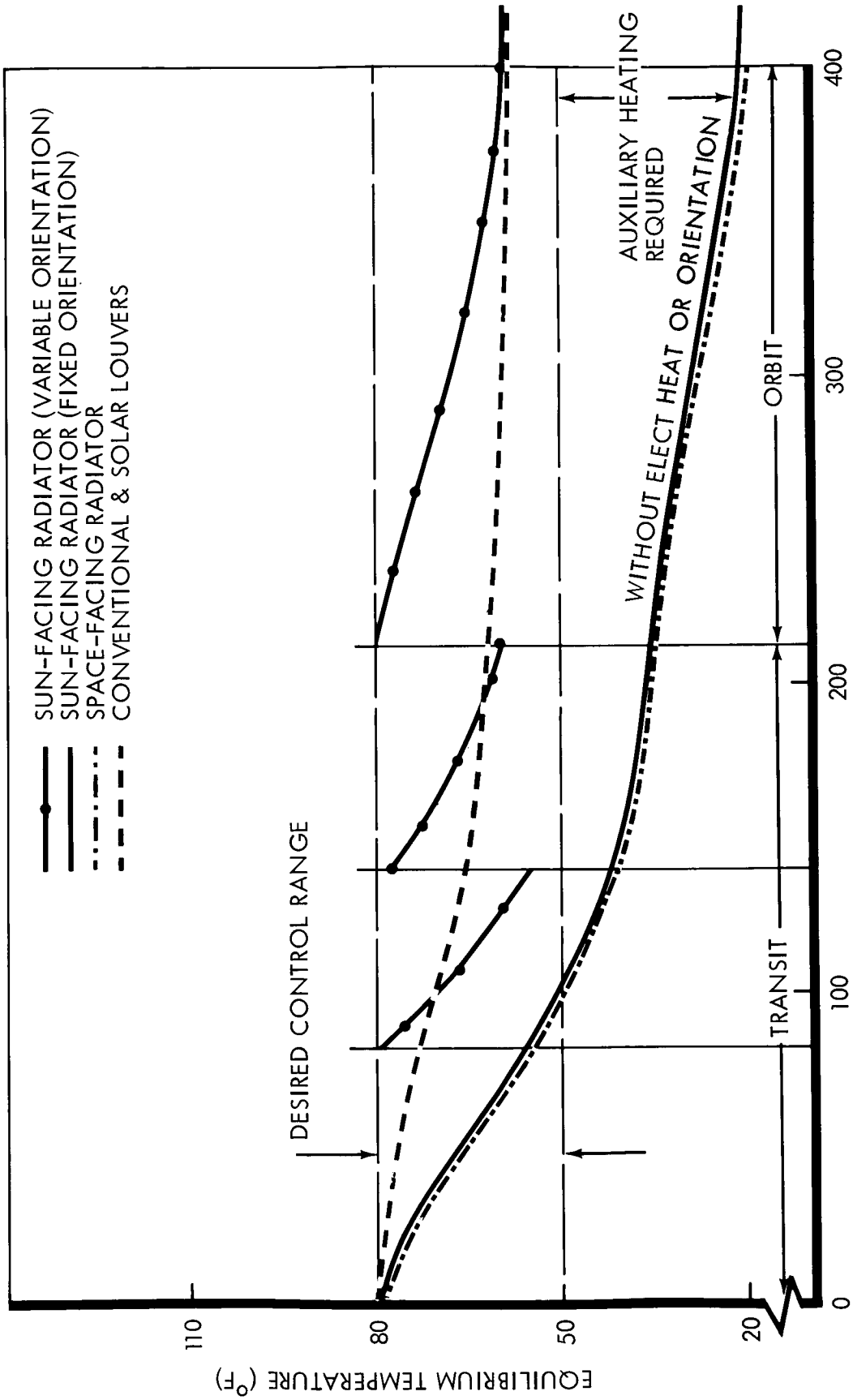

Figure 4.4-3: Steady-State Temperature Performance

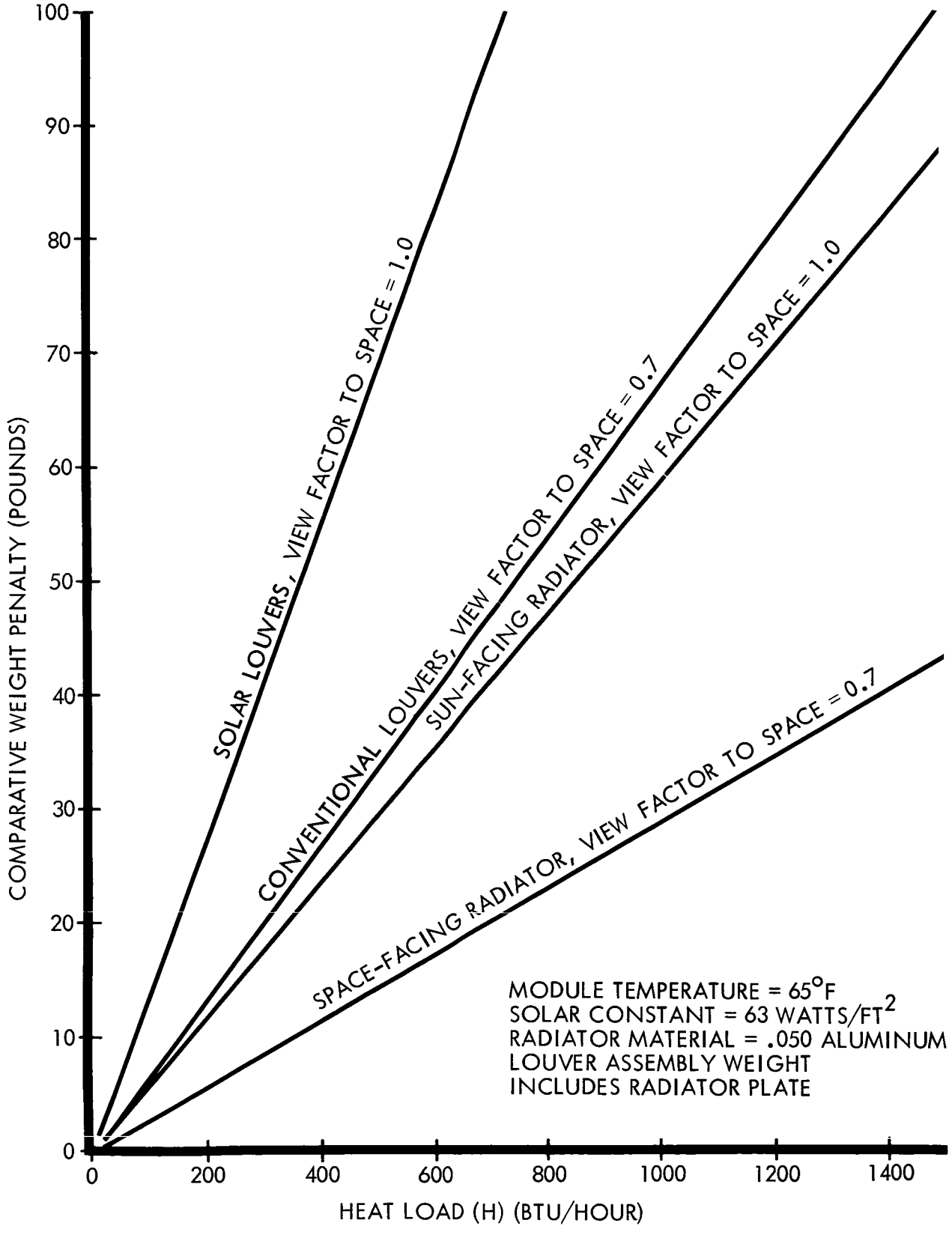

Figure 4.4-4: Temperature Control Concept Weight Penalty

Btu/hr, T_{min} = 50°F (50° to 80°F control range), and a weight penalty for the solar panels of 0.625 pounds per watt. Table 4.4-5 summarizes the weight penalty for the four concepts.

Table 4.4-5

Concept	Weight Penalty
Space-facing radiator	85
Sun-facing radiator	76
Solar louvers	180
Conventional louvers	88

Off-Design Performance--To ensure that temperature margins are adequate for all components, it is essential that the performance of all alternates be considered with respect to off-design conditions and uncertainties. Off-design conditions are represented by external environment transients, power failures, temperature control failures, and material and performance deviations. The temperature response, $\Delta T/\Delta \tau$, of each concept during transient external conditions is illustrated in Figure 4.4-5. The capability of the louvers to adjust to variable conditions results in the lowest $\Delta T/\Delta \tau$ for these concepts. Hence, for the case of transient external conditions, louvers provide a substantial degree of damping to the response generated by the thermal forcing function.

The space-facing radiator concept is dependent on design power levels. Deviation from specified power levels or local failure of heat dissipating components directly influences the temperature of the assembly. The Sun-facing radiator concept is subject to the greatest uncertainty, since

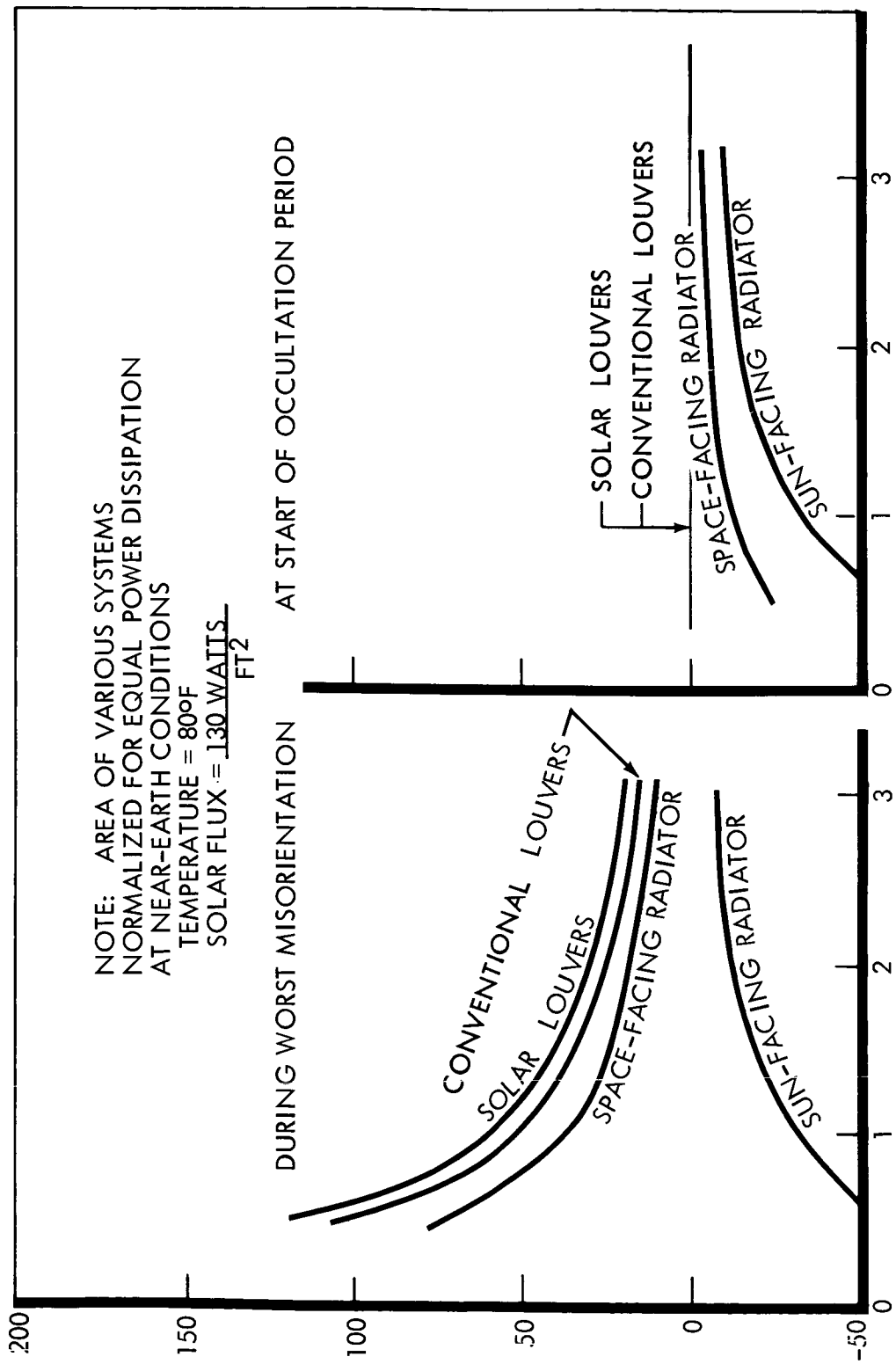

Figure 4.4-5: Internal Equipment Temperature Change Rate Comparison

thermal balance of this system is dependent on the α/ε of the radiator coating. The absorptance properties of the coating may be subject to considerable uncertainty as indicated in Figure 4.4-6. For instance, at the time Voyager reacher Mars, the "best estimate" shows a $\Delta\alpha$ of .14 corresponding to an 84 percent loss of design margin. The uncertainty of the estimate requires a design capable of encompassing 60 to 125 percent loss in design margin. Similarly, solar louvers depend on the reflective properties of the blades and are subject to uncertainties in surface degradation.

Although power failures have an effect on the conventional louver performance, their modulating characteristic will usually compensate for this variation. A failure of more concern is that of a single louver blade. Figure 4.4-7 shows temperature-control degradation as a function of the number of blade failures. Because the louver blades are independently actuated, louver assemblies are inherently redundant and provide a greater probability of temperature control subsystem success than a totally passive system.

Justification of Selected Concept--The conventional louver concept is preferred for temperature control of the internal equipment. The strongest factors that favor this concept are its operational development status and its proven reliability. Conventional louvers are an accepted thermal control approach and have been space-proven on Nimbus, Pegasus, Mariner II, Mariner IV and Ranger spacecraft. Conventional louvers are capable of providing temperature control within the narrow range (50° to 80°F) established for components with temperature-dependent failure rates.

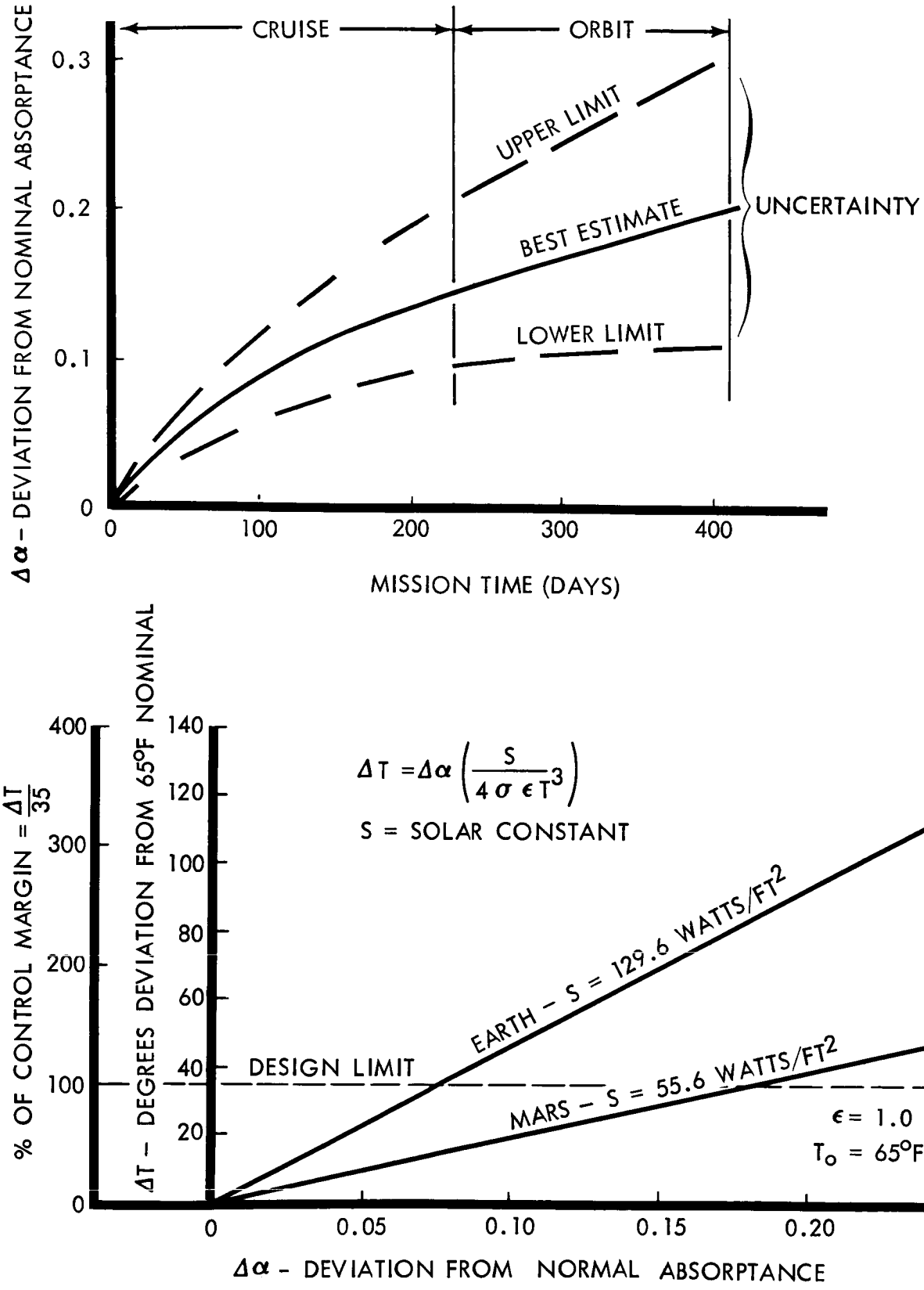

Figure 4.4-6: Coating Absorptance Degradation — Effect of Absorptance Variations on Temperature

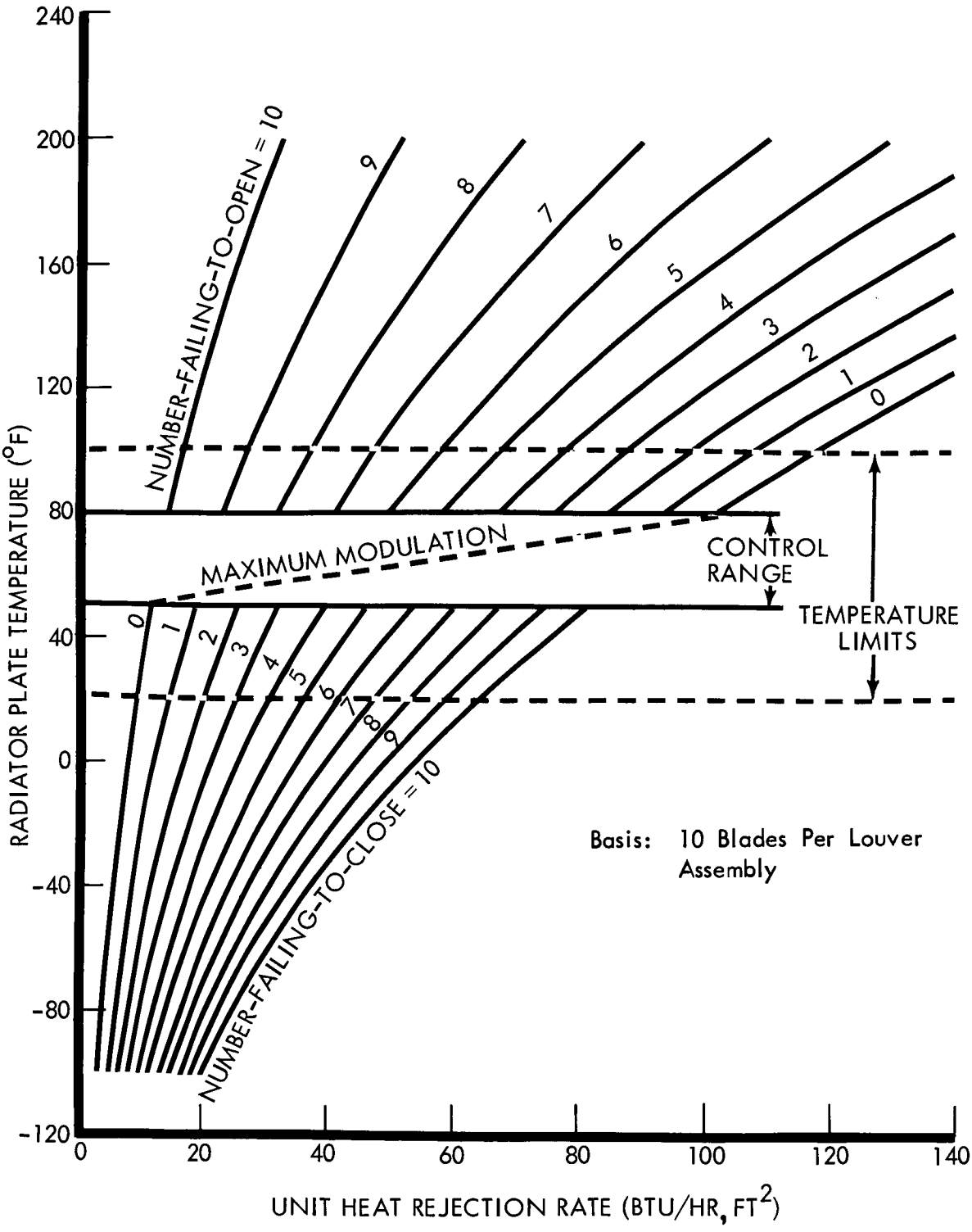

Figure 4.4-7: Conventional Louver– Failed-Blade Performance

The modulation capability affords the greatest compensation for off-design internal and external conditions and uncertainties. The inherent redundancy of a multiple blade louver assembly provides high reliability. As shown in Table 4.4-5, conventional louvers are comparable with the other concepts on the basis of weight.

4.4.1.2 External Equipment

External equipment includes small, independently-mounted reference sensors, equipment support (booms), solar panels and antennas. Table 4.4-6 is a list of representative equipment included in this category and the temperature limits.

Table 4.4-6

	T_{min} (°F)	T_{max} (°F)	Classification
High-Gain Antenna	0	167	Large Equipment
Solar Panels	-250	+175	Large Equipment
Ionization Chamber	- 22	158	Small Equipment
Trapped Radiation Detector	14	132	Small Equipment
Helium Magnetometer	14	132	Small Equipment
Magnetometer Boom	-175	+300	Equipment Support (Booms)
High-Gain Antenna Boom	-175	+300	Equipment Support (Booms)

Based upon the temperature requirements, this group has been subdivided into: Large Equipment, Small Equipment, and Equipment Support. These classifications are such that the components within a group lend themselves to a single thermal control treatment.

This equipment all protrudes from the main bus structure. Therefore, it is subject not only to the solar, planetary albedo and emission environments described in Section 2.0 of Volume A, but also to heating from the orbit insertion engine exhaust plume.

Large Equipment--This group includes the solar panels and the high-gain antenna. Effects of normal mission environments are not critical, require no trades, and are described in Section 4.4.1 of Volume A. The heating effect of the solid-propellant orbit-insertion engine is considered in this section. The two concepts considered were the engine oriented in the two directions along the Z axis of the space-craft. Shields were evaluated for each of the two concepts. The shields are shown in Figure 4.4-8. The evaluation criteria are weight and protection afforded to the solar panels and antenna.

To determine solar panel and antenna temperatures resulting from the exhaust-plume emission, the following preparatory analyses were completed:

1) Particle temperature and distribution using the two-phase flow computer program (used data from Burner II engine);
2) Exhaust-plume incremental radiosity based on similarity to a detailed study on Minuteman exhaust-plume;
3) Radiation view factors using the Boeing Monte Carlo Direct View Factor Computer Program.

These analyses resulted in a description of the exhaust-plume in terms of geometry and thermal characteristics, and view factors to solar panels and antenna.

Figure 4.4-9 shows the view factors calculated from the plume to the solar panels for various configurations considered. This geometric study clearly demonstrated that there was much to be gained by locating

Figure 4.4-8: Typical Shielding Concepts

the engine such that the exhaust was directed away from the sun-facing side of the spacecraft (+Z axis) and thus was the greatest distance from the external equipment (see Configurations 3, 4, 5, Figure 4.4-9).

Figures 4.4-10 and 4.4-11 show the temperature-time traces for the solar panels and antenna based on engine orientation only. The small insert on the figure shows radial distribution of the temperature normalized to any maximum. The solar-panel temperatures were based on the results of radiosities calculated by similarity to the Minuteman study and are designated V-I and V-II in the figure. These curves correspond to nozzle expansion ratios of 30 (nozzle length of 23 inches) and 75 (nozzle length of 35 inches). These characteristics encompass the solid engines considered for Voyager.

The results indicate that only engines with high expansion ratios produce heating rates compatible with solar-panel requirements (+175°F). The antenna proves to be no problem, since during engine operation the highly reflective backside will be displayed toward the exhaust plume.

The shield concepts shown in Figure 4.4-8 each weigh slightly under 100 pounds. Figure 4.4-12 shows the potential gain in temperature margin to be achieved by the use of shields. The shields for the engine oriented in either direction reduces the heating rates on the solar panels such that either solid engine can be used.

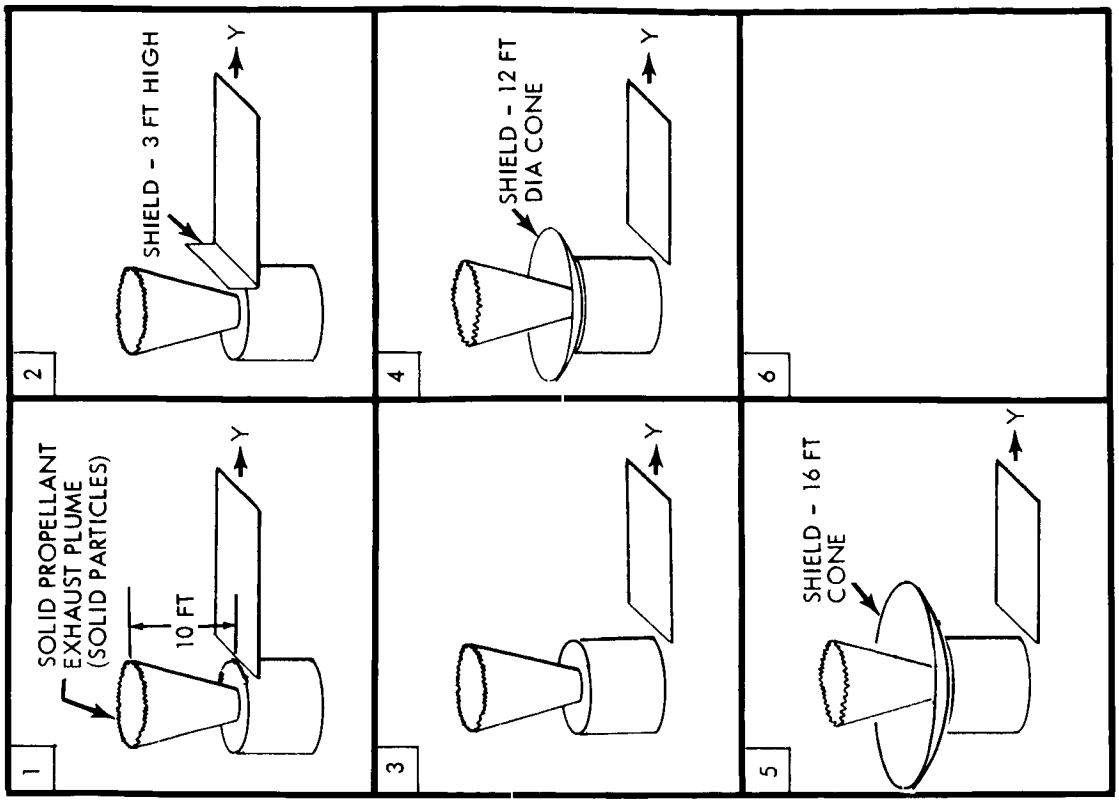

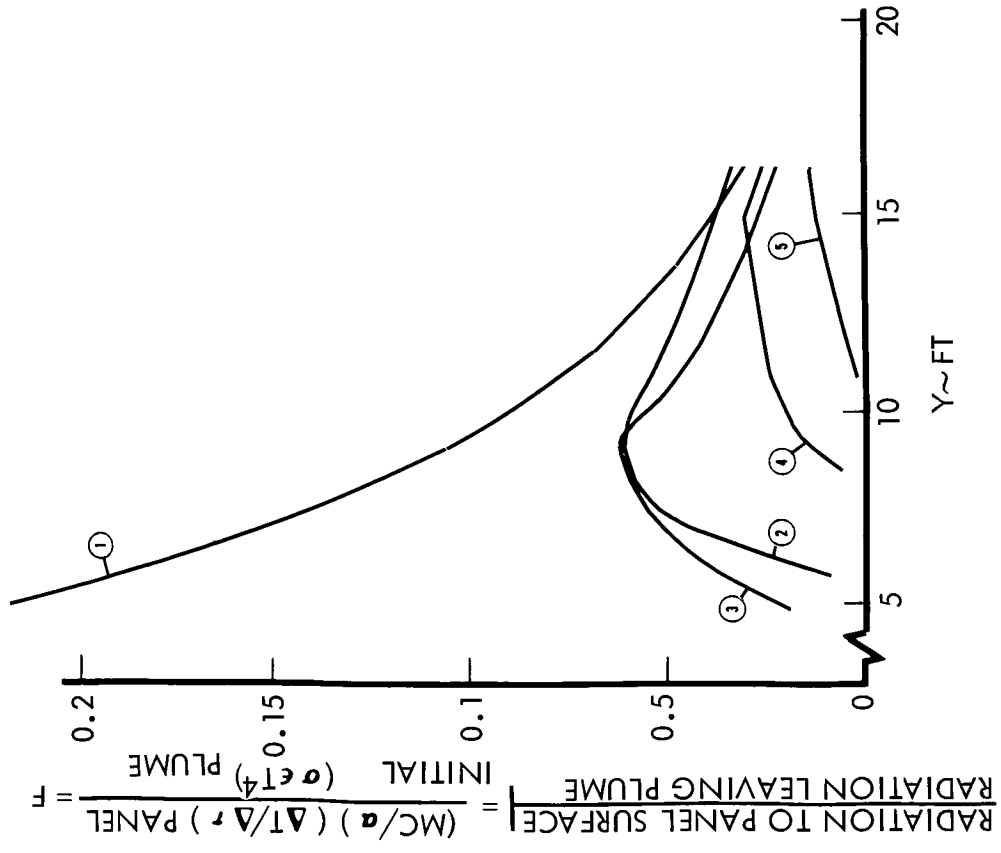

Figure 4.4-9: Solar Panel Exhaust – Plume View Factors

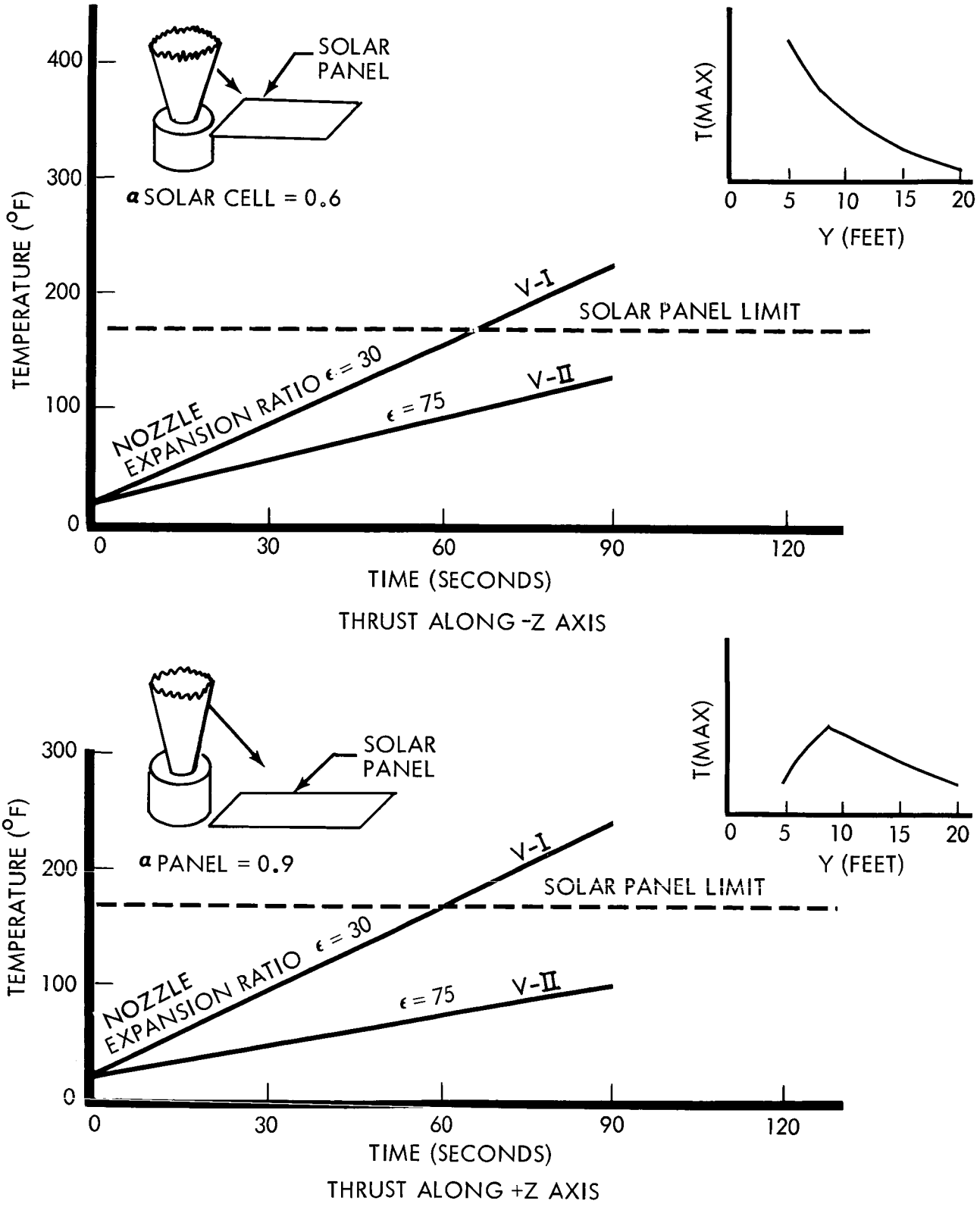

Figure 4.4-10: Solar Panel Transient Temperature Without Shields

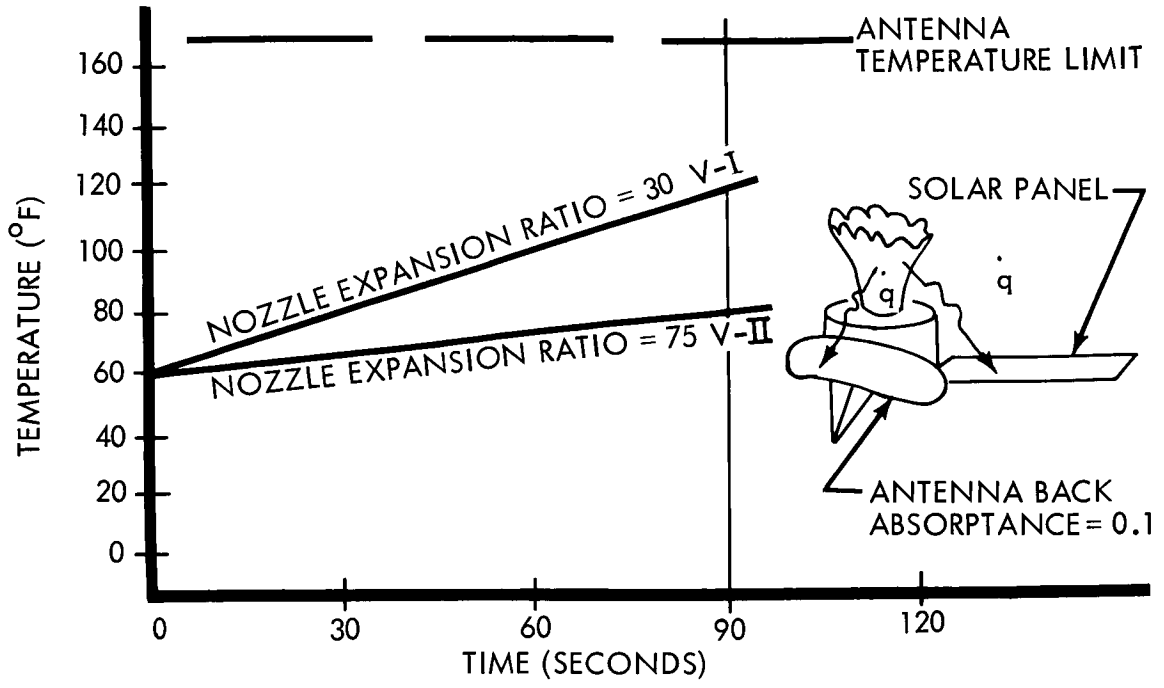

THRUST ALONG -Z AXIS

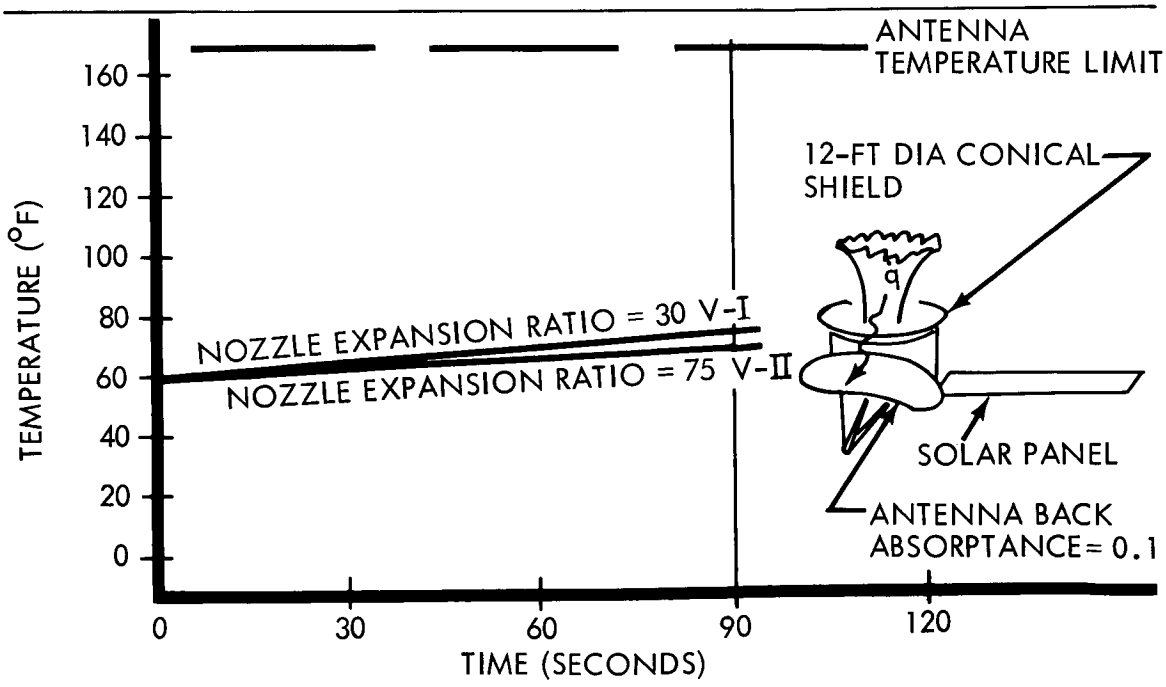

THRUST ALONG +Z AXIS

Figure 4.4-11: High-Gain Antenna Transient Temperatures

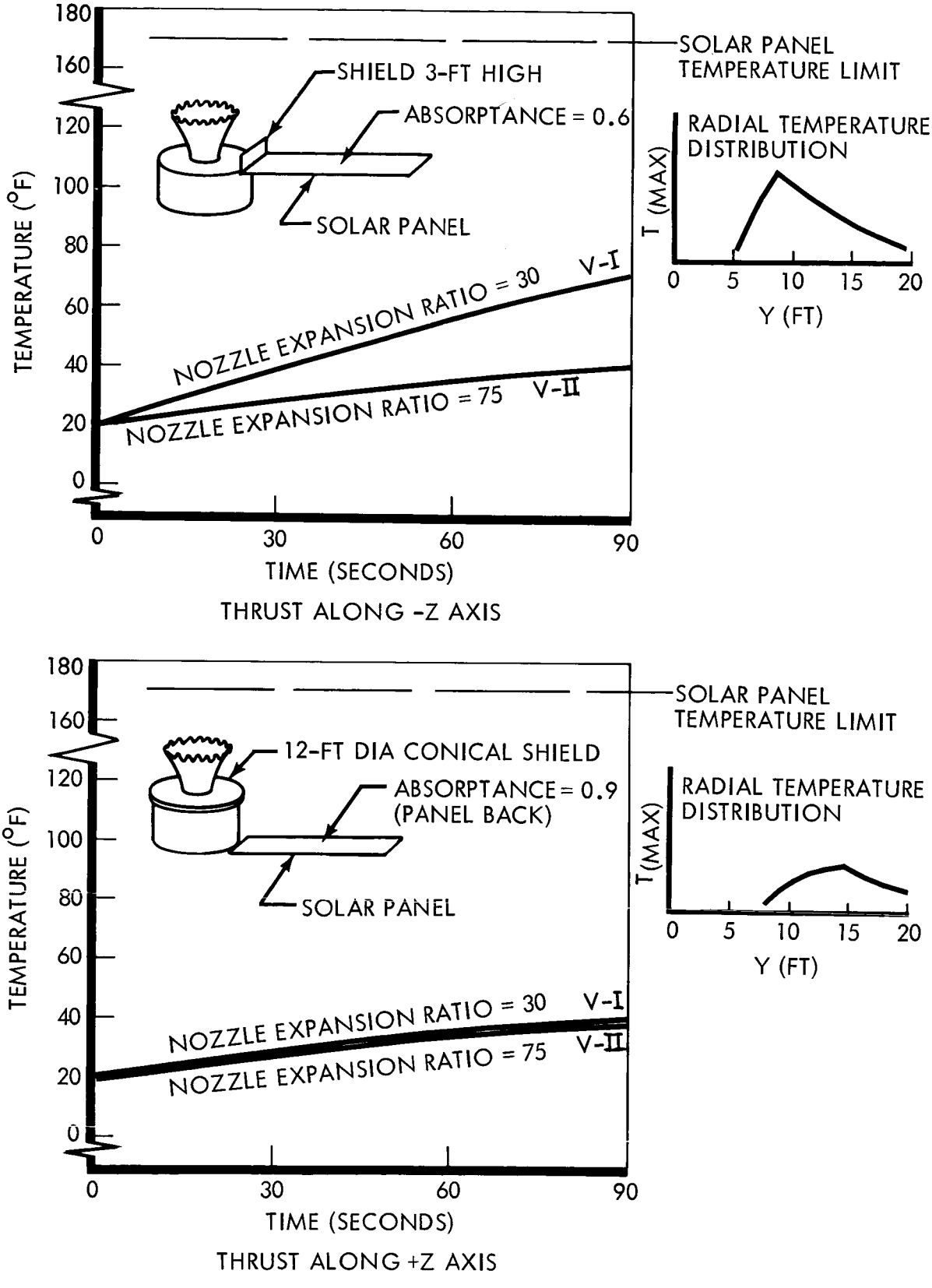

Figure 4.4-12: Solar-Panel Transient Temperature (With Shields)

On the basis of the above data, the solid-propellant orbit-insertion engine was located with the thrust line along the +Z axis. With the selection on propulsion considerations of an engine with a large expansion-ratio, the solar panels have a temperature margin of 90°F without a heat shield. Therefore, the heat shield was not required.

Small Equipment--Included are the magnetometer, low-gain antenna head, actuator motors, and remote science sensors. Two alternate concepts considered were solar shields and coating. These are characterized as follows:

Solar Shield	Coating
Black Solar Shield	Selected α/ε coating
Insulation	Insulation
	Electric heater element

In the first approach, the solar shield reduces the effect of variable solar flux while the insulation restricts the heat lost to space and damps transient effects. In the coating approach, the operation is similar, except that a selected α/ε coating is used on the Sun-side surface. The concepts are compared on the basis of temperature margins, weight and performance verification.

Figure 4.4-13 shows the temperature profiles for the plasma probe, micrometeorite detector, trapped-radiation detector, and magnetometer for the solar-shield concept. These curves lie well within the operating temperature limits of 14° to 132°F. Corresponding curves

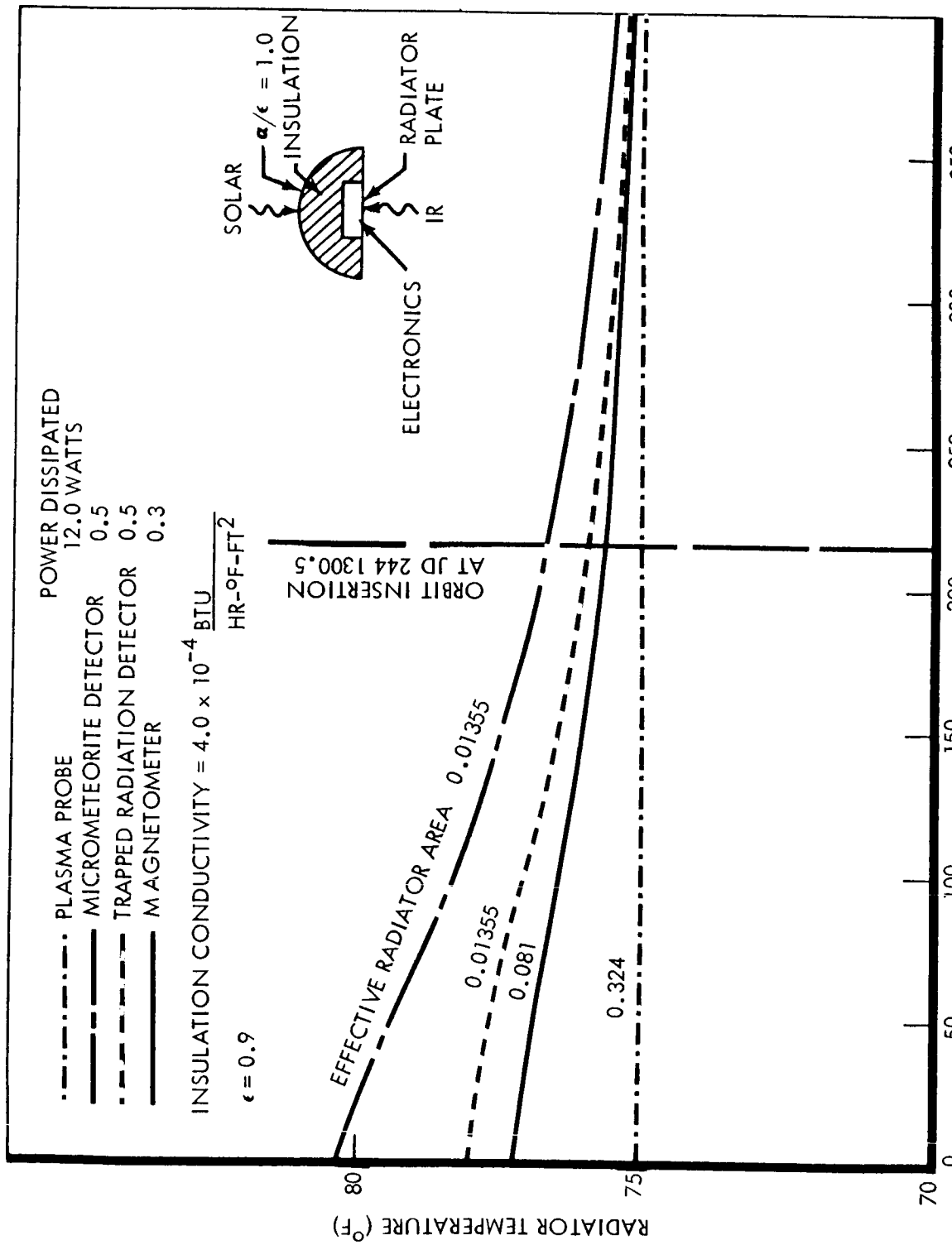

Figure 4.4-13: Temperature Profiles of Externally Mounted Instruments - Solar Shield Concept

for the coating concept appear in Figure 4.4-14. With the proper α/ϵ, the temperature of the instruments will remain within operating limits during transit. Further decrease of solar flux during orbit dictates the use of electric heat to maintain minimum temperatures. The power requirements are shown in Figure 4.4-15.

Figure 4.4-13 shows that the shield concept provides substantially greater temperature margins and, hence, is the preferred approach for small equipment. Since the heat-leak area is obviously less for this concept, it will undergo smaller temperature decreases during occultation and misorientation. There is no heater power weight penalty with this approach. Furthermore, the use of a black outer surface on the shield reduces testing problems and uncertainties regarding coating degradation.

Equipment Support (Booms)--The high-gain antenna and magnetometer booms have "not to exceed" requirements of 2^{o} and 1^{o}, respectively. Figure 4.4-16 compares deflections of booms for specular, gray, and black coatings. Results show that only the specular surface meets the requirements for the magnetometer boom, whereas any of these surfaces would be acceptable for the high-gain antenna boom. Since the specular surface results in the minimum deflection, it is preferred as the surface treatment for all booms.

4.4.1.3 Propulsion Module

The propulsion module includes tankage plumbing, nozzles, and structure associated with the RCS, midcourse and orbit-insertion propulsion. It is located in the center of the spacecraft with the orbit insertion

ERRATA

The Boeing Company Document D2 82709-2
Voyager Spacecraft System Final Technical Report

VOLUME B

"Alternate Designs Considered for Flight Spacecraft and Hardware Subsystems"

Page No.	Paragraph, Table, or Figure No.	
3-24	Table 3-2	Add to "Injection" line: Under Column "1σ B_{MAX}" add ">4 (10^5)" Under Column "1σ B_{MIN}" add ">5 (10^3)" Under Column "Θ MAX" add "26.9" On Line "5 125" under Column "$1\sigma \Delta V$" change "0.107" to "1.07" On Line "5 125 175," under Column "$1\sigma T_F$" change "0.00" to "0.003" Add to last line on page "in meters per second"
3-28	Para. 3.1.3.2	Midcourse Guidance Accuracy Analysis Add: "Δ" in second line to read: "ΔVproportional errors;"
3-57	Table 3-6	Last entry in Column "Δt_p" add "$.7 \cdot 10^{-6}$" (hrs)
3-63	Figure 3-24	Change ordinate label to read: "Error in Ω, 1σ (degrees) Add abscissa label to read: "Hours"
3-67	Para. 3.1.7	Line 11: Delete: "(3Δ)" Add: "(3σ)"
3-81	Para. 3.2.2	Line 5: Delete: "high-low"
3-89	Para. 3.2.4.2	Last line on page: Delete ". No" Change: "risk) no appreciable difference in the assessments existed."

ERRATA (Continued)

VOLUME B

Page No.	Paragraph, Table, or Figure No.	
3-90	Figure 3-30	Add in third entry in third column under "Configuration" to read "0.73" Delete: Second column under Configuration Probability of Success Add: 0.25 0.62 0.73 0.83
3-108	Para. 3.3.4.4	Line 22: Delete sentence "The estimated failure rate... ." Add: "The estimated failure rate is reported in Section 6, Volume A, to be 5 in 100,000 with a component reliability of 0.9999945."
4.1-87	Para. 4.1.4.3	Delete "doubt" from last line on page
4.1-95	Para. 4.1.5	Line 12: Delete: "Figure 4.1-10" Add: "Figure 4.1.11"
4.1-100	Para. 4.1.5.3	Last line on page: Change "Section 4.1.6.1" to "Section 4.1.5"
4.1-111	Para. 4.1.5.4	Delete last sentence on page Add: "The d.c.-to-d.c. converter with its high-voltage power switching circuits, is not adaptable to subcomponent redundancy techniques."
4.1-116	Para. 4.1.5.4	Line 11: Delete "Summary--Table 4.1-10" Add: "Summary--Figure 4.1-13"
4.1-119	Table 4.1-11	Mode 3: Change: "Capsule Engineering Data" from "100 bps" to "10 bps" Change: "Stored Spacecraft Engineering Data" from "50 bps" to "100 bps"

ERRATA (Continued)

VOLUME B

Page No.	Paragraph, Table, or Figure No.	
4.1-127	Para. 4.1.6	Line 19: Change Section "4.1.1" to "4.1.3"
4.1-174	Para. 4.1.8	Line 8: Change "page 112" to "page 4.1-166"
4.2-6	Para. 4.2.1	Line 13: "This will permit... missions." Add" "(See reference 4)"
4.2-9	Para. 4.2.2.2	Delete Item 2) "The V-ridge, although... etc."
4.2-31	Para. 4.2.6	Add Reference 4 "4) Voyager Spacecraft Alternate Radioisotope Thermoelectric Electrical Power Subsystems, EOS Document No. EOS-V-1040, 29 July 1965."
4.3-5	Para. 4.3	Line 18: Change "30 pounds" to "38 pounds"
4.3-12	Para. 4.3.2.1	Line 3 from bottom of page: Change: "Subsystem component test" to "Subsystem component list"
4.3-32	Figure 4.3-6	Delete: " B HYD OIL ACCUM"
4.3-35	Table 4.3-14	Change Acceleration, Max. (G's) Orbit Trim from "0.36" to "0.036" Change Acceleration, Min. (G's) Orbit Trim from "0.34" to "0.034"
4.3-36	Table 4.3-15	Change Maximum Thrust/Weight Monopropellant from "0.36 (Orbit Trim)" to "0.036 (Orbit Trim)"
4.3-54	Para. 4.3.3.1	Line 12: Change "However, the ellipsoidal motor velocity has per-" to "However, the ellipsoidal motor has per-"
4.3-85	Para. 4.3.3.2	Line 6: Change "(Volume A, Section " To: "(Volume A, Section 3.8)"

ERRATA (Continued)

VOLUME B

Page No.	Paragraph, Table, or Figure No.	
4.5-14	Para. 4.5.1.3	Line 5: Change "field of view of ±2.5" To: "field of view of ±5"
4.5-57	Table 4.5-10	Under "Analog Alternate No. 1, Major Advantages" Add: 1. Space-proven 2. Low Drift Under "Analog Alternate No. 2, Major Advantages" Add: 1. Space-proven 2. Low power